Controls on rift-climax sedimentation: impact of sediment sources, sea-level change and tectonics. Examples from the Gulf of Suez Rift, Egypt.

A thesis submitted to the University of Manchester for the Degree of PhD in the Faculty of Engineering and Physical Sciences.

2009

Paul Woodman

School of Earth, Atmospheric and Environmental Sciences

CONTENTS

SECTION ONE: INTRODUCTION AND BACKGROUND

SECTION TWO: MIOCENE SUEZ RIFT, EGYPT

Word count = 75,163

FIGURE LIST

TABLE LIST

APPENDICES

ENCLOSURES

ABSTRACT

The aim of this project is to investigate the controls on syn-rift sedimentation during the latter stages of rifting by integrating sedimentary, stratigraphic and structural data from a variety of structural settings within the Oligo-Miocene Suez Rift, Egypt. In particular, this project examines the syn-rift depositional systems associated with the late rift climax Upper Rudeis Formation to address the nature of local structural, and more regional (e.g. sea-level, sediment supply) controls that interact to influence geomorphology, sediment supply and sequence stratigraphy of depositional systems that are deposited around active normal faults.

Although recent advances have been made in understanding small-scale depositional systems associated with drainage networks that develop locally around active normal faults, little attention has been paid to larger-scale, regional drainage systems and associated depositional systems at a fault block (20-30 km long by 5-10 wide) and rift-wide scale. This is addressed through a comprehensive subsurface dataset from the present day offshore axis of the rift, integrated with extensive exposures along the eastern rift margin, located within the Sinai Peninsula. Regionally consistent, key sequence stratigraphic surfaces within a biostratigraphic framework are used to subdivide the Upper Rudeis Formation into a series of high-resolution, stratal units, which are then correlated from the rift axis to rift margin. This allows for the spatial and temporal variability of the Upper Rudeis Formation to be compared across the main structural domains characteristic of rift basins. As a result, this study provides a model for contemporaneous linked tectono-stratigraphic evolution of late rift-climax syn-rift depositional systems across a rift basin.

Consistent with conceptual tectono-stratigraphic models for rift evolution, (e.g. Gawthorpe and Leeder, 2000), the facies, thickness and stratigraphic variability of late rift climax deposits are shown in this study to be fundamentally controlled by the evolving nature of tectonically-generated relief, with normal fault populations defining the location and extent of sediment source areas, transport pathways and depocentres. However, in addition to the role provided by this local structural template, the identification of regionally consistent key surfaces, associated facies shifts, thickness variations and compositional data are suggestive of a series of more regional-natured controls upon the deposition of the Upper Rudeis Formation.

Using thickness, facies, and compositional data, this study documents the presence and spatial extent of a series of regionally extensive depositional systems transporting material from the margin to the axis of the rift. Sourced from a major hinterland provided by the uplifted rift shoulder, these extensive sedimentary systems are in marked contrast to those locally-derived from individual uplifted footwall blocks and have a complex interaction with individual fault zones due to the interplay between rates of fault-generated accommodation space and sediment supply. As a result, varying stratigraphic, thickness and facies distributions are observed at differing structural locations. The temporal evolution of these regional depositional systems is recorded through the regional correlation of the key surfaces identified, which delineate a series of consistent basinward and landward shifts in facies. These rift-wide shifts are interpreted to reflect regional fluctuations in relative sea-level, and a potential role for glacio-eustasy against a backdrop of waning tectonic activity is considered.

The results of this study have general implications for tectono-stratigraphic development and variability during rift basin evolution. In particular, this study highlights the importance of investigating syn-rift variability from a variety of structural settings within a rift, thus allowing for contrasting responses to the complex interplay of tectonics and other controls to be recorded and thereby allowing for a truly basinwide synthesis for the distinct evolutionary phases of rift basin development.

DECLARATION

No portion of the work referred to in this thesis has been submitted in the support of an application for another degree or qualification of this or any other university or other institute of learning.

Paul David Woodman

ACKNOWLEDGEMENTS

I would like to thank the many people who have been associated in one way or another the last few years with this PhD project.

Firstly, thanks to Rob Gawthorpe for providing me with the opportunity to undertake such a varied and interesting research project. Moreover, I have greatly appreciated his time and expertise both in the field and in guiding me through the epic that has been the production of this thesis. Thanks also to all the members of the Basin Research Group who I've come across over the years, with particular thanks to guys who have made fieldwork in Egypt so fun and informative. In this regard, thanks to Chris Leppard, Dave Hodgetts, Ivan Fabuel-Perez, Paul Wilson, Frank Rarity and Lorna Strachan. Other Manchester folk who have been friends and colleagues both in and out the office, at conferences (and their associated road trips) and during the time I spent commuting have included Laura Adams, Ruth Underdown, Nadine Mader, Chris Edwards, Vicky Coker and Vicky Catteral.

Very sadly, our driver and guide in the field, Sayed Good passed away in late 2008. However, Sayed was more than just a driver or guide – I always felt he acted as *loco-parentis* to all the numerous students Rob has sent out to wander the desert over the years, and I was no exception. He had an especially challenging time with me in my choice of field area, as the local bedouins in the area did not always take kindly to our interruptions into their prolific agri-business activities. As such, Sayed frequently added bodyguard, negotiator and getaway driver to his list of job titles. He will be sorely missed. Thanks must also go to Sayed's brother Gamal, and his son, Bilal, for also taking me around in the desert and for the preparation of what must be a frighteningly large number of tuna sandwiches that I've eaten in the field.

I would like to thank to the many friends and colleagues who have helped me in Egypt over the past few years, both on visits and for the 15 months Rob exiled me there to work at GUPCO. The help of Sammy, Yagieh, Anwar, Gammal Amar, Mohammed Tarek, Mohammed Zahran, and the numerous Biostrat guys was invaluable. Additionally I must thank the Hawagas in the exploration team; Ashley Price and Graeme Bagley for giving me a job, Joe Piombino for his comprehensive subsurface knowledge and willingness to give my ideas some push back, Simon Payne for his help in deciphering the years of voluminous (and varying) biostratigraphic datasets, Tom Mason for chats about the Asl and also Karl Henck for his insights into the southern GOS.

I would finally like to thank my family for their help and encouragement over the last few years. And a special mention for my wife, Rachel, who has continually and unfailingly supported me over the course of this work.

SECTION ONE
INTRODUCTION AND BACKGROUND

CHAPTER ONE
INTRODUCTION

CHAPTER 1
INTRODUCTION

1.1. RATIONALE

This thesis utilises an extensive database comprising 3D seismic, borehole and fieldwork-derived data to investigate sedimentation within a rift basin setting deposited during the latter stages of the main phase of rift development and the range of controls on facies distribution and stratigraphic development.

Syn-rift deposits (i.e. those sediments deposited synchronously during an active phase of rifting) have been shown to provide a valuable insight into the evolution of extensional settings; the varying distribution of facies types, thicknesses and nature of stratigraphic geometries reflect the complex interplay of primary local tectonic and more regional controls (e.g. sea/lake level, climate and sediment supply) upon deposition. Characterised by a high preservation potential, such deposits therefore may provide an important record about the temporal and spatial variability of the mechanisms controlling the basin fill (e.g. Gawthorpe & Leeder, 2000). A major focus of previous research, analysis of syn-rift deposits has impacted both on our current understanding of nucleation, growth and linkage of normal fault systems, whilst also providing more specific information on syn-rift depositional systems, aiding the reconstruction of local palaeoenvironments and palaeoclimates (e.g. Leeder and Gawthorpe, 1987; Eliet and Gawthorpe, 1995; Ravnås and Bondevik, 1997; Ravnås et al., 1997; Gawthorpe and Leeder 2000).

In addition, rift basins provide vast economic reserves of natural resources. Syn-rift deposits form potential reservoirs, which due to potentially marked variability over relatively short distances (< 100's m), require careful study to enable accurate delineation. With specific respect to hydrocarbons, rift basins contain a disproportionate amount of oil and gas reserves for the 5% volume of the sedimentary basin record that they represent (e.g. Landon, 1994; Katz, 1995).

Published models for the linked tectonic and stratigraphic evolution of rift basins commonly divide the syn-rift infill into broad *initiation* and *climax* stages (e.g. Prosser, 1993); consistent with models for the development of normal fault systems in which the initial radial propagation of individual isolated faults is followed by interaction and linkage of fault segments to form hard-linked fault arrays (e.g. Cowie et al., 2000; Gawthorpe & Leeder, 2000). Both rift initiation and climax stratigraphy has been the

subject of considerable previous research, utilising outcrop (e.g. Jackson et al., 2006; Young et al., 2000), subsurface (e.g. Dawers & Underhill, 2000; Corfield & Sharp, 2000; Young et al., 2001) and numerical modelling methods (e.g. Cowie, 1998; Gupta et al., 1998; Cowie et al., 2000). These studies have documented how the evolution of local normal fault systems within a rift increasingly provides a dominant control upon coeval depositional systems and thus the resultant stratal geometries and architectures developed. Distinct early, mid and late sub-phases have been described for both the larger initiation stage (e.g. Cowie et al., 2000) and climax stage (e.g. Nottvedt et al., 1995; Ranvas and Steel, 1997; Ranvas et al., 2000), with the main focus to date for this research having been placed on the initiation stage and the subsequent switch to climax stages. In contrast, the latter part of the rift climax stage, prior to the onset of post-rift and the associated abatement of fault activity has not been significantly discussed.

During this 'late rift climax' phase as defined in this thesis, there is potential for fault activity to become reduced and for more episodic faulting to occur in response to the transition to a post-rift scenario. Whilst the structurally-defined relief inherited from the previous main period of rift climax remains important, in some parts of a rift, this episodic and reduced rate of fault displacement may result in more non-tectonic controls having a greater relative impact upon deposition, e.g. eustatic sea-level change, climate and sediment supply. Thus in contrast to a simplistic model in which stratigraphy deposited during the rift climax period is completely dominated by first-order structural control, in fact the final part of this phase may be characterised by a complex interplay of both regional and local controls. Also the relative importance of these controls is likely to vary greatly across the different structural domains throughout the rift. Recognising this change from a dominant, purely structural control to a more complex scenario may greatly impact upon the accuracy of predictive models for sedimentary systems deposited during this phase of rift evolution. The different structural domains which form the principal study areas of this thesis and the range of scales at which they are investigated, offer a unique opportunity to evaluate the complex interaction of controls upon sedimentation within a late rift climax phase.

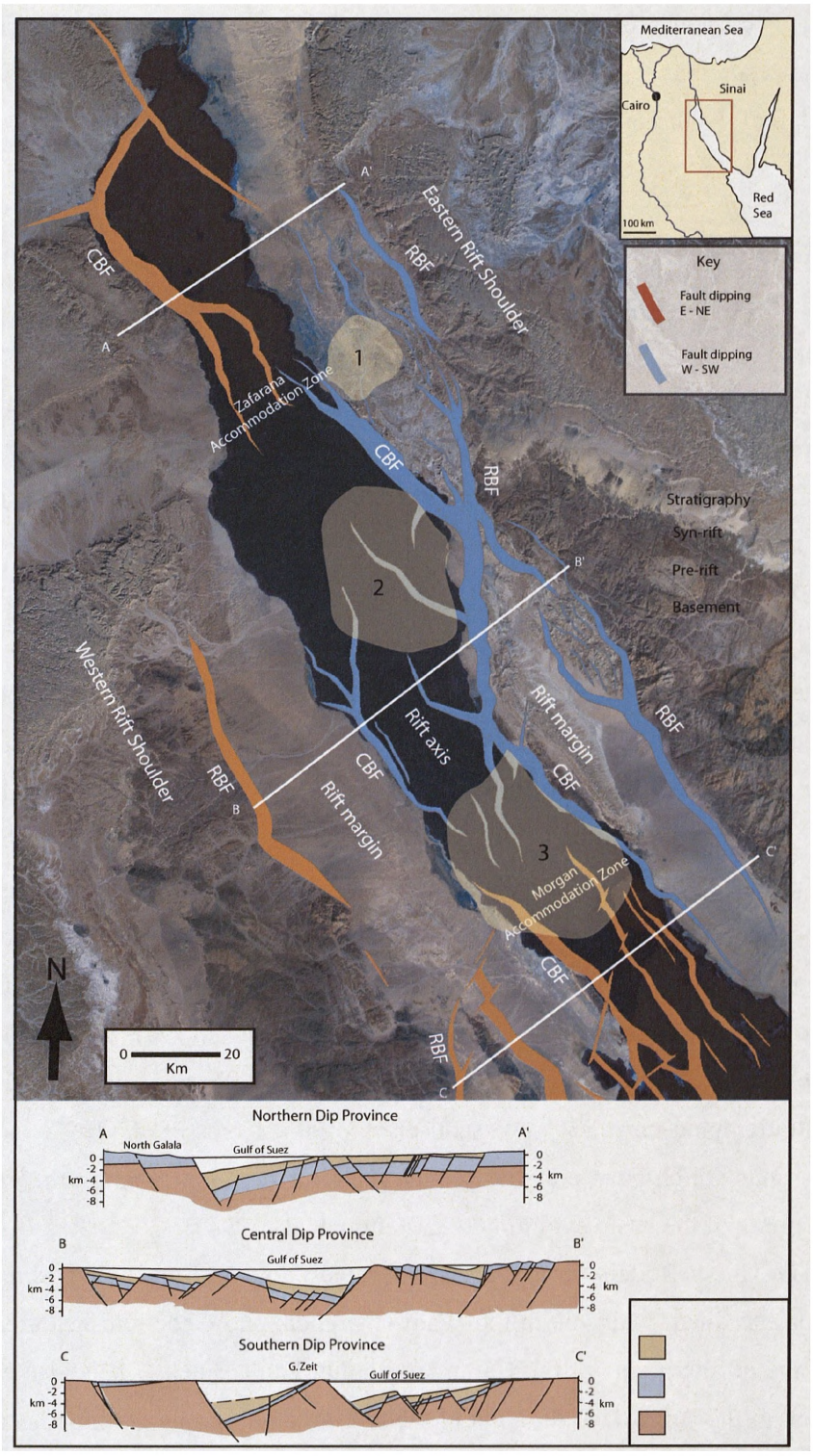

Figure 1.1. Landsat image of the Suez Rift, displaying main structural elements for the northern, central and southern dip provinces in addition to the intervening Zafarana and Morgan Accommodation Zones. Regional faults modified after Younes and McClay, 2002 (RBF = Rift Border Fault; CBF = Coastal Boundary Fault). The location of the three principal study areas are highlighted: 1) Wadi Gharandal - Gebel Gushea; 2) October area and 3) Morgan Accommodation Zone. Lines A-A' to C-C' after Patton et al., 1994. Corner inset displays regional context of the rift location.

This chapter proceeds to outline the scope, principal aims and objectives of this PhD study, summarises the available datasets and methodologies and finishes with a description of the thesis layout.

1.2. PROJECT SCOPE

This project utilises some of the superbly exposed Oligocene to Miocene syn-rift stratigraphy on the Sinai Peninsula within the Suez Rift in addition to a comprehensive subsurface database provided by an industrial sponsor company, the Gulf of Suez Petroleum Company (GUPCO), the largest operating petroleum company within the Suez Rift, comprising 3D seismic, wireline, core and detailed biostratigraphic data from beneath the present day offshore Gulf of Suez (Fig. 1.1).

This study was envisaged to build upon recent studies of syn-rift deposits along the margin of the Suez Rift, which have previously been broadly defined as part of the rift climax succession (Sharp et al., 2000, Young et al., 2000; 2002; Gawthorpe et al., 2003; Leppard and Gawthorpe 2006). A key aspect of this thesis research was to examine both the rift margin and rift axis, through outcrop based studies in the Hammam Faraun Fault Block along the rift margin in the Sinai Peninsula, and to provide a linkage to contemporaneous deposits within the rift axis, primarily though a subsurface dataset provided for the offshore October Fault Block. The principal stratigraphic interval of focus has been referred to previously as the Upper Rudeis Formation (e.g. Garfunkel and Bartov, 1977; Patton et al., 1994), the Asl and Hawara Formations or Members (Dolson et al., 1996; Pivnik et al., 2003) and tectonostratigraphic unit 'S30' (Wescott et al., 1996; Krebs et al., 1997), and directly precedes units which have previously been interpreted as representing the onset of the post-rift phase of the basin evolution (e.g. Patton et al., 1994).

The Upper Rudeis Formation is extensively exposed on the western margin of the rift on the Sinai Peninsula in the Wadi Gharandal and Gebel Gushea areas, located towards the northern part of the Hammam Faraun Fault Block. It is also extensively penetrated in the subsurface throughout the rift, highlighting its potential as a principal syn-rift hydrocarbon reservoir. As outlined in Chapter 3, which reviews the overall geological setting of the Suez Rift, the Upper Rudeis Formation markedly differs from the preceding rift climax Lower Rudeis Formation. The Lower Rudeis Formation is dominated by fine-grained hemipelagic sediments and intervening localised coarse-

grained clastics, therefore conforming to conceptual facies models for tectonically controlled rift climax deposits. In contrast, previous studies of the Upper Rudeis Formation have shown it to mark a regional change in depositional style, to more proximal, coarser-grained clastic sediments within both the rift margin and axis. In order to investigate the nature of this marked change in syn-rift deposition, observations of sedimentological, stratigraphic and thickness variability of the Upper Rudeis Formation from three principle study areas within the rift are integrated to determine the varying impact of both local (e.g. localised fault evolution) and more regional controls (e.g. variations in sediment supply or sea-level) on deposition.

1.3. DATASET AND METHODOLOGY

Three principal study areas within the Suez Rift were considered as part of this thesis, (Fig 1.1.). An outcrop-based study area located towards the northern part of the Hammam Faraun Fault Block on the eastern margin of the rift in the Sinai Peninsula was complemented by two subsurface study areas located on the October Fault Block, and the Morgan Accommodation Zone respectively (Fig.1.1)

In the rift margin study area, exposures of the Upper Rudeis Formation within the Wadi Gharandal and Gebel Gushea areas offer a readily accessible dataset to be investigated through fieldwork techniques, based on geological mapping, integrated with analysis of SPOT and QUIKBIRD satellite imagery for a study area of approximately 158 km^2. Vertical sedimentary successions were logged, with the recording of principal sedimentological and thickness data. A laser range finder was used to measure gross stratal sections, for largely inaccessible, vertical sections. Measured sections were correlated by the tracing or 'walking-out' of key stratal surfaces and utilising photomontages.

With respect to the rift axis study areas, the October Fault Block provided an initial focus subsurface dataset. The data from the October area comprised 131 wells with a variable suite of wireline logs, core, accompanying high resolution biostratigraphic data and the NGOSMEGA pre-stack depth-migrated 3D seismic survey covering an area of 450 km^2. Existing GUPCO horizon interpretations for the present day structure of the October Fault Block were used as a primary template with which to delineate the variability of the Upper Rudeis Formation primarily due to the very poor quality of the seismic data. These horizon interpretations were tested against the extensive borehole data.

Six wells located in the hangingwall of the October Fault Zone provided cored intervals of the Upper Rudeis Formation; approximately 275 m was examined and logged at a scale of 1:50, with relevant sedimentological and ichnofabric information recorded and accompanying petrographic analysis of thin sections. Subsequent lithofacies and process-based facies associations, identified within cored intervals, were calibrated to the wireline logs, allowing for the development of a process-based facies model. Key surfaces identified at both the core and wireline log scales were then used to aid correlation within the larger study area to offer an interpretation for the linked structural and stratigraphic evolution of the October Fault Zone during the deposition of the Upper Rudeis Formation.

A second rift axis dataset associated with a major structural accommodation zone, termed the Morgan Accommodation Zone became available during the course of the study as part of a 15 month placement at the sponsor company. Covering an area of approximately 1600 km^2, the dataset consists of two regional, depth pre-stack depth-migrated 3D seismic volumes, N2MERGE and SHMBVA. Regionally mapped major seismic horizons and structures throughout the study area were used in this study to help constrain sub-seismic resolution variations in the Upper Rudeis Formation. A comprehensive suite of borehole data for 324 wells which significantly penetrate the focus interval was utilised to determine key surfaces, intervening stratal units and related variations in facies types, facies stacking patterns and thickness. Integration of the sedimentary and stratigraphic data with structural interpretations were then used to interpret the evolution of both individual faults and depositional systems active within the study area during deposition of the Upper Rudeis Formation.

1.4. AIMS AND OBJECTIVES

The overall aim of this project is to document the nature of Upper Rudeis Formation depositional systems from differing structural settings within the rift. This is in order to determine the role of local structural, and more regional (e.g. sea-level, sediment supply) controls that interact to influence geomorphology, sediment supply and sequence stratigraphy of depositional systems that are deposited around active normal faults, during the latter part of the climax stage of rift basin evolution. This overall aim is addressed through a series of specific key objectives:

1) Examine the sedimentology, facies and stratigraphy of late rift climax deposits of the Upper Rudeis Formation associated with a major rift axis, crustal-scale fault zone and associated tilted fault-block within the axis of the Suez Rift (i.e. the October Fault Zone). Define the extent of any regional or local syn-rift depositional systems and the controls upon their development.

2) Map stratigraphic thickness and facies variability of the Upper Rudeis Formation around the October Fault Zone, to integrate these observations with interpretations for the present day structural configuration of the October Fault Zone in order to provide a model for its linked tectonostratigraphic evolution.

3) Identify key facies, stratal units, and bounding surfaces within the Upper Rudeis Formation consistent with a biostratigraphic framework within the rift axis component of a major structural accommodation zone (the Morgan Accommodation Zone). Correlate these key stratal surfaces throughout the study area.

4) Map the regional thickness variability of the high resolution stratal units for the Upper Rudeis Formation identified within the Morgan Accommodation Zone study area. Use these thickness maps to determine the timing of activity upon a series of major block bounding fault zones, and furthermore with the integration of facies information, to document the scale and evolution of depositional systems entering the rift axis.

5) Examine the sedimentology, stratigraphy and thickness variability of rift initiation to late rift climax deposits within the proximal part of a major structural accommodation zone (the Zafarana Accommodation Zone). Contrast the nature of controls upon rift climax sedimentation in such an area of subtle and diffuse structure with contemporaneous deposits elsewhere along the margin of the rift.

6) Integrate the observations of late rift climax deposits studied in the three differing structural positions within the rift, i.e. rift axis fault block (October Fault Zone), rift axis component of structural accommodation zone (Morgan Accommodation Zone) and the rift margin part of a structural accommodation zone (Zafarana Accommodation Zone). Combine with previously published data for contemporaneous deposits elsewhere

within the rift to produce a regional, rift-wide sequence stratigraphic model for late rift climax deposition

7) Provide a synthesis of the observations and interpretations of this study and discuss their general implications for tectonostratigraphic models for syn-rift sedimentation.

1.5. THESIS LAYOUT

This thesis is organised into three sections. **Section 1** provides an introduction to the research conducted as part of this study, and comprises this initial introductory chapter (**Chapter 1**), a background literature review with respect to the current understanding of processes of sedimentation and tectonics within extensional basins (**Chapter 2**), and an additional detailed review of the published record of the overall geological setting and evolution of the Suez Rift (**Chapter 3**), which provides the principle study area.

Section 2 contains the main research chapters, and is structured around three main principle focus areas studied within the rift. Each chapter is presented as a self-contained paper with individual introductions and pertinent descriptions of the geological setting, which are followed by observations and subsequent interpretations which are then discussed and summarised. **Chapter 4** provides a detailed model for the sedimentological and tectonostratigraphic evolution of the late rift climax Upper Rudeis Formation associated with the October Fault Zone, a major block-bounding fault zone with a maximum of 2 km displacement, located in the northern part of the central dip province within the rift axis. Regional versus local-scale depositional systems are identified on the basis of differing compositions, indicative of differing sediment provenances and linked to the structural evolution of the fault zone. This study demonstrates that in axial rift settings, localised late rift climax faulting is episodic and the main focus of displacement varies spatially through time, resulting in marked variations in active sediment transfer pathways and depocentres. In addtion to this local structural control, variations in relative regional sea-level, sediment source area and sediment entry points into the rift axis combined to control the location, magnitude, extent and composition of individual late rift-climax depositional systems.

Chapter 5 examines the variability associated with regional-scale, late rift climax, depositional systems within the rift axis component of a major structural accommodation zone associated with a flip in the polarity of the dominant dip direction

of major seismogenic faults and associated fault blocks. Using a regionally extensive, biostratigraphy supported stratigraphic framework for the Upper Rudeis Formation, this chapter documents the spatial and temporal variability of regional-scale late rift climax depositional systems entering the rift axis via structurally controlled entry points associated with the major structural Morgan Accommodation Zone. This study demonstrates that during the late rift climax stage, the evolution of the structural template was episodic and directly controlled the location of sediment transport pathways and depocentres, whilst more regional relative sea-level variations controlled the magnitude and resulting spatial extent of major syn-rift depositional systems entering the rift axis.

Chapter 6 provides a regional-scale (158 km^2) study of rift initiation to late rift climax deposits located within the proximal, rift margin component of the Zafarana Accommodation Zone, centred upon the Wadi Gharandal and Gebel Gushea areas to the north of the Hammam Faraun Fault Block. This chapter highlights the primary importance of a complex structural template on facies and thickness distributions associated with intra-block faults, syn-sedimentary growth faults, and fault-related folding. However, the distributed deformation in the accommodation zone results in subtle topography and shallower bathymetry compared to the major fault blocks in the adjacent northern and central dip provinces. This reduced topography in the accommodation zone results in a stronger relative sea-level signal compared to the hangingwalls of the main block-bounding faults.

Chapter 7 takes the observations of Upper Rudeis Formation variability from the preceding chapters of Section 2, and integrates them with previously published studies to provide a sequence stratigraphic model for late rift climax deposits in a variety of tectonostratigraphic settings. Whilst observed to have varying stratigraphic architectures at differing structural locations, the regionally correlated key surfaces identified in this chapter delineate consistent rift-wide basinward and landward shifts in the location of principal Upper Rudeis depositional systems. Previous studies, based heavily upon examined exposures at the rift margin, have linked the onset of deposition of the Upper Rudeis Formation to a major tectonic reorganisation of the rift, the cause of which proved controversial. Rather than a response to an isolated episode, this study suggests that the Upper Rudeis Formation reflects marked changes in regional relative sea-level, largely driven by glacio-eustasy, upon syn-rift sedimentation during a period of reduced and episodic fault activity. This chapter provides an example of the

contemporaneous variability of sediments deposited during a period of late rift climax in response to the interplay of evolving structurally controlled phyisography and bathymetry, variations in regional base-level and differing sediment source areas and transfer pathways.

Section 3 contains the final, concluding chapter (**Chapter 8**) of this thesis, which presents a synthesis of the results from Chapters 4 to 7, together with the main conclusions and recommendations for future work.

CHAPTER TWO
TECTONICS AND SEDIMENTATION IN RIFTS

CHAPTER 2
TECTONICS AND SEDIMENTATION IN RIFTS

2.1. INTRODUCTION

This chapter aims to provide a background context for this PhD research project by briefly reviewing the current understanding and concepts of the relationships between tectonics and sedimentation within a rift basin setting, which will be built upon in this thesis. This literature review chapter is divided into three sections in which: (1) the proposed mechanisms for the development of rift basins are summarised and resulting structural characteristics are described, (2) the dynamic nature of normal fault evolution within rifts is considered and (3) the interaction of structural and other controls upon the deposition of coeval syn-rift deposits and their resulting variability are discussed.

2.2. RIFT BASIN DEVELOPMENT AND ARCHITECTURE

2.2.1 Rift forming processes

Basins formed due to the extension and rupture of the continental lithosphere form part of an evolutionary sequence in which intracontinental rifts form in response to the earlier stages of extension, and are commonly referred to as failed or aborted rifts if they do not achieve crustal separation. Continued extension results in successful rifting and the subsequent development of a conjugate pair of passive margins and an intervening new oceanic basin (e.g. Allen and Allen, 1990; Ziegler and Cloetingh, 2004). The term rift was coined by Gregory (1894) working in the East African Rift System, and can be broadly defined as an elongate depression above a site of extensional lithospheric rupture, bounded by normal faults (e.g. Burke, 1980; Nelson et al., 1992). Well documented examples include the Rhine Graben and the Lake Baikal, East Greenland, Corinth, Suez, North Sea and East African Rifts, which contrast with broader zones of extension, such as the Basin & Range Province, USA.

The process of rifting has traditionally been discriminated into two distinct, idealised end-member processes, *active* and *passive* rifting (e.g. Sengor and Burke, 1978; Turcotte, 1983; Wilson, 1989; Allen and Allen, 1990). Active rifting is thought to occur as a result of the impingement of a thermal anomaly at the base of the lithosphere. Subsequent lithospheric thinning may result in isostatic uplift, with subsequent tensional stresses resulting in crustal extension. Alternatively passive rifting is thought to occur when tensional stresses within the continental lithosphere cause thinning and brittle failure

in the upper crust, resulting in the upwelling of hot aesthenosphere. Both these models account for the presence of a thermal anomaly at depth below many present day rift basins associated with a shallow Moho, and therefore it may be difficult to distinguish between either a 'passively' or 'actively' formed rift (Allen & Allen, 1990). Furthermore, recent studies have argued whether such a distinction is wholly justified, (e.g. Zeigler and Cloetingh, 2004).

Irrespective of the manner of rifting, traditionally two main mechanisms have been considered to accommodate the passive stretching of the lithosphere, i.e. the *pure* and *simple* shear models, (Fig. 2.1). McKenzie (1978) proposed a pure shear model of uniform stretching, were an initial rapid period of uniform mechanical lithospheric stretching accommodated by fault controlled subsidence is followed by a period of post rift thermal subsidence, resulting in a highly symmetrical rift basin, (Fig. 2.1). Simple shear models such as that of Wernicke (1981) suggest that extension may be accommodated along a major through-going low angle detachment fault, extending from the Earth's surface to either the base of the lithosphere or within the upper aesthenosphere.

2.2.2 Structural characteristics of rift basins

Areas of active lithospheric extension, such as rift basins, are characterised by the presence of normal fault populations, which typically show a sub-parallel direction of strike, perpendicular to the vector of extension (e.g. North Sea, Gulf of Suez, Central Greece, Basin and Range) (e.g. Garfunkel & Bartov, 1977; Stewart, 1980; Jackson & McKenzie, 1983). These faults accommodate the extension associated within the brittle, and therefore seismogenic upper crust above the ductile, aseismic lower crust. Thus the thickness of this brittle layer is fundamental to the length of major crustal-scale normal faults and the width of intervening fault blocks, as faults may only have dimensions comparable to or less than the brittle crust in which they are contained (Jackson et al., 1988). These major crustal-scale normal faults are typically planar, associated with dips between 30 and 60 , whilst commonly having length-scales of ca. 100 km and are typically ca. 20 km apart (Jackson et al., 1988; Roberts & Jackson, 1991). Fault trace lengths may be in excess of 100 km, but commonly display a discontinuous geometry along strike, with individual traces up to 30 km in length with distinct bends, "jogs" and areas of low displacement which are interpreted to reflect an en-echelon fault array composed of initially individual, but subsequently linked fault segments, (Eyidogan & Jackson, 1985; Stein & Barrientos, 1985; Jackson, 1987; Jackson et al., 1988; Jackson &

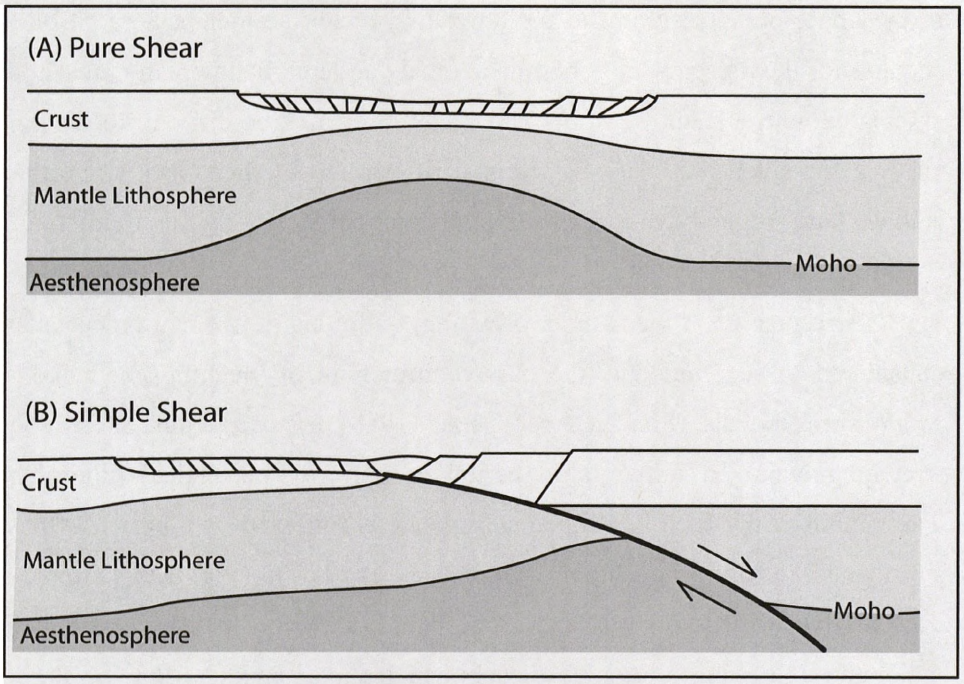

Figure 2.1. (A) Pure Shear and (B) Simple shear models of lithospheric stretching. From Allen and Allen (1990).

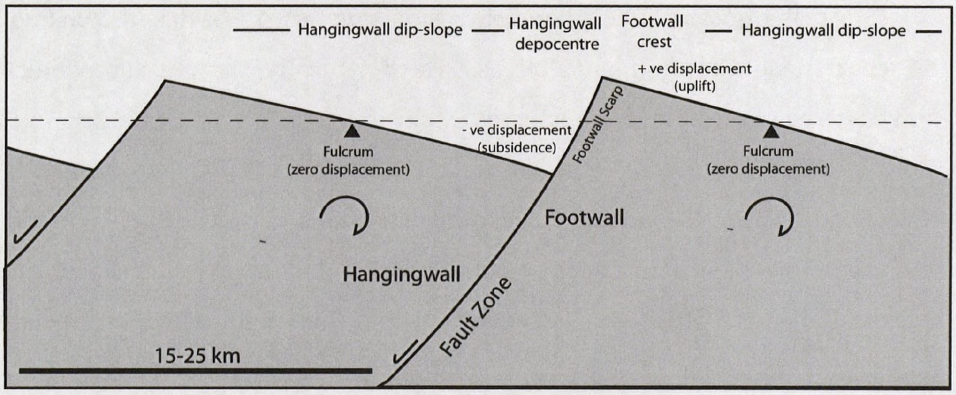

Figure 2.2. Simple 2D line sketch through a series of tilted fault blocks showing areas of uplift and subsidence and key terminology associated with structural relief and gradients.

White, 1989). This segmented nature is reaffirmed in studies of active fault zones, e.g. central Greece or the Basin and Range, which indicate that the faults are segmented along-strike, comprising a series of 20-30 km long segments separated by segment boundaries that inhibit or disrupt fault ruptures (e.g. Schwartz & Coppersmith, 1984; Jackson, 1987; Jackson & White, 1989; dePolo et al., 1991; Crone & Haller, 1991; Machette et al., 1991; Zhang et al., 1991; Gawthorpe & Hurst, 1993; Roberts, 1996).

The intervening area between two sub-parallel, synthetically dipping faults defines a fault block, which due to vertical motion associated with each of the bounding faults, typically results in a tilted or half-graben morphology. Thus, the classic model of rift basin structure is that of the rotating domino model for planar faults (e.g. Barr, 1987), which results in a series of tectonically induced slopes and asymmetric subsidence (Fig. 2.2). Fault blocks associated with major, crustal-scale bounding faults are typically in the order of 15 -25 km in width and 20 -35 km in length, and may contain numerous mesoscale (< 500 m displacement) synthetic and antithetic fault zones (e.g. Sharp et al., 2000a). Individual faults zones may be characterised by transfer zones or relay ramps which transfer displacement between individual fault segments along strike (e.g. Rosendahl et al, 1986, Rosendahl, 1987; Morley et al, 1990; Gawthorpe & Hurst, 1993; Morley, 1995), whilst broader structural accommodation zones, typically 10's km wide, allow for the separation of structural domains containing faults and fault blocks with opposite senses of dip polarity (e.g. Moustafa, 1976; Bosworth, 1995).

2.3. NORMAL FAULT SYSTEMS

As discussed in the previous section, the development of a rift basin is associated with extension accommodated by subsidence on basin bounding, long-lived, planar, seismogenic, normal fault arrays, (e.g. Jackson et al., 1988), which therefore provide a first order control on the temporal and spatial evolution of the basin extent and internal geomorphology. It is therefore of paramount importance to understand the evolution of normal fault arrays with respect to the mechanisms of individual fault growth, interaction and linkage, in order to determine the nature of the structural control upon syn-rift sediment dispersal patterns and stratigraphic development.

2.3.1 Mechanisms of Fault Growth

Extensional fault systems are spatially and temporally dynamic (e.g. Mcleod et al., 2000). It is widely understood that isolated faults evolve through time from isolated

segments to a linked, through-going fault array (e.g. Cowie et al., 2000; Gawthorpe & Leeder, 2000), but the mechanism(s) by which this is attained has been the subject of much debate as detailed data for this temporal evolution is still poorly constrained, (Gawthorpe & Leeder, 2000).

Two principal models exist for the initiation and development of normal faults. The first model suggests that the trace length of the fault increases with displacement, with initially isolated faults linking along strike forming longer faults (Cartwright et al., 1995; Cowie et al., 2000; Gawthorpe et al., 2003). A second model, more applicable to the reactivation of fault zones, suggests that faults attain their final trace length during the earliest stage of development, with final offsets representing the cumulative displacement on a fault that has had an approximate constant length during the majority of its evolution (e.g. Nicolet al., 2005; Bull et al., 2006; Manzocchi et al., 2006). Within the first model for fault growth, two distinct mechanisms are recognised (Cartwright et al., 1995) (1) radial propagation, (e.g. Walsh & Watterson, 1988) and (2) segment linkage (e.g. Anders & Schlische, 1994) with recent models suggesting a combination of both.

Growth by radial propagation follows a prescribed growth or scaling law, (Cartwright et al., 1995). Several studies (e.g. Peacock & Sanderson, 1991; Dawers & Anders, 1995; Cartwright et al., 1995) using both outcrop and subsurface data, have been based on the structural geometry of the fault trace, and quantitative data from ancient fault systems have indicated that maximum fault displacement (D) scales with fault trace length (L), (Fig. 2.3). Such models propose that increasing displacement accumulation on the fault surface is coupled with increased fault trace length, following the D-L ratio, (e.g. Walsh et al., 2002), and that maximum displacement occurs at the centre of the fault, reducing along the length of the fault to zero at the tip points. Implicit in this model is that the earliest formed faults had much shorter lengths initially than their final length, (Walsh et al., 2002). Whilst Dawers & Anders (1995) proposed that $D \propto L$, from studies of brittle fault populations, it is now generally accepted that conventional models of fault growth follow the growth law, $D = cL^n$ (e.g. Schlische et al., 1996; Walsh et al., 2002), in which c is a constant related to rock properties, including shear modulus (Cowie & Scholtz, 1992a, b; Scholtz et al., 1993; Dawers et al., 1993; Cartwright et al., 1995), and n is a scaling exponent, which varies between 1 and 2, (e.g. Watterson, 1986; Walsh & Watterson, 1988; Marret & Almendinger, 1991; Gillespie et al., 1992; Cowie & Scholtz, 1992a, b; Gudmundsson, 1992; Dawers et al., 1993; Dawers & Anders, 1995; Schlische et al., 1996).

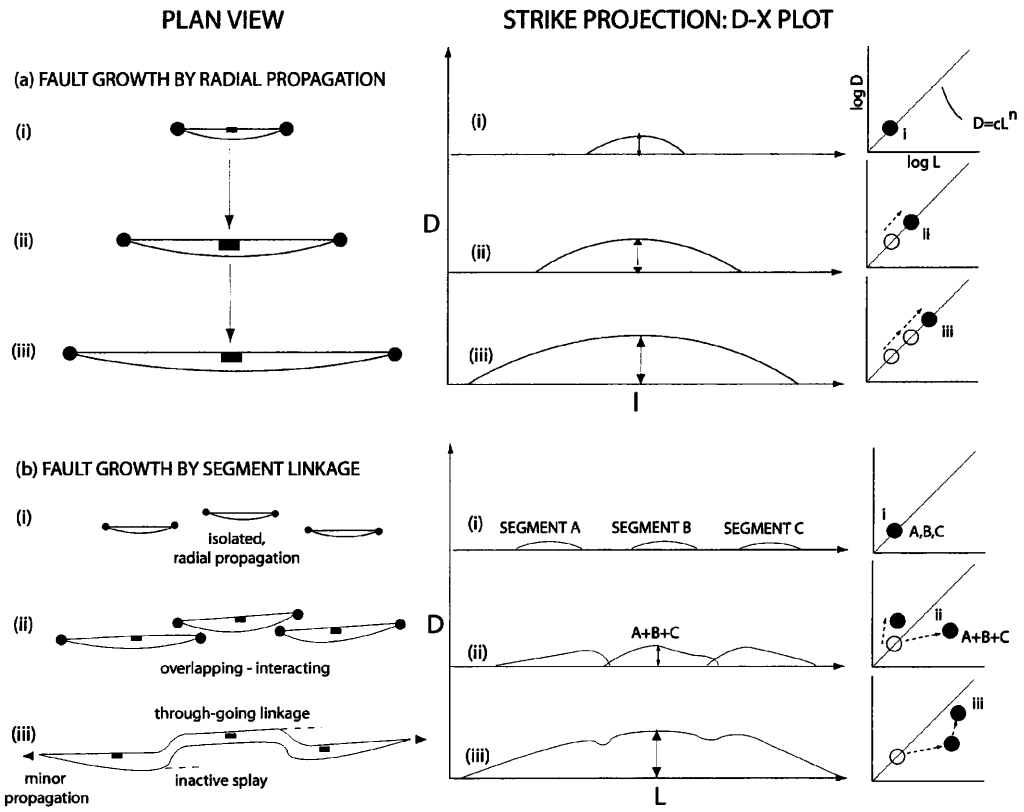

Figure 2.3. A comparision between two models of fault growth: a) radial propagation, and b) via segment linkage. Both models of fault growth are compared for displacement (d) against distance (l), and on a log maximum displacement (D) vs log trace length (L) plot. It is shown in a), that bilateral radial propagation produces a linear relationship, whilst segment linkage results in stepped deviations, b). Interaction of segments may lead to deviation above the idealised line, but the entire fault will show deviation below the line, as a longer trace length is produced for only a limited increase in maximum displacement. (from Cartwright et al., 1995).

Therefore, a D vs log L plot as shown in Figure 2.3, would show that for incremental increases in D and L, a linear growth path would be produced for the radial propagation of a fault. Variations in the value of n have been attributed to problems associated with *D-L* data compilation, mainly as scatter in D against L; Cartwright et al., (1995) proposed four explanations for this scatter of *D-L* data; (1) inaccurate data and sampling, (2) variations in material properties, (3) isostatic restoring forces imposing a limitation on displacement accumulation and (4) measurement biases. Using data from the Canyonlands graben of SE Utah, they showed how the scatter in *D-L* data could be attributed to the growth of a fault through initial isolated radial propagation, followed by subsequent interaction and linkage of fault segments, rather than trying to be reconciled entirely with radial, bilateral propagation (following the scaling law $D = cL^n$) of a single fault (Fig. 2.3).

Thus linkage of initially isolated normal fault segments is now understood to be the dominant mechanism of fault growth rather than simple radial propagation (e.g. Segall & Pollard, 1980; Segall, 1984; Pollard & Aydin, 1984; Granier, 1985; Watterson, 1986; Gudmundsson, 1987; Walsh & Watterson, 1988; Martel et al., 1988; Peacock & Sanderson, 1991; Marrett & Almendinger, 1991; Cowie & Scholtz, 1992a; Dawers et al., 1993; Gawthorpe & Hurst, 1993; Anders & Schlische, 1994; Jackson & Leeder, 1994; Trudgill & Cartwright, 1994; Cartwright et al., 1995) and has been documented in numerous subsurface and outcrop studies, (e.g. Dawers & Underhill 2000; McLeod et al., 2000; Young et al., 2001; Jackson et al., 2002).

Fault-related folding

Also associated with the propagation and linkage of normal fault systems is the development of fault-related folding, which can be considered as either longitudinal or transverse types with respect to the orientation of an underlying fault (e.g. Schlische, 1995).

Transverse folds, alternatively termed hangingwall anticlines or synclines and intra-basinal highs or lows, are linked to the along-strike variation in displacement associated with segmented fault systems (e.g. Schlische, 1995). Areas of lower displacement, such as between segment boundaries between overlapping segments may be characterised by anticlinal structures, whilst areas of higher displacements are typically associated with synclinal geometries (e.g. Anders & Schlsche, 1994; Schlische, 1995; Morley, 1999). As a result, the overall hangingwall of a segmented fault array can be characterised by a series of synclinal basins defining the centres of active fault segments, separated by anticlinal areas of displacement "deficit" defining fault segment boundaries (Fig. 2.4).

In contrast, longitudinal or alternatively termed drag or fault propagation folds may form either at the lateral tip points of surface ruptured faults, or above upward propagating, blind normal faults (e.g. Corfield & Sharp, 2000) (Fig. 2.4). In this scenario, a monoclinal fold may develop in response to the earliest stages of hangingwall displacement and coeval footwall uplift. Continued propagation leads to the rupture of the monocline and the development of a surface breaking fault; the remnant of the monocline forming a fault sub-parallel hangingwall syncline (e.g. Withjack et al., 1990; Schlische, 1995; Gawthorpe et al., 1997; Hardy & McClay, 1999; Sharp et al., 2000b). As normal fault zones are segmented, a surface ruptured fault may occur contemporaneously with a lateral tip propagation fold along strike, (Gawthorpe et al., 1997).

2.3.2 Evolution of normal fault systems

Analysis of the stacking patterns and stratigraphic architectures of coeval syn-rift deposits led to the identification of distinct tectono-stratigraphic phases associated with the development of normal fault systems (e.g. Prosser, 1993; Nottvedt et al., 1995; Ranvas and Steel 1997; Ranvas et al., 2000). In a broad sense, *rift initiation*, *rift climax* and *post-rift* periods have been discerned from syn-rift infill (Prosser, 1993) (Fig. 2.5), and have provided a basis for understanding the nature of the temporal and spatial evolution of extensional fault populations. Recent research has utilised numerical modelling (e.g. Cowie, 1998; Gupta et al., 1998; Cowie et al., 2000), outcrop (e.g. Sharp et al., 2000a; Gawthorpe et al., 2003) and subsurface studies (e.g. Dawers & Underhill, 2000; Corfield & Sharp, 2000; Young et al., 2001) to achieve this.

In this study, the term 'late rift climax' is used to describe the latter part of the rift climax period which is characterised by increasingly waning and episodic fault activity prior to the post-rift period. Comparable to the 'late-rift' stage of Ranvas and Steel (1998), the syn-rift deposits in this study show marked differences in facies and stratigraphic relationships than those typically ascribed to the main period of rifting. However, a subdivision of the rift climax period is preferred in this study rather than a separate tectono-stratigraphic period, as the structurally defined geomorphology within a rift defined during the main rifting phase, in addition to episodic faulting, may still potentially provide a dominant control upon sedimentation until the subsequent post-rift period. Furthermore, this nomenclature is consistent with other previous studies of fault array evolution, which having typically focussed on the onset of rifting, have subdivided the rift initiation period into early-, mid- and late-rift initiation sub-stages (e.g. Cowie et al. 2000).

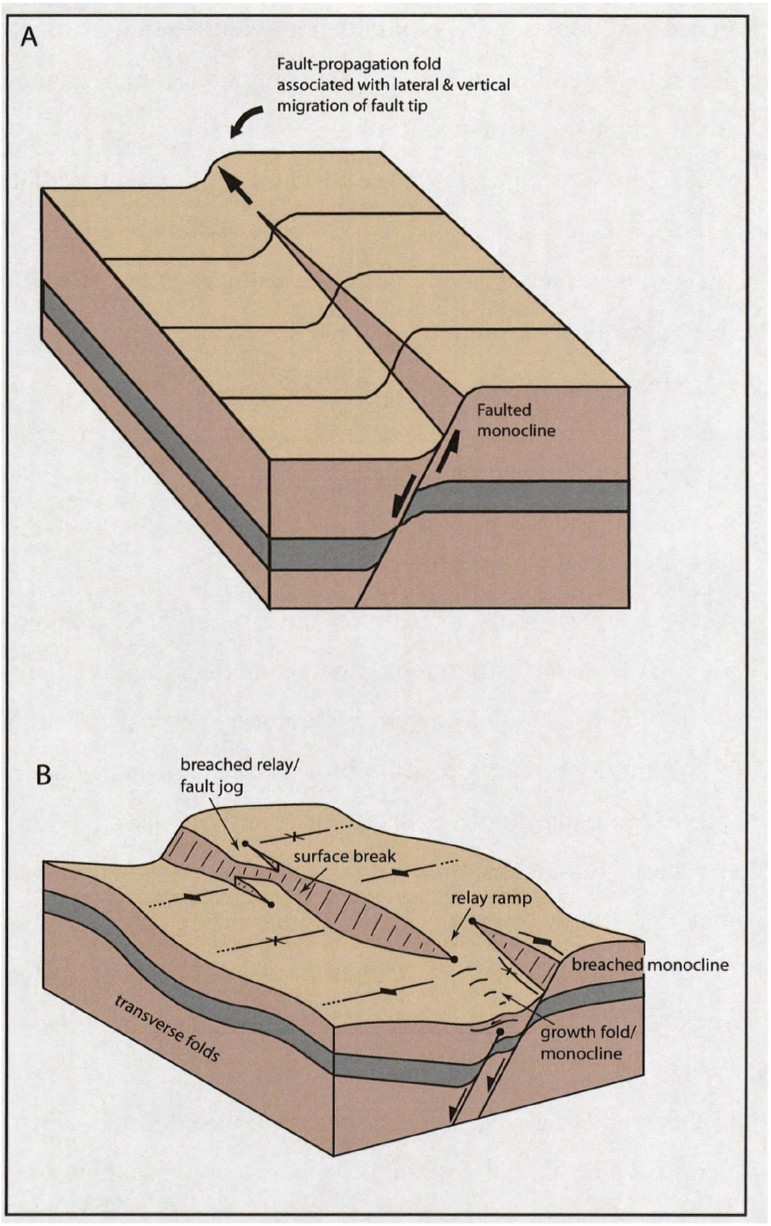

Figure 2.4. (A) Folding due to vertical and lateral propagation of a normal fault. Propagation of the fault tip results in the eventual surface rupture of the monocline, as with continued vertical propagation of a blind fault at depth. Modified from Walsh and Watterson, 1987; and Schlische, 1995. No scale. (B) Block diagram to show the significant structural elements of a rift basin, half-graben geometry, fault scarps, hangingwall dip slopes, relay ramps (transfer zones) and associated fault propagation folds. Modified from Larson(1988); Trudgill & Cartwright, (1994) and Schlische (1995).

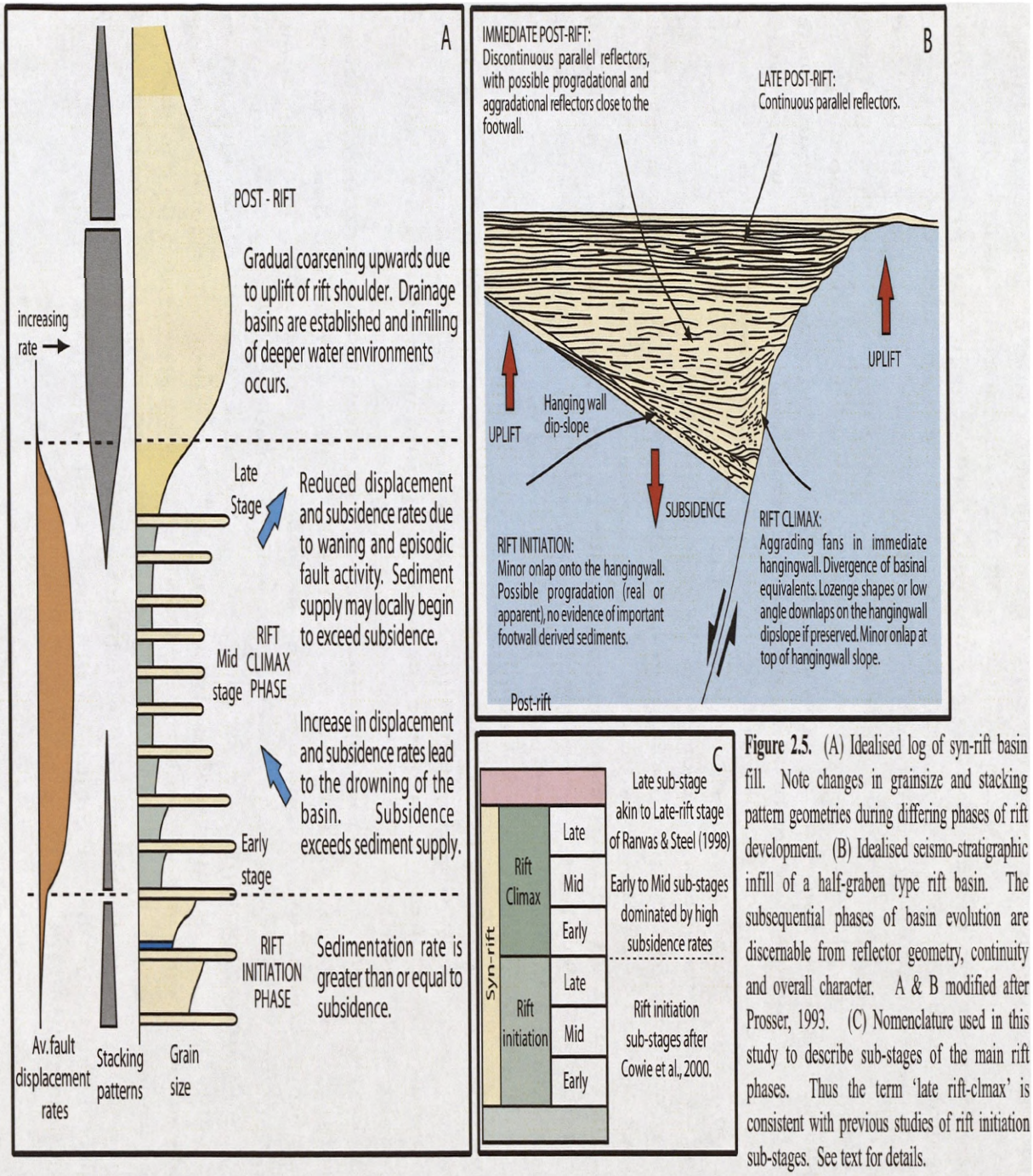

Figure 2.5. (A) Idealised log of syn-rift basin fill. Note changes in grainsize and stacking pattern geometries during differing phases of rift development. (B) Idealised seismo-stratigraphic infill of a half-graben type rift basin. The subsequential phases of basin evolution are discernable from reflector geometry, continuity and overall character. A & B modified after Prosser, 1993. (C) Nomenclature used in this study to describe sub-stages of the main rift phases. Thus the term 'late rift-climax' is consistent with previous studies of rift initiation sub-stages. See text for details.

The framework of this tectono-stratigraphic nomenclature is further described in Figure 2.5.

A key theme predicted by numerical modelling and documented in subsurface and outcrop studies, is the progressive localisation of displacement through time as the rift event progresses (Fig 2.6). During the initiation of extension, local crustal weaknesses provide for the nucleation of numerous isolated fault segments which grow by bilateral tip propagation and are characterised by small, typically uniform displacements (e.g. Cowie et al., 1998; Gupta et al., 1998; Cowie et al., 2000). Continued nucleation and propagation of these isolated segments leads to an increase in the fault population and subsequent onset of segment linkage events. A fault population of several longer segments with numerous smaller ones is developed; the larger segments forming early hangingwall depocentres. Higher subsidence rates are produced within the central section of the fault segments producing a characteristic asymmetric along-strike displacement profile. These larger faults grow more rapidly, whilst the numerous smaller faults fall within the stress shadows of the larger linked segments, resulting in their cessation, (Nicol et al., 1997; Gupta et al., 1988). Gupta et al. (1998) explain the subsidence pattern associated with normal fault arrays in terms of a feedback mechanism; as fault linkage progresses, the stress shadows associated with the larger faults result in the cessation of fault growth in the immediate hangingwalls and footwalls of the structure. As a result, displacement rates increase on the remaining active structures to accommodate a constant strain rate. The transition to the rift climax phase sees the wholesale switching of displacement onto a series of fully linked, 'through-going' fault arrays, with the cessation of minor fault activity within their respective stress shadows.

A key observation of the numerical model of Cowie et al. (2000) is that the accumulation of displacement through the evolution of the fault population is inherently episodic along strike, i.e. as one segment shows rapid subsidence, another adjacent segment may be tectonically acquiescent. Dawers & Anders (1995) show that even in dominant fault linkage settings, the overall *D-L* scaling is essentially that expected for a single isolated fault of similar length, reflecting the alternation of tectonic activity and cessation between segments through time. Cowie et al. (2000) suggest this is due to the complex interactions between the fault population and results in irregular pulsed subsidence along basin bounding faults, which is likely to have a major impact on the synrift architecture; in that it might control the abrupt transitions between stratal units characterised by different stacking patterns.

2.4. CONTROLS ON SEDIMENT DISTRIBUTION, ARCHITECTURE AND SEQUENCE STRATIGRAPHY IN EXTENSIONAL SETTINGS.

In this section the controls on syn-rift sedimentation within an extensional basinal setting are considered. The evolution of normal fault systems within a rift has been shown to provide a fundamental control on the architecture and distribution of coeval stratigraphy (e.g. Leeder and Gawthorpe, 1987; Gawthorpe and Leeder 2000), and is thus outlined first. The interaction of this dominant structural control upon sedimentation with additional controls such as variations in climate, sediment supply and sea-level change has also been highlighted in previous research (e.g. Gawthorpe et al., 1994; Collier et al., 2000). These controls are discussed with particular reference to the resultant variability for available accommodation space and subsequent sequence stratigraphic architectures (e.g. Gawthorpe et al., 1994; Howell and Flint, 1996).

2.4.1 Structural control upon drainage and resultant depositional systems

The temporal and spatial evolution of normal fault systems has been shown in section 2.3 to have a profound control upon the development of the structural characteristics of a rift basin. Patterns of differential uplift and subsidence associated with a series of normal faults determine the location and geometry of topographic (or bathymetric) relief and the nature of tectonically-generated slopes (e.g. Leeder et al., 1991; Leeder and Jackson, 1993; Eliet and Gawthorpe, 1995). As previously outlined, rifts are commonly characterised by a series of rotated fault-bounded blocks with a resultant asymmetric dip-section profile of hangingwall subsidence and footwall uplift (e.g. Barr, 1987). Considering a dip-direction oriented profile for this model across a single fault envisages: (1) an uplifted footwall crest, (2) a steeply dipping, spatially constricted footwall scarp slope, marking the footwall to hangingwall boundary, (3) a subsided hangingwall basin and (4) a broad gentle hangingwall dip-slope, up-dip of which is the immediate footwall crest of the adjacent fault zone (Fig 2.2). The boundary between the areas of this hangingwall dip-slope characterised by either net uplift or net subsidence forms a fulcrum, i.e. an area of zero displacement. Tectonic gradients parallel to the strike of a fault zone vary with respect to varying displacement in the hangingwall and uplift in the footwall. With respect to a single fault segment, maximum displacement and coeval

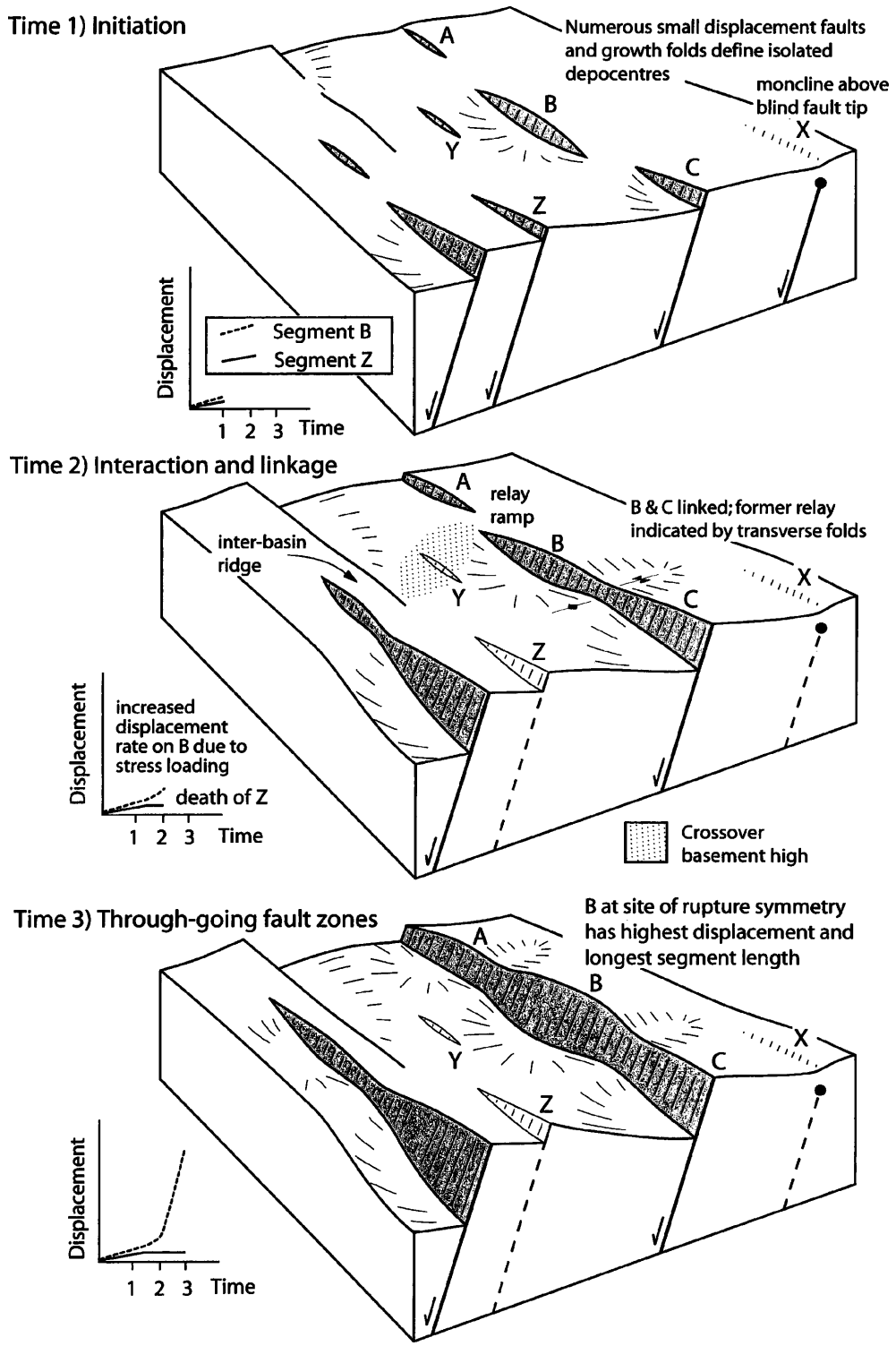

Figure 2.6. Schematic 3-D evolution of fault populations or arrays during rifting (cf. Cowie et al. 2000) and associated displacement vs time graphs highlighting the histories of segments B and Z. Both segments B and Z show increasing displacement accumulation at time 1. At time 2, segment B has linked with C and shows increased displacement, whilst Z has become inactive. Time 3 shows linking of A, B and C to form a through going fault array, leading to a large increase in displacement accumulation, (modified from Gawthorpe and Leeder 2000).

uplift has been shown to be located towards the centre of the segment, and reducing towards the fault tips. As a result, gradients around a single isolated fault segment are thought to be concave towards the hangingwall basin centre and convex towards the central footwall crest. Overlapping segment tips impact upon this simplistic scenario, as transverse folding resulting in intra-basinal highs and relay ramps also provide varying tectonic gradients.

As a result, the nature of drainage systems within a rift are the product of the amount of tilting, fault spacing and fault overlap produced by normal faulting (Fig. 2.7). Broadly though, four main drainage types are generally recognised: (1) transverse, (2) axial, (3) antecedent and (4) reversed (e.g. Leeder and Jackson, 1993; Gawthorpe et al., 1994; Collier and Gawthorpe, 1995). Transverse drainage systems can be further divided between those sourced from the uplifted footwall and down the footwall scarp, and those focussed along the hangingwall dip-slope. Those associated with the steep footwall scarp are typically small scale, yet greater in number than larger drainage systems developed on the more gentle hangingwall dip-slope (e.g. Leeder and Jackson et al., 1993; Gawthorpe et al., 1994; Eliet and Gawthorpe, 1995). Footwall sourced depositional systems are therefore characterised by a sharp change in gradient from the steep footwall scarp to the hangingwall basin, which is typically associated with the first available accommodation space for deposition. This is reflected in the development of aggradational depositional systems, which are typically locally restricted (< 100's metres) (Fig 2.7). Sub-aerial settings may be characterised by high gradient alluvial fans, and talus deposits whereas in lacustrine to marine settings, fan deltas to slope aprons may occur. Erosion and modification of the footwall may result in the production of fault scarp degradation complexes (e.g. Underhill et al., 1997; Leppard and Gawthorpe, 2006). Areas of fault overlap, characterised by relay ramps provide a localised footwall topographic low, and typically may act as a focus for drainage systems to cross a fault zone from a uplifted footwall to hangingwall depocentre (e.g. Leeder and Gawthorpe, 1987; Morley et al., 1990; Gawthorpe and Leeder 2000). These relay ramps may therefore provide a major conduit for fluvial systems in continental settings (e.g. Gawthorpe and Leeder 2000) or submarine fan depositional systems in marine rift settings (e.g. Bruhn and Vagle, 2005) (Fig 2.7). In contrast, hangingwall dip-slope deposition systems are typically subject to a gentler gradient, with accommodation space being down-dip of the fulcrum point. Dependant upon the structural elevation of the fault block and intersection with regional base-level, the hangingwall dip-slope may be subject to both net erosion and deposition (e.g. Ranvas

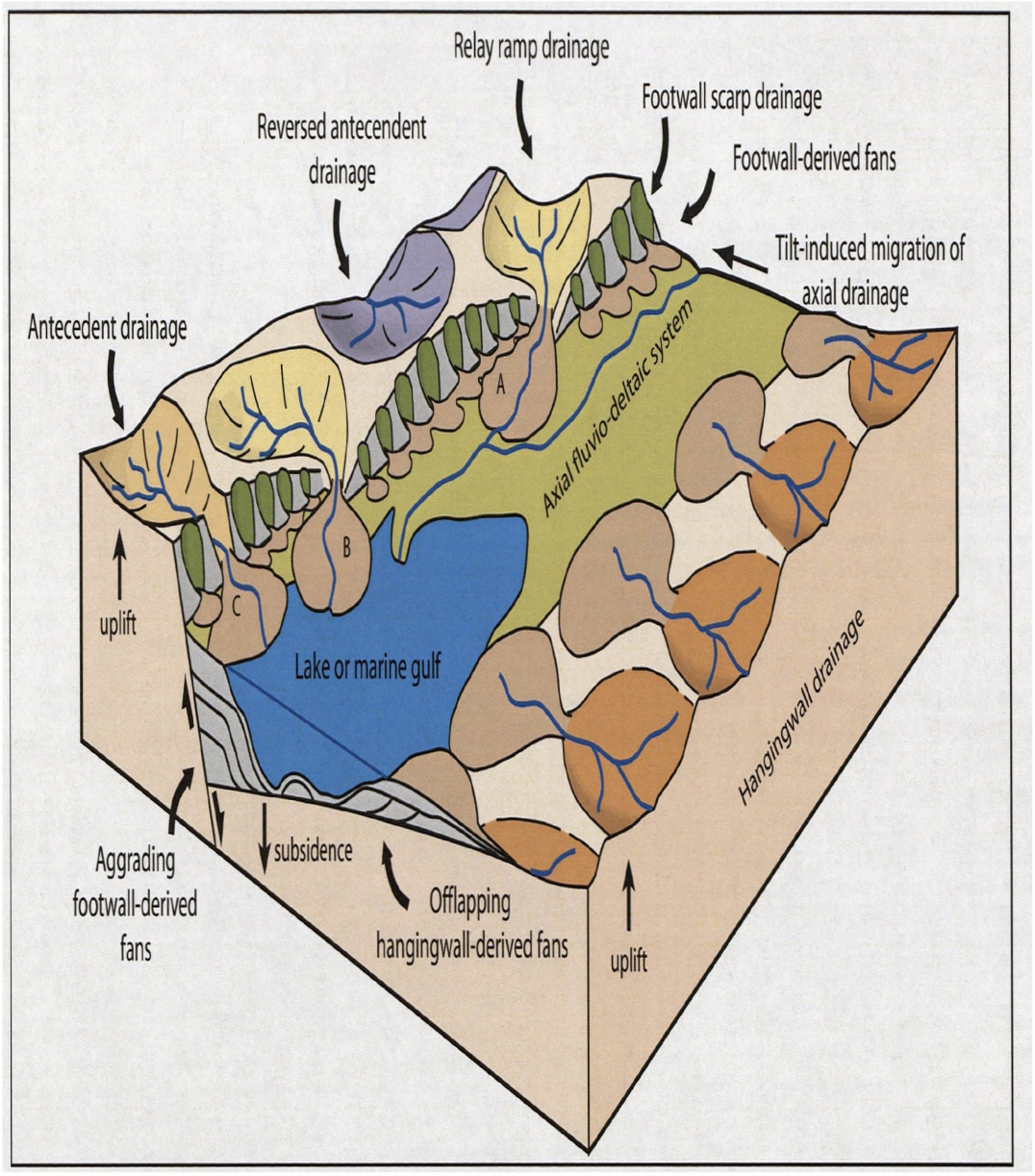

Figure 2.7. Block model illustrating the key areas of sediment source, drainage, deposition and basin physiography, i.e. tectonic slopes and fault segments. Model illustrated depicts a transition from a continental to marine gulf rift basin. The major bounding fault consisting of three fault segments, with lengths of 12-50 km, (vertical scale is greatly exaggerated). Axial, footwall and hangingwall dervied drainage and associated depositional systems are shown. Both Fans A and B represent footwall hinterland derived allovial fans, reaching the basin via relay ramp; C is a fan delta sourced from antecedent drainage (from Gawthorpe et al., 1994).

et al., 2000). In a scenario were base-level intersects a tilted hangingwall dip-slope at the fulcrum point between overall uplift or overall subsidence, the slope above this point may be characterised by bypass and incision. Below this, the amount of accommodation space would increase to a maximum within the immediate hangingwall of the fault. As a result, in continental rift settings, hangingwall dip-slopes may be characterised by fluvial channels feeding down-dip alluvial fans and fan deltas into fluvial to lacustrine environments contained within the hangingwall basin (e.g. Gawthorpe and Leeder, 2000). In a marine scenario, shallow marine and prograding, down-stepping, broad sheet-like delta lobes may occur, contrasting sharply with the stacked architecture of those sourced from the footwall (Fig.2.7), (Gawthorpe and Leeder, 2000).

Axial drainage is orientated parallel to strike of the bounding fault and is typically focussed into the immediate hangingwall. Common in both continental and marine rifts, these depositional systems are associated with lakes or floodplain deposits and fan deltas or submarine fans respectively. In continental settings, the sensitivity of the axial system to the rotation of the hangingwall dip slope may lead to the migration of fluvial channels towards the footwall slope and the subsequent stacking of fluvial deposits (Fig 2.7) (e.g. Leeder and Gawthorpe, 1987).

Antecedent drainage forms where there is a high density of pre-existing down-cutting drainage pathways and/or where bedrock lithologies are more easily erodable, and therefore fault activity has little impact on the course of this existing drainage. Essentially these drainage systems are therefore able to incise into the newly uplifted topography or bathymetry (e.g. Gawthorpe et al. 1994). In contrast, where this rate of downcutting is insufficient to maintain the pre-existing drainage pathway, the drainage system may become diverted or reversed (e.g. Gawthorpe et al., 1994). The onset of reversed drainage systems is commonly cited as evidence for doming associated with thermal uplift prior to the onset of rifting.

2.4.2 Role of bedrock lithology and climate variations

Variations in bedrock lithology within a rift are important to understand as they fundamentally control the compositional signature of the depositional systems that result, in addition to modifying tectonically-generated relief due to the nature of their resistance to erosion. As bedrock lithologies may vary from crystalline igneous and metamorphic basement to pre-rift carbonates, pre-rift clastics and also earlier deposited syn-rift units, subsequent depositional systems may vary in architecture and extent due to the ability for

sediment liberation and transport mechanisms to entrain and sustain prolonged sediment influxes. Whilst the unroofing history of a rift can be typically derived from the inverse stratigraphy of the syn-rift infill (e.g. the Suez Rift, Evans, 1990), care has to be taken to differentiate periods of genuine sediment supply switch-off from the sourcing of fine-grained bedrock lithologies (e.g. Leppard and Gawthorpe, 2006).

With respect to the ability of a bedrock lithology to resist erosion, examples from central Greece show that there is a marked bias in transverse footwall drainage catchments size along the strike of many faults, due to differential bedrock properties within the footwall. Here, Pliocene – Pleistocene deposits prove to be more easily eroded than adjacent crystalline basement or Mesozoic carbonates (e.g. Leeder et al., 1991; Collier and Gawthorpe, 1995; Eliet and Gawthorpe, 1995).

Changes in climate may result in both variations in the nature of clastic sediment supply and the potential for climatically sensitive facies to be deposited within the syn-rift infill. In continental rifts, climate directly impacts upon fluvial discharge within drainage systems, the nature of any vegetation, and principal current directions associated with aeolian and lacustrine deposits. In marine rifts, the expression of climate, most notably through temperature, has a direct control on the development of biogenic carbonates and evaporites in the form of sabkhas and basinal evaporites, such as observed in the Suez and Red Sea Rifts.

2.4.3 Sequence stratigraphy

Sequence stratigraphy is a methodology for sub-dividing the stratigraphic record into a series of genetically linked stratal units bounded by chronostratigraphic key surfaces of erosion, non-deposition or their correlative conformities (e.g. sequence boundaries, transgressive surfaces, or maximum flooding surfaces). The underlying principle of sequence stratigraphy is that the availability of accommodation space which allows for an influx of sediment to be deposited within a basin, is based on cyclical variations in relative sea-level, which is a function of the combined effects provided by eustatic sea-level change and tectonic uplift or subsidence. This results in cycles of deposition which can be punctuated by surfaces which represent periods of maximum rates of accommodation space creation (maximum flooding surfaces) and maximum rates of accommodation space removal (sequence boundaries) (e.g. Vail et al., 1977; Posamentier et al., 1988; Galloway, 1989). Individual systems tracts within this cycle, defined by distinct stratal relationships and architectures of component stratal units and the nature of their stacking patterns, e.g.

aggradational, progradational and retrogradational, reflect different periods associated with the relative sea-level curve when relative sea-level was rising (transgressive and highstand systems tracts) and falling (forced regressive and lowstand systems tracts). A complete *sequence* is thus defined as comprising the stratal record of one such period of relative sea-level rise and fall, although different workers have debated which chronostratigraphic surfaces are best used to bound this. Thus *depositional sequences* are recognised, bounded by the major hiatal surfaces of erosion and their correlative conformities, and termed sequence boundaries in the Exxon scheme (e.g. Vail et al., 1977; Posamentier et al., 1988; Van Wagoner et al., 1988) as are *genetic sequences* bounded by surfaces reflective of maximum flooding (e.g. Galloway, 1989).

In addition to the controls provided by changes in relative sea-level (thus encompassing eustatic and tectonic effects), the stratal relationships and architectures within stratal units are also recognised to be controlled by basin margin physiography, sediment supply, climate and compaction upon burial (e.g. Vail et al., 1977; Jervey, 1988; Posamentier et al., 1988; Galloway, 1989; Van Wagoner et al., 1988; 1990; Hunt & Tucker, 1992; Schlager, 1993; Posamentier & Allen, 1993). However, as classic sequence stratigraphic models developed during the 1970's to early 1990's were originally defined from passive margin or intra-cratonic settings with relatively simple patterns of subsidence (e.g. the Tertiary Gulf of Mexico, Galloway 1989; Van Wagoner et al., 1990), the role of eustatic sea-level changes was proposed to exert the primary control on stratigraphic development and geometry (Vail et al., 1977, 1984; Haq et al., 1988; Posamentier et al., 1988; Van Wagoner et al., 1990).

2.4.4 Sequence stratigraphic variability in rifts

In a rift basin, characterised by variable subsidence and uplift associated with the growth of normal fault systems, the spatial and temporal variability of the constituent stratal units of depositional sequences is likely to be complex, as these structures, rather than eustasy, are the primary control upon the availability of accommodation space (Fig 2.8) (e.g. Lambiase, 1990; Schlishe & Olsen, 1990; Prosser, 1993; Anders & Schlische, 1994; Gawthorpe et al., 1994; Howell and Flint, 1996; Contreras et al., 1997; Gawthorpe & Leeder, 2000). For example, within the centre of a fault segment where displacement rates are greatest, the rate of a glacio-eustatic sea-level fall may be outpaced by the rate of fault-related subsidence (e.g. Gawthorpe et al., 1994). As a result, the relative sea-level may increase, so that this hangingwall location is characterised by the continual

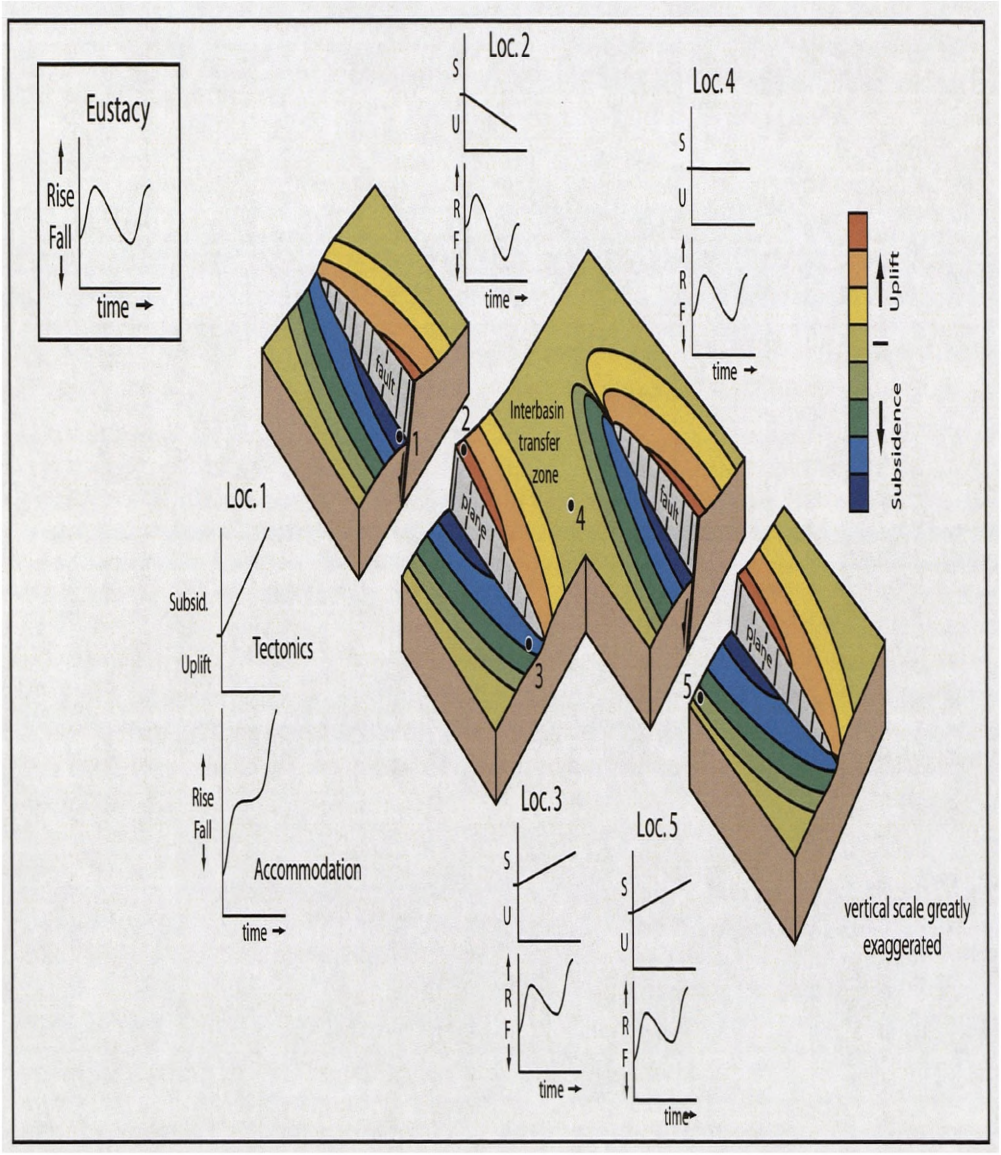

Figure 2.8. Spatial variation in accommodation around a schematic segmented normal fault zone. Two half-graben basins are separated by an interbasin transfer zone. The typical length of the border fault segments is 12-50 km. Note how the amount of deformation decays away from the centre of the fault zone to the segment boundaries (transfer zone) and away from the fault zone. the pairs of graphs for locations 1 to 5 illustrate the variation in uplift or subsidence (top) and the resulting accommodation (bottom) for different structural locations. The inset shows a simplified fourth-order glacio-eustataic sea-level curve (based on Quaternary glacio-eustatic sea level which was used to generate the accommodation curves (Gawthorpe et al., 1994)

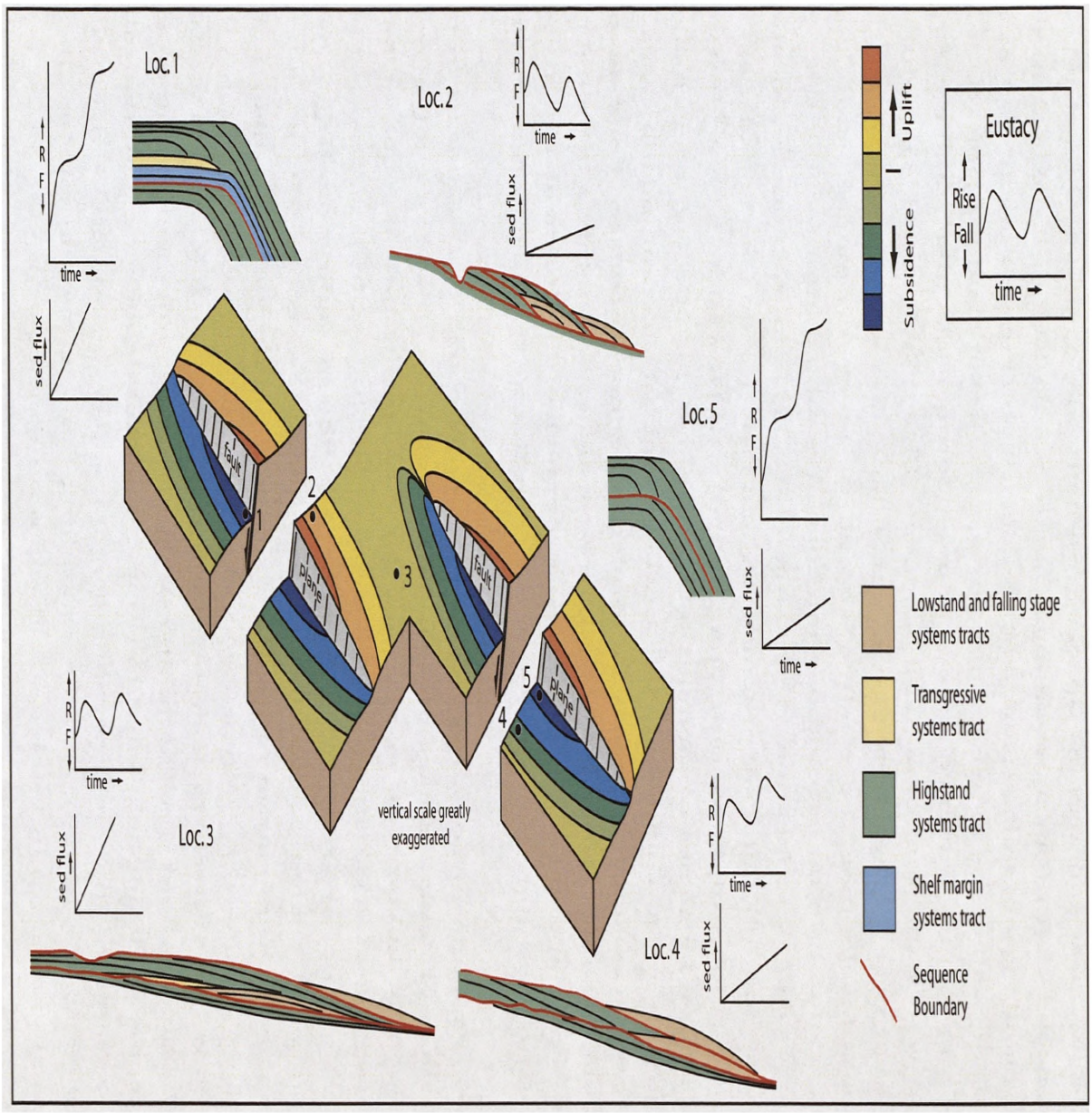

Figure 2.9. Contemporaneous sequences and key surfaces for selected locations, (1-5) in a rift basin complex, composed of two fault segments, approximately 12 - 50 km in length. Inset shows background eustatic curve. Each location (1-5) is summarised by a pair of graphs displaying relative sea-level (hence accommodation space) and sediment supply. This figure highlights the marked spatial variation of system tract and key surface development within rift basin settings. See text for discussion. Gawthorpe et al., (1994)

development of new accommodation space; resultant depositional highstand or transgressive sequences being of an aggradational nature whilst lacking type 1 sequence boundaries and lowstand system tracts (Gawthorpe et al., 1994) (Fig. 2.9 locations 1 & 5). In contrast, uplifted footwall crests may be subject to aerial exposure and incision resulting in the formation of an apparent sequence boundary, even during a glacio-eustatic rise (Fig. 2.9, location 1). Towards the tips of a fault segment (Fig. 2.9, location 3), uplift or subsidence rates are lower. Therefore eustasy may have a more prominent role in accommodation space development, i.e. a fall in eustatic sea-level may outpace subsidence in the hangingwall, resulting in no accommodation space creation and/or destruction. On hangingwall dip slopes (Fig. 2.9, location 4) and structural relay ramps, (Fig. 2.9, location 3), sequences may develop full suites of system tracts and type 1 sequence boundaries. A key observation in the studies of Gawthorpe et al., (1994) and Howell and Flint (1996) is that due to the differing relevancies of tectonic subsidence and eustatic sea-level changes spatially within the basin in controlling the development of accommodation space, differing key surfaces and systems tracts may be formed contemporaneously. For example, highstand systems tract development in a footwall derived succession within a hangingwall depocentre may be contemporaneous with sequence boundary development and forced regressions in a hangingwall dip-slope derived succession during a single period of base level fall.

The temporal variation of coeval syn-rift stratal architectures can be linked to the progressive localisation of fault displacement as normal fault populations evolve from isolated segments to fully linked fault arrays, and the subsequent shift in locus of fault controlled depocentres (e.g. Cowie et al., 2000; Davies et al., 2000; McLeod et al., 2000; Sharp et al., 2000a; Young et al., 2001). The early propagation of faults from depth, may lead to the development of related flexural folding as discussed in section 2.3. Resultant monoclinal structures have been shown to invoke a stratigraphic response in which strata onlap and *thin* towards the fault. In contrast, once the blind fault breaks, i.e. ruptures the surface, synrift strata will conversely *thicken* towards a fault, (Fig. 2.10) (Gawthorpe et al., 1997; Sharp et al 2000b; Corfield and Sharp, 2000). With the development of numerous, and isolated fault segments during this initiation stage, resultant depocentres are typically small, and locally constrained in their immediate hangingwalls (e.g. Anders & Schlische, 1994; Schlische, 1995; Morley, 1999). As the controlling faults grow and interact, these previously isolated sub-basins begin to merge and enlarge. Consequently the oldest syn-rift units will often form more restricted sequences that are thickest in the centres of the

originally active fault-controlled depocentres, in contrast to younger syn-rift units, which deposited after fault linkage, will form more extensive sequences that are thickest in the centre of the newly linked fault array and thus the site of highest fault-generated subsidence.

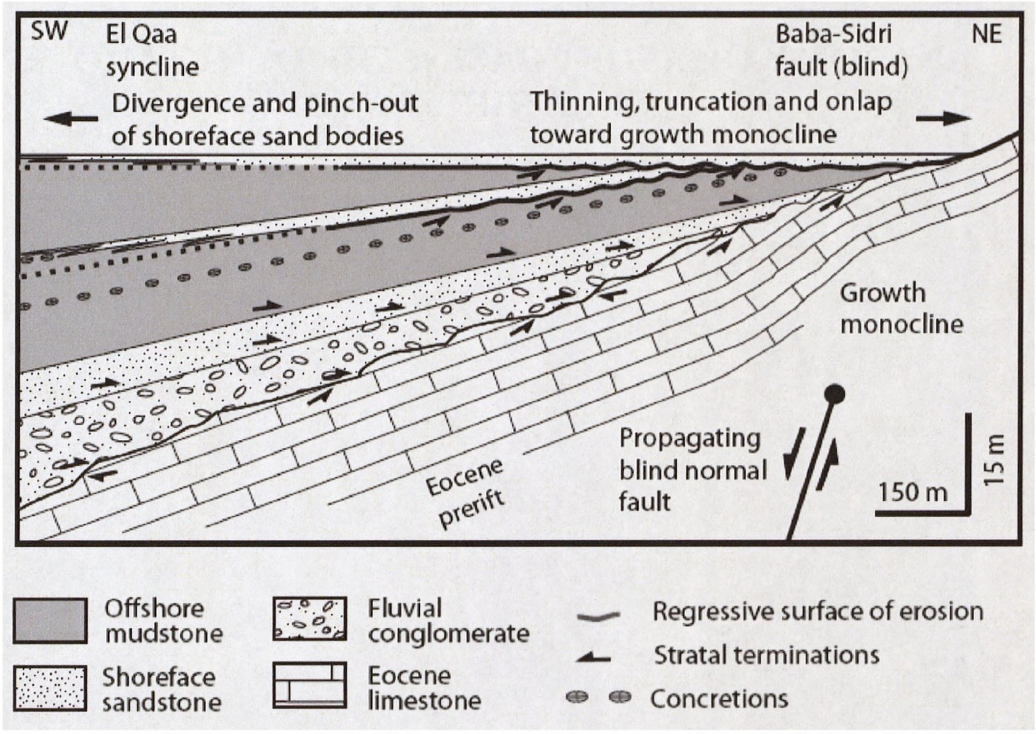

Figure 2.10. Tectono-stratigraphic development of a propagating blind fault tip; the Baba-Sidri fault zone, El-Qaa fault block, Suez Rift. Note initial onlap, thinning and truncation of syn-rift strata due to the active growth and rotation of the monocline. Modified from Gawthorpe et al., (1997).

CHAPTER THREE

ANATOMY OF A RIFT BASIN: THE OLIGO-MIOCENE SUEZ RIFT, EGYPT

CHAPTER 3

ANATOMY OF A RIFT BASIN: THE OLIGO-MIOCENE SUEZ RIFT, EGYPT

3.1. INTRODUCTION

The Suez Rift is a classic example of a failed intracontinental rift system and through numerous studies, has provided a fertile testing ground for the development of our current understanding of the linked tectono-stratigraphic evolution of rift basins (Fig. 3.1). Uplifted margins of the rift, and notably the eastern margin of the rift located on the Sinai Peninsula, specifically within the Hammam Faraun and El Qaa Fault Blocks, provides for a well preserved succession of both pre-rift and syn-rift units in addition to non-inverted rift-related structures. Moreover, present day arid climatic conditions preclude the development of extensive vegetation whilst incision due to ephemeral flash-flood events has formed a complex wadi drainage network. This results in a series of continuous, kilometre-scale exposures which can be locally constrained in pseudo three-dimensional geometries where intersected by the drainage network.

In contrast, the axis of the rift is characterised by the modern day Gulf of Suez, and is associated with a major prolific hydrocarbon province. With respect to the rift axis, this study utilises an extensive subsurface dataset provided by the Gulf of Suez Petroleum Company (GUPCO), the largest hydrocarbon company operating within the rift. A fundamental problem within the subsurface is the quality of available seismic reflection datasets. Extensive, intercalated evaporites and clastics of the Zeit Formation, up to 4.3 km in thickness, and layers of massive halite in the South Gharib Formation associated with the shallowest levels of the syn-rift infill of the rift, account for heavy seismic attenuation (e.g. Zaki 1990). Resultant datasets are often therefore severely affected by multiples and poor reflector definition with increased depth, especially within the pre-Miocene section (Fig. 3.2). Extensive processing (e.g. Sercombe et al., 1997; Dolson et al., 1997) and ground-truthing provided by borehole data is therefore required to accurately constrain the present day structural configuration of the rift, upon which observed syn-rift thicknesses and facies variations may be constrained, and interpreted. Recent advances have seen the use of mult-azimuth, ocean bottom cable seismic surveys to reduce this effect. Despite the difficulties in imaging the subsurface, when extensive subsurface datasets are coupled to the excellent exposures at the rift margin, a unique, variable-scale dataset therefore exists with which to investigate the spatial and temporal evolution of

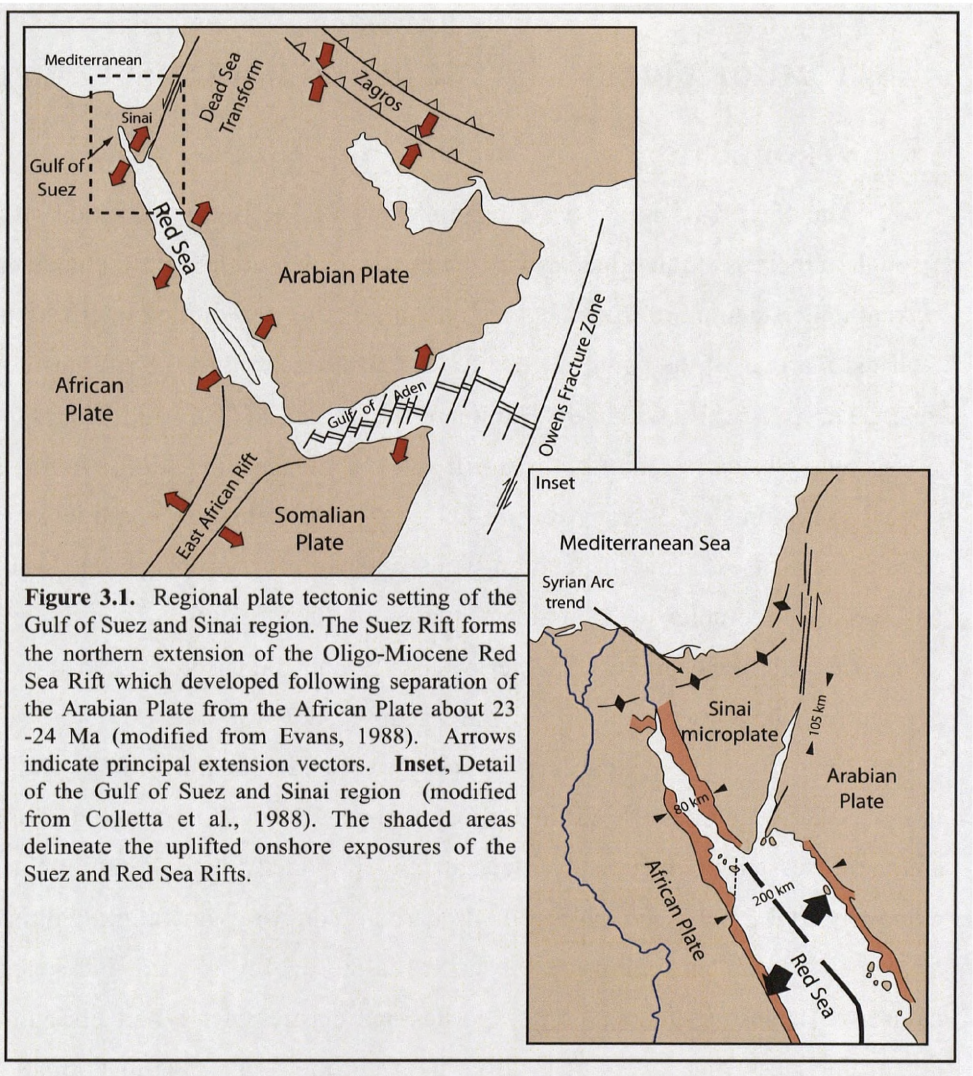

Figure 3.1. Regional plate tectonic setting of the Gulf of Suez and Sinai region. The Suez Rift forms the northern extension of the Oligo-Miocene Red Sea Rift which developed following separation of the Arabian Plate from the African Plate about 23 -24 Ma (modified from Evans, 1988). Arrows indicate principal extension vectors. **Inset**, Detail of the Gulf of Suez and Sinai region (modified from Colletta et al., 1988). The shaded areas delineate the uplifted onshore exposures of the Suez and Red Sea Rifts.

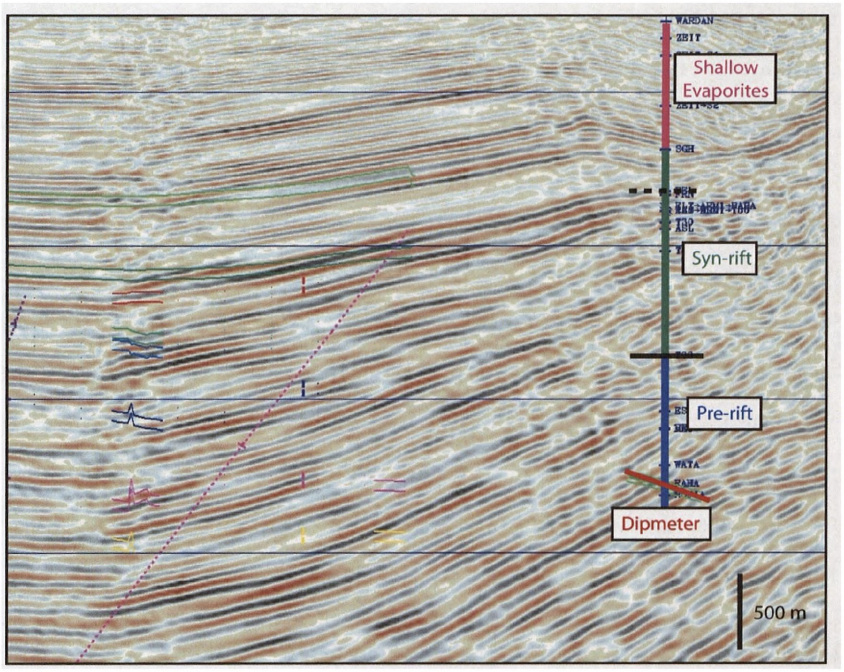

Figure 3.2. Seismic section from the subsurface axis of the Suez Rift, illustrating the potential for poor reflector definition at deeper levels (> 1000 m) due to shallow intercalated evaporites and clastics. Note how primary reflectors in the pre-rift section apparently dip to the left, whilst the borehole dipmeter determines a regional pre-rift dip to the right. Image courtesy of Brian Barley, BP Egypt.

normal fault systems and the nature, extent and controls upon coeval syn-rift sedimentation patterns within an extensional setting.

The aim of this chapter is to provide a detailed account of the geological setting of the rift, which provides the study area for this thesis; the rationale being to expand upon the limited descriptions provided in each of the individual research chapters in Section 2. The tectonic setting of the rift and the observed present day structural configuration is discussed initially, followed by an outline of the stratigraphic framework. Together, these elements provide a basis for a broad model for the linked tectono-stratigraphic evolution of the Suez Rift. The principal emphasis in this section is placed upon the development of the Upper Rudeis and Kareem Formations which form the key focus intervals of this thesis and evidence for the classification of these two formations as being deposited during a late rift climax to rift acquiescence phase is discussed.

3.2. REGIONAL TECTONIC SETTING AND PRESENT DAY STRUCTURAL CONFIGURATION

Orientated NW-SE with an approximate width of up to 80 km and some 300 km in length, the Suez Rift is a northern continuation of the 2000 km long Cenozoic Red Sea Rift (e.g. Gawad 1970; Schutz, 1994; Patton et al., 1994), bounded by two sets of marginal faults, with exposed Palaeozoic-Tertiary strata and Precambrian basement either side and which separates the African plate and Sinai microplate. Today, the margins of the rift are exposed onshore in the Eastern and Sinai Deserts respectively, whilst the inner axial trough of the rift contains the marine Gulf of Suez (Fig. 3.1).

The initiation of the Suez Rift is currently estimated to have occurred in the Late Oligocene and into the Early Miocene, during the separation of the African and Arabian plates, (e.g. Robson, 1971; Garfunkel & Bartov, 1977; Colletta et al., 1988; Patton et al., 1994) with associated limited basalt intrusions and flows dated between 23 and 20 Ma (Garfunkel & Bartov, 1977). The dominant normal fault trend within the rift mirrors the NW – SE orientation of the rift (e.g. Patton et al., 1994) and the majority of models indicate that the regional extension that formed the rift was therefore simplistically perpendicular, with north-eastwards dominant extension (e.g. McKenzie et al., 1970; Robson et al., 1971; Garfunkel and Bartov 1977; Lyberis 1988; Patton et al., 1994). In contrast, some studies suggest an initial strike-slip component of movement (e.g. Jarrige et al., 1986; Montenat et al., 1986; 1988), however this is not convincingly supported by an

analysis of fault geometries, fault kinematics and early syn-rift sedimentation patterns (Bosworth and McClay, 2001).

The onset of the Dead Sea – Aqaba Transform fault, at ca. 15.5 Ma is thought to have inhibited this initial phase of rifting (e.g. Richardson and Arthur, 1988; Bosworth et al., 2005), whilst the Red Sea Rift continued opening to the present day with the onset of seafloor spreading (Cochran, 1983). Renewed fault activity and associated subsidence is suggested from ca. 8 Ma within the axis of the rift by observations of displaced strata younger than 15.5 Ma within individual fault blocks (e.g. Gawthorpe et al., 2003). A concentration of displacement upon the major fault zones forming the present day shoreline of the Gulf of Suez is indicated by recording the largest displacements within the rift (up to 4 km), and a thickened post-Miocene section (Gawthorpe et al 2003). Uplifted Quaternary marine terraces (e.g. Garfunkel and Bartov, 1977) and historical earthquakes (e.g. Jackson et al., 1988; Hussein et al., 2006) suggest that referring to the Suez Rift as currently inactive is erroneous.

The dominant NW-SE trending fault system, commonly referred to as the 'Clysmic trend' (after the Roman city of Clysmia, located near to the present day city of Suez, (Lelek et al., 1994) markedly contrasts with a predominantly W-E to WSW-ENE trending system of earlier, inverted normal faults and associated anticlines stretching across from Cyrenaica into the northern part of Egypt: specifically through the Western Desert, the greater Cairo area and into the northern part of the Sinai Peninsula (e.g. Moustafa and El Shaarawy, 1987; Zahran and Meshref, 1988; Moustafa and Khalil, 1995, Moustafa, 1997). This northern Egypt fold belt is interpreted to have formed as a response to Santonian to Late Eocene compressive events inverting previous Jurassic E-W trending extensional structures (Guiraud & Bosworth, 1999). Forming part of the larger Syrian Arc fold belt of Krenkel (1925), this trend continues into the northern Levant, where these structures are observed to sweep into a SSW-NNE to N-S trend (Aqaba trend) associated with the major left-lateral Dead Sea – Aqaba Transform (Fig. 3.1).

In addition to the Clysmic trend, northwest oblique, north oblique and cross fault trends are recognised (Patton et al., 1994). The interaction of the Clysmic and oblique trends allows for a transfer of displacement between major fault systems and produces a characteristic zig-zag pattern of faults within the gulf, (e.g. Garfunkel & Bartov, 1977; Lelek et al., 1990; Patton et al., 1994; McClay and Khalil, 1998) which are easily identifiable on LANDSAT satellite images of the region (Lelek et al., 1994). For example, recorded observations of fault trends within the Precambrian basement exposed towards

the southern half of the Sinai Peninsula clearly show a subordinate north oblique trend in addition to the Clysmic trend (P. Whitehouse, pers. comm.).

In addition to the longitudinal compartmentalisation of the rift into axial and margin components, the Suez rift can also be arbitrarily divided into three transversely orientated structural provinces or half grabens, defined as the northern, central and southern dip provinces (Fig. 3.3). Within these structural provinces, smaller scale fault blocks, (10-15 km wide, by 20-30 km long) and associated bounding faults show a consistent dip orientation (e.g. Moustafa 1976; 2002; Patton et al., 1994). From north to south, major faults within the northern province dip to the northeast, those in the central province to the southwest, with a return to a northeast dip direction in the southern province. Tilted pre-Miocene strata within individual fault blocks typically exhibit average dips of $10\text{-}15^0$, but dips may reach up to 45^0 in the southern part of the rift, reflective of an increased amount of extension in the south (Moustafa 2002). Indeed, estimates of total extension within the rift vary from 16 km ($\beta = 1.33$) in the north, to 30 km ($\beta = 1.51$) in the southernmost part (Patton et al., 1994), consistent with Africa-Arabia-Sinai plate reconstructions (cf. Bosworth and McClay, 2001 and references therein). This northwest to southeast variance in extension and increase in fault block dip angle has been cited to suggest that the southwards increase in extension is the result of a continuous 'scissors-like' opening process of the rift from the south (Colletta et al., 1988). Alternatively, a model for two extensional domains separated by the Late Cretaceous, Syrian arc Wadi Araba inversion structure is proposed by Patton et al., (1994).

The dip provinces are linked by two diffuse (approximately 15 – 50 km wide) accommodation zones (*sensu* Younes and McClay, 2002) which extend transversely across the rift and accommodate the changes in dip direction observed to occur along the axis of the rift between the structural provinces (e.g. Moustafa 1976; 1997; 2002; Coffield and Schamel, 1989; Patton et al., 1994; Younes and McClay, 2002). From north to south, these zones of structural accommodation are variously termed the Zafarana (or alternatively the Gharandal or Galala-Zenima) and Morgan (or Sufr El Dara) Accommodation Zones respectively (Fig 3.3). The presence and location of these accommodation zones are attributed to the presence and rejuvenation of pre-existing pre-rift faults, Syrian Arc anticlinal structures and the thickness of Cambrian to Eocene pre-rift sedimentary cover upon the basement (Moustafa, 1997; 2002; Younes and McClay, 2002). The Morgan Accommodation Zone separating the southern and central dip provinces is interpreted to have localised here as a response to left lateral strike slip movement upon pre-existing

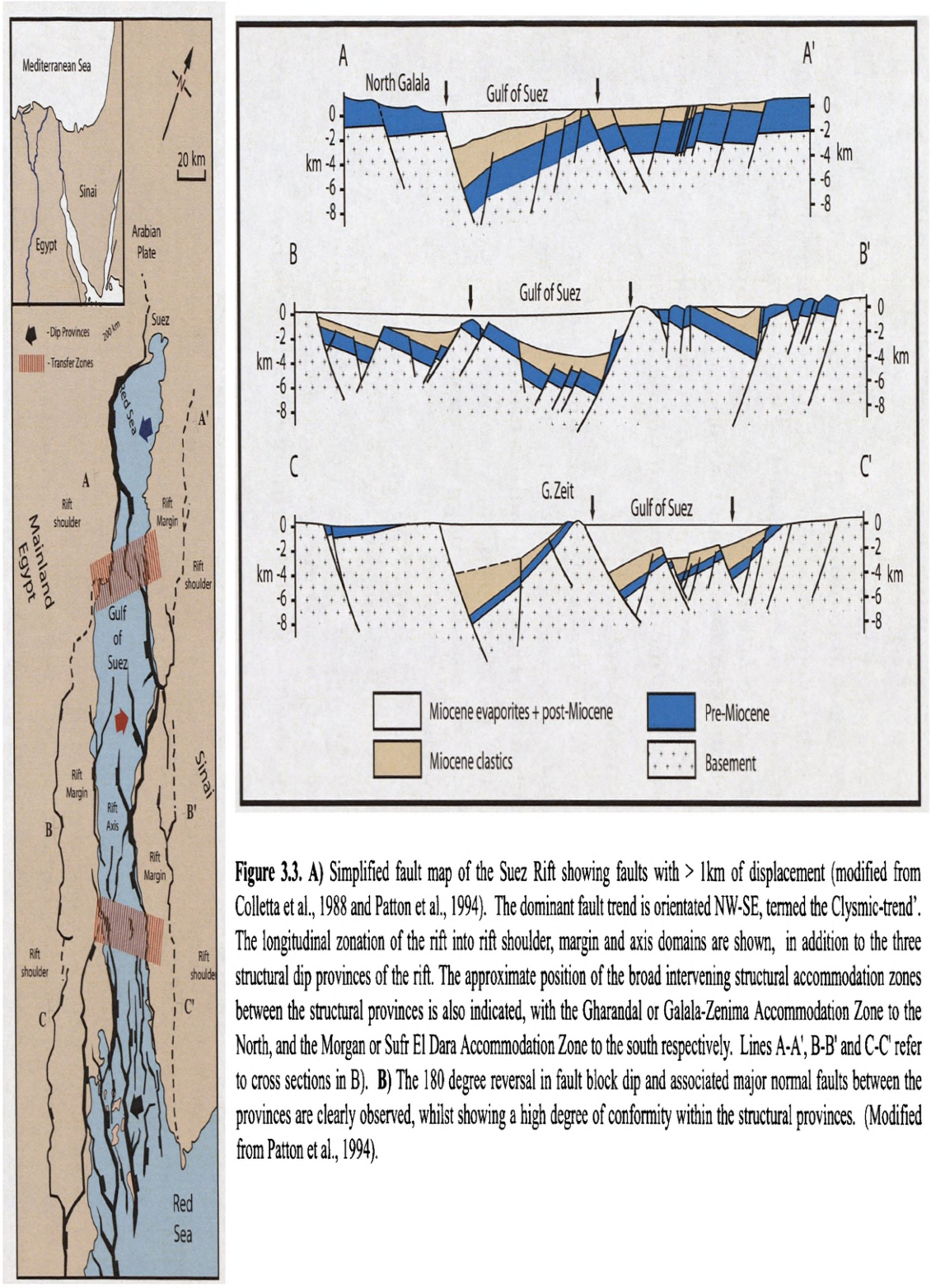

Figure 3.3. A) Simplified fault map of the Suez Rift showing faults with > 1km of displacement (modified from Colletta et al., 1988 and Patton et al., 1994). The dominant fault trend is orientated NW-SE, termed the Clysmic-trend'. The longitudinal zonation of the rift into rift shoulder, margin and axis domains are shown, in addition to the three structural dip provinces of the rift. The approximate position of the broad intervening structural accommodation zones between the structural provinces is also indicated, with the Gharandal or Galala-Zenima Accommodation Zone to the North, and the Morgan or Sufr El Dara Accommodation Zone to the south respectively. Lines A-A', B-B' and C-C' refer to cross sections in B). **B)** The 180 degree reversal in fault block dip and associated major normal faults between the provinces are clearly observed, whilst showing a high degree of conformity within the structural provinces. (Modified from Patton et al., 1994).

faults; contrasting with the Zafarana Accommodation Zone which is thought to be largely controlled by the pre-rift, Syrian Arc thick-skinned inversion fold located at Wadi Araba (e.g. Moustafa 1997; 2002).

In addition to the larger-scale accommodation zones separating dip provinces and intrarift faults of opposed polarity, individual faults and fault blocks are observed to form transfer zones, i.e. areas of lower displacement connecting individual faults, regardless of dip direction; designated as fault-to-fault transfer zones by Moustafa (2002). Synthetic transfer zones with associated relay ramps (e.g. the Bir El Markha monocline, Moustafa, 2002), and transfer faults (e.g. Gebels Abu Durba and Araba, Moustafa and Khalil, 1987; McClay and Khalil, 1998) are common within the dip provinces and are typically associated with local to major syn-rift sediment entry points into the rift.

3.3. STRATIGRAPHIC FRAMEWORK

The Suez Rift encompasses stratigraphy from Precambrian to Holocene in age and may be divided into three principle megasequences (Fig 3.4) (e.g. Sharp et al., 2000a). The initial megasequence is comprised of predominantly Cambrian to Lower Cretaceous Nubian sandstones, lying unconformably upon a complex Precambrian crystalline basement (e.g. Schutze, 1994). The second megasequence is comprised of mixed carbonate – clastic strata of Mesozoic to Tertiary age, whilst the final megasequence is comprised of mixed clastic, carbonate and evaporitic units. Megasequences one and two are composed of pre-rift strata, whilst megasequence three contains syn-rift units which are consistent with a model of coupled tectonostratigraphic development, *sensu* Prosser, (1993). Lithostratigraphic names outlined here are in accordance with the EGPC Stratigraphic Committee (1964) and the National Stratigraphic Sub-Committee (1974).

3.3.1 Megasequence 1 (Pre-rift)

A major package of siliciclastic sandstones loosely referred to as the Nubia Formation, are observed to unconformably overlie a Precambrian crystalline basement (Fig 3.4) (e.g. Schutze, 1994). Consisting of units from Cambrian to Lower Cretaceous in age, these deposits reflect the position of the northeastern Africa craton as a passive margin to the Palaeotethys and succeeding Neotethys oceans to the north (e.g. Guiraud & Bosworth, 1999). In a lithostratigraphic sense, the oldest deposits immediately overlying the peneplained basal surface above basement are locally preserved shallow marine deposits of the Araba Formation, and comprises of interbedded fine to medium grained yellowish

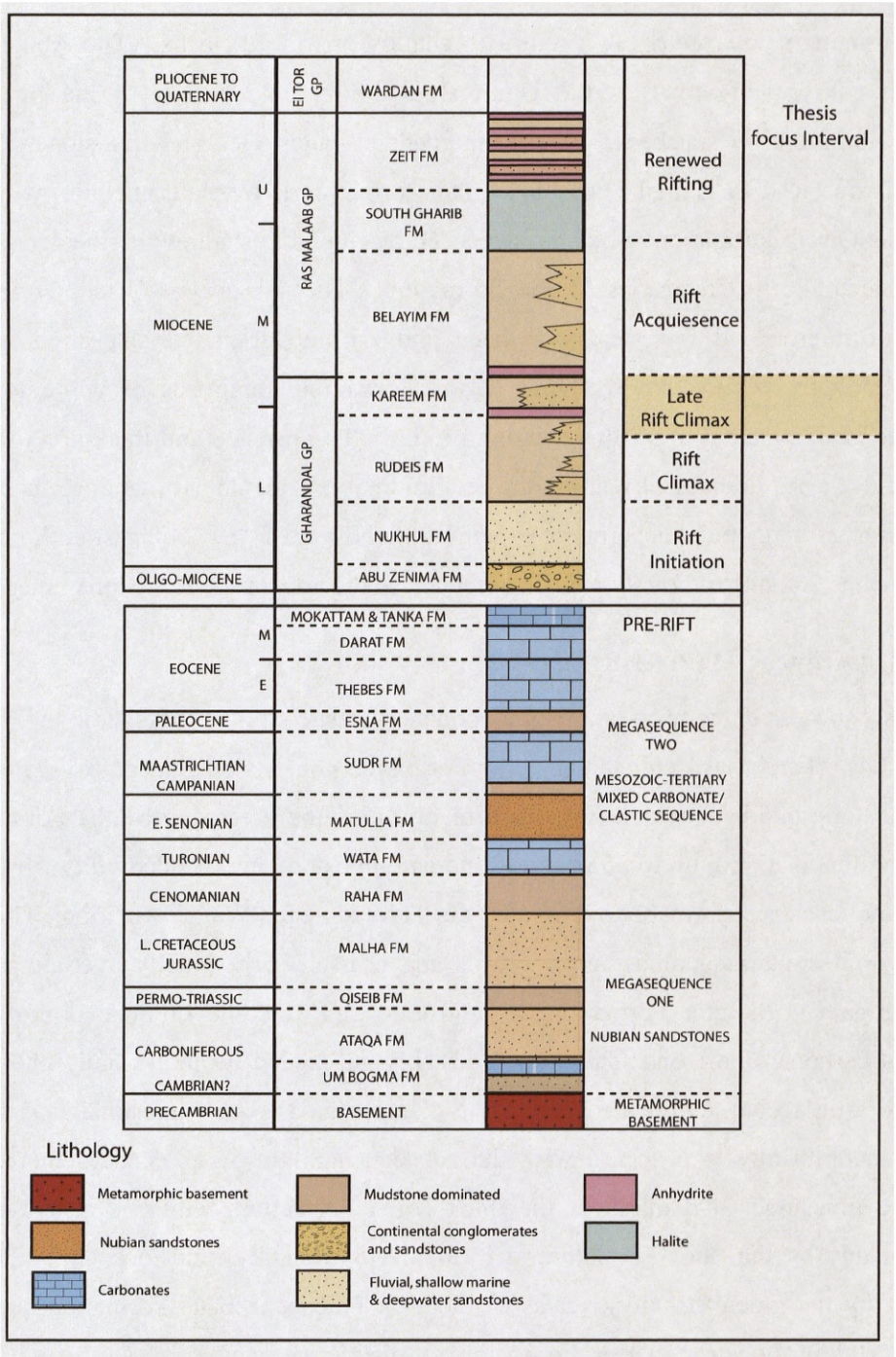

Figure 3.4. Broad stratigraphic framework for the Suez Rift. The pre-rift succession comprises two megasequences and the syn-rift infill an additional third.

to white sandstones and grey to greenish mudstones. The subsequent Naqus Formation is conformably overlying and comprises thick pebbly and cross bedded sandstones interpreted as continental in origin. This formation is in turn overlain unconformably by the Early Carboniferous aged, interbedded, highly calcareous marl and dolomitic Umm Bogma Formation, interpreted as a return to shallow marine deposits. The Abu Durba Formation conformably overlies the Umm Bogma Fm and consists of marine black mudstone units and is succeeded by the interbedded sandstones and mudstones of the shallow marine Rod El Hamal Formation. This formation is overlain unconformably by the Triassic Qiseib Formation, which is succeeded by fluvial to shallow marine deposits of the Jurassic to Early Cretaceous Malha Formation. The subsequent Qiseib Formation consists of interbedded red sandstone beds and purple variegated shales containing paleosol horizons, whilst the overlying Malha Formation comprises of white to grey sandstones of continental to shallow marine origin. The presence and thickness of these Nubia facies varies dramatically along the longitudinal axis of the rift, as does their age; with a major thinning and diachronous younging trend towards the southeast until units of Megasequence 2 come to directly overlie basement in the area of the Ras Mohammed Arch.

3.3.2 Megasequence 2 (Pre-rift)

This succession comprises mixed carbonate – clastic strata of Mesozoic to Tertiary age (Fig 3.4). The basal Cenomanian Raha Formation consists of glauconitic shales and white sandstone interbeds which rest conformably upon the preceding Malha Formation. Succeeding this is a thin, up to 25 m sandstone and mudstone interbedded unit of the Abu Qada Formation, unconformably overlain by the Turonian aged Wata Formation. This is a carbonate unit containing mudstone interbeds and is itself subsequently overlain by the Early Campanian Matulla Formation; a sandstone and siltstone dominated unit with occasional carbonate horizons. This is conformably succeeded by the initially chert-rich then more argillaceous carbonate unit of the Campanian Brown Limestone Formation. Another unconformity is observed with the subsequent highly argillaceous, cherty and phosphatic limestones and marls of the thick Duwi Formation, which is also overlain unconformably by the Sudr Formation, a brilliant white chalky limestone unit. This is succeeded by the greenish - grey shales of the Late Paleocene Esna Formation, and the Early to Middle Eocene Thebes Formation, a distinctive white limestone unit with ubiquitous chert bands and concretions. Overlying this is the Middle Eocene thinly bedded, marl-rich limestone of the Darat Formation, the variegated marls of the Khaboba

Formation and the Middle to Upper Eocene white micritic pelloidal limestones of the Tanka Formation. The Tanka Formation is capped by a biostratigraphically defined non-depositional unconformity at the base of the Tayiba Formation; comprising shelf to offshore carbonate-rich clastic and carbonate deposits (Jackson et al., 2006). This Lower Oligocene unit which forms the uppermost part of the pre-rift succession is only locally preserved in the hangingwalls of several intra-block faults within the Hammam Faraun Fault Block and is observed up to a maximum of 56 m in thickness.

3.3.3 Megasequence 3 (Syn-rift)

The syn-rift infill of the Suez Rift ranges in age from Late Oligocene to the present day and forms three groups: the basal Gharandal Group, overlying Ras Maalab Group and the younger El Tor Group (Fig 3.4). The earliest syn-rift units of the Gharandal Group are Late Oligocene continental red bed facies and localised volcanics of the Abu Zenima Formation. These deposits show an upward transition to the initially fluvial and increasingly marginal marine facies of the Aquitanian to Burdigalian Nukhul Formation, whilst in the southern part of the rift, extensive anhydrites are observed (e.g. Winn et al., 2001; Orszag-Sperber et al., 1998; Carr et al., 2003). The overlying Lower Rudeis Formation is characterised by a sharp switch to offshore marine fine-grained facies with localised areas of coarser-grained clastic input (e.g. Gawthorpe et al., 1990; Patton et al., 1994; Sharp et al., 2000; Leppard and Gawthorpe, 2006). This dramatic change from shallow marine to dominantly open marine conditions is confirmed by observations of abundant pelagic foraminifera (e.g. Schutze, 1994). A major basinwide unconformity referred to as the mid-Clysmic or mid-Rudeis unconformity (e.g. Garfunkel & Bartov 1977; Patton et al., 1994; Wescott et al., 1996; Krebs et al., 1997) is commonly cited to precede a marked change in the nature of deposition recorded within the Burdigalian to Langhian Upper Rudeis Formation (also previously termed the Hawara and Asl Formations, e.g. Pivnik et al., 2003). At this time, increased clastic input was delivered into the rift resulting in proximal point-sourced fan delta facies along the rift margin and submarine fan facies in hangingwall depocentres within the rift axis, (e.g. Garfunkel & Bartov, 1977; Allen et al., 1984; Evans, 1988; Smale et al 1988; Elbaz and Handley, 1994; Dolson et al., 1996; Young et al., 2002; Pivnik et al., 2003). The Langhian to Serravalian Kareem Formation comprises interbedded sandstones, mudstones, carbonates and minor evaporites deposited in proximal shallow carbonate platforms and contemporaneous alluvial, deltaic and submarine fan systems which prograded into the axis of the rift (e.g. Rine et al., 1988;

Salah and Alsharhan, 1997; El-Ashry, 1972; Plaziat et al., 1998). The base of the Kareem Formation is typically observed within the rift axis to be associated with the Markha Anhydrite Member: a generally isopachous, laterally extensive, up to 30 m thick, subaqueous deposited evaporate (e.g. Orszag-Sperber et al., 1998). Cited to be diachronous (e.g. Beleity, 1982), stacked packages of this evaporite separated by fine-grained mudstones are observed within the rift axis towards the northern area of the central dip province and also locally towards the eastern margin of the axis in the southern dip province.

The onset of the Ras Malaab Group, signified by the deposition of the Serravallian Belayim Formation is characterised by a major switch to intercalated evaporitic, carbonate and clastic deposition, which is commonly subdivided into the Baba, Sidri, Feiran and Hammam Faraun Members (e.g, Schutze, 1994). The subsequent South Gharib Formation, largely of Tortonian age, is observed primarily within the axial subsurface of the rift and is dominated by halite with thin interbeds of anhydrite, mudstone and sandstones, whereas the overlying Tortonian to Messinian Zeit Formation is dominated by anhydrite, with clastic interbeds. Together, these two formations attain up to 3 km in thickness within the rift axis, yet according to most authors are not observed in the marginal areas of the rift (e.g. Patton et al., 1994).

The El Tor Group records deposition during the Pliocene to Pleistocene and is characterised by the basal Wardan Formation and overlying deposits of the Quaternary, although the boundary is difficult to pick (Bosworth & McClay 2001 and references therein). The Wardan Formation is typically up to 2 km thick in the rift axis, contains interbedded clastics, thin evaporites and carbonates, and shows spatial variations linked to the position of active sediment input points. The overlying Quaternary succession covers topographically low areas at the rift margin, predominantly as ephemeral wadi gravel deposits and related alluvium, which are often indistinguishable from those deposited in wadis and often located in identical positions present day; reflecting a continuous process of drainage network formation. Semi-lithified wind-blown sand dunes are also observed, usually preserved within sheltered wadi locations. Along the present day margin of the Gulf of Suez (i.e. the margin of the rift axis) fan deltas are observed to be associated with these extensive wadi systems, whilst raised beaches and reefs are also observed.

Biostratigraphic framework for Megasequence 3 (Syn-rift)

The requirement to accurately correlate contemporaneous syn-rift deposits both within the subsurface and exposed rift margin, which may display rapid lateral and vertical facies variations led to extensive research into age-specific biostratigraphic data, principally through the investigation of benthic foraminifera and nanoplankton (e.g. Souaya, 1966; Beleity, 1982; Wescott et al., 1996; 1998; Krebs et al., 1997). Whilst accurate, high resolution ages are difficult to establish due to considerable variations in both published and non-published reference standards, principle foraminiferal assemblage zones have been recognised which are largely accepted by various workers within the rift (Fig. 3.5).

A principal advance in this endeavour was made by Amoco / GUPCO workers in the 1980's through the use of the graphic correlation method of Shaw (1964) with respect to abundant foraminiferal data. Despite inherent difficulties in this method with respect to defining accurate composite standards, the ability for the taxa to be affected by environmental conditions and again, uncertainties associated with accurate dating, this method allowed for the recognition of significant hiatuses within the syn-rift succession, at a scale independent of individual structures (e.g Beleity, 1982). Outlined in the schemes of Wescott et al., 1996; 1998 and Krebs et al., 1997, this work used such hiatuses (termed hiatal terraces) due potentially to erosion, non-deposition and condensed sections, to bound intervening 'biostratigraphic sequences' of continuous deposition, which were then broadly related to the large-scale tectonostratigraphic evolution of the rift, e.g. rift initiation versus rift climax (*sensu* Prosser 1993). These sequences, whilst not corresponding to depositional sequences (*sensu* Vail et al., 1977) and also being largely equivalent to the previously defined lithostratigraphic based formations, provided a first order basis for constraining regional correlations for syn-rift facies and thickness variations and an initial movement away from previous, purely lithostratigraphic schemes.

Within the framework of Wescott et al., 1996; 1998 and Krebs et al., 1997, the initial rift break-up unconformity is designated T_{00} with the early syn-rift strata of the Abu Zenima Formations corresponding to Sequences S_{05} and S_{10}. Hiatal terrace T_{10} defines the onset of the climax phase of rifting, with the main rift climax deposits of the Lower Rudeis Formation comparable to Sequence S_{20}. Of specific interest to this study, the mid-Clysmic unconformity of Garfunkel and Bartov (1977) is designated as equating to terrace T_{20}, and the Upper Rudeis Formation corresponds to Sequence S_{30}. Sequence S_{30} is capped by the

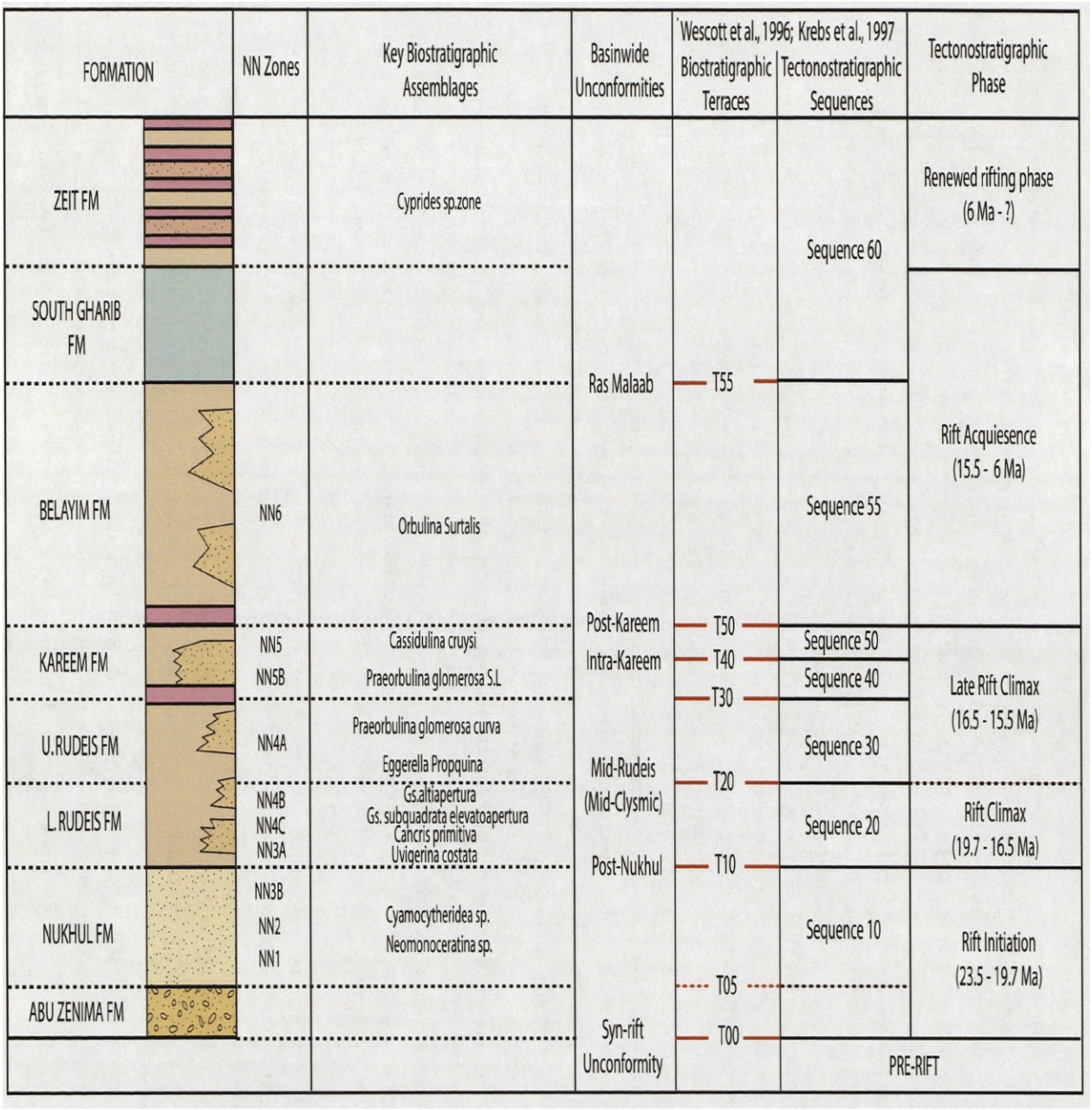

Figure 3.5. Key biostratigraphic zones, unconformities, tectono-stratigraphic sequences and interpreted phases of rift development for the syn-rift infill of the rift. Key to lithologies is in Figure 3.4.

T_{30} hiatal terrace, which is typically placed at the base of the lithostratigraphic Markha Anhydrite member of the Kareem Formation. Sequence S_{40} incorporates the lower part of the Kareem Formation and is capped by a regional flooding surface denoted by a landward shift in facies, which equates to hiatal terrace surface T_{40}. The upper part of the Kareem Formation corresponds to Sequence S_{50} and is capped by a major sequence boundary at the base of the Belayim Formation, T_{50}. The overlying Ras Malaab and El Tor Groups consist of Sequences S_{55}, S_{60} and S_{70} which equate to the Belayim, South Gharib plus Zeit and Wardan Formations respectively (Fig 3.5).

Unpublished Gulf of Suez Petroleum Company (GUPCO) trial studies during the early 2000's utilising nanoplankton data to further subdivide these biostratigraphic sequences were conducted, but ultimately not pursued. However, early results conducted on borehole-derived information for the Upper Rudeis Formation (Sequence S_{30}) in the rift axis were highly suggestive of the presence of a number of higher resolution stratal units. This is an interpretation consistent with, and independently derived from, the high-resolution stratal units defined for the Upper Rudeis Formation in Section 2 of this thesis.

3.4. LINKED TECTONOSTRATIGRAPHIC EVOLUTION

In this section, observations of structure, facies and stratigraphy are integrated with evidence from subsidence models (e.g. Steckler, 1985; Evans 1988; Richardson and Arthur 1988; Steckler et al., 1988) to outline the coupled tectonostratigraphic models for the evolution of the Suez Rift. Also, a brief outline of the principle events that occurred within the area prior to Oligo-Miocene extension is described.

3.4.1 Pre-rift

A complete review of the pre-rift events within the area of the Suez Rift is outside the scope of this chapter. For a comprehensive pre-rift review see Giraud and Bosworth, (1999) who provide a regional perspective for the evolution of north-eastern Africa and north-western Arabia. The salient points summarised here focus upon the uppermost pre-rift section of Megasequence 2. The late Cretaceous (Santonian) to late Eocene was characterised by a major NW-SE compressive event due to the onset of continental collision between the Africa-Arabian and Eurasian plates and the closure of the Neo-Tethys Ocean towards the North (e.g. Patton et al., 1994; Giraud and Bosworth, 1999). Older E-W striking faults associated with earlier Jurassic extension were reactivated and a series of folds developed from northern Cyrenaica to the Levant, commonly referred to as 'Syrian Arc' structures (after Krenkal, 1925). These structures provided an important topographic control upon contemporaneous and subsequent deposition, an example being the major Syrian Arc structure located at Wadi Araba, located on the western margin of the rift. During the Late Cretaceous a topographic high associated with a major ENE-WSW trending anticline provided a focus for a Campanian to Maastrichian aged carbonate rimmed shelf towards the south (Scheibner et al., 2001), whilst at the crest of the evolving structure the earliest units of Megasequence 2 were eroded and subsequent units not deposited (e.g. Zahran & Meshref, 1988; Moustafa & Khalil, 1995).

The Cretaceous – Palaeocene boundary is marked in the area by a marked marine transgression reflected in the deposition of the fine-grained mudstones of the Esna Formation and the subsequent development of shallow marine platforms. By the onset of the Eocene, a large stable carbonate platform represented by the Thebes Formation extended across North Africa to the northeastern part of the Arabian platform. The subsequent Eocene-aged deposits of the Darat, Khaboba and Tanka Formations represent an overall upwards-shallowing transition from outer to middle and inner nertic

bathymetries (Abu Nasr, 1987). A major Late Eocene compressive event is also recorded along the earlier broadly E-W Syrian Arc trend and is associated with uplift and the development of fold and thrust structures (e.g. Giraud and Bosworth, 1999). The Eocene – Oligocene boundary is characterised in the Suez Rift by a biostratigraphically defined unconformity, separating the shallow limestones of the Tanka Formation from the offshore shelf to shallow marine facies of the Tayiba Formation (Jackson et al., 2006). These rarely preserved deposits have previously proved controversial as some workers have attributed them to reflecting the onset of the first phase of the rift event; the localised preservation of this unit within intra-block fault zones is cited as evidence for an early rift tectonic control (e.g. Abu-Nasr, 1990; Refaat & Imam, 1999). However, the fully marine nature of this unit is in direct contrast to the overlying continental facies of the incontrovertible early syn-rift deposits of the Abu Zenima Formation. Furthermore Jackson et al., (2006) demonstrated that the Tayiba Formation is consistent with the underlying Eocene succession in that it does not display any variations in thickness or facies with respect to any individual, early rift related fault-segments.

3.4.2 Rift initiation (c 23 – 19.5 Ma)

The earliest stratigraphic expression of rifting is marked by a regional angular unconformity (T_{00} in the scheme of Wescott et al., 1996; Krebs et al., 1997) with pre-rift Eocene to Lower Oligocene units overlain by the continental red beds of the Late Oligocene to Early Miocene Abu Zenima Fm. The level of erosion associated with this syn- to pre-rift unconformity varies across the rift with respect to both local and regional structural position. Whilst locally within the eastern rift margin Hammam Faraun Fault Block the Late Oligocene Tayiba Formation forms the uppermost pre-rift unit within preserved early depocentres, typically Eocene carbonates form the uppermost preserved pre-rift unit. Along the rift margins, the age of the subcropping units are variable: for example limestones of the Upper Eocene Tanka Formation are observed in Wadi Gharandal, Wadi Wasit and Gebel Gushea areas towards the Zafarana Accommodation Zone on the Eastern rift margin, contrasting with the Lower Eocene Thebes Formation in locations such as at Wadi Baba in the El Qaa Fault Block (eastern margin) and Gebel El Zeit (western margin) (e.g. Winn et al., 2001; Jackson et al., 2006). In the rift axis, subsurface well penetrations indicate that the crests of individual fault blocks are typically variably characterised by the subcrop of the Darat and Thebes Formations. The age of the T_{00} unconformity is cited to vary along the axis of the rift, consistent with the 'scissors-

like' opening model of Colletta et al., (1988) from South to North (e.g. Bosworth and McClay, 2001). Dates range from: 27-25 Ma for the southernmost part of the rift; 23 Ma $\pm$ 2Ma for the central part constrained by K-Ar dating of rare basaltic sills, dykes and flows in the Abu Zenima Formation (e.g. Steen, 1984; Moussa 1987); and 23.5 Ma for the northernmost part of the rift (Bosworth and McClay, 2001).

During the subsequent initiation stage of rift development, rift-wide subsidence models (e.g. Steckler, et al., 1988; Evans, 1988; Richardson and Arthur, 1988) suggest that overall displacement and subsidence rates were relatively low, in the order of 9 m Ma^{-1}. This is consistent with integrated structural and stratigraphic studies, both fieldwork and subsurface based, which suggest that extension was initially distributed upon numerous, short (1-10 km long) and low displacement (<1 km) individual fault segments (Sharp et al., 2000; Gawthorpe et al., 2003; Carr et al., 2003; Young et al., 2003; Jackson et al., 2002; 2005). Consistent with models of fault growth by radial propagation and segment linkage (e.g. Walsh and Watterson, 1988; Cartwright et al., 1995; Dawers and Anders, 1995; Cowie, 1998; Ackermann et al., 2001; Mansfield and Cartwright, 2001), these fault segments coalesced through time to increasingly form longer, through-going fault arrays. As part of this evolution, the role of fault propagation folds, both monoclinal folds above upwards-propagating blinds faults (*sensu* Walsh and Watterson, 1987; Schlische, 1995) and hangingwall transverse synclines and anticlines associated with along-strike displacement variations (*sensu*, Anders and Schlische, 1994), are recognised upon the thickness distribution and stratigraphic architecture of the rift initiation deposits (Gawthorpe et al., 1997; Sharp et al., 2000b; Khalil and McClay, 2001).

The Abu Zenima Formation (Sequence S_{05}: Wescott et al., 1996; Krebs et al., 1997) is characterised throughout the rift by a continental fluvio-lacustrine succession consisting of channelised conglomerates, calcrete-bearing siltstones, variegated mudstones, cross bedded sandstones and poorly-sorted sheet-gravels (e.g. Patton et al., 1994; Jackson et al., 2002; 2006; Young et al., 2003). The change from marine facies of the pre-rift Tayiba Formation to the continental facies of the Abu Zenima Formation associated with the T_{00} surface is suggestive of a major fall in relative sea-level and has been attributed to either a tectonic or eustatic origin. The tectonic model invokes a response to an active rifting scenario, with the impingement of a mantle plume at the base of the crust causing a long-wavelength flexural uplift (Steckler 1985; Steckler et al. 1988) as suggested for other rifts such as the Jurassic North Sea Rift (Underhill and Partington, 1993) and is consistent with the presence of both intrusive and extrusive igneous bodies (Jackson et al., 2006 and

references therein). The studies of Garfunkel and Bartov (1977) and Steckler et al., (1985) argue against any stratigraphic evidence for significant uplift prior to rifting, whereas a period of basement unroofing is suggested from apatite fission track dating during the transition from the Eocene to Oligocene (c. 34 Ma) (Steckler and Omar, 1994; Omar and Steckler 1995). Alternatively, a Mid-Oligocene major eustatic sea-level fall (32 – 30 M.a) as suggested in the global eustatic curves of Haq et al., (1987) and Abreu & Anderson (1998), would be consistent with variable preservation of Middle Oligocene deposits across North Africa (Jackson et al., 2006 and references therein). Locally, erosional palaeovalleys are recognised at the base of the Abu Zenima Formation within the Hammam Faraun Fault Block at Wadi Tayiba (Jackson et al., 2002; 2006), Wadi Nukhul and Wadi Thal (Sharp et al., 2000), the hangingwall of the centre of the rift bounding Thal Fault at Gebel Musaba Salaama (Young et al., 2003) and within the Zafarana Accommodation Zone at Wadi Gharandal (this study: Chapter 6). The orientation of these palaeovalleys is inferred not to have been constrained by fault-related topography during this earliest phase of rift initiation, as they largely trend perpendicular to the Clysmic fault trend (Jackson et al., 2006), i.e. NE to SW.

The subsequent Nukhul Formation (Sequence S_{10} Wescott et al., 1996; Krebs et al., 1997) is overall trangressive, showing a transition from fluvial to marginal marine, tidally-influenced clastics in the rift margin Hammam Faraun Fault Block. The base of the formation is bounded by an erosive trangressive surface, designated T_{05}, which is typically characterised by marked angular unconformity (e.g. Evans & Moxon 1986; Krebs et al., 1997). Observed facies associations at the rift margin have been interpreted to reflect deposition across a genetically-linked succession of fluvial, estuarine, and shoreface to offshore environments; whilst stratigraphic and thickness variability suggests that deposition occurred within a series of structurally-controlled, elongate narrow depocentres (e.g. Carr et al., 2003; Jackson et al., 2005). In comparison, in the southern dip province of the rift, the Nukhul Formation consists of reefal carbonates, anhydrites and fluvial sandstones (e.g. Saoudi and Khalil, 1984; Winn et al., 2001). Within the axis of the rift, isopach and facies data for the Nukhul Formation are suggestive of an overall younging from South to North (e.g. Saoudi and Khalil, 1986; Meshref and Khalil 1986; Richardson and Arthur, 1988; Patton et al., 1994). Like the rift margin, the Nukhul Formation is interpreted as a transition from initially fluvial to shallow marine members. A basal fluvial Shoab Ali Member is overlain by marls and anhydrites of the Ghara Member, the October marine sandstones and Gharamul reefal limestones (Saoudi and Khalil, 1986; Bosworth

and McClay, 2001). These lithostratigraphically defined members are likely to be diachronous, and the basal members may actually be time equivalent to the Abu Zenima Formation as defined at the rift margin (Bosworth and McClay, 2001).

3.4.3 Rift Climax (c 19.5 – 16.5 Ma)

A marked rift-wide switch in facies from the shallow marine Nukhul Formation to the offshore Lower Rudeis Formation (Sequence S_{20} Wescott et al., 1996; Krebs et al., 1997) is universally agreed to represent the stratigraphic response to the onset of the climax phase of the rift event, (e.g. Beleity, 1984; Evans and Moxon 1986; Evans, 1988; Patton et al., 1994; Gupta et al, 1998; Gawthorpe et al., 2004). The hiatal surface between the older rift initiation deposits and the Lower Rudeis Formation is designated T_{10} in the schemes of Wescott et al., (1996) and Krebs et al., (1997) and has been described as a 'drowning unconformity' and reflects a major surface of marine transgression and subsequent switch-off in sediment supply.

Subsidence histories for the rift are unequivocal in suggesting a marked increase in subsidence rates from c. 19.5 Ma (e.g. Scott and Govean, 1986; Moretti and Colletta 1987; Richardson and Arthur, 1987; Evans, 1987), with suggested maximum fault displacement rates of between 125 m/Myr (Steckler et al., 1988) and 400 m/Myr (Richardson and Arthur, 1988). Field based studies have shown that this is in response to a marked period of fault linkage, with the development of larger, through-going fault arrays and the concentration of displacement onto crustal-scale faults; previously active smaller, medium-scale displacement (50-350 m) fault segments associated with the earlier rift initiation stage having become part of the larger fault arrays or abandoned (e.g. Sharp et al., 2000; Gawthorpe et al., 2003). These authors document the subsequent rotation of such medium-scale faults within larger half-grabens (in the order of 25 km wide by 40 km long) defined by the crustal scale faults (Fig.3.6).

Different authors have suggested varying deep-water palaeobathymetries during the rift climax stage deposition of the Lower Rudeis Formation: with ranges from 200 m, Scott and Govean (1986); 550 m, Beleity, (1984) and 1000 m, Evans, (1988). What is clear is that the Lower Rudeis Formation is characterised by offshore, basinal mudstones both within the rift axis and margin (e.g. Patton et al., 1994). Garfunkel and Bartov, (1977) cited the absence of coarse-clastics adjacent to the rift border fault system upon the rift margin as evidence for the absence of any uplifted rift shoulders. However, more recent studies have shown that the Lower Rudeis Formation contains significant coarser-grained

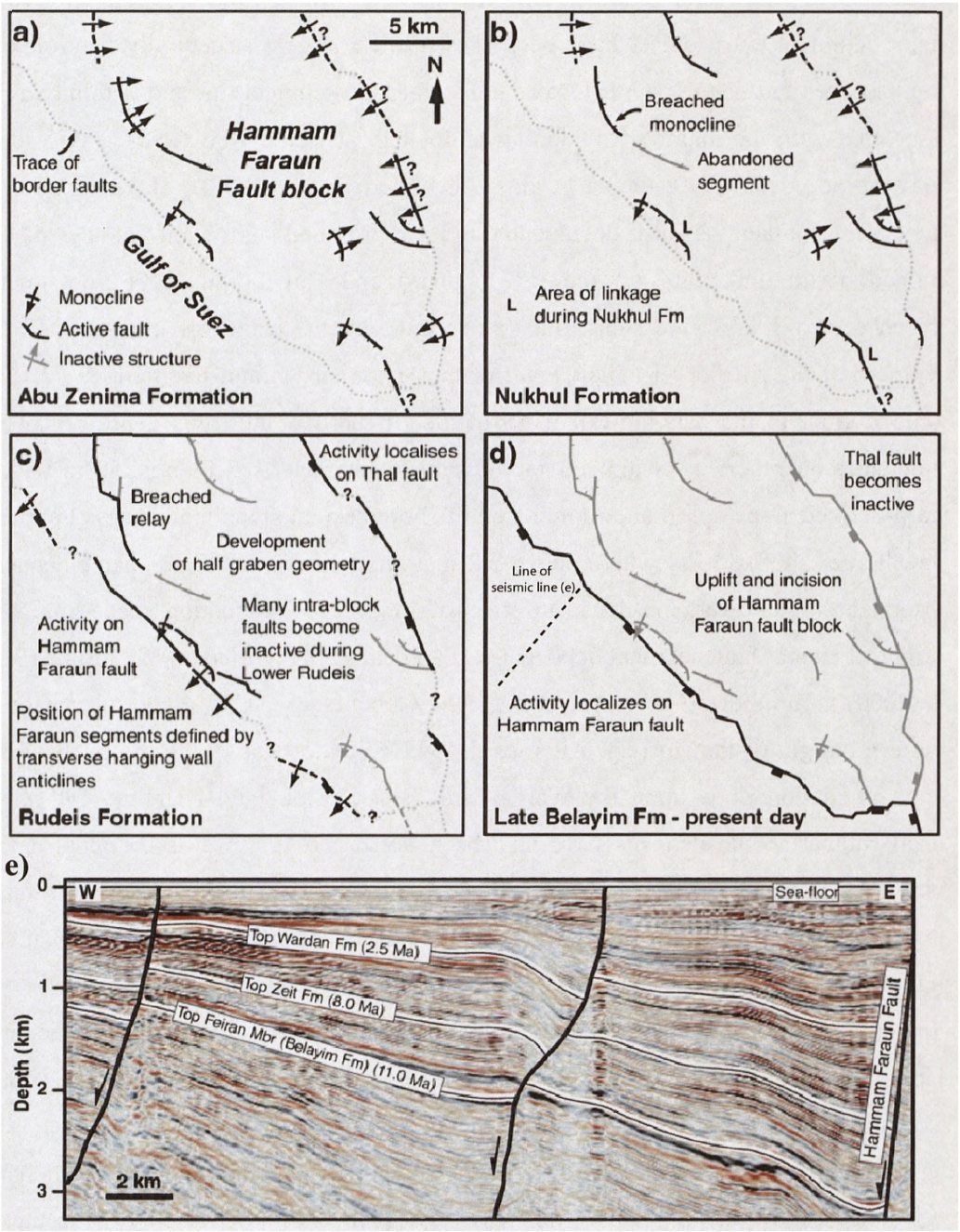

Figure 3.6. Interpreted evolution of the fault population within the rift margin Hammam Faraun Fault Block. Key stages are: (a) Early rift initiation (Late Oligocene - Early Miocene), (b) Mid to late initiation (Lower Miocene), (c) Rift climax (Lower to Middle Miocene), (d) Second phase of rifting (Middle Miocene to Recent). This 2nd rift phase is demonstrated in (e) with marked thickening of post Belayim Fm strata into the hangingwall of the Hammam Faraun Fault Zone. Figure modified after Gawthorpe et al., 2003.

clastic facies throughout the rift, i.e. both in marginal and axial areas which are typically associated with major sediment entry points (e.g. Evans, 1988). At the rift margin, such major sediment entry points have been shown to be largely structurally controlled, with point sourced fan-delta systems located at both at fault segment tips and within relay zones associated with the major rift bounding faults, e.g. at Gebel Abu Alaqa and Wadi Baba (Gawthorpe et al., 1990; Gupta et al., 1999; Sharp et al., 2000). However, long-lived antecedent drainage has also documented to have provided significant volumes of coarse-grained clastic material into the rift. Leppard and Gawthorpe (2006) document the presence of a 1 km wide submarine fan complex at the centre of the Sabut El Gamal Segment of the rift border (Thal) Fault of the Hammam Faraun Fault Block. Extending some 2 km into the hangingwall basin of the rift border fault, this depositional system punctuates an otherwise sediment-starved setting, characterised by a <250 m wide fault scarp-derived slope apron and more distal offshore basinal slope mudstones (Leppard and Gawthorpe, 2006). Elsewhere on the rift margin, examples of these coarse deposits are observed as shallower, fan-deltas in areas of lower accommodation space compared to Sarbut El Gamal fault segment depocentre. Fan deltas are reported at Wadi Baba (Sharp et al., 2000), Wadi Sidri, (Gawthorpe et al., 1990; Gupta et al., 1999), in the subsurface of the western margin of the rift (e.g. Allen et al., 1984; Smale et al 1988) and in the Zafarana Accommodation Zone upon the Warda Fault Block (Elbaz and Handley, 1994). More distal submarine fan deposits have also been noted further towards the axis of the rift within the Lower Rudeis succession; extensive, up to 200 m thick, submarine sandstones observed on the crest of the present day major block-bounding fault of the July Fault Block in the central dip province (Pivnik et al., 2003). Overall stacking patterns for these coarse-grained depositional systems in both the rift axis and margin are largely dependant upon the nature of the local structural configuration and the rate at which the fault-controlled accommodation space was generated. In a rift-wide sense, these Lower Rudeis depositional systems consistently show aggradational to retrogradational stacking, reflecting an overall series of trangressive sequence sets associated with the rapid subsidence of the rift climax phase.

3.4.4 The Mid-Clysmic or Mid-Rudeis event (c. 16 - 16.5 Ma)

A major erosional unconformity, referred to as the 'mid-Clysmic' or 'mid-Rudeis' unconformity has been cited to overlie the Lower Rudeis Formation and separate it from the overlying Upper Rudeis Formation. This is typically dated between 16-16.5 Ma (e.g.

Bosworth and McClay, 2001). First documented by the field mapping of Garfunkel and Bartov (1977) within the Sinai Peninsula, the magnitude, extent, and the significance of this unconformity with respect to the tectonic evolution of the Suez rift has been controversial (Patton et al., 1994). This has not been helped by confusion in the literature ascribing differently aged hiatal events to the mid-Clysmic event, and the confusion surrounding the potential for composite unconformities in structurally elevated positions, e.g. the Middle Miocene Kareem Formation resting unconformably upon pre-rift Middle Eocene Darat Formation limestones in part of the footwall crest of the October Fault Block (Chapter 5).

The mid-Clysmic unconformity is commonly observed at the rift margin as a marked change in the nature of deposition from the underlying Lower Rudeis Formation, with an observed abrupt increase in sediment input being delivered into the rift in the overlying Upper Rudeis Formation, suggesting a major relative sea-level fall (Garfunkel and Bartov, 1977). Whilst the margin does display a marked change in the style of deposition, there is no evidence of any contemporaneous disruption in sedimentation style having occurred at various structural locations within the axis (Patton et al., 1994; this thesis). The axial equivalent to the rift margin unconformity is typically observed within a mudstone-dominated succession, as a biostratigraphically defined hiatal terrace, designated T_{20} in the schemes of Wescott et al., (1996) and Krebs et al., (1997), discussed below. In addition to the shift in facies types, Garfunkel and Bartov (1977) made the observation that mesocale faults commonly tip out below or at the unconformity surface, whilst calculated subsidence models are typically shown to display a variable reduction in subsidence rate (e.g. Richardson and Arthur, 1988; Evans, 1988; Steckler et al., 1988; Wescott et al., 1996). However, as discussed in the preceding rift climax section, the abandonment of mesoscale faults is consistent with a model for the *progressive* localisation of displacement onto crustal-scale block bounding fault zones (Sharp et al., 2000). This combination of an abrupt change in facies types and the reduction in fault activity at the rift margin have been variably interpreted to be the result of a major structural reorganisation of the rift, either characterised by a localisation of displacement onto larger fault blocks (Garfunkel and Bartov, 1977) or alternatively signifying a much more fragmented rift system (Montenat et al., 1986; Richardson and Arthur, 1988; Smale et al., 1988). The underlying cause of this tectonic event has principally been attributed to the onset of rift shoulder uplift during the main rift climax phase (e.g. Garfunkel and Bartov, 1977; Moretti and Colletta, 1988; Steckler et al., 1988), with suggested mechanisms including: passive isostatic rebound

(Wescott et al., 1996), a 45^0 clockwise rotation of the regional stress field (Lyberis et al., 1988), an end of early strike-slip component of faulting and transition to pure dip-slip motion (Montenat et al., 1988; Jarrige et al., 1990) or the onset of transform movement associated with the Gulf of Aqaba (e.g. Patton et al., 1994 and references therein). A review of these mechanisms by Bosworth and McClay (2001) found no consistent evidence for a transition from previous strike-slip motion (e.g. Montenat et al., 1988; Jarrige et al., 1990), poor age constraint for a proposed rotation of the regional stress field (Lyberis et al., 1988), and that the common citing of coeval onset of transform movement associated with the Gulf of Aqaba (e.g. Patton et al., 1994) is unsuitable, as better age constraints suggest this initiated during the deposition of the subsequent Kareem Formation at ca. 15.5 Ma (e.g. Richardson and Arthur, 1988). Thus this leaves isostatic rebound as the plausible proposed tectonic mechanism for potential uplift at this time; Wescott et al., (1996) cite the mid Clysmic unconformity as a specific episode of uplift linked to maximum crustal thinning, shallowing of the transition zone between the brittle and ductile crust, with subsequent wholesale fault block rotation. However, one of the key contentions of this thesis is that to extrapolate observations derived solely from the rift margin to define a rift-wide model evolutionary model is inappropriate. The rotation of fault blocks is more likely to have been progressive as suggested in the models of Sharp et al., (2000) and Gawthorpe et al., (2003) rather than as a response to a single tectonic episode. This is supported by the lack of a major erosion unconformity within the subsurface of the rift associated with the biostratigraphically defined T_{20} hiatal surface between the Lower and Upper Rudeis Formations upon both footwall locations that might be expected with fault block rotation.

A potential alternative mechanism to account for the observations made both within the rift margin and axis is the combination of an overall decrease in extension rates within the rift following the 16.5 – 16 Ma (Richardson and Arthur, 1988; Patton et al, 1994) and the role of a major 30 - 100 m fall in eustasy during the Langhian, (e.g. Haq et al., 1987; Abreu and Anderson 1998; Miller et al., 2005). Whilst this eustatic fall has been previously cited (e.g. Evans 1988; Richardson and Arthur, 1988; Smale et al., 1988), it has not been regarded as a principal mechanism in itself to explain the mid-Clysmic unconformity. This theme is explored in Chapters Seven and Eight.

3.4.5 Late rift climax to rift abatement (c 16.5 – 15.5 Ma)

Directly above the mid-Clysmic or mid-Rudeis unconformity at the rift margin and the synonymous T_{20} hiatal surface in the rift axis are the deposits of the Upper Rudeis Formation which form the principle interval of interest for this thesis (Sequence S_{30} Wescott et al., 1996; Krebs et al., 1997) and the succeeding Kareem Formation (Sequences S_{40} and S_{50}). As documented in Section 2, the Upper Rudeis and Kareem Formations are associated with an overall marked basinward shift in depositional systems throughout the rift; with coarse-grained proximal fan deltas and submarine fans being established within the rift margin and rift axis respectively, typically displaying a progradational stacking geometry in marked contrast to the aggradational to retrogradational stacking patterns of previous depositional systems associated with the rift climax Lower Rudeis Formation (e.g. Evans, 1990; Gawthorpe et al., 1990; Pivnik et al., 2003). This period of the rift evolution is interpreted to be associated with decreasing tectonic activity reflected in subsidence studies which typically document reduced rates of subsidence, albeit with variations due to differing structural locations (e.g. Steckler et al., 1988; Richardson and Arthur, 1988; Evans 1988). Detailed studies of individual fault blocks have also recorded the episodic nature of activity upon individual fault zones during this period and the subsequent response in Upper Rudeis depositional systems, e.g. on the July Fault Block (Pivnik et al., 2003).

The base of the Kareem Formation is associated with the first regional deposition of an evaporitic facies since that associated with the Nukhul Formation in the southern part of the rift. This is characterised by a relatively isopachous, 0-50 m thick unit of anhydrite, although some thickening into fault hangingwalls is observed, referred to as the Markha Anhydrite. Commonly referred to as a sabkha deposit (e.g. Wescott et al., 2000), a preferred interpretation is that this unit reflects a period of restricted basinal conditions within the rift (e.g. Orszag-Sperber et al., 1998; Chapter 4).

By the time of deposition of the succeeding Belayim Formation, tectonic activity within the rift had largely abated and transferred to the Aqaba transform (e.g. Lyberis, 1988; Patton et al., 1994; Bosworth and McClay, 2001). The interbedded evaporitic and clastic deposits and their resultant complex and rapid facies relationships within this unit are interpreted to reflect a complex interplay between remnant structural and previous depositionally generated relief and fluctuations in regional sea-level. The basin became

increasingly evaporitic and experienced the deposition of the thick halite deposits of the South Gharib Formation.

3.4.6 Renewed phase of rifting (6 Ma to present)

Following the period of tectonic acquiescence which is associated with the deposition of the Belayim and South Gharib Formations linked to the onset of activity upon the left lateral Aqaba Transform at ca. 15.5 Ma, a second phase of renewed extension is recorded in the Suez Rift ca. 6 Ma during the Late Miocene to Early Pliocene. This activity was manifested by both the reactivation of fault zones associated with the earlier phase of extension, and the development of younger, shallower fault systems which display differing growth histories to underlying deeper seated fault zones upon which they are localised, e.g. the October Fault Block (Jackson, 2002, unpublished Ph.D thesis). This phase of tectonic subsidence was principally concentrated onto the fault zones separating the rift axis from the rift margin, i.e. the present day coastal boundary fault systems which display a final vertical offset of up to 4 km. Marked thickening of Pliocene strata into hangingwall depocentres of the coastal boundary fault system is observed, although the role of halokinesis associated with the underlying South Gharib Formation may mask the timing of fault activity, particularly in the southern part of the rift where salt diapirs are observed (e.g. above the 'B-trend' system of fault blocks (e.g. Helmy, 1993). This renewed Late Miocene to Pliocene phase of subsidence has been kinematically linked to continued extension in the Red Sea Rift, and a phase of sinistral strike-slip movement along the Aqaba Transform (Bosworth and McClay, 2001).

Uplift of Quaternary terraces, earthquake activity and recent GPS data suggest that the Suez Rift remains an area of active normal extension to the present day, with a clustering of historical and recent earthquakes towards the southern part of the rift (Jackson et al., 1988; Bosworth and Steckler, 1997; Hussein et al., 2006). Estimates for the rate of extension and subsidence are in the order of 1 – 1.5 mm per year contrasting with rates of 8-9 mm per year for the Red Sea rift (Steckler et al., 1988; Mahmoud et al., 2005; Hussein et al., 2006). Continued extension today is likely to be related to the continuing northwards movement of the Sinai microplate / Arabian plate away from the similarly northwards-moving, albeit at a slower rate, African plate.

CHAPTER FOUR

SEDIMENTOLOGY AND EVOLUTION OF RIFT AXIS DEPOSITIONAL SYSTEMS: THE LATE RIFT CLIMAX UPPER RUDEIS FORMATION, OCTOBER FAULT ZONE, SUEZ RIFT, EGYPT

CHAPTER 4

SEDIMENTOLOGY AND EVOLUTION OF RIFT AXIS DEPOSITIONAL SYSTEMS: THE LATE RIFT CLIMAX UPPER RUDEIS FORMATION, OCTOBER FAULT ZONE, SUEZ RIFT, EGYPT

4.1. ABSTRACT

Within extensional basins, syn-rift sedimentation during the climax phase of rifting is dominantly controlled by the evolution of normal fault systems and the resultant basin physiography produced, interacting with more regional variations in eustasy and sediment supply. This chapter highlights the spatial and temporal variability of rift climax deposits within a marine rift axis setting, by examining the linked sedimentological and tectonostratigraphic evolution of the Miocene Upper Rudeis Formation associated with the October Fault Zone, Suez Rift, Egypt. Utilising an extensive subsurface database comprising wireline logs, biostratigraphic information and core, the primary sedimentology and stratigraphic framework of the Upper Rudeis Formation is characterised and a process-based depositional model developed. Integrated with stratigraphic unit thickness maps, major facies and thickness variations are identified which, when related to interpretation of the present day structural configuration, reveal the sequential structural and palaeogeographic evolution of the October Fault Zone during the *ca.* 0.8 Myr deposition of the Upper Rudeis Formation.

Deposition of the Upper Rudeis Formation associated with the rift axis October Fault Zone was characterised by three contemporaneous depositional systems: 1) a background offshore basinal system, with thickness and facies variation reflecting the inherent asymmetry of half-graben style basin physiography; 2) a calcarenite-rich submarine fan system sourced from potentially both the uplifted October Fault Block footwall crest and the adjacent rift margins, and 3) a siliciclastic-rich submarine fan, regionally sourced from a major sediment entry point, 57 km to the North. Whilst the structural evolution of the October Fault Zone, characterised by the growth and linkage of individual fault segments had a profound impact upon the distribution of the depositional systems, the recognition of correlatable, regional scale, key stratigraphic surfaces and associated variations in sediment flux into the rift axis is indicative of additional regional-scale controls upon the deposition of the Upper Rudeis Formation. Variations in relative regional sea-level, sediment source area and sediment entry

points into the rift axis combined to control the location, magnitude, extent and composition of individual late rift-climax depositional systems.

4.2. INTRODUCTION

The spatial and temporal variability of syn-rift deposits within marine rift basins results from an interaction of both local and regional scale controls upon sedimentation. The fundamental local control upon deposition is the physiography of the basin, determined by the evolution of basin bounding normal fault systems. Marked spatial variations in tectonic subsidence and uplift provide a template, upon which further local controls (e.g. bedrock lithology and drainage network evolution) and more regional controls (e.g. variations in eustatic sea-level, climate and sediment supply) interact (Gawthorpe and Leeder, 2000).

During the climax phase of rifting (*sensu* Prosser, 1993), normal fault systems have been shown to increasingly interact and form a series of fully linked, through-going fault zones, (e.g. Gupta et al., 1998; Cowie et al., 2000; McLeod et al., 2000; Gawthorpe and Leeder, 2000; Gawthorpe et al., 2003). With maximum rates of displacement being achieved upon basin bounding faults during this period, related hangingwall subsidence outpaced sedimentation. Consequentially, marine rift hangingwall depocentres may be characterised by deepwater bathymetries, sediment starvation and are therefore underfilled. This is reflected in the nature of associated hangingwall syn-rift deposits, typified by an abundance of fine-grained hemipelagic sediments with intervening coarse clastic, gravity flow deposits derived from both local intra-basinal topographic highs (uplifted footwalls) and basin margins (e.g. Ranvås & Steel, 1997; Gawthorpe and Leeder, 2000; Leppard and Gawthorpe, 2006).

Generic tectono-stratigraphic models for rift climax marine sedimentation (e.g. Gawthorpe and Leeder, 2000) provide an important conceptual tool in recognising and predicting potential variations in syn-rift facies types and resultant stratal geometries within the context of a series of evolving normal faults; whilst specific facies models for deposits adjacent to an individual fault zone (e.g. Surlyk, 1989; Young et al., 2000; 2002; Leppard and Gawthorpe, 2006) provide both a quantitative description of the extent and thickness of depositional systems and an indication of the localised controlling factors upon their development. However, such detailed facies models have tended to focus upon a discrete section of a single fault zone, whereas few studies have documented the nature of high-

resolution syn-rift facies variations at a regional fault block scale, i.e. ca. 30 km long by 25 km wide.

Specific to the Suez Rift, detailed rift climax facies models (e.g. Gupta et al,. 1999; Sharp et al., 2000; Young et al., 2000; 2002; Leppard & Gawthorpe, 2006) have focussed on the exposed major rift boundary fault zones or mesocsale intrablock faults within the rift margin Hammam Faraun and El Qaa Fault Blocks (Fig 4.1). These workers have documented depositional systems of both a limited extent, ca. 250 m from the rift border fault zone linked to linear footwall scarp degradation, (e.g. Leppard & Gawthorpe, 2006), and larger, ca. 1.5 – 5 km point sourced, fan delta and submarine fans systems associated with relay and antecedent drainage networks, (e.g. Gupta et al., 1999; Young et al, 2002; Leppard & Gawthorpe, 2006). However, the suitability of rift-margin-based models to accurately characterise and predict the full nature of regional, potentially multiple-sourced depositional systems within the rift axis is questionable.

This chapter aims to investigate the temporal as well as spatial sedimentological and stratigraphic variability of rift climax deposits deposited within an axial rift location associated with an evolving regional scale fault block by examining the Upper Rudeis Formation associated with the October Fault Zone, located in the present day axis of the Gulf of Suez Rift. A rift axis, process-based facies model is presented for the late rift climax depositional systems active during deposition of the Upper Rudeis Formation, which together with a model for the tectono-stratigraphic development of the October Fault Zone, allow for potential variations in sediment source and transfer pathways to be defined and the role of different controlling mechanisms upon rift climax sedimentation, both at a local and regional scale to be evaluated.

4.3. DATASET AND METHODOLOGY

This study utilises an extensive subsurface database provided by the Gulf of Suez Petroleum Company, (GUPCO), comprising approximately 200 wells with a variable suite of wireline logs, core, accompanying high resolution biostratigraphic data and a depth pre-stack converted 3D seismic survey covering the study area. Within the rift axis, shallow syn-rift intercalated clastic and evaporite units produce significant seismic attenuation and result in

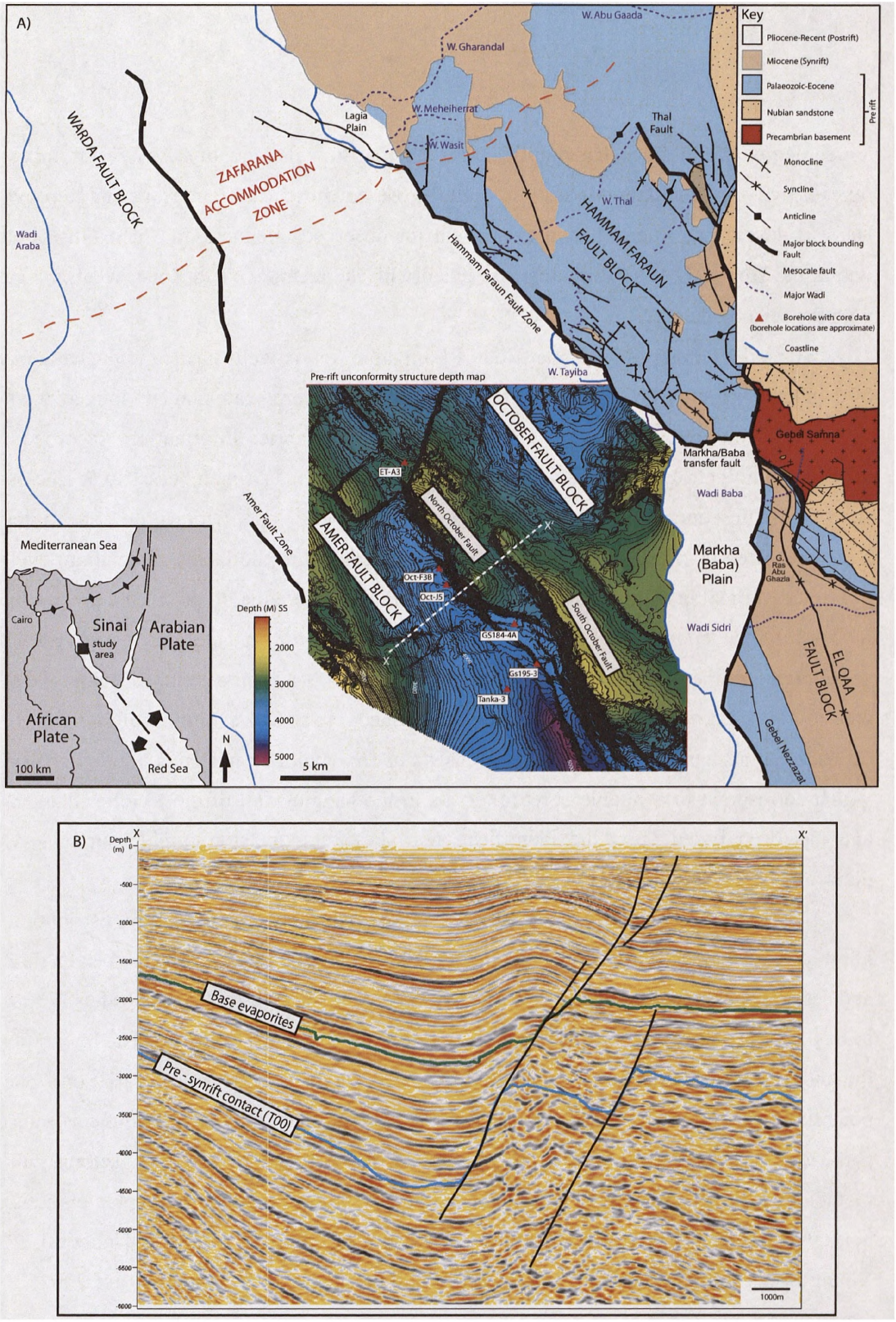

Figure 4.1. A) Simplified geological map of the Hamman Faraun and El Qaa Fault Blocks (modified after Moustafa, 1993; Sharp et al., 2000), with the location of the October Fault Zone shown by a depth structure map on the pre-rift to syn-rift unconformity. Wells with cored intervals. Inset shows geographic location. B) Seismic dip line through the OFZ. Seismic quality is severely reduced below the base of the evaporite package.

a high degree of multiples that significantly reduce seismic data quality. As a result, this study relies heavily on well data to constrain both the present structural framework and to provide a basis to develop an interpretation to account for observed thickness and facies distributions within the Upper Rudeis Formation associated with the October Fault Zone, when integrated with the seismic dataset.

Cored intervals of the Upper Rudeis Formation for six wells located in the hangingwall of the October Fault Zone, approximately totalling 275m were examined and logged at a scale of 1:50, with relevant sedimentological and ichnofabric information recorded and accompanying petrographic analysis of available thin sections (Appendices 1 to 3; Enclosures A to G). Subsequent lithofacies and process-based facies identified within cored intervals were calibrated to wireline log signatures (typically linked to the facies association level due to limited vertical resolution) and correlated within the study area, to produce a process-based model for the deposition of the Upper Rudeis Formation. In addition, a high resolution stratigraphic framework for the Upper Rudeis Formation has been developed within the study area to aid in correlation and evaluate the palaeogeography and evolution of late rift climax depositional systems. This framework consists of five major stratal units, the lower three of which correspond to available cored intervals in the hangingwall of the October Fault Zone, and has been based upon the identification of key regional stratigraphic surfaces which delineate major facies shifts within the study area.

Analysis of mapped variations in both stratal unit thickness and facies distribution has allowed for a model of the linked tectono-stratigraphic evolution of the October Fault Zone and active depositional systems associated with the deposition of the Upper Rudeis Formation to be developed at the scale of an individual fault block (40 km x 25 km). The integration of thickness and facies data allows for the differentiation of thickness variations due to potentially fault-controlled subsidence and the proximity to major sediment transport pathways; an important distinction within an underfilled half-graben setting, and a methodology in accordance with previous studies of linked tectono-stratigraphic evolution of normal faults both in the subsurface (e.g. Davies et al., 2000; Dawers & Underhill, 2000; Young et al., 2001; Bruhn and Vagle, 2005) and at outcrop (e.g. Young et al., 2002, 2003; Gawthorpe et al., 2003).

4.4. GEOLOGICAL SETTING

4.4.1 Structure

The Suez rift is a failed NW-SE trending intracontinental extensional rift system up to 80 km wide and 300 km long, which developed as a northern continuation of the Cenozoic Red Sea Rift (e.g. Colletta et al., 1988; Patton et al., 1994). The present day Gulf of Suez occupies only the inner axis of the rift, with marginal rift flanks exposed onshore (Fig. 4.1a). The main phase of rifting is estimated to have been initiated in the Late Oligocene to earliest Miocene, (c. 24 Ma) in response to the separation of the African and Arabian plates, with the main phase of rifting ending at the time when significant plate motion transferred to the Dead Sea – Aqaba transform (c. 15.5 Ma), (e.g. Richardson & Arthur, 1988; Colletta et al., 1988; Patton et al., 1994; Moustafa 2002).

The Suez rift can be divided into three structural provinces, defined as the northern, central and southern dip provinces, that comprise several major crustal-scale fault blocks, 10-15 km wide and 20-30 km long, and their associated bounding normal faults showing a consistent dip orientation each province, (Fig. 4.1a), (e.g. Moustafa 1976; 1993; Patton et al., 1994; Pivnik et al., 2003). The dip direction of the structural provinces changes from north to south along the rift, with major faults within the northern province dipping northeast, those in the central province to the southwest, and a return to a northeast dip direction in the southern province. The dip provinces are separated by two accommodation zones, which extend transversely across the rift, and accommodate the change in dip direction between the provinces and are termed the Zafarana and Morgan accommodation zones in the north and south respectively, (Moustafa, 2002).

The October Fault Block is located in the central dip province and is a large, ca. 40 km long by ca. 25 km wide, tilted fault block (Moustafa & Abdeen, 1992. It forms the hangingwall dip-slope to the rift margin bounding Hammam Faraun Fault Zone towards the northeast, whilst in the southwest it is bounded by the October Fault Zone; the associated hangingwall dip-slope of which is formed by the adjacent Amer Fault Block (Fig. 4.1a). In a dip orientated cross sectional view, (Fig. 4.1b), the October Fault Zone displays two distinct geometries: a shallow listric geometry associated with the late middle Miocene to Recent section, contrasting with a more deep-seated fault geometry characterised by a steep planar dip,

ca. 60° in the pre-rift to late syn-rift succession. Syn-rift strata associated with this deeper geometry are observed to both thicken in the hangingwall and thin onto the footwall crest, confirming the October Fault Zone was active during the main phase of syn-rift activity.

In plan view, (Fig. 4.1), the present day trace of the October Fault Zone at the pre-rift-syn-rift contact has an overall dominant NW-SE trend (referred to as the Clysmic trend, e.g. Lelek et al.,1994) and is approximately 30 km in length and displays a maximum throw of 2 km. In detail however, the fault zone is observed to consist of two large overlapping faults, (< 20 km in length), termed the North October and South October Faults. Based upon their plan view geometry, both these large faults can be considered to be made up of a series of smaller (< 5 km in length), NWW to SEE, Clysmic, NNW-SSE and N-S orientated segments (Fig 4.1), which appear comparable in scale and orientation to similar segments identified in previous studies on the rift margin (e.g. Gawthorpe et al., 2003). Dense well control through the fault zone and into the footwall provides a relatively good constraint for the present day geometry of the South October Fault. Approximately 20 km in length, this NNW-SSE trending major fault exhibits a maximum of 2 km of vertical throw, and is interpreted at the pre- syn-rift contact to consist of a series of individual fault terraces. Limited well control within the hangingwall makes accurate mapping of individual fault terraces difficult, however at the level of the top of the Upper Rudeis Formation, the South October Fault is considered to be comprised of up to five smaller segments based upon their plan view geometry. The North October Fault is approximately 15 km in length, with a maximum throw of 1450 m, and similarly based upon trace geometry can also be considered to be comprised of five main identifiable fault segments.

4.4.2 Stratigraphy

The stratigraphy of the northern Gulf of Suez is summarised in Fig. 4.2. The pre-rift succession is comprised of two megasequences, with the initial megasequence containing predominantly Cambrian to Lower Cretaceous Nubian sandstones, lying unconformably upon a complex Precambrian crystalline basement (e.g. Schutze, 1994). These deposits reflect the position of the northeastern Africa craton as a passive margin to the Palaeotethys and succeeding Neotethys oceans to the north (e.g. Guiraud & Bosworth, 1999). Megasequence 2

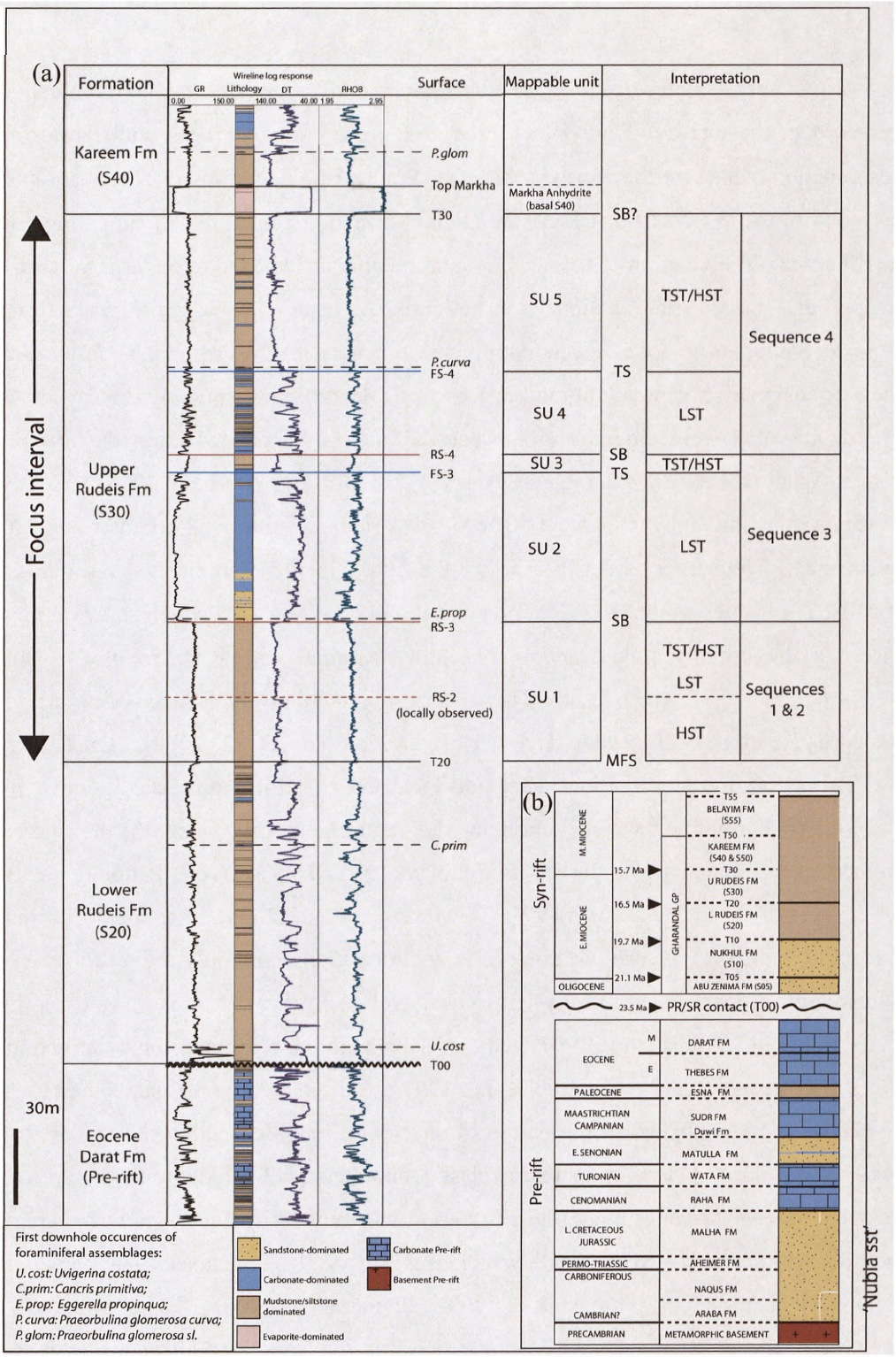

Figure 4.2. (a) Type well section (OCT-J5) for the syn-rift succession within the hangingwall of the October Fault Zone. Key surfaces, accompanying biostratigraphic data and interpretation is indicated. Refer to text for details. (b) General stratigraphic column for the October Fault Block, which places (a) into context. Stratigraphic ages are taken from Krebs et al., 1997 and Bentham et al., 1996.

consists of mixed carbonate–clastic strata of Cenomanian to Oligocene age, with typically 900 m preserved in the October Fault Block area. This markedly contrasts with the Zafarana Accommodation Zone to the north, where at Wadi Araba and its offshore component associated with the Warda Fault Block, the Nubia Formation constitutes the uppermost layer of pre-rift strata. The location of the accommodation zone is believed to be largely controlled by the presence of a Syrian arc inversion anticline (Moustafa 1997), which formed as the response to Santonian to Late Eocene compressive events inverting previous Jurassic E-W trending extensional structures (Guiraud & Bosworth, 1999). Consequently the earliest units of Megasequence 2 were eroded and subsequent units not deposited upon the Syrian arc anticline at Wadi Araba, (e.g. Zahran & Meshref, 1988; Moustafa & Khalil, 1995).

Syn-rift stratigraphy of Late Oligocene to Middle Miocene age comprises a third megasequence. The earliest syn-rift units are the Late Oligocene continental red bed facies and localised volcanics of the Abu Zenima Formation (24 – 21.5 Ma) which show an upward transition to the initially fluvial and increasingly marginal marine facies of the Nukhul Formation (21.5 – 19.7), which are thought to correspond to slow subsidence rates during rift initiation (e.g. Patton et al., 1994; Krebs et al., 1997; Sharp et al., 2000). Overlying the Nukhul Formation are deep marine facies and localised areas of coarse clastic input of the Lower Rudeis Formation, which represent the stratigraphic response to the increased subsidence rates associated with the onset of climax (19.7 – 16.5 Ma) (e.g. Patton et al., 1994; Krebs et al., 1997; Gupta et al, 1998; Gawthorpe et al., 2004). A major basinwide unconformity is cited to overlie the Lower Rudeis Formation commonly referred to the mid-Clysmic or mid-Rudeis unconformity (e.g. Garfunkel & Bartov 1977; Patton et al., 1994; Wescott et al., 1996; Krebs et al., 1997) and correlates with the biostratigraphic-defined hiatal terrace, T_{20}, (Wescott et al., 1996; Krebs et al., 1997). Subsequent to this hiatal event, several authors cite a marked change in the nature of deposition recorded within the Upper Rudeis Formation (16.5 – 15.7 Ma), with increased clastic input being delivered into the rift; proximal point sourced fan delta facies along the rift margin and submarine fan facies in hangingwall depocentres within the rift axis, (e.g. Garfunkel & Bartov, 1977; Evans, 1988; Smale et al 1988; Dolson et al., 1996; Young et al., 2002; Pivnik et al., 2003). The Upper Rudeis Formation is defined in this study as being analogous to Sequence S30 in the schemes of Wescott et al,. (1996) and Krebs et al., (1997), i.e. a biostratigraphic sequence defined by the

graphic correlation method, bounded at the base and top by rift-wide hiatal terraces termed T_{20} and T_{30} respectively.

The subsequent Kareem, Belayim, South Gharib and Zeit Formations record the progressive evaporitic nature of deposition, reflecting the overall abatement of the rift event and increasingly complex interplay between eustatic and tectonic effects, (Bosworth & McClay, 2001).

4.5. SEDIMENTOLOGY

The Upper Rudeis Formation deposited around the October Fault Zone is characterised by three different cotemporaneous depositional systems: i) offshore basinal, ii) calcarenite-rich submarine fan and iii) siliciclastic-rich submarine fan (Fig. 4.3). The submarine fan depositional systems reflect the episodic influx of largely rift margin derived sediment which punctuated the largely sediment starved facies of the offshore basinal depositional system within the rift axis.

Examination of cored intervals highlights considerable compositional variation within these three depositional systems ranging from i) calcareous mudstones, ii) subarkosic to quartz rich siliciclastic sandstones, iii) skeletal, bioclastic grainstones, packstones to wackestones and iv) calcareous sandstones (Fig. 4.3). The siliciclastic sandstones and bioclastic carbonate clastic lithofacies identified form the end members of a siliciclastic – carbonate mixing continuum, similar in concept to that identified by Dorsey and Kidwell, (1999). Lithofacies groupings and subsequent lithological terms used in this study are based upon approximate ratios of siliciclastic to carbonate components (Table 4.1), which whilst arbitrary, affords a shorthand basis to allow for the temporal and spatial variation in the lithofacies components to be quantified. This provides important data with which to investigate the interplay of local versus regional sediment sources and delineate locally axial versus transverse sediment transfer pathways. Process-based facies are summarised in Table 4.2.

4.5.1 Offshore basinal system

Three facies associations reflect the nature of deposition within a largely sediment starved, series of offshore marine half-grabens. The inherent asymmetry associated with a tectonically controlled hangingwall dip slope (typically 15 - 25 km in width) and associated

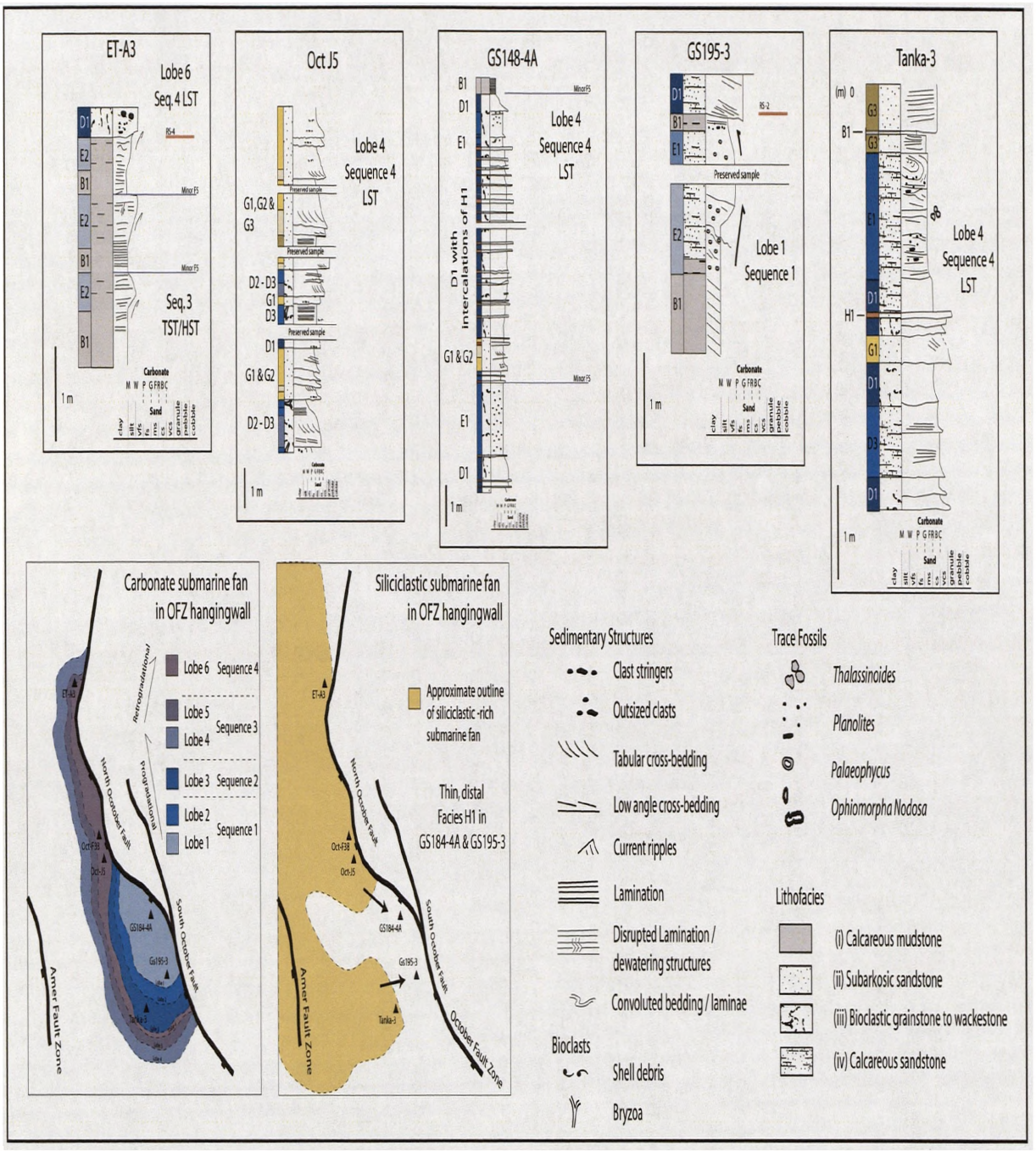

Figure 4.3. Temporal and spatial variability of the two major Upper Rudeis submarine fan depositional fan systems identified within the hangingwall of the October Fault Zone. Graphic sedimentary logs (A-E) show the varying intercalated nature of siliciclatic and carbonate dominated process-based and lithological-based facies, see text for details. Maps F and G illustrate how a series of fan lobes of carbonate-rich submarine fan are centred between North and South October Faults, contrasting with a more axially orientated siliciclastic-rich submarine fan, sourced from the North.

Lithofacies	Lithology -(ies)	Composition	Texture	Wireline response	Other
(i)	**Calcareous mudstone**	Fine grained carbonate material and comminuted shell material.	Fine grained, dark coloured, massive and laminated. Body fossils or trace fossils rare or difficult to observe.	Core to wireline log calibrations are characterised by high gamma ray responses of >50 API, with accompanying formation density and neutron porosity logs typically displaying a wide separation, with generally high density values, >2.5 g/cm^3 respectively.	Observed up-to 7 m thick in core.
(ii)	**Subarkosic sandstone** (Dominantly siliciclastic deposit, i.e. >60% silicic material, with common values being >80).	Predominantly undulose quartz (>50%), with variable lesser amounts of plagioclase feldspar, chert, lithic fragments, glauconite and carbonate bioclasts.	Grains are variable in size from very fine to granule grade, sub-rounded to angular and display a range of sorting from medium to poor. Plagioclase feldspars when present are similarly shaped and sized as the quartz grains and account for a maximum of 10%. Carbonate bioclasts are identical to those in Lithofacies (iii)	Gamma ray responses are typically lower than 40 API whilst calibration with formation density logs suggest a typical maximum density cut-off of approximately <2.4g/cm^3, usually accompanied with a neutron-density crossover.	Observed intergranular porosities are generally good with infilling calcite cement proportional to the amount of carbonate bioclasts present.
(iii)	**Bioclastic grainstone, packstone and wackestone** (>80% carbonate material)	Skeletal bioclasts with varying amounts of carbonate mud material. Bioclasts include bivalves, bryozoans, echinoids, red algae, forams and disarticulated shell fragments. Increasing amounts of fine grained material are characteristic of packstone and wackestone lithologies.	Sizes range from fine grained fragments to coarse bioclasts, and sorting from medium to poor. Quartz grains are observed; generally comprising 5 – 10%, and are usually very fine to medium grained and sub to well-rounded.	Generally low API values for the gamma ray, typically less than 40 API, akin to Lithofacies (ii), with increasing values related to increased clay material associated with packstone and wackestones, whilst formation density log values are typically greater than 2.4g/cm^3	Observed porosities are poor, being primarily of mouldic nature as pore spaces are typically cemented with calcite cement.
(iv)	**Calcareous sandstone** (Carbonate material 40 – 80% and siliciclastic, component of 60 – 20%).	Comprises elements of both lithofacies (ii) & (iii). Bioclastic material is identical in type to Lithofacies (iii). Plagioclase feldspars are not observed, whilst quartz typically account for 25-30%.	Bioclastic material is generally finer grained in comparison to Lithofacies (iii). Quartz grains are akin to those in Lithofacies (ii).	Calibrated wireline log signatures are similar to those for Lithofacies (iii).	Porosities are generally poor, dominated by mouldic examples with limited examples of intragranular pore spaces typically infilled by calcite cement.

Table 4.1. Table of lithofacies identified from cored sections of the Upper Rudeis Formation within the hangingwall of the October Fault Zone. Lithological terms are based upon ratio of siliciclastic to carbonate components present, and in reality form a mixing continuum.

footwall scarp is characterised by a facies association belt, within which, condensed section associated with a sediment starved fault-block crest (A), is observed to pass down-dip into passive basin infill facies (B) and the locally footwall derived coarse clastics of the slope apron (C).

Facies Association A: Fault-block crest

Facies Association A is characterised by dominantly fine-grained deposits within a section which is demonstrably dramatically thinned and not consistent with alternate interpretations of eroded or faulted-out section (Table 4.2). This facies association is comprised of a single facies, *Condensed section (A1)*, which whilst not viewed directly in core, is identified in wireline logs as packages typically from 0 – 60 m thick, with log responses indicating a dominance of calcareous mudstones of Lithofacies (i). Commonly intercalations of thin, (< 5 m) high gamma-ray packages are observed, reflecting the most distal elements of the other two coarser clastic contemporaneous depositional systems. The condensed nature of Facies A1 is consistent with the identification of traceable marker horizons and an observed amalgamation of biostratigraphic zones identified by individual foraminiferal assemblages. Correlations of wells containing Facies A1 commonly display a thinning and inferred onlapping relationship onto structural highs and may be laterally equivalent to areas of interpreted erosion and non-deposition onto underlying units. These condensed sections are spatially significant; individual areas of condensed section inferred from well control to have maximum areas in excess of 5 km^2.

Interpretation of Facies Association A

The highly condensed nature and lateral extent in the absence of stratigraphy reflects a location that experienced markedly reduced sedimentation rates, with the dominance of mudstone suggesting primary deposition occurred through hemipelagic suspension fall out. This is typical of structurally high locations associated with the footwalls of major normal faults and in this study, wells that contain Facies Association A are all located on present day structural highs, with demonstrable, correlative thick successions preserved in adjacent hangingwall locations. An example in this study is the EGB-1 well located on the present day Amer Fault footwall crest, where 56 m of Upper Rudeis Formation is inferred between the Lower Rudeis and Kareem Formations, contrasting markedly with 430 m in the adjacent

hangingwall. Examples of condensed basinal sedimentation upon fault block locations are commonly recognised in other rift basins, where the structurally high footwall location is in an offshore location, (c.f. the Late Jurassic of the Northern North Sea, e.g. Ranvås & Steel, 1997; Ranvås et al., 2000).

Facies Association B: Passive basinal infill

Facies Association B comprises packages of laminated to massive mudstones (B1), calcareous marl (B2) and massive anhydrite (B3) (Table 4.2). Facies B1 is observed extensively both throughout the study area and throughout the studied interval, contrasting with Facies B2 and B3 which whilst similarly spatially widespread, are observed to be present only at the uppermost section of the Upper Rudeis Formation. Although Facies B2 and B3 therefore have a time specific connotation, the widespread nature of these facies suggests against a local limiting control. Facies B2 and B3 are also observed to occur in a greater range of different structural settings across the study area when compared to Facies B1.

Laminated to massive mudstones (B1) viewed in core occurs within packages up to 7 m thick, consists of fine-grained, dark, laminated to massive mudstone of Lithofacies (i) and contains variable amounts of very finely comminuted shell debris (Fig. 4.4b). Trace and body fossils are rare, with the bioturbation index (BI) (*sensu* Taylor & Goldring 1993) being between 0-1, with sparse occurrences of *Chondrites* isp. Centimetre-scale normal faulting highlighted by laminae offsets together with similar sized slump folds is commonly observed. Calibration to wireline logs show that Facies B1 forms units tens of metres in thickness with consistently high γ-ray values, typically > 50 API. Isolated intercalated low γ-ray peaks (typically <5m) are observed, which are interpreted to represent the most distal elements of the calcarenite-rich submarine fan and siliciclastic-rich submarine fan depositional systems.

Calcareous marl (B2) is not viewed in core, but is clearly identified from wireline log signatures and cutting descriptions. The calcareous fine-grained nature of Facies B2 is characterised by a distinctive 'bow' or 'barrel' wireline log motif and relatively high sonic log responses of 100-120 μsec/m and density log values greater than 2.4g/cm^3. Packages of this facies can be traced regionally throughout the study area and may occur in excess of 100 m with little or no variation and are typically succeeded by Facies B3.

Massive anhydrite (B3) like Facies B2 is not observed in core, but is readily identified by a characteristic 'box-shape' wireline log motif and accompanying cuttings information. The pure anhydrite nature of this facies is reflected by consistently very low γ-ray and sonic

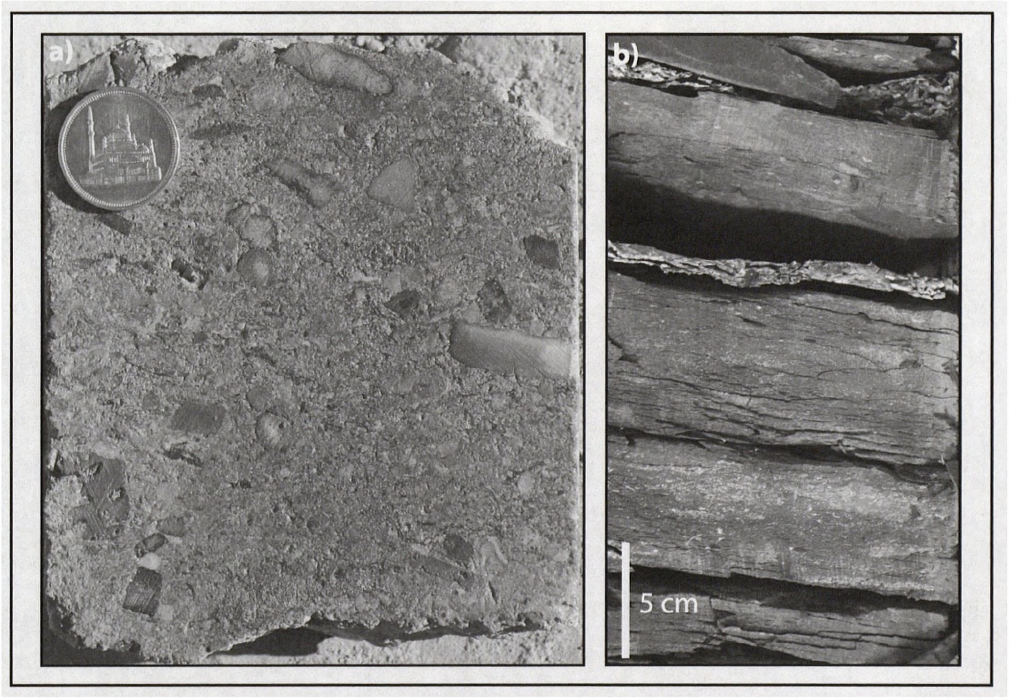

Figure 4.4. Cored section photographs highlighting examples of the offshore basinal depositional system identified within the hangingwall of the October Fault Zone. A) Coarse bioclastic breccia of slope apron Facies C1 located in the immediate hangingwall. B) Calcareous mudstone of Facies B1, rich in highly comminuted bioclastic material.

log responses (<10 API and 50 μsec/m respectively) and high density values (2.98 to 3 g/cm^3), with packages ranging in thickness from 5 -30 m

Interpretation of Facies Association B

The fine-grained nature of Facies B1 and the lack of wave or current generated structures suggest that this facies was deposited in low energy, relatively deep water conditions, i.e. below the storm wave base, via hemipelagic suspension fall-out. The low level of bioturbation suggests a stressed environment, with a limiting factor for colonisation (Taylor et al., 2003). Syndepositional deformation in the form of centimetre-scale faulting and slumping suggests deposition occurred within a basinal, unstable setting, potentially linked to fault slip triggered seismic events or alternatively instability associated with the hangingwall dip slope.

Considered in isolation, the calcareous marls of Facies B2 are not diagnostic of any specific environment, and the lack of a cored interval does not aid interpretation. When considered with the overlying pure anhydrite of Facies B3, both Facies B2 and B3 are inferred to represent a restriction of marine waters within the axis of the rift. The lack of intercalated clastics within both facies suggests limited sediment supply, with the wireline log signature of Facies B2 consistent with a carbonate rich, condensed pelagic unit representing sediment starvation within the rift, (c.f. the Late Miocene/Pliocene Akri Formation of the Taranki Basin, New Zealand, Hansen & Kamp, 2004).

Facies B3 is analogous to the lithostratigraphic unit which has been previously termed the 'Markha Anhydrite' (e.g. Beleity 1982), and represents the first onset of regional evaporitic conditions during late to post rift climax associated with the end of Upper Rudeis Formation deposition. A model of subaqueous deposition, rather than that of a sabkha, is preferred for Facies B3, as sabkha style tidal flats would be difficult to establish due to the large variations in fault controlled relief upon coastal margins within the rift (Orszag-Sperber et al., 1998), whilst furthermore, the pure anhydritic nature of Facies B3, i.e. the lack of intercalated clastic facies is not what would be expected within a sabkha deposit (Kendall & Harwood, 2002).

Facies Association B therefore reflects the passive infill of the offshore rift axis, with Facies B1 representing a dominant background hemipelagic process of deposition. Facies B2 and B3 document the increasing restriction of marine waters within the rift axis towards the

end of deposition of the Upper Rudeis Formation, culminating in a basin dominated by evaporite deposition.

Facies Association C: Slope apron

Facies Association C consists of a single facies (Table 4.2). Viewed in core in the OCT-J5 well in the immediate hangingwall of the October Fault Zone, *Bioclastic breccia (C1)* comprised decimetre thick beds of massive, poorly sorted bioclastic angular breccias, clasts including angular pebble grade quartz, glauconite and disarticulated bioclasts within a calcareous sandstone matrix (Fig. 4.4a). No bioturbation is observed. Occurrences of Facies C1 are rare, and are observed to have a sharp contact with underlying and overlying facies associations of the other depositional systems.

Interpretation of Facies Association C

The immediate hangingwall position and immature nature of Facies C1 is interpreted to reflect proximal deposition of a slope apron at the base of an active footwall scarp within the October Fault Zone, analogous to a subaerial talus cone (Richards et al., 1998). The bioclastic and glauconitic components may reflect reworking of uppermost Eocene to early syn-rift deposits exposed within the footwall scarp, or the erosion of contemporaneous relatively shallow biogenic carbonate production upon the footwall crest. Potentially linked to tectonic activity associated with activity along the October Fault Zone, or alternatively general mass wasting processes, gravity driven transport and subsequent deposition occurred; with a concentrated density flow (sensu Mulder & Alexander, 2001), providing a viable mechanism. Rapid deposition, suggested by both the lack of sorting and subsequent bioturbation may have been linked to the marked change in gradient at the base of the footwall scarp, thereby rapidly reducing the competency of the flow.

Whilst the spatial extent and thickness of these deposits is difficult to determine due to limited borehole constraint and sub-seismic nature, these deposits are likely to form discrete lobate cones which may coalesce from the broad linear source provided along the footwall scarp of the October Fault block and are also likely to be of limited extent perpendicular from the fault zone. Leppard & Gawthorpe (2006) documented slope apron deposits adjacent to the interpreted emergent rift border and associated Thal Fault, in the order of less than 150 m. It is therefore probable that slope aprons associated with the October Fault Zone are likely to have been of comparatively reduced extent, reflecting an offshore rift axis position, and thus

an overall low sediment supply from an adjacent submerged footwall block (e.g. Ranvås & Steel, 1997).

4.5.2 Calcarenite-rich submarine fan

Three facies associations dominated by carbonate Lithofacies (iii) and (iv) comprise this submarine fan depositional system. Sourced regionally from the rift margin and potentially with additional material locally from the October Fault Block, proximal to mid fan (D), distal fan (E) and pro-fan (F) elements of six stacked, lobate submarine fans are recognised to transversely extend into the rift axis; individual lobe thicknesses attaining a maximum of approximately 50 m within the immediate hangingwall of the October Fault Zone.

Facies Association D: Proximal to mid fan

Facies Association D consists of three facies types (Table 4.2). *Normal graded bioclastic grainstones, packstones and calcarenites (D1)* are characterised by sharp to erosive based massive, fining upwards packages over ~ 0.5 m, comprising calcareous Lithofacies (iii) and (iv) (Fig. 4.5 a and b). Bioturbation is generally rare with isolated occurrences of *Ophiomorpha Nodosa* isp and *Planolites* isp. (BI = 0-1). *Cross bedded bioclastic grainstones and calcarenites (D2)* display similar characteristics to Facies D1, albeit with unidirectional cross bedding of varying size (forests typically <10 cm), whilst *Laminated packstones (D3)* consists of millimetre-scale laminated packstone with increased mud content. Both Facies D2 and D3 are not observed to be bioturbated.

This facies association is generally organised into depositional fining upwards sequences within stacked packages which exhibit progradational, aggradational or retrogradational geometries. An idealised complete depositional sequence comprises a repeatable succession of sedimentary features: basal, erosive coarse-grained grainstones fining upwards to massive packstones and calcarenites (Facies D1), which may alternatively display pervasive decimetre-scale cross bedding (Facies D2) before passing into fine laminated packstones, reflective of increased mud content (Facies D3). Complete depositional sequences are generally rare with truncation either by the next overlying sequence or intercalations of the siliciclastic submarine fan depositional system.

At the wireline log scale, Facies Association D is typified by low γ-ray (<50 API) packages ~ 50-100 m thick, with accompanying formation density log values >2.4g/cm^3. The

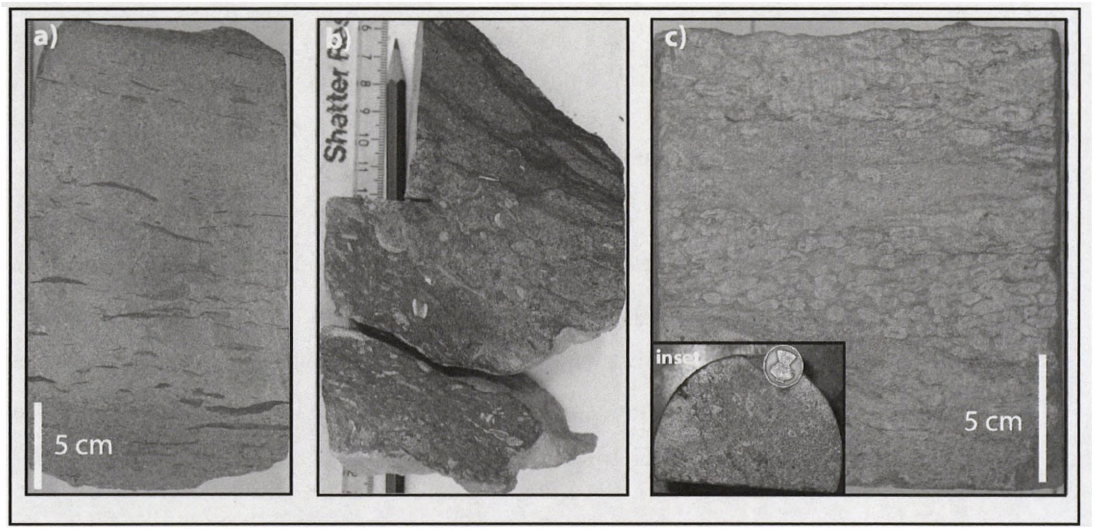

Figure 4.5. Cored section photographs highlighting examples of the calcarenitic-rich submarine fan. A) Normal graded, calcareous sandstone bioclastic Facies D1, with abundant mud rip-up clasts. B) Very coarse bioclastic grainstone to packstone example of Facies D1. C) Heavily bioturbated bioclastic packstone of Facies E1, displaying 'J' shaped tubular traces, confirmed in vertical section (inset) interpreted as the deposit feeder ichnotaxa Schaubcylindrichnus isp.

packages display basal contacts which are typically sharp, reflecting an abrupt decrease in API values from underlying packages of Facies B1. The tops of the packages are commonly observed as either gradual or sharp increases in API values, therefore displaying a range of symmetrical, boxcar and bell trends (e.g. Emery & Myers, 1996).

Interpretation of Facies Association D

Facies Association D is interpreted to reflect deposition by progressive aggradation of sediment from concentrated density flows (Mulder & Alexander, 2001) within a relatively deep water environment, forming a series of submarine fans lobes; consistent with the lack of sedimentary structures associated with shallower environments and the limited, low diversity nature of observed bioturbation. Facies D1 reflects an initially erosive, then depletive and increasingly waning flow and is akin to the T_a unit within Bouma (1962) or Lowe (1982) sequences. The unidirectional cross-bedding of Facies D2 represents deposition under a tractional flow, (Unit S_2, Lowe, 1982), whilst Facies D3 reflects subsequent deposition under upper flow regime condition (Unit T_c, Bouma, 1962). The low γ-ray signature, and formation density log values reflect the carbonate clastic dominated nature of Facies Association D, suggestive of a carbonate dominated provenance. The variation in the ratio of bioclastic components, thus defining a spectrum between Lithofacies (iii) and (iv) is suggestive of initial variations in entrained sediment compositions and /or subsequent compositional sorting during deposition.

Facies Association E: Distal fan

This facies association consists of two facies (Table 4.2). *Bioturbated packstones and calcarenites (E1)* are characterised by typically <4 m thick individual units of variable bioturbated (BI = 1-6) fine grained, mud rich packstones and calcarenitic sandstones which are generally massive, but contain some millimetre-scale laminations. The cored interval within Well GS216-1 contains multiple depositional units of Facies E1, with a maximum thickness of 10 m for stacked individual smaller depositional packages. Trace fossils identified include *Palaeophycus* isp. *Schaubcylindrichus* isp. (Fig. 4.5c), *Ohiomorpha Nodosa* isp. *Ohiomorpha Irregulaire* isp. *Phycosphion* isp. *Techicnus* isp. and *Thalassinoides* isp. Facies E1 is typically preceded by elements of Facies Association D, and is observed to show a gradation into Facies B1. *Reverse graded siltstone and wackestone (E2)* show an increase in grainsize from the calcareous mudstones of Facies B1, and are generally <0.5 m thick. Bioturbation is variable

(BI = 0-2) with *Ohiomorpha Nodosa* isp. and *Thalassinoides* isp. recognised. Facies E2 is observed to either gradate into Facies D1, or to be sharply truncated by a return to Facies B1. Correlation with wireline logs indicate Facies E1 is represented by subtly increased API values in the γ-ray log in comparison to Facies Association D, reflecting increased mud content, with accompanying changes in the formation density and neutron porosity logs. Facies E2, conversely displays a characteristic 'cleaning up trend' in the γ-ray response, i.e. a decrease in API values from underlying high γ-ray packages of Facies B1.

Interpretation of Facies Association E

With the gradation from underlying proximal to mid fan deposits of Facies Association D and into the overlying succession of background hemipelagic mudstones of Facies B1, Facies E1 is interpreted to represent waning deposition within the distal portion of the calcarenite-rich submarine fan system. The fine grained nature of Facies E1 is indicative of deposition from sediment gravity flows with low sediment concentrations, i.e. turbidity currents (*sensu* Mulder & Alexander, 2001). The pervasive and often high bioturbation suggests that the progressive aggradation of these deposits were by low frequency, short lived flow events, thus allowing for extensive subsequent colonisation by the numerous tracemakers identified, potentially reflecting prolonged periods of lobe abandonment. Conversely, Facies E2, with a reverse graded, coarsening upwards character from underlying mudstones of Facies B1, represents the progradation and onset of deposition of the distal elements of the calcarenite-rich submarine fan.

Facies Association F: Pro fan turbidite

Facies Association F is characterised by a single facies (Table 4.2). *Thin, sharp based calcarenites (F1).* Facies F1, whilst not observed in cored examples from proximal hangingwall locations of the October Fault Zone, is recognised at more distal locations within the rift axis at the wireline log scale as thin, typically <5 m isolated peaks of low γ-ray (<50 API) and accompanying peaks in the sonic (~ < 60 μsec/m) and formation density logs (>2.4g/cm^3) within overall larger packages of Facies B1, and which can be often be correlated to larger packages of Facies Associations D and E in more proximal locations.

Interpretation of Facies Association F

Facies F1, given the thin, sharp based nature of the observed calcarenitic deposits in addition to the distal nature, low thickness to large spatial extent ratio and observation of being within overall packages of Facies B1, is interpreted to reflect pro submarine fan deposition. Waning flow associated with surge-like turbidity currents, punctuated distal hemipelagic dominated deposition to deposit thin, extensive sheet-like beds of calcarenitic clastic material ahead of the various prograding fan lobes associated with the calcarenite-rich submarine fan depositional system.

4.5.3 Siliciclastic-rich submarine fan

This third depositional system is characterised by a dominance of subarkosic sandstones of Lithofacies (ii), intercalated with deposits of the offshore basinal and calcarenite-rich submarine depositional systems. Cored intervals located in the hangingwall of the October Fault Zone, allow for two facies associations to be recognised within an axially orientated, sheet-like fan, which reflect variation in distance from the provenance of the submarine fan from proximal to mid sheet (G) to distal to pro sheet turbidite (H).

Facies Association G: Proximal to mid fan

Viewed within core, siliciclastic dominated sandstones of Facies Association G comprise four main facies types, organised within packages of typically 1-10 m (Table 4.2). *Coarse to very fine normal graded sandstones (G1)* are characterised by a sharp or erosive base, are normal graded and generally structureless, typically up to a maximum of 1 m in thickness. Variable sorting is observed from poor to well sorted, with outsized clasts being common at the coarser-grained and erosive base. Subordinate calcareous clasts represented by bioclastic debris are identical to those in the calcarenite-rich submarine system. The amount of bioturbation is generally low (BI = 0–2), with a low diversity of ichnotaxa, with isolated occurrences of *Ophiomorpha Nodosa* isp. *Thalassinoides* isp. and *Palaeophycus* isp. representing typical trace types. *Cross bedded sandstones (G2)* are medium to coarse grained, display varying bed thicknesses (0.3-1 m) and unidirectional cross bedding with set sizes 5-10 cm. Facies G2 is commonly erosively based and grades into either Facies G1 or G3. No occurrences of bioturbation are observed. *Thinly bedded sandstones (G3)* are fine to very fine grained, with interbedded finer grained mudstones, with bed thicknesses typically 1-3 cm. Bioturbation is low with isolated occurrences of *Ophiomorpha Nodosa* isp. (BI = 0–2), whilst

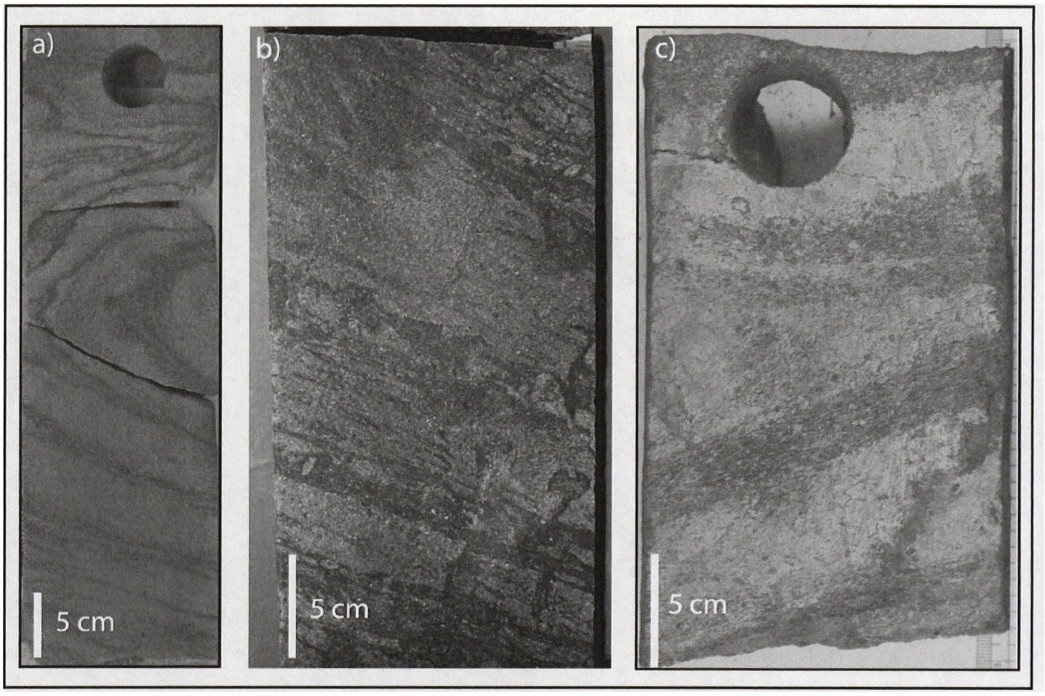

Figure 4.6. Cored section photographs highlighting examples of the siliciclastic submarine fan. A) Convoluted bedding picked out by variable hydrocarbon staining of Facies G4. B) Disrupted laminae of subfacies G3i, interpreted to reflect rapid dewatering upon deposition. C) Thin, coarse grained distal Facies H1 intercalated within calcarenite deposits of Facies Association E at the distal margin of the sheet depositional system

a subfacies *(G3i)* is recognised, which documents disruption of the thin beds by dewatering (Fig. 4.6b). *Convoluted bedded sandstones (G4)* are characterised by medium to coarse sandstone packages, up to 60 cm thick, with convoluted and folded bedding (Fig. 4.6a). Depositional packages, typically ~1 m thick are recognised showing a succession from either Facies G1 or G2, through to G3. More commonly, the erosional nature of subsequent deposits results with incomplete preserved depositional packages.

Calibrated to the wireline log scale, Facies Association G is characterised by metre scale packages (<10 m) with low γ-ray values (<10 API), corresponding formation density and neutron porosity displaying a neutron-density crossover, with low density values, (< 2.4 g/cm^3). In the hangingwall of the October Fault Zone, these packages are intercalated with deposits of the calcarenite-rich submarine fan, within larger (>50 m thick) low γ-ray packages, and it is probable that thinner elements of Facies Association G below the resolution of the formation density and neutron porosity logs are not identified.

Interpretation of Facies Association G

Facies Association G is interpreted to reflect deposition through the progressive aggradation of sediment from concentrated density flows (Mulder & Alexander, 2001) within a relatively deep water environment, forming an axial, sheet like deposit, thickening into active hangingwall depocentres. Therefore the processes are interpreted to be analogous to those active upon deposition of Facies Association D of the calcarenite-rich submarine fan depositional system. This is supported by the lack of sedimentary structures associated with shallower environments and the limited, low diversity nature of observed bioturbation. Facies G1 reflects an initial erosive, then depletive and increasingly waning flow and is akin to the T_a unit within Bouma (1962) or Lowe (1982) sequences. The unidirectional cross bedding of Facies G2 represents deposition under a tractional flow, (Unit S_2, Lowe, 1982), whilst Facies G3 subsequent deposition under upper flow regime (Unit T_c, Bouma, 1962). Dewatering structures associated within Subfacies G3i record fluid escape upon rapid deposition, whilst Facies G4 suggests synsedimentary deformation, potentially reflecting slope instability or fault related earthquake activity.

Facies Association H: distal to pro fan turbidite

Facies Association H consists singularly of *Thin, sharp and erosive based sandstones (H1)* comprising relatively thin 1-2 cm to thicker ~30 cm beds of medium to coarse sandstones

of Lithofacies (ii), generally intercalated with facies of calcarenite-rich submarine fan depositional system (Fig. 4.6c) (Table 4.2). The beds are observed to be typically sharp or erosive based and often with down-cutting geometries. Bioturbation is not observed (BI = 0). Given the thin nature of this facies association, it is below resolution at the wireline log scale.

Interpretation of Facies Association H

Facies Association H reflects deposition from an initially erosive then waning turbidity surge (sensu Mulder & Alexander, 2001), reflecting the distal component of an evolving flow from the concentrated density flows depositing Facies Association G. The thin bed size relatively small compared to flow size is consistent with short duration surges occurring from the distal part to ahead of the siliciclastic-rich submarine sheet-like fan.

4.6. DEPOSITIONAL MODEL FOR THE UPPER RUDEIS FORMATION

In this section, interpretations from borehole-derived sedimentological data adjacent to the October Fault Zone, are integrated with the physiography and potential provenance areas associated with this half-graben setting, to provide a synthesis for the three depositional systems active during deposition of the Upper Rudeis Formation, (Fig. 4.7).

Located within a submerged, sediment-starved rift axis setting, Upper Rudeis deposition adjacent to the October Fault Zone was dominated by an offshore, basinal depositional system. Thickness and facies variations within this basinal depositional system throughout the study area clearly reflect the structurally defined physiography associated with the asymmetric tilted fault-block setting for the October and adjacent fault blocks. Thinned and condensed sections are observed upon fault-block crests reflecting reduced sedimentation rates (Facies A1), and locally also areas of non–deposition and even net erosion (Fig. 4.7). Coeval strata are demonstrated to thicken down hangingwall dip slopes and into hangingwall depocentres through the identification of stratal units bounded by key foraminiferal assemblages. Expanded sections within hangingwall depocentres are dominated by calcareous mudstones (Facies B1), indicative of background hemipelagic sedimentation, whilst the presence of minor base of slope aprons are also inferred from bioclastic breccia, deposited by sediment gravity flows (Facies C1). This facies was sourced from immediately adjacent footwall scarps and crests, therefore consisting of a mixture of contemporaneous benthic faunas and earlier, reworked syn-rift and pre-rift material. These deposits may reflect fault scarp instability, and/or tectonic activity associated with ongoing fault propagation in addition

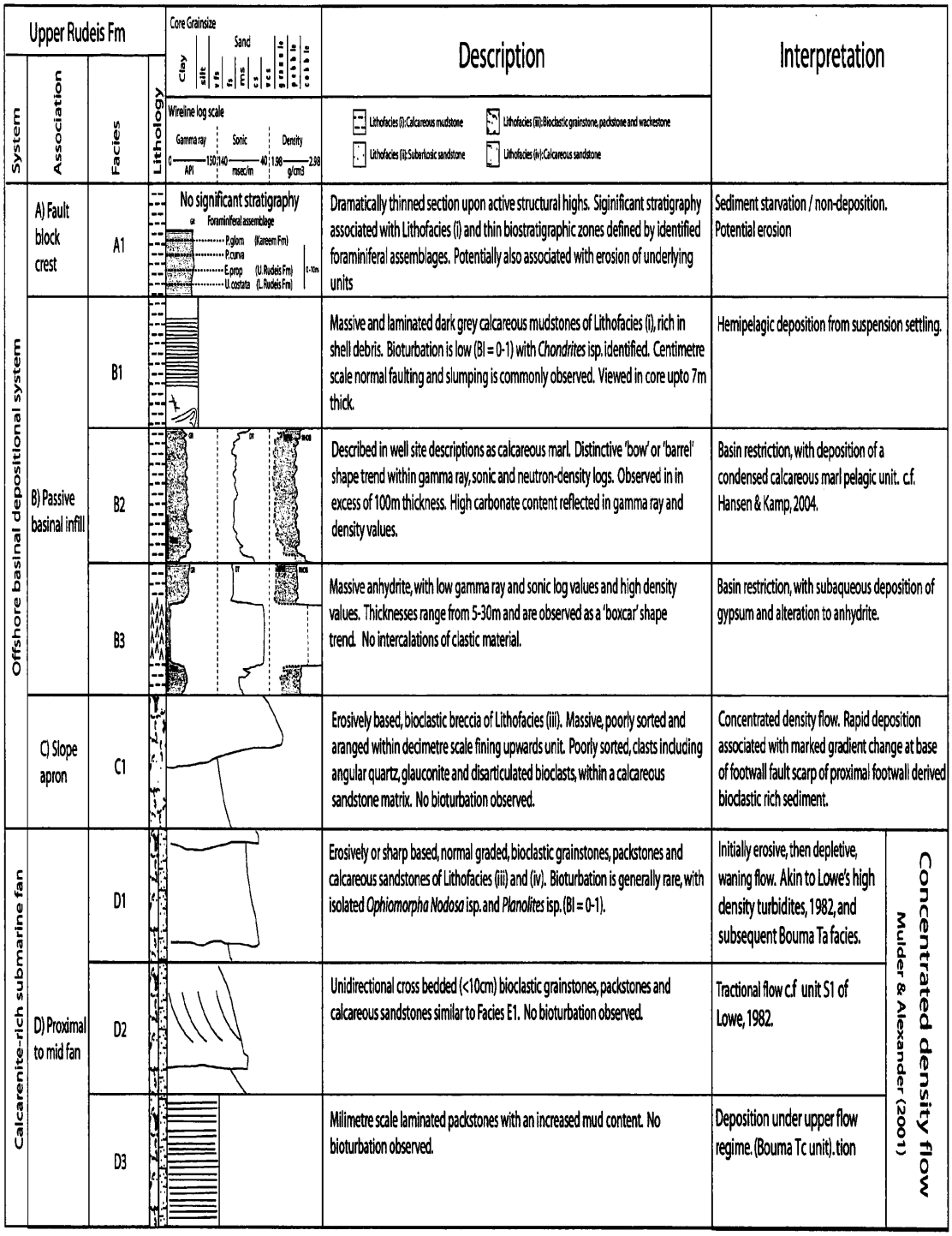

Table 4.2. Process-based facies associations and individual facies observed both from cored section and wireline log responses within the Upper Rudeis Formation. Graphic lithology reflects both lithofacies identified within cored section (Table 4.1) and inferred from wireline log response.

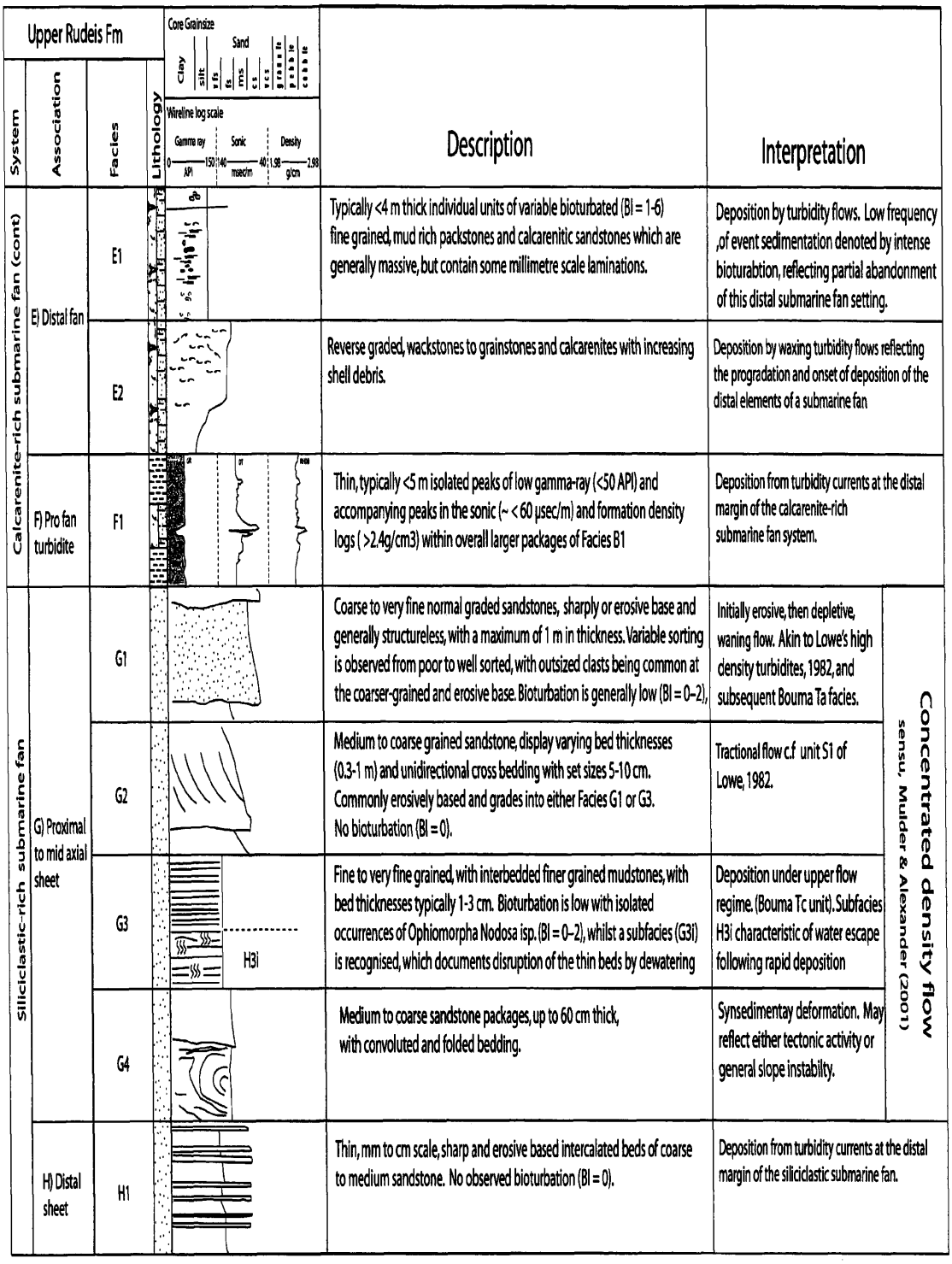

Table 4.2 continued.

to potential storm wave action for the highest fault crest locations. Prolonged periods of sediment starvation and restriction of marine waters in both hangingwall depocentres and footwall locations are recorded during the latter stages of deposition of the Upper Rudeis Formation. This reduction in sediment supply is characterised by a switch in the nature of the fine-grained background infill of the rift axis; from the calcareous mudstones of Facies B1 to calcareous pelagic marls (Facies B2) and massive anhydrite facies (Facies B3).

In addition to the offshore, fine-grained basinal sedimentation, two major coaser-clastic depositional systems with contrasting principal compositions were active within the rift axis, and formed as a result of sediment transport from the rift margins. The deposits of these depositional systems are observed to thicken into hangingwall depocentres, whilst thin up-dip upon hangingwall dip-slopes. The first of these coarser-grained depositional systems consists of a series of calcarenite-rich submarine fans which prograded into the rift axis. Dominated by carbonate material, sourced from contemporaneously produced bioclasts, eroded pre-rift Eocene limestones and reworked early syn-rift calcarenites (Lithofacies iii and iv), this submarine fan depositional system was deposited by a spectrum of concentrated density to turbidity flows reflected in proximal to mid fan deposits (Facies Association D), distal fan deposits (Facies Association E) and pro-fan turbidites (Facies Association F). Regional well correlations suggest that these calcarenite-rich submarine fans were principally sourced from the rift margin, and are thus related to regional sediment transfer pathways into the rift axis, in addition to potential local sources from rift axis footwall crests such as the October Fault Block. Locally within the hangingwall of the October Fault Zone, the calcarenite-rich depositional system is characterised by a series of transverse orientated, stacked, lobate submarine fans, with six individual fan lobes recognised (Fig. 4.3). The fan lobes thicken towards the October Fault Zone, whilst conversely thinning up the October hangingwall dip-slope towards the footwall crest of the Amer Fault Zone. Both overall progradation of the fan lobes (lobes 1 to 4) and retrogradation (lobes 5 and 6) are observed, with local sediment transport pathways interpreted to be focussed through structural relay ramps and around the tips of active fault segments. This role in focussing sediment transport pathways is consistent with similar structural settings documented in other rifts (c.f. the North Sea Rift, e.g. Underhill, 1995; Bruhn and Vagle, 2005).

The second coarse-clastic depositional system is characterised by siliciclastic submarine fan deposits. Dominated by a relatively immature subarkosic compositional signature (Lithofacies ii) suggestive of a basement or Nubia Formation source terrain, deposits

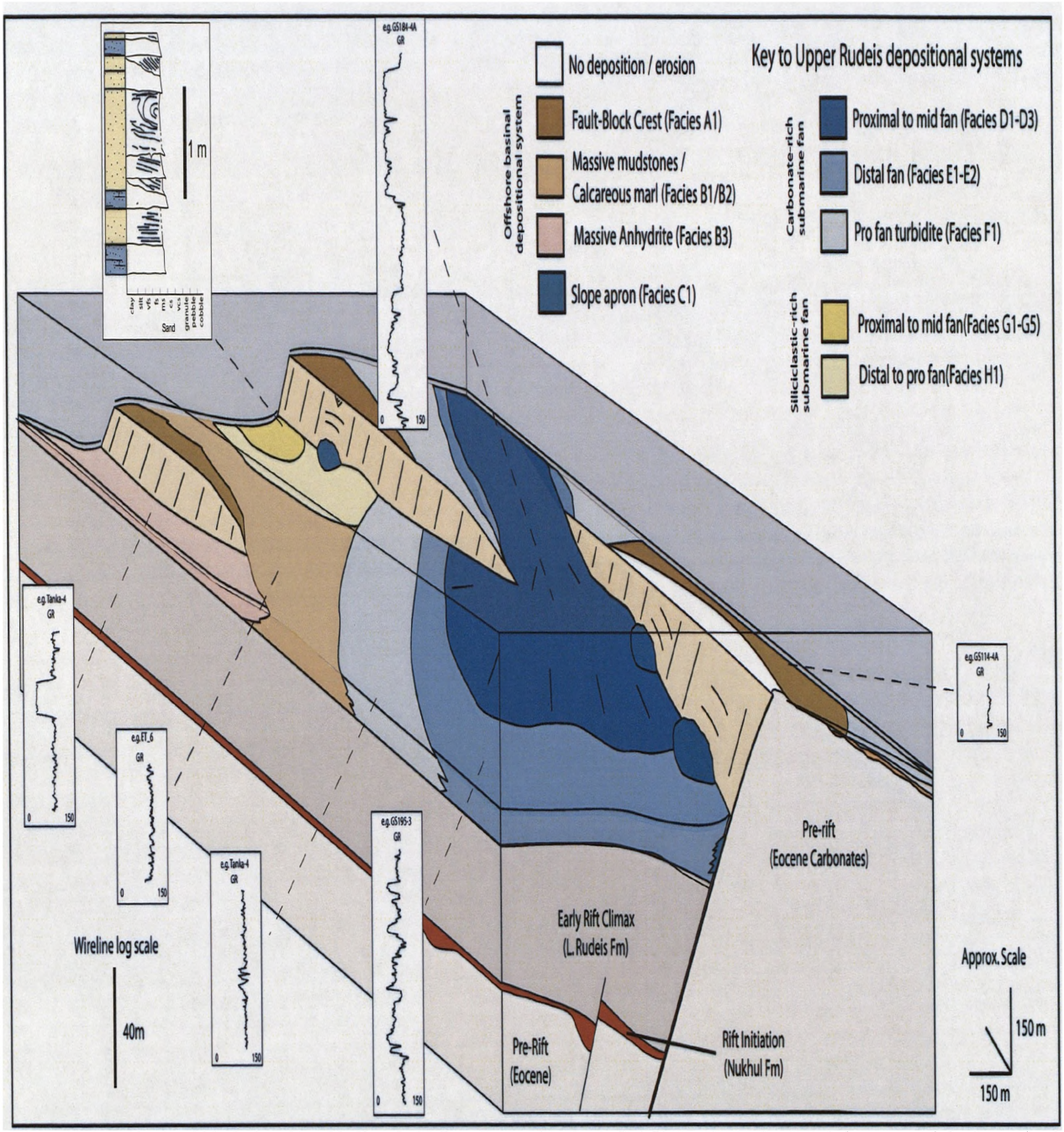

Figure 4.7. Depositional model for the depostition of the Upper Rudeis Formation around the October Fault Block, with examples of principal gamma-ray wireline log motifs and a core log. A segmented fault system, deposition was dominated by a background, fine-grained offshore depositional system. This was punctuated by a major carbonate-rich submarine fan principally entering the hangingwall via a major relay ramp between the North and October Faults. In contrast, a siliciclatic-rich submarine fan entered the hangingwall axially from the north. Local bathymetric variations due to the underlying nature of the tilted fault blocks provided a fundamental control on deposition and therefore thickness and stratal variability.

of this depositional system are intercalated with those of the calcarenite-rich depositional system. Within the hangingwall of the October Fault Zone, deposition of this siliciclastic-rich submarine fan depositional system was largely centred in the immediate hangingwall of the North October Fault, characterised by a sheet-like geometry, with thickening into active fault-controlled depocentres. Similar to the calcarenite facies, the deposits of this siliciclastic-rich system were the result of both concentrated density flows (Facies G1-G3) and turbidity flows (Facies H1), with slope instability or fault activity reflected by synsedimentary deformation (Facies G4). A gross isochore map for siliciclastic sandstone in the Upper Rudeis Formation suggests an entry point at Wadi Araba to the north of the study area, and subsequent axial transport to the south (Fig 4.8). This is consistent with the observation that the Nubia Formation forms the uppermost pre-rift unit at Wadi Araba, and is directly overlain by Upper Rudeis Formation deposits immediately offshore in the Warda Fault Block (Elbaz and Handley, 1994).

Determining an accurate estimate of water depths for both the footwall and hangingwall locations of the October Fault Zone during deposition of the Upper Rudeis Formation is difficult. In the hangingwall settings, sediment gravity flows associated with the three depositional systems may have potentially occurred in a wide range of bathymetric environments. The only unequivocal conclusion that can be derived from the observed suite of sedimentary structures (and absence of structures indicating significant wave action) present from hangingwall derived cored sections is that deposition occurred somewhere below the storm wave base. Proprietary GUPCO studies investigating both benthonic and planktonic foraminifera from the cored interval within the Oct-J5 well suggest that water depth was in excess of 130 m, a conclusion based upon the low diversity nature of the assemblages observed and the rarity or absence of typically dominant shallow water taxa. Macro fossil assemblages observed, whilst indicative of shallower depths, are consistently fragmented, thus consistent with reworking, transport and deposition into the deeper hangingwall depocentres of the October Fault Zone.

In comparison, fine-grained and condensed or even locally absent stratigraphy, upon footwall crestal locations along the October Fault Zone reflect limited deposition. This is consistent with again, typically relatively deep water conditions, i.e. below storm wave-base also upon footwall locations. Crestal footwall erosion may have been linked to areas being episodically above the storm wave base, therefore allowing for net erosional conditions. There is no evidence that footwall erosion was associated with emergence at any time, as there

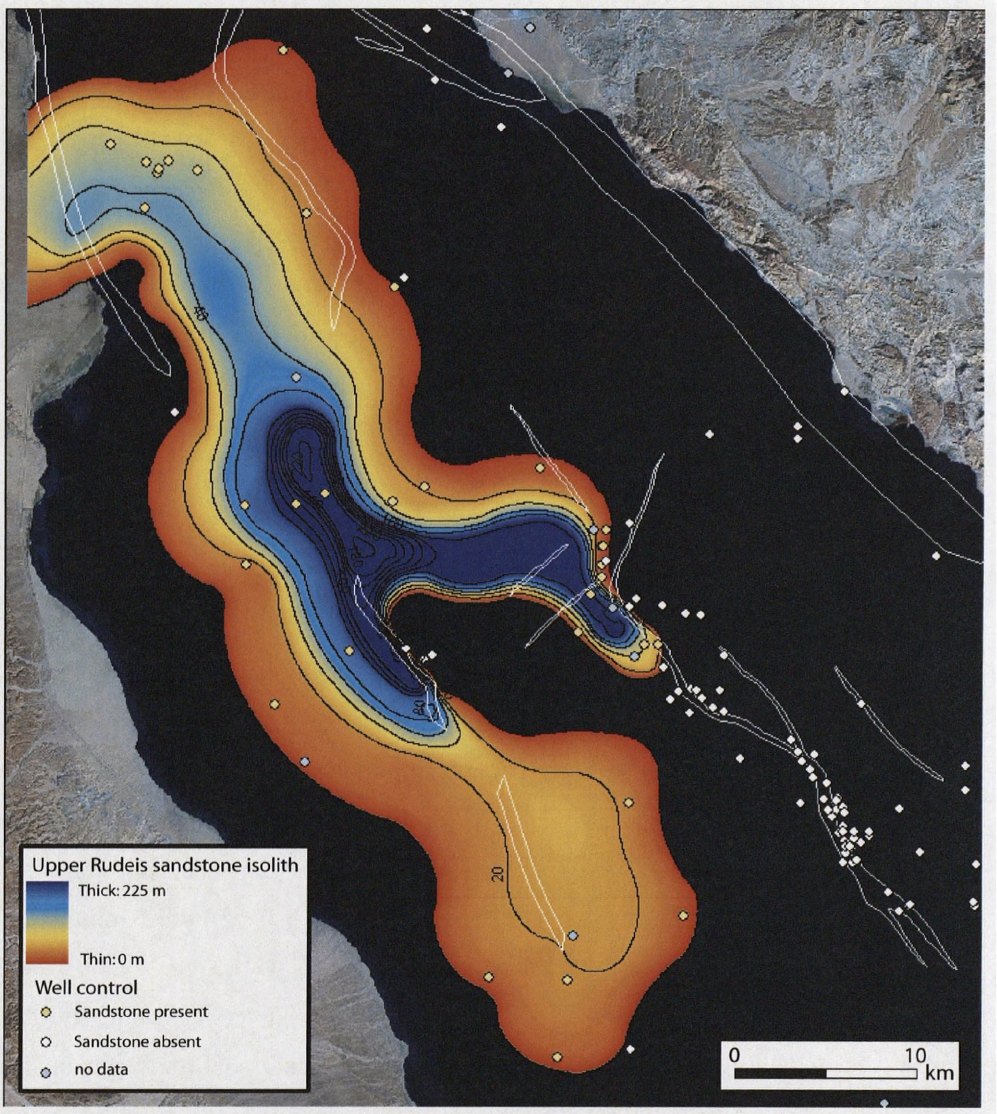

Figure 4.8. Landsat image of part of the northern Gulf of Suez with superimposed gross Upper Rudeis siliciclastic isolith. Fault polygon outlines shown are major faults interpreted at top of the Upper Rudeis Formation. A clear north to south axial trend in shown, with an interpreted sediment entry point associated with Wadi Araba on the western rift margin.

is a demonstrable lack of any associated shallow water facies that might be expected further down the associated hangingwall dip-slope. Limited biogenic carbonate production is interpreted to have occurred upon local footwall crestal locations, inferred from the coarse nature of disarticulated bioclasts within hangingwall locations.

4.7. STRATIGRAPHIC FRAMEWORK

This section outlines the stratigraphic framework utilised to subdivide the Upper Rudeis Formation, which is later used to analyse variations in thickness and facies in order to determine the tectono-stratigraphic evolution of the October Fault Zone.

Within the study area, the Upper Rudeis Formation is composed of five stratal units bounded by regionally extensive and key stratal surfaces in well Oct-J5 (Fig 4.2). These stratal units are often typified by consistent wireline log signatures, albeit with variations resulting from spatial changes in facies types, and are supported by a biostratigraphic framework based on the first downhole occurrences of key foraminiferal assemblages (Fig. 4.2). The key stratal surfaces are interpreted to reflect either basinward or landward shifts in facies. Surfaces interpreted to reflect basinward shifts in facies are erosive to sharp based in nature, regionally correlatable, delineate a marked downshift from more distal facies from below the surface to more proximal facies above and are typically associated with a major renewal of clastic input into the basin (e.g. surfaces RS-3 and RS-4 in Fig. 4.2). Given the regional extent of these major downshift surfaces, they are interpreted as sequence boundaries. In contrast, marine flooding surfaces associated with an abrupt landward shift in facies, are typically marked by a regionally extensive widespread onset of more basinal, fine-grained Facies B1, abruptly overlying the coaser-grained facies of either of the two submarine fan depositional systems (e.g. FS-3 and FS-4, Fig. 4.2). The widespread nature of these flooding surfaces is interpreted to reflect a major decrease in the rate of sediment supply associated with a switch overall transgression and are therefore interpreted as trangressive surfaces.

Stratal Unit 1 (SU1) within the study area is bounded at its base by the T20 hiatal event, marking the boundary with the underlying Lower Rudeis Formation. The T20 surface is picked at an interpreted maximum flooding surface often within a uniform mudstone package or at the top of a cleaning-upwards unit related to an increase in grainsize, and is consistently placed between the benthic foraminiferal assemblages of *Eggerella propinqua* and *Globigerinoides altiapertura* or interpreted older foraminferal assemblages (Fig. 4.2). A major downshift surface, (RS-2) is observed locally within Stratal Unit 1 adjacent to major

sediment entry points and associated with a subsequent influx of coarse clastics of the submarine fan depositional systems. This contrasts with sediment starved locations, which are typically dominated by offshore basinal mudstones with RS-2 therefore not observed. The top of Stratal Unit 1 is characterised by a regionally extensive downshift surface, (RS-3), generally linked to the first downhole occurrence of the *Eggerella propinqua* assemblage. Stratal Unit 1 is therefore interpreted to be comprised of both a highstand systems tract of an earlier sequence (Sequence 1) and a second complete sequence (Sequence 2) (*sensu* Vail et al., 1977).

Sequence boundaries, represented by downshift surfaces RS-3 and RS-4, form the basal surfaces of stratal units interpreted as being the lowstand systems tract components of Sequences 3 and 4 (Fig. 4.2). Calibrated in core, these sequence boundaries are characterised by a sharp to erosive contact between offshore basinal facies (Facies B1), and coarser overlying facies of the calcarenite or siliciclastic-rich submarine fans (typically Facies D1 or G1), dependant upon location. The succeeding lowstand deposits consist of variably intercalated deposits of the two submarine fan depositional systems and isolated occurrences of offshore basinal mudstones (Facies B1) and slope apron bioclastic breccia (Facies C1). Within corresponding core intervals, individual depositional packages are recognised which are dominantly retrogradational in nature, i.e. showing an overall fining-upwards character from proximal and mid fan facies (Facies Associations D or G), to distal fan facies (Facies Associations E and H).

Both lowstand stratal units within Sequences 3 and 4 are capped by major transgressive flooding surfaces, FS-3 and FS-4, and are characterised by regionally consistent marked increase in γ-ray values, which in core are represented by a sharp return to offshore basinal mudstones (Facies B1) or pelagic marls (Facies B2). These overlying fine-grained facies are interpreted as the onset of the transgressive and highstand systems tracts within rift axis (Fig. 4.2). The transgressive and highstand stratal unit of Sequence 3 (Stratal Unit 3) is generally observed as a relatively thin (10 – 40 m thick) package of offshore basinal mudstones (Facies B1) adjacent to the October Fault Zone and is sharply to erosively overlain by the lowstand deposits of Sequence 4. In contrast, the transgressive to highstand stratal unit of Sequence 4 is typically thicker (> 240 m) and dominated by calcareous pelagic marls of Facies B2. The top of Sequence 4 is typically denoted by the presence of massive anhydrite (Facies B3), lithostratigraphically termed the 'Markha Anhydrite', the base of which

corresponds to the T_{30} hiatal surface and thus the base of the Kareem Formation (e.g. Patton et al., 1994; Wescott et al., 1996; Krebs et al., 1997).

4.8. UPPER RUDEIS THICKNESS VARIATION AROUND THE OCTOBER FAULT ZONE AND ADJACENT FAULT BLOCKS

A number of key inferences can be made about the palaeostructure of the October Fault Zone during the deposition of the Upper Rudeis Formation. These will be described with respect to the present day observed geometric segments (Fig 4.9a), using well-derived isochores for the individual defined stratal units of the Upper Rudeis Formation (Fig.4.9b to e). In addition, the more regional distribution of thickness variations in adjacent fault blocks are considered in order to identify major sediment source entry points into, and transport pathways within the rift axis.

4.8.1 October Fault Zone

The gross thickness isochores for the Upper Rudeis Formation (Fig. 4.9b-e) clearly delineate the principle footwall and hangingwall locations associated with the two major, > 20 km long faults forming the present day October Fault Zone. At the level of the seismically mapped top Upper Rudeis Formation horizon, both the South and North October Faults are observed to be comprised of at least five, generally < 5 km long fault segments, based upon plan view geometry (Fig. 4.9a). The South October Fault is comprised of Segments 1 to 5, whilst the North October Fault consists of Segments 6 to 10. Orientated NWW-SEE, Segment 6 appears to act as a linking fault between the overall Clysmically orientated North and South October Faults.

The present day footwall crest of the South October Fault is defined by an area, approximately 17 km^2, inferred from borehole penetrations which do not encounter any stratigraphic section associated with the Upper Rudeis Formation, but rather Kareem Formation deposits lying unconformably upon pre-rift limestones of the Darat Formation. Approximately 3 to 4 km down dip of the footwall crest towards the northeast, east and southeast, a biostratigraphically confirmed Upper Rudeis condensed section (Facies A1) about 50 m thick is encountered. Over an additional 3.5 km down dip, the Upper Rudeis section thickens (up to 170 m thick) and is characterised by offshore basinal mudstones (Facies B1) and distal facies associations of the calcarenite-rich submarine fan depositional system (Facies Association E and F). This contrasts strikingly with the hangingwall of the South October

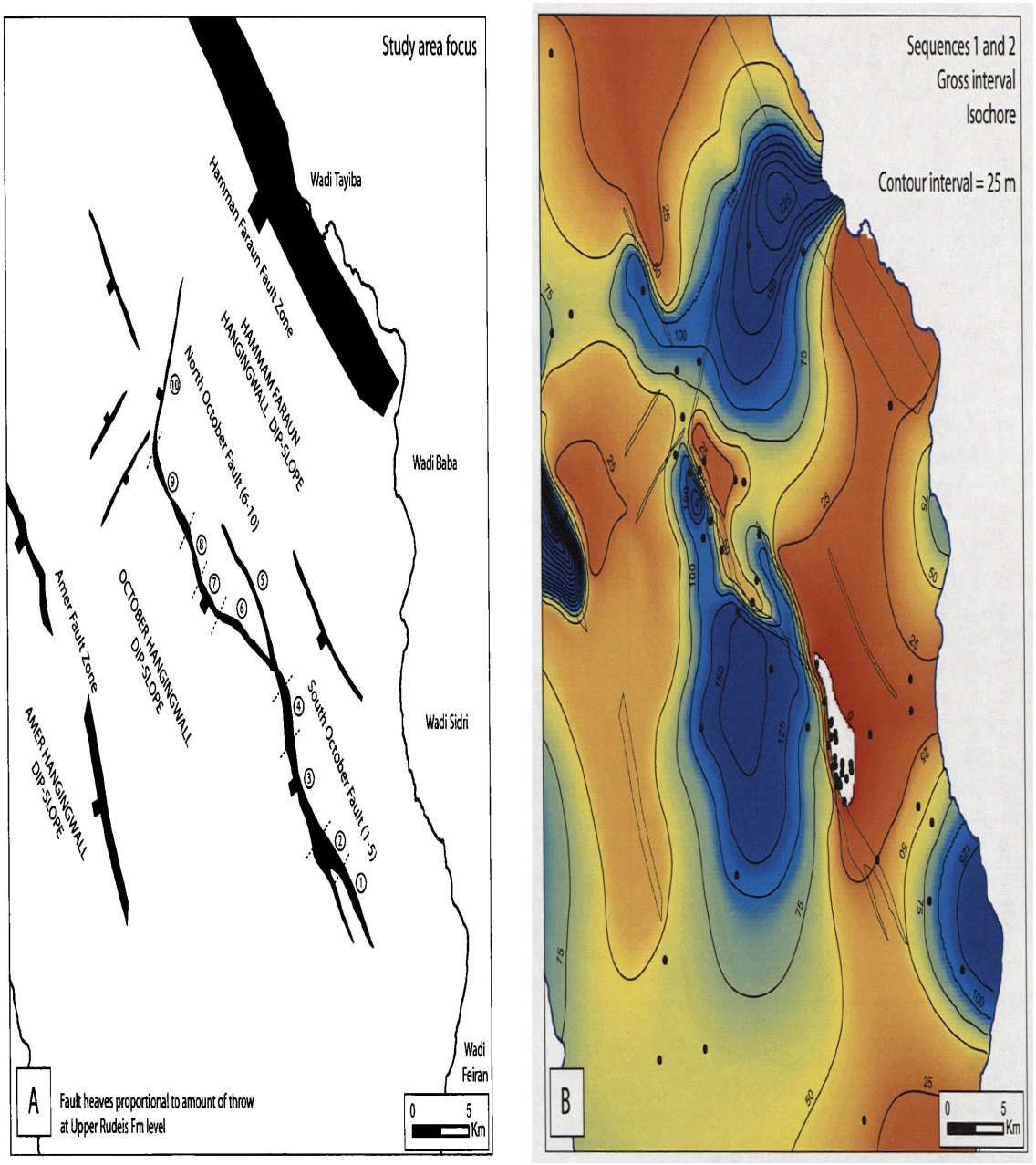

Figure 4.9. Well-derived, subjectively-contoured gross interval isochore maps for individual stratal units. Available well control for each complete section is posted and contour interval is set at 25 m. A) Sketch basemap of focus study area. Interpreted major fault heaves are at top Upper Rudeis Fm level. B) Composite isochore for Sequences 1 and 2. Principal isochore thicks are identified in the hangingwalls of the Amer and October Fault Zones, in addtion to a series of isochore thicks located basinward of three present day fan-deltas associated with Wadis Tayiba, Baba, Sidri and Feiran drainage systems (identified in A). Refer to text for detailed descriptions.

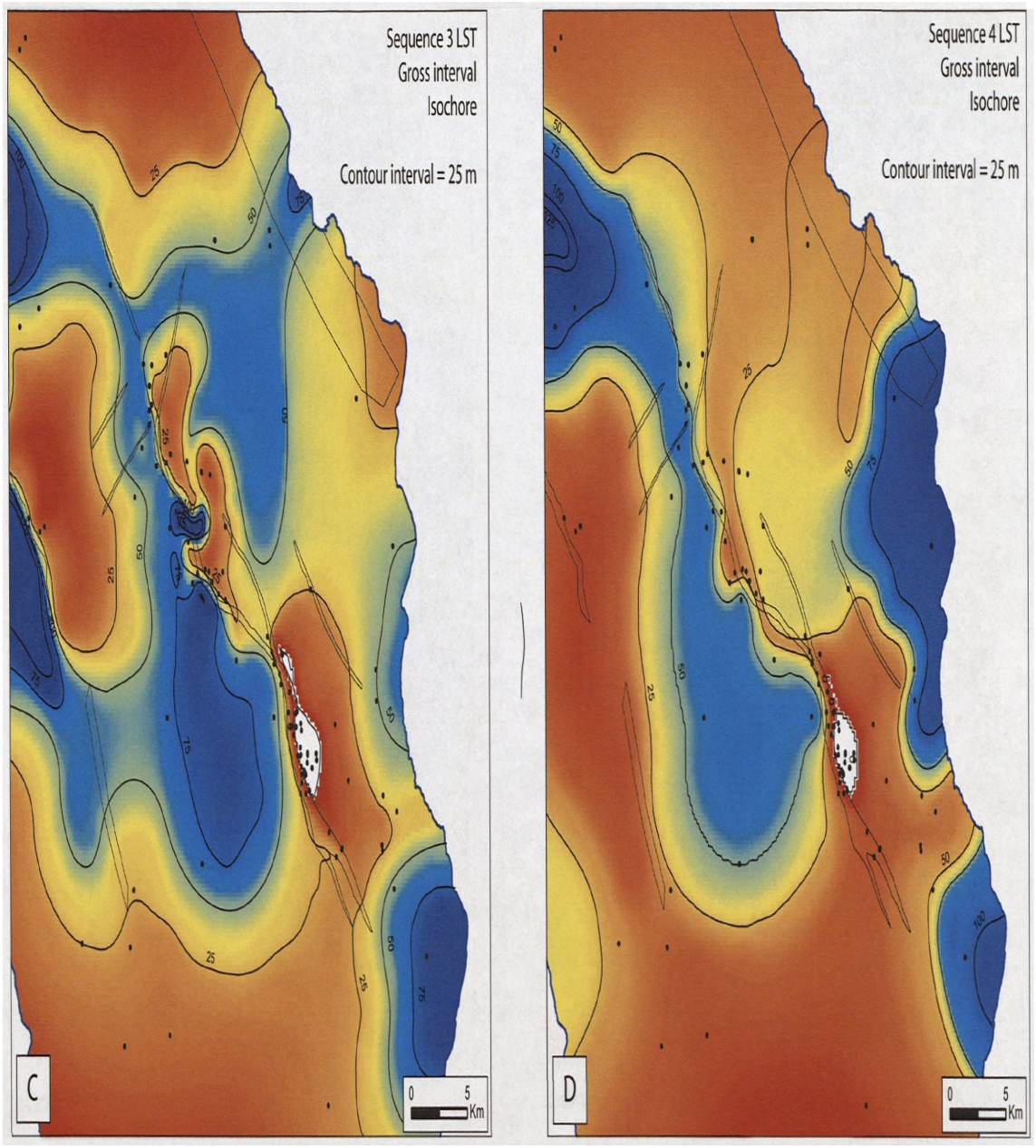

Figure 4.9. continued. C) Sequence 3 lowstand and D) Sequence 4 lowstand. Note overall reduction in thicknesses associated with both the hangingwalls of the Amer and October Fault Zones from the lowstands of Sequence 3 to Sequence 4. Refer to text for detailed descriptions.

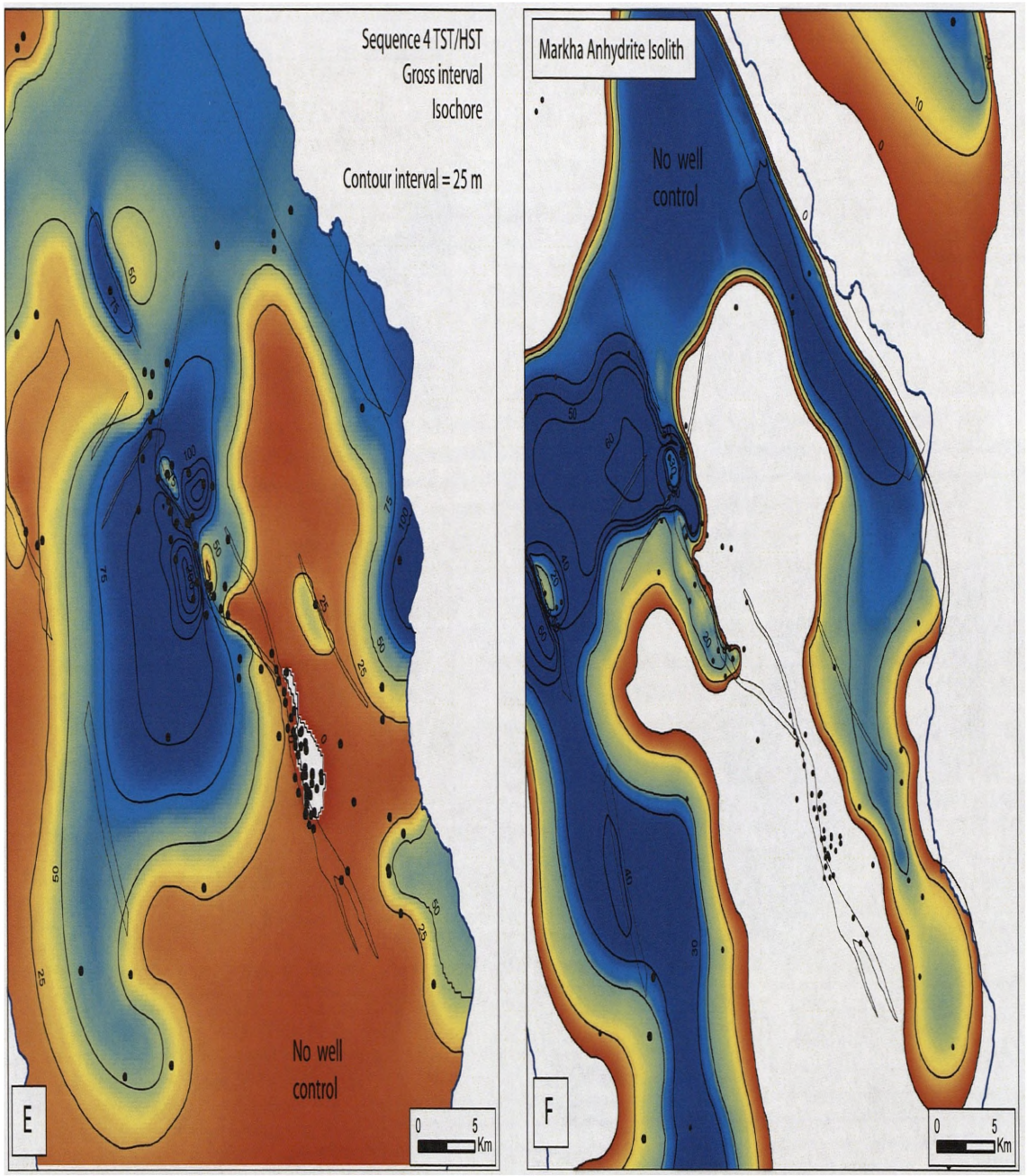

Figure 4.9. continued. E) Sequence 4 trangressive and highstand periods. Largest thicknesses are inferred to be associated with the northern part of Segment 8. F) Thickness isolith for the basal Kareem Formation Markha Anhydrite (Facies B3). An inner fairway associated with the South October Fault is observed to contain no massive anhydrite facies. Note change in contour interval to 10 m See text for discussion.

Fault, where overall gross thicknesses are observed in the order of 200-250 m (Fig. 4.10), comprising a series of six stacked lobes of the calcarenite-rich submarine fan depositional system (Facies Associations D, E and F), intercalated with offshore basinal mudstones (Facies B1) (e.g. Well GS193-5; Fig. 4.10). The lack of any small-scale (5-10 km) along-strike variability in gross thicknesses observed in the immediate footwall is inferred to be largely mirrored within the immediate hangingwall. Thus whilst in the footwall, observations show a consistent thinning and subsequent lack of Upper Rudeis section towards a single, large (17 km^2) crestal culmination, Upper Rudeis section within the hangingwall is inferred (due to limited well control) to gently thin from the observed thick of 250 m within the hangingwall of Segment 4 in well GS195-3 (Fig.4.10), to less than 100 m towards the southern tip of the Fault (Segments 1 & 2). With respect to thickness variations associated with each of the individual stratal unit thickness maps (Fig 4.9 b to e), Segments 1 to 5 comprising the South October Fault largely show little variation, i.e. a consistent distribution of Upper Rudeis Formation thickness (Fig. 4.9).

As with the South October Fault, the hangingwall and footwall areas associated with the North October Fault are broadly defined by the gross Upper Rudeis Formation isochores (Fig. 4.9). However in contrast, considerable thickness variability is observed in the individual stratal unit isochores for the smaller scale (< 5km long) segments which comprise the October Fault Zone (Fig. 4.9b to e). This variability is observed in the immediate footwall of the North October Fault which is characterised by a significant total gross Upper Rudeis section, ranging in thickness from approximately 45-100 m and with two main crestal areas defined by, along-strike isochore thins, approximately 4.5 km apart. The first isopach thin is centred in the footwall to the Clysmically orientated Segment 7, and is consistently observed as such in the isochore map for each stratal unit (Fig. 4.9b-e). Characterised by an approximate total gross 45 m of proximal to distal facies associations of the calcarenite-rich submarine fan depositional system (Facies Associations D and E), the Upper Rudeis section is observed to thicken down-dip to the northeast to approximately 200 m thick in the immediate hangingwall of the northern tip of the South October Fault; over a distance of some 2.7 km. In the immediate hangingwall of Segment 7, gross Upper Rudeis Formation thickness is approximately 400 m and is observed as a consistent principle sediment thick throughout Sequences 1 to 4, (e.g. well NO183-1, Figs. 4.9b to d, 4.10). The identified lowstand stratal units are characterised by the six stacked lobes of the calcarenite-rich submarine fan system (Facies Associations D and E) with intercalated basinal mudstones (Facies B1) (Fig. 4.10).

The second identified isochore thin located in the immediate footwall is also associated with a Clysmic orientated segment, Segment 9, where a maximum gross Upper Rudeis thickness of 73 m contrasts with some 340 m in the immediate hangingwall (Wells GS160-2 & Oct-J5, Figs. 4.10a, 4.11). The footwall is characterised by 19 m of condensed section (Facies A1) during Sequences 1 to 3 and the lowstand stratal unit of Sequence 4. The transgressive to highstand stratal unit for Sequence 4 marks the onset of significant deposition on the footwall to Segment 9, with a 54 m thick package of calcareous marl (Facies B2) present (Fig. 4.11). In the immediate hangingwall of Segment 9, Sequences 1 and 2 comprise 89 m of basinal mudstones of Facies B1, and are erosively overlain by the lowstand stratal unit of Sequence 3 (Well Oct–J5, Fig. 4.11). This lowstand package is approximately 98 m thick and is characterised by intercalated elements of the siliciclastic-rich and calcarenite-rich submarine depositional systems (Figs. 4.10, 4.11). The overlying transgressive to highstand stratal units of the sequence are represented by a thin, approximately 10 m package of offshore basinal mudstones (Facies B1). Overlying Sequence 4 is composed of 53 m of calcarenite-rich submarine fan lowstand deposits and an ensuing 100 m of calcareous marl (Facies B2).

In addition to the two Clysmic orientated segments (Segments 7 and 9), Upper Rudeis thickness is observed to vary adjacent to the remaining approximately N-S and NWW-SEE orientated segments of the North October Fault. Within the hangingwall of Segment 6, which forms the NWW-SEE orientated link between the North and South October Faults, the Upper Rudeis section attains a gross thickness of approximately 400 m (Fig. 4.10), and remained a consistent, major sediment thick during each of the stratal units (Fig. 4.9b to e). Correlation of well GS184-4A located here with well GS195-3 from the South October Fault hangingwall (Fig. 4.10) shows an increase in proximal calcarenite-rich submarine fan Facies Associations D and E within stacked fan lobes within the lowstand components of Sequences 1 to 4. Thin, intercalated distal elements of the siliciclastic-rich submarine fan depositional system (Facies H1) are also observed in cored interval of GS184-4A, but are generally below the resolution of the associated wireline logs.

A single borehole (well Oct-D7ST2, Fig. 4.9c) penetrates the immediate footwall to the northern part of the NNW-SSE orientated Segment 8, and indicates the southwards continuation of the isochore thick located in the hangingwall of Segment 9 during Sequence 3 (Fig. 4.9d). This approximately 130 m isochore thick upon the present day footwall is characterised by proximal facies associations of the calcarenite-rich submarine fan and the distal elements of the siliciclastic-rich submarine fan (Facies Associations D and H). In the

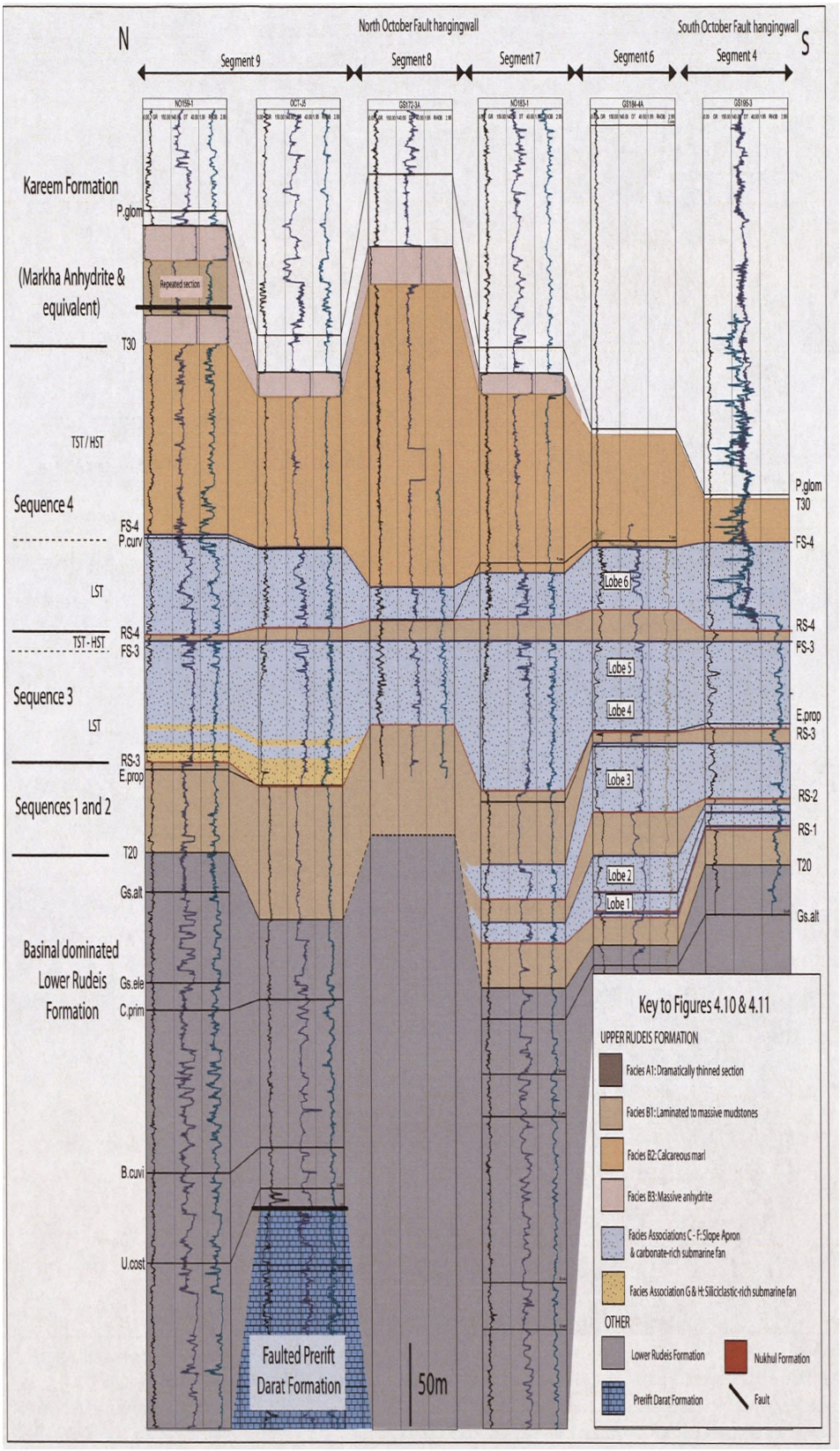

Figure 4.10. Strike orientated. wireline log correlation panel within the hangingwall of the OFZ, showing spatial thickness and facies variability within the Upper Rudeis Formation. Key observations include the north to south progradation of the siliciclastic rich submarine fan depositional system (Facies Associations H & I) and the centring of the calcarenite-rich subarine fan depositional system, identified in six separate fan lobes, towards the overlap of the two faults. In addition a marked reduction in thicknesses for Sequences 1 to 3 and the lowstand of Sequnce 5 is associated with the hangingwall of Segment 8 (well GS172-3A). Subsequently in the trangressive to highstand period of Sequence 4, this site became a major sediment thck within a uniform fine-grained succession throughout the October Fault Zone hangingwall. See Figure 4.2 for key to biostratigraphic names.

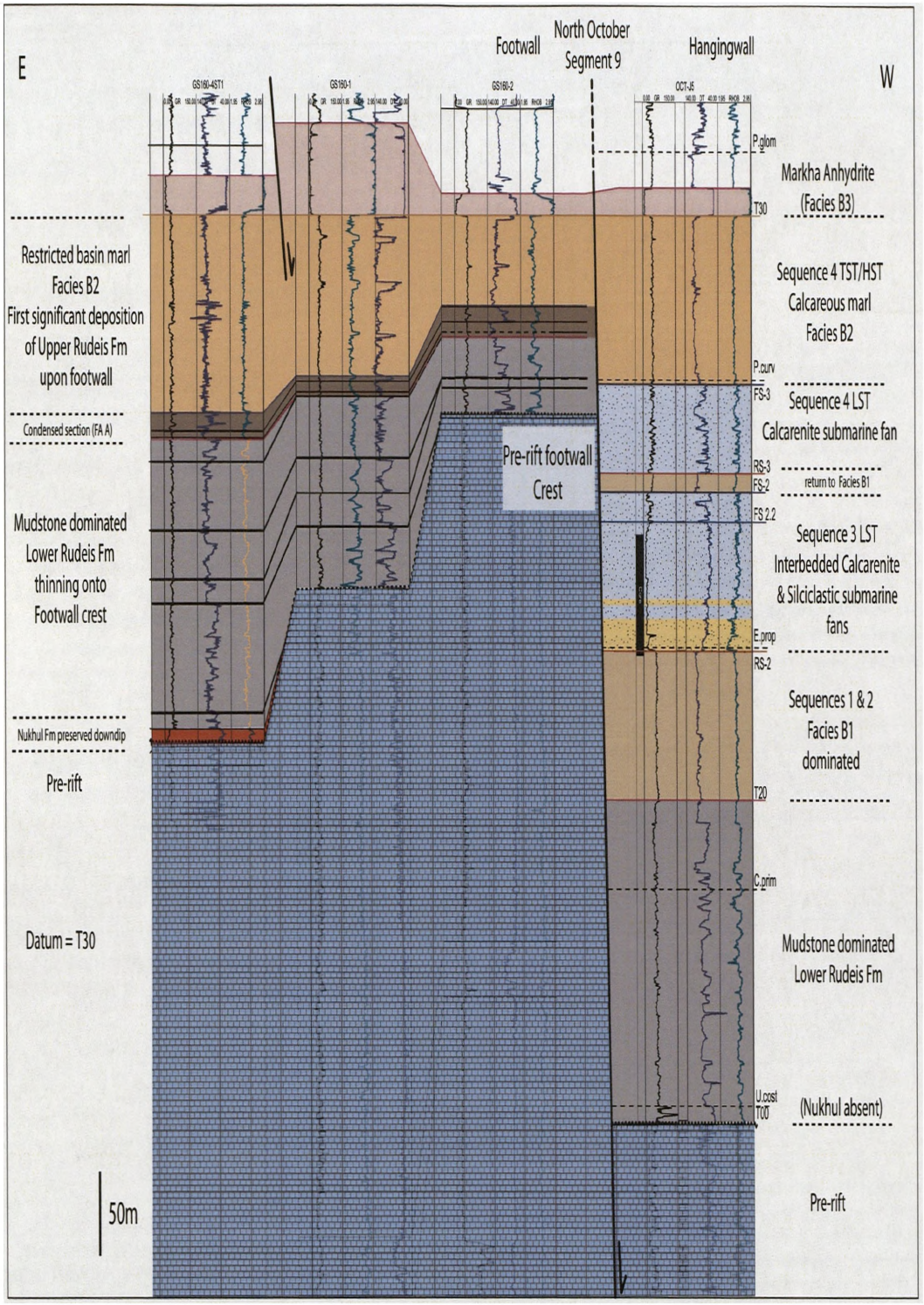

Figure 4.11. Dip orientated wireline log correlation panel across Segment 9 of the North October Fault. Previously marked thickness variations in the Lower Rudeis Formation between footwall and hangingwall is continued during deposition of the Upper Rudeis Formation. Sequences 1 to 3 and the lowstand of Sequence 4 are characterised by fine-grained mudstones of condensed Facies Association A upon the footwall, contrasting with a major depocentre in the hangingwall. Significant deposition first occurs on the footwall during the trangressive to highstand period of Sequence 4, but thickness variations across the fault zone indicate the segment was still potentially active, or at least provided a significnt bathymetric feature. During deposition of the Markha Anhydrite (Facies B3), Segment 9 is intepreted to be largely inactive, contrasting with a newley developed fault bewteen wells GS160-4st1 and GS160-1.

southernmost part of the hangingwall of Segment 8, Sequences 1 to 3 and the lowstand of Sequence 4 show a marked thinning to approximately 170 m (Figs, 4.9b to d, 4.10), containing thin, distal elements of the calcarenite-rich submarine fan system, i.e. Facies Associations E and F and a greater proportion of basinal mudstones (Facies B1). Subsequent deposits of the transgressive to highstand stratal units of Sequence 4 shows a marked increase in thickness compared to that exhibited in both Segment 7 and Segment 9 (Fig. 4.10).

The southernmost part of the NE-SW trending Segment 10 has thick Upper Rudeis section within the hangingwall, with a maximum of 320 m, and proximal to distal facies of the calcarenite-rich submarine fan (Facies Associations D and E) and the siliciclastic-rich siliciclastic submarine fan (Facies Associations G and H), akin to the hangingwall of Segment 9. Although no well penetrations exist within the immediate footwall of the segment, further to the north overall thickness distribution does not suggest any major, abrupt thickness variations associated with the segment during each of the defined Upper Rudeis stratal units.

4.8.2 Adjacent Fault Blocks

In addition to Upper Rudeis Formation thickness variations associated with the October Fault Zone, the isochore maps in Figure 4.9 also suggest major thickness changes in the hangingwall dip slopes to the adjacent Amer and Hammam Faraun Fault Zones. Within the immediate hangingwall of the northern part of the Amer Fault Zone, a gross Upper Rudeis thickness of over 450 m is observed, contrasting with a thickness of 56 m in the immediate footwall. This paired hangingwall-thick and footwall-thin is similarly observed during the deposition of the high resolution stratal units defining Sequences 1 to 3 (Fig 4.9 b to c). Sequence 4 displays a marked change, with thicknesses in both the hangingwall and footwall areas ranging from approximately 10-15 m during the earlier lowstand, and 25 m in the ensuing transgressive and highstand periods.

The limited well control within the hangingwall dip-slope of the Hammam Faraun Fault Zone is consistent with an overall general thickening down-dip towards the Hammam Faraun Fault Zone from the footwall crestal areas of the October Fault Zone. In addition, three principle concentric-like isochore thicks are also consistently observed towards the eastern margin of the present day gulf coastline in each of the thickness maps for the Upper Rudeis Formation stratal units (Fig. 4..9). Offshore of Wadi Tayiba (see Fig. 4.1 for location), a consistent lobate isochore thick is observed during Sequences 1 and 2, > 200 m thick (Fig. 4.9b) and the lowstands of Sequences 3 (~75 m thick) and 4 (~ 40 m thick). Further to the

southeast and offshore of Markha Plain containing Wadis Baba and Sidri, a second isochore thick attains a maximum thickness of ~ 80 m during the lowstand of Sequence 4 (Fig 4.9d). The third isochore thick is located offshore to the north of Wadi Feiran is consistently observed in each of the stratal units mapped (Fig 4.9) to be in the order of 75 – 100 m in thickness.

4.9. LINKED STRUCTURAL AND SEDIMENTARY EVOLUTION OF THE OCTOBER FAULT ZONE

In this section, the tectono-stratigraphic evolution of the October Fault Zone during the deposition of the Upper Rudeis Formation is reconstructed through a series of palaeogeographic maps. This is achieved by integrating observations and interpretations of thickness variations, with a process-based facies model and provenance data within a high resolution sequence stratigraphic framework.

4.9.1 Sequences 1 and 2

The base of the Upper Rudeis Formation, comprising of the highstand of Sequence 1 and Sequence 2, reflects the renewed influx of multiple sourced clastic systems into the hemipelagic dominated offshore rift axis (Fig. 4.12a), following the end of Lower Rudeis deposition, ca. 19.5 Ma. The concentrated density and turbidite flow deposits of the siliciclastic-rich siliciclastic dominated submarine fan, sourced from exposed Nubia Formation within Wadi Araba (Fig. 4.8), reached the hangingwall depocentre of the active Amer Fault Zone, a distance of approximately 37 km, whilst isochore and facies data suggest that four contemporaneous calcarenite-rich calcareous submarine fans prograded from both the western and eastern rift margins, fed via sediment entry points associated with a series of present days wadis, i.e. Wadi Tayiba, Wadi Baba, Wadi Sidri, Wadi Feiran and Wadi Uldahal (Fig. 4.1).

Thickness and facies variations within the hangingwall of the October Fault Zone are indicative of variations in displacement along-strike. The South October Fault was clearly active along much of its present day length and acted as a single linked fault. Differential subsidence and uplift associated with this structure formed a hangingwall bathymetric low which acted as a major depocentre for a large calcarenite-rich submarine fan system, juxtaposed to a major footwall bathymetric high characterised by condensed to non-deposition. The lack of any shallower water facies types around the South October Fault crest confirming that the immediate footwall was not emergent and was sediment starved. The rift margin

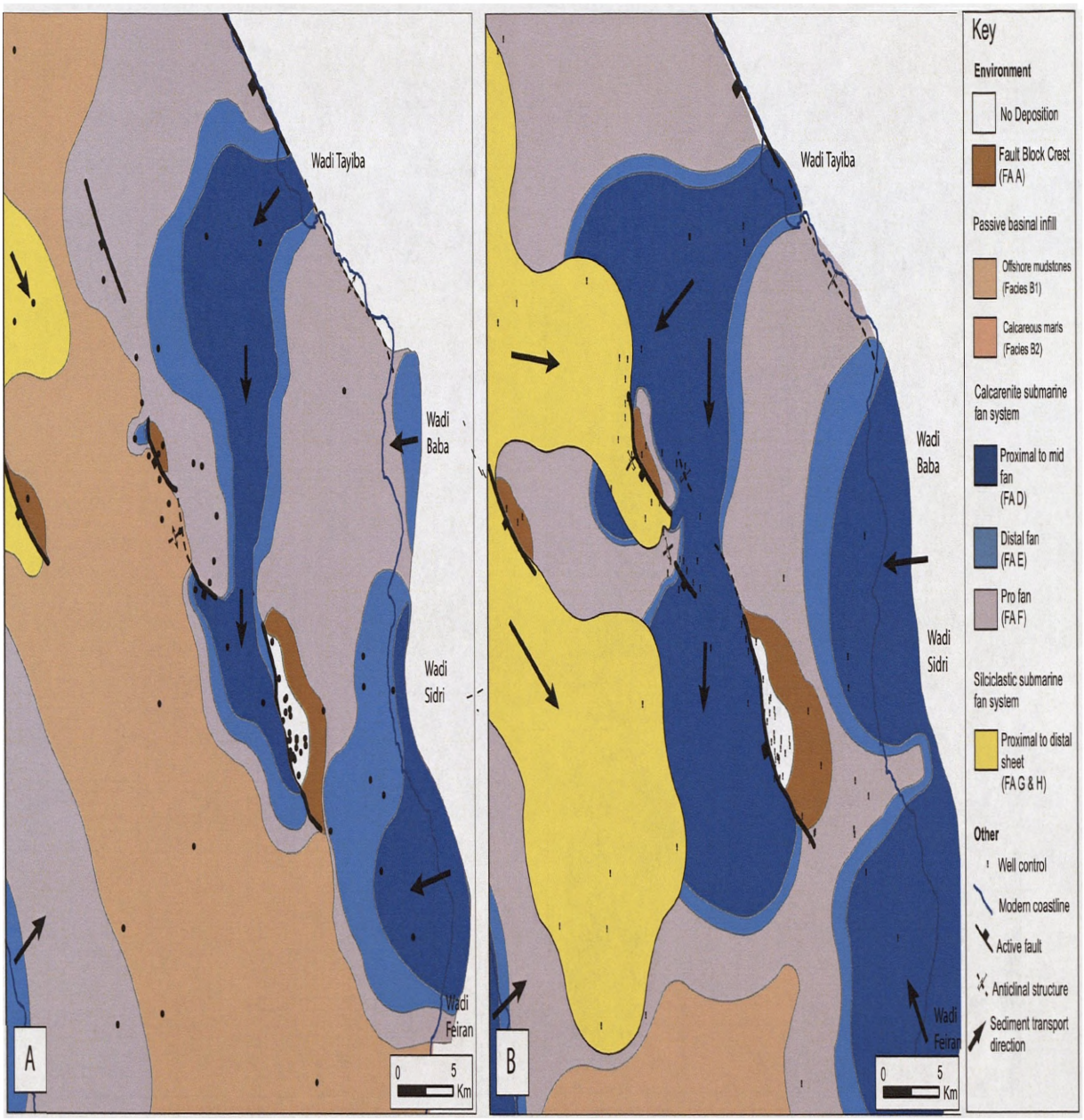

Figure 4.12. Palaeogeographic maps for the deposition of the Upper Rudeis Formation during periods of maximum regression. Well control is indicated. A) Sequence 2 lowstand. Two large calcarenitic dominated submarine fans prograded from the eastern margin of the rift axis from the Wadi Tayiba and Wadi Feiran entry points. The Wadi Tayiba system fed the series of calcarenite fans observed within the hangingwall of the October Fault Zone via a relay ramp between the South October Fault and Segment 6 of the North October Fault. The siciclastic submarine fan is at this time located towards the northwest. B) Sequence 3 lowstand. Marked progradation of all depositional system into the rift axis, , with the silciclastic submarine fan reaching its maximum extent into the depocentres of October Fault Zone. Activity upon the Hammam Faraun Fault Zone after Gawthorpe et al., (2003).

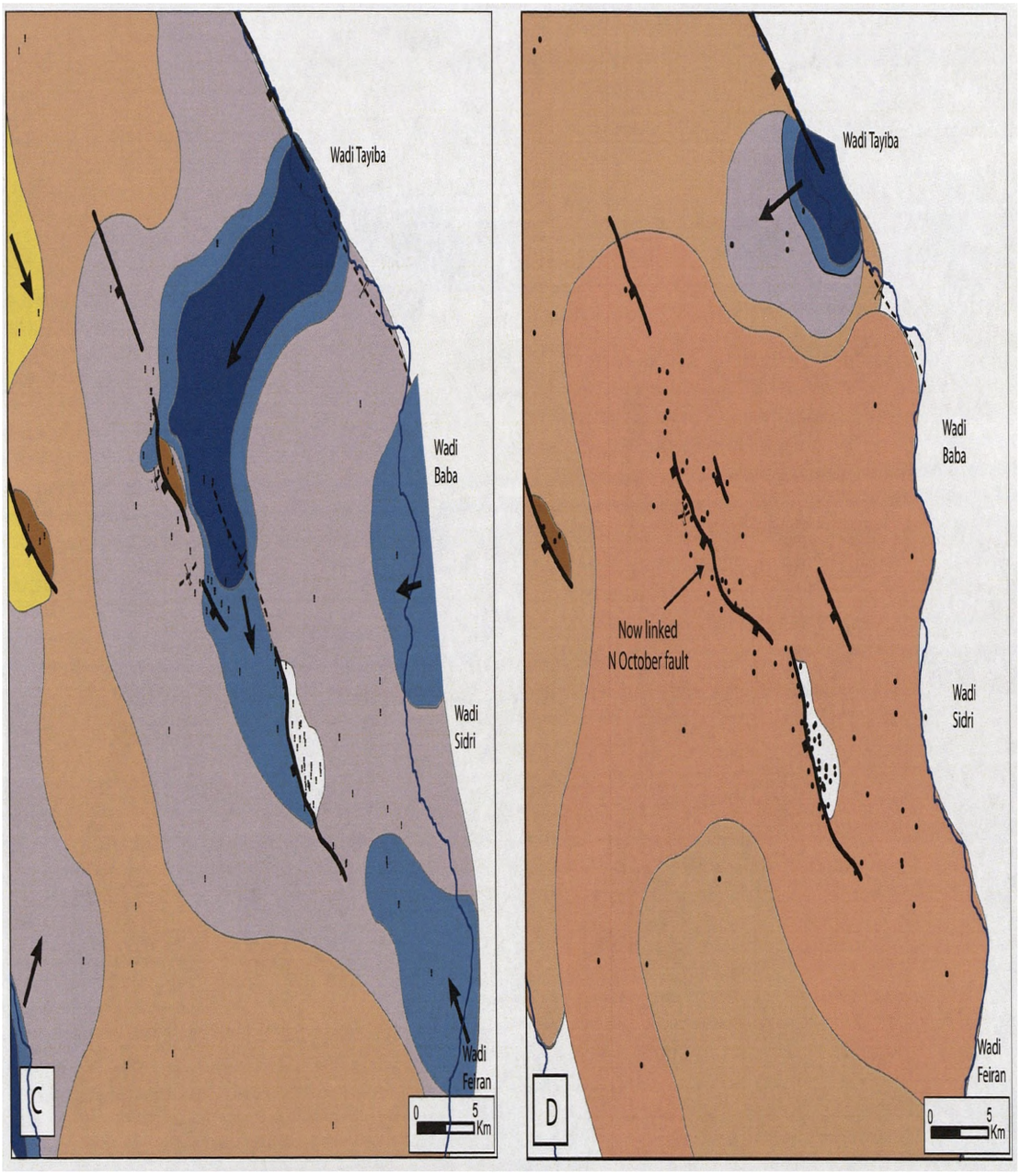

Figure 4.15. continued. C) Sequence 4 lowstand. Renewed progradation of active depositional systems, but not as pronouced as during the previous lowstand The siliciclastic submarine fan was centred in the hangingwall of the Amer Fault. With respect to the eastern margin derived calcarenitc submarine fans, the Wadi Tayiba and North Feiran fans providing the main supply of sediment into the axis. The relay ramp bewteen the South October Fault and Segment 6 of the North October Fault still provided a major sediment transport pathway into the hangingwall of the October Fault Zone. D) Sequence 4 trangression and highstand. A period of basin restriction, with a single, marginally confined calcarenitic submarine fan sourced from Wadi Tayiba entering the rift axis. The North October Fault became fully hard linked during this period. Furthermore a new, clysmically orientated fault within the October Fault Zone Footwall is interpreted to have become active (c.f. Figure 4.11).

derived calcarenite-rich submarine fan sourced from Wadis Baba and Sidri extended ~ 10 km to the west, and northwest, with its most distal part onlapping onto the hangingwall dip-slope down-dip of the South October Fault footwall crest (Fig. 4.12a). In contrast to the South October Fault, the North October Fault is interpreted to have consisted of a series of unlinked active surface breaking fault segments and associated fault propagation folds along-strike. The second calcarenite-rich submarine fan sourced from western rift margin via the Wadi Tayiba sediment entry point along the rift margin prograded at least 27 km to the south. The distal portion of this depositional system onlapped onto an eastwards tilted hangingwall dip-slope down dip of the Segment 9 of the North October Fault before passing into a thinned and condensed section upon the immediate footwall crest. Similarly, the Clysmically orientated Segment 7 is also interpreted to have been active, with thinned, distal pro-fan Facies F of the Wadi Tayiba calcarenite-rich submarine fan, characterising deposition upon the footwall crest. A major, approximately 1.5 km wide, relay ramp between the Segment 7 and the fully linked South October Fault formed a sediment transport pathway to allow for the deposition of three stacked calcarenite-rich fan lobes within the hangingwalls of Segment 7 and the South October Fault (Figs. 4.3; 4.10), which are estimated from available well control to have a maximum extent of 6 km to the northwest, 5 km to the southwest and 10 km to the southeast. These calcarenite-rich submarine fan lobes are inferred to be connected to the Wadi Tayiba sourced depositional system as volumetrically they cannot have been derived solely from the uplifted portions of the October Fault Block.

In contrast to the hangingwalls of the South October Fault and Segment 7, the hangingwall of Segment 9 was largely sediment starved, with deposition dominated by basinal mudstones of Facies B1 (Fig. 4.11), with a minor area of distal fan Facies E towards the northern tip of the fault segment, and likely to be sourced from the Wadi Tayiba calcarenite-rich fan system (Fig. 4.12a). Along strike towards the southeast, the hangingwall of Segment 8 is characterised by marked northwest-southeast stratigraphic thinning and switch to basinal mudstones of Facies B1 from the calcarenite-rich submarine fan lobes associated with the hangingwall of Segment 7 (Fig. 4.10). This suggests that this fault segment was an area of displacement deficient, potentially expressed as a hangingwall anticline with associated onlapping and limited deposition (e.g. Gawthorpe and Hurst, 1993; Gawthorpe et al., 1994; Anders and Schlische, 1994; Gawthorpe et al., 1997).

4.9.2 Sequence 3: Lowstand

This lowstand stratal unit documents a major regionally extensive basinward shift of the depositional systems into the rift axis compared to Sequences 1 and 2 (Fig. 4.12b). With respect to the siliciclastic-rich submarine fan, this depositional system exhibited a marked progradation into the hangingwall depocentres of the North October Fault segments 7 and 9, whilst it also prograded southwards in the hangingwall of the active Amer Fault Zone, and reached a maximum extent of 57 km from its source at Wadi Araba, with distal elements reaching into the hangingwall of Segment 6 of the North October Fault (Figs.4.8 & 4.9). The calcarenite-rich submarine fan sourced from the Wadi Tayiba entry point similarly prograded during this period towards the rift axis, thinning, and onlapping onto the hangingwall dip-slope, down dip of Segment 9. Sediment within this depositional system was also transported across the October Fault Zone and into the hangingwall of Segment 9, potentially from both around the northern and southern tips of the active fault segment.

Segment 7 continued to be active, with the calcarenite-rich submarine fan sourced from Wadi Tayiba supplying sediment onto both the Hammam Faraun Fault hangingwall dip-slope immediately down dip of the footwall crest of this segment (Fig. 4.12b). Likewise, the October Fault Zone remained a major bathymetric feature; condensation and non-deposition characterising the immediate footwall, whilst the hangingwall formed a major depocentre for the Wadi Tayiba calcarenite-rich submarine fan focussed via the previously identified major 1.5 km wide relay ramp associated with this fault and Segment 7. The calcarenite-rich submarine fan deposits located here in this major hangingwall depocentre formed two stacked fan lobes, thus extending a total of approximately 35 km from the Wadi Tayiba entry point into the rift axis. Additionally the Wadi Baba and Wadi Sidri derived calcarenite-rich submarine fans, also shifted basinward onto the hangingwall dip-slopes down dip of the South October Fault footwall crest (Fig. 4.12b).

4.9.3 Sequence 3: Transgression and highstand

This uppermost stratal unit of Sequence 3 is regionally consistent within the study area with a sharp return to basinal mudstone Facies B1 overlying the major transgressive flooding surface (FS-3) and typically ranging 2-50 m in thickness. This large range in observed thicknesses is interpreted to reflect both bathymetric response to structural location, the proximity to main submarine fan depositional fairways and the level of subsequent erosion associated with the overlying regressive surface RS-4. The regional nature of this return to

Facies B1 across independently sourced, regional depositional systems precludes a scenario invoking the role of an increase in localised tectonic activity and subsequent variations in sediment transport pathways, or an unroofing history associated with a change to a fine-grained bedrock lithology (c.f. Leppard & Gawthorpe, 2006) as potential causal mechanisms. Thus, the period of effective sediment supply switch off and resultant dominance of background hemipelagic deposition which characterises the trangressive to highstand period of Sequence 3 within the rift axis is interpreted to have been largely controlled by a major, basinwide rise in relative sea-level. Coaser-grained sediment was likely to have been increasingly trapped within depocentres within the rift margin, reflecting the increased amount of available accommodation space associated with the rift-wide rise in base-level.

4.9.4 Sequence 4: Lowstand

The period defined by this stratal unit marks a renewal of significant clastic sediment into the rift axis associated with regressive surface RS-4, but not being as extensive as the previous lowstand of Sequence 3 (c.f. Figs. 4.12b and c). The southernmost extent of the siliciclastic-rich submarine fan sourced from Wadi Araba (Fig. 4.8) was focussed within the hangingwall of the Amer Fault Zone, whilst not reaching the active segments of the North October Fault (Figs. 4.9; 4.12c).

Deposition within the hangingwall depocentres of the October Fault Zone was dominated by pro fan (Facies Association G) and distal submarine fan (Facies Association F), being sourced from the Wadi Tayiba entry point and primarily transported through the major relay ramp between the South October Fault and Segment 7 of the North October Fault. The proximal to mid submarine fan facies of Facies Association E were concentrated upon the hangingwall dip slope of Segments 9 and 7, with a minor sediment transfer pathway around the tip of Segment 9 into the immediate hangingwall.

The South October Fault Zone continued to experience non-deposition upon its footwall crest, whilst the calcarenite-rich submarine fan sourced from Wadi Sidri entry point had limited progradation and onlapped onto its hangingwall dip slope, dominated by Facies Association G. To the south of the October Fault Zone, away from the major relay ramp supplying calcarentic material into the rift axis, basinal hemipelagic deposition was dominant.

4.9.5 Sequence 4: Transgression and highstand

This uppermost stratal unit of Sequence 4 documents a period of sediment starvation within the rift axis, with both hangingwall depocentres and hangingwall dip-slopes typically dominated by calcareous marl Facies B2 and basinal mudstones Facies B1 (Fig. 4.12d). The siliciclastic submarine depositional system is not observed within the study area (Fig. 4.10), whilst the western margin Wadi Baba and Wadi Sidri and eastern margin Wadi Ulahdal sourced calcarenite-rich submarine fans appear to have also been switched-off. Only the Wadi Tayiba sourced calcarenite-rich submarine fan is observed to be have active, albeit with a markedly reduced extent, with a maximum of 10 km from the rift margin sediment entry point associated the Hammam Faraun Fault Zone.

The South October Fault was still a major bathymetric high associated with a lack of deposition, whereas a marked change is observed with thickness variations associated with the North October Fault. In contrast to Sequences 1 to 3 and the lowstand of Sequence 4, the hangingwall of Segment 8 was characterised by a major sediment thick (Fig. 4.10). This suggests that the previously identified area of displacement deficient now recorded the maximum displacement along a fully linked, North October Fault comprising of Fault Segments 7, 8 and 9. The presence of fine-grained Facies B2 within this interval (Fig. 4.13) throughout the hangingwall locations of the North October Fault further supports this interpretation of fault segment linkage and a shifting in the locus of subsidence as it precludes the role of shifting sediment input as a cause of the change in thickness distributions. The widespread presence and considerable thicknesses of Facies B2 in both the hangingwall and footwall locations of the North October Fault may be indicative that the bathymetric differential across this fault was also becoming increasingly reduced, i.e. accommodation space was being progressively infilled as a result of reduced subsidence rate. Alternatively, it may be that the deposition of Facies B2 was unaffected by bathymetry, and therefore cannot be used to discriminate palaeobathymetric variations.

4.9.6 Immediate Post Upper Rudeis Formation: the Markha Anhydrite

Following the deposition of Sequence 4 and the subsequent T_{30} hiatal event marking the end of Upper Rudeis deposition, the onset of restricted marine evaporitic conditions at the beginning of Kareem Formation is marked by the deposition of the Markha Anhydrite (Facies B3) (Fig 4.9f). Accurately correlating Facies B3 with other contemporaneous facies types with the current biostratigraphic resolution is difficult and beyond the scope of this study, but

some key inferences about palaeobathymetry can be made from examining the thickness and distribution of this evaporitic facies (Fig. 4.9f). With respect to the North October Fault, Facies B3 is centred within the immediate hangingwall ca. 20 m thick, but is also observed in the adjacent footwall, with limited thickness variation across the fault (Fig. 4.11). Like Facies B2 during Sequence 4, this may suggest a limited bathymetric differential across the fault, or that deposition was not affected by bathymetry. However in contrast, the South October Fault is associated with basinal mudstones within the hangingwall and condensed Kareem aged facies upon the footwall. This suggests that the South October Fault was still a major bathymetric feature, with unrestricted marine conditions within a deep hangingwall depocentre, and coeval limited deposition upon the uplifted fault-block crest.

Regionally, the distribution of the Markha Anhydrite (Fig. 4.9f) is centred upon NW-SE orientated depocentres associated with the Amer Fault and Hammam Faraun Fault Zone in addition to the North October Fault Zone. The lack of anhydrite within the centre of the rift axis and presence of fine-grained basinal mudstones Facies B1 is suggestive of an unrestricted marine axial fairway within the centre of the rift. This regional distribution is largely consistent with the relationship between restricted calcareous marl Facies B2 and Facies B1 during the trangressive to highstand uppermost stratal unit of Sequence 4.

4.10. IMPLICATIONS FOR UNDERSTANDING THE CONTROLS UPON LATE RIFT CLIMAX SEDIMENTATION

Models for rift climax sedimentation have previously highlighted the importance of a local structural control upon the spatial and temporal distribution of sedimentary depositional systems within rift basins (e.g. Ranvås et al., 2000; Gawthorpe and Leeder, 2000). Similarly in this study, integration of observations of structural, stratigraphic thickness and facies variations during deposition of the Upper Rudeis Formation suggests that the October Fault Zone provided a first order control upon the distribution of three differing depositional systems. The resultant bathymetric variations around the October Fault Zone determining the nature of available accommodation space, slope gradients and thus the locations of sediment source areas, transport pathways and depocentres. Additionally, more regional controls upon sedimentation are recognised in this study which can be linked to both regional structure and variations in basinwide relative sea-level. Therefore whilst providing new insights into rift climax structural and stratigraphic interactions directly applicable to the Suez Rift, this study also has implications for generic rift basin development.

4.10.1 Local variability associated with the October Fault Zone

The high-resolution sequence stratigraphic interpretation used in this study has allowed for the development of a model for the linked tectono-stratigraphic development of the Upper Rudeis Formation around the October Fault Zone. Dominated by offshore hempelagic fine-grained deposition, the variably uplifted, yet wholly submerged footwall crests of the fault zone provided sites of both local erosion and limited, condensed sedimentation. In contrast, hangingwall bathymetric lows along the fault zone were either locally sediment starved or provided depocentres for restricted slope apron deposits sourced locally via the adjacent footwall scarp or more regional sourced submarine fan depositional systems. Along-strike variations in displacement along the fault zone formed both relay ramps which acted as conduits for sediment fluxes across the fault zone and also transverse intra-basinal highs which acted as bathymetric barriers which were characterised by limited deposition. Similar palaeogeographic settings associated with tilted fault blocks have been documented in other rift settings such as the North Sea Rift (e.g. Underhill, 1994; Gabrielsen et al., 1995; Ranvås & Steel, 1997; Ranvås et al., 2000). In addition, to locally derived sediment, the nature of the structurally defined bathymetric template also controlled the location of the two major, compositionally distinct regional depositional systems which entered the rift axis from the rift margin via a series of point sourced sediment entry points discussed below. These calcarenite-rich submarine fan systems provided the main volumetric influxes of coarser-grained sediment into the hangingwall dip-slopes of the more marginal Hammam Faraun Fault and Amer Fault Zones and subsequently the hangingwall depocentres of the more axial positioned October Fault Zone. This is confirmed where hangingwall depocentres were 'in the shadow' of major sediment transport pathways associated with these depositional systems, such as hangingwall depocentres north of the major relay ramp between the North and South October Faults, which were more prone to being sediment starved and thus dominated by fine-grained basinal deposition.

Thickness and facies variations associated with the high resolution stratal units defined in this study along the October Fault Zone also document the temporal structural evolution of the fault zone. During the latter stages of the rift climax phase, some 7.5 Ma after the onset of rifting, the October Fault Zone was active as a surface-breaking fault zone comprising a series of 1.5-20 km fault segments with intervening relay ramps. Continued fault interaction during an approximate period of 0.8 Myr led to the linkage of individual segments along the October

Fault Zone, resulting in two large-scale fault segments (> 20 km in length). This progressive development of the fault array is consistent with models for the growth of normal fault zones by segment linkage (Walsh and Watterson, 1988; Cartwright et al., 1995; Dawers and Anders, 1995; Cowie et al., 1998; Ackerman et al., 2001; Mansfield and Cartwright, et al., 2001; Young et al., 2001). However the important implication for the structural evolution of normal faults suggested by this study is that the October Fault Zone was still highly segmented late in the development of the rift. Comparison with onshore studies upon the rift margin in the adjacent Hammam Faraun Fault Block shows that this is consistent with a model for the localisation of activity along major block-bounding fault zones similarly during the deposition of the Upper Rudeis Formation, with subsequent migration of the locus of faulting towards the rift centre (e.g. Sharp et al., 2000; Young et al., 2002; Gawthorpe et al., 2003).

4.10.2 Regional controls upon late rift climax deposition

In addition to the localised structural control of the October Fault Zone, this study suggests a significant role for a series of more regional controls upon late rift climax deposition. Firstly, a regional structural control is recognised in controlling the position of major sediment entry points for the two regional depositional systems entering the rift axis. Previous studies have suggested that the increasingly linked nature of through-going fault zones during the rift climax phase, displacement is concentrated onto a series of major crustal-scale faults in conjunction with the death of smaller scale intra-block faults, with the result that regional fault blocks became increasingly rotated (e.g. Sharp et al., 2000). Thus, regional scale fault blocks with half-graben geometries may become largely self-contained depocentres during the rift climax phase, typically hindering the transverse orientated movement of sediment from an uplifted rift shoulder to the basin axis and leading to the dominance of axial palaeoflows. Consequently, both rift-wide structural accommodation zones of reduced faulting, such as the Zafarana Accommodation Zone (Fig. 4.1), smaller scale sites of individual fault linkage, e.g. relay ramps and long-lived antecedent drainage networks form the dominant sediment input points into a rift. In this study, the palageographic maps presented in Figure 4.12 show the presence of a series of consistent, long-lived sediment entry points from the rift margin over the deposition of several sequences of the Upper Rudeis Formation and associated with present-day wadi drainage systems. For example, Wadi Tayiba on the western margin of the rift in the Hammam Faraun Fault Block, demonstrated to have been a consistent sediment entry point for a series of Upper Rudeis calcarenite-rich submarine

fan systems prograding into the rift axis, has also been shown to be linked to a Late Oligocene palaeo-valley within the Abu Zenima Formation (Jackson et al., 2006). Therefore Wadi Tayiba has acted as a major sediment transport pathway from the earliest stages of the rift event and continues to do so today, with the development of a fan-delta into the present day Gulf of Suez. The potential for the importance of axial palaeoflows within a rift for sediment dispersal is also highlighted in this study by the identification of the siliclastic-rich submarine fan depositional system. Sourced from the eastern rift margin, via the rift wide Zafarana Accommodation Zone, this depositional system became increasingly axially orientated and at its maximum extent into the hangingwall of the North October Fault, covered a distance of some 57 km from its rift axis sediment entry point.

A second regional control upon the late rift climax Upper Rudeis Formation is suggested by the recognition of regionally extensive, consistent surfaces of regression and flooding that can be correlated between structural locations. These surfaces interpreted as sequence boundaries and transgressive surfaces are associated with stratal units which define systems tracts associated with consistent periods of sediment-switch off (trangression & highstand) and increased sediment fluxes (lowstand) Thus, variations in regional relative sea-level independent of the scale of evolution of individual structures with the rift is recognised. The potential mechanism for this relative sea-level variability is therefore a combination of regional subsidence and uplift history of the rift and changes in glacio-eustasy. The role of changes in sea-level and particularly glacio-eustasy in controlling syn-rift sedimentation has typically been considered subordinate to the role of local structure within a rift during the climax phase. However in this study it has been shown to provide a first order control upon the timing and magnitude of sediment influxes into the rift, which when combined with the evolving structural template, produces the resultant stratigraphic and thickness variability of the Upper Rudeis Formation.

A third and final regional control is recognised in the compositional variability of the submarine fan and basinal depositional systems identified in this study. Directly a function of the nature of the lithology of the source terrain, resultant syn-rift lithofacies can have widely varying compositional signatures, and as in this study, can be utilised to discriminate between differing syn-rift depositional systems. Understanding the distribution of both pre-rift and syn-rift lithologies associated with potential sediment source terrains is therefore an important aspect to studying syn-rift depositional systems.

4.11. SUMMARY

This study has investigated the linked sedimentological, stratigraphic and structural evolution of the Miocene rift climax Upper Rudeis Formation associated with the October Fault Zone located in the axis of the Suez Rift. This chapter demonstrates how in an area of poor seismic resolution, abundant well control with corresponding core information can be utilised to constrain present day structural configuration, provide a higher resolution stratigraphic subdivision of larger syn-rift tectonostratigraphic sequences and develop a process based facies model. Integrating these products can be used to outline the linked tectonostratigraphic evolution of a major fault zone and associated depositional systems. Based upon observations made during this study, four main summary points can be drawn:

1). The Upper Rudeis Formation associated with the October Fault Zone was deposited within three contemporaneous depositional systems, with facies and thickness variations reflecting the inherent asymmetry associated within half-graben marine rift basins, and subsequent variations in available accommodation space. Examination of cored intervals and accompanying wireline log data have enabled a offshore basinal system, dominated by passive infill to be recognised, with intercalations of both axial and calcarenite-rich submarine fan depositional systems being preferentially deposited in active hangingwall depocentres of the October Fault Zone.

2). Four principal lithofacies have been identified consisting of calcareous mudstones, subarkosic sandstones, bioclastic grainstones to packstones and calcareous sandstones which indicate multiple provenances for deposits of the Upper Rudeis Formation. Wadi Araba, on the western margin of the rift within the Zafarana Accommodation Zone formed an entry point for a major ~ 57 km long, dominantly axially orientated siliciclastic dominated submarine fan depositional system, which reached the hangingwall of the North October Fault. This contrasted with calcarenite-rich calcareous submarine fans sourced from the eastern rift margin, entraining contemporaneous biogenic material and reworking both earlier syn-rift deposits and the carbonate dominated units of uppermost pre-rift succession. These fans prograded and onlapped onto the hangingwall dip slopes of the Hammam Faraun Fault Zone, whilst also entering into the hangingwall of the October Fault Zone, principally via a major 1.5 km wide relay ramp between the North and South October Faults. A third, local intra-basinal October Fault Zone footwall crestal source for contemporaneous or reworked biogenic

material is inferred from coarse bioclastic units immediate within the hangingwall and is interpreted as limited extent (<150 m), base of slope aprons.

3. Regionally consistent surfaces of regression and flooding consistent within a biostratigraphic framework define five stratigraphic units, within which facies and thickness variations have been mapped to discern the linked tectonostratigraphic evolution of the October Fault Zone and associated depositional systems during a ca. 0.8 Ma period. During this period, the October Fault Zone evolved, from a single major (>10 km long) fault and further along-strike, isolated and smaller scale (< 2 km long) fault segments, to two, increasingly interacting major faults (~ 20 km long).

4. Whilst the evolving local structural configuration of the October Fault Zone provided a first order control for the distribution of facies types and stratigraphic thickness variations, a series of more regional natured controls upon deposition are recognised. The regional half-graben structure nature of the rift inhibited sediment fluxes directly entering into the rift axis from the rift margin, highlighting the importance of both structural and long lived antecedent drainage sediment entry points between the two major structural domains. Furthermore, variations in basinwide relative-sea level are recognised to be a major control on the extent and timing of the progradation of late rift climax clastic depositional systems into the rift axis. The importance of regional variations in provenance lithology is highlighted in controlling subsequent variations in the resultant nature of syn-rift lithofacies.

CHAPTER FIVE

MULTISCALE VARIABILITY OF LATE RIFT CLIMAX DEPOSITIONAL SYSTEMS ASSOCIATED WITH A MAJOR STRUCTURAL ACCOMMODATION ZONE, MIOCENE SUEZ RIFT, EGYPT

CHAPTER 5: MULTISCALE VARIABILITY OF LATE RIFT CLIMAX DEPOSITIONAL SYSTEMS ASSOCIATED WITH A MAJOR STRUCTURAL ACCOMMODATION ZONE, MIOCENE SUEZ RIFT, EGYPT

5.1. ABSTRACT

Rift-wide structural accommodation zones have been typically associated with syn-rift sediment transport pathways which link otherwise structurally isolated depocentres within a rift. However, few studies have documented in detail the controls upon the sedimentological and stratigraphic variability of syn-rift depositional systems within an area of more distributed fault-controlled subsidence and uplift. This study uses a high-resolution sequence stratigraphic framework to investigate the variability of the late rift-climax deposits of the Upper Rudeis and Kareem Formations within the Morgan Accommodation Zone, located in the Suez Rift, Egypt. This chapter documents the existence of a series of major, regional scale syn-rift depositional systems, which entered the axis of the rift from more marginal areas via a number of structurally controlled sediment entry points within the accommodation zone. A regional, basinwide-scale control is additionally recognised, determined the magnitude and timing of a series of sediment fluxes into the rift linked to variations in relative sea-level. These sediment fluxes were manifested as a series of submarine fan to fan-delta depositional systems, the dispersal patterns of which, and resultant distribution of facies, thicknesses and stratigraphic architectures, resulted from a complex interplay between the availability of fault-generated accommodation space and sediment supply. The results of this study suggest that during higher rates of sediment supply, fault-generated accommodation may be quickly infilled, so that syn-rift depositional systems orientated transversely to a major fault zone may be able to prograde across fault zones and blanket the uplifted footwall. In contrast, axially transported depositional systems are more likely to be continually constrained within hangingwall depocentres.

5.2. INTRODUCTION

Within extensional rift basins, the evolution of normal fault systems is a fundamental control on syn-rift facies distribution, stratigraphic thickness and stratal geometry. The development of normal fault populations through the processes of segment growth and linkage are characterised by marked spatial and temporal variations in slip (e.g. Peacock and Sanderson, 1991; Cartwright et al., 1995; Dawers and Anders, 1995; Cowie, 1998;

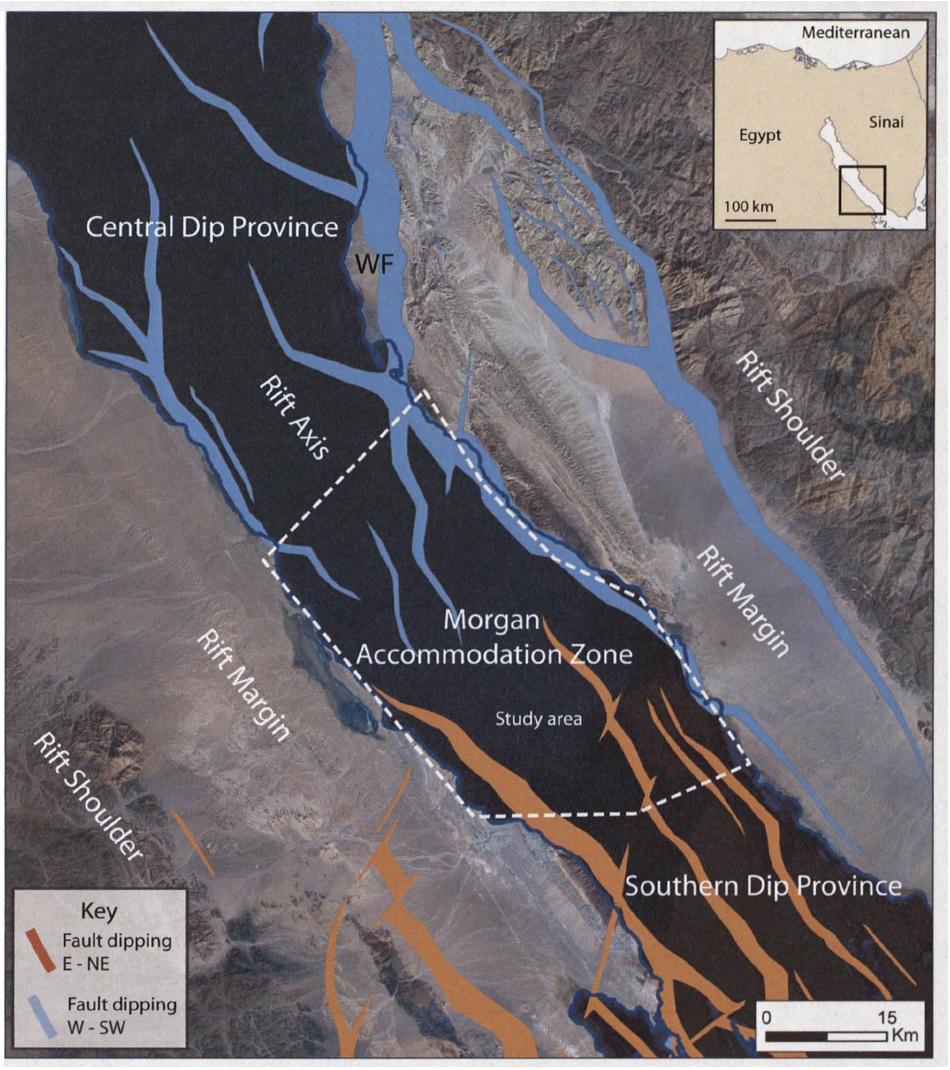

Figure 5.1. Landsat image with main structural elements for the central and southern dip provinces in addition to the intervening Morgan Accommodation Zone superimposed (modified after Younes and McClay, 2002). The location of this study is within the dashed polygon. Corner inset displays regional context of the rift location. WF = Wadi Feiran.

Cowie et al., 2000). As a result in the spatial and temporal variation in displacement, uplift and subsidence of footwalls and hangingwalls respectively create a complex three-dimensional relief. The interaction of this structurally defined rift physiography with additional local (e.g. bedrock lithology) and more regional controls (e.g. climate; sea/lake level) on sedimentation, combine to determine the location of primary sediment source terrains, transport pathways and depocentres for syn-rift depositional systems (e.g. Gawthorpe and Leeder, 2000).

During the main phase of rifting, often termed the rift climax phase (e.g. Prosser, 1993), the concentration of displacement onto major, through-going normal fault zones, results in the structural configuration of a rift being characterised by a series of 10-30 km wide, tilted fault-blocks, typically contained within larger structural domains which exhibit consistent overall dip directions (e.g. Patton et al., 1994, Sharp et al., 2000). Conceptual tectono-stratigraphic models for syn-rift sedimentation during this climax phase of the rift evolution typically differentiate between: (1) local depositional systems directly sourced from uplifted footwall scarps with steep gradients or gentler gradient hangingwall dip slopes, with sediment transported transversely into adjacent hangingwall depocentres and (2) those sourced more distally and characterised by the regional transport of sediment that is often axial and through several sub-basins (e.g. Leeder and Gawthorpe 1987; Ranvas and Steel 1998; Gawthorpe and Leeder, 2000). Sediment entry points into fault-bounded basins associated with both these local and regional-scale depositional systems are typically located within areas of overall lower displacement. At a local scale, these sediment entry points are typically associated with relay ramps between individual fault segments (e.g. Leeder and Gawthorpe, 1987; Morley et al., 1990; Gawthorpe and Hurst, 1993; Morley, 1995; Bruhn and Vagle 2005). At a larger scale, they are typically characterised by a broad region (5 – 20 km wide) of overall low subsidence that may be associated with a switch in polarity of fault dip, characterising what have been termed structural accommodation or transfer zones (e.g. Bosworth, 1985; Rosendahl, 1987; Morley et al., 1990; Lambiase and Bosworth 1995; Moustafa, 1997). These rift-wide structural accommodation zones have often been cited as providing a major role in transferring regional sediment fluxes across different structural domains within a rift; particularly from major rift shoulder hinterlands, across the rift margin and into the central axis of a rift (e.g. Lambaise and Bosworth, 1995; Gawthorpe and Leeder, 2000). However, few studies have documented, in detail, the regional extent, variability and evolution of rift climax syn-rift depositional systems within a major rift-wide accommodation zone. Thus

the aim of this study is to utilise an extensive subsurface database from the Morgan Accommodation Zone within the Oligo-Miocene Suez Rift, Egypt to demonstrate how the local spatial and temporal evolution of normal fault zones interact with more regional controls to determine the nature of regional-scale syn-rift sediment fluxes within a major structural accommodation zone.

5.3. GEOLOGICAL SETTING

5.3.1 Regional structure and stratigraphy

The Suez rift is a failed intracontinental rift, trending NW-SE and is up to 80 km wide and 300 km long (Fig.5.1). Developed as a northern continuation of the Cenozoic Red Sea Rift (e.g. Colletta et al., 1988; Patton et al., 1994), the main phase of rifting is commonly estimated to have initiated in the Late Oligocene to earliest Miocene, *c.* 24 Ma, in response to the separation of the African and Arabian plates, and subsequently abating when significant plate motion transferred to the Dead Sea – Aqaba transform *c.* 15.5 Ma, (e.g. Courtillot et al., 1987; Richardson & Arthur, 1988; Colletta et al., 1988; Patton et al., 1994; Moustafa 2002). A second renewed phase of faulting, concentrated within the axis of the rift is suggested during the Pliocene to Recent by observations of displacement of late Middle Miocene post-rift strata, marked expansion of the Pliocene succession within fault hangingwalls and observations of modern day seismicity (e.g. Jackson et al., 1988; Hussein et al., 2006).

Along the axis of the rift, three structural domains are observed, termed the northern, central and southern dip provinces, which consist of several major crustal-scale, tilted fault blocks, typically 10-15 km wide and 20-30 km long, which with their associated bounding normal faults, show a consistent dominant dip orientation within each province, (e.g. Moustafa 1976, 1993; Patton et al., 1994). The dip direction of the structural provinces changes from north to south along the rift, with major faults within the northern and southern provinces dipping northeast, whilst those in the central province dip to the southwest. These provinces are separated by two structurally diffuse accommodation zones, which extend transversely across the rift, and accommodate the change in dip direction between the structural provinces. Termed the Zafarana and Morgan accommodation zones in the north and south respectively, these accommodation zones are 15-50 km in width and are characterised by smaller scale fault blocks compared to the

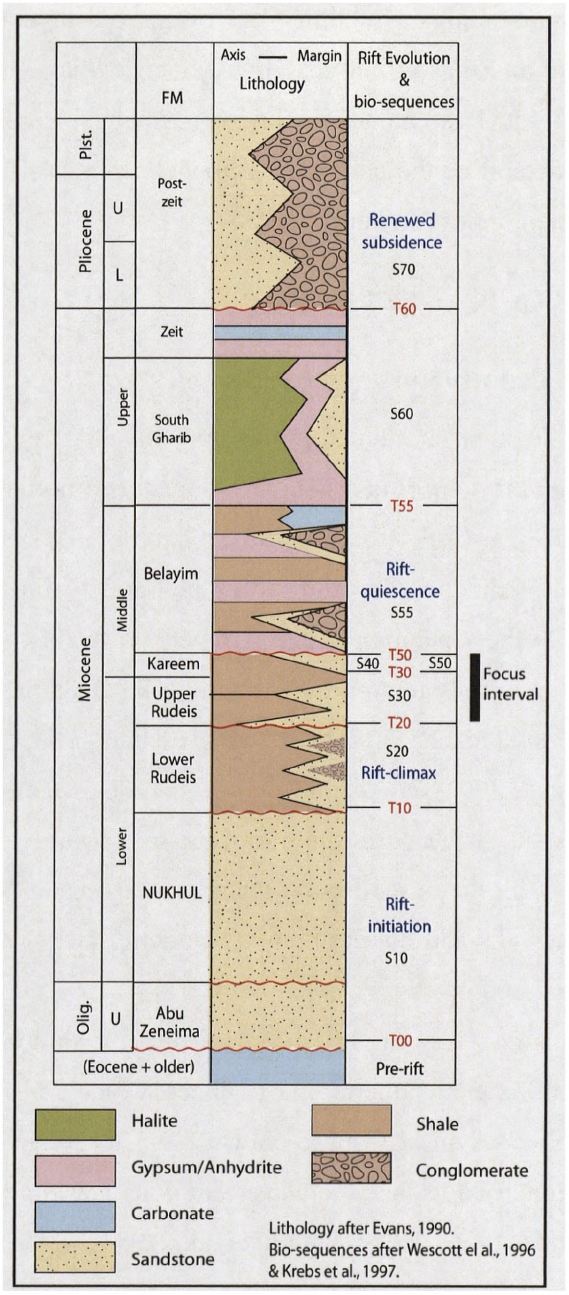

Figure 5.2. Late Oligocene to Pleistocene stratigraphic column for the synrift to postrift infill of the Suez rift, showing typical lithofacies (after Evans, 1990), lithostratigraphic based formations and the biostratigraphic defined hiatuses and intervening sequences of Wescott et al., (1996) and Krebs et al.,(1997). These biostratigraphic sequences correspond to the major tectonic evolutionary stages of the rift. The Upper Rudeis and Kareem Formations form the focus interval for this study.

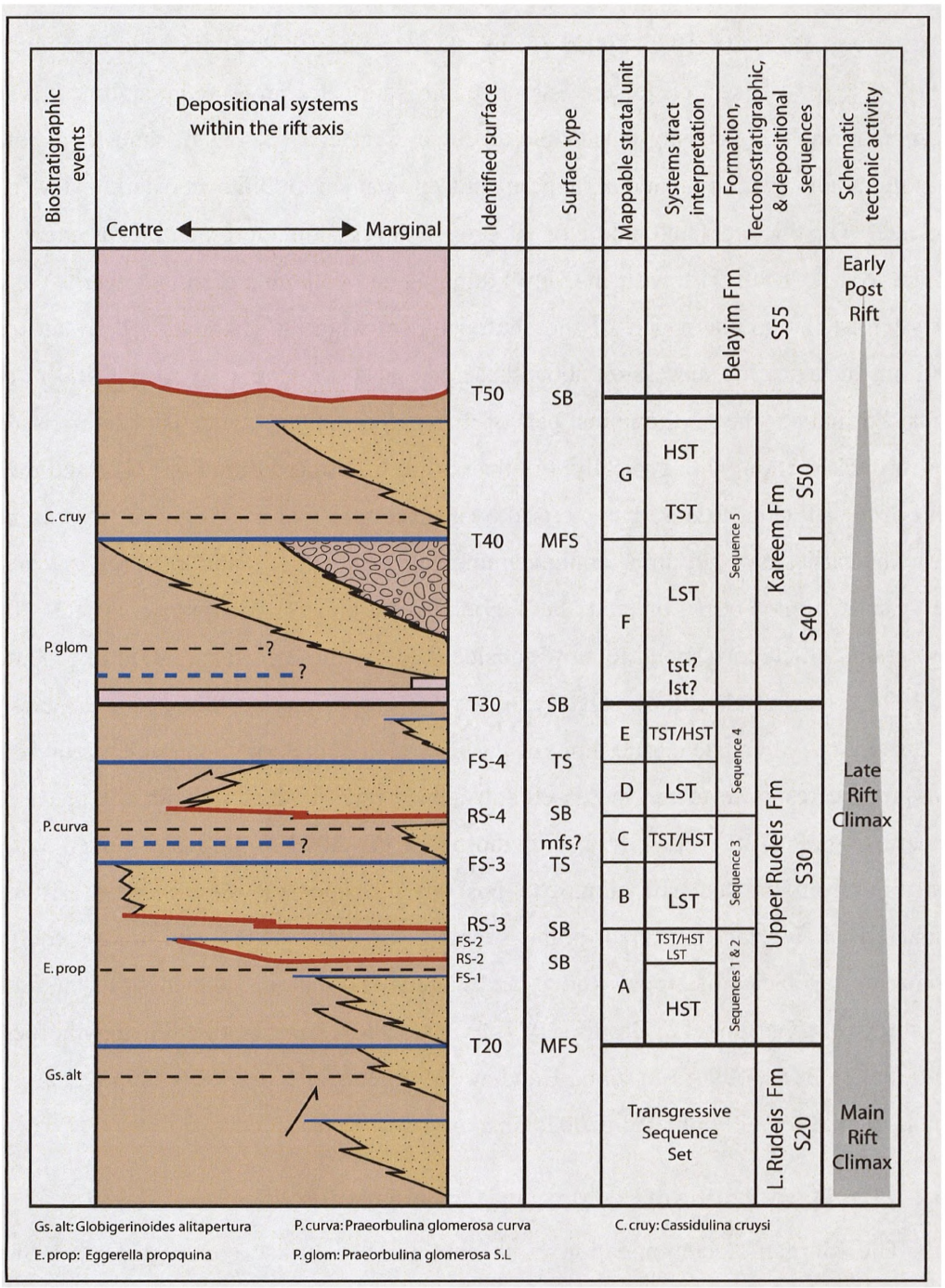

Figure 5.3. Idealised stratigraphic column for the Upper Rudeis and Kareem Formations, highlighting facies stacking patterns, key surfaces and resultant stratigraphic packages. The Upper Rudeis and Kareem Formations reflect the sedimentary response to an overall decrease in tectonic activity associated with the transition from the rift climax (Lower Rudeis Formation) to post-rift periods (Belayim Formation). Identified system tracts within the focus interval form seven stratal units which can be mapped regionally through-out the study area. See Fig. 5.2 for key to lithologies.

structural provinces, typically 1-5 km wide and overlapping fault segments of alternate polarity (e.g. Moustafa, 1976, 2002; Coffield & Schamel, 1989; Younes and McClay 2002).

The pre-rift section for the Suez rift consists of Precambrian crystalline basement, an unconformably overlying Palaeozoic to Lower Cretaceous series of sandstones referred to as the Nubia Formation and an uppermost Cenomanian to Oligocene carbonate – clastic package. The thickness and nature of the pre-rift succession overlying the basement varies along the strike of the rift, with an overall thinning and younging of units towards the south. Thus whilst the southern part of the central dip province is characterised by an overall +900 m thick pre-rift succession above basement and contains in excess of 400 m of the Nubia Formation, the northernmost part of the southern dip province is characterised by a 250 m thick section, with typically less than 50 m of Nubia Formation. The sedimentary infill of the rift (Fig. 5.2) is characterised by a succession of Late Oligocene to present day age. The earliest syn-rift units are the continental red bed facies and localised volcanics of the Abu Zenima Formation and the fluvial to marginal marine facies of the Nukhul Formation, which correspond to slow subsidence rates during rift initiation (e.g. Patton et al., 1994; Sharp et al., 2000). Overlying are the deeper marine, fine-grained facies with localised areas of coarse clastic input of the Lower Rudeis Formation, which represent the stratigraphic response to the increased subsidence rates associated with the onset of rift climax, (e.g. Patton et al., 1994; Gawthorpe et al., 2004). Deposits linked with the transition from the late rift climax to post-rift phase of the first pulse of rifting are characterised by the proximal point sourced fan-delta facies and distal equivalent submarine fan facies of Upper Rudeis and Kareem Formations, which form the basis of this study (e.g. Garfunkel & Bartov, 1977; Evans, 1988; Smale et al 1988; Gawthorpe et al., 1990; Patton et al., 1994; Elbaz and Handley 1994; Dolson et al., 1996; Gupta et al., 1999; Young et al., 2002; Pivnik et al., 2003; Chapter 4).

5.3.2 Structural setting of the Morgan Accommodation Zone

The Morgan Accommodation Zone comprises a diffuse convergent zone of fault polarity change, with the dominant dip direction of major faults changing from northeast to southwest, consistent with the change in dip polarity of major structures from the central to southern dip provinces. Figure 5.4 shows a fault interpretation map for the study area at the top of the Kareem Formation, which is the deepest horizon at which the major structures may be confidently identified from current seismic datasets without extensive borehole control. Two main fault trends are recognised: a dominant NW-SE trend,

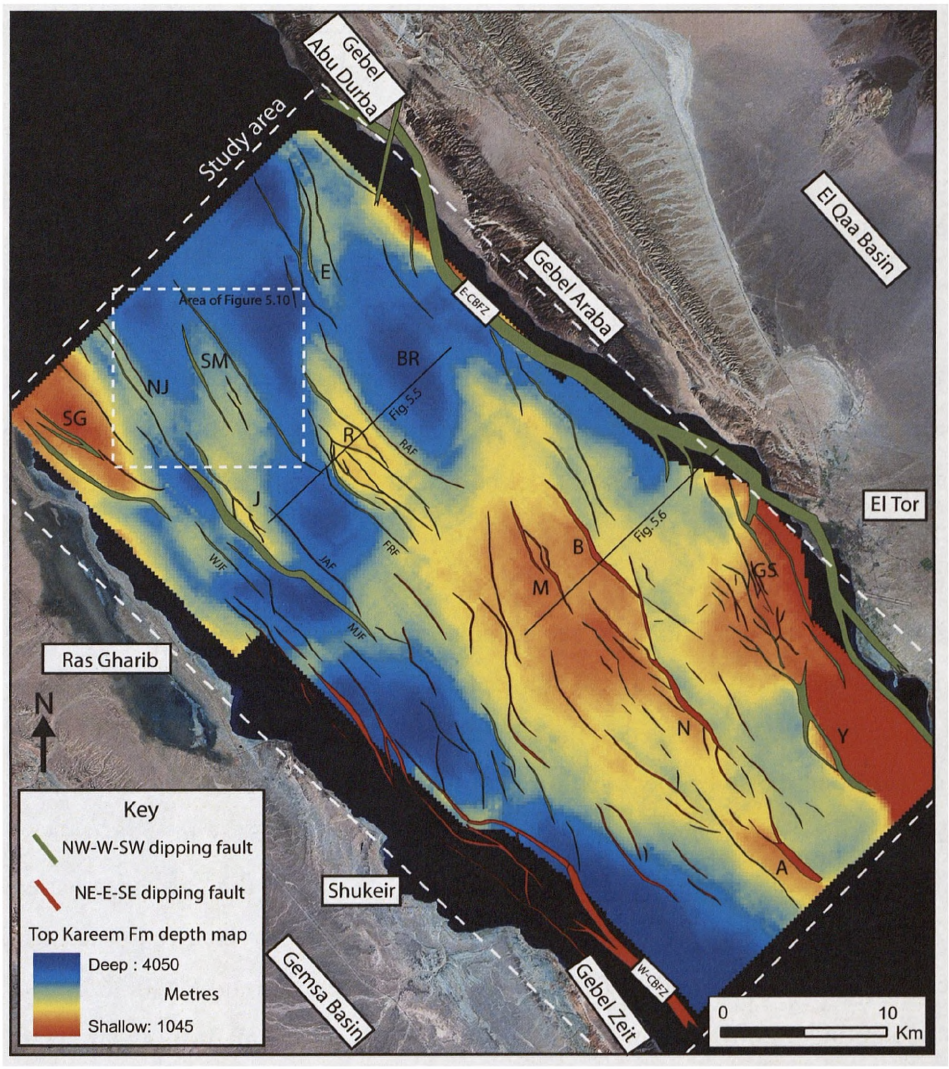

Figure 5.4. Depth surface at top Kareem Formation with associated present day structural framework for the study area superimposed on a regional Landsat image. Fault heaves are coloured by dip direction and thicknesses are proportional to amount of displacement. Fault block listed are: SG = SG300 Fault Block; NJ = North July Fault Block; SM = Safa-Mawa Fault Block; E = Eagle Fault Block; J = July Fault Block; R = Ramadan Fault Block; M = Morgan Fault Block; B = Badri Fault Block; N = Nessim Fault Block; A = Amal Fault Block; GS = GS306 Fault Block; Y = Younis Fault Block. Individual faults listed are: WJF = West July Fault; MJF = Main July Fault; JAF = July Antithetic Fault; FRF = Frontal Ramadan Fault; RAF =Ramadan Antithetic Fault; CBFZ=Coastal Boundary Fault Zones. BR = Back Ramadan synclinal area.

commonly referred to as the 'Clysmic trend', (e.g. Patton et al., 1994), indicative of the principal perpendicular (SW-NE) extension vector, and a second, subordinate N-S trend commonly observed to hard-link Clysmic NW-SE trending segments. This second, N-S trend is believed to reflect an inherited, pre-existing pre-rift trend, as illustrated in measurements of pervasive fault and dyke geometries observed in satellite maps for basement exposures upon the rift shoulder (P. Whitehouse. Pers. comm).

The study area is bounded by two large, NW-SE trending, coastal delineating fault zones and associated major tilted fault blocks, with footwall crests exposed onshore as major topographic highs: Gebel Araba on the eastern margin and Gebel El Zeit on the western margin. Both fault zones, herein referred to as Coastal Boundary Faults display maximum displacements in excess of 4 km, and are interpreted to tip out towards the accommodation zone and form a series of splay faults which rapidly lose displacement. Contained within the rift axis component of the accommodation zone, second order faults ($\geq$ 500 m displacement) and associated fault blocks are observed to display reduced displacement and reduced spacing (1-2 km apart) towards the centre of the accommodation zone from that typically observed in the central and southern dip provinces. Principal fault blocks towards the north of the study area i.e. within the southernmost part of the central dip province, are the July and Ramadan Fault Blocks (Fig. 5.5), whilst to the south, the Amal, Badri, Nessim and Morgan Fault Blocks (Fig. 5.6) form the northernmost elements of the 'B' trend series of fault blocks of the southern dip province (e.g. Helmy, 1990). Antithetic faults are observed within both dip provinces, the July and Ramadan Fault Blocks containing significant antithetic faults down-dip of the main footwall crest. In the southern dip province, the Amal Fault Block is characterised by an asymmetric horst, whilst the Younis Fault Block is observed to be a large, antithetically orientated, > 4 km wide fault block.

5.4. DATASET AND METHODOLOGY

The area studied covers an area approximately 1600 km^2 and is located in the present day offshore component of the rift, encompassing the southern portion of the central dip province, the Morgan Accommodation Zone and the northern portion of the southern dip province (Fig. 5.1). The study area contains some of the most prolific oilfields in the Suez rift (e.g. Morgan Field, Rine et al., 1988; July Field, Pivnik et al., 2003) and thus utilises an extensive subsurface database provided by the Gulf of Suez Petroleum Company (GUPCO). Part of this database consists of two regional, depth converted 3D

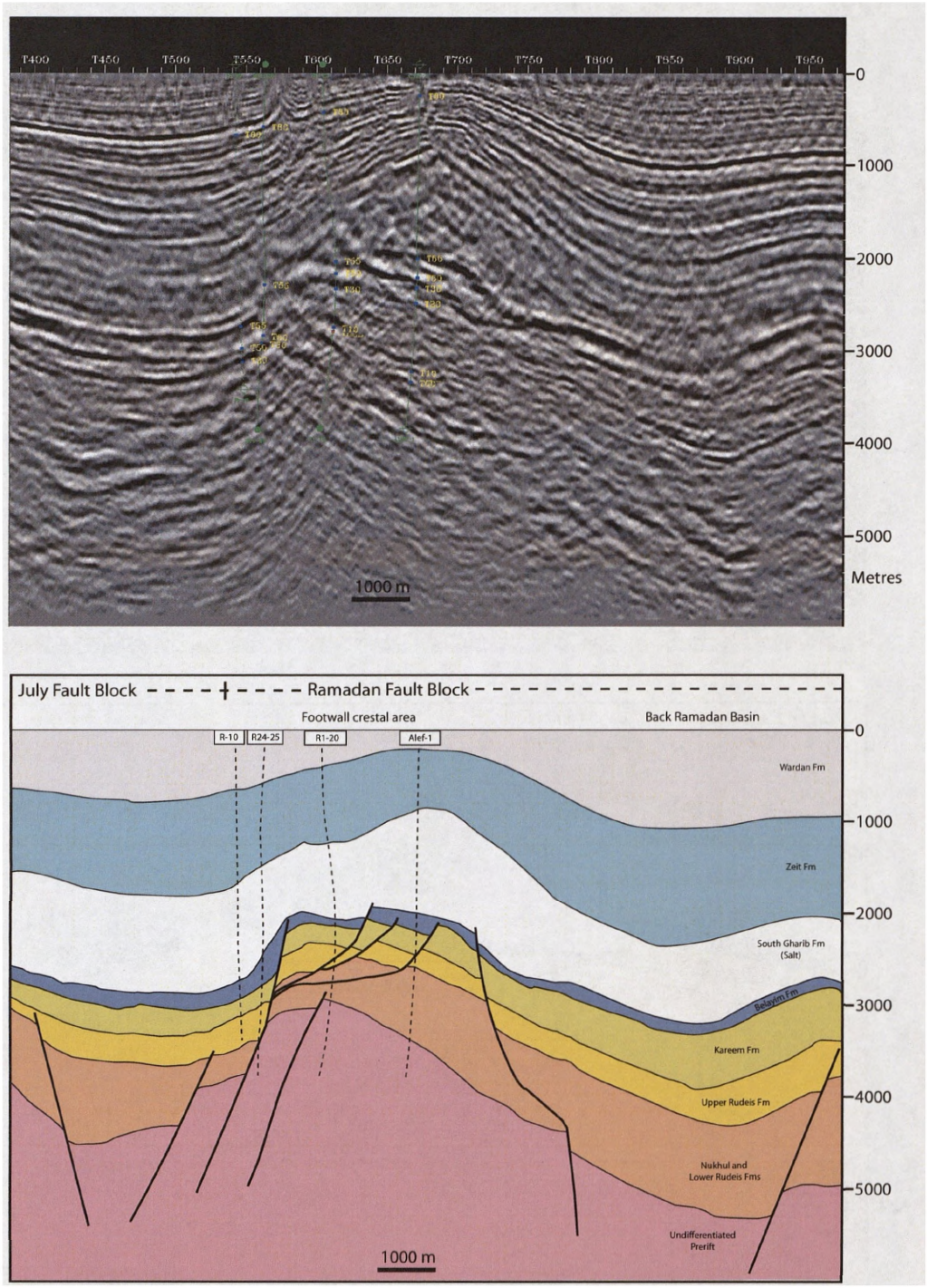

Figure 5.5. Dip section across the Ramadan Fault Block, see Figure 5.4. for location. Borehole penetrations aid the definition of the footwall crestal area and indicate the presence of a series of listric faults within the syn-rift succession. Prinicple thickness variations are associated with the Lower and Upper Rudeis Formations. The synclinal area, termed the back Ramadan basin, down the hangingwall dip-slope is mapped an isochore thick, but is poorly constrained.

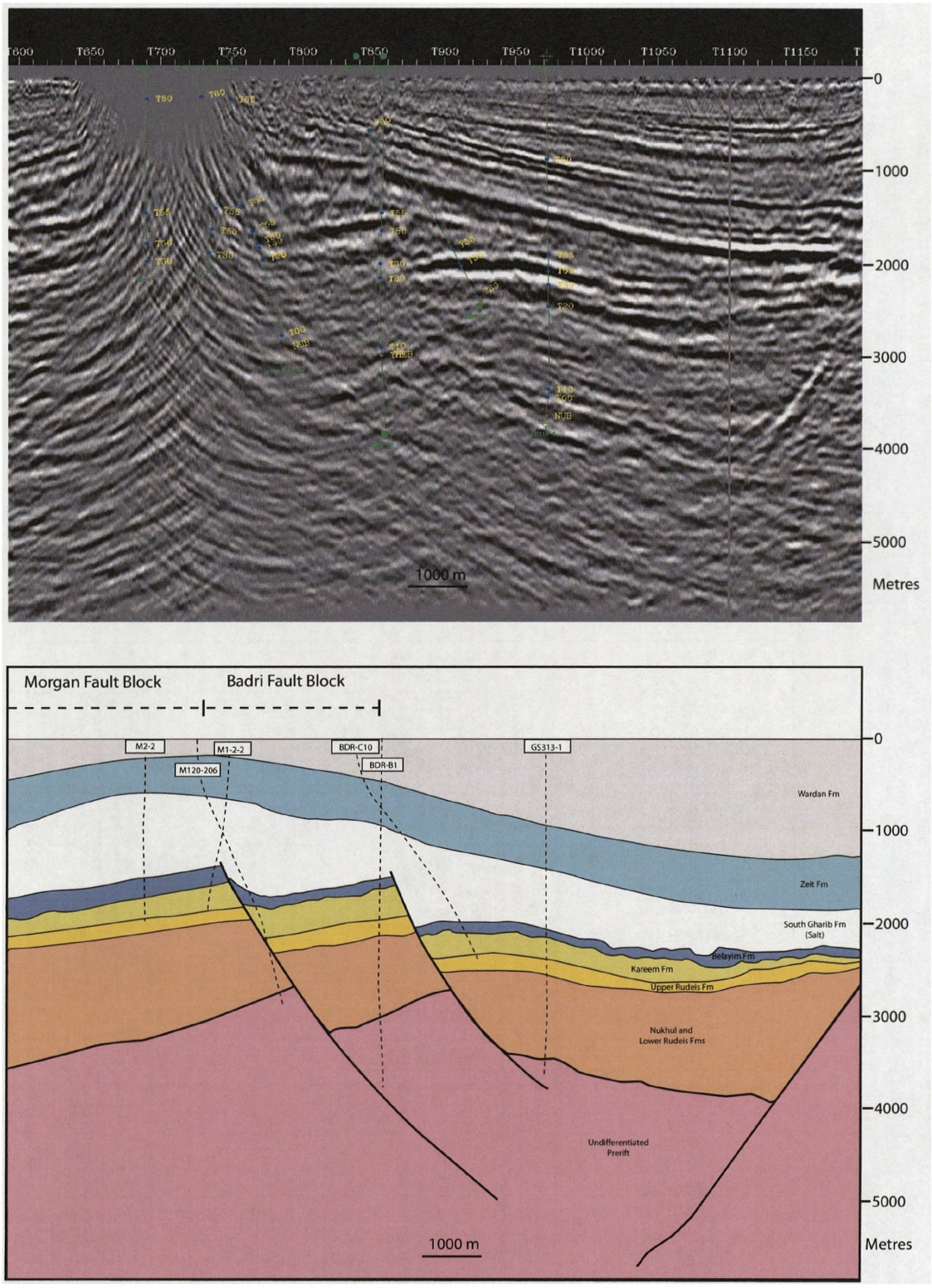

Figure 5.6. Dip section across the Morgan and Badri Fault Blocks, see Figure 5.4. for location. Well correlations across the Morgan and Badri Faults show localised thickness variations for mapped stratal units of the Upper Rudeis and Kareem Formations. In contrast, the overlying Belayim Formation is relatively isopachous.

seismic projects, orientated to reflect the strike and dip directions of the Suez rift. However, as shallow syn-rift intercalated clastic and evaporite units produce significant seismic attenuation and result in a high number of multiples that significantly reduces seismic data quality, extensive borehole data is heavily relied upon to constrain both the present structural framework and interpretations of syn-rift thickness and facies variations. This combination of extensive borehole control and primary reflector interpretation was used to map key horizons throughout the study area which are interpreted to approximate to the bounding hiatal surfaces of the Upper Rudeis and Kareem Formations. Whilst the top Kareem Formation (T50) is consistently observed to be associated with a paired set of high and low amplitude reflectors, the top of the Upper and Lower Rudeis Formations (T30 and T20 respectively) are characterised by locally variable and typically multiple-affected reflectors. Thus whereas resultant broad-scale seismic isochore mapping of the Upper Rudeis and Kareem Formations identifies large-scale (0-600 m) thickness variations, the poor data quality for this subsalt section precludes the effective use of seismic data alone in accurately defining the tectono-stratigraphic evolution of the study area.

To address this, interpretations for the structural configuration and associated mapped seismic horizons within the study area were integrated with a comprehensive suite of borehole-derived, wireline log, core and biostratigraphic data to correlate late rift climax thickness and facies variations at a sub-seismic resolution. Approximately 320 wells in the study area have significant penetration within the Upper Rudeis and Kareem Formations, and were examined to determine lithology and facies and develop a high-resolution stratigraphic framework. True stratigraphic thicknesses for both gross interval and net sandstone for the key stratigraphic units defined were then calculated. Principal lithologies were determined from cored intervals and calibrated wire-line logs. A petrophysical definition for sandstone, calibrated to available cored section, was used to provide a fair approximation of the siliciclastic-dominated sandstones observed within the study area; with the calcarenitic sandstones observed elsewhere in the rift largely absent in the study area (c.f. Chapter Four). Gross interval and sandstone isopachs were constrained by biostratigraphic supported wire-line log correlation of key stratal surfaces, seismic mapping, published onshore datasets and analysis of present day drainage systems through satellite imagery and bathymetric maps. Observations of facies variations were then incorporated with interpretations of fault activity and the location of depositional systems derived from the isopach maps to generate interpretive palaeogeographic maps, providing a model for the tectono-stratigraphic development of the Morgan Accommodation Zone

during the Early to Middle Miocene. Ultimately these maps are limited by the spatial distribution of available borehole data (Appendix 4) and thus contain areas of poorly understood structural configuration.

5.5. SEDIMENTARY FRAMEWORK

A detailed sedimentological study of the key intervals is outside the scope of this chapter. However, analysis of consistent wire-line log motifs, core and cuttings data for the Upper Rudeis and Kareem Formations, integration with previously published studies within the study area (e.g. Rine et al., 1988; Pivnik et al., 2003) and comparison with contemporaneous deposits elsewhere in the rift axis (e.g. the October area in the northern part of the central dip province, Chapter 4) allows for the identification of four main facies associations (Table 5.1). The Upper Rudeis and Kareem Formations within the study area comprise fine-grained mudstones and marls, with varying-thickness units of intervening coaser-grained sandstones, conglomerates and evaporites.

Facies Associations

Facies Association (A): Offshore Basinal Mudstones

Viewed in core, Facies Association A is characterised by thick, metre-scale packages of calcareous mudstones and marls, which may be laminated or massive and are sparsely bioturbated. Calibrated to wire-line logs, Facies Association A consistently shows high gamma-ray values, typically > 50 API, whilst accompanying neutron and formation density logs exhibit a wide separation. Packages of Facies Association A are observed as both thick, 10's of metres uninterrupted successions and as smaller, 1-2 m thick units intercalated between the other facies association identified. The lack of any shallow water indicators, in addition to a dominance of benthic forams suggests that Facies Association A was deposited in a relatively low energy setting through suspension settling; envisaged as an offshore marine environment below the storm wave base.

Facies Association (B): Submarine Fan

Cores, cuttings and wire-line logs document the presence of significant packages of sub-arkosic sandstones within the Upper Rudeis Formation. The interbedding of these sandstones in the axis of the rift with the offshore basinal mudstones of Facies Association A, the typically normal-grading of grainsize, the low diversity nature of trace fossils such

	GR / NPHI RHOB / DT	Key observations	Environment
Facies Association D	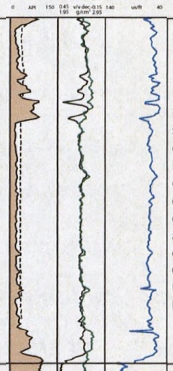	Stacked packages, 15 to >50 m thick, of overall reducing-upwards gamma-ray and sonic log motifs. This is interpreted as a coarsening-upwards trend within a dominantly sandstone or coarser-grained succession. Both gamma-ray and sonic log values are typically low, with smaller, approximately 10 m thick, individual coarsening-upwards trends observed within the larger overall package. Core descriptions document this facies association as poorly-sorted, thick, pebbly and graded sandstones with interbedded basinal offshore mudstones. Wave ripples and a diverse shallow marine trace fossil assemblage are observed, which distinguish these deposits from the deepwater, submarine fan Facies Association B. Other Fan-deltaic deposits are identified elsewhere in the axis of the rift during the Upper Rudeis Formation, e.g. on the Warda Fault Block in the Northern Dip Province, (Elbaz and Handley, 1994).	Fan-delta
Facies Association C		Massive anhydrite with a characteristic 'box-shape' wireline log motif, packages ranging in thickness from 5-30 m. The pure anhydrite nature of this facies is determined from cuttings data and is reflected by consistently very low gamma-ray and sonic log responses (<10 API and 50 µsec/m respectively) and high density values (2.98 to 3 g/cm3).	Restricted evaporitic basin
Facies Association B — Facies B4		Very thick (> 50 m), massive packages of very low gamma-ray and sonic values which are interpreted to indicate sandstones with little or no fine-grained content. Typically Facies B4 displays both a sharp basal and top surface contacts with packages of the offshore basinal mudstone Facies Association A. Typically observed to proximal to the sediment entry points.	Proximal submarine fan
Facies Association B — Facies B2 (ii)		Sharply based from underlying offshore mudstones with a low gamma-ray and sonic log response calibrated in core to medium- to coarse-grained sandstones. A subsequent overall increasing-upwards gamma-ray and sonic log 'bell-like' profile over packages 5-20 m thick is interpreted as fining-upwards trend, reflecting a gradual return to the offshore mudstones of Facies Association A	Mid submarine fan: lobe
Facies Association B — Facies B2(i)		Stacked, 5 -10 m thick, sharply based, low gamma-ray and sonic log 'boxcar' packages. Intercalated with 1-5 m thick units of offshore mudstones of Facies Association A. Correlations indicate a generally tabular nature to sheet-like nature over several km.	Mid submarine fan: sheet
Facies Association B — Facies B1		Decreasing-upwards motif in gamma-ray and sonic logs interpreted as a coarsening-upwards from underlying mudstones of Facies Association A. The low gamma-ray packages at the top of this package are typically 5-10 m thick and show a sharp top surface with overlying packages of offshore basinal mudstones.	Progradational distal submarine fan
Facies Association A		Metre-scale packages of calcareous laminated or massive mudstones and marls and are sparsely bioturbated. High gamma-ray values, typically > 50 API, whilst accompanying neutron and formation density logs exhibit a wide separation. maximum uniterrupted thicknesses of 10's of metres. No shallow wave-generated structures observed in cored section	Offshore Basinal mudstones

Table 5.1. Facies Association scheme. Consistent wireline log signatures, accompanied by core and biostratigraphic data allows for the Upper Rudeis and Kareem Formations to be subdivided into four main facies associations.

as *Ophiomorpha*, and *Thallasinoides* in addition to the lack of wave-generated sedimentary structures which would be evidence for shallow water deposition (c.f. Pivnik et al., 2003; Chapter Four) suggest that deposition occurred from sediment gravity flows below the storm wave base as a series of submarine fans. Wire-line log trends allow for the discrimination of five log facies: *Progradational distal fan Facies (B1)* is characterised by a decreasing-upwards motif in gamma-ray and sonic logs interpreted as a coarsening-upwards from underlying mudstones of Facies Association A. The low gamma-ray packages at the top of this package are typically 5-10 m thick and show a sharp top surface with overlying packages of offshore basinal mudstones. *Mid Submarine fan Facies (B2)* is split into two subfacies based upon geometry: *Mid fan sheet (B2i)* is characterised by a series of stacked, 5 -10 m thick, sharp based and topped, low gamma-ray and sonic log 'boxcar' packages intercalated with 1-5 m thick units of Facies Association A. Correlations between wells confirm the sheet-like, tabular nature of these sandstone packages. In contrast, *Mid fan lobe (B2ii) Subfacies* is generally characterised by a sharp base from underlying mudstones with a low gamma-ray and sonic log response calibrated in core to medium- to coarse-grained sandstones. A subsequent overall increasing-upwards gamma-ray and sonic log 'bell-like' profile over packages 5-20 m thick is interpreted as fining-upwards trend, reflecting a gradual return to the offshore mudstones of Facies Association A. *Proximal submarine fan Facies (B4)* is distinguished from Facies B3 by very thick (> 50 m), massive packages of very low gamma-ray and sonic values which are interpreted to indicate sandstones with little or no fine-grained content. Typically Facies B4 displays both a sharp base and top with surrounding packages of the offshore basinal mudstone facies association.

Facies Association (C): Restricted basinal evaporite

Occurring predominantly at the base of the Kareem Formation, this facies association is identified by a characteristic 'box-shape' wireline log motif, with packages ranging in thickness from 5-30 m. In some locations, stacked packages of this facies association are observed with intervening offshore mudstones. The pure anhydrite nature of this facies is determined from cuttings data and is reflected by consistently very low gamma-ray and sonic log responses (<10 API and 50 μsec/m respectively) and high density values (2.98 to 3 g/cm^3). This facies association has been widely documented in the literature and has lithostratigraphically been referred to as the 'Markha Anhydrite' and has been variably interpreted as a being deposited within a tidal flat or sabkha environment

(e.g. Patton et al., 1994), or alternatively within a restricted marine basin (e.g. Orszag-Sperber et al., 1998; Salah and Alsharhan, 1997). The latter interpretation is preferred in this study given the lack of interbedded clastics that might be expected within a sabkha setting rather than the pure anhydritic nature of this facies association (e.g. Kendall & Harwood, 2002).

Facies Association (D): Fan-delta

Facies Association D is characterised by stacked packages, 15 to >50 m thick, of overall reducing-upwards gamma-ray and sonic log motifs. This is interpreted as a coarsening-upwards trend within a dominantly sandstone or coarser-grained succession. Both gamma-ray and sonic log values are typically low, with smaller, approximately 10 m thick, individual coarsening-upwards trends observed within the larger overall package. Rine et al., (1988) focussing upon this type of facies association within the area of the Morgan and Badri Fault Zones, describe a dominance of poorly-sorted, thick, pebbly and graded sandstones with interbedded basinal offshore mudstones. Facies association D is distinguished from the submarine fan sandstones of Facies Association B principally on the basis of core data which contain evidence for shallow water deposition, which includes: wave ripples and a diverse shallow marine trace fossil assemblage.

5.6. STRATIGRAPHIC FRAMEWORK

The Upper Rudeis and Kareem Formations are equivalent to the biostratigraphically defined tectono-stratigraphic sequences S30, S40 and S50 of Wescott et al., (1996) and Krebs et al., (1997). The biostratigraphic sequences are bounded by surfaces which have been identified as representing a hiatal biostratigraphic lacune or terrace in the graphic correlation method of Shaw (1964) and do not correspond to the depositional sequences of Vail et al., (1977), but rather can be broadly related phases associated with the large-scale tectono-stratigraphic evolution of the rift (Wescott et al., 1996).

Within the study area, the Upper Rudeis Formation is subdivided into a number of higher resolution stratigraphic units, bounded by regionally extensive key stratal surfaces identified by consistent facies changes, which represent landward or basinward shifts in facies (Fig. 5.3). Flooding surfaces (FS-2, FS-3 etc) are characterised by a pronounced, widespread shift to distal, fine-grained facies, whereas downshift surfaces (RS-2, RS-3 etc) are sharp and marked by an abrupt shift to more proximal facies. The overall regional

nature of these surfaces, the integration of observations for the facies stacking patterns within intervening stratal units allows for the recognition of high-resolution depositional sequences and component system tracts (Fig. 5.3). Both surfaces and intervening stratal units may display marked variability between different structural locations. Within hangingwall depocentres, stratal units display expanded thickness bounded by key stratal surfaces, whereas, strata; surfaces may amalgamate and become composite and intervening stratigraphic units become thin and condensed upon structural highs.

In contrast, the Kareem Formation (biostratigraphic tectono-sequences S40 and S50), due to a scarcity of diagnostic zonal fossil assemblages within the typically coarse-grained nature of the succession, is considered at the previously defined principal tectono-stratigraphic sequence levels of Wescott et al., (1996) and Krebs et al., (1997).

Upper Rudeis Formation

The Upper Rudeis Formation is interpreted to consist of four high-resolution depositional sequences (*sensu* Vail et al., 1977), which can be regionally mapped within five stratal units (Stratal Units A-E) (Fig 5.3). The Lower Rudeis Formation is typically mudstone-dominated within the centre of the rift axis, with a coeval series of coarsening-upwards submarine fan packages located towards the marginal areas of the rift axis and which are typically retrogradationally stacked. The T_{20} surface defining the contact between the Lower and Upper Rudeis Formations is typically picked either within a uniform mudstone package or at the base of a mudstone interval capping a the uppermost Lower Rudeis coarsening-upwards submarine fan package. The T_{20} surface is placed between the benthic foraminiferal assemblages of *Eggerella propinqua* and *Globigerinoides altiapertura* or older Lower Rudeis foraminferal assemblages and is interpreted to be a maximum flooding surface.

The lowermost part of the Upper Rudeis section is typically mudstone dominated within the centre of the rift axis, whereas markedly progradational submarine fan deposits observed towards the marginal areas of the rift axis, adjacent to the principal sediment entry points (discussed below), contrast to those associated with prior Lower Rudeis Formation. This lowermost part of the Upper Rudeis Formation is thus interpreted as a relative highstand following the T_{20} maximum flooding surface, and forms the uppermost part of an initial depositional sequence (Sequence 1). A marked downshift surface (RS-2) is observed locally adjacent to the sediment entry points located towards the margin of the rift axis and is associated with a marked basinward shift in facies to submarine fan

sandstones. Thus RS-2 is interpreted as a sequence boundary marking the onset of lowstand deposition within the rift axis associated with a second depositional sequence (Sequence 2). The submarine fan sandstones associated with RS-2 are capped by a sharp switch to fine-grained offshore mudstones which are interpreted to reflect the ensuing development of the transgressive and highstand system tracts of Sequence 2. Away from the sediment entry points within the axis of the rift, Sequences 1 and 2 may be locally mudstone dominated and RS-2 cannot be identified. Thus over most of the study area, it is difficult to define Sequences 1 and 2 and these are mapped within a single stratal unit (Stratal Unit A) (Fig 5.3).

The base of Sequence 3 is formed by the major, rift axis wide downshift surface, (RS-3) marked by the most extensive influx of siliciclastic submarine fan sandstones into the rift axis associated with the Upper Rudeis Formation. Forming a second mappable stratal unit (Stratal Unit B), these lowstand are capped by sharp flooding surface (FS-3) and landward facies shift, with the rift axis being dominantly characterised by an abrupt switch to fine-grained offshore mudstones, and with coarser sandstone submarine fan deposits being restricted towards the margin of the rift axis. Flooding surface FS-3 is therefore interpreted as a transgressive surface, linked to a switch-off in coaser-grained sediment supply largely throughout the rift axis and a return to offshore basinal mudstones forming the transgressive to highstand deposits of Sequence 3. Containing the first down-hole occurrence of the foraminiferal assemblage *Preaorbulina glomerosa curva,* these deposits form Stratal Unit C (Fig 5.3).

A further regional downshift surface (RS-4) and linked basinward shift to submarine fan facies forms the base of the fourth depositional sequence identified in the Upper Rudeis Formation. Akin to those associated with RS-3, these submarine fan deposits are interpreted as reflecting a period of lowstand, albeit the spatial extent of these submarine fan facies above RS-4 are not as widespread as those associated with the base of Sequence 3. An abrupt landward shift to offshore mudstones and marls above flooding surface FS-4 caps this lowstand unit (Stratal Unit D) and similarly to Stratal Unit C, this fine-grained interval is interpreted as a series of transgressive to highstand deposits, which form the uppermost part of Sequence 4 and thus Stratal Unit E (Fig 5.3).

Kareem Formation

The Kareem Formation has previously been subdivided into two, biostratigraphically defined sequences: S_{40} and S_{50} (e.g. Wescott et al., 1997 and Krebs et

al., 1997). The lack of biostratigraphic data associated with this typically coaser-grained formation makes any further higher resolution sub-division difficult. The Kareem Formation is therefore considered as a single depositional sequence (Sequence 5), with the two biostratigraphically defined intervals forming Stratal Units F and G (Fig 5.3).

The lowermost section of the Kareem Formation within the study area is typically associated with a sharp transition from the offshore mudstones and marls of Facies Association A within the uppermost part of the Upper Rudeis Formation (Stratal Unit E) to the restricted evaporites of Facies Association C or the Markha Anhydrite. The basal boundary of this evaporitic unit forms the T_{30} hiatal surface and is a candidate sequence boundary which has been described a regionally diachronous throughout the rift (e.g. Beleity, 1982). Where the Markha Anhydrite is locally absent, T_{30} is commonly placed below a package of offshore basinal mudstones containing the first downhole occurrence of the *Preaorbulina glomerosa* foraminiferal assemblage. Locally the lowermost part of the Kareem Formation is dominated by extensive deposits of the submarine fan and fan-deltaic Facies Associations (B and D), which occur in gross packages up to 50 m thick. This lower Kareem Formation package is capped by a markedly abrupt landward shift in facies to offshore basinal mudstones, and an initial restriction of coarser-grained sediments back towards the marginal areas of the rift axis. The intervening surface is designated S_{40} in the Wescott et al, (1996) and Kreb et al, (1997) schemes and interpreted as a transgressive to maximum flooding surface. Therefore the lower part of the Kareem Formation is interpreted to reflect deposition during a period of overall lowstand of Sequence 5 and forms mappable Stratal Unit F.

The overlying uppermost section of the Kareem Formation contains the diagonsotic benthic foramiferal assemblage *Cassidulina cruysi* and is associated within its uppermost part with an overall progradation of submarine fan depositional systems from the margin towards the centre of the rift axis. Bounded by the locally erosional unconformity associated with the base of the intercalated clastics and evaporites of the Belayim Formation which is interpreted as a major regional sequence boundary; the uppermost part of the Kareem Formation forms Stratal Unit G and is interpreted as a reflecting deposition during transgression and subsequent highstand of Sequence 5.

5.7. LATE RIFT CLIMAX THICKNESS AND FACIES VARIABILITY

In this section, seismic and borehole data derived, regional isochore and higher resolution, borehole-based, isopach maps for the variations in stratal units identified within

the study area are used to determine regional-scale fault activity. These data are also integrated with facies data to evaluate the temporal and spatial development of the major Early to Middle Miocene sedimentary depositional systems within the rift axis part of the Morgan Accommodation Zone.

5.7.1 Gross interval thickness variations

Figure 5.7 shows a pair of seismic and borehole derived isochore maps for the Upper Rudeis (S30) and Kareem Formations (S40 & S50) which highlight a series of consistent regional thins and thicks within the study area. These identified thickness variations are described below and then compared to a set of borehole-derived isopachs for a series of higher resolution stratal units. The largest thicknesses observed at this scale in both maps in Figure 5.7 are typically associated with the hangingwalls of present day major faults in the southern part of the central dip province (e.g. West July, July, Ramadan, Safa-Mawa Faults), whereas principal thin areas are present upon present day major footwall locations (e.g. on the SG300, July, GS306, Amal and Younis Fault Blocks). See Fig. 5.4 for locations.

The Upper Rudeis Formation (S30) isochore, between the T20 and T30 horizons, shows thickness variations within the study area from approximately 0 – 620 m (Fig. 5.7a). Thicknesses of >500 m are observed in large-scale hangingwall depocentres associated with faults associated with the July and Ramadan Fault Blocks, (labelled as Depocentres 1-4 in Fig 5.7a). Depocentre 1 is up to 540 m thick in the hangingwall of the NW-SE orientated West July Fault, whilst a series of smaller, circular depocentres are observed along strike within the immediate hangingwall of the present day principal July Fault, (labelled 1i, 1ii and 1iii; Fig 5.7a). To the E – ENE of Depocentre 1, a thickness of 400 m is recorded in Depocentre 2 which is located in the hangingwall to the similarly orientated frontal Ramadan Fault. Approximately 5-10 km to the north of Depocentre 2, Depocentre 3 is up to 470 m thick, elongated N-S and wedge-shaped towards the south, and is located within the hangingwall to a N-S trending series of fault segments from the Ramadan and Eagle Fault Blocks. Depocentre 4 is up to 620 m thick, within the synclinal hangingwall-dip slope, termed the Back Ramadan Basin, located between the Ramadan Antithetic Fault and the eastern Coastal Boundary Fault on Fig 5.7a. Note that this is in an area of relatively poor quality seismic data and there are no boreholes for corroboration (Fig. 5.5). Towards the south and in the part of the southern dip province covered in this study, the variation in thicknesses is markedly reduced, but two principal sediment thicks are

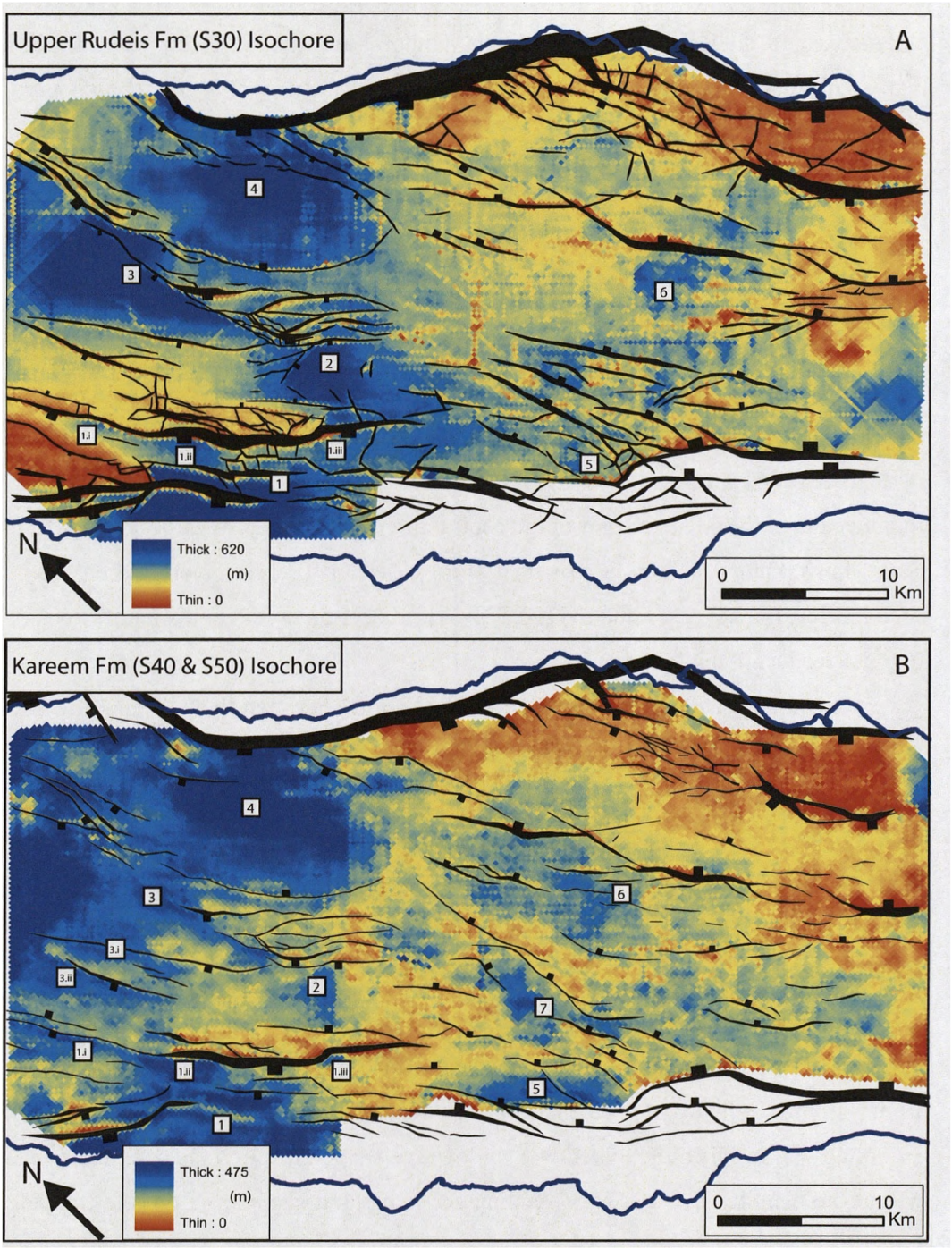

Figure 5.7. Seismic derived isopach maps for the Upper Rudeis and Kareem Formations within the study area. Principal isochore thicks / sediment depocentres are numbered.

observed, (Depocentres 5 and 6; Fig 5.7a). Depocentre 5 is located offshore of the Shukeir area, within the hangingwall to the Coastal Boundary Fault and shows a diffuse area up to 285 m, whereas Depocentre 6 is located downdip of the footwall of the Badri Fault, and is up to 308 m thick.

The Kareem Formation (S40-S50) isochore, calculated between horizons T50 and T30, is observed to show approximate thickness variations from 0-475 m (Fig. 5.7b). Depocentre 1 is up to 380 m thick, and is observed to link into the previous smaller depocentre 3.ii, within the hangingwall of the main July Fault, whilst depocentres 3.i and 3.iii remain isolated. Depocentre 2 is reduced in extent, whereas Depocentre 3 is still a significant, > 300 m thick, albeit, narrower and more elongate. Smaller scale depocentres (3.i and 3.ii) are recognised associated with faults within the Safa-Mawa Fault Block. Depocentre 4 is again inferred from seismic data alone to be a major thick, up to 475 m, whilst Depocentre 5 is more spatially extensive, elongated NW-SE along the hangingwall of the Coastal Boundary Fault, and up to 370 m thick. The locus of Depocentre 6 has shifted some 2 km to the west, and is up to174 m thick. Compared to the Upper Rudeis Formation, the Kareem Formation contains a new area of thick sediment accumulation located in Depocentre 7, which is approximately 6 km to the NE of Depocentre 5 and up to 180 m thick.

Figure 5.8 depicts a series of well-based, gross interval isopach maps for high resolution Stratal Units A, C and D within the Upper Rudeis Formation and Stratal Units F-G of the Kareem Formation (Fig. 5.3). The gross interval isopachs for Upper Rudeis Formation Stratal Units A, C and D (Fig. 5.8a - c) show thickness variations of 0-214 m, 0-147 m and 0-207 m respectively. Depocentre 1 previously identified in Figure 5.7 is observed to be part of a larger consistent sediment thick extending to the present day onshore Ras Gharib area. Initially contained by the West July Fault during Stratal Units A, this large sediment thick during Stratal Units C and D and E and F shows an N-NE movement towards the hangingwall of the Main July Fault, the immediate footwall of which remained a consistent relative thin during the deposition of the Upper Rudeis and Kareem Formations. Similarly, Depocentre 5 is interpreted to extend onto the present day onshore Shukeir area throughout Stratal Units A, C, and D-F, consistent with well data observed on the western rift margin outside of the study area and other published studies (e.g. Smale et al., 1988). In each of the isopach maps, (Fig 5.8), the present day onshore and immediate offshore area between the Ras Gharib and Shukeir is corroborated by several wells to be a relative isopach thin separating the two isopach thicks. Basinward,

Depocentre 5 extends to the NE, linking to Depocentres 2 and 7 during Stratal Units A and B, but is increasingly restricted during Stratal Unit D. During Stratal Unit F of the Kareem Formation, Depocentre 5 forms part of a major, rift axis wide, sediment thick extending from the onshore Shukeir area to the SW and a major paired depocentre associated with the Morgan and Badri Faults, incorporating Depocentre 6 and the onshore El Tor area on the eastern rift margin. The two principal isopach thicks associated with the Badri and Morgan Fault Zones, are mapped as lobes up to 300 m, separated by a smaller concentric isopach thin, up to 85 m thick. A major sediment thick extending from the onshore El Tor area to the Morgan and Badri Fault Zones is also observed in older Stratal Units C and B, but not in the earliest Upper Rudeis Formation Stratal Unit A. In contrast during Stratal Unit G, the Shukeir and Depocentre 5 sediment thicks are more isolated, with no major sediment thicks associated with the El Tor area, or Morgan and Badri Fault Zones.

Depocentre 2, located within the hangingwall of the Frontal Ramadan Fault is shown during Stratal Units A and B to be linked to both Depocentre 5 towards the south, and also Depocentre 3, to the North, which continues to the north and the onshore Abu Durba area. During Stratal Unit C, the link between Depocentres 2 and 5 is interpreted to be broken, whilst the link to Depocentre 3 towards the north is still present. Continuing into Stratal Units F and G of the Kareem Formation, Depocentre 2 becomes increasing isolated. As previously described, Depocentre 3 is interpreted to be N-S orientated and located in the hangingwall of the similarly orientated fault zones bounding the northern part of the Ramadan and Eagle Fault Blocks. This depocentre is interpreted to be present, and connected to the onshore Abu Durba area throughout Upper Rudeis Formation Stratal Units A, B and D, whilst being less pronounced during Kareem Formations Stratal Units F and G.

Two other principle sediment thicks are shown in Figure 5.8 in areas of no or limited available borehole data. Firstly, a consistent sediment thick is shown throughout each of the mapped Stratal Units in the Back Ramadan Basin, as suggested by seismic mapping. Secondly, a less consistent sediment thick, being principally mapped in Stratal Units A and B and potentially Stratal Unit D, but not during Stratal Units F and G is located to the NW of the study area, within the centre of the rift axis. This area of poor data is inferred to be a sediment thick due to observed wells outside of the study area to the NW and is consistent with facies distributions described below. Other notable thickness variations include the consistent principal isopach thins associated

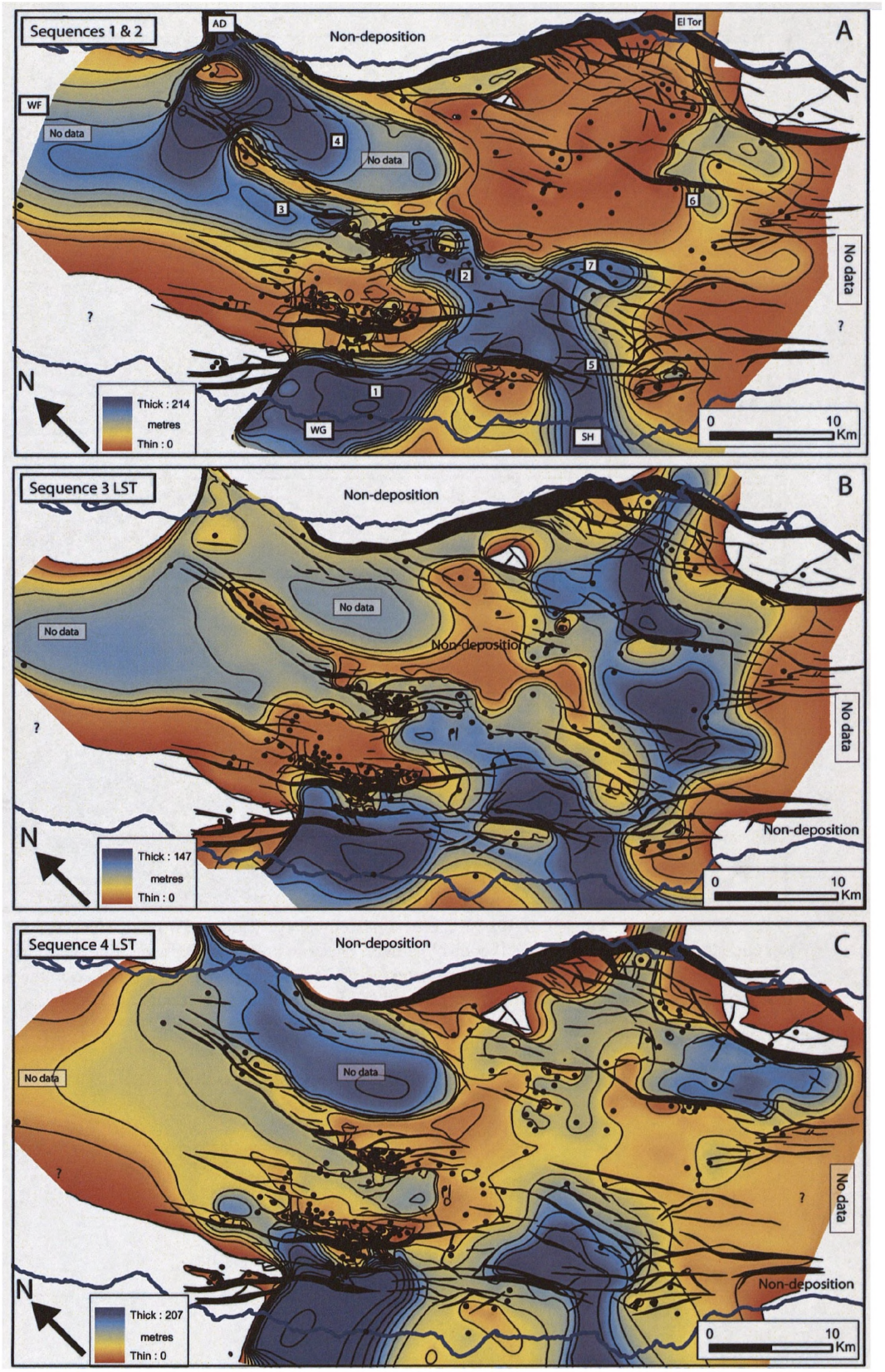

Figure 5.8. Gross interval borehole isopach maps for key Upper Rudeis Stratal Units. Onshore areas highlighted: WF= Wadi Feiran; AD=Abu Durba; WG=Wadi Gharib; SH=Shukeir & El Tor. Seismic derived depocentres 1-7 listed. Refer to Figure 5.7 for fault throw directions.

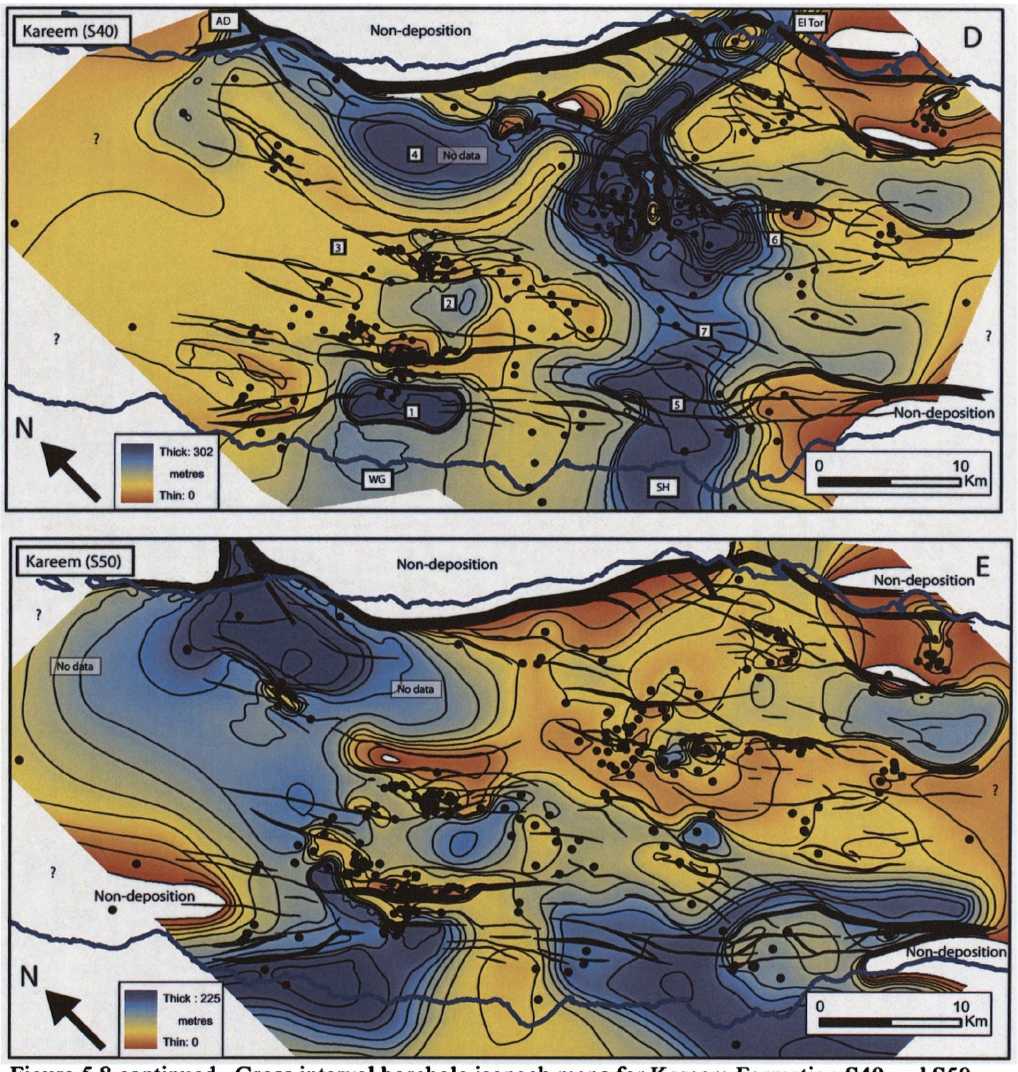

Figure 5.8 continued. Gross interval borehole isopach maps for Kareem Formation S40 and S50 tectono-stratigraphic units with well control shown. Onshore areas highlighted: WF= Wadi Feiran; AD=Abu Durba; WG=Wadi Gharib; SH=Shukeir & El Tor. Depocentres 1-7 identified in the seismic isochores are also listed. Refer to Figures 5.4 and 5.7 for fault throw directions.

with footwall locations and sediment thicks within the adjacent hangingwalls of the SG300, GS306, Badri, Nessim, Younis and Gebel El Zeit Fault Blocks.

5.7.2 Sandstone distribution

Figure 5.9 shows a series of isopach maps documenting the distribution of siliciclastic sandstones for selected stratal units of the Upper Rudeis Formation, and the two stratal units of the Kareem Formation (Fig. 5.6). In large part, these maps for sandstone thickness mirror the trends observed in the gross interval isopachs. Stratal Unit A of the Upper Rudeis Formation displays thickness variations of 0-35 m (Fig. 5.9a). The principle series of isopach thicks are interpreted to be both axial sourced from the NW and the Abu Durba area, incorporating Depocentres 3 and 4. Depocentre 3 is partly controlled by the Eagle and northern Ramadan Fault segments, linking to up to 22 m of sandstone on the present day, uplifted Ramadan Fault Block. Depocentres 2 and 7 are interpreted to be linked by an elongate, 4 km wide E-W trending sandstone thick, up to approximately 23 m thick. However for this interval, there is no evidence for significant sandstones reaching Depocentre 5. Depocentre 1 forms part of a large isopach thick, up to 35 m, sourced from Ras Gharib and extending onto the northern footwall of the Main July Fault. Depocentre 6 is part of a large sediment isopach thick, sourced from the El Tor area. Principal thicknesses here are inferred in the hangingwall of the Nessim Fault, and the southern part of the footwall; contrasting with no reservoir further North within the footwall. Additionally, an isolated, approximately 13 m thick, is observed within the immediate hangingwall of the eastern Coastal Boundary Fault, thinning towards the footwall of the GS306 Fault Block.

Stratal Unit B (Fig. 5.9b), is characterised by a marked influx of sandstones into the rift axis, locally up to 115 m thick having a greater spatial extent, c.f. Stratal Unit A. During this interval, an isopach thick extending from the onshore Shukeir area to Depocentre 5 is interpreted to be present, and is linked axially to the North and Depocentre 2 within the hangingwall of the Ramadan Frontal Fault.

The next major influx of siliciclastic sandstones into the axis is recorded during Stratal Unit D (Fig. 5.9c). Although sandstone thicknesses reach up to 170 m, their spatial extent is generally reduced from that observed during Stratal Unit B. Both the onshore Shukeir area linked to Depocentre 5, and the El Tor sourced thick demonstrate this. During Stratal Unit D the isopach thick associated with Depocentre 1, some 170 m in maximum thickness and still extending onto the onshore Ras Gharib area, shows a marked

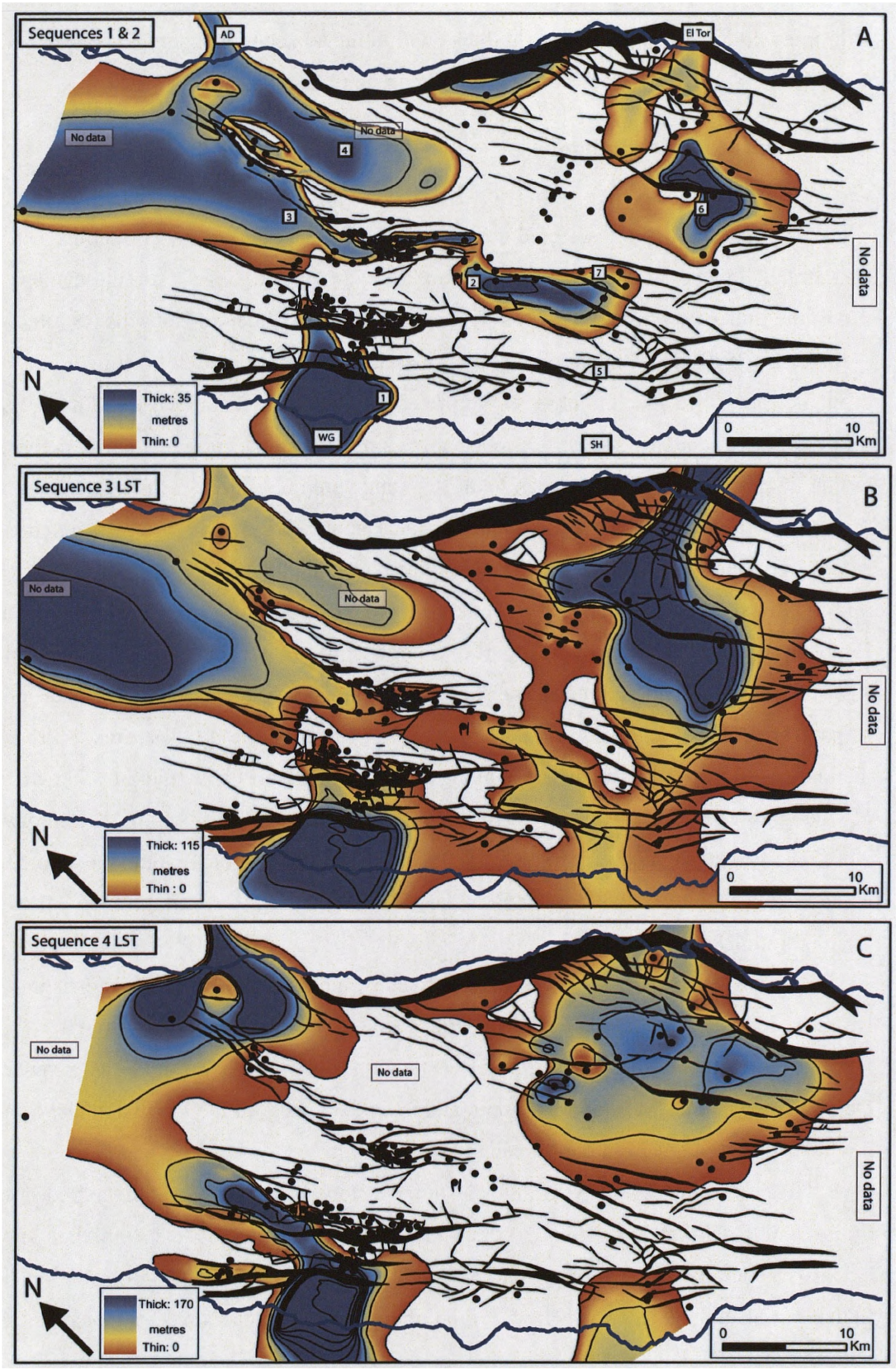

Figure 5.9. Sandstone isopach maps for key Upper Rudeis Stratal Units. Onshore areas highlighted: AD=Abu Durba; WG=Wadi Gharib; SH=Shukeir & El Tor. Position of seismic isochore depocentres 1-7 are shown. Refer to Figure 5.7 for fault throw direction.

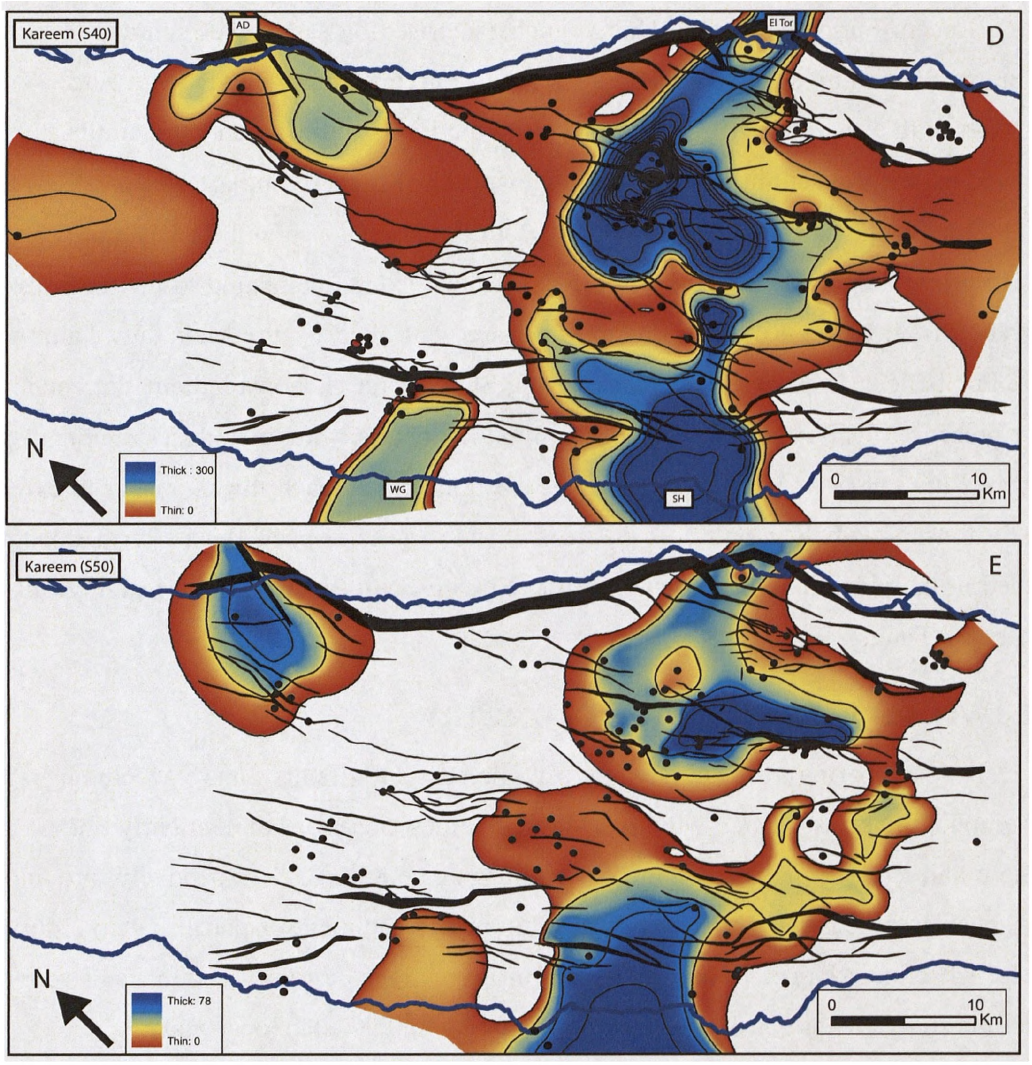

Figure 5.9 continued. Sandstone isopach maps for the Kareem Formation. Onshore areas highlighted: AD=Abu Durba; WG=Wadi Gharib; SH=Shukeir & El Tor. Refer to Figures 5.4 and 5.7 for fault throw direction.

change from Stratal Unit B in that it extends further to the North, linking in with an axial orientated isopach thick to the NW extending from the Abu Durba area.

Kareem Formation Stratal Unit F is characterised by sandstones sourced from the El Tor and Shukeir areas, with thickness variations ranging from 0-300 m (Fig. 5.9d). Two major lobate thicks are observed associated with the Badri and Morgan Fault similar to the observed geometries within the gross interval isopach (Fig 5.8d) and are sourced from the El Tor area on the eastern side of the rift. Both the Ras Gharib and Abu Durba sourced isopach thicks are markedly reduced in thickness and extent, compared to the thicknesses observed in the Upper Rudeis Formation and are controlled by the Main July Fault and Eagle Fault Block respectively. The overlying Stratal Unit G shows a dramatic reduction in the presence of siliciclastic sandstones within the rift axis, with thicknesses ranging from 0-78 m (Fig. 5.9e). Akin to Stratal Unit F, the principal isopach thicks appear to extend into the onshore Shukeir and El Tor areas. The largest isopach thick, 78 m thick, is attained in the immediate hangingwall of the Nessim Fault, linking to the hangingwall of the Morgan Fault.

5.8. LATE RIFT CLIMAX FAULT GEOMETRY

By comparing thicknesses across present-day faults and accounting for stratigraphic thicks associated with depositional bodies close to sediment entry points, the isochore and isopach maps in Figure 5.7 and Figures 5.8 and 5.9 respectively, provide a mechanism to reconstruct the structural evolution and sediment dispersal patterns during the late rift climax Upper Rudeis and Kareem Formations. In this section, fault activity within the study area is considered at both a regional- and detailed local-scale.

5.8.1 Regional-scale fault activity

At a regional-scale, thickness variations associated with the isochore and isopach maps indicate the principal active faults during the deposition of the Upper Rudeis and Kareem Formations. These include segments of the western and eastern Coastal Boundary Fault Zones delineating the rift margin from rift axis. The thick Upper Rudeis and Kareem successions within the hangingwalls to these major fault zones contrast with the present day uplifted footwalls either side of the rift axis, e.g. Gebel Abu Durba and Gebel Zeit (Fig 5.4), which do not display any preserved syn-rift section within the immediate footwall. Within the respective rift margin half-graben basins formed between these major fault zones and the fault zones bounding the rift shoulder, i.e. the El Qaa and Gemsa basins

upon the western and eastern margins respectively (Fig. 5.4), dramatically thinned and condensed section observed at outcrop upon the hangingwall dip-slopes is coeval with thick late rift climax successions encountered in the subsurface within the hangingwall depocentres to the rift bounding fault systems (e.g. Allen et al., 1984; Evans & Moxon, 1986; Smale et al., 1988; Bosworth, 1995; McClay and Khalil, 1998; Khalil and McClay, 2001; Winn et al., 2001).

Within the rift axis and towards the northern part of the of the study area principal active structures interpreted from mapped Upper Rudeis and Kareem Formation thickness variations include: the West and Main July Faults towards the west, associated with Depocentre 1; elements of the July Antithetic, Frontal Ramadan and Ramadan Antithetic Faults associated with Depocentres 2 and 4; northern elements of the Ramadan Fault Block and the Eagle Fault Block controlling the N-S elongate Depocentre 3. Whereas in the southern part of the study area, variable activity upon the Morgan, Badri, Nessim and Amal Faults is interpreted (See Figure 5.4 for locations). In addition the Younis, GS306 and SG300 Fault Blocks are interpreted to have been dominant palaeo-bathymetric highs, with limited or no deposition upon their crestal footwall locations throughout Upper Rudeis to Kareem times.

5.8.2 Detailed fault growth: North July – Ramadan areas

Previous work by Pivnik et al,. (2003) on the July Fault Block for the Upper Rudeis and Kareem Formations determined that the late rift climax to early post rift activity upon individual structures within the study area was episodic in nature. Detailed analysis of thickness variations depicted in each of the isopach maps presented in this study (Figs. 5.8 & 5.9), similarly allow for the episodic evolution of activity upon individual structures to be identified. In this section, the structural evolution of the area immediately to the North of the main July Fault Block (i.e. the study area of Pivnik et al., 2003) and the resultant impact on late rift climax deposition is considered.

North July-Ramadan area

The north July-Ramadan area, located towards the northwest of Morgan accommodation zone, (Figs. 5.4 and 5.10) is approximately some 200 km^2, with the present day structural configuration characterised by the northern most parts of the eastwardly dipping North July, Safa-Mawa and Ramadan Fault Blocks (Fig. 5.11). The North July Fault Block, a northern extension of the main July Fault Block (Pivnik et al.,

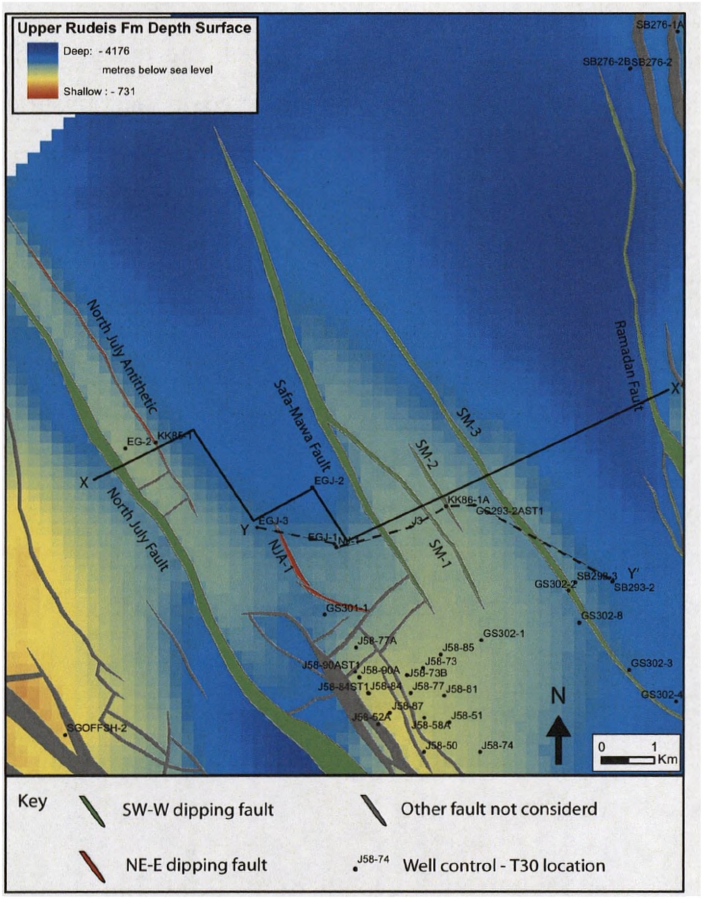

Figure 5.10 Top Upper Rudeis Formation depth surface (Surface T30) within the North July area (located in Figure 5.4). Line X-X' is the location of the seismic section in Figure 5.11. Line Y-Y' is the location of the well correlation in Figure 5.12.

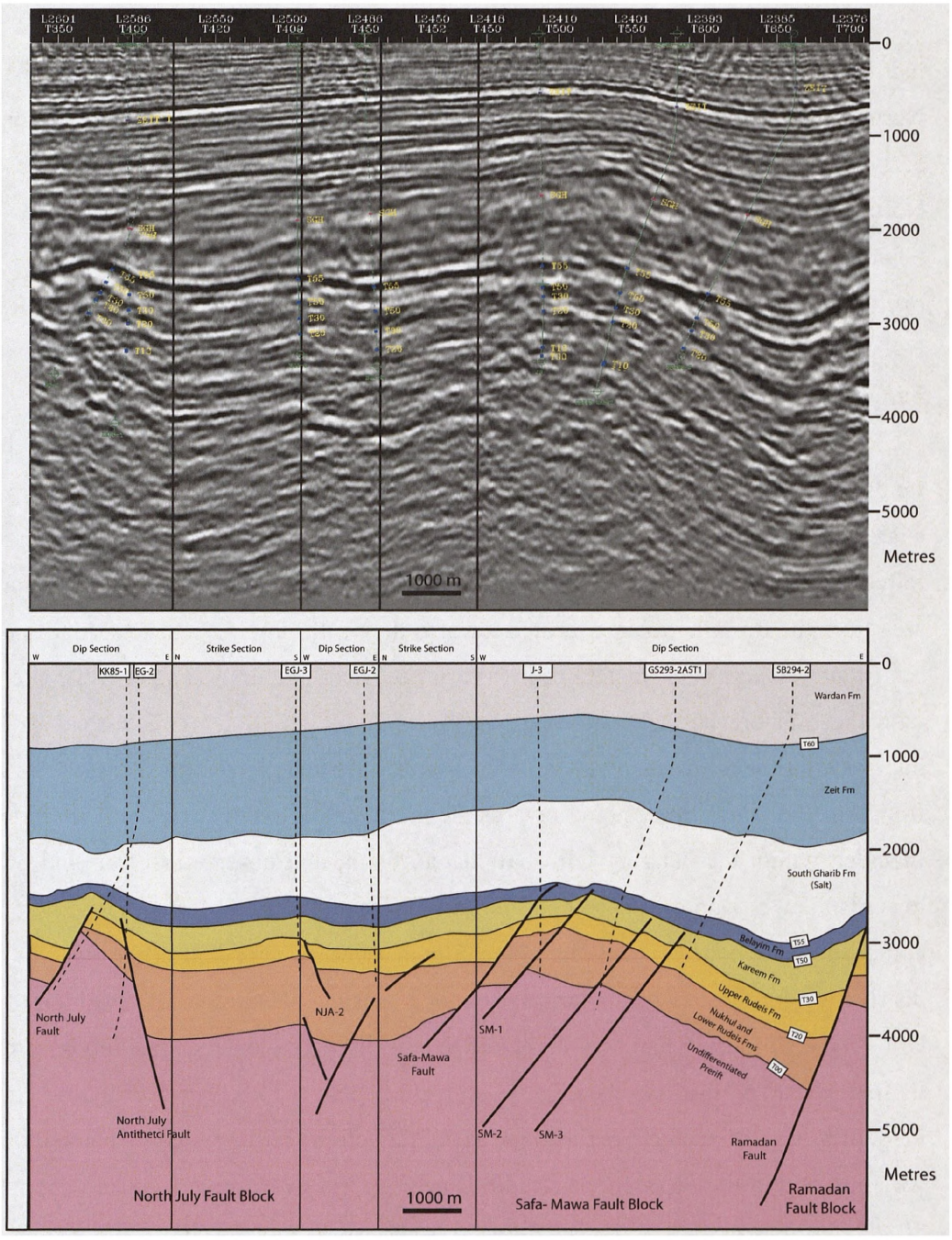

Figure 5.11 Composite dip and strike seismic lines across the North July and Safa-Mawa Fault Blocks. Line of section shown in Figure 5.10.

2003), is approximately 3.7 km wide and bounded to the west by the westward dipping North July Fault, with a 720 m wide horst block at its crest, bounded to the east by the North July Antithetic Fault. This antithetic fault displaces the pre-rift syn-rift contact by 550 m and controls the local thickness of the Lower Rudeis Formation. To the east of the North July Fault Block, the Safa-Mawa Fault Block is approximately 5.5 km wide and bounded by the Safa-Mawa Fault. The Lower Rudeis to Kareem Formations show an overall thickening trend into this fault and additionally the bounding fault of the Ramadan Fault Block to the east, whereas little thickness variation is observed across three synthetic intra-block faults (SM-1, SM-2 and SM-3).

During Stratal Unit A of the Upper Rudeis Formation, two separate submarine sandstone packages are recognised within the area (Fig 5.12). The lower package, characterised by progradational submarine fan sandstones (Facies B1), is interpreted to reflect the distal part of a prograding highstand submarine fan system into the North-July area from the Ras Gharib area located towards the south (Fig. 5.4). The second submarine sandstone package is characterised by a series of sheet-like units (Facies B2i), intercalated with the offshore basinal mudstones of Facies Association A. This second package is interpreted to be a lowstand deposit of Sequence 2 above surface RS-2 (Fig. 5.3), sourced from the Abu Durba entry point towards the north, and is axially orientated north to south, focussed within the hangingwall of Ramadan Fault, and observed to thin and pinch-out towards the west and the present day footwall crest of the Safa-Mawa Fault (Fig. 5.12). A composite sandstone isopach map for Stratal Unit A (Fig. 5.13a) shows the spatial distribution for these two submarine sandstone packages. During the deposition of Stratal Unit A, the North July Fault is interpreted to have been active; no deposition is observed in its immediate footwall (wells KK85-1 and EG-2, Fig. 5.14a). The North July Antithetic Fault may have been active at this time, as earlier activity is suggested by marked thickness variation within the older Lower Rudeis Fm (Fig 5.11). However with no deposition of Stratal Unit A recorded in the hangingwall to the North July Antithetic Fault (Fig. 5.14a), suggesting that the local bathymetry was dominated by longer-wavelength uplift of the footwall to the North July Fault. The highstand depositional system sourced from the Ras Gharib shows no apparent thickness change across the Safa-Mawa Fault, suggesting that the southern part of this fault was also inactive at this time (5.12).

Upper Rudeis Formation Stratal Unit B, which represent the lowstand deposits of Sequence 3 (Fig. 5.3) records the pronounced basinal shift of the two depositional systems and facies associations previously identified in Stratal Unit A into the North July-Ramadan

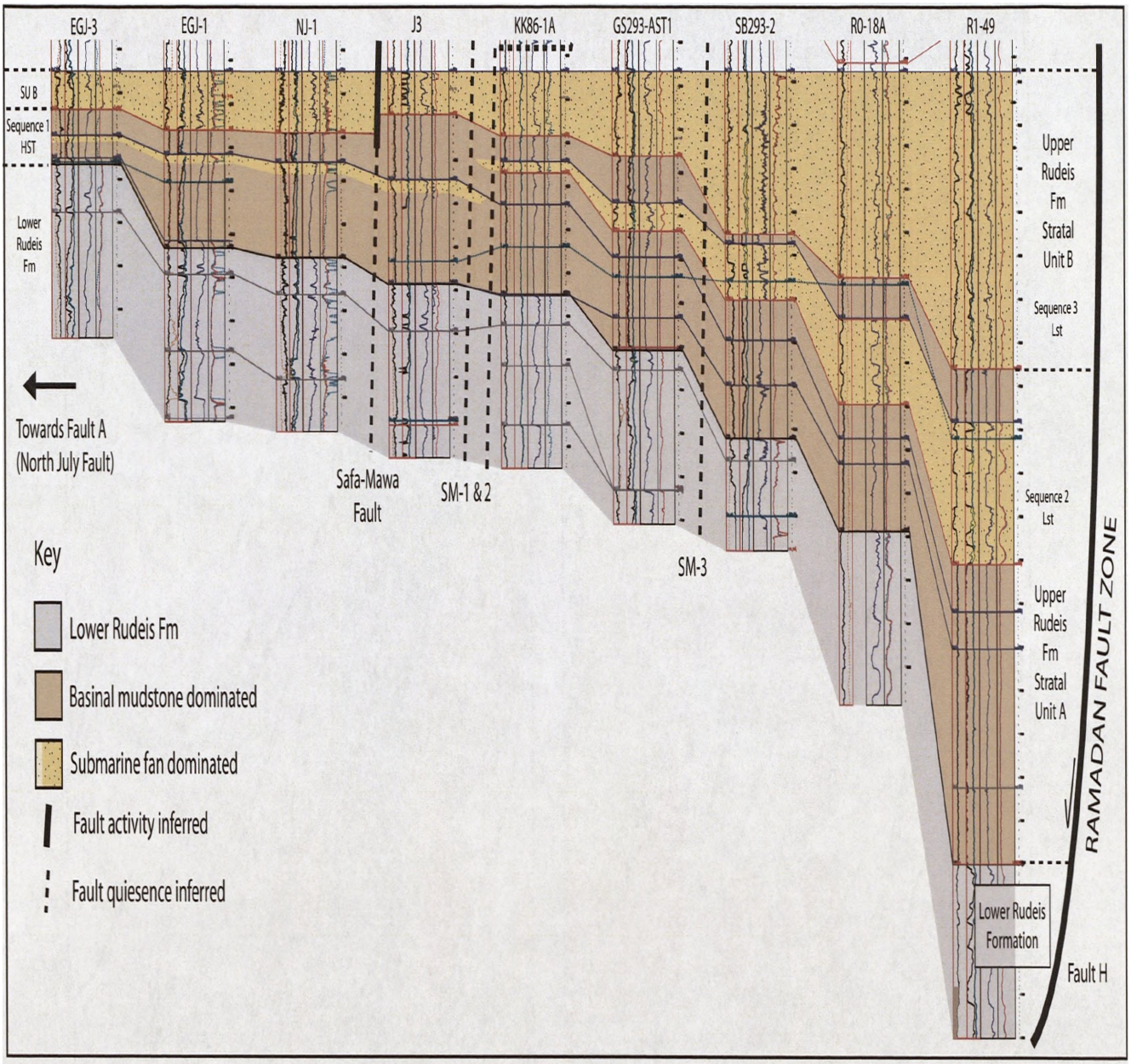

Figure 5.12. Dip orientated well correlation panel for Stratal Units A and B of the Lower Rudeis Formation in the North July-Ramadan area. See Figure 5.10. for location.

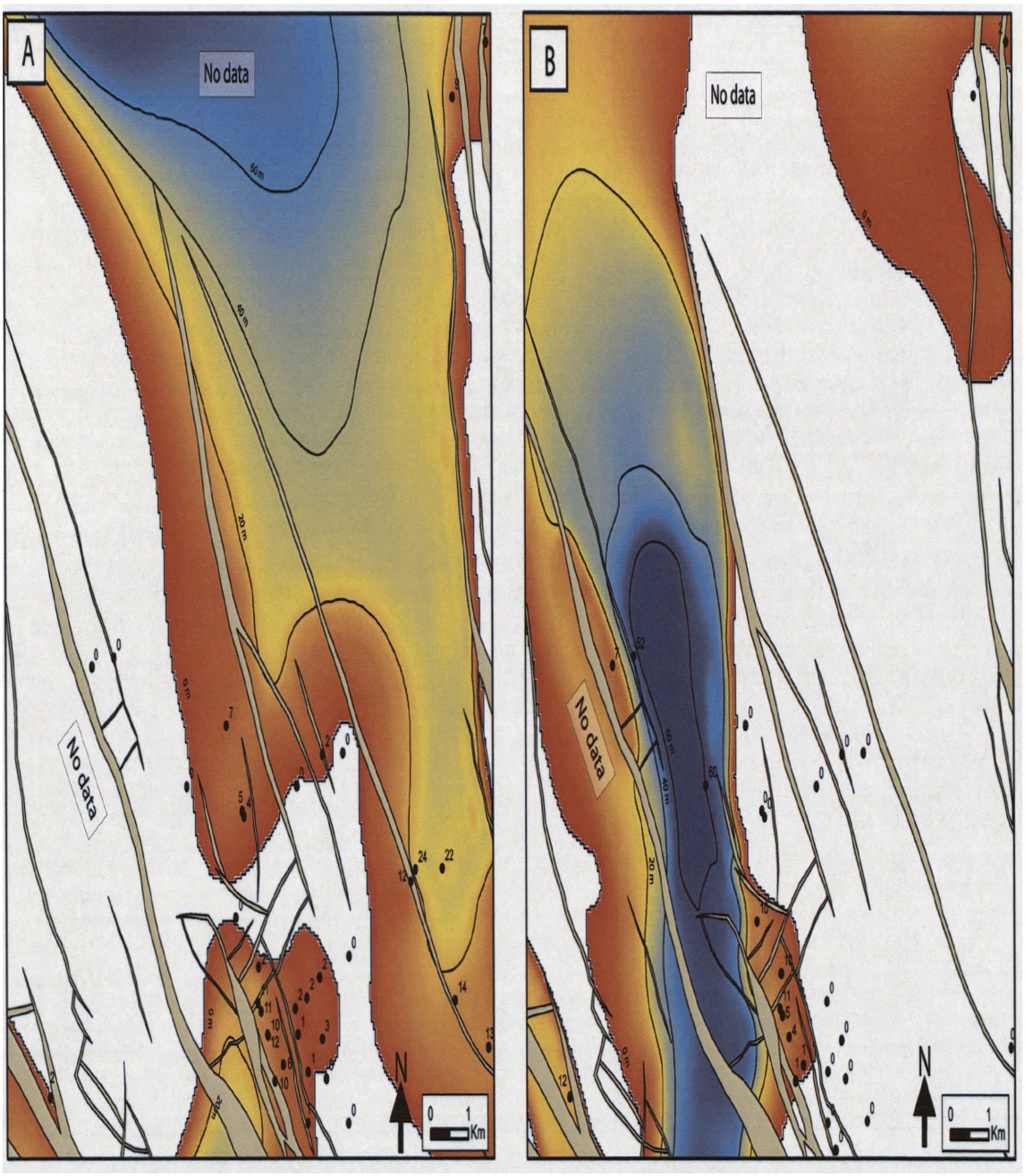

Figure 5.13. Sandstone isopach maps for the North July-Ramadan area: A) Upper Rudeis Stratal Unit B; B) Upper Rudeis Stratal Unit D. Contour interval 20 m.

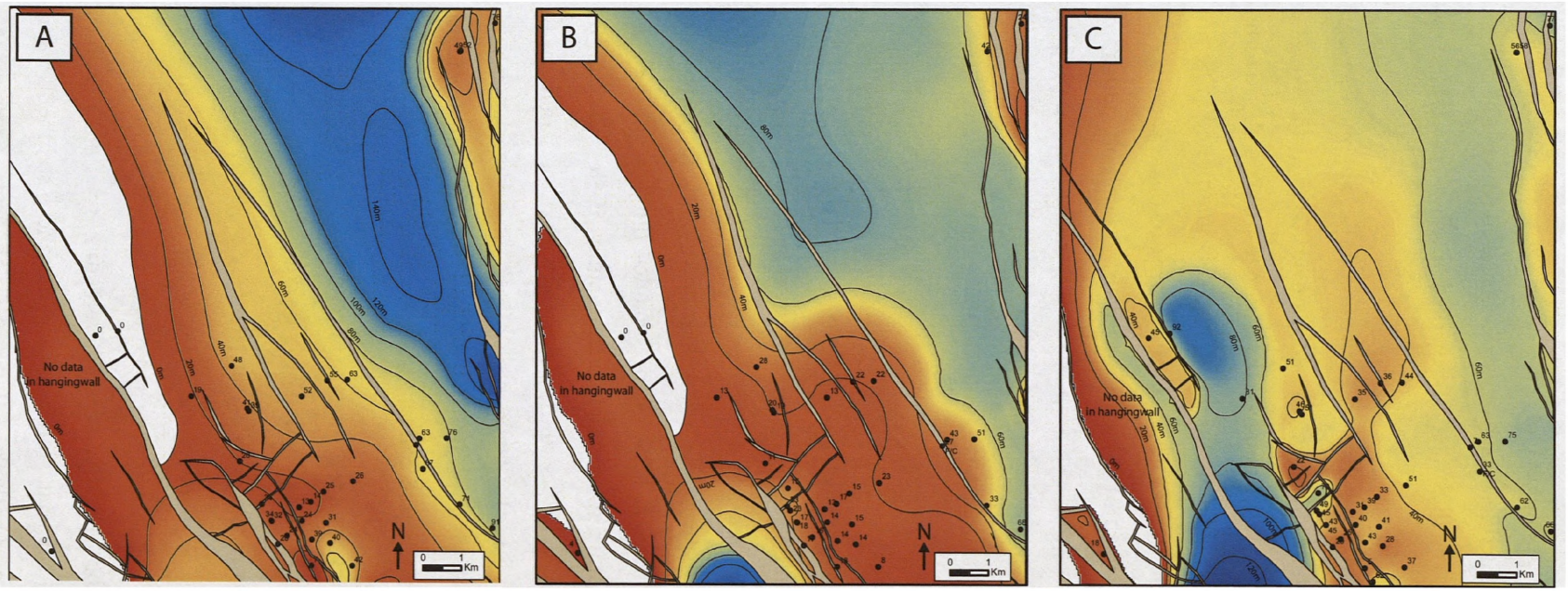

Figure 5.14. Gross interval isopach maps for the North July-Ramadan area: A) Upper Rudeis Stratal Unit A; B) Upper Rudeis Stratal Unit B; C) Upper Rudeis Stratal Unit D. Contour interval 20 m.

area (5.14b). With respect to fault activity, thickness variations suggest that the North July, and Ramadan Faults continued to be active, whilst the Safa Mawa Fault is shown in Figure 5.12 to have become active, illustrated by marked thickness variations across from its hangingwall to footwall.

Stratal Unit D of the Upper Rudeis Formation, reflecting the lowstand of Sequence 4 (Fig. 5.3) records a variable renewal of sediment influx into the North July-Ramadan area (Fig. 5.13c). The axial depositional system sourced from the Abu Durba entry point is not encountered within any wells within the area, and is interpreted to be not as regionally extensive as during Stratal Unit B. Thus, a limited area of distal submarine fan deposition is postulated towards the north of the area, but with no borehole constraint (Fig. 5.13c), whereas the Ras Gharib sourced system in contrast shows a marked progradation into the area. Activity upon the North July Antithetic Fault and an additional minor antithetic fault, NJA-2, is interpreted during the deposition of Stratal Unit D, and controlled the main locus of submarine fan sandstone facies deposition (Figs 5.13c and 5.14c). The sandstones of Stratal Unit D are interpreted to thin and onlap towards the footwall crest of the antithetic minor NJA-2 Fault, as suggested by well GS301-1 (Fig 5.14c), which acted as a topographic barrier diverting sediment transport away from the immediate hangingwall of the Safa-Mawa Fault, and focussed it into the hangingwall of the North July Antithetic Fault. This switching of the primary depocentre for Stratal Unit D towards the west away from the hangingwall of the Safa-Mawa Fault, enabled the deposition of distal submarine sandstone facies upon both the crestal horst structure of the North July Fault Block, defined by wells EG-2 and KK85-1 and potentially within the hangingwall of the North July Fault (Figs 5.13c and 5.14c). This contrasts with the earlier deposited Stratal Units 1 and 2 which saw the crestal footwall of the North July Fault characterised by either sediment starvation, or very limited condensed deposition.

5.9. TECTONO-SEDIMENTARY EVOLUTION OF THE MORGAN ACCOMMODATION ZONE DURING RIFT CLIMAX

Gross interval and sandstone isopachs, (Figs 5.8 and 5.9) are strongly suggestive of the existence of regional-scale depositional systems transporting sediment across from the rift margin to the rift axis which were focussed within the Morgan Accommodation Zone during the deposition of the Upper Rudeis and Kareem Formations. Both the volume and composition of the siliciclastic sandstones suggest that these sediments were derived from the hinterland provided by the flanks or shoulders of the rift, rather than from locally

derived uplifted fault blocks within the rift. In this section, firstly the key sediment entry points into the rift axis are described, and the controls upon their location discussed. Secondly, the evidence for fault activity is integrated to provide a model for the late rift climax tectono-sedimentary evolution of the Morgan Accommodation Zone

5.9.1 Sediment entry points and source areas

Major sediment entry points into the rift axis can be identified based on the mapped isopach thicks within the proximal areas of the rift axis (Figures 5.8 and 5.9), gross thickness data for both borehole and fieldwork datasets within the adjacent rift margin, and modern day drainage and bathymetric patterns. Four principal sediment entry points from the rift margin into the rift axis are identified within the study area located at the Shukeir, Ras Gharib, El Tor and Abu Durba areas (Fig. 5.4). An additional fifth entry point is suggested to be located at Wadi Feiran (Fig 5.1), located outside of the study area to the north, to account for a significant southward axial flux of sand-grade sediment documented in Figure 5.9.

Each of the four sediment entry points, two on each side of the rift, are interpreted to be largely structurally controlled. The location of the Shukeir and El Tor entry points, on the western and eastern margins respectively, are controlled by activity upon the El Zeit and Araba Faults respectively. Principal sediment thicks suggested by both onshore well and fieldwork datasets (e.g. Evans & Moxon, 1986; Smale et al., 1988; Bosworth 1995; Winn et al., 2001) within the rift margin have been extended offshore into the rift axis in this study, linking with significant gross interval isopach thicks and sandstone distributions (Figs. 5.8 & 5.9).

The Ras Gharib sediment entry point, located to the north of the Shukeir entry point on the western rift margin, is located towards the southern most part of the central dip province. The area between the two sediment entry points forms the onshore expression of the Morgan Accommodation Zone, forming a region characterised by fault polarity reversal, and thus an area of lower displacement associated with a major basement eastwards dipping structural nose, forming a local structural high in the Gebel Gharamul area (Coffield and Schamel, 1989). This interpretation of a major entry point at Ras Gharib is consistent with previously published sandstone isopachs for the Upper Rudeis Formation within subsurface of the rift margin, which indicate an overall east to west transport of sediment from the rift shoulder (Allen et al., 1984), and which are interpreted in this study to extend into the rift axis in the area of Depocentre 1 (Fig 5.7).

Both the fourth and fifth sediment entry points identified are located on the eastern rift margin, with the geometry of isopach thicks suggesting axial sediment transport towards the south. The downthrown side of the NE-SW trending Abu Durba transfer fault within the Coastal Boundary Fault Zone (e.g. Moustafa & Khalil, 1987; McClay & Khalil, 1998; Moustafa, 2002) is observed to have acted as a principal sediment entry point, focussing sediment into an axial fairway associated with the Eagle and Ramadan Fault Blocks. Further axially transported sediment associated with this series of isopach thicks is interpreted to be sourced via another major entry point, potentially located at Wadi Feiran (located on Fig. 5.1) (e.g. El-Heiny & Enani, 1990), although this is poorly constrained by limited available borehole information.

5.9.2 Tectono-sedimentary evolution

In this section, observations of thickness and facies variability for the mapped stratal units of the Upper Rudeis and Kareem Formations are integrated with interpretations for palaeo-structural activity and the location and extent of regional depositional systems entering the axis of the Suez. Through a resultant set of palaeogeographic maps, a model for the linked tectono-stratigraphic evolution of the Morgan Accommodation Zone during the latter stages of the rift climax phase is presented.

Upper Rudeis Formation

Following the main rift climax phase reflected in the basinal dominated transgressive sequence sets of the Lower Rudeis Formation (Fig. 5.3), the Upper Rudeis Formation in the Morgan Accommodation Zone was characterised by a series of major submarine fan depositional systems entering the axis of the rift via a number of structurally-controlled sediment entry points. The volume and siliciclastic nature of the deposits indicate that the primary provenance of these depositional systems was uplifted Precambrian basement and sandstones of the pre-rift Nubia Formation upon the rift shoulder (Fig 5.1), rather than from individual uplifted fault blocks within the rift, characterised by an uppermost pre-rift succession of Eocene carbonates. Thus in contrast to the other locations within the rift axis, large thicknesses of calcarenitic syn-rift sediments are not observed (c.f. the October Fault Zone, Chapter Four). Once within the rift axis, sediment transport and submarine fan deposition was controlled by bathymetric gradients associated with the episodic growing and linking of faults with deposition concentrated within hangingwall depocentres.

The extent of sediment influxes associated with the highstand of Sequence 1 and ensuing lowstand of Sequence 2, mapped as composite Stratal Unit A, are shown in Figure 5.15a. The depositional systems extending from western margin Shukeir and Ras Gharib sediment entry points are associated with submarine fan facies associations which are shown to have extended back into the western rift margin in the previous subsurface studies (e.g. Allen et al., 1984; Smale et al., 1988), with more proximal, small catchment fan-deltas potentially being located within the rift margin, juxtaposed to the fault segments defining the rift border. Examples of these facies as documented in both the Lower and Upper Rudeis Formations within the eastern rift margin at Gebel Gushea (e.g. Young et al., 2002) Wadi Baba (e.g. Sharp et al., 2000a) and Abu Alaqa (e.g. Gawthorpe et al., (1990); Gupta et al., (1999).

The Ras Gharib submarine fan depositional system extended transversely across from hangingwall to the footwalls of a series of active faults associated with present-day July and Ramadan Fault Blocks, suggesting that the rate of sediment accumulation was often equal to or greater than the rate of fault-generated accommodation space. In contrast to the Ras Gharib area, erosion and bypass is inferred in proximal part of rift axis of the Shukeir entry point, with submarine fan facies being contained within the hangingwall of a series of active segments of the western Coastal Boundary Fault Zone. This submarine fan extended towards the north onto the Ramadan Fault Block, amalgamating with the sheet facies of an axial submarine fan system sourced from the Abu Durba and ?Wadi Feiran entry points. The El Tor entry point was also active at this time, with more distal sheet-like facies extending westwards towards the Morgan and Badri areas, and also towards the south into the hangingwall of the active Younis Fault.

During the lowstand of Sequence 3 (Stratal Unit B), each of the active depositional systems in Stratal Unit A shifted significantly basinward into the centre of the rift axis and attained their maximum extent in the Upper Rudeis Formation (Fig. 5.15b). Proximal fan facies are observed to extend into the Morgan and Badri areas from the El Tor entry point, potentially reflecting a reorganisation of drainage pathways within the eastern rift margin as a response to major fall in relative sea-level. The El Tor entry point possibly provided an outlet into the rift axis for sediment being transported axially down the southern axial plunge of the rift margin El Qaa Fault Block. This sediment was likely to be sourced from extensive drainage systems in the rift shoulder and fed via proximal fan deltas such as at Abu Alaqa, which show a marked switch from aggradational to progradational stacking patterns with the switch from the Lower to Upper Rudeis Formations (e.g. Gawthorpe et al.,

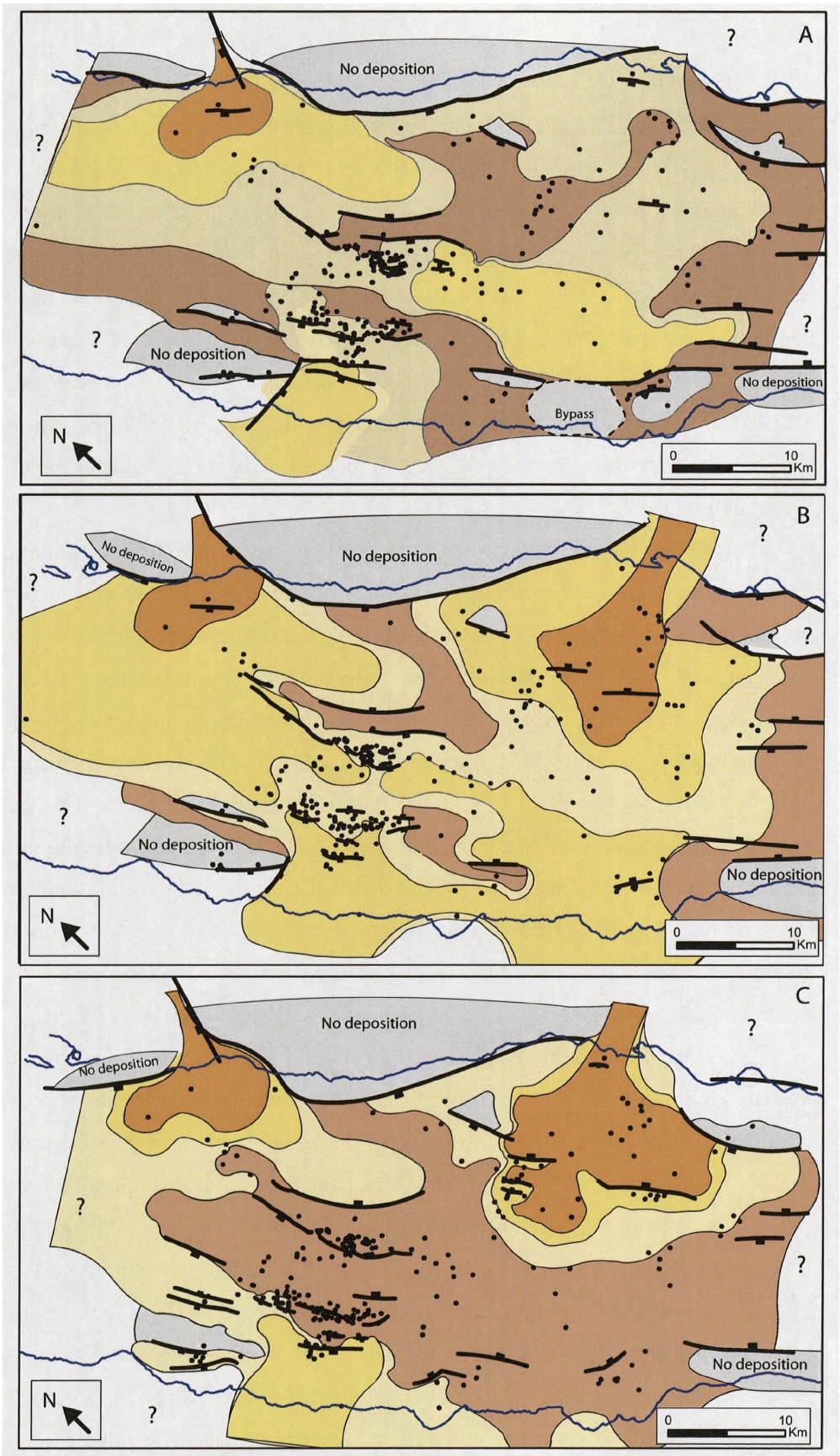

Figure 5.15. Palaeogeographic maps for the Upper Rudeis and Kareem Formations. A) Upper Rudeis Stratal Unit A; B) Stratal Unit B; C) Stratal Unit D. (c.f. Figure 5.3). Key to environments on page 174.

1990; Gupta et al., 1999). The Abu Durba and Shukeir entry points during the lowstand of Sequence 2 fed axial orientated submarine fan depositional systems into the centre of the rift axis, centred upon the area of the present day Ramadan Fault Block, whilst the Ras Gharib system continued to supply sediment transversely towards the present day July Fault Block. Here, the rate of sediment supply consistently outpaced the rate of fault displacement associated with the West July Fault and blanketed the footwall of the fault block with mid to distal submarine fan sandstones (Fig 5.15b).

Stratal Unit C characterised a rift-axis wide switch to deposition of the fine-grained offshore basinal mudstones of Facies Association A during the transgressive to highstand systems tracts of Sequence 3, with a similar marked facies shifts to fine-grained mudstones recorded within the western rift margin in the subsurface study of Allen et al., (1984). The ensuing lowstand deposits of Sequence 4 (Stratal Unit D) are characterised by a renewed basinward shift of depositional systems into the rift axis, albeit at a lower magnitude that during Stratal Unit B. During Stratal Unit D, (Fig. 5.15c) sediment supply associated with the Shukier entry point was switched-off in contrast to the Abu Durba and El Tor entry points, which are associated with more extensive proximal submarine fan deposits. In the case of the El Tor sourced system, proximal fan deposits are observed in the hangingwalls of the Morgan, Badri, Nessim and Younis Faults. The Ras Gharib-sourced depositional system was at this time contained within the hangingwall of the now active, present-day main bounding fault of the July Fault Block, as the rate of fault-generated accommodation space along this structure outpaced sediment supply (Pivnik et al., 2003). This resulted in the diversion of this depositional system into North July - Ramadan area and into depocentres formed by the active North July, North July Antithetic and Safa-Mawa Faults.

Kareem Formation

During the lower part of the Kareem Formation, (Stratal Unit F), influx of clastic material into the rift axis continued from the Ras Gharib, Shukeir, Abu Durba and El Tor sediment entry points (Fig 5.15d) With respect to the transverse depositional system sourced from the El Tor entry point, a major fan-delta is observed to have extended into the rift axis at this time, with two principal fan lobes centred around the area of the present-day Morgan and Badri Fault Zones, within both hangingwall and footwall locations. The shallowing of water depths in the Morgan – Badri area suggested by the presence of this major fan-delta was probably a result of the combination of: (1) the reduction of sea-floor bathymetry due to earlier submarine fan deposition reducing differential sea-floor

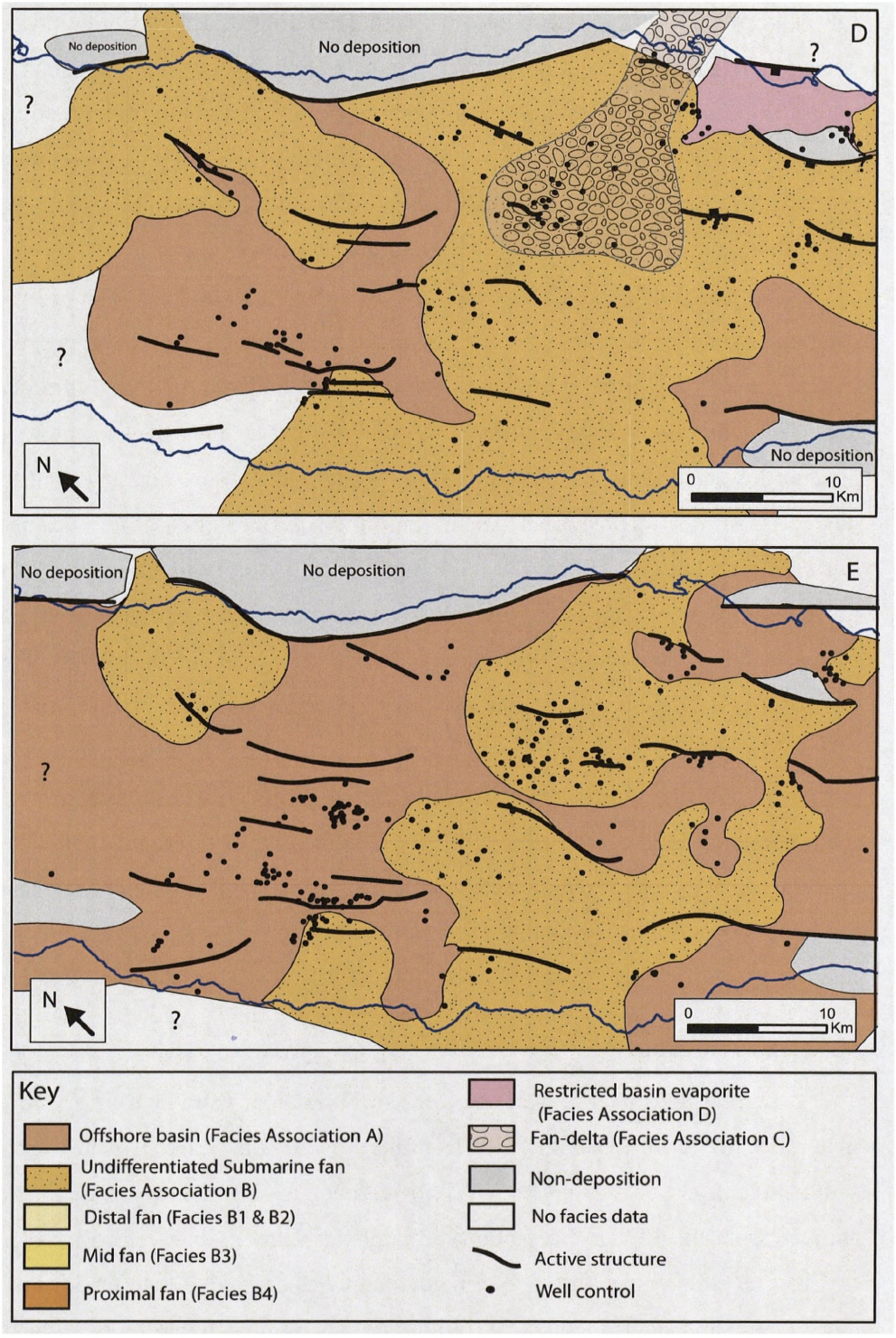

Figure 5.15 continued. Palaeogeographic maps for the Kareem Formation, D) Stratal Unit F; E) Stratal Unit G

bathymetry, suggesting that the rates of displacement of active faults at this time were lower than rates of sediment supply similar to the July Fault block example discussed previously, and (2) the regional fall in relative sea-level allowing for a fan-delta to prograde across a stable slope.

Adjacent to El Tor entry point to the south, upon the Younis Fault Block, prolonged restricted basinal conditions are documented by stacked packages of anhydrite Facies Association C. This restriction may have been caused by the marked progradation of the Morgan fan-delta effectively closing off the hangingwall dip-slope down-dip of the Younis footwall crest from more open marine conditions within the rift axis. Similar restriction and development of restricted evaporites is observed in the Kareem Formation in the rift margin to the north of Wadi Sidri. The Abu Durba entry point continued to be active, and like the western margin entry points associated with the Ras Gharib and Shukeir areas, appear to be characterised by a broad amalgamated areas of submarine fan sandstone deposition.

Following the extensive influx of clastic material into the rift axis during the Stratal Unit F, interpreted to reflect the lowstand period of Sequence 5, the ensuing Stratal Unit G is interpreted to reflect a marked switch to overall transgressive to highstand conditions (Fig. 5.3). Stratal Unit F is characterised by an increase in the extent of the deposition of finer-grained offshore basinal mudstones and a marked restriction in the spatial extent of the main coarser-grained submarine fan depositional systems, with the El Tor sourced depositional system showing a change from fan-deltaic to submarine fan facies (Fig.5.15e).

5.10. DISCUSSION

Previously accepted conceptual models for distribution of syn-rift depositional systems and resultant stratigraphic architectures have cited major structural accommodation zones as having a significant impact in the transfer of sediment across differing half-graben sub-basins within a rift (e.g. Lambaise and Bosworth, 1995; Gawthorpe and Leeder et al., 2000). However, most detailed studies looking at this tectonic setting have focussed on the structural style of accommodation zones, with little work done on the sedimentological and stratigraphic variability of active depositional systems within a marine rift. This chapter addresses this by using an extensive subsurface dataset to document the thickness, facies and stratigraphic variability within the major, rift wide Morgan Accommodation Zone within the Suez Rift. This has implications for

understanding the variable controls upon syn-rift sedimentation in an area of relatively reduced fault controlled subsidence in a rift.

5.10.1 Structural control

The results of this study show that during the latter stages of the climax phase of the rift event during the late Early to Middle Miocene, a series of regionally extensive depositional systems prograded into the rift axis within the Morgan Accommodation Zone via a series of structurally controlled sediment entry points. Compositionally, these regional fluxes of sediment into the rift were linked to the progressive unroofing of a major hinterland associated with the rift shoulder, rather than from isolated or uplifted fault blocks within the rift itself. Uplifted local fault blocks of Eocene pre-rift carbonates are likely to have provided an additional source of sediment flux; however they appear to not be volumetrically significant in this setting. This may reflect the more distributed nature of faulting within the accommodation zone, i.e. with numerous lower displacement faults contrasting with the larger, rotated fault blocks that might be expected in an adjacent domain characterised with a more classical half-graben geometry.

The underlying structure of the accommodation zone largely controlled the position of the regional depositional systems identified in this study. The locations of the sediment entry points from the rift margin to axis typically remained consistent throughout the studied interval and were linked to areas of displacement minima, typically towards the tips of major faults zones forming the boundary between the rift margin and central axial trough. Moreover, subsequent sediment transfer pathways within the rift axis were controlled by the bathymetric gradients and available accommodation space generated by the underlying and evolving structural template, consistent with traditional models for the distribution of syn-rift sediments in areas of fault-controlled subsidence. Akin to several other published examples of rift basins, subsided hangingwalls provided primary depocentres, whereas sediment was routed around areas of relative uplift (e.g. Leeder et al., 1991; Leeder and Jackson, 1993). The evolution of this spatial structural control, linked to the growth and linkage of normal faults has been shown in previous studies to play a profound control on the temporal variability of syn-rift sediments. These studies have typically documented the change from numerous, low displacement faults with isolated depocentres to fewer, larger, through going fault zones with larger, coalesced depocentres during the transition from rift initiation to rift climax (e.g. Cowie et al., 2000; Davies et al., 2000; McLeod et al., 2000; Sharp et al., 2000a; Young et al., 2001). The detailed example

discussed in this chapter for the North July-Ramadan area similarly shows the role that evolving fault activity can play on coeval depositional systems. In this case, the shifting onset and death of activity associated with a series of fault zones during the latter stages of the rift provided a profound impact on the distribution of Upper Rudeis depositional systems. Moreover, it highlights the importance of discriminating the syn-rift succession into the highest resolution stratal units possible. Investigating the variability of the Upper Rudeis Formation in the North July-Ramadan at a larger, biostratigraphic tectono-sequence level (e.g. S30 *sensu* Wescott et al., 1996; Krebs et al., 1997), might fail to recognise subtle thickness and facies variations that reflect change in structurally-generated relief.

5.10.2 The interplay of additional controls

In addition to the role provided by structure, the regionally extensive nature of the key stratal surfaces identified and the associated consistent basinwide shifts in facies and depositional systems is suggestive of a role for a more rift wide control upon sedimentation, interpreted to reflect changes in relative sea-level, with marked periods of sea-level fall and rise. Periods of relative sea-level fall are thought not to be typically observed in areas of fault-controlled subsidence, given that subsidence rates may outpace rates of sea-level fall (Gawthorpe et al., 1994; Howell and Flint, 1996). However, with the overall reduction in rates of fault activity associated with the late climax phase of the rift, coupled with more distributed deformation within an accommodation zone setting, this is a plausible scenario. Any sea-level changes are also likely to have extended into the rift margin, and may be expected to result in a reorganisation of drainage systems there. This is potentially demonstrated with marked changes in the stacking patterns of proximal fan-delta depositional systems being observed along the eastern rift margin between the Lower and Upper Rudeis Formations (e.g. Wadi Sudr, unpublished; Gebel Abu Alaqa, Gawthorpe et al., 1990 and Gebel Gushea, Young et al., 2000, 2002).

These fluctuations in sea-level acted to control the timing and magnitude of sediment fluxes into the rift. This resulted in a complex interplay between sediment supply rates and fault-generated accommodation space within several depocentres of the rift axis. Typically, major depositional systems such as those transported from the El Tor and Ras Gharib sediment entry points, and which were orientated transversely towards the strike of active fault zones, were periodically associated with rates of sediment accumulation that outpaced fault-displacement. Thus for locations such as the July and Morgan – Badri areas during lowstand periods such as Stratal Unit B and F, coarse-grained submarine fan to fan-

delta deposition was able to prograde across from hangingwall locations into the immediate footwall. During periods of reduced sediment supply, active structures prevented sediment reaching footwall locations, with the resulting deflection of the sediment transport pathways, e.g. during the lowstand of Stratal Unit D in the area of the Main July Fault. In contrast, axially orientated sediment transport, such as that associated with the depositional systems sourced from the Abu Durba entry point, may be continually localised to hangingwall depocentres.

CHAPTER SIX

SYN-RIFT SEDIMENTATION WITHIN RIFT ACCOMMODATION ZONES: AN EXAMPLE FROM THE ONSHORE ZAFARANA ACCOMMODATION ZONE, SUEZ RIFT, EGYPT

CHAPTER 6

SYN-RIFT SEDIMENTATION WITHIN RIFT ACCOMMODATION ZONES: AN EXAMPLE FROM THE ONSHORE ZAFARANA ACCOMMODATION ZONE, SUEZ RIFT, EGYPT

6.1. ABSTRACT

This chapter investigates the variability of facies, thickness and stratal surfaces associated with the rift initiation to late rift climax succession within the proximal, rift margin component of a major rift wide structural accommodation zone. The results of sedimentological analysis of principle syn-rift facies within the study are described and interpreted, allowing for a depositional model based upon genetic-relationships to be developed. The temporal distribution of facies observed is consistent with traditional models for syn-rift development which link the transgression from continental or shallow marine facies to increasingly deeper marine facies to the change from rift initiation to rift climax phases. The subsequent late rift climax stage is marked by a series of basinward shifts to coarser-grained, more proximal depositional systems linked to falls in relative sea-level following erosion and bypass. The response in this relatively low accommodation setting is for the amalgamation of key stratal surfaces, forming a significant composite unconformity. With respect to the variability of facies, thickness and stratal units adjacent to evolving structures, this chapter highlights how the magnitude and timing of fault activity within a structural accommodation zone may 'lag' in comparison to a more classical half-graben model. This may result in the presence of structures and associated stratigraphic responses in the latter stages of the rift development, which are otherwise thought to typically occur earlier in the evolution of the rift.

6.2. INTRODUCTION

Intracontinental rift basins are generally characterised by domains in which all or most major normal faults and intervening tilted fault blocks show a consistent dominant dip direction. Well documented examples include the North Sea rift (e.g. Roberts et al., 1990), Gulf of Thailand Rift (e.g. Kornsawan and Morley, 2002) and the Suez Rift, (e.g. Moustafa, 1976, Patton et al., 1994). Changes in the polarity of these structural dip domains typically occur across diffuse zones, 5 - 30 km wide, which may extend across an entire rift (e.g. Moustafa, 1976, Patton et al., 1994). These diffuse zones may be characterised by faults with

reduced displacements in comparison to those in the adjacent dip domains, increased observations of fault propagation folds associated with blind (i.e. non-surface breaking) faults and overlapping fault zones of opposing dip polarity (e.g. Coffield and Schamel, 1989; Morley et al., 1990). The nomenclature for these zones is varied, they are referred to as transfer zones (e.g. Moustafa, 1976; Morley, 1990), accommodation zones (e.g. Bosworth, 1985; Rosendahl et al., 1986; Ebinger, 1989; Faulds and Vaga, 1998; Younes & McClay, 2002) or fault-domain boundaries (Schlische and Withjack, 2008). In this chapter, the term structural accommodation zone is preferred as it implies no sense of timing with respect to activity along individual faults (Morley, 1995, Peacock et al., 2000).

Numerous studies have investigated the linkage between fault growth and thickness and stratigraphic variability of coeval depositional systems adjacent to major normal fault zones (e.g. Gawthorpe et al., 1994; Leeder and Gawthorpe, 2000; Dawers & Underhill 2000; McLeod et al., 2000; Young et al., 2001). Typically these studies have been focussed within dip-domains characterised by crustal-scale tilted fault blocks or half grabens and highlight the first-order controlled provided by local structure upon sedimentation (e.g. Gawthorpe et al., 1994; Gawthorpe and Leeder 2000). Within structural accommodation zones, the control upon facies and thickness distributions is likely to be provided by a more complex interplay of local and regional controls. Here, the structural template is likely to be characterised by relatively widely distributed deformation thus forming more subtle relief and associated lower topographic or bathymetric gradients when compared to major fault blocks in adjacent dip domains. Consequently, variations in eustasy, climate and sediment supply may have a more pronounced effect than that observed with more discrete fault zones (e.g. Gawthorpe et al., 1994). As accommodation zones may provide an important conduit for regional-scale sediment fluxes within a rift (e.g. Lambiase and Bosworth, 1995; Gawthorpe and Leeder, 2000), understanding the relative importance of these interacting controls may have a profound implication for characterising or predicting rift-wide syn-rift sediment dispersal patterns.

The uplifted eastern margin of the Suez Rift, within the Sinai Peninsula, provides an excellent example of a preserved, non-inverted rift system. Present day arid desert conditions precluding the development of extensive vegetation, combined with ephemeral wadi incision provides for kilometre-scale outcrops, often characterised by pseudo three-dimensional exposure. This study utilises traditional fieldwork methods to investigate the sedimentological, stratigraphic and thickness variability of syn-rift deposits associated with the present day

onshore exposure of the Zafarana Accommodation Zone within the Suez Rift, centred upon the Wadi Gharandal area to consider the nature of controls upon syn-rift sedimentation in an area of fault polarity change.

6.3. GEOLOGICAL SETTING OF THE ZAFARANA ACCOMMODATION ZONE

6.3.1 Structure

The Suez rift is a failed intracontinental rift formed by the separation of the Arabian and African plates during the late Oligocene to Early Miocene, *c.* 23.5 Ma (e.g. Colletta et al., 1988; Patton et al., 1994). Trending NW – SE, the rift is approximately 80 km wide and 300 km long. The inner, axial, portion of the rift contains the present day Gulf of Suez, whereas the uplifted margins of the rift are exposed in the Eastern Desert and Sinai Peninsula respectively (Fig 6.1). The main phase of rifting activity is generally considered to have abated *c.*15.5 Ma, coinciding with the onset of extension on the Dead Sea - Aqaba transform (e.g. Richardson and Arthur, 1988). However, modern seismic activity and uplifted Quaternary marine terraces indicate that some of the major faults are still active present day (e.g. Gawthorpe et al., 2003). Along its longitudinal axis, the rift can be divided into three major dip-domains (e.g. Moustafa 1976; 1993; Patton et al., 1994) (Fig 6.1). Within each dip-domain, tilted fault blocks, typically 10-15 km wide by 20-30 km long, and bounding major normal faults, display a consistent dip polarity. The northern and southern dip-domains contain major faults dipping towards the northeast, whereas major faults within the central dip-domain dip south-westwards. The changes in polarity between the dip domains occur across two rift wide structural accommodation zones, termed the Zafarana and Morgan Accommodation Zones in the north and south respectively (e.g. Moustafa, 1976; Patton et al., 1994; Younes & McClay, 2002).

This study focuses on the Zafarana Accommodation Zone, which has also been referred to as the Galala-Zenima (Moustafa 1976) or Gharandal transfer zone (Moustafa 1997; 2002), which extends transversely across the rift between the northern and central dip domains. It is approximately 40 to 50 km wide and encompasses the pre-rift Late Cretaceous to Early Tertiary-aged inversion anticline located at Wadi Araba on the western margin of the rift, and its eastward extension offshore into the rift axis (e.g. Moustafa and Khalil, 1995). Moustafa (1976, 1997, 2002) has suggested that this pre-existing structure provided the focus area for

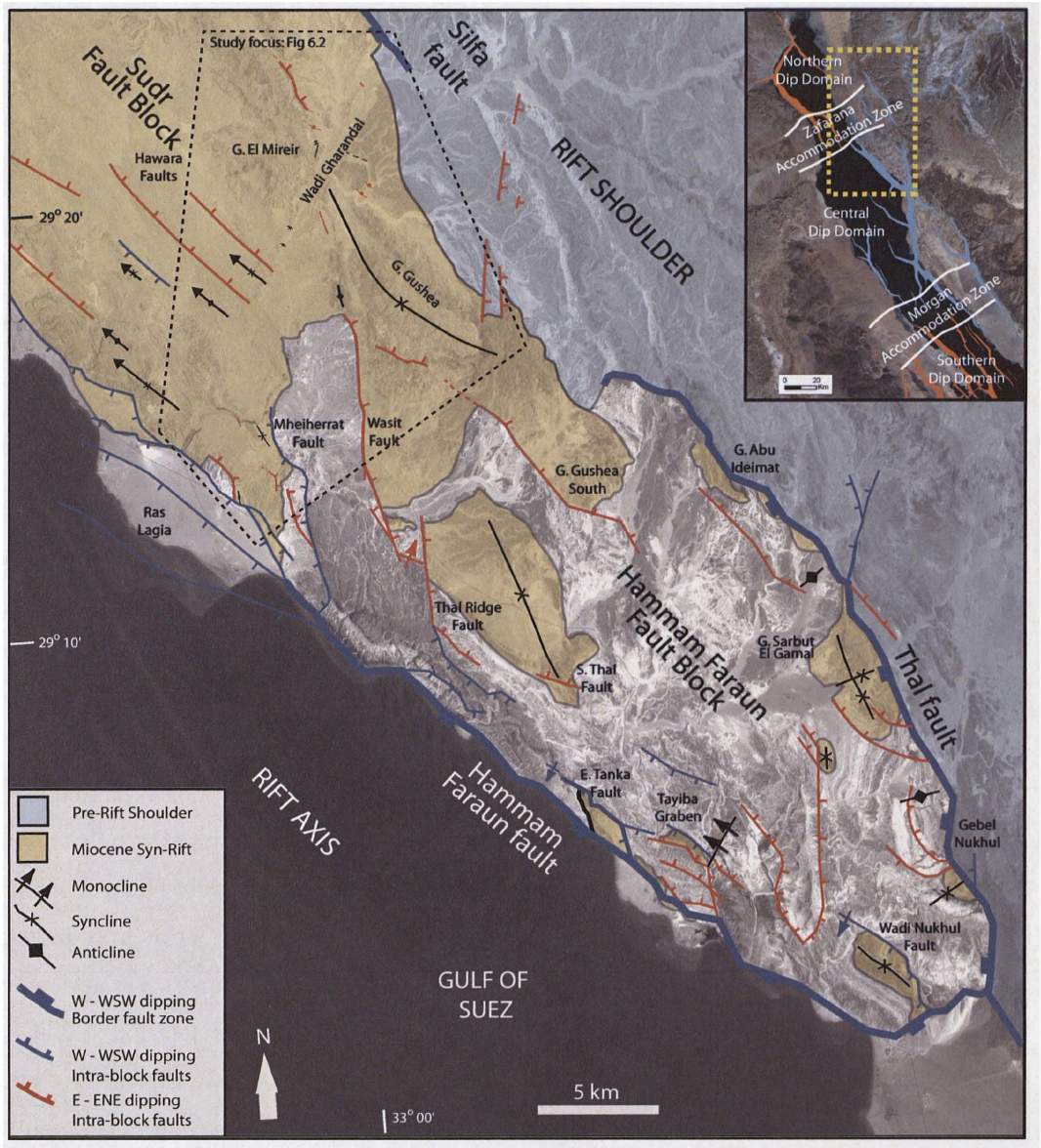

Figure 6.1. Location of study area (outline dashed) in relationship to the Hammam Faraun and Sudr Fault Blocks of the rift margin. Strutural elements modified from Moustafa and Abdeen, (1992). Corner inset shows regional context within the Suez Rift.

the transfer of throw between the rift bounding faults of the northern and central dip domains and thus the constraint upon the position of the Zafarana Accommodation Zone.

The study area, (centred upon Wadi Gharandal) is located towards the northernmost part of the Hammam Faraun Fault Block (Fig 6.2). Here, extensive syn-rift deposits are exposed over a wide area (approximately 158 km^2), contrasting with other preserved syn-rift deposits throughout the fault block, which are typically more spatially constrained and which have formed the basis for several recent detailed studies (e.g. Sharp et al., 2000a; Young et al., 2000, 2002, 2003; Jackson et al., 2002, 2005, 2006a, 2006b; Gawthorpe et al., 2003; Leppard and Gawthorpe., 2006). The main part of the Hammam Faraun Fault Block to the south is bounded along its eastern margin by the Thal Fault, and the Hammam Faraun Fault at its western margin. The Thal Fault is approximately 30 km in length and has a highly sinuous pattern of en echelon longer rift parallel and shorter oblique segments. Its maximum displacement of 1.4 km is at the southeast and displacement decreases towards its northern tip, located towards the southern part of Gebel Gushea, (Young et al., 2000; 2003). Towards the northwest of the Thal Fault, a large, 13 km wide relay ramp is present; no major rift bounding fault observed until Wadi Silfa, (Moustafa, 1976; 2003) herein termed the Silfa Fault (Fig 6.2). The western margin of the Hammam Faraun Fault Block is defined by the present day coastal boundary forming Hammam Faraun Fault Zone. With a maximum of approximately 4 km displacement towards its centre, the Hammam Faraun Fault Zone similarly loses displacement northward and is interpreted from both outcrop and subsurface data to form a series of synthetic splays in the Wadi Wasit to Ras Lagia area (Fig 6.2). The Hammam Faraun Fault Block also contains a series of mesoscale intra-block fault zones and fault-related folds. These intra-block faults are both synthetic and antithetic to the dominant W-WSW dip of the fault block and are up to 11 km in length, with maximum throws of less than 1 km (e.g. Sharp et al., 2000a). North of Wadi Gharandal these intra-block faults typically show a change in dip, dipping to the E-ENE, consistent with the transition into the Sudr Fault Block of the northern dip province.

Previous mapping of the study area has delineated the large-scale structural framework and has thus provided a basis for this study, with principal structures observed within the study area shown in Figure 6.2. (e.g. Theibaud & Robson, 1979; Moustafa and Abdeen 1992; Moustafa, 1996; 2003). Principal structures are: (i) the Wasit synthetic (with respect to the Hammam Faraun Fault Zone) and Mheiherrat antithetic intra-block faults and associated fault-related folds; (ii) the Ras Lagia series of synthetic splays within the Hammam Faraun Fault

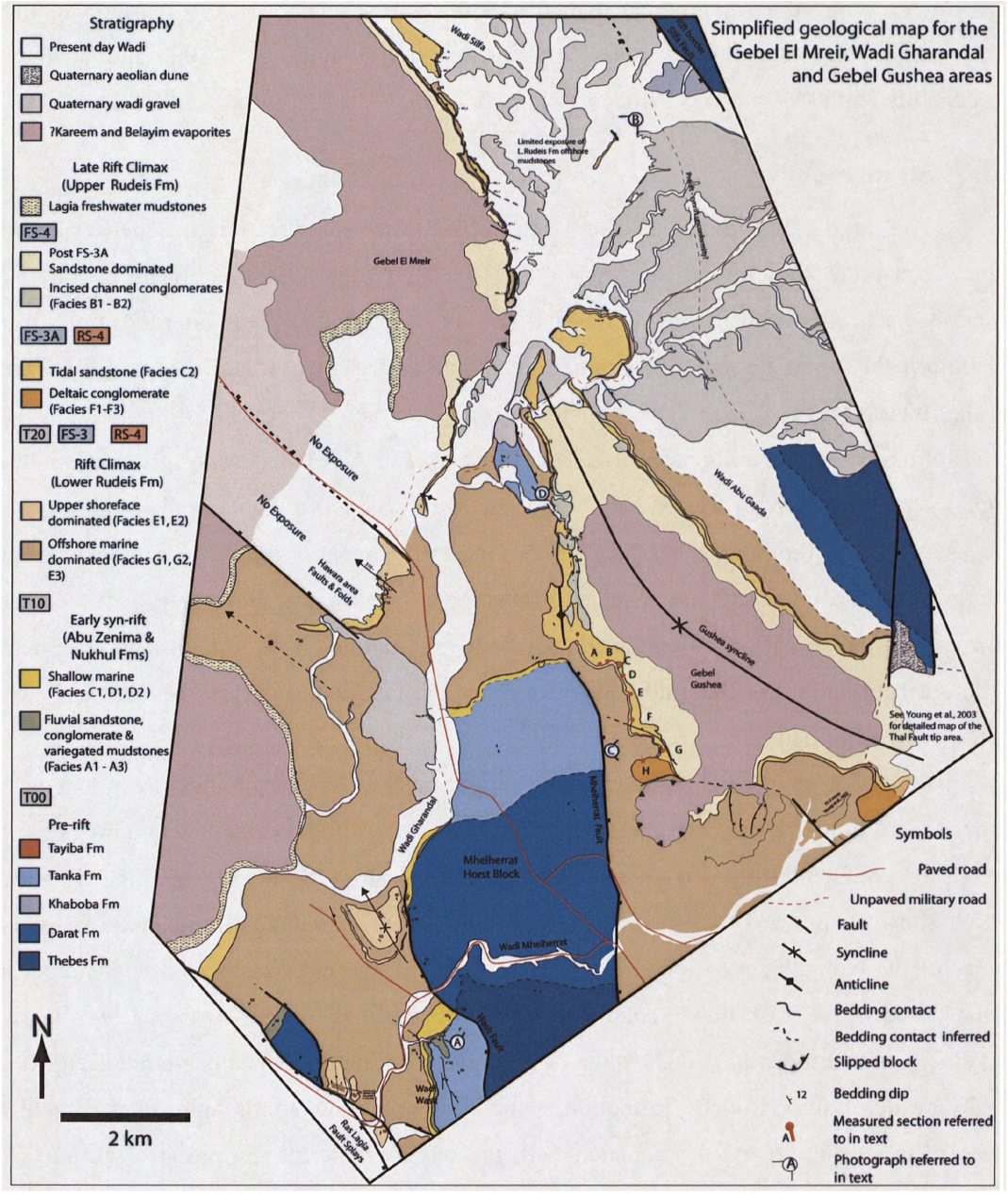

Figure 6.2. Simplified geological map for the Gebel El Mreir, Wadi Gharandal and Gebel Gushea areas. Regional Fault trends modified after Moustafa and Abdeen, (1992). For regional context, see Figure 6.1.

Zone; (iii) the major Gushea Syncline, orientated parallel to the rift shoulder; (iii) the Hawara ENE-dipping intra-block faults and related fold structures; (iv) a series of listric detachment faults which sole out within the syn-rift succession (c.f. Young et al., 2003 and (v) the rift border Silfa Fault (Moustafa, 1996).

6.3.2 Stratigraphy

The stratigraphy of the northern Suez rift consists of three megasequences, two of which constitute the pre-rift succession and the final one, the syn-rift infill (Fig 6.3). Megasequence One consists of Cambrian to Lower Cretaceous Nubian sandstones, lying unconformably upon a complex Precambrian crystalline basement (e.g. Schutze, 1994; Patton et al., 1994). Megasequence Two consists of mixed carbonate – clastic strata, with a lower series of mudstone and carbonate formations of Cenomanian to Palaeocene age, overlain by an uppermost succession of Eocene to Oligocene carbonates. Key outcropping units of this megasequence within the study area from oldest to youngest are: the pelagic chert-rich micricitc wackestones of the Thebes Formations; the muddy limestones of the Darat Formation; the mudstone dominated Khaboba Formation; the brilliant white micritic pelletoidal limestones of the Tanka Formation and the interbedded mudstones and sandstones of the Tayiba Formation.

Megasequence Three contains Late Oligocene to Quaternary aged syn- to post-rift deposits. Within the rift margin, the initial phase of rifting is documented by the Late Oligocene continental red bed facies and localised volcanics of the Abu Zenima Formation which show an upward transition to the initially fluvial and increasingly marginal marine facies of the Nukhul Formation, reflecting slow subsidence rates associated with numerous, isolated and widely distributed, smaller scale normal faults (e.g. Patton et al., 1994; Sharp et al., 2000; Gawthorpe et al., 2003). Overlying these rift initiation deposits are the deep marine facies of the Lower Rudeis Formation, which represent the stratigraphic response to an increase in subsidence rates associated with the onset of the climax phase of rifting, (e.g. Patton et al., 1994; Gupta et al, 1998). A major basinwide unconformity overlies the Lower Rudeis Formation, commonly referred to the mid-Clysmic or mid-Rudeis unconformity (e.g. Garfunkel & Bartov 1977; Patton et al., 1994; Wescott et al., 1996; Krebs et al., 1997). Subsequently, an increased amount of clastic input into the rift, characterised by proximal point sourced fan delta facies along the rift margin and submarine fan facies in hangingwall depocentres within the rift axis forms the Upper Rudeis Formation (e.g. Garfunkel & Bartov,

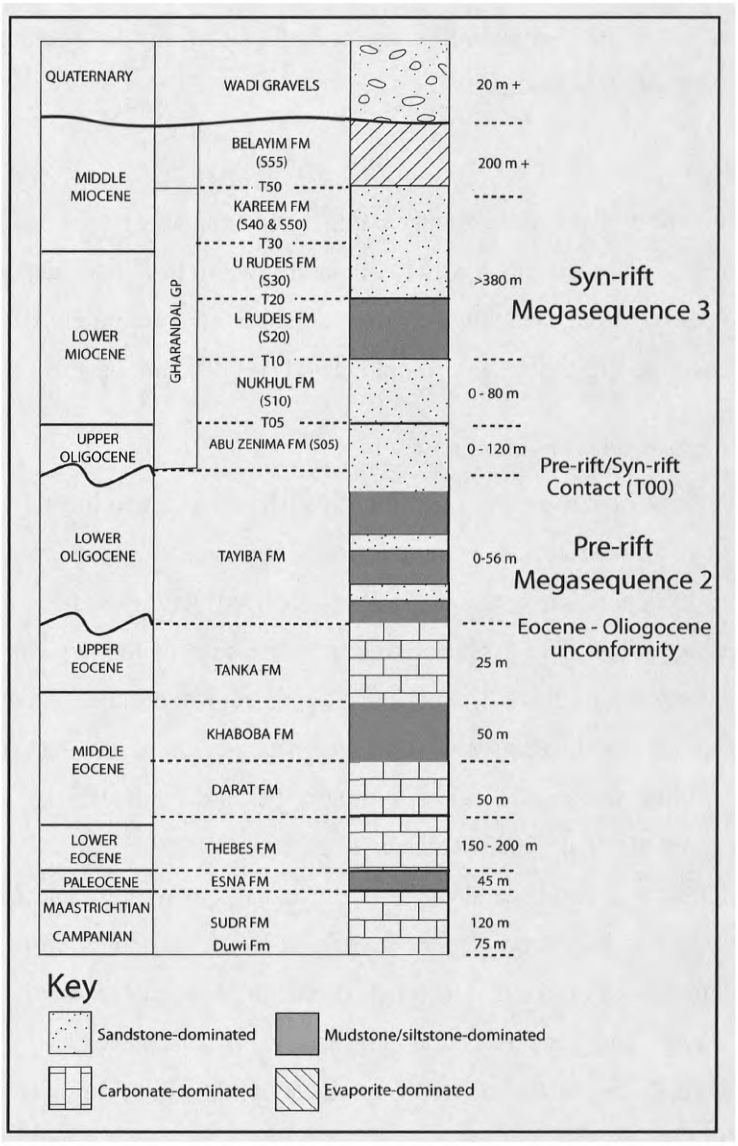

Figure 6.3. Stratigraphic column for the eastern rift margin of the Suez Rift, depicting the uppermost pre-rift succession (Megasequence 2) and subsequent syn-rift stratigraphy (Megasequence 3). Thickness estimates taken from Sharp et al., (2000a) and Jackson et al., (2006a).

1977; Evans, 1988; Smale et al 1988; Pivnik et al., 2003). The subsequent Kareem and Belayim Formations record the progressive evaporitic nature of deposition, reflecting the overall waning of the rift event and increasingly complex interplay between eustatic and tectonic effects, (Bosworth & McClay, 2001).

6.4. SEDIMENTOLOGY

Detailed examination of the syn-rift succession within the study area has allowed for the identification of six facies associations which are interpreted to have been deposited within four principal, genetically-linked depositional environments: (i) continental, (ii) shallow marine to offshore transition, (iii) deltaic to pro-deltaic and (iv) offshore basinal.

6.4.1 Continental depositional environment

Two distinct facies associations are recognised which reflect a continental environment of deposition. Facies Association A is characterised by sandstone, conglomerate and mudstone which record depositional processes that occurred within a fully non-marine, alluvial to fluvial setting. This facies association sits at the base of the syn-rift succession, immediately above the pre-rift to syn-rift unconformity and represents the rift initiation Abu Zenima Formation (Fig 6.4, log i). The three facies identified here have also been consistently recorded elsewhere within the rift margin Hammam Faraun Fault Block at the same stratigraphic level (e.g. Young et al., 2003; Jackson et al., 2006a).

Facies Association B is constrained to the northern parts of western and eastern limbs of the Gushea Syncline, and is observed to be contained within a maximum, 2.5 km wide trough-like feature, which has a markedly erosional contact into underlying marine sandstones of the rift climax Lower and Upper Rudeis Formations (Fig 6.4, log iii). Individual thicknesses for the two differing facies that represent the fluvial infill of an incised valley are difficult to constrain but the overall package attains a maximum thickness of approximately 25 m and can be traced laterally for approximately 2.5 km and 700 m over the western and eastern limbs of the syncline respectively, before pinching out into interbedded shoreface sandstone and offshore mudstone.

Facies Association A: Alluvial to fluvial

Facies A1: Variegated mudstones. This facies is composed of massive to bedded mudstones and siltstones that have a variegated red to purple colour and commonly contain

pale white to grey, cemented carbonate nodules typically less than < 5 cm in diameter. The nodules are observed to be both randomly located throughout the facies, or associated with individual bedding horizons. Ranging in thickness from 1-15 m and laterally extensive up to 200 m, this facies is interbedded and commonly incised by the other two facies of this facies association.

Facies A2: Poorly-sorted conglomerate. Interstratified with the variegated red mudstones of Facies A1 and sandstones of Facies A3 (described below) are variable clast- to-matrix supported conglomerates forming erosively based units up to 6 m thick. These units form either laterally extensive-sheets, up to 200 m wide, or more laterally constrained channel-like forms up to 50 m wide and 5 -10 m deep. Clasts are typically representative of the uppermost pre-rift succession, being dominantly composed of brilliant-white Eocene Tanka Formation limestones (> 90 %) and pale white to brown Darat Formation muddy limestones (>10). Importantly, no significant volumes of either chert or basalt clasts are observed. Clasts are very poorly sorted, generally angular to sub rounded and range in size from granule grade to 50 cm in diameter with typical sizes in the order of 10-20 cm. The intervening matrix is formed of fine-grained sandstones to mudstones, and overall the conglomerates may be arranged in crude metre scale beds, with indications of a general fining-upwards trend within the more constrained channelised forms. Localised imbrication of clasts and gutter marks provide indication of unidirectional palaeoflows. There is no indication of marine fauna other than those associated within clasts of the reworked pre-rift lithologies.

Facies A3: Pale green to buff sandstones. Fine to very coarse-grained, light green to buff coloured sandstones often with up to 10 cm thick interbeds of the conglomerates of Facies A2. The sandstones of Facies A3 are arranged into sharp- or erosively-based beds, generally < 1 m thick, which commonly fine upwards. At larger-scale exposures, these beds are commonly arranged as lenticular, sigmoidal sandstone beds with inclined bounding surfaces. Internally, tabular cross bedding, unidirectional ripples and parallel lamination are also observed within individual beds. Sorting varies from well to moderate, with outsized clasts typically observed. In addition basal lags are common at the base of units of Facies A3 which are dominantly composed of late pre-rift carbonate lithologies mirroring the conglomerates of Facies A2, although rare basaltic clasts are observed at North Wadi Tayiba variegated red mudstone intraclasts of Facies A1 are also common. No bioturbation or marine bioclastic material is observed within this facies.

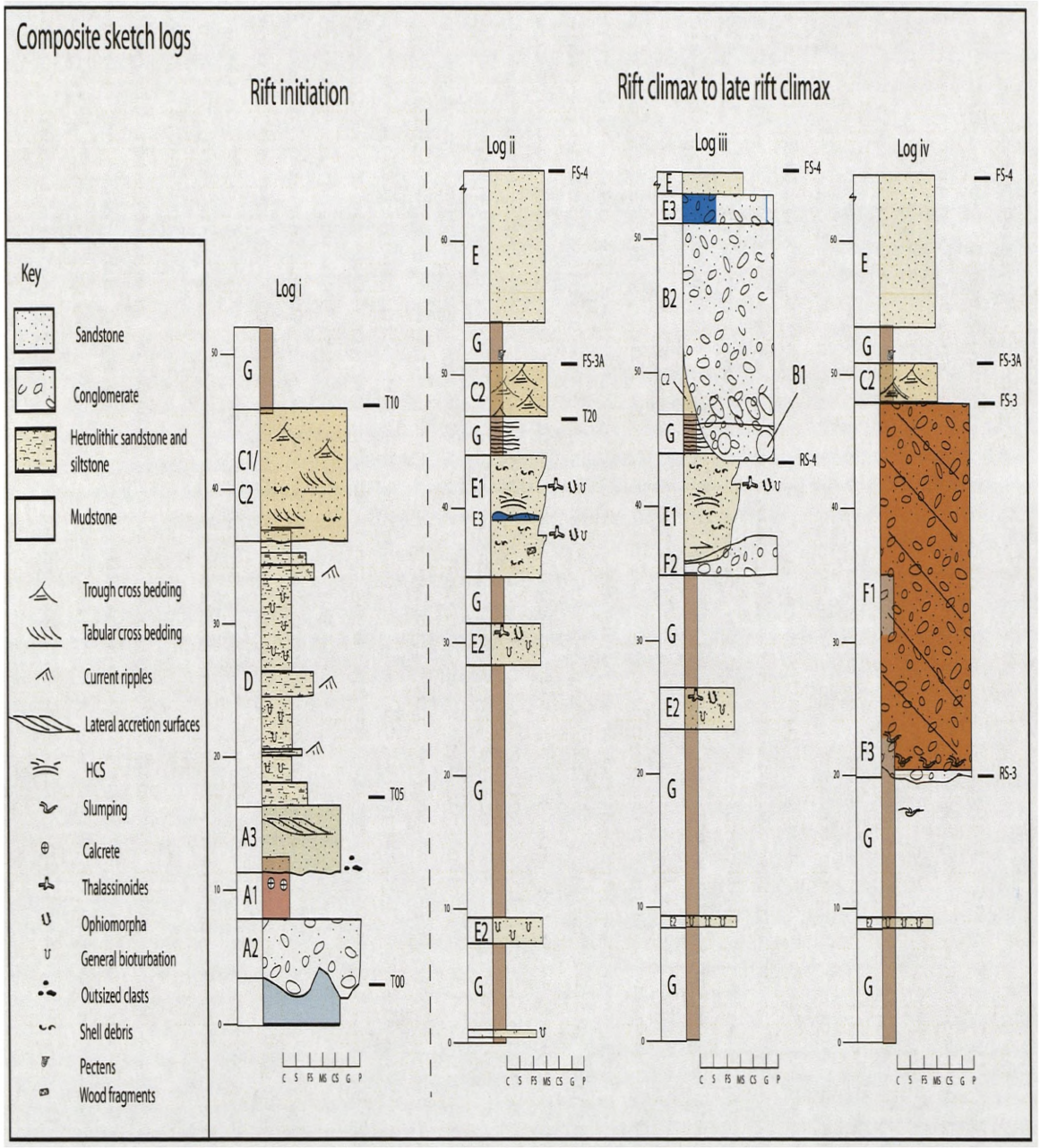

Figure 6.4. Composite sketch logs illustrating key facies types and vertical relationships for the rift initiation (i) and rift climax to late rift climax (ii-iv) succession.

Interpretation of Facies Association A

The lack of marine fauna and bioturbation indicate that Facies Association A was deposited within a non-marine depositional setting, corroborated by the interpretation of the carbonate nodules observed in Facies A1 as pedogenic calcretes. The intervening conglomerates of Facies A2 arranged in either broad sheets or within incised channel-like features are interpreted to have been deposited within a fluvial system, with the poorly sorted nature of this facies indicative of limited transport and the palaeocurrent data from clast imbrication, gutter marks suggesting unidirectional stream flows. The broad sheets are suggested to have been deposited as gravel-sheets or bars given their coarse-grained, planar nature and lack of internal cross bedding (e.g. Boothroyd, 1972; Nemec and Postma, 1993; Jo et al., 1997). The fining upwards motif associated conglomerates constrained within the incised channels is suggestive of waning flow during deposition. Deposition here in the confined channel axis may have occurred in response to the switching of main flow to an alternate channel (e.g. Church, 1983). The interbedded green to buff coloured sandstones of Facies A3 is further consistent with deposition within a fluvial system. The tabular cross-bedded and rippled sandstones of this facies potentially reflect the migration of two-dimensional straight crested dunes and ripples, whilst the sigmoidal sandbodies are thought to represent lateral accretion at channel margins.

The compositionally immature nature of the clast types in Facies A2 and A3, i.e. being dominantly composed of Tanka Formation clasts, is consistent with the initial stages of unroofing of the pre-rift succession during the onset of the rift event. The lack of chert clasts indicate that there was no sourcing of the older Thebes Formation at this time, whereas the presence of basaltic clasts in Facies A3 at North Wadi Tayiba suggests for erosion of locally present Late Oligocene basaltic sills (e.g. Jackson et al., 2006a). The bedded mudstones and siltstones of Facies A1 are interpreted to be the overbank deposits within the fluvial system. The interbedded nature of the mudstones and siltstones of Facies A1 indicates the shifting of this system with periods of channel abandonment following deposition characterised subsequent suspension settling. Ensuing non-deposition within an arid to semi-arid climate regime allowed for the evaporation of a carbonate-rich groundwater to form the calcrete carbonate nodules observed (e.g. Retallack, 1986; Rhee et al., 1998).

Facies Association B: Rift climax incised channel infill

Facies B1: Matrix-supported calcareous-rich conglomerate. Facies B1 forms the lowermost unit of this facies association and is located above a highly erosive contact into underlying tidally-influenced cross bedded sandstones of Facies C2 and shoreface sandstones of Facies E1 (described below). Poorly sorted, matrix-supported clasts of Thebes Formation (>70%) limestone and subordinate clasts of chert (20-30%) form the dominant component of this facies (Fig 6.5). Clasts are typically angular to sub angular, with sizes ranging from 4-50 cm, (average size 15-20 cm), with chert clasts being typically smaller than the limestone clasts. The intervening matrix is composed of medium to coarse-grained sandstone with outsize chert clasts. Additional rare intraclasts of Facies C2 sandstones are also observed. The unit has a thickness of 2 - 5 m, but is difficult to distinguish from the overlying conglomerates of Facies B2 throughout the mapped extent of this facies association. No primary bedding is observed, with an overall chaotic appearance for the distribution of clasts within the unit.

Facies B2: Clast-supported calcareous-rich conglomerate. This facies sharply overlies the matrix-supported conglomerate of Facies B1 and is differentiated by a switch to overall clast support. The composition, size and overall sorting of clasts throughout the unit is identical to the underlying facies and similar clast sizes are present. However, this unit differs in that it is much thicker, attaining a maximum thickness of approximately 20 m, and is composed of metre-scale beds. Typical sedimentary features include a degree of fining upwards, crude metre-scale cross bedding and clast imbrication; all palaeocurrent indicators suggesting a W to NW trend.

Interpretation of Facies Association B

The location of the mapped exposures of Facies Association B and palaeocurrent data from clast imbrications and cross bedding in Facies B2 points to the development of a major 1-2.5 km wide incised valley with flow and the long axis orientated to W-NW.

The local downcutting of the lower bounding surface of Facies B1 into immediately underlying tidally-influenced sandstones of Facies C2 and older bioturbated shoreface sandstones of Facies E1 (described below) suggests for an initial period of non-deposition associated with fluvial erosion and sediment bypass, with sediment being most likely transported directly into the axis of the rift. Facies B1 forms the earliest infill within the incised valley, with the lack of marine fauna and the poorly sorted and chaotic nature of

matrix supported clasts is interpreted to be the product of a debris flow associated with a major fluvial discharge event, (e.g. Nemec and Steel, 1984). The subsequent deposition of Facies B2, characterised by more organised bedding, crude cross bedding and clast imbrication indicates the subsequent establishment of a major fluvial depositional system, characterised by unidirectional, turbulent streamflows (Nemec and Steel, 1984). The compositional dominance of Thebes Formation limestone and chert clasts within both facies indicates to a major sourcing of this pre-rift formation at this time, potentially within the uplifted rift shoulder. The W-NW palaeocurrent direction indicated from clast imbrication and cross bedding suggest subsequent transport from this shoulder towards axis of the rift.

6.4.2 Shallow marine to offshore transition environments

Three facies associations are recognised which reflect deposition within a shallow marine to offshore transition environment. Facies Associations C and D record deposition within high and low energy sub-tidal settings, whereas Facies Association E reflects the transition from lower shoreface to offshore. The dominant lithologies observed are sandstones, siltstones and rare conglomerates; Facies C1, C2 and Facies Association D characterise the rift initiation Nukhul Formation, whereas Facies C1, C2 and D1 to D3 comprise parts of the rift climax Lower and Upper Rudeis Formations (Fig 6.4).

Facies Association C: Tidally-influenced high energy setting

Two distinct facies comprised of variably-scaled cross bedded sandstone are recognised in this facies association:

Facies C1: Decimetre-scale cross bedded sandstone. This facies is characterised by well-cemented, medium- to very coarse-grained and often granule-rich sandstone. Outsized granule-sized clasts of sub-angular to sub-rounded chert, bioclastic shells and coral debris commonly form a lag at the base of individual beds. The intervening matrix is composed of sub-angular to sub-rounded quartz and limestone clasts, which are poorly to moderately well-sorted, with little or no mud content. Tabular to trough-cross bedding is ubiquitous throughout this facies, with decimetre-scale sets dominating, whilst herring-bone sets are also commonly observed. Larger beds are typically 0.5-1 m thick, and are also arranged in stacked packages, with a maximum thickness of 7.5 m, which are laterally continuous for up to 600 m. Basal bedding surfaces are sharp to erosive and may be associated with loading into underlying units. Bioturbation is rare, with a bioturbation index (BI) of 0-2 (*sensu* Taylor and Goldring, 1993),

and is dominantly characterised by simple vertical burrows *Skolithos* and the nodular *Ophiomorpha,* which are typically beneath the basal surfaces of individual beds. In contrast, top bedding surfaces are typically associated with extensively symmetrically rippled, fine to medium-grained sandstone.

Facies C2: Metre-scale cross bedded sandstone. Facies C2 forms a distinctive cliff forming unit, with sharp to erosive bases and characterised by metre-scale, tabular to trough cross bedded sandstones directly overlying, an intercalated succession of Facies Associations D and F (Fig 6.5). Forming a laterally extensive sheet 5-15 m thick, this facies can be traced over several kilometres within the study area, with local thickening into fault hangingwalls and syncline axes. Facies C2 is locally associated with interbedded lenses of conglomerate (Facies F2), and also may display a gradation into underlying shoreface sandstones of Facies E1. Individual sets are up to 30 cm thick, arranged in metre-scale cosets (1-3 m) bounded by major reactivation surfaces, and are picked out by variable cementation. Laterally, prominent cross beds can be traced over 3 to 5 m. Two main palaeocurrent directions are typically identified, a dominant W-NW trend and a subordinate SE trend (Appendix 5). In general, the dip directions of the cross beds are typically the same as those of the master bounding reactivation surfaces. Texturally, Facies C2 is characterised by moderately to well-sorted, medium- to very coarse-grained limestones and chert grains, which are typically sub-rounded to angular, with no evidence for a mud to silt grade fraction. The intervening finer-grained intervals show characteristics in common to Facies E1, with fine- to medium-grained, mottled sandstone displaying variable *Ophiomorpha* and *Planolites* bioturbation (BI = 0-3), with increased levels of bioturbation particularly above major reactivation surfaces.

Interpretation of Facies Association C

The ubiquitous presence of marine shell debris and bioturbation in both facies indicates a fully marine depositional environment for this facies association. The presence of cross stratification within Facies C1 suggests deposition under periods of active current flow; with the migration of 2D to 3D dune and ripple scale bedforms inferred from foresets which represent simple avalanche sets. The presence of symmetrical ripples and herringbone cross-bedding indicate marked periods of reversal in flow direction, thereby suggestive of deposition under a tidal regime. The lack of mud content and presence of large outsized clasts indicates relatively high energy conditions, consistent with the concentration of trace fossils to the interfaces between beds, reflecting colonisation during lower energy periods. Thus Facies

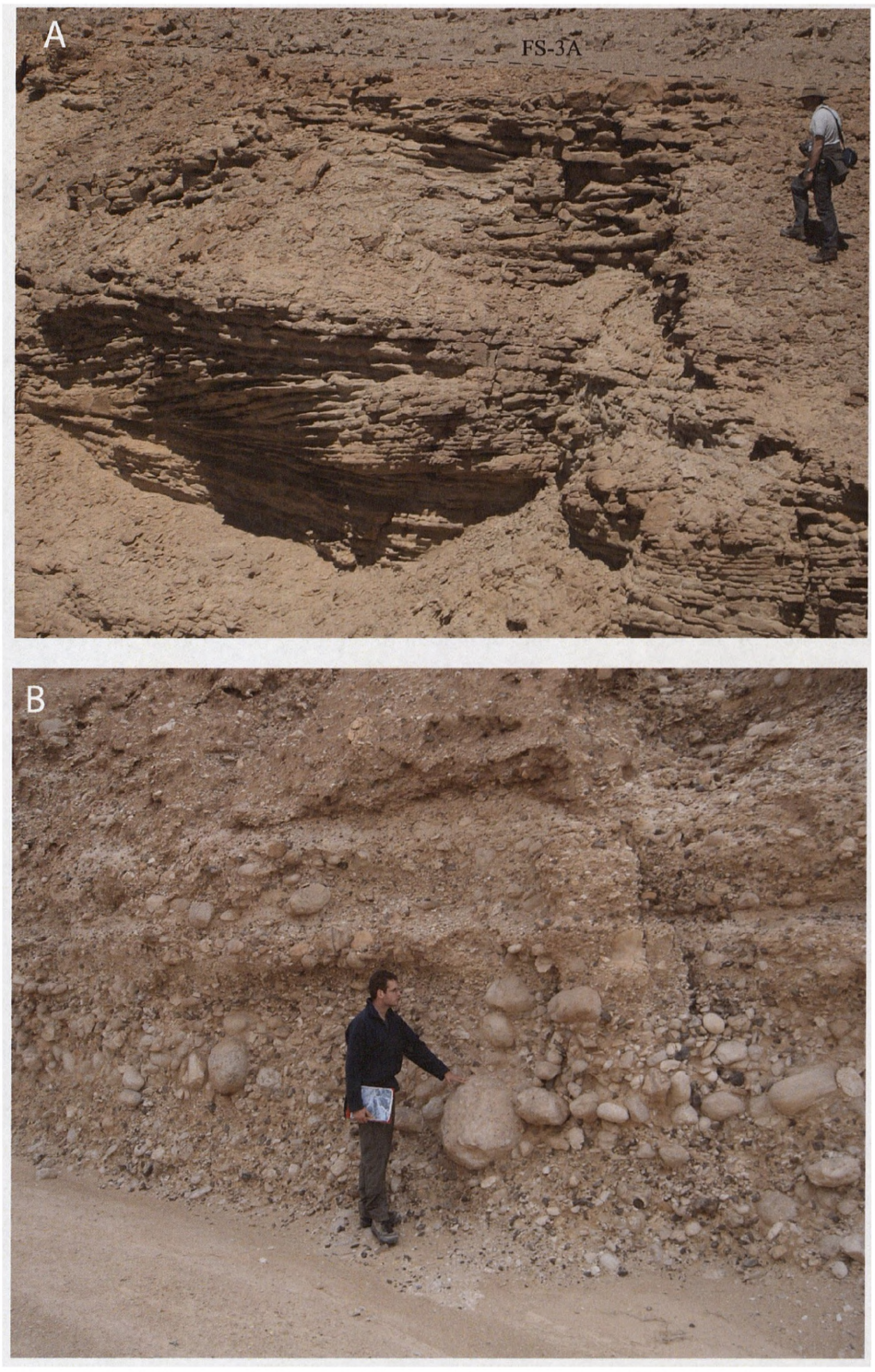

Figure 6.5. A) Photograph of cross bedded sandstones of Facies C2. Flooding Surface FS-3A is picked out by the reddish stained cemented layer. B) Poorly sorted, chaotic fluvial conglomerates of Facies B1 within the palaeovalley to the NW of Gebel Gushea.

C1 is interpreted to have been deposited in a relatively shallow, high-energy, tidally-influenced marine setting.

The metre-scale cross bedded sandstones of Facies C2 are similarly thought to reflect the migration of a sediment as a series of sub-tidal, dune-scale bedforms by tidal currents within a shallow marine setting (e.g. Allen and Homewood 1984; Ashley 1990), albeit at larger-scale than those associated with Facies C1. The shared dip direction of foresets with bounding master surfaces and the lack of any observed channels bodies suggests that this facies records the deposition of subtidal compound dunes, i.e. with a bedform long axis orientated transversely to flow direction, rather the deposition of flow parallel tidal bars (*sensu* Houbolt, 1968). The kilometre-scale extent of this facies suggests that the deposition of these large dune forms occurred over a wide-scale area, dominated by alternations of higher and lower energy tidal currents, as indicated by the observed vertical stacking of dominant and subordinate sets in two contrasting dip directions, overall lack of bioturbation and coarse-grained nature of the succession. The dominant palaeoflow direction to the NW is away from the rift shoulder and is interpreted to document the role of a dominant ebb tidal flow.

Facies Association D: Tidally-influenced low energy setting

Facies Association D is comprised of two facies which are interbedded, forming heterolithic units up to 5 m thick and which are laterally traceable up to approximately 500 m (Fig 6.7). Facies Association D is commonly vertically intercalated and laterally adjacent to the decimetre-scale cross bedded sandstones of Facies C1 (Fig. 6.4, log i).

Facies D1: Rippled sandstone. This facies is comprised of thinly bedded, typically 5 cm thick, very fine to medium-grained sandstones, which display pervasive symmetrical ripples and rarer planar lamination. Bioturbation within the sandstone bed varies from low to moderate (BI = 0-2).

Facies D2: *Bioturbated siltstone.* Interstratified with Facies D1, this facies consists of orange to green mottled siltstone, which display moderate to high levels of bioturbation, (BI = 2-4). Principal traces recognised are *Thalassinoides, planolites*, and *Ophiomorpha.*

Interpretation of Facies Association D

The sedimentary structures, variable bioturbation and linkage to the decimetre-scale cross bedded sandstones of Facies C1, suggests that Facies Association D is similarly interpreted to deposition within a sub-tidal setting, albeit one experiencing alternating periods

of high and low energy conditions. The thin sandstones are interpreted to have been deposited as subtidal, wave-reworked current ripples during higher energy periods, whilst the siltstones are thought to represent periods of when tidal currents were diverted from the area; thus allowing for subsequent colonisation.

Facies Association E: Shoreface to offshore transition

Facies E1: Pale 'ribbed' bioturbated bedded sandstone. This facies is composed of typically coarse to very coarse, poorly to moderate-sorted pale brown sandstones, arranged in tabular, sheet-like units up to 16 m thick which are traceable over several kilometres. It is interbedded with units dominated by the mudstones and sandstones of Facies Association G and subordinate beds of Facies E3 (Fig 6.6). Although superficially structureless and massive, Facies E1 is comprised of decimetre-scale beds, which are sharp to erosive based and commonly display an overall coarsening-upwards motif. Individual beds contain floating out-sized clasts of chert and pre-rift limestone, which are generally less than 10 cm in diameter and commonly observed as lags at the base, in addition to mud rip-up clasts and shell debris. Bioturbation is generally moderate to low, typified by *Planolites, Thalassinoides and Ophiomorpha* (BI = 0-3), although the top of each bed may be characterised by a marked increase (BI = 5-6) (Fig 6.8). Evidence for sedimentary structures is generally poor, although faint erosional surfaces and rarely observed examples of HCS (Fig 6.8). Lenticular beds of the bioclastic conglomerate Facies E2 are also commonly interbedded within larger packages of Facies E1, typically towards the base of individual beds.

Facies E2: Calcarenitic reefal conglomerate. This facies is occasionally observed within the bedded sandstones of Facies E1 as lenticular, coquina-like packages of white, bioclastic-rich conglomerates up to 2 m thick and 10's of metres in lateral extent (Fig 6.4, log ii). This facies is also observed overlying the clast supported conglomerates of Facies B2 as a 1-2 m thick bedded layer (Fig 6.4, log iii). The conglomerate of Facies E2 is typically clast supported, with a matrix of medium- to coarse-grained sandstone. Clasts are 1-50 cm in diameter, with an average of 20 cm, and include sub-rounded to well-rounded chert, pre-rift limestones and varying bioclasts, including oysters and colonial coral. The top surface of Facies E2 is typically characterised by a sharp transition into the sandstones of Facies E1.

Facies E3: Orange to buff mottled bioturbated sandstone. Facies E3 is characterised by orange to buff coloured, mottled sandstones arranged in isolated beds up to 3 m thick, which are intercalated within metre-scale thick units of Facies Association G and are laterally

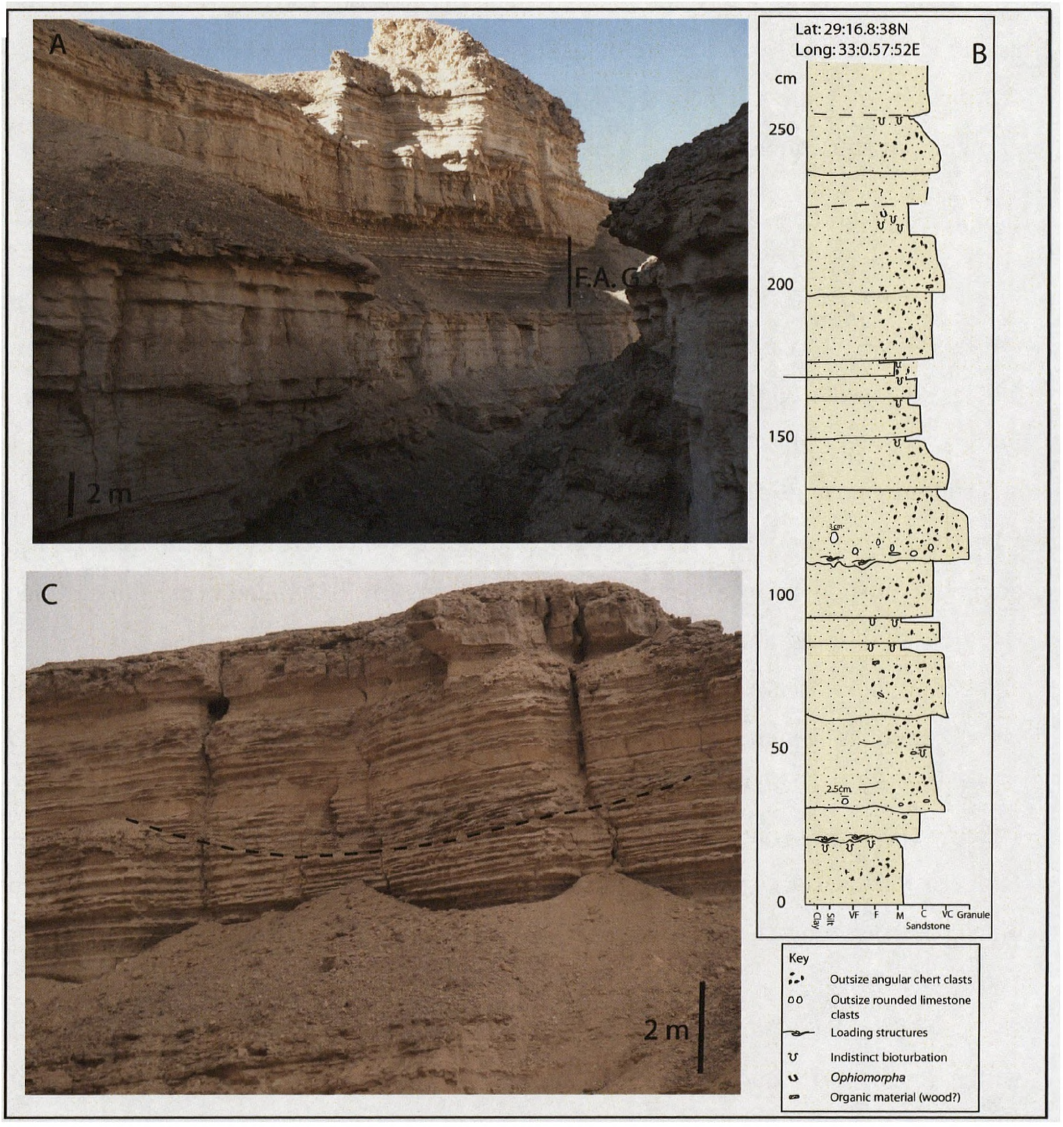

Figure 6.6. Nature of the bedded sandstones of Facies E1. A) Photograph showing tabular, sheet-like nature of Facies E1, interbedded with packages of Facies Association G. B) Detailed log of part of lower unit of Facies E1 in photograph A. Log shows a series of sharp- erosive based beds, which contain outsized chert and limestone clasts in addition to shell debris and wood fragments. Tops of individual beds show increased levels of bioturbation which include Ophiomorpha. C) Photograph showing nature of erosive surfaces observed in Facies E1. Differential cementation linked to grain size variations results in a distinct 'ribbed' weathering profile. A clear down cutting surface can be seen, infilling the erosional scour with what appear to be lateral accretion surfaces.

extensive over several kilometres. The sandstones of this facies are medium to fine-grained and moderately to well-sorted, with rare out-sized chert and pre-rift limestone clasts and bioclastic shell fragments. Bioturbation is moderate to intense, (BI = 2-5) and dominated by *Planolites, Thalassinoides* and *Ophiomorpha* which results in an indistinct homogeneous structureless appearance. The underlying basal contact of Facies E3 may be either gradational or sharp with respect to the underlying mudstones of Facies G1, whereas the top of the facies is sharp and overlain by fine-grained facies of Facies G1.

Interpretation of Facies Association E

Facies E1 to E3 are interpreted to have been deposited within a shallow marine setting extended across lower shoreface to offshore transition environments. The thickly-bedded sandstones of Facies E1 are interpreted to reflect deposition in a lower shoreface setting. The sharp to erosive nature of basal surfaces, rare HCS and intraformational mud rip-up clasts, coarse-grained lags and shell debris suggest relatively high energy conditions. The generally low to moderate levels of bioturbation reflect this, although periodic fair-weather conditions, during which time colonisation of the substrate could occur, are indicated by the increased concentration of bioturbation towards the tops of individual beds.

The bioclastic dominated conglomerates of Facies E2, interbedded within larger packages of lower shoreface sandstones of Facies E1, are identical to those which have been identified as channel infill or chute deposits in the study of Young et al., (2003) located further south within the Hammam Faraun Fault Block (*their Facies 3b).* The erosive basal nature of the lenticular packages of this facies located within the sandstones of Facies E1 is consistent with the influx and deposition of coarse-grained material following high energy, erosional flow events. Young et al., (2003) proposed two potential mechanisms: a) as either tidal or rip channels or b) shoreface cutting chutes associated with ephemeral discharge events. Either of these mechanisms would have allowed for the transport of bioclastic material from a shallower, more proximal setting through the shoreface.

The gradational to sharp based nature of isolated bioturbated sandstone beds of Facies E3 containing outsized clasts, shell debris and occurring within overall packages of offshore marine mudstone (Facies G1) suggests that this facies was deposited by during relatively higher energy events against an otherwise low energy, offshore marine background. Facies E3 is therefore interpreted as representing the transition from lower shoreface to offshore marine, dominated by storm event or tempestite deposition (e.g. Hamblin and Walker 1979). The high

degree of bioturbation within this facies supports this interpretation, and is likely to be related to extended periods dominated by quiet, fairweather conditions (e.g. Reading and Collinson, 1996). The sharp top surfaces observed above this facies record the sharp. abrupt switch back to low energy conditions following the storm event.

6.4.3 Deltaic and pro-delta environment

A deltaic to pro-deltaic depositional environment is represented by deposits composed of interbedded conglomerates and pebbly sandstones which form a single facies association (Facies Association F) that is interbedded with, and eroded into Facies Associations C, D and F. This Facies Association forms part of the rift climax Lower and Upper Rudeis succession which is centred within the Gebel Gushea area (Fig 6.4, logs iii, iv).

Facies Association F: Deltaic conglomerate

Facies F1: Chert-rich clinoformal conglomerate. This facies forms the main component of this facies association and forms up to 30 m thick, and laterally 400 m wide units. Facies F1 is characterised by dominantly clast supported, poorly to moderately sorted, sub-angular to rounded clasts which typically range in size from < 1 cm to > 50 cm. Clasts compositions are typically: chert (60%), pre-rift limestones (30-40%) and bioclastic debris (5-10%) with a matrix formed by medium- to coarse-grained sandstones. Crude, 1-2 m thick bedding is defined by poorly-defined normal grading of clasts. Facies F1 shows a markedly incised basal surface which is often associated with a convolution into the underlying deformed pebbly sandstones of Facies F3, whilst crude metre-scale clinoformal beds also commonly downlap onto this basal surface. A major package of Facies F1 is located towards the southern part of Gebel Gushea is located within an overall trough-like feature, 400 m wide; its northwestern margin characterised by up to 30 m of incision into underlying stacked units of shallow to offshore marine deposits of Facies Association E and G, whereas its south-eastern margin is bounded in the hangingwall of a major detachment fault within the syn-rift succession.

Facies F2: Lenticular chert-rich conglomerate. Facies F2 is identical in clast composition and texture but has a significantly differing morphology which merits distinction. This facies is characterised by packages which are arranged as sheets to mound-shaped lenses, which are up to 8 m thick and laterally extensive over distances ranging from 100 – 200 m. Sharp to erosive surfaces denote the basal contact of Facies F2, which may laterally grade into,

2-3 m thick beds of Facies C2, and may also be onlapped by the shoreface sandstones of Facies E1 and interbedded mudstones and siltstones of Facies Association G.

Facies F3: Deformed pebbly sandstone. Up to 30 m thick and with a lateral continuity of up to approximately 300 m, this facies occurs laterally adjacent to and also underlies the conglomerates of Facies F1. Facies F3 is characterised by a chaotic mixture of contorted medium to coarse-grained pebbly sandstones, typically structureless and bioturbated akin to Facies C1, with isolated bodies of Facies F3, up to 1 m thick. Isolated bedding is observed, but overall the facies is dominated by recumbent metre-scale folding of individual sandstone beds

Interpretation of Facies Association F

Facies F1 and F2 are directly analogous to other coarse-grained conglomerate packages which have been identified within the rift margin and have regularly been interpreted as deltaic deposits, some of which are directly to the south of the study area (e.g. Gawthorpe et al., 1990; Gupta et al., 1999; Young et al., 2000; 2002). This interpretation is consistent with the intercalation of Facies Association F with facies interpreted in this study to reflect an overall shoreface to offshore marine depositional setting. The coarse-grained, poorly sorted nature of the deposits of Facies F1 and F2 are suggestive of a relatively proximal depositional system, close to sediment transport pathways and sourced from the uplifted rift shoulder; the dominance of chert clasts indicating that the pre-rift Thebes Formation provided the principal provenance lithology. The metre-scale clinoformal geometries of Facies F1 reflect the basinward progradation of the deltaic bodies away from the rift shoulder, with the poorly to moderately sorted conglomerates within an a medium- to coarse-grained sandstone matrix suggesting transport via cohesionless debris-flows, with deposition occurring as the result of frictional flow freezing. (e.g. Nemec and Steel, 1984; Orton 1988). The crude scale bedding observed may reflect either seasonal or ephemeral variations in sediment supply within the feeder drainage system, similar to that experienced by the wadi-fed fan deltas, building out into the present day gulf (Roberts, 1987). The occurrence of Facies F2 as sharp based lenses and laterally extensive sheets within packages of cross bedded sandstones of Facies C1, C2 and shoreface sandstones of Facies D1, is interpreted as being the more distal equivalents of Facies F1, reflecting unconfined debris flows deposited ahead of the main delta front.

The chaotic and disrupted nature of Facies F3 is indicative of syn-sedimentary deformation ahead of the progradation of the coarse-grained delta characterised by Facies F1,

Subfacies (i) into underlying shoreface marine deposits. This deformation is likely to have been linked to the loading of the overlying coarse-grained deltaic material, and the escape of pore fluid from the depositing cohesionless debris flows into the substrate upon deposition (e.g. Nemec and Steel, 1984; Postma, 1988). Additionally, considering the overall setting, instability associated with earthquake events may have also contributed to the observed deformation.

6.4.4 Offshore marine environment

Mudstones, siltstones and fine-grained sandstones comprise the lithologies deposited within this fully offshore marine setting form two principal interbedded facies.

Facies Association G: Background hemipelagic and intervening turbidites

Facies asscociation G consists of two interbedded facies (Fig 6.7):

Facies G1: Laminated mudstone. This facies consists of dark green to grey coloured, massive to laminated mudstones arranged in packages 5-10 m thick which are laterally correlatable over distances of >2 km. The packages are typically arranged between units of the shoreface to offshore deposits of Facies Association E and display sharp basal and sharp to erosive overlying contacts (Fig 6.4, logs ii-iv). Bioturbation and body fossils are rare; individual sharks teeth reported in the analogous facies identified in the study of Young et al., (2002) to the south of Gebel Gushea. Packages of Facies G1 are typically interbedded with the siltstones to fine-grained sandstones of Facies G2. Syn-sedimentary deformation is common, with decimetre-scale normal faulting and recumbent folding observed.

Facies G2: Thinly bedded sandstone and siltstone. This facies is characterised by thin beds, typically 2 - 25 cm thick, and laterally continuous over 10's of metres, of pale grey to buff coloured siltstone and fine-grained sandstone, interbedded in metre scale packages of fine-grained Facies G1. Texturally well sorted and sub-rounded to rounded, clasts are composed of both quartz and carbonate fragments. Basal surfaces of the individual beds are typically sharp to erosive into the underlying mudstones of Facies G1 and are commonly associated with scour and tool marks. Internally the beds may be massive or show a transition of sedimentary structures from massive, through cross lamination, to planar lamination. Upper contacts with overlying mudstones are sharp. Individual beds often display a concave, 'gutter-like' geometry, associated with thickened areas of the individual bed. Bioturbation is generally rare, whilst plant and bioclast fragments are more commonly observed.

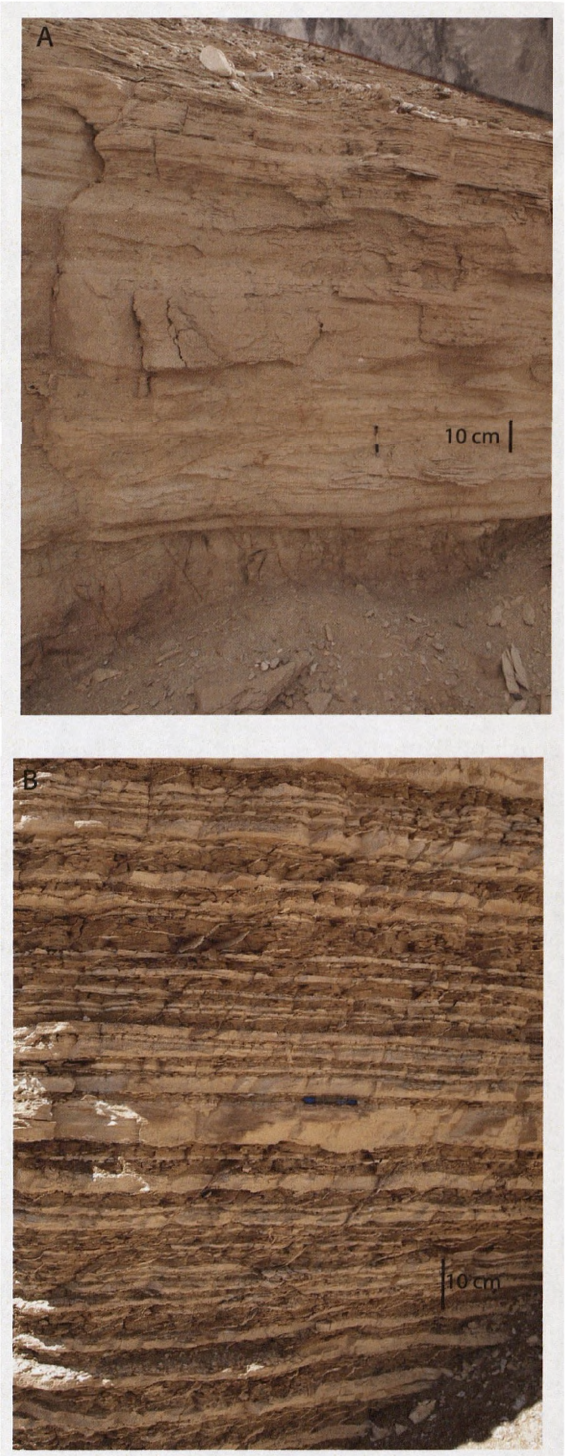

Figure 6.7. A) Photograph of the hetrolithic interbedded sandstone and siltstone facies of Facies Association D. The base of the section appears more massive, whilst the top shows increasing lamination and current ripples. B) Photograph of the interbedded offshore marine Facies Association G. Greenish to grey mudstones of Facies G1 are interbedded with siltstone to very-fine sandstones of Facies G2.

Interpretation of Facies Association G

The dominantly fine-grained, low bioturbated nature of the background mudstone Facies G1 is indicative of deposition within a low energy setting. The mudstone succession was therefore likely to have been the product of suspension-fall out, hemipelagic sedimentation below the storm wave base (e.g. Stow, 1994). The sharp to erosive based nature of interbedded, thin very fine sandstones and siltstones of Facies G2 are suggestive of punctuating periods of higher energy conditions. Depositional structures within these individual beds are consistent with deposition under changes from upper to lower flow regimes associated with distal turbidity currents potentially linked to ephemeral storm input. (e.g. Bouma, 1962; Lowe, 1982, Mulder and Alexander, 2001).

6.5. DEPOSITIONAL AND STRATIGRAPHIC SYNTHESIS

6.5.1 Depositional model

A schematic depositional model is summarised in Figure 6.8, based on the genetic relationships for the facies associations described above. This model illustrates how rift initiation to late rift climax deposits within the study area were deposited across a range of environments from continental, shallow marine, fan-deltaic and to fully offshore marine settings. During the rift initiation phase, earliest deposition was alluvial to fluvial in nature, with drainage systems incising into and being sourced from locally uplifted terrains. The coarse-grained and immature nature of the earliest fluvial deposits suggests that their associated drainage catchments areas were typically of limited extent (Facies A2). The continued erosion of fault-generated areas of uplift led to the establishment of increasingly wider-reaching drainage systems, with the resulting deposits showing a more diverse assemblage of clasts (Facies A3). Adjacent to fluvial channels, locally overbank deposits formed in what appears to have been a largely arid environment (Facies A1).

Continued rifting saw the first onset of a marine transgression into the study area. Tidal current activity led to the migration of subtidal dune-scale bedforms (Facies C1), whilst areas of lower energy, typically away from focus of current activity, were extensively colonised by marine fauna (Facies D2), with periodic interruptions of higher energy conditions (Facies D1) (Fig 6.8). During later periods, areas of extensive shallow marine embayment were present, where larger dune-scale bedforms, often referred to as sandwaves (e.g. Ashley,

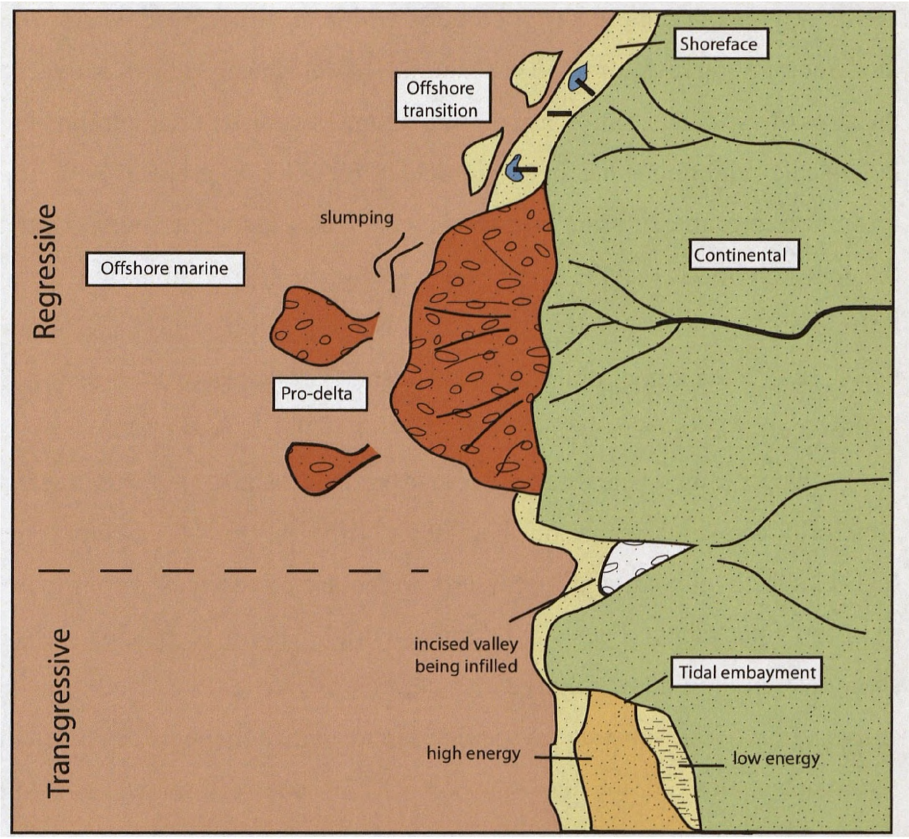

Figure 6.8. Depositional model for the facies identified in this study. Two main suites of systems are recognised: transgressive and regressive.

1990) migrated (Facies C2). Largely within a widespread sheet, these bedforms locally thickened into areas with higher accommodation space, such as active fault hangingwalls and the axes of synclines. Similar structural amplification of tidal currents and the development of large-scale tidal dunes has been previously recorded in areas of both active extensional basin formation, e.g. the Jurassic Bearreraig Formation associated with a series of half grabens in the Inner Hebrides (Mellere and Steel, 1996), the Upper Jurassic-Lower Cretaceous Raukelv Formation East Greenland (Surlyk and Noe-Nygaard, 1991) and compressional thrust top basins, e.g. the subtidal dunes of the Eocene Baronia Sandstone of the Ager piggyback basin in the Central Pyrenees (e.g. Mutti et al., 1985; Olariu, et al., 2008).

Deposition of medium to coarse grained sandstones was deposited within the study area reflecting shallow marine shoreface to offshore transitional environments (Fig. 6.8). The high bioclastic content and highly erosive nature of surfaces within these coarsening upwards sandstone packages (Facies E1) reflects high energy conditions associated with a lower shoreface environment. Intervening periods of fairweather conditions allowed for extensive colonisation of the substrate by marine fauna. Tidal channels or chutes through this shoreface setting also allowed for the transport of this coarser-grained, contemporaneous bioclastic material basinward, which were deposited a sheet-like deposits and small mounds (Facies E3). The planar, regionally laterally extensive nature of these lower shoreface sandstones indicates that accommodation space throughout the study area was being periodically infilled. Continuing basinward, sandstones were deposited following storm events which punctuated lower energy, basinal conditions, and which were extensively colonised during the subsequent return to lower energy periods (Facies E2).

Fluvial drainage located on the rift shoulder hinterland fed coarse-grained, proximal fan-delta systems via structurally controlled sediment pathways (Fig 6.8). The pre-rift Thebes Formation was exposed at this time in the rift shoulder, providing chert which from the dominant clast type for a series of progradational, clinoformal fan-deltas (Facies F1). Locally infilling incised topography, associated with an earlier period of sediment bypass, these fan-deltas were preceded by more distal coarse-grained sediment fluxes which were transported as unconfined sheets and lobes (Facies F2) down an unstable pro-delta slope (Facies F3). Other periods of regression are observed in the study area, with marked channel incision into underlying shallow marine deposits and subsequent infilling by fluvial conglomerates (Facies B1 and B2) following the associated basinward shift in facies. Subsequent transgression led to

marine incursion into these lowstand incised valleys, recognised by the deposition of bioclastic conglomerates (Facies E3) and subsequent shoreface sandstones.

Basinward, away from the rift shoulder, offshore hemipelagic sedimentation dominated with the deposition of fine-grained mudstones (Facies G1) (Fig 6.8). Distal turbidites periodically deposited siltstones to very fine-grained sandstones, and may have been the result of seasonal variations in sediment supply and/or storm events (Facies G2). Sparse bioturbation suggests a limiting factor upon colonisation within this basinal setting.

6.5.2 Key stratal surfaces and temporal facies distribution

A series of key stratal surfaces associated with either marine flooding or regression and associated facies shifts are recognised within the study area (Fig 6.9). The physical correlation (i.e. walking out) of these surfaces shows them to be regionally persistent within the study area and are thus used to subdivide the syn-rift succession into a number of stratigraphic packages. Marine flooding surfaces may be sharp and are associated with a regional typically landward shift in facies, (e.g. from shoreface sandstone into offshore basinal mudstones), whereas regressive surfaces are characterised by a basinward facies shift (e.g. from shoreface to fluvial sandstone) and may be associated with truncation and/or erosion. The nomenclature assigned to these surfaces in this study reflects the incorporation of two schemes which have assessed syn-rift stratigraphy in the Suez Rift at differing scales. A number of major surfaces are described below, which are designated T00 through to T30 (*sensu* Wescott et al., 1996 and Krebs et al., 1997). These surfaces have been previously recognised throughout the rift as regional, basinwide unconformities which are corroborated by biostratigraphic data and define the main tectonostratigraphic phases of the evolution of the rift (e.g. Patton et al., 1994; Wescott et al., 1996; Krebs et al., 1997). The remaining surfaces utilised in this study, designated RS-3, FS-3 FS-3A, RS-4 and FS-4 are linked to higher resolution stratal units which have been used to subdivide the late rift climax Upper Rudeis Formation in the present day offshore axis of the rift (Chapters Four and Five). Unpublished propriety biostratigraphic data obtained from the Gulf of Suez Petroleum Company (GUPCO) within the study area, allows for the direct correlation of the Upper Rudeis Formation here with the coeval deposits within the rift axis (Chapter Seven).

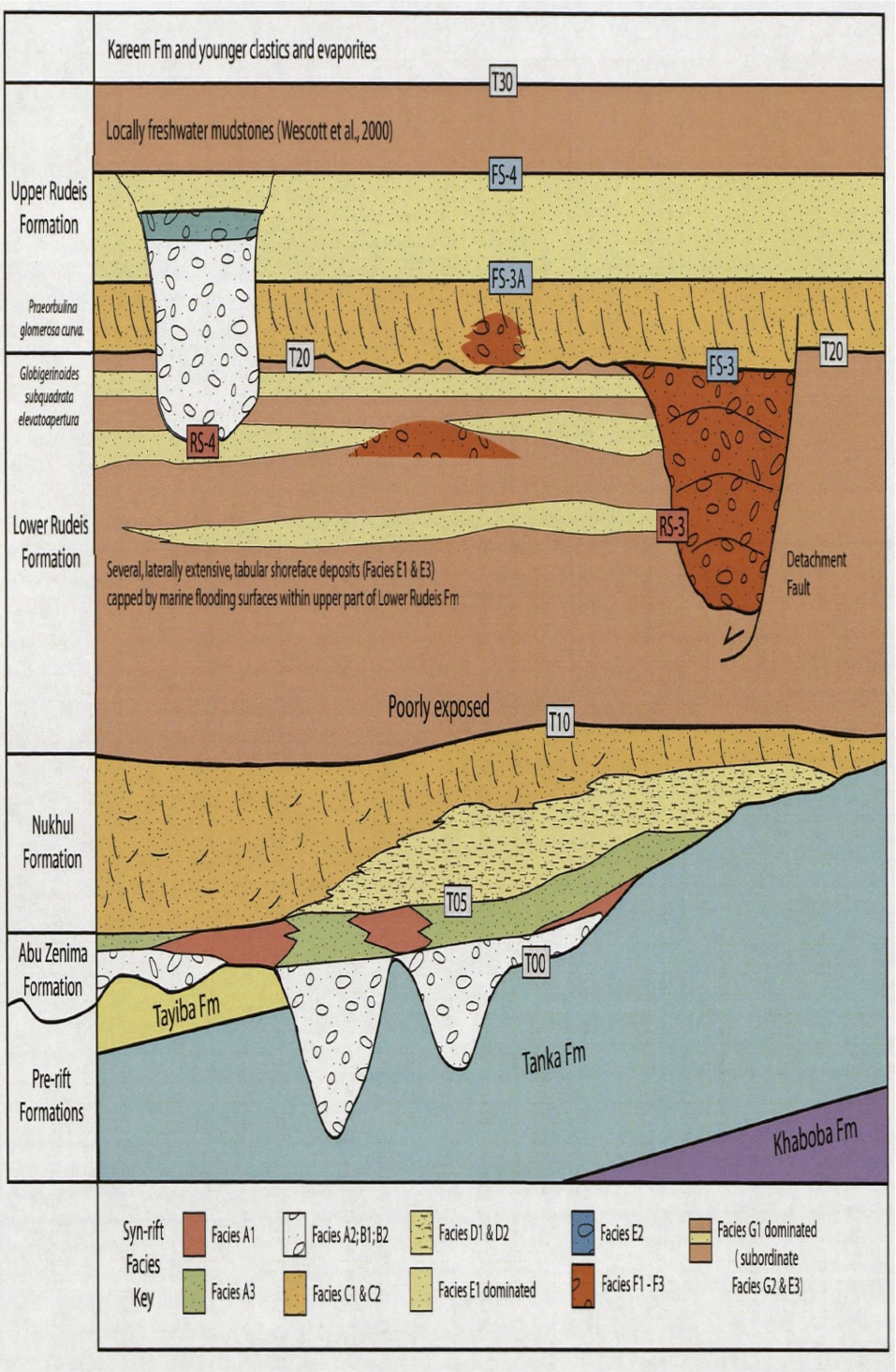

Figure 6.9. Schematic illustration of the key relationships between facies and key stratal surfaces identified in this study. Surfaces T00, T10, T20 and T30 are based on the nomenclature of Wescott et al., (1996) and Krebs et al., (1997). No scale implied.

Pre-rift to syn-rift contact (T00), and early rift marine transgression (T05)

A major erosional unconformity is identified at the base of the Oligo-Miocene syn-rift succession within the eastern margin of the rift (e.g. Garfunkel and Bartov, 1977; Patton et al., 1994; Jackson et al., 2006a) (Fig 6.9). Dated as late Early to early Late Oligocene in the Hammam Faraun Fault Block to the south, (Jackson et al., 2006a), the pre-rift to syn-contact (T00 in the schemes of Wescott et al., and Krebs et al., 1997) is observed at several differing locations within the study area with varying expressions. The base of the early syn-rift deposits characterised by the Abu Zenima and Nukhul Formations varies from a sharp contact characterised by onlap, to a markedly erosional contact associated with incision, along the uppermost surface of the underlying pre-rift. The uppermost units of the pre-rift succession are typically characterised by the Eocene carbonates of the Thebes, Darat and Tanka Formations, whereas locally, the shallow marine facies of the younger Tayiba Formation are located beneath the contact (Fig. 6.9). The hiatus associated with this major unconformity is interpreted to be diachronous throughout the rift (e.g. Patton et al., 1994), and this is mirrored at a smaller-scale, with differing relative ages for the rift initiation facies observed to lying unconformably above the contact across the study area (outlined below).

The switch from the continental facies of the Abu Zenima Formation (Facies Association A) to the shallow marine Nukhul Formation (Facies C1, and D1-D2) is generally characterised by a diachronous surface of transgression, T05 (Wescott et al., 1996; Krebs et al., 1997). Locally, such as in the immediate hangingwall of the Wasit Fault and on the Mheiherrat horst block, this trangressive surface marks the first onset of syn-rift deposition onto the underlying pre-rift and therefore becomes composite with T00.

Onset of the rift climax phase: (T10)

The syn-rift stratigraphic response to the onset of the rift climax phase during the Lower Rudeis Formation, associated with progressive fault linkage, the localisation of displacement onto fewer, larger faults and resultant increase in rift-subsidence rates (e.g. Garfunkel and Bartov, 1977; Steckler et al., 1988; Arthur and Richardson et al., 1988; Sharp et al., 2000a; Gawthorpe et al., 2003), is characterised in the study area by the major T10, trangressive flooding surface (Wescott et al., 1996; Krebs et al., 1997). Poorly exposed, this surface is characterised by a shift from shallow marine sandstones of Facies C1 and heterolithic Facies D1-D2, to a succession dominated by the offshore mudstones of Facies G1,

interbedded with siltstones to very-fine sandstones of Facies G2 and the shoreface to offshore transition sandstones of Facies Association E. Locally, coarser-grained conglomerates of Facies E3 and F2 occur as downlapping, sharp based lenticular lobes (Fig 6.9).

Composite unconformity (T20)

The abrupt switch associated with the transition from the rift climax Lower Rudeis Formation to the late rift climax Upper Rudeis Formation observed on the eastern rift margin has been the subject of much controversy (e.g. Patton et al., 1994). Termed the 'mid-clysmic' or 'mid-rudeis' unconformity after Garfunkel and Bartov, (1977) and comparative to the T20 hiatal terrace of Wescott et al., (1996) and (Krebs et al., 1997), exposures in the study area suggest this is a composite unconformity, and comprises of at least two other stratal surfaces which can be observed in the study area (Fig 6.9).

Regressive surface RS-3 & Flooding surface FS-3

Regressive Surface RS-3 is an erosive surface with a least 35 m of erosional relief towards the south of Gebel Gushea. The surface is characterised by an abrupt truncation of offshore basinal mudstones (Facies G2) and interbedded shoreface sandstones (Facies E1) containing the foraminiferal assemblage *Globigerinoides subquadrata elevatoapertura* and a shift to the chert-rich fan-deltaic conglomerates of Facies F1. Similar scale erosive surfaces at the same stratigraphic level and the associated facies shift to fan-deltaic, chert-rich conglomerate packages are documented to the south of the study area, in the area of the tip of the rift border Thal Fault (e.g. the Surface A of Young et al., 2000 and surface RS-4 of Young et al., 2002). Like the analogous surfaces to the south, RS-3 is interpreted to reflect a major fall in relative sea-level, with subsequent subaerial erosion, incision and bypass. Relative sea-level falls in extensional settings have the potential to be recorded in areas of reduced displacement, e.g. towards the tips of a fault zone, where subsidence rates may be outpaced by the rate of sea-level fall (e.g. Gawthorpe et al., 1994). The example observed in this study is poorly constrained being within the immediate hangingwall of a detachment fault within the syn-rift succession to the south, whereas to the immediate north of this conglomeratic body, RS-3 is observed to downcut through the uppermost part of the Lower Rudeis Formation present, before amalgamating with flooding surface FS-3. The infilling conglomerates of Facies F1 are approximately 35 m thick and laterally extensive over approximately 350 m. Flooding surface FS-3 is observed immediately above the chert-rich conglomerates of Facies

F1 towards the south of Gebel Gushea, and is characterised by a sharp switch to a 15 m thick package of metre-scale cross bedded sandstones of Facies C2. Throughout most of the study area, RS-4 and FS-3 are coincident and located towards the base of the sheet-like unit of Facies C2, which is interpreted as a combined surface of regression and transgression and equivalent to the T20 hiatal surface of Wescott et al., (1996) and Krebs et al., (1997).

Flooding surface FS-3A,

Located at the top of the sheet-like unit of metre-scale cross bedded sandstones of Facies C2, flooding surface FS-3A is characterised by a distinct reddish-coloured, carbonate cemented hard-ground, associated with extensive colonisation by marine fauna, typically by oysters, Pectens and benthic foraminifera (Fig 6.5; 6.9). In addition, Thalassinoides and Ophiomorpha burrows are also commonly observed at this surface, which marks a landward shift to interbedded packages of shoreface sandstones and offshore mudstones which contain the foraminiferal assemblage *Praeorbulina glomerosa curva*. These observations suggest that FS-3A represented a period of non-deposition or marked reduction in the rates of sediment accumulation. During this time, diagenesis beneath the immediate sediment water interface produced a hard substrate for the colonising fauna observed, (c.f. Taylor & Gawthorpe, 1993; Taylor et al., 1995). This interpretation is consistent with correlations of FS-3A into the axis of the rift with a candidate maximum flooding surface within a package of mudstones containing the first downhole occurrence of *Praeorbulina glomerosa curva* (Chapter Seven).

Regressive surface: RS-4

This regressive surface is characterised by marked incision into underlying units of metre-cross bedded sandstones Facies C2, the shoreface to offshore transition deposits of Facies Association E and offshore marine Facies Association G within the northern part of the Gushea Syncline (Fig 6.9). At least 25 m of erosional relief is observed over an area extending laterally up to 2.5 km, with the subsequent infilling of the resultant trough by the calcarenitic-rich, fluvial conglomeratic facies of Facies Association B, reefal-rich conglomerate Facies E2 and interbedded shoreface to offshore mudstones. The highly erosive nature and overall trough-shaped morphology of RS-3 and its subsequent fluvial to shallow marine infill, indicative of a major basinward facies shift, is consistent with the formation and subsequent backfilling of a major incised valley or channel during a period of relative sea-

level lowstand within the rift margin (e.g. Zaitlin et al., 1994). Laterally, RS-4 becomes amalgamated with flooding surface FS-4.

Flooding surface FS-4

Surface FS-4 is a prominent marine flooding surface which marks a landward facies shift from shoreface sandstones and interbedded offshore mudstones to an overall finer-grained package to offshore mudstones (Fig 6.9). The uppermost part of this post FS-4 succession towards Gebel El Mreir is associated with localised brackish to freshwater lacustrine mudstones (Wescott et al., 2000) before being capped by the basal evaporites of the Kareem Formation which approximately denote the T30 hiatal terrace (c.f. Wescott et al., 1996).

6.6. THE EVOLUTION OF FACIES DISTRIBUTION AND STRATIGRAPHIC ARCHITECTURE WITHIN THE ACCOMMODATION ZONE

In this section, the distribution of facies, the nature and thickness and architectural variability of key chronostratigraphic stratal units and their bounding surfaces outlined above, are described in relation to a number of the key structural elements within the study area. This evolution is considered at two stages: (1) rift initiation (Abu Zenima and Nukhul Formations) and (2), rift climax to late rift climax (Lower and Upper Rudeis Formations. Measured palaeocurrent data referred to is contained in Appendix 5.

6.6.1 Rift initiation

Two significant exposures of the rift initiation succession crop out at localities within the study area (Fig. 6.2). These are: (i) in the immediate hangingwall of the Wasit Fault (Figs. 6.2; 6.10) and (ii) at the northern confluence of the present day Wadi Silfa and Wadi Gharandal.

Wasit Fault hangingwall

The succession in the hangingwall of the Wasit Fault (Fig. 6.2, photopoint A) is characterised by an overall upwards trangressive vertical profile from the conglomerates, siltstones and sandstones of Facies Association A, to the hetrolitithic deposits of Facies Association D, and finally the cross bedded sandstones of Facies C1 and C2 (Fig 6.10). Structurally, the syn-rift succession lies unconformably above the pre-rift Tanka Formation,

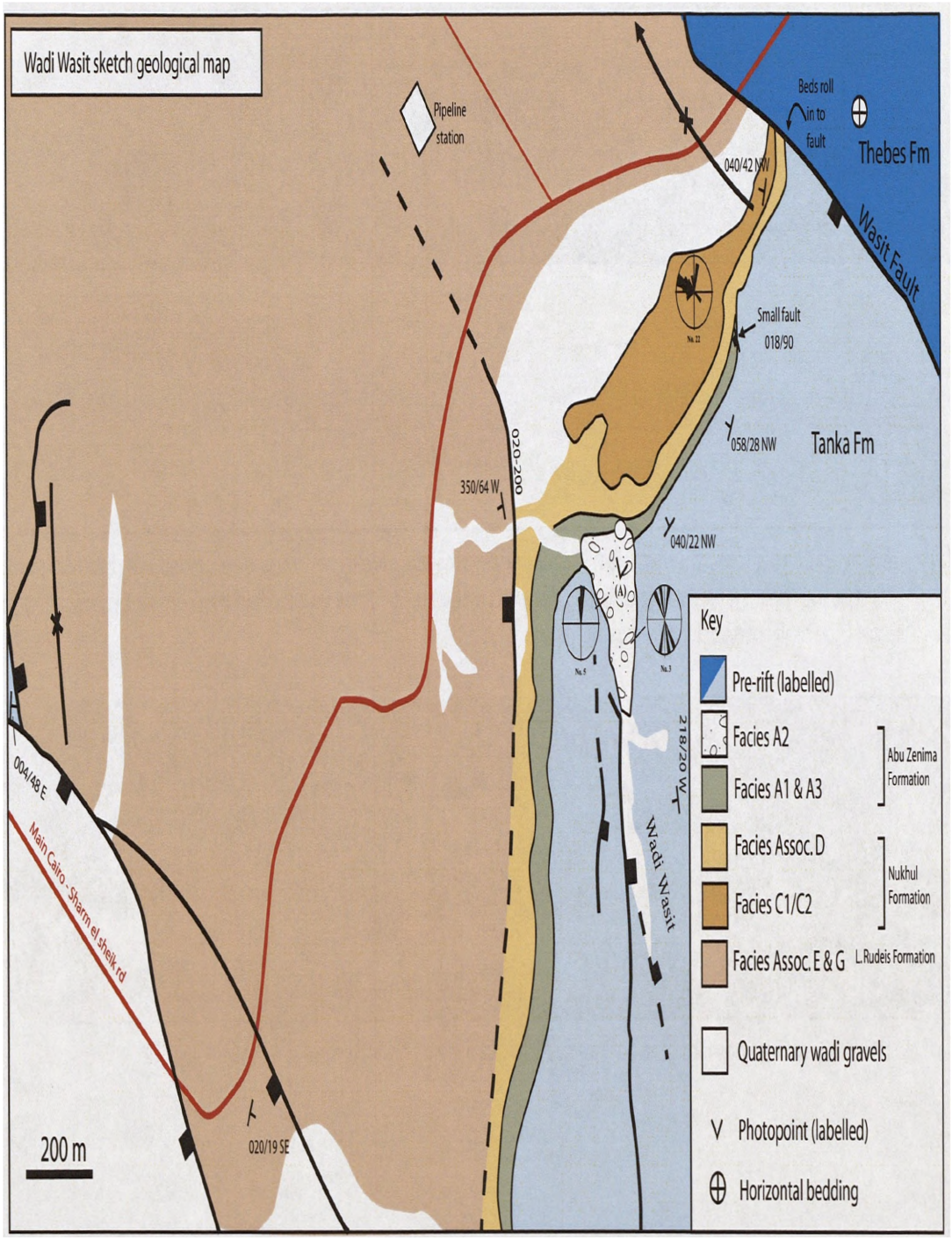

Figure 6.10. Simplified geological map of Wadi Wasit. Here early synrift deposits comprising a trangression from fluvial facies (Abu Zenima Fm) to shallow marine facies (Nukhul Fm) are observed onlapping onto a series of faulted pre-rift fault blocks. See text for discussion. Photopoint (A) is Figure y

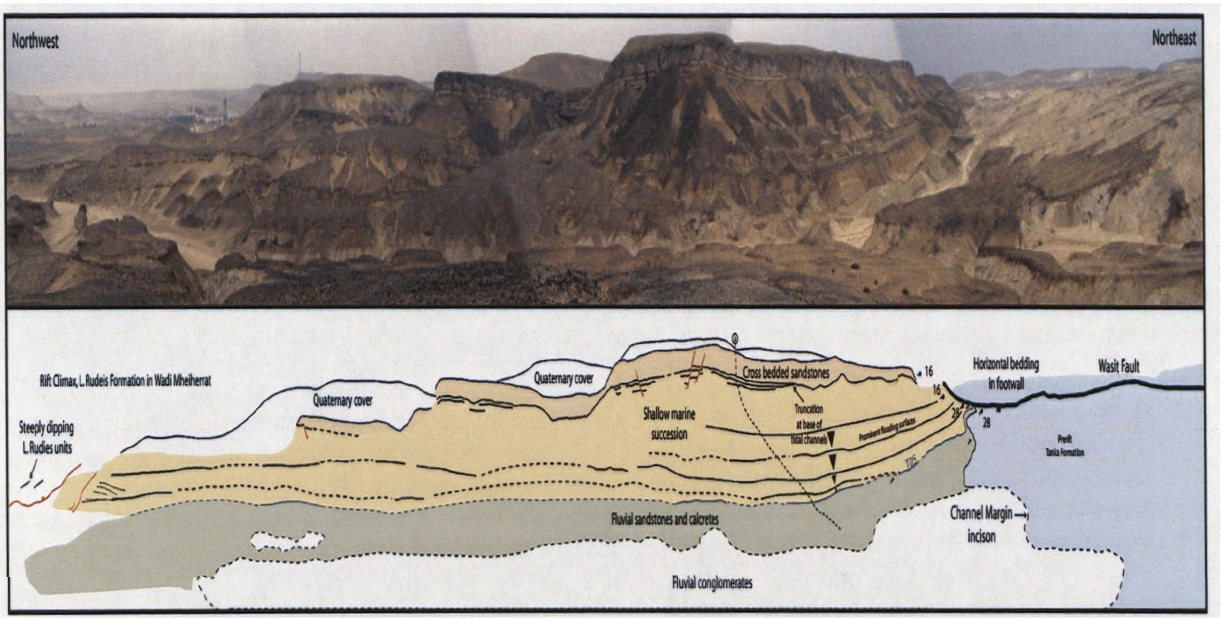

Figure 6.11a Photograph and associated line drawing interpretation to illustrate onlapping relationships of early syn-rift units onto the pre-rift Tanka Formation towards the immediate hangingwall of the Wasit Fault. Syn-rift facies present consist of an overall trangression from fluvial facies and intervening palaeosol development to shallow marine facies, culminating in the highly cemented cliff forming unit of tidal sandstones.

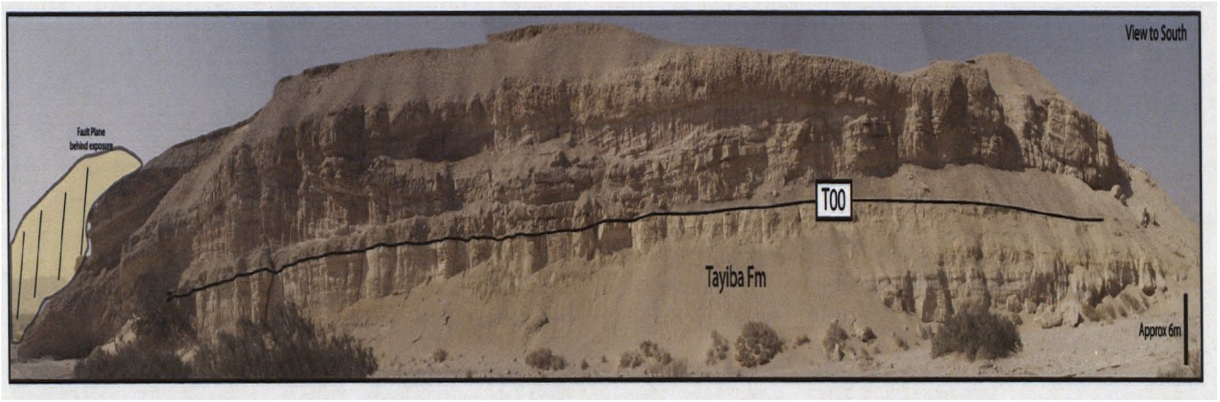

Figure 6.11b Photograph of early continental syn-rift deposits overlying the shallow marine pre-rift Tayiba Formation at Wadi Silfa - Gharandal.

which dips between 40-60° to the NW, and has a synclinal geometry in the immediate hangingwall of the fault, which plunges to the NNW. In contrast, the immediate footwall of the block is characterised by the Thebes Formation, which is sub-horizontally bedded, although beds immediately adjacent to the fault, appear to begin to dip towards the fault by a few degrees. The nature of the T00 contact in the hangingwall varies in a dip-orientated sense away from the fault zone. Approximately 700 m away from the fault, the T00 contact is associated with marked, channel incision. Here a > 100 m wide channel contains the limestone-rich conglomerates of Facies A2, which pass vertically in siltstones and sandstones of Facies A1 and A3 respectively (Figs. 6.10; 6.11). Clast imbrications indicate a dominant from S to the N palaeocurrent trend, whilst bi-directional gutter marks show a similar N-S orientation. The overlying fluvial sandstones (Facies A3) similarly are limestone clast dominated, but additionally contain rarer basaltic clasts. This facies can be traced laterally to the NE and towards the fault for approximately 400 m before pinching out (Fig.6.10). From this point to the fault, the T00 surface becomes coincident with the T05 surface marking the base of the shallow marine Nukhul Formation. Dominated by the hetrolithics of Facies association D, this succession is capped by tidal cross bedded sandstones of Facies C1/C2, with palaeocurrents from cross-bedding showing a dominant trend to the NW, and subordinate NNE and SEE trends. As with the underlying continental facies association, these shallow marine facies thin and progressively onlap towards the fault, whilst their associated dips show an up-section decrease. To the NW and across the main Cairo to Sharm El-Sheik road, the syn-rift succession passes into the mudstone dominated units of the Lower Rudeis Formation, where two major packages of Facies Association E form the limbs of a fault-parallel hangingwall anticline towards the tip of the Wasit Fault (Fig. 6.2).

Wadi Silfa – Wadi Gharandal confluence

At this location (Fig. 6.2, Photopoint B), the red continental siltstones and white conglomerates of the Abu Zenima Formation markedly contrast to the otherwise uniform buff to white gravels of locally extensive Quaternary cover. A linear exposure, approximately 25-30 m in length of these earliest rift initiation deposits are downthrown by a NE dipping fault, with Lower Rudeis Formation mudstones of Facies G1 in the immediate footwall (Fig. 6.12). The exposure is characterised by a approximately 15 m thick, interbedded succession of variegated mudstones (Facies A1), planar conglomerate sheets (Facies A2 and lenticular sandstone bodies (Facies A3). The T00 contact here is characterised by a sharp to erosional

contact between the of Facies A1 and laterally adjacent fluvial conglomerates and an underlying package of marine mudstones and sandstones interpreted to be the rarely preserved Tayiba Formation (e.g. Jackson et al., 2006a). Palaeocurrent data at this locality suggests an overall transport direction to the S-SSW.

6.6.2 Rift climax - late rift climax

The area considered in this chapter encompasses an extensive series of expousure of the rift climax to late rift climax deposits of the Lower and Upper Rudeis Formations. In this section, two localities are described: (i) western Gebel Gushea in the hangingwall to the antithetic Mheiherrat Fault and (ii) the incised palaeovalley at the northern part of Gebel Gushea (Fig. 6.2).

Mheiherrat Fault hangingwall: western Gebel Gushea

At this locality (photopoint C, Fig. 6.2), the antithetic Mheiherrat Fault bounding the Mheiherrat Fault Block to the west, strikes approximately N-S, and contains a thick Lower Rudeis and younger section in its hangingwall which dips away from the fault in the order of 2-5° to the E-NE. The immediate footwall of the fault is comprised of pre-rift Thebes and Tanka Formation limestones, which dip 5-10° to the W-NW. Approximately 180 m to he north of photopoint C in Figure 6.2, the Mheiherrat fault is mapped to tip out, and is characterised by an along-strike, fault-parallel anticline within the Lower and Upper Rudeis Formations.

Within the hangingwall to the Mheiherrat Fault, the Lower and Upper Rudeis Formations are characterised by marked along-strike variability (Fig. 6.12). Dominated by the fine-grained mudstones of Facies G1, the Lower Rudeis succession contains a series of stacked packages, typically up to 10 m thick, of shoreface sandstones (Facies E1 and E3) which are capped by prominent, and laterally extensive flooding surfaces. A number of coarser-grained, conglomeratic, lenticular packages of Facies F2 are occur at differing stratigraphic levels, and which are commonly onlapped by overlying shoreface sandstones. Laterally along-strike, these conglomerates grade into the tidally cross bedded sandstones of Facies C1 and C2. The T20 surface within this hangingwall setting is typically picked out by a sharp to locally erosive basal surface, bounding a 15 m thick, laterally extensive sheet of metre-scale cross bedded sandstones (Fig. 6.12). However, to the south, this package onlaps the large fan-deltaic body (Facies F1), with up to 35 m of associated incision at its base which

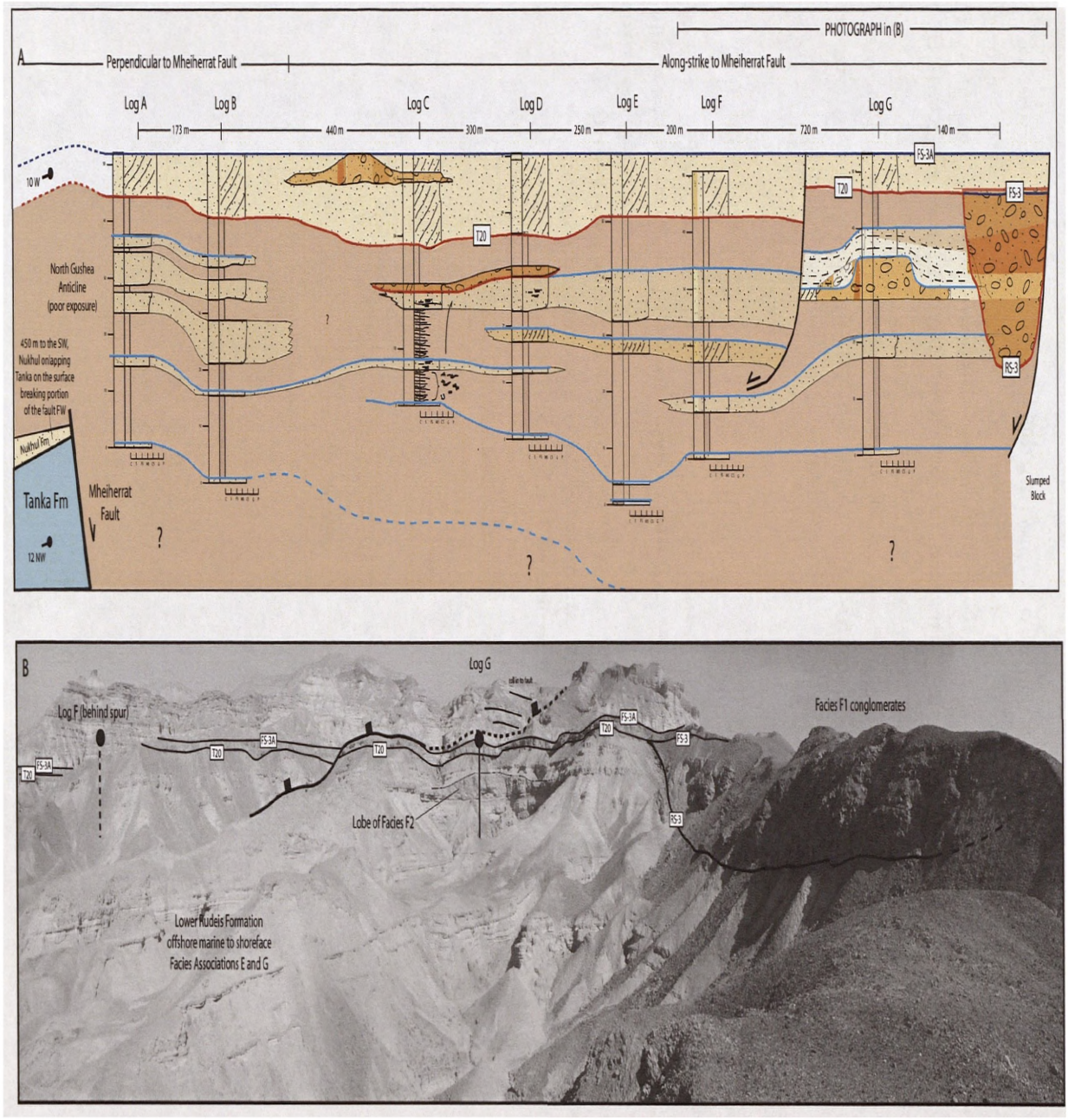

Figure 6. 12. A) Correlation panel initially along-strike, and then perpendicular to the Mheiherrat Fault and associated anticline towards its northern tip. Datum = FS-3A. Logs A-G located in Figure 6.2. For key to facies, see Figure 6.9. B) Photopan centred on Log G.

has been referred to previously. Clear incision into underlying units is observed on the northern side of this coarse-grained unit, however the southern margin appears to be in part controlled by the location of a detachment fault within the syn-rift succession. As shown in Figure. 6.12, logs F to G, other detachment faults are recorded within the hangingwall of the Mheiherrat Fault which control thickness variations.

To the northern tip of the fault, (Fig 6.12, logs B and A), both the Lower Rudeis and Upper Rudeis intervals are inferred to thin toward the fault, and form part of a fault tip fold (Fig. 6.2).

North Gebel Gushea – Palaeovalley

Figure 6.13 shows a regional panorama orientated towards the North along the north-western limb of the Gebel Gushea syncline (located in Fig. 6.2 photopoint D). This regional viewpoint illustrates how the offshore to shallow marine Lower and Upper Rudeis succession, sub FS3-A, is truncated and replaced along strike by the thick, up to 25 m, coarse-grained, white fluvial conglomerates of Facies Association B. The marked basinward shift in facies here is consistent with the observations made with respect to the other main principle coarse-grained conglomerates of Facies F1, the significance of which is discussed below.

Figure 6.13. Photograph showing stratal relationships towards the NW limb of the Gushea Syncline. A major erosive surface, RS-4 cuts down into underlying marine sandstones and mudstones of Facies C2 ,Facies Associations E and G, and bounding surfaces T20 and FS-3A . Immediatly above RS-4, a thick package of the fluvialc onglomerates of Facies Association B, thin and onlap towards the north. The upper-most part of the succession is characterised by interbedded mudstones and shoreface sandstones, capped by FS-4.

6.7. DISCUSSION: EARLY RIFT TO RIFT CLIMAX EVOLUTION OF THE ZAFARANA ACCOMMODATION ZONE WITHIN THE EASTERN RIFT MARGIN

The observations of the distribution of facies, thicknesses, and stratal surfaces described in this study, both temporally through the syn-rift succession and spatially adjacent to individual structures, are consistent with previous models for the linked tectono-stratigraphic evolution of normal fault zones. These models suggest that fault populations may evolve from numerous, isolated faults with limited displacement, to fewer, but increasingly linked fault arrays with increased displacement rates (e.g. Cowie et al., 1998; Gupta et al., 1998; Cowie et al., 2000; Gawthorpe and Leeder, 2000; Dawers and Underhill, 2000). This is broadly reflected in the syn-rift succession within the study area, and its overall trangressive nature from initially continental through to shallow marine and subsequently deeper marine facies; thus mirroring classical models for syn-rift infill (e.g. Prosser, 1993).

With respect to the four specific localities discussed, the two rift initiation exposures show facies and stratal relationships which readily conform to accepted tectono-stratigraphic geometries for rift initiation times listed above. Within the hangingwall to the Wasit Fault, early incision of the pre-rift Tanka Formation with NW-orientated sediment transport reflected localised uplift by a series of present-day low displacement blocks within the Tanka Formation immediately to the south. Continued faulting led to the development of more extensive drainage pathways which sourced Oligocene volcanics, documented to the south, just outside the study area (Wescott et al., 1998). The Wasit Fault during this earliest syn-rift stage was expressed at the surface as a flexural monocline in response to the fault being blind at depth, thus accounting for the classical onlap and truncation observed towards the hangingwall of a subsequently surface-breaking fault (*sensu* Gawthorpe et al., 1997; Sharp et al., 2000b). Palaeocurrents, bedding dips and continued stratal unit thinning towards the fault indicate that the Wasit Fault persisted as a non-surface breaking monocline well into the deposition of the shallow Nukhul Formation, with rupture likely to have occurred during the subsequent deposition of the rift climax Lower Rudeis Formation. This is corroborated by the presence of Facies Association G in the hangingwall further to the NW, juxtaposed to the Tanka Formation in the footwall.

The locality at Wadi Silfa – Gharandal, located as it is in the present day major wadi system is evidence for the existence of a major, long-lived sediment transport pathway within

the accommodation zone from the rift shoulder to axis, from Late Oligocene time to the present day. In fact, the palaeocurrent data obtained here mirror the same trend as the present day wadi and link to observed thickness variations offshore of the Ras Lagia area (Fig 6.1). This is interpreted to be linked to the lack of a single, major rift border fault zone within the study area. As shown in Figure 6.2 to the north of photopoint B, the tip of the rift border Silfa Fault marks the beginning of a major, 15 km wide structural relay ramp from the rift margin to the tip of the Thal Fault tip (Fig. 6.1), as documented in the studies of Young et al., (2002, 2003). Thus, this relay ramp has focussed sediment input from the rift shoulder from the Late Oligocene and Early Miocene to the present day. The proximal part of the Zafarana Accommodation Zone is therefore likely to have continually been an area with a high sediment supply to accommodation space ratio relative to other locations along the rift margin. This is shown by the laterally extensive and sheet-like nature of many of the subsequent rift climax to late rift climax packages of Facies Associations C and E throughout the study area, which can be correlated over 10's of km's. This is in marked contrast to locations within the immediate hangingwall of the rift border fault to the Hammam Faraun Fault Block, which are interpreted to have a lower sediment to fault-generated accommodation space ratio. In these locations, such as Sarbut El Gamal, facies and thickness variations are comparatively rapid, occurring over distances of 500 – 1000 m (e.g. Leppard and Gawthorpe et al., 2006).

The other two specific localities described in this chapter, with reference to the rift climax to late rift climax part of the succession, illustrate two principal differences to generally accepted models for the tectonostratigraphic development of rift basins: (i) the role of relative sea-level falls within a rift and (ii) the relative timing of fault activity during the rift and resultant stratigraphic architectures.

Previous research has documented how rates of eustatic sea-level fall may be outpaced by contemporaneous or higher rates of fault related subsidence along normal fault systems (Gawthorpe et al., 1994). Combining this understanding with other studies which have discounted previously proposed eustatic fluctuations in extensional settings in favour of tectonic activity (e.g. during the Jurassic of the North Sea and Greenland Rifts, e.g. Underhill, 1991; Surlyk, 1991), may lead to disregarding the importance of relative sea-level falls upon syn-rift sedimentation. However, it is important to recognise that regional changes in base-level may have a major impact at lower accommodation settings within a rift, i.e. at fault tips and within a rift-wide scale, diffuse structural accommodation zone. This study documents a series of basinward shifts during the late rift climax phase, marked by broad incision and the

coalescence of key stratigraphic surfaces, as shown by the composite nature of the T20 hiatal surface (Fig 6.9). As a result, correlation of areas across a rift with differing levels of fault-generated accommodation space requires detailed examination of surfaces, and how these surfaces and associated facies shifts vary laterally. Furthermore, this study illustrates how using surfaces and associated facies shifts from a single tectonic setting in a rift, specifically at the rift margin, may not provide a full account of tectono-stratigraphic evolution of a rift, and requires comparison with higher accommodation space settings, e.g. the rift axis.

The second important distinction provided by this study, is the observation that mesoscale (*sensu* Sharp et al., 2000a), intra-block faults may remain active late in the evolution of a rift within a diffuse accommodation zone setting. This is demonstrated by the thickness variations both along strike within the hangingwall and across the intra-block Mheiherrat Fault, the tip of which is associated with a fault propagation fold of the Lower and Upper Rudeis Formations. This is in marked contrast to observations in discrete fault blocks, such as the Hammam Faraun Fault Block to the south, which are characterised by classical half-graben geometries. Several studies of this fault block have demonstrated how models of fault displacement localisation can be applied to the timing of activity upon major, through-going fault zones during the rift climax period (e.g. Sharp et al., 2000a, Gawthorpe et al., 2003). These studies show how the major half-graben bounding faults became the principle sites of fault-displacement and thus provide the main control on coeval depositional systems. In contrast, within the more structurally diffuse Zafarana Accommodation Zone, both small mesoscale faults and fault-related folding continued to control syn-rift thickness, facies and stratal architecture until relatively late into the rift's history.

6.8. Conclusions

Three generic conclusions from this chapter for syn-rift sedimentation within accommodation zones are:

1) Structural accommodation zones within rifts may be associated with prolonged, high fluxes of sediment supply from rift initiation to late rift climax. Due to the diffuse nature of structural activity, resultant relief may be characterised by more gentle gradients compared to a half-graben setting. This may result in broad, extensive depositional systems which rapidly infill the limited accommodation space generated by the distributed, and low

displacement fault-generated subsidence. Resultant deposits may be sheet-like in nature and strongly progradational.

2) This relatively low nature of structural relief within a structural accommodation zone compared to adjacent, larger half-graben domains, may be registered during periods of relative sea-level fall, (regardless of mechanism) by marked incision, bypass and amalgamation of key stratal surfaces within the syn-rift succession. This is in marked contrast to higher accommodation space settings, where a contemporaneous relative sea-level fall may not be recorded.

3) The relative timing of structures within an accommodation zone may effectively 'lag' behind those within an adjacent half-graben structural domain. This can be manifested in the development of syn-rift stratal geometries that models might suggest for the earliest phases of rift evolution. Thus the roles of low displacement faults and fault propagation folds can continue to impact upon rift climax to late rift climax depositional systems within a structural accommodation zone.

CHAPTER SEVEN

SEQUENCE STRATIGRAPHY OF LATE RIFT CLIMAX DEPOSITS: RIFT-WIDE OBSERVATIONS OF THE IMPACT OF REGIONAL SEA-LEVEL VARIATIONS UPON THE UPPER RUDEIS FORMATION, SUEZ RIFT, EGYPT.

CHAPTER 7: SEQUENCE STRATIGRAPHY OF LATE RIFT CLIMAX DEPOSITS: RIFT-WIDE OBSERVATIONS OF THE IMPACT OF REGIONAL SEA-LEVEL VARIATIONS UPON THE UPPER RUDEIS FORMATION, SUEZ RIFT, EGYPT.

7.1. ABSTRACT

This chapter provides an analysis of the sedimentology and sequence stratigraphy of the late rift climax Upper Rudeis Formation using observations derived from the central dip province and northern structural accommodation zone of the Oligo-Miocene Suez Rift. A comprehensive subsurface dataset from the present day offshore axis of the rift is integrated with extensive exposure within the onshore component of the northern accommodation zone and compared to previously examined outcrops elsewhere along the Sinai margin. Regionally consistent key stratal surfaces, calibrated by biostratigraphic data are used to subdivide the Upper Rudeis Formation into a series of high-resolution stratal units, which are then correlated from the rift axis to rift margin. This allows for the spatial and temporal variability of the Upper Rudeis Formation to be compared across the main structural domains characteristic of rift basins. As a result, this study provides a model for contemporaneous linked tectono-stratigraphic evolution of late rift-climax syn-rift depositional systems across a rift basin.

The Upper Rudeis Formation is characterised by an overall transisition from shallow to offshore marine facies from the rift margin to rift axis and is comprised of both regionally extensive depositional systems sourced from a major hinterland present along the rift shoulder, and more locally limited deposits, derived from individual uplifted footwall blocks. Whilst observed to have varying stratigraphic architectures at differing structural locations, the regionally correlated key surfaces delineate consistent basinward and landward shifts in the location of principal Upper Rudeis depositional systems. Previous studies, based heavily upon examined exposures at the rift margin, have linked the onset of deposition of the Upper Rudeis Formation to a major tectonic reorganisation of the rift, the cause of which has proved controversial. Rather than a response to an isolated episode, this study suggests that the observed variability of the Upper Rudeis Formation reflects marked changes in regional relative sea-level, largely driven by glacio-eustasy, upon syn-rift sedimentation during a period of reduced and episodic fault activity.

This chapter provides an example of the contemporaneous variability of sediments deposited during a period of late rift climax in response to the interplay of evolving structurally controlled phyisography and bathymetry, variations in regional base-level and differing sediment source areas and transfer pathways. The importance of regional controls upon sedimentation documented in this study has implications for the development of syn-rift tectono-stratigraphic models.

7.2. INTRODUCTION

Within extensional basins, the principal control upon the availability of accommodation space, and likewise the location of consequent drainage networks and resultant sediment dispersal patterns associated with syn-rift sedimentation, is the marked spatial and temporal variation in tectonic subsidence or uplift linked with the evolution of normal fault zones (e.g. Gawthorpe & Leeder, 2000). General models for the linked tectonic and stratigraphic development of rift basins distinguish between three broad evolutionary phases: a rift initiation phase, characterised by numerous, small, isolated faults with low displacement rates, succeeded by fewer, but increasingly linked, larger faults with higher rates of displacement during a rift climax phase, and finally, a period of waning fault activity and reduced overall subsidence associated with the transition to the post rift phase (e.g. Prosser, 1993; Cowie et al., 1998, 2000; Gawthorpe and Leeder, 2000). The interaction of this localised evolving tectonic control within extensional basins with more regional changes in eustasy and climate has been suggested to result in a complex distribution of syn-rift sedimentary facies types and stratigraphic architectures (e.g. Gawthorpe et al., 1994; Howell and Flint, 1996; Ravnas and Steel, 1998; Gawthorpe and Leeder 2000). Therefore high resolution studies of syn-rift sequence stratigraphic and facies variability have been typically conducted at the discreet fault zone or individual fault block scale. Moreover, regional rift-wide tectonostratigraphic models have largely been conceptual in nature, comprising data from differing sub-basins within a rift, with the potential for marked contrasts in relative ages.

The Oligo-Miocene Suez Rift provides an ideal setting to study high resolution, contemporaneous variations in syn-rift sedimentation and resultant sequence stratigraphic architectures at a regional, rift-wide scale. Excellent, non-inverted exposures at the rift margin may be confidently correlated with extensive industry subsurface penetrations within the rift

axis within the resolution of a robust biostratigraphic framework. Previous workers have identified and correlated high resolution stratigraphic surfaces associated with the rift climax succession, both at the main rift bounding and intra-block faults within the exposed Hammam Faraun and El Qaa Fault Blocks of the rift margin, (e.g. Gawthorpe et al., 1990; Gupta et al., 1999; Sharp et al., 2000a, b; Young et al., 2000, 2002; Gawthorpe et al., 2003; Leppard and Gawthorpe 2006) and individual subsurface fault blocks within the rift axis (e.g. Dolson et al., 1996; Pivnik et al., 2003). However, these studies have been largely considered in isolation and are therefore unable to accurately distinguish local versus regional controls upon stratigraphic and sedimentary response to a regional series of growing fault arrays. Previous attempts to address this through the development of regional correlation schemes within the rift have considered the entire syn-rift megasequence and are therefore relatively low in resolution (e.g. Wescott et al., 1996; Krebs et al., 1997).

The aim of this chapter is to develop a regional, contemporaneous rift-wide, high-resolution sequence stratigraphic synthesis for the late rift climax Upper Rudeis Formation to assess the role of regional versus local competing controls upon syn-rift depositional systems and stratigraphic development in differing structural settings within the Suez Rift.

7.3. DATASET AND METHODOLOGY

This chapter draws upon data and observations from both published sources and examples documented in this study which are located within three principal tectono-stratigraphic domains: (a) rift axis, (b) rift margin and (c) major structural rift accommodation zones (Fig. 7.1). Both the rift axis and margin settings are typified by classic tilted half-graben geometries, whilst the transverse orientated accommodation zones are considered as a separate setting as they are characterised by more distributed deformation style, resulting in subtle topography and therefore reduced topographic or bathymetric gradients compared to the major fault blocks in adjacent dip provinces.

Within the present-day offshore rift axis, two regional scale subsurface datasets comprising a combined total of approximately 500 wells, with 6 cored intervals totalling some 275 m of core and a comprehensive suites of wireline log and biostratigraphic information was examined. These data were complimented by structural interpretations derived from a number of depth migrated 3D seismic surveys, extensively constrained by borehole information as

shallow, intercalated evaporitic and clastic sediments of the later part of the syn-rift succession hinder accurate imaging of the majority of the pre- and syn-rift succession and the structural configuration at depth (e.g. Zaki et al., 1990). Principal fault blocks examined in this chapter within the rift axis include the October and adjacent Amer Fault Blocks in the northern part of the central dip province, and the West July, July, Safa-Mawa and Ramadan Fault Blocks located towards the southern part, whilst the western part of the offshore component of the Zafarana Accommodation Zone on the Warda Fault Block is additionally examined (Fig 7.2).

Upon the exposed eastern rift margin in the Sinai Peninsula, considered study areas include Wadi Feiran, located within the El Qaa Fault Block (Wescott et al., 1998), the South Gebel Gushea and Gebel Gawher areas located towards the northern end of the Hammam Faraun Fault Block (Young et al., 2000, 2002) and Wadi Gharandal within the diffuse Zafarana Accommodation Zone, between the Hammam Faraun and Sudr Fault Blocks (this study; Chapter 6) (Fig. 7.2). Widespread exposure of the Upper Rudeis Formation within the outcropping portion of the Zafarana Accommodation Zone is associated with arid climatic conditions and extensive ephemeral wadi incision. Resultant excellent pseudo three-dimensional exposure allows for the correlation of sedimentary and thickness data through the direct tracing or 'walking out' of key surfaces between measured sections, thereby documenting lateral facies and stratigraphic variations in the order of > 1000's m.

7.4. GEOLOGICAL SETTING

The Suez rift is a failed intracontinental rift between the North African and Arabian plates which developed as a northern continuation of the Red Sea rift (Fig.7.1). Rifting is estimated to have initiated in the Late Oligocene and Miocene, (ca 24 Ma), with a cessation in fault activity thought to coincide with transfer of significant extension to the Dead Sea – Aqaba transform (ca 15.5 Ma), (e.g. Colletta et al., 1988; Richardson & Arthur, 1988; Patton et al., 1994; Moustafa 2002). Trending NW-SE, the Suez rift is up to 80 km wide and 300 km long and is commonly divided into three structural provinces, defined as the northern, central and southern dip provinces. Within each province, smaller scale fault blocks (10-15 km wide, by 20-30 km long) and associated bounding faults display a consistent dip direction, with 180° switches in polarity observed across two structurally diffuse structural accommodation zones. Termed the Zafarana and Morgan Accommodation Zones in the north and south respectively,

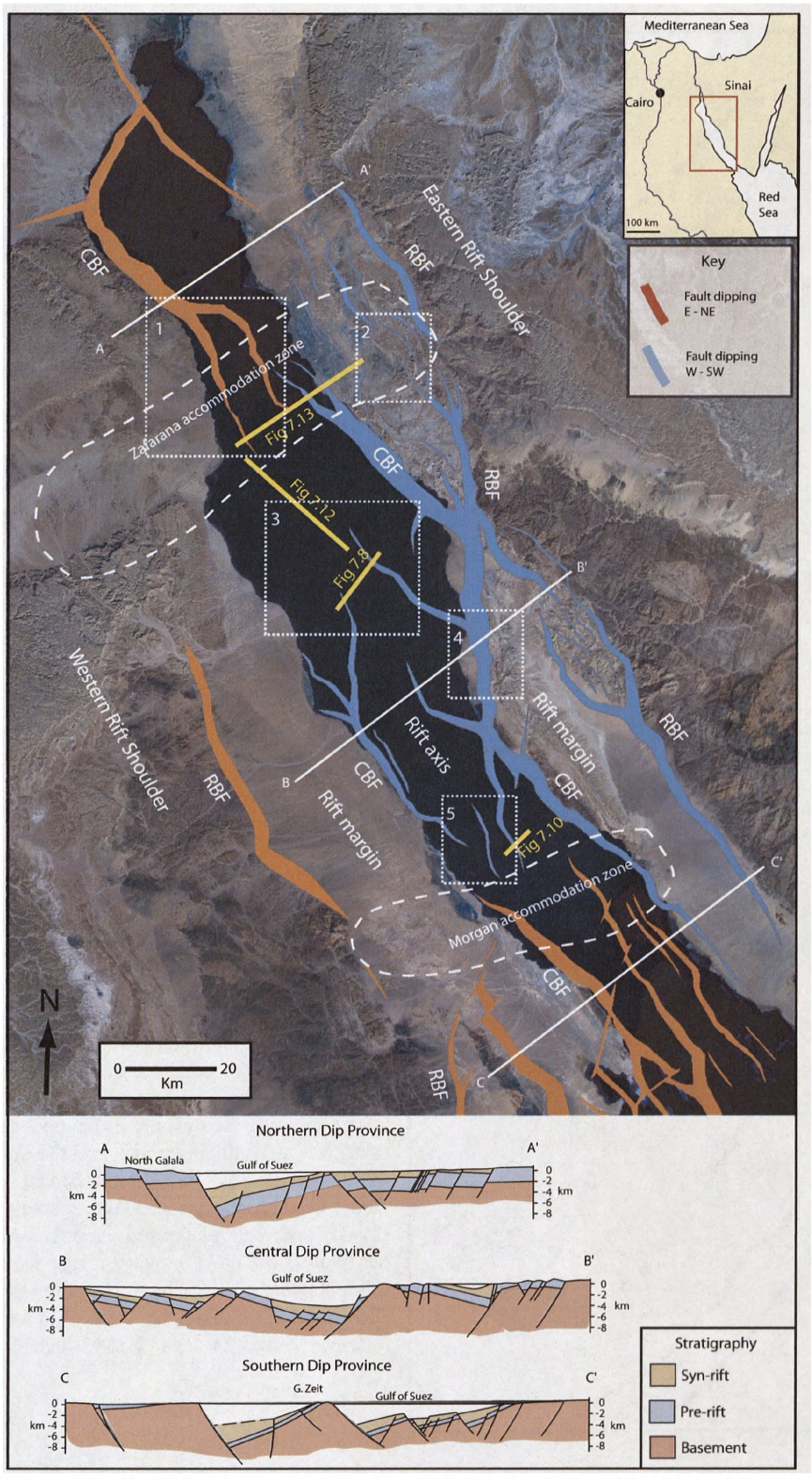

Figure 7.1. Simplified fault map of the Suez Rift showing faults with > 1km of displacement (modified after Younes and McClay, 2002) superimposed upon a regional landsat image. RBF= Rift Border Fault system; CBF = Coastal Boundary Fault system. Corner inset displays regional context of rift location. Lines A-A', B-B' and C-C' refer to cross sections which highlight the change in dip between the three structural dip provinces (after Patton et al., 1994), whilst the location of the northern (Zafarana) and southern (Morgan) accommodation zones are shown. Inset boxes 1-5 refer to specific locations discussed in this study, shown in Figure 7.2. Approximate lines of section for Figures 7.8, 7.10, 7.12 and 7.13 are also indicated.

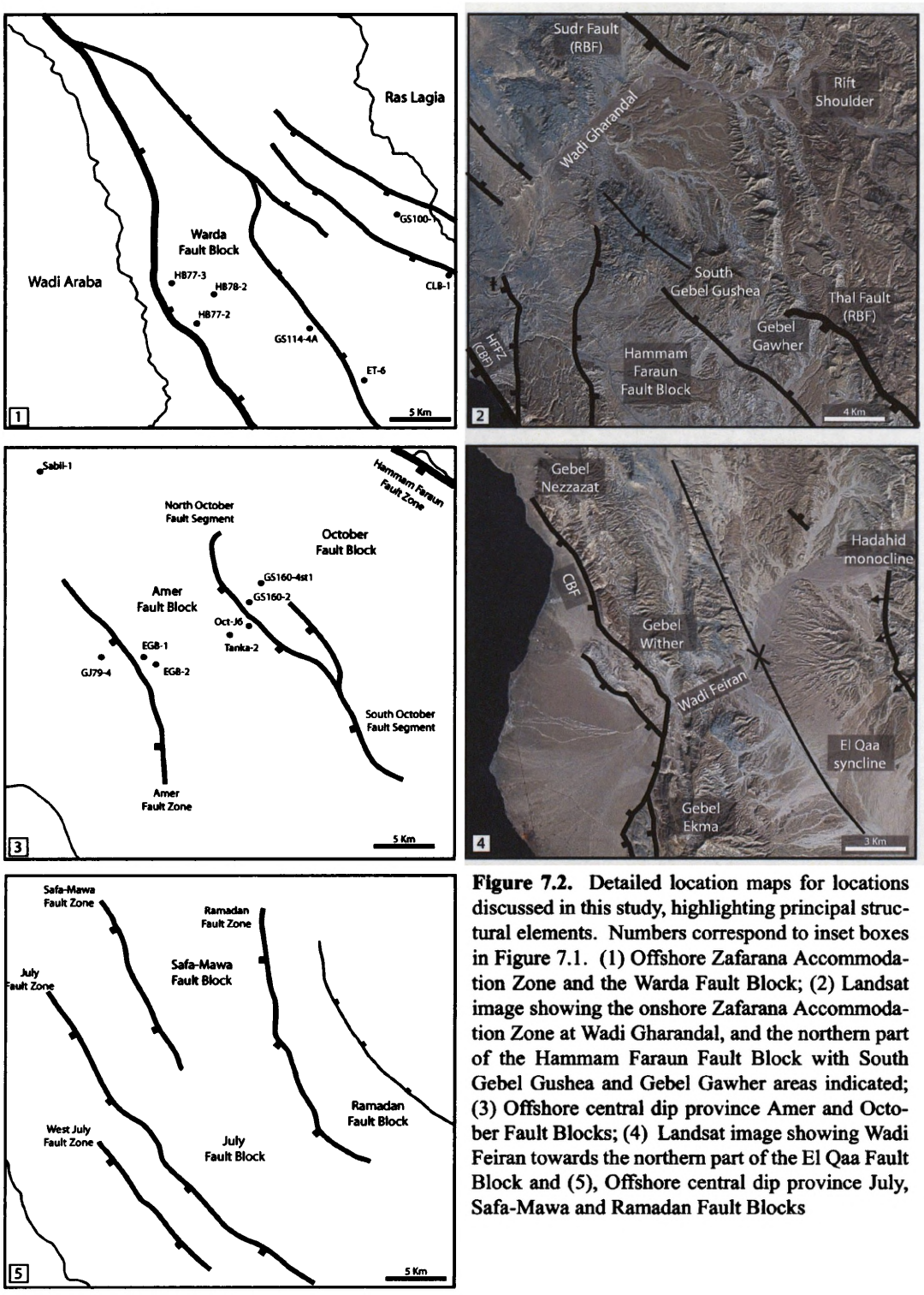

Figure 7.2. Detailed location maps for locations discussed in this study, highlighting principal structural elements. Numbers correspond to inset boxes in Figure 7.1. (1) Offshore Zafarana Accommodation Zone and the Warda Fault Block; (2) Landsat image showing the onshore Zafarana Accommodation Zone at Wadi Gharandal, and the northern part of the Hammam Faraun Fault Block with South Gebel Gushea and Gebel Gawher areas indicated; (3) Offshore central dip province Amer and October Fault Blocks; (4) Landsat image showing Wadi Feiran towards the northern part of the El Qaa Fault Block and (5), Offshore central dip province July, Safa-Mawa and Ramadan Fault Blocks

these zones may be approximately 15 to 50 km in width and extend transversely across the entire rift (e.g. Moustafa 1976, 1993; Patton et al., 1994; McClay et al., 1998; Coffield and Schamel 1989; Younes and McClay 2002). The rift can be further divided into rift marginal and axial components along its NW-SE axis, with the western and eastern margins exposed within the Eastern Desert and Sinai Peninsula respectively, bounded by a major (> 2 km scale displacement) Rift Border Fault System, outboard of the rift shoulder. The present-day marine Gulf of Suez occupies the inner axial portion of the rift and is separated from the rift margin by another series of major km scale displacement faults referred to as the Coastal Boundary Fault System (Fig. 7.1).

The Oligocene to Early Miocene syn-rift succession consists of an overall deepening succession from continental, through shallow marine to deeper marine facies that is interpreted to reflect the sedimentary response to an increase in fault-related subsidence from rift initiation to rift climax times (e.g. Patton et al., 1994; Sharp et al., 2000; Gawthorpe et al., 2003), and which is consistent with models for overall subsidence within the rift (Moretti and Colletta 1987; Evans, 1988; Steckler et al., 1988; Richardson and Arthur, 1988). Graphic correlation of foraminiferal assemblages has identified a series of biostratigraphic terraces interpreted to reflect major, basinwide hiatuses (Wescott et al., 1996; Krebs et al., 1997). The intervening biostratigraphic sequences (Fig. 7.3) do not correspond to depositional sequences, (*sensu* Vail et al., 1977) but rather can be broadly related to the large-scale tectonostratigraphic evolution of the rift (Wescott et al., 1996).

The Upper Rudeis Formation which provides the focus for this study (Fig. 7.3), is equated to Sequence S_{30} in the scheme of Wescott et al (1996) and Krebs et al (1997), and is bounded above and below by the biostratigraphically-defined hiatal surfaces T_{30} and T_{20} respectively. The T_{2o} hiatal surface is commonly equated to a proposed major tectonically-generated unconformity, termed the mid-Clysmic or mid-rudeis event (e.g. Garfunkel & Bartov, 1977; Patton et al., 1994), the nature and origin of which has proved controversial (see discussions in Patton et al., 1994 and McClay and Bosworth, 2001). Several authors have suggested that the subsequent Upper Rudeis Formation records an overall basinward shift in facies from those of the preceding deeper-marine dominated, rift climax Lower Rudeis Formation (S_{20}) (e.g. Garfunkel & Bartov, 1977; Evans, 1988; Smale et al 1988; Pivnik et al., 2003; Young et al., 2000; 2002; Chapters 4, 5 and 6). The Upper Rudeis Formation was

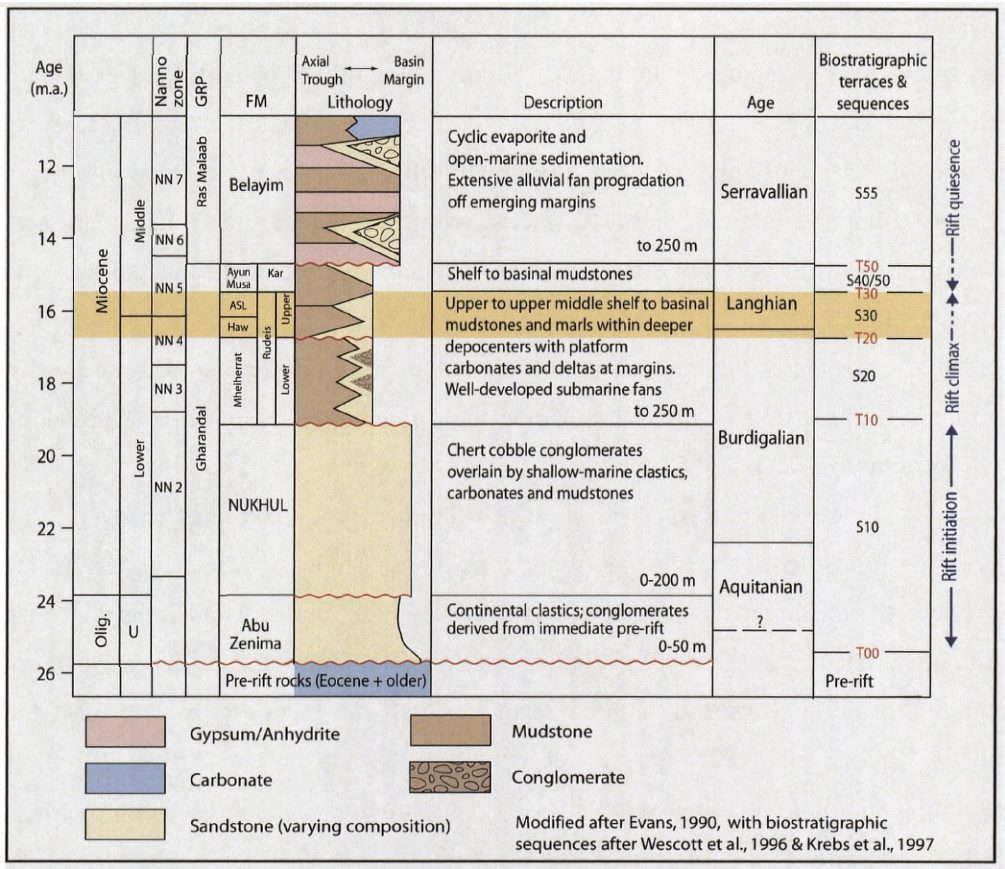

Figure 7.3. Late Oligocene to Middle Miocene stratigraphic column for the synrift infill of the Suez rift, showing typical lithofacies, lithostratigraphic based formations and the biostratigraphic defined hiatuses and intervening sequences of Wescott et al., (1996) and Krebs et al.,(1997). These biostratigraphic sequences correspond to the major tectonic evolutionary stages of the rift. The Upper Rudeis Formation, the focus interval of this study is bounded by the T20 and T30 hiatal surfaces and succeeds the onset of rift climax associated with the basinal mudstones and submarine fans of the Lower Rudeis Formation. Modfied from Evans (1990).

deposited during the latter stages of the main rift climax phase (*ca.* 16.6 to 15.8 Ma), characterised by a switch to waning and more episodic fault activity associated with an overall transition to Middle Miocene tectonic quiescence, a view supported by both subsidence models (e.g. Steckler et al., 1988; Evans et al., 1988; Richardson and Arthur, 1988) and detailed studies of individual fault activity (e.g. Pivnik et al., 2003). Increasing tectonic quiescence is reflected in the deposition of the Kareem (S_{40}-S_{50}), Belayim (S_{55}), the progressive evaporitic nature of which is thought to represent an increasingly complex interplay between eustatic and tectonic effects, (Bosworth & McClay, 2001).

7.5. OVERVIEW OF THE SEDIMENTOLOGY OF THE UPPER RUDEIS FORMATION

Although a detailed sedimentological study of the Upper Rudeis Formation is outside the scope of this chapter, understanding the main facies associations and their variable distribution within the rift is necessary for constraining the nature of stratigraphic surfaces identified, (Table 7.1). Table 7.1 documents the nature of the main sedimentary facies associations observed and summarises the principle observations and interpretations from this study (Chapters 4, 5 and 6) and previous research (Smale et al., 1988; Evans, 1988, 1990; Allen et al., 1994; Gawthorpe et al., 1990; El-Heiny and Enani, 1990; Elbaz and Handley, 1994; Patton et al., 1994; Young et al., 2000, 2002; Pivnik et al., 2003), allowing for a basinward synthesis for the deposition of the Upper Rudeis Formation.

7.5.1 Principal Facies Associations

Within the rift margin, tidally-influenced shelf, coarse-grained fluvial-deltaic, shallow marine shoreface and offshore basinal mudstone Facies Associations are recognised at outcrop. In the subsurface of the rift axis, localised examples of the coarse-grained deltaic Facies Association, and more regionally extensive submarine fan Facies Association against a background dominated by the offshore basinal mudstone Facies Association are recognised in cored section and calibrated wireline logs.

The tidally-influenced shelf Facies Association is characterised by regionally extensive (< 25 km) sheet-like series of tabular and trough-cross bedded sandstones typically up to 20 m thick at South Gebel Gushea (Fig. 7.4a), within the Zafarana Accommodation Zone at Wadi Gharandal and

Facies Association	Key Observations	Examples
(A) Tidally influenced shelf	Characterised by metre-scale, tabular to trough cross bedded sandstones with a commonly sharp to erosive base. These deposits can be traced regionally over several kilometres, with thicknesses up to 20 m, associated with thickening into fault hangingwalls and fault related synclines. Locally associated with interbedded lenses of deltaic conglomerate facies and also may infrequently display a gradation into underlying and laterally adjacent shoreface sandstones. Texturally, these sandstones are characterised by moderately to well-sorted, medium to very coarse-grained clasts of limestone and chert, which are typically sub-rounded to angular, with no evidence for a mud to silt grade fraction. Individual cross beds are up to 10's cm thick, arranged in metre-scale sets, bounded by major reactivation surfaces Laterally, these prominent cross beds can be traced over a few metres, and are observed as both showing wholly consistent directions, but may also display subordinate sets of opposing dip. In general, the dip directions of the cross beds are the same as those of the master bounding reactivation surfaces.	Wadi Sudr, Sudr Fault Block (Patton et al., 1994); Wadi Feiran, El Qaa Fault Block (Wescott et al., 1998; Carr et al., 1999); South Gushea, Hammam Faraun Fault Block (Young et al., 2002); Wadi Gharandal (this thesis, Chapter 6).
(B) Coarse-grained fluvial-deltaic	Major conglomeratic bodies, up to 10's m thick and extending up to 5 km away from source areas. Dominated by clast supported, massive and crudely, metre-scale bedded conglomerates often arranged in clinoformal geometries, the conglomerate bodies may show overall aggradational to progradational geometries. Generally texturally immature, the conglomerate facies are typically comprised of chert, pre-rift limestones, pre-rift Nubia and basement and rhodolith-rich limestone clasts. Intercalated facies may be minor biogenic reefal carbonates, calcareous mudstones, bedded, pebble rich and cross bedded sandstones. Sandstone facies range from very coarse to medium-grained with variable bioturbation and marine bioclasts.	Wadi Sidri, El Qaa Fault Block (Gawthorpe et al., 1990; Gupta et al., 1999); South Gushea – Gebel Gawher, Hammam Faraun Fault Block (Young et al., 2000; 2002); Warda Fault Block (Elbaz and Handley, 1994); Wadi Feiran, El Qaa Fault Block (Wescott et al., 1998; Carr et al., 1999).

Table 7.1: Summary of sedimentary facies associations observed within the Upper Rudeis Formation, with key referenced examples.

(C) Shallow marine shoreface	The dominant facies of this facies association is characterised by highly bioturbated fine-grained sandstones and siltstones with a resultant homogenised appearance and containing abundant marine fossils, including sharks teeth, bivalves, echinoids, gastropods and comminuted shell hash. Principle trace fossils observed include *Thalassinoides, Skolithos, Planolites* and *Ohiomorpha* burrows. This facies occurs in packages of up to 5 m thick, and which are laterally extensive in the order of 7 km. Subordinate facies include calcareous mudstones and muddy, up to 2 m thick tempestite sandstones characterising the shoreface to offshore transition.	Wadi Feiran, El Qaa Fault Block (Wescott et al., 1998; Carr et al., 1999)
(D) Submarine fan	Includes both siliciclastic and detrital carbonate lithofacies which display similar process derived sedimentary structures. Viewed in core to be arranged over metre scale, sharp to erosive-based fining upwards units <1-10 m thick, principle sedimentary features include massive intervals, mudstone rip-up clasts, cross bedding (unidirectional arranged in sets 5-10 cm) and thinly bedded to laminated intervals. Convoluted and dewatering structures are also common. Upwards facies transitions from massive and cross bedded to thinly bedded and laminated sandstones are consistently repeated. Overall, gross packages observed at the wireline log scale are up to 120 m thick, which are laterally extensive over 10's kilometres. Bioturbation is variable, from rare isolated occurrences of *Ophiomorpha Nodosa* and *Planolites* within the siliciclastic sandstones, bioclastic grainstones and calcarenites to highly bioturbated packstone intervals containing *Palaeophycus, Schaubcylindrichus, Ohiomorpha Nodosa, Ohiomorpha Irregulaire, Phycosphion, Techicnus* and *Thalassinoides*.	Rift axis, (Evans, 1990); July Fault Block (Pivnik et al., 2003); October Fault Block (this study, Chapter 4); Morgan Accommodation Zone (this study, Chapter 5).
(E) Offshore basinal	Dominated by fine-grained calcareous mudstones and marls, with intercalated of coarser clastics variably comprised of siliciclastic and detrital carbonate lithofacies, which may be 10's m thick. Viewed in core, calcareous mudstones are typically massive or laminated, containing finely comminuted carbonate shell material and rare bioturbation. Calcareous marls are principally defined from wireline log response and cuttings information.	Rift axis, (Evans, 1990); July Fault Block (Pivnik et al., 2003); October Fault Block (this study, Chapter 4); Morgan Accommodation Zone (this study, Chapter 5).

Table 7.1 continued.

within the Sudr Fault Block to the North in the northern dip province (Chapter 6; Patton et al., 1994; Young et al., 2002). The coarse-grained deltaic Facies Association is found within the Northern part of the Hammam Faraun Fault Block, upon the hangingwall dip-slope of the El Qaa Fault Block at Wadi Feiran and locally within the Zafarana and Morgan Accommodation Zones (e.g. Allen et al., 1984; Chapter 6; Wescott et al., 1998; Young et al., 2000; 2002). Within the rift axis, local examples adjacent to the Coastal Boundary Fault systems are recognised in the studies of El-Heiny and Enani, (1990) and Elbaz and Handley, (1994). A major outcrop example located at the tip of the Thal Fault Segment of the Rift Border Fault System at Gebel Gawher (e.g. Young et al., 2000; 2002). Here, a major conglomeratic body, up to 65 m thick, and extending approximately 5 km from the rift shoulder, is dominated by clast supported, massive and crudely metre-scale bedded conglomerates arranged in clinoformal geometries. Additional rift shoulder-derived coarse-grained conglomerates are associated with the Abu Alaqa Fan complex in the Wadi Sidri area of the El Qaa Fault Block (Gawthorpe et al., 1990; Gupta et al., 1999). Extensive shallow marine shoreface deposits are located on the hangingwall dip-slopes of the El Qaa Fault Block up to 5 m thick, and which are laterally extensive over 7 km (e.g. Carr et al., 1993; Wescott et al., 1998). The dominant facies observed here are generally tabular with little internal structure; characterised by highly bioturbated fine-grained interbedded sandstones and siltstones with a resultant homogenised appearance and containing abundant marine fossils.

Within the subsurface of the present day offshore rift axis, fine-grained calcareous mudstones and marls of the offshore basinal Facies Association dominate the Upper Rudeis succession, reflecting background, low sedimentation rates dominated by suspension settling (e.g. Evans, 1990; Pivnik et al., 2003; Chapters 4 and 5). Occurring in packages 10's of metres thick, these mudstones are intercalated by the coarser-grained clastics of the submarine fan Facies Association (e.g. Evans, 1990; Pivnik et al., 2003; Chapters 4 and 5). Siliciclastic and calcarenitic-rich compositional lithofacies are recognised, reflective of variable pre-rift and earlier syn-rift source provenances throughout the rift. Submarine fan packages range from <1- 120 m thick, with proximal and more distal elements recognised, with a consistent suite of process based facies viewed in core (Fig 7.4b) indicative of deposition from subaqueous sediment gravity flows.

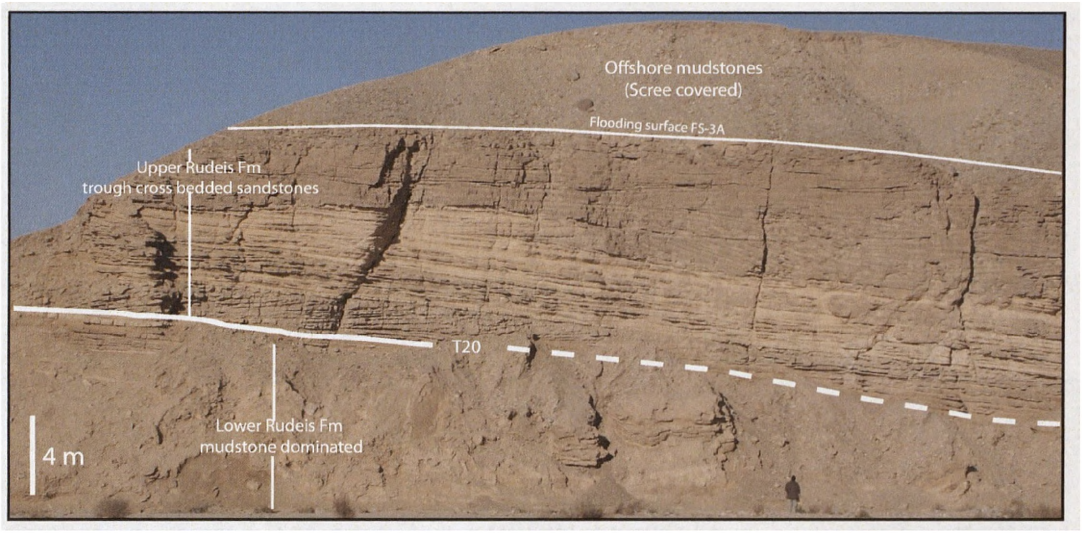

Figure 7.4a. Photograph showing change in facies types between the Lower Rudeis and Upper Rudeis Formation within the proximal part of the rift accommodation zone at Wadi Gharandal (see Figure 7.2 for location). Underlying offshore mudstones and interbedded calcarenitic shoreface sandstones are overlain by trough cross-bedded sandstones, interpreted as shallow marine sandwaves. The mid-clysmic surface (akin to T20) is interpreted to be represented by the basal downlap of the cross bedded units.

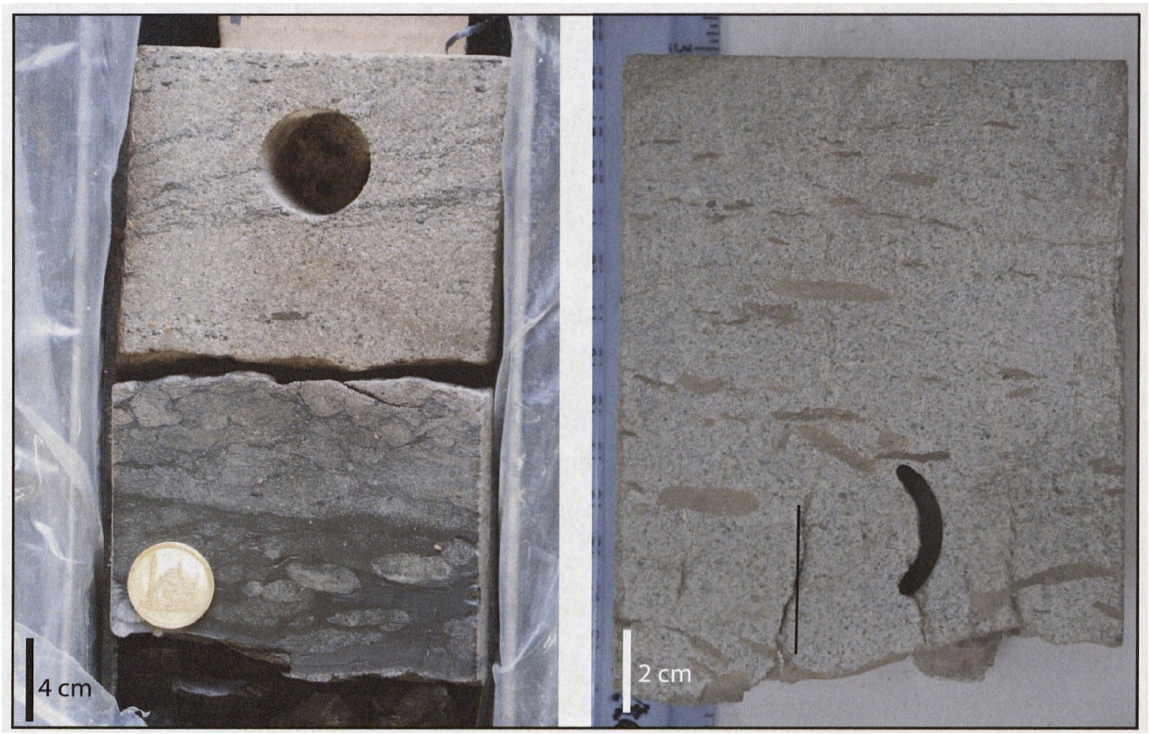

Figure 7.4b. Examples of offshore marine facies types observed in cored section of the Upper Rudeis within the rift axis. (i) Fine-grained background basinal mudstone facies containing Thalassinoides burrows defined by coarser-grained infill, overlain by coarser-grained well cemented sandstone. Well SG310-5A, July Fault Block hangingwall. (ii) Well cemented calcarenitic sandstone with mudstone rip-up clasts, indicative of erosive flow prior to deposition. Well Tanka-3, October Fault Block hangingwall.

7.5.2 Depositional synthesis

Figure 7.5 drawn to illustrate a time of maximum regression, highlights the greatest spatial extent and variability for the principal sedimentary systems of the Upper Rudeis Formation. Deposition within the rift was fundamentally controlled by structural location, which provided a first order control upon potential sediment source areas, transfer pathways and depocentres. Differences in sediment sources and therefore provenance lithology are also observed to impact upon the compositional nature of resultant depositional systems.

At the rift margin, the immediate hangingwall of the Rift Border Fault system was characterised by proximal point-sourced fan delta and potentially submarine fan facies, reflecting varying along-strike tectonically controlled bathymetry. Areas of low subsidence, such as at fault segment tips and associated relay ramps provided a focus for coarse-grained deltas to extend from the rift shoulder (Gawthorpe et al., 1990; Young et al., 2000; 2002). In contrast, the immediate hangingwalls in the centre of the fault segments were dominated by offshore basinal mudstones, with localised point-sourced submarine fan depositional systems fed from the rift shoulder (e.g. Leppard & Gawthorpe et al., 2006). Shallow margin fault blocks with low clastic input are likely to have provided a site for the development of carbonate platforms, with associated reefal and embayment carbonate deposits in addition to detrital carbonate talus deposits upon the steep footwall scarp slopes (e.g. Burchette 1988). Faults zones such as the Hammam Faraun Fault Zone, forming part of the Coastal Boundary Fault system, have been interpreted to have developed into major fault zones by Upper Rudeis time (Gawthorpe et al., 2003). Likely to have been locally emergent, footwall islands supplied sediment down the associated hangingwall dip-slope to be deposited in shallow marine to deltaic environments. Contrastingly, the immediate hangingwall depocentres of this fault system may have been locally sediment starved, with isolated, limited-scale fault scarp sourced fan deltas, mirroring present day fan-delta systems building out into the Gulf of Suez (e.g. Roberts 1987).

Within the subtle, reduced topography of the structural accommodation zones, significant sediment fluxes from the rift shoulder extended into the rift axis (e.g. Smale et al., 1988), in addition to that sourced through relay ramps between fault segments of the Costal Boundary Fault System (e.g. El-Heiny & Enani, 1990; Chapter 5). In the rift marginal

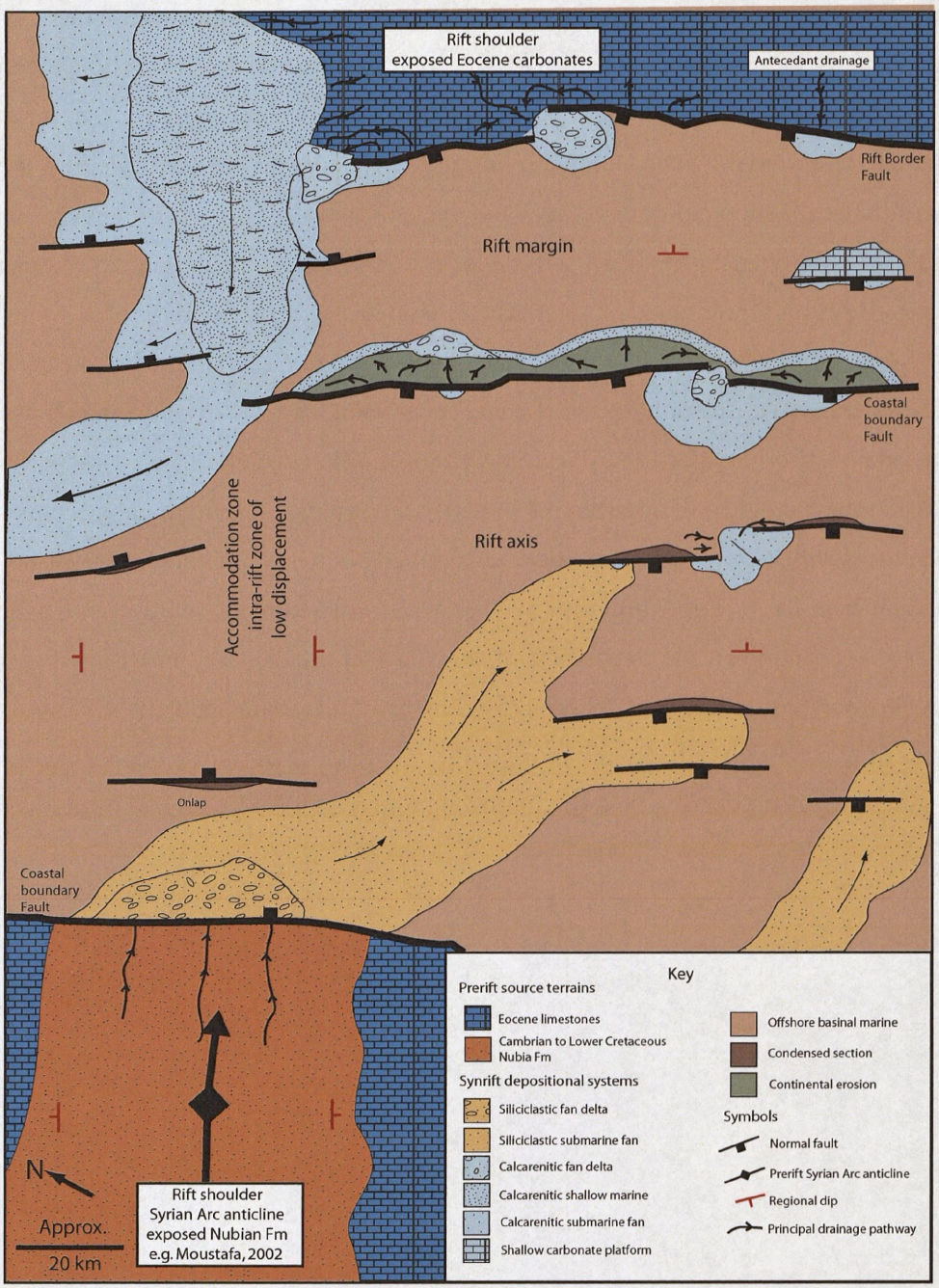

Figure 7.5. Schematic representation of a depositional synthesis for the Upper Rudeis Formation. Principal depositional systems are shown in relation to rift climax structural configuration. Prerift source terrains, controlled by thickness variability and inherited prerift structure, are shown to directly impact upon the composition of subsequent synrift deposits.

component of the structural accommodation zones, shallow marine and tidally influenced depositional systems formed the proximal equivalent to more distal submarine fan depositional systems located within the rift axis. Contrastingly, coarse-grained depositional systems were also present towards the margin of the rift axial component of the structural accommodation zones, having been sourced by drainage systems in part controlled by pre-rift structures within the rift shoulder (Elbaz and Handley, 1994).

In the rift axis tilted half-graben settings of the main structural provinces, submarine fan depositional systems prograded into areas dominated by offshore basinal hemipelagic deposition (Evans 1990; Pivnik et al., 2003; Chapter 4). Regionally sourced submarine fan depositional systems were spatially extensive and locally display both transverse (e.g. West July system) and axial orientations (e.g. Warda – October siliciclastic system). Preferentially deposited within the hangingwall depocentres of active structures, these regional systems were intercalated with more locally-restricted footwall derived footwall-sourced slope aprons and relay ramp submarine fans. Footwall crests with low rates of sediment supply were typically sediment starved, resulting in the deposition of thinned and condensed fine-grained section. Conversely, footwall crests adjacent to major sediment input points into the rift axis (e.g. footwall crest of West July Fault, Pivnik et al., 2003; Chapter 5) provided depocentres, once the initial bathymetry differential across the fault zone into the hangingwall had been balanced.

7.6. A HIGH RESOLUTION REGIONAL STRATIGRAPHIC FRAMEWORK FOR THE UPPER RUDEIS FORMATION

This section documents a stratigraphic framework for the Upper Rudeis Formation for the three principle tectonostratigraphic settings within the rift: (a) rift axis, (b) rift margin and (c) rift accommodation zone. The nature of key surfaces and the geometry and thickness variability for intervening stratigraphic units are described and integrated with facies and facies stacking patterns to allow for the sequence stratigraphic evolution of the Upper Rudeis Formation to be discussed. Particular emphasis is placed upon hangingwall depocentres within the rift axis as these areas are likely to record the most continuous preserved successions and therefore define a 'type section' of key surfaces and stratigraphic units (Fig. 7.6).

7.6.1 Rift axis

Deposits of the Upper Rudeis Formation within the axis of the rift are placed within three specific structural locations, which reflect a half-graben, tilted-fault block geometry: (i) hangingwall depocentre, (ii) footwall crest, and (iii) hangingwall dip-slope. Studied examples within the central dip province of the rift axis are the Amer and October Fault Blocks towards the north and the West July, July, Safa-Mawa and Ramadan Fault Blocks within the southern part (Figs. 7.1 and 7.2). The Amer and October Fault Blocks are 10.5 km and 25 km in width and their bounding fault zones display a maximum of 800 m and 2000 m offsets at the prerift-syn-rift contact respectively. The West July, July, Safa-Mawa and Ramadan Fault Blocks display widths up to 2 km, 5.2 km, 5.4 km and 8 km, which are bounded by fault zones with 600 m, 2000 m, 400 m and 1200 m final displacement respectively.

Hangingwall depocentre

Examples of rift axis hangingwall depocentres described in this section are those associated with the October, Safa-Mawa and West July Fault Blocks (Fig.7.2). The Upper Rudeis Formation observed within these locations consists of five high-resolution stratigraphic units bounded by regionally extensive key stratal surfaces (Fig. 7.6).

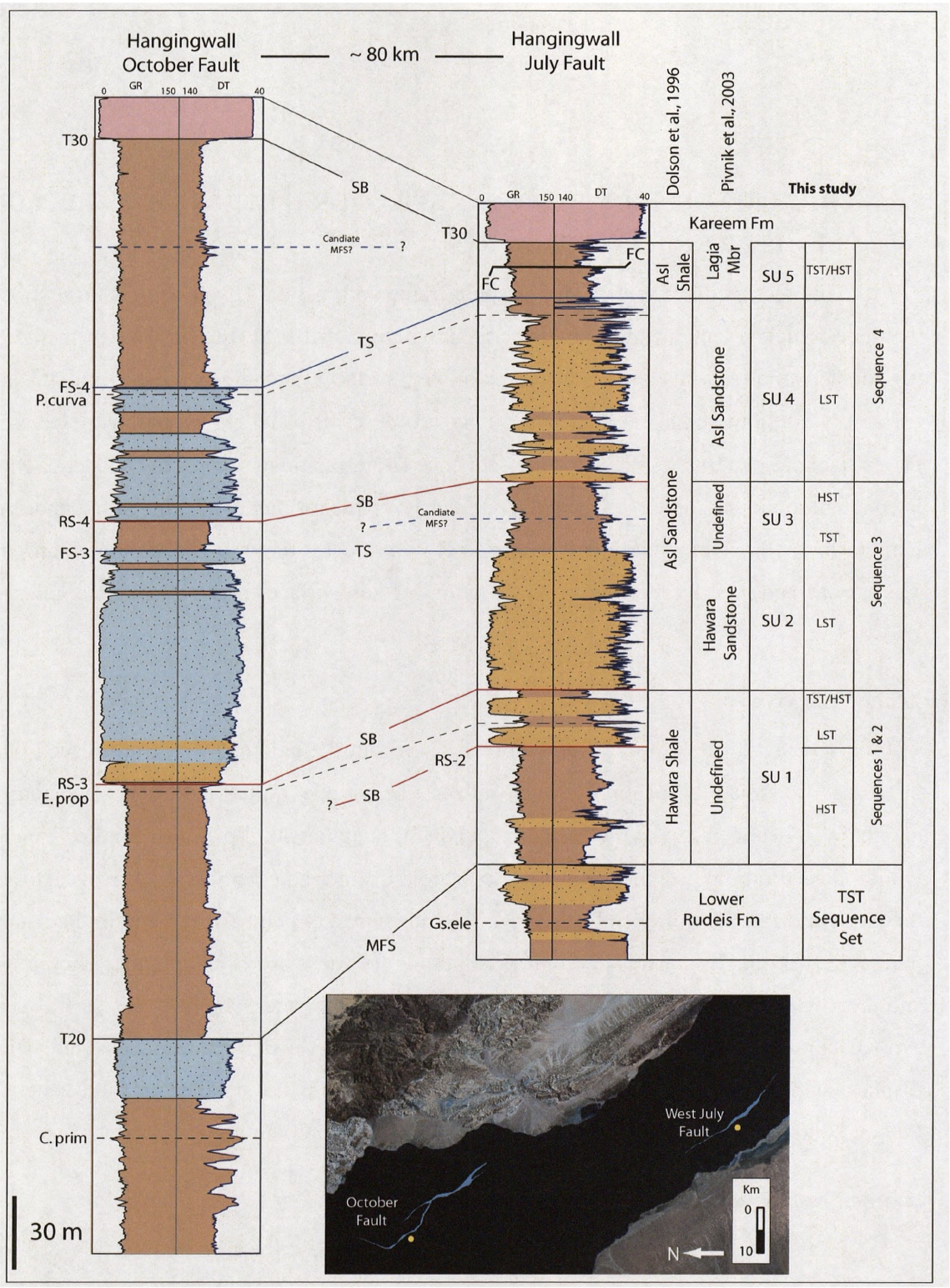

Figure 7.6. Stratigraphic framework for the Upper Rudeis Fm, derived from prinicpal rift axis hangingwall depocentres. Five stratal units are defined, bounded by key surfaces which can be correlated regionally within a supporting biostratigraphic framework. Two wells depicted are located within the hangingwalls of the October and West July Fault Zones, a distance of some 80 km. See Figure 7.5 for key to facies scheme. Lithostratigraphic schemes of Dolson et al., (1996) and Pivnik et al., (2003) are shown for comparison.

Stratal Unit 1

The T_{20} hiatal terrace (sensu Wescott et al., 1996) defining the base of the Upper Rudeis Formation and Stratal Unit 1 is consistently placed between the benthic foraminiferal assemblages of *Eggerella propinqua* and *Globigerinoides altiapertura* or older foraminferal assemblages within the Lower Rudeis Formation. It is either characterised by a discrete high value spike in the gamma-ray and sonic wireline logs, within a uniform basinal mudstone package, or is coincident with the top of a cleaning upwards log motif. In the hangingwall to the West July Fault, the previous Lower Rudeis Formation, is characterised by a series of similar individual progradational cleaning-upwards cycles, arranged in an overall retrogradational stacking pattern, contrasting with overall typically aggradational to progradational geometries observed within Stratal Unit 1 above the T_{20} surface. A cored example of T_{20} within well EGJ-2 located in the hangingwall to the Safa-Mawa block bounding fault is characterised by calcareous nodules within an otherwise mudstone dominated package.

Stratal Unit 1 throughout the rift axis is dominated by the deposition of basinal, hemipelagic mudstones which typically contain the benthic foraminiferal assemblage of *Eggerella propinqua* (Fig. 7.6). The proportion of any coarser-grained submarine fan deposits within this stratal unit greatly varies based on structural location and also proximity to interpreted sediment entry points. For example, in the hangingwall to the October Fault Block, marked along strike variation is observed suggesting variable sediment supply to a series of active fault segments (Chapter 4). Within the hangingwall of the North October Fault Segment, 80 m of uninterrupted basinal mudstones contrasts markedly with the hangingwall of the major South October Fault Segment to the south, typified by three spatially extensive calcarenitic submarine fan lobes (> 60 km^2), with a combined thickness of 75 m, intercalated with 50 m of basinal mudstones. These calcarenitic submarine fan deposits, sourced from the crest of the October Fault Block are interpreted to have been sourced through the synthetic relay ramp between northern and fault southern segments. The hangingwall of the north fault segment is interpreted to have been effectively sediment starved due to southerly plunge of this relay ramp which would deliver sediment southwards (Fig.7.7). The hangingwall of the

West July Fault is also observed to contain significant submarine fan deposits within Stratal Unit 1, some 80 km to the south (Fig. 7.6) (Chapter 5).

The abrupt shift from typically basinal mudstones to coarser-grained clastics associated with the base of this submarine fan package defines a major, yet locally observed regressive surface, RS-2 (Fig. 7.6). Correlations of RS-2 within the rift axis are suggestive of a marked influx of sediment along roughly the same sediment transport routes as those observed in the Lower Rudeis Formation. Away from the major submarine fan systems in more sediment starved locations, e.g. the hangingwall of the North October Fault Segment, there is little facies change and the correlative conformity of RS-2 is interpreted to be located within an overall package of background basinal mudstones. As such, RS-2 cannot be confidently used to define a regionally consistent stratal unit, and is thus constrained within Stratal Unit 1.

Stratal Unit 2

Regressive Surface 3 (RS-3) defines the base of Stratal Unit 2 and is generally characterised by a marked, abrupt increase in grainsize, typically observed in core as a sharp, erosively based shift to coarse to medium siliciclastic sandstones, bioclastic grainstone or calcarenitic sandstones. RS-3 is regionally extensive and for previously sediment starved locations, signifies the first major influx of submarine fan facies, e.g. within the hangingwall of the North October Fault segment (Fig 7.6). Facies correlation within Stratal Unit 2 documents a marked, regional progradation of clastic depositional systems into the rift axis. Figure 7.7 highlight this regional extent, with a correlation between the hangingwalls of the North October Fault Segment and West July Fault, a distance of some 80 km along strike. Stratal Unit 2 is observed with up to 110 m of submarine fan siliciclastic sandstones and detrital carbonates observed within the axial hangingwall depocentres of the rift axis. Maximum gross interval thickness observed is ~140 m.

Stratal Unit 3

The base of Stratal Unit 3 is typically observed as a sharp, regional reduction in grainsize associated with Flooding Surface 2 (FS-3) (Fig. 7.7). FS-3 is typically associated with an abrupt switch from submarine fan facies of Stratal Unit 2 to basinal mudstones facies in core, consistent with markedly sharp increases in calibrated gamma ray and sonic logs. Within some rift axis hangingwall depocentre locations, the otherwise monotonous log

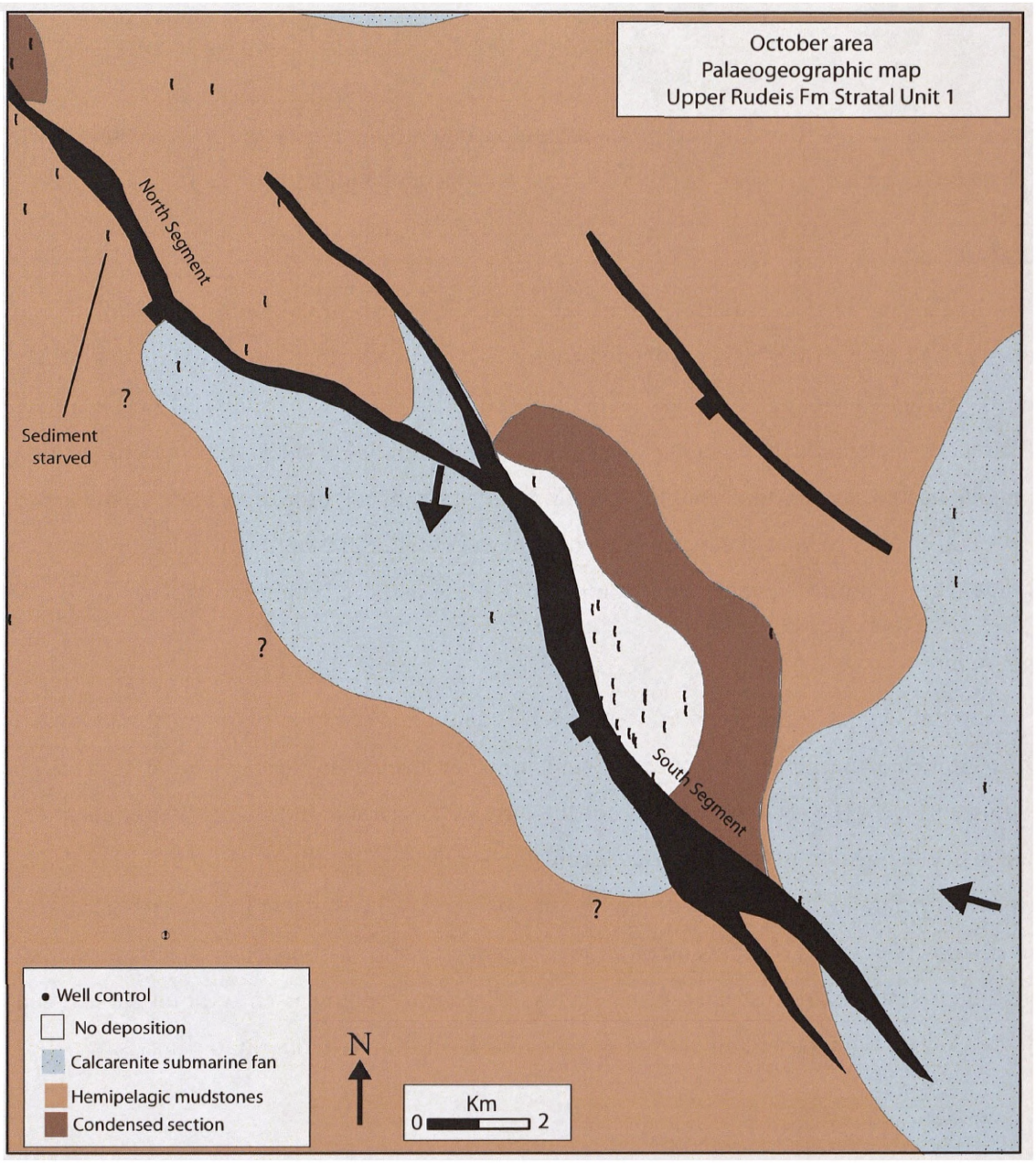

Figure 7.7. Palaeogeographic map for Upper Rudeis Stratal Unit 1 in the October Fault area (See Figure 7.2 for location), superimposed with the present day Upper Rudeis Fm level fault geometry. During this time, gross interval thickness maps suggest North and South fault segments were unlinked, with a synthetic relay ramp between them,with core and wireline log data indicative of a calcarenitic submarine fan lobe being sourced via this relay ramp, which principally prograded towards the southeast, into the hangingwall of the South October Fault Segment. This contrasts with locations in the hangingwall of the North October Fault Segment, which display uninterupted hemipelagic basinal mudstone deposition, suggestive of sediment starvation.

responses associated with these basinal mudstone packages, which may reach up to 30 m thick, are observed to contain a major, but thin high gamma-ray and equivalent low sonic log spike.

Stratal Unit 4

Regressive Surface 4 (RS-4) forms the basal surface of Stratal Unit 4, is locally sharp to erosive and akin to RS-3, is associated in core and wireline log motifs with a regionally extensive influx of submarine fan facies into the rift axis (Fig. 7.7) as shown at both October and West July hangingwall locations. Stratal Unit 4 is up to 207 m thick and contains the first downhole occurrence of the benthic foraminiferal assemblage of *Preaorbulina glomerosa curva*. Regional correlations suggest that the renewed submarine fan depositional systems at this time were of limited spatial extent compared to those mapped within Stratal Unit 2.

Stratal Unit 5

Stratal Unit 5, similarly to Stratal Unit 3, is again marked by a regional, abrupt switch to fine-grained facies from the coarser submarine fan facies of Stratal Unit 4 (Fig. 7.7). Flooding surface 4 (FS-4) therefore defines the base of this stratal unit, which is characterised by extensive deposition of basin restricted calcareous marl facies, observed up to 112 m thick. Correlation of Stratal Unit 5 towards the margins of the rift axis suggest that the whilst absent from rift axis hangingwall depocentres, coarser-grained clastics associated with submarine fan depositional systems are restricted immediately adjacent to sediment entry points associated with the Coastal Boundary Fault system and the transition from rift margin to rift axis.

T30 Surface

The top of the Upper Rudeis Formation and Stratal Unit 5 is defined by the T30 hiatal surface, which is overlain by the Kareem Formation (Fig. 7.7). Commonly, T30 is placed at the base of the Markha Anhydrite Member. Although cited as being regionally diachronous (Beleity, 1984; Patton et al., 1994), the first appearance of anhydrite associated with this member is fairly isopachous in large parts of the axis, typically in the order of 20 m. Thickening into some hangingwall locations is common, whilst in some areas multiple stacked packages of anhydrite are observed. Where the Markha Anhydrite is absent, the lowermost part of the Kareem Formation are characterised by basinal mudstones and localised sandstones

containing the first downhole occurrence of the foraminiferal assemblage of *Preaorbulina glomerosa circularis.*

Interpretation

Thickness and facies data indicate that hangingwall locations in the rift axis provided primary depocentres for the offshore basinal and submarine fan depositional systems active during the Upper Rudeis Formation. The transition from the preceding Lower Rudeis Formation marked by surface T_{20} within hangingwall depocentres is interpreted to represent a maximum flooding surface (Fig. 7.7). High gamma-ray and low sonic log values are consistent with the cored example of the calcareous nodules in well EGJ-2 suggesting a significant condensed interval representing a prolonged period of limited or no sedimentation. The switch in overall stacking patterns for the progradation of individual submarine fan lobes, shown as a cleaning-upwards trend in wireline logs, from retrogradational to either aggradational or progradational across the T_{20} surface is suggestive of a marked change in relative sea-level.

Rift axis hangingwall depocentres recorded three main basinward shifts associated with the influx of coarse clastics into the rift axis and linked to the development of regional surfaces of regression (RS-2, RS-3 and RS-4). Although regionally correlatable, the magnitude of these basinward shifts varied, indicated by the spatial extent and typical thicknesses of submarine fan deposits associated with each event. The localisation of generally thinner submarine fan deposits associated with surface RS-2 in Stratal Unit 1 within hangingwall depocentres, typically located proximally to major sediment entry-points contrasts with the more widespread and thicker deposits linked to surface RS-3 in Stratal Unit 2 and subsequently, but more spatially limited, submarine fan deposits of Stratal Unit 4 related to surface RS-4. Conversely, Stratal Units 3 and 5, characterised by abrupt, regionally consistent switches to dominantly fine-grained, basinal deposition, are interpreted to signify a wholesale, regional shutdown of the submarine fan depositional systems within the axis and periods of significant sediment starvation. The observed spike in the gamma-ray and sonic logs in some wells during basinal mudstone dominated Stratal Unit 3 is interpreted as a candidate maximum flooding surface.

Regardless of local thickness variations, a similar regional stratigraphic development, i.e. expression of key surfaces and facies stacking patterns within the resolution of biostratigraphic control, is highlighted in Figure 7.7 for the Upper Rudeis Formation. Being located in two separate hangingwall depocentres associated with the October and West July Faults over 80 km apart, this similarity in the Upper Rudeis succession strongly suggests that in addition to broadly similar depositional systems having been active along strike within the rift axis, a further, more regional control independent of fault array evolution, must have acted to organise the timing and magnitude of sediment influxes and alternatively periods of sediment starvation within the rift axis.

Footwall crest

The lack of evidence for shallow marine facies and thickness observations are consistent with progressive thinning and onlap of the Upper Rudeis succession onto examined crestal footwall locations within the rift axis and suggest that these locations were completely submerged, and below the influence of the storm wave base. The footwall crests of the Amer, October and West July Fault Zones highlight two principle Upper Rudeis depositional scenarios: (i) high topographic differential and low sediment supply, and (ii) low topographic differential and high sediment supply.

High topographic differential: low sediment supply

This end member of footwall crest stratigraphic style is illustrated by the footwalls to the South October Fault Segment (Fig. 7.7), North October Fault Segment and Amer Fault (Fig. 7.8) located within the northern part of the central dip province (Fig. 7.2). The South October Fault Segment is approximately 30 km in length and exhibits a maximum throw of 2 km at the pre – syn-rift contact (Chapter 4). In this location, no Upper Rudeis Formation is present upon the crestal location, with deposits of the younger syn-rift Kareem Formation lying uncomformably upon the pre-rift limestones of the Darat Formation. Further down-dip, upon the associated hangingwall dip slope, section correlated with the Upper Rudeis Formation is observed to consistently thin back up-dip, before depositionally pinching out some 0.5 – 2 km before the footwall crest. This lack of Upper Rudeis section upon the immediate footwall differs with the North October Fault Segment footwall crest, which is associated with a highly condensed (< 15 m thick) interval, confirmed by the presence of

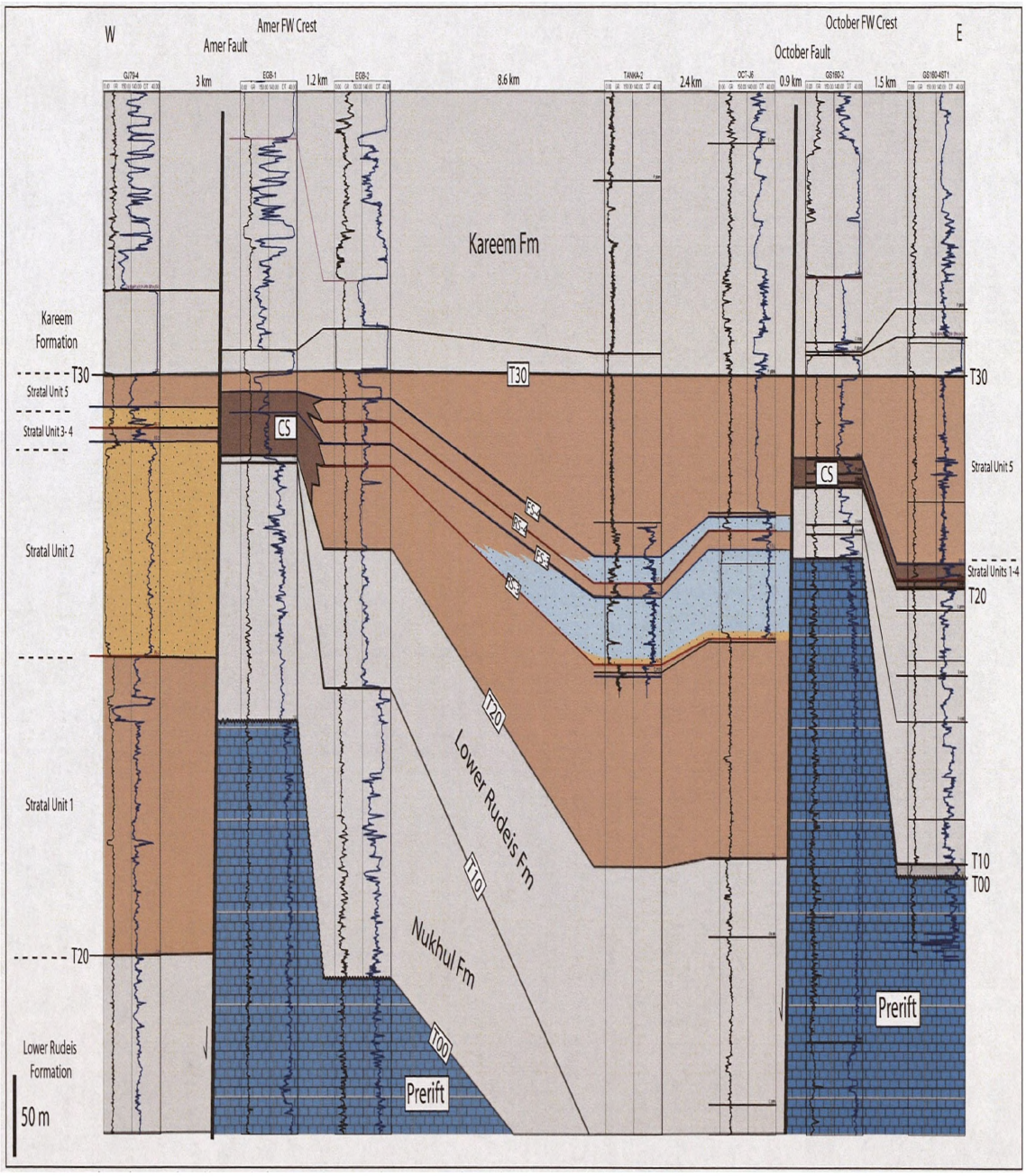

Figure 7.8. Dip-orientated well correlation panel across the Amer and October Faults to highlight Upper Rudeis Formation stratal unit facies and thickness variability, see Figure 7.1 for location. The hangingwall of the Amer Fault displays expanded thickness for Stratal Units 1 and 2, but interepreted to be relatively sediment starved during Stratal Units 3 to 5. Upon the adjacent footwall crest, Stratal Units 1to 4 are significantly condensed, with only overlying Stratal Unit 5 readily identifiable. Clear expansion is observed to the east and into the hangingwall of the October Fault. Upon the October Fault Zone footwall, condensation of Stratal Units 1 to 4, is observed, extending up to some 1.5 km away downdip upon the hangingwall dip slope.

amalgamated foraminiferal assemblages and dominated by offshore basinal mudstone facies. Like at the more basinward Amer Fault footwall crest, individual key surfaces upon the North October Fault Segment footwall are difficult to identify within this condensed interval and markedly contrasts with the expanded section of intercalated mudstones and submarine fan deposits in the immediately adjacent hangingwall depocentre (Fig. 7.8).

Low topographic differential: high sediment supply

Alternatively, crestal footwall locations adjacent to major, regional sediment input points into the rift axis are observed to contain significant Upper Rudeis Formation stratigraphy, e.g. the footwall crest of the West July Fault (Fig. 7.2) (Pivnik et al., 2003; Chapter 5). At this location high-resolution correlation of interpreted minor flooding surfaces associated with individual fining-upwards packages within Stratal Units 1, 2 and 4 associated with a major submarine fan depositional system between hangingwall and footwall locations show that deposition was not wholly constrained within the hangingwall (Fig. 7.9). The July submarine fan system, sourced from the western margin and roughly perpendicular to the NNW-SSE-orientated West July structure can be traced into adjacent half-grabens associated with the July and Ramadan Faults. Key surfaces defining the main stratal units identified in this study are confidently correlated within this depositional system across the West July and adjacent structures.

Interpretation

Facies and stratigraphic variability associated with footwall crestal locations primarily reflects the interplay of the fault-controlled bathymetric differential across the fault zone and style and volume of sediment supply. In the October Fault Zone examples, both northern and southern fault segments appear to have been established surface breaking faults associated with marked topography throughout deposition of the Upper Rudeis Formation. Regionally and locally-sourced coarse clastic deposition was progressively concentrated within the immediate hangingwalls to both fault segments, contrasting markedly with limited to no sediment accumulation upon the footwall crest. This is suggests that a relatively low rate of sediment supply associated with the distal nature of the submarine systems to the immediate hangingwall could not reduce the pre-existing and developing bathymetric differential across the two faults. As a result, the footwall locations experienced limited sedimentation or overall

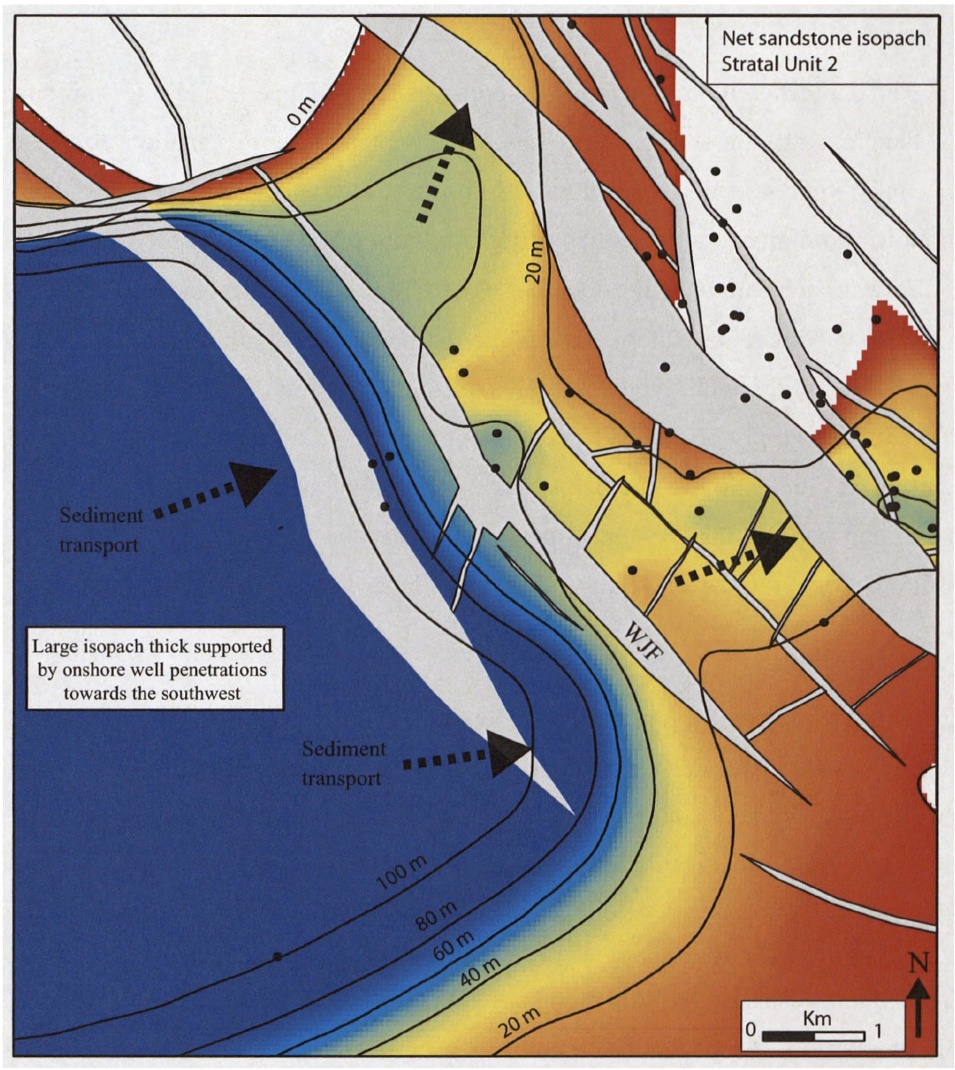

Figure 7.9. Net sand isopach map for Stratal Unit 2 in the July Fault Block area. Sediment transport is inferred from west to east (confirmed by onshore wells not shown), sub-perpendicular to the strike of the main controlling faults. Whilst a gradual thinning to the east is observed, individual depositional packages can be traced across the West July Fault (WJF), indicating that the rate of sediment supply was episodically able to outpace the rate of tectonic accommodation space creation. Contour interval is 20 m, with the location of borehole datapoint control indicated. Upper Rudeis Fault map after Pivnik at el., 2003.

starvation. The depositional thinning and onlapping nature of Upper Rudeis section down the associated hangingwall-dip slope argues against an alternative explanation for extensive erosion of Upper Rudeis section upon the footwall crest. In contrast, the West July Fault was located in close proximity to a major depositional system providing a marked contrast to the nature of footwall deposition at the October Fault Zone. This depositional system, with sediment transport directions interpreted to be perpendicular with respect to the strike direction of the West July Fault, whilst initially constrained within the hangingwall depocentre, the rate of sediment supply episodically outpaced the rate of fault-generated accommodation space, resulting in the healing of the bathymetric differential across the fault. This allowed the submarine fan depositional system to prograde across the fault onto the footwall and the hangingwall dip-slope into the next half-graben to the East.

Hangingwall dip-slope

Rift axis hangingwall dip-slope, like footwall settings are considered with respect to sediment supply, with two depositional style end-members recognised: (i) low sediment supply and (ii) high sediment supply. The two examples considered are the hangingwall dip-slopes associated with the October and Ramadan Fault Zones (Fig. 7.2).

Low sediment supply

The October hangingwall dip-slope, with a maximum width of approximately 12 km from the footwall of the Amer Fault to the October Fault Zone provides the sediment starved example (Fig. 7.8). Well OCT-J6 in the immediate hangingwall of the northern segment of the October Fault Zone, records an overall Upper Rudeis Section approximately 300 m thick, contrasting with 70 m on the immediate footwall crest of the Amer Fault (well EGB-1, Fig. 7.8). Stratal Units 2 and 4 within the October Fault Zone hangingwall are characterised by stacked intercalated deposits of regional, axially sourced siliciclastic submarine fan sandstones and locally, footwall derived detrital submarine fan carbonates. These coarse-grained facies can be traced 2.4 km, up the dip-slope away from the fault zone with a small reduction in thickness and increase in finer-grained, basinal mudstone facies (e.g. well TANKA-2). Further up the dip-slope, the coarse clastic facies are interpreted to thin and pinch out over a distance of 8.6 km, being replaced with offshore basinal mudstone for the entire Upper Rudeis Formation succession (e.g. well EGB-2). With respect to tracing key surfaces defined in the

October hangingwall depocentre on the October hangingwall dip-slope, Well EGB-2 illustrates how both flooding and regressive surfaces are inferred from marked inflections in otherwise monotonous, interpreted mudstone wireline log responses, before becoming amalgamated within a condensed section, 1.2 km towards the Amer Fault footwall crest.

High sediment supply

The Ramadan hangingwall dip-slope in contrast experienced a higher rate of sediment supply, particularly during Stratal Units 1 and 2 of the Upper Rudeis Formation. Well log motifs and correlations indicate that an axially orientated siliciclastic submarine fan depositional system focussed upon and progressively infilled the accommodation space in the hangingwall of the Ramadan Fault Zone (Fig.7.10). Two principle coarse-grained clastic dominated packages are observed. The older package within Stratal Unit 1 shows an overall thickness change from 20 m in the immediate hangingwall of the Ramadan Fault Zone, and pinches out approximately 4.4 km up-dip on the hangingwall dip-slope, with evidence for onlapping of internal depositional packages. The second package comprising Stratal Unit 2 also thins up-dip from 67 m in the immediate hangingwall, but extends up the hangingwall dip-slope and still has 16 m thickness on the immediate footwall crest of the Safa-Mawa Fault (well J-3, Fig. 7.10). Continued correlation into the hangingwall of the Safa-Mawa Fault indicates that this submarine fan depositional extended a further 1.5 km to the west (well NJ-1).

Interpretation

Stratigraphic and facies variability in rift axis hangingwall dip-slope locations is a function of both the gradient of this tectonically generated slope and the nature of regional sediment supply. In sediment restricted settings like on the October hangingwall dip-slope, kilometre scale changes in facies and stratal surfaces can be directly traced down-dip to hangingwall depocentres. The change from fine-grained offshore facies to coarser-grained submarine facies, down this dip-slope, reflects the roles of slope gradient and available accommodation space in focussing both regional, axially sourced and local, footwall derived sediment into a hangingwall depocentre. In this example, an initially large, and continuing bathymetric gradient associated with the hangingwall dip-slope resulted in active submarine fan depositional systems being principally centred upon the available accommodation space in

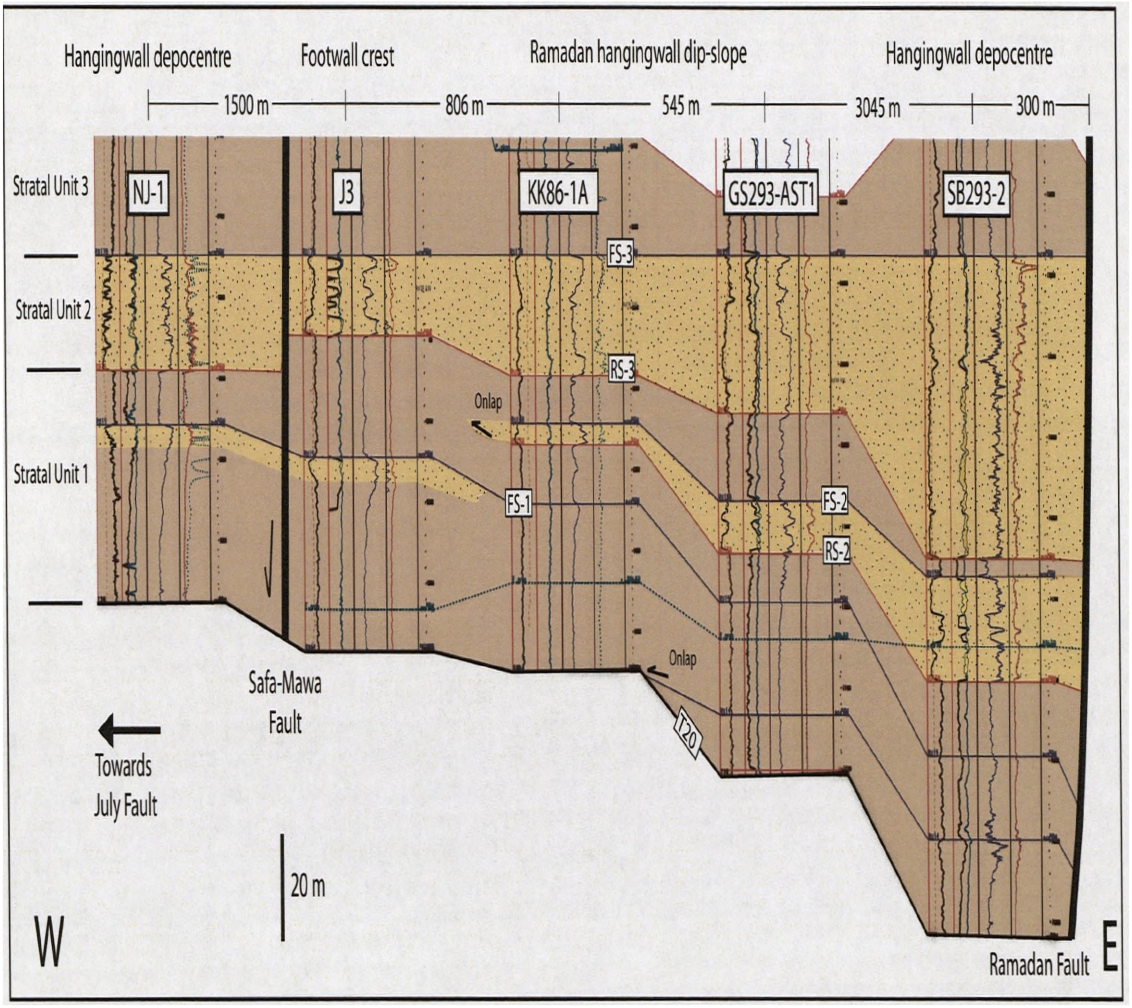

Figure 7.10. Well correlation panel orientated west to east from the hangingwall depocentre of the Safa-Mawa Fault, adjacent footwall crest and down the hangingwall dip-slope towards the Ramadan Fault Zone, see Figure 7.1 for location. Thining, onlap and pinch-out of submarine fan sandstones upon the hangingwall dip-slope are associated with the uppermost part of Stratal Unit 1, contrasting with an increased supply of coarse-grained sediment during Stratal Unit 2.

the October Fault Zone hangingwall. The relatively low rate of sediment supply within this half graben, reflecting a distal position with respect to the regional rift margin hinterland and limited nature of a local, intra-rift axis October Fault Block source, was therefore unable to allow for these coarser-grained depositional systems to deposit further up on the hangingwall dip-slope.

In areas with higher regional sediment supply, the potential for facies variation is reduced, as shown in the Ramadan hangingwall dip-slope example. Whilst coarse-grained submarine facies within Stratal Unit 1 were focussed down-dip towards the Ramadan Fault Zone, increased sediment flux during Stratal Unit 2 may have also potentially reduced the bathymetric gradient due to a subsequent infilling of accommodation space within the hangingwall depocentre. Thus, a second series of Upper Rudeis submarine fan deposits were able to progressively deposit upon the entire hangingwall dip-slope and into the adjacent half-graben. In both sediment supply scenarios discussed for the rift axis, key surfaces can be confidently traced across the hangingwall dip slope, although there is the potential for increasingly condensed section further up the dip-slope in the sediment starved scenario.

7.6.2 Rift margin

Extensive deposits of the Upper Rudeis Formation crop out on the eastern rift margin within the tilted half-graben settings of the Hammam Faraun and El Qaa Fault Blocks (Fig. 7.2). The locations considered in this study are principally associated with areas of low fault-generated subsidence and therefore low accommodation space. Two structural scenarios are examined: (i) Rift border fault tip and (ii) hangingwall dip-slope.

The Gushea and South Gushea areas are located towards the northern end of the Hamman Faraun Fault Block, adjacent to the northerly tipping out Thal Fault segment of the Rift Border Fault System (Fig 7.2). The northern tip of this segment is characterised by throw estimates of 0-300 m, contrasting with maximum throws of 1436 m further to the south along this *ca.* 30 km long rift bounding fault zone (e.g. Young et al., 2002). Further to the south, Wadi Feiran is located upon the hangingwall dip-slope of the El Qaa Fault Block, in the region of Gebels Nezzazat, Wither and Ekma segments of the eastern Coastal Boundary Fault System (Fig. 7.2). The rift margin examples of the Upper Rudeis Formation studied are dominantly

calcarenitic in nature, having been sourced from Eocene prerift carbonates and containing Miocene aged bioclastic material.

Rift border fault tip

The Upper Rudeis succession associated with the northern end of the Hamman Faraun Fault Block, and the associated tipping out rift bounding Thal Fault (Fig. 7.2) has previously been examined in the studies of Young et al (2000, 2002). Key surfaces utilised in their studies to constrain the architecture and stratigraphic evolution of a coarse grained delta at Gebel Gawher (their South Gushea area) and similarly deltaic and associated coeval depositional systems towards the northwest, at South Gebel Gushea (their Gushea area), adjacent to the northern tip of the rift bounding Thal Fault, can be correlated with those used to define the stratigraphic framework defined in this study (Fig. 7.11).

Deposits of Stratal Unit 1, containing the foraminiferal assemblage of *Eggerella propinqua* are not observed at both areas. The contact between the Upper and Lower Rudeis Formations, which therefore corresponds to the T_{20} hiatal terrace of Wescott et al (1996); Krebs et al (1997), is marked by bypass and erosion. Young et al (2000, 2002) determine up to 25 m of incision occurred at Gebel Gawher, (their surface RS-2) with deposits interpreted to be equivalent to Stratal Unit 2 directly overlying the Lower Rudeis Formation. Young et al (2002) placed the entire Upper Rudeis succession here at Gebel Gawher within a single stratal unit (their stratal unit 2), and interpreted it to reflect the back-filling of previously generated erosional topography, whilst also suggesting that subsequent overlying parts of the Upper Rudeis Formation have been not been preserved. The isolated nature of this exposure and lack of biostratigraphic subdivision due to the coarse-grained nature of the succession make any regionally consistent, high-resolution subdivision difficult. However, comparison with stratigraphy 7 km further to the north at South Gebel Gushea area and the ability to confidently correlate this section with biostratigraphic data within the Zafarana Accommodation Zone, a further 20 km to the north, provides the rationale for placing the coarse-grained facies at Gebel Gawher within Stratal Unit 2. At South Gebel Gushea, Stratal Unit 2 is similarly dominated by deltaic and pro-deltaic conglomerates, up to a maximum of 65 m thick. Capping this coarse-grained succession is a tabular, sheet-like series of tidally-influenced cross bedded sandstones, some 20-60 m thick. The sharp contact between the

underlying coarse-grained facies association and cross bedded sandstones is the expression of flooding surface FS-3 on the rift margin (flooding surface FS-3 of Young et al., 2002). These tidal sandstones are themselves capped by a prominent and extensive, red-stained flooding surface associated with a sharp switch to intercalated mudstones and shallow marine shoreface sandstones, which can be traced into the rift marginal exposures of the Zafarana Accommodation Zone (Fig. 7.5a). This surface associated with a landward shift in facies types, is defined as flooding surface FS-3A in this study (ca.f. surface FS-5 of Young et al., 2002).

Interpretation

Along the rift margin, the tips of the Rift Border Fault System are characterised by extensive periods of erosion and sediment bypass for the lowermost stratal units of the Upper Rudeis Formation. The boundary between the Lower Rudeis and Upper Rudeis Formations at the Thal Fault tip is recognised to be a composite unconformity. The < 25 m of incision into the underlying Lower Rudeis Formation at Gebel Gawher and the subsequent non-deposition of sediments equivalent to Stratal Unit 1 indicate a lack of available accommodation space at the fault tip, resulting in sediment bypass and transportation further into the rift. Thus the underlying contact of the Upper Rudeis succession comprises the T_{20} hiatal surface, RS-2 and RS-3 and is therefore is interpreted to be a major sequence boundary.

This is consistent with a major fall in regional sea-level, estimated to be in the order of < 100 m (Young et al., 2002), the rate of which outpaced the low rate of fault-controlled subsidence at the fault tip during Stratal Unit 1. The overlying fan-deltaic bodies of Stratal Unit 2 at both South Gebel Gushea and Gebel Gawher are interpreted to reflect infilling of previous incision during an ensuing lowstand, and subsequent rise in relative sea-level. At South Gebel Gushea, continued regional base-level rise is observed with the initial switch to shallow marine, trangressive tidally influenced sandwave deposition, the subsequent development of FS-3A and change to shoreface sandstones and offshore mudstones during Stratal Unit 3.

Hangingwall dip slope

At Wadi Feiran, located upon the hangingwall dip-slope of the El Qaa Fault Block (Fig. 7.2), unpublished studies by Wescott et al (1998) and Carr et al (1999) document the

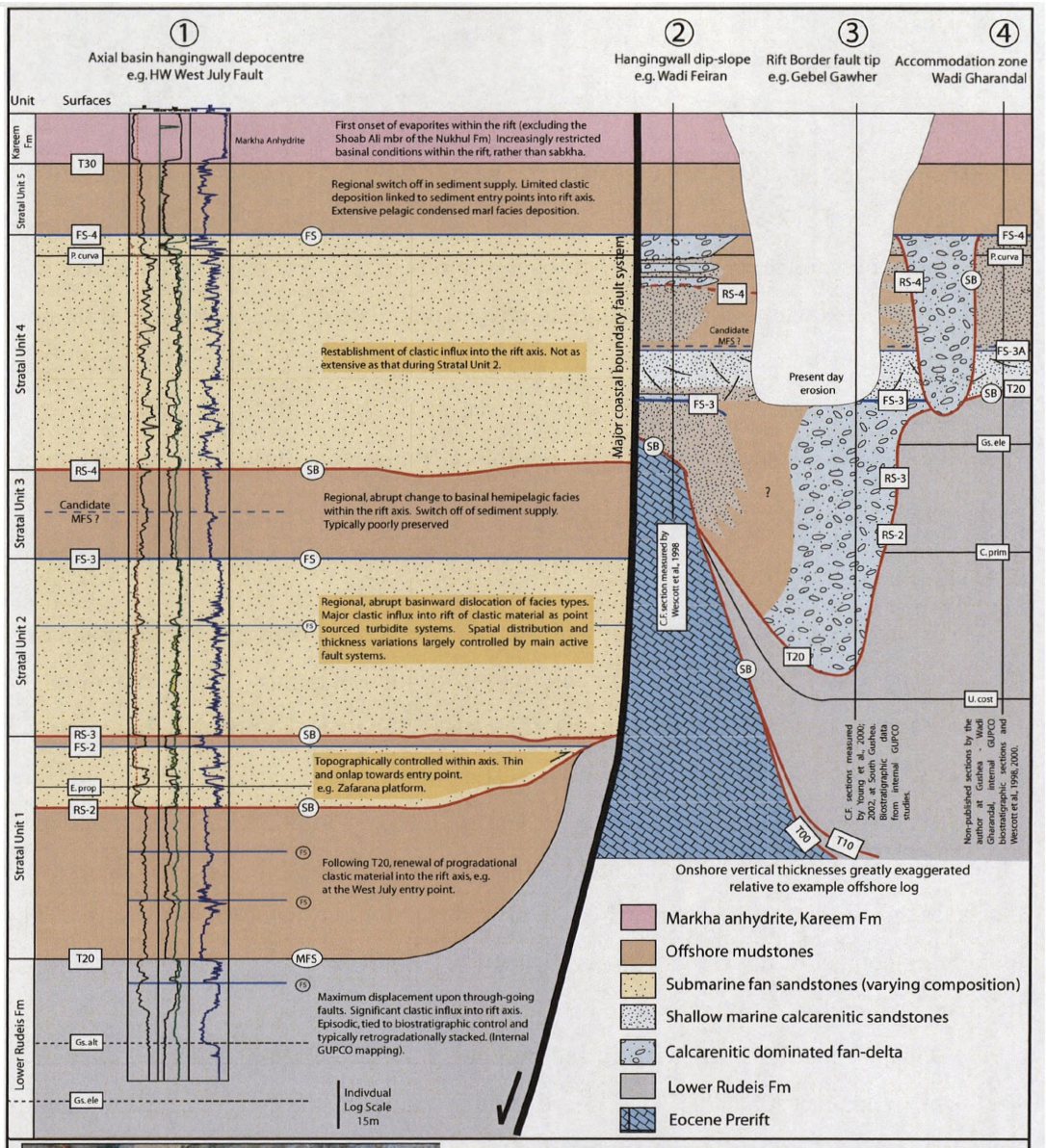

Figure 7.11. (A) Comparison of key surfaces between locations within a rift axis hangingwall depocentre, hangingwall dip-slope, Rift Border Fault tip and proximal accommodation zone within the rift margin located on the map in (B). In hangingwall depocentres, the T20 hiatal surface is interpreted as a maximum flooding surface overlying aggradational to retrogradational stacked coarsening-upwards packages. This contrasts with the rift margin, where the T20 surface is observed as a varyingly composite (dependant upon structural location) sequence boundary,. **(B)** Map showing approximate locations for areas highlighted in (A).

presence of up to 100 m of Upper Rudeis Formation section, directly overlying prerift Eocene limestones. Whilst the lack of available detailed biostratigraphic data makes accurate correlation of the succession here into the stratigraphic framework difficult, observations of facies variations and stacking patterns, with comparison with similar organised deposits at the Thal Fault tip and within the proximal part of the Zafarana accommodation zone are used to achieve a best fit model (Fig.7.11).

The basal hiatal T_{20} surface of the Upper Rudeis Formation is coincident with both the pre-rift – syn-rift unconformity surface, T_{00} and the switch from rift initiation to rift climax deposits delineated by surface T_{10}. The earliest Upper Rudeis deposits, approximately 18 m in thickness are assigned to Stratal Unit 2, based upon the recognition of overlying surfaces consistent with major flooding surface FS-3 and minor flooding surface FS-3A. Stratal Unit 2 is characterised by a transition from initially fluvial to deltaic facies to overlying shoreface deposits. Flooding surface FS-3 is picked by the switch to the characteristic tidally-influenced cross bedded sandstone facies, akin to those at the South Gebel Gushea area at the Thal Fault tip, and within the proximal Zafarana Accommodation Zone at Wadi Gharandal. This facies therefore denotes the onset of Stratal Unit 3. Flooding surface FS-3A is recognised, with a shift to a 5 m thick package of offshore mudstones

Above this, is a 50 m, overall upwards coarsening package of shoreface sandstones and intercalated deltaic conglomerates which passes into a thick package of deltaic conglomerates, up to 10 m, which are capped by an abrupt switch to a 20 m thick package of offshore mudstones. This major flooding surface is confidently interpreted as FS-4, and therefore this thicker mudstone package as Stratal Unit 5, as the T30 hiatal surface defined by the Markha Anhydrite Member of the lowermost part of the Kareem Formation, (but see Wescott et al., 1996), subsequently overlies this mudstone package. A major regressive surface, akin to RS-4 in the subsurface is not easily recognised, and may be associated with the base of one of the deltaic conglomerate packages in the 30 m below FS-4 (Fig. 7.11).

Interpretation

The lack of any preserved older syn-rift deposits associated with the rift initiation and climax phases, in addition to Stratal Unit 1 at Wadi Feiran is indicative of persistently reduced or lack of accommodation upon this hangingwall dip-slope setting. This reflects both the

limited nature of tectonically generated subsidence, and the ability for regional variations in base-level to remove previously deposited material. Thus the regional sea-level fall interpreted at Gebel Gushea South and Gebel Gawher at the Thal Fault tip, may also account for the lack of Stratal Unit 1 at Wadi Feiran. Stratal Unit 2 here is of the order of 18 m, and potentially therefore only represents the uppermost part of equivalent aged deposits of the stratal unit within the rift axis. The overall succession of Stratal Units 2 is thus interpreted to signify a period of transgression, culminating in the deposition of offshore basinal mudstones. Wescott et al (1998) interpret the presence of a maximum flooding surface within this 5 m thick mudstone package, which mirrors the candidate maximum flooding surfaces observed in Stratal Unit 3 within the rift axis hangingwall depocentres (Fig. 7.6). The subsequent, gradational coarsening-upwards nature of the overlying shoreface to deltaic succession is further consistent with a slowing rate of relative sea-level rise, allowing for the progradation of hangingwall derived sediments down the hangingwall dip-slope into the El Qaa half-graben. The return to offshore mudstone deposition during Stratal Unit 5 is interpreted to reflect a renewed increase in relative sea-level and mirrors a similar switch off in coarse-grained sedimentation observed in several locations throughout the rift.

7.6.3 Rift accommodation zones

Accommodation zones spanning across a rift and separating structural provinces with different dip-polarity have been recognised to be important structural domains within rift basins (e.g. Lambiase and Bosworth, 1985; Rosendahl et al., 1986; Patton et al., 1994; Morley et al., 1995) and like the two transverse orientated accommodation zones present with the Suez Rift (Fig. 7.1), may encompass both rift margin and rift axis components. In this section, the results of fieldwork conducted within the Zafarana Accommodation Zone, along the western rift margin in the vicinity of Wadi Gharandal (Fig. 7.2) are integrated with subsurface data from the accommodation zone within the rift axis on the Warda Fault Block (Fig. 7.2), to determine the stratigraphic and sedimentary nature of the Upper Rudeis Formation.

Wadi Gharandal, located towards the northern end of the central dip province of the Hammam Faraun Fault Block, provides a type locality within the proximal, rift margin component of the accommodation zone, with extensive exposure of the Upper Rudeis Formation allowing correlation of key surfaces and facies variations both across Gebel Gushea

and the northern tip of the Thal Fault, 20 km to the south, and conversely 5 km towards the north and into the Sudr Fault Block of the northern dip province (Fig. 7.2). The Warda Fault Block is located towards the western margin of the rift axis part of the Zafarana Accommodation Zone, downthrown some 2400 m against a segment of the Coastal Boundary Fault system and dips 15-20^0 towards the east-southeast (Elbaz & Handley, 1994). Several wells upon the fault block have penetrated a thick package of siliciclastic sandstones within the Lower Rudeis to Kareem Formation succession.

Rift margin

As with previously described localities within the rift margin, the Upper Rudeis Formation exposed within the rift marginal component of the Zafarana Accommodation Zone is dominantly calcarenitic in nature. The underlying contact beneath the Upper Rudeis Formation at Wadi Gharandal is characterised by a sharp, abrupt change from interbedded offshore mudstones and lower shoreface deposits of the Lower Rudeis Formation, to 5 - 10 m of sheet-like, metre-scale tabular cross bedded, tidally influenced sandstones which are similarly observed at South Gebel Gushea (Figs. 7.5a & 7.11). Whilst locally intercalated with conglomeratic deltaic lobes, this facies is capped by a prominent red, cemented flooding surface, which is directly correlated to flooding surface FS-3A at South Gebel Gushea. Thus, the lowermost deposits of the Upper Rudeis Formation are placed within Stratal Unit 3, with therefore Stratal Units 1 and 2 not present.

Directly overlying FS-3A is an overall fining upwards, 30 m thick unit comprising intercalated shoreface sandstones and offshore mudstones containing the foraminiferal assemblage of *Preaorbulina glomerosa circularis* (unpublished GUPCO sections). As with the hangingwall dip-slope location at Wadi Feiran, a subsequent overall coarsening upwards package, 50 m thick consisting of shoreface sandstones, is capped by the FS-4 major flooding surface. Overlying FS-4, Stratal Unit 5 is up to 230 m thick and is characterised by brackish to lacustrine marls indicated by the presence of non-marine diatoms and freshwater algae (Wescott et al., 2000). The T_{30} surface is again linked to the first appearance of the Markha Anhydrite, here up to 30 m in thickness.

Surface RS-4 and associated deposits of Stratal Unit 4 are not easily identified at Wadi Gharandal. Tracing of key units onto Gebel Gushea towards the south (Fig. 7.2) documents

the presence of a series of fluvial to deltaic conglomerates infilling incised topography into underlying Stratal Unit 3, and the Lower Rudeis Formation (Chapter 6). This fluvial-deltiac package is comprised of initially poorly sorted, angular to sub angular clasts, predominantly of pre-rift limestones, but also clasts of underlying tidal cross bedded sandstones of Stratal Unit 3. Increased sorting and the development of crude cross bedding and imbrication of clasts is observed in the younger part of this package. These conglomerates are then clearly onlapped by a shallow marine to offshore succession of Stratal Unit 5 (Fig.7.11).

Interpretation

The relatively low subsidence setting of the accommodation zone in a rift margin setting at Wadi Gharandal was initially characterised by erosion and bypass during the earlier stages of Upper Rudeis Formation deposition. The direct juxtaposition of the Lower Rudeis Formation with overlying deposits of Stratal Unit 3 suggests a more composite surface than that at South Gebel Gushea and Gebel Gawher, comprising the T_{20} hiatal terrace and all surfaces and units of the Upper Rudeis Formation older than FS-3. The relatively low subsidence setting at Wadi Gharandal, like at the Thal Fault tip, was characterised by erosion and bypass during the earlier stages of Upper Rudeis Formation deposition. Considering the offshore to lower shoreface nature of the previous underlying Lower Rudeis Formation, this again is further suggestive of a relative sea-level fall during Stratal Units 1 and 2. Similarly to both the Thal Fault tip and Wadi Feiran, the renewal of deposition at Wadi Gharandal was during Stratal Unit 3, linked to a subsequent overall marine transgression. The base of Stratal Unit 3 deposited here is characterised by the tidally influenced shelf Facies Association, with a continued rise in base-level documented by FS-3A and the succeeding package of shoreface sandstones and offshore mudstones. RS-4 is interpreted to be mainly coincident with FS-4 within the Wadi Gharandal area, contrasting sections at the northern part of Gebel Gushea. Here, RS-4 is picked at the base of major incision into Stratal Unit 3 and even into the Lower Rudeis Formation, with subsequent infilling by fluvial to deltaic conglomerates. This is suggestive of a major regression, with the development of local incised valleys. The angular to sub angular nature of the earliest clasts dominated by pre-rift limestone clasts is suggestive of renewed erosion at the rift shoulder, whilst the presence of clasts sourced from the

underlying facies is consistent with the interpretation for incision. The valley fill presents the onset and return to overall transgression continued into overlying Stratal Unit 5.

Rift axis

Located towards the western margin of the Zafarana Accommodation Zone within the rift axis, the sub-horizontal platform of the Warda Fault Block has several wells which penetrate extensive siliciclastic sandstones within the Lower Rudeis to Kareem Formations. This succession has been interpreted as a proximal fan delta depositional system, downthrown against the easterly dipping Coastal Boundary Fault System, with individual, coarsening-upwards depositional cycles correlated locally on the fault block through minor flooding surfaces (Elbaz and Handley, 1994). The more basinward footwall crest of the Warda Fault Block, determined by well GS114-4A (Fig. 7.2), is dominated by finer-grained offshore mudstones, suggesting considerable thinning and onlap of these coarse-grained facies towards the footwall crest.

Within the hangingwall of the Coastal Boundary Fault System, the Lower Rudeis Formation is dominantly aggradational and contrasts with the marked progradational nature of the Upper Rudeis Formation (Fig. 7.12). Stacking patterns and tracing of key surfaces allows for the five Upper Rudeis Formation stratal units defined within the rift axis to be delineated in this area, despite the poor biostratigraphic control associated with the coarse-grained facies. The T_{20} surface is characterised as a major flooding surface capping the aggradationally stacked, Lower Rudeis fan-deltaic deposits, with the overlying Stratal Unit 1 represented by a thin package, < 20 m thick of offshore mudstones. Seventeen kilometres to the southeast towards the rift axis, Stratal Unit 1 contains thin, distal silciclastic turbidites, bounded at the base by surface RS-2, which are inferred to thin and onlap back towards the Warda Fault Block (well Sabil-1, Fig. 7.12). Stratal Unit 2, markedly progradational, is comprised of predominantly siliciclastic sandstones, arranged within a series of up to seven, 5-50 m thick, coarsening upwards cycles, which abruptly overlie Stratal Unit 1. The distal equivalent of these deposits is the siliciclastic submarine fan facies observed in the hangingwall of the October Fault Zone, some 40 km to the south. Capping Stratal Unit 2, flooding surface FS-3 denotes a shift to basinal mudstones, up to 20 m thick, of Stratal Unit 3. Renewed siliciclastic sandstone deposition occurs in Stratal Unit 4, although not as extensive as during Stratal Unit

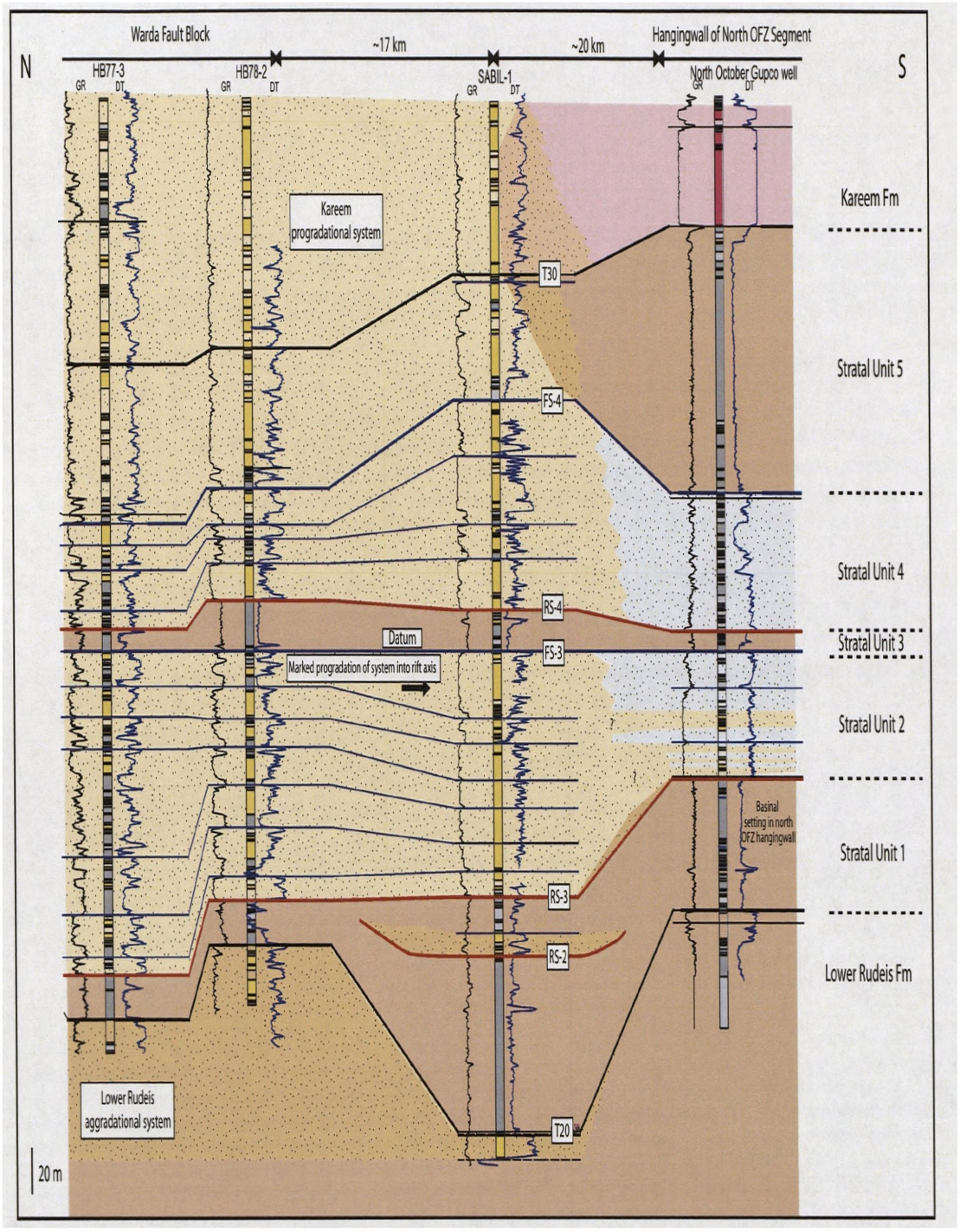

Figure 7.12. Well correlation panel from the Warda Fault Block to rift axis hangingwall depocentre of the northern segment of the October Fault Zone. See Figure 7.1 for location. Stratal Unit 1 is charaterised at the Warda Fault Block by thin, mudstone deposition with coeval submarine fan deposition ~17 km downdip into the rift axis. Stratal Unit 2 records a marked progradation into the rift, with distal siliciclastic submarine fan deposits intercalated with alternatively sourced calcarenite submarine sandstones in the hangingwall of the October Fault Zone.

2, with for example, entirely locally derived calcarenitic submarine fan deposits in the hangingwall depocentres of the October Fault Zone (Fig. 7.12). The presence of extensive siliciclastic sandstone deposits upon the Warda Fault Block within Stratal Unit 5 contrasts with common observations made within the rift axis, where this stratal unit is typically dominated by a pelagic rich, calcareous marl facies.

Interpretation

The hangingwall nature of the Warda Fault Block setting with respect to the Coastal Boundary Fault within the Zafarana Accommodation Zone provides an almost complete record of the role this structurally diffuse zone played in focussing regional sediment fluxes from the rift margin hinterland into the rift axis, contrasting with the erosionally dominated rift marginal setting at Wadi Gharandal (Fig. 7.13). The siliciclastic composition of deposits on the Warda Fault Block, in sharp contrast to the calcarenitic nature of the syn-rift deposits located within the western margin, reflects a clear difference in prerift provenance lithology to that provided by uppermost pre-rift Eocene carbonates, early syn-rift and contemporaneous carbonate sources. This compositional signature, reflecting the sourcing of prerift Cambrian to Lower Cretaceous Nubian sandstones upon the eastern margin (Chapter 4; Elbaz and Handley, 1994) is mirrored in the composition of more distal submarine fan deposits further within the rift axis (Chapter 4). Thus the observation that whilst Stratal Unit 1 upon the Warda Fault Block is dominated by fine-grained mudstones, the presence of thin siliciclastic submarine fan sandstones, some 17 km in the central dip province, (well Sabil-1, Fig. 7.12) suggests a period of sediment bypass during Stratal Unit 1 upon the Warda Fault Block. Potentially, the topographic gradient associated with the footwall of the basinward Warda bounding fault combined with a regional southerly dip towards the central dip province in focusing the sediment influx associated with Stratal Units 1, 2 and 4 largely towards the south into the rift axis, rather than directly basinward into the axis (well ET-6, Fig. 7.13). The period of observed sediment switch off in rift axis hangingwall depocentres during Stratal Unit 3 is similarly mirrored upon the Warda Fault Block, supportive for a regional shutdown in sediment supply into the rift axis at this time. This differs to Stratal Unit 5, which while similarly observed to reflect sediment starvation in the rift axis, is observed to significant, yet restricted coarse-grained sedimentation upon the Warda Fault Block.

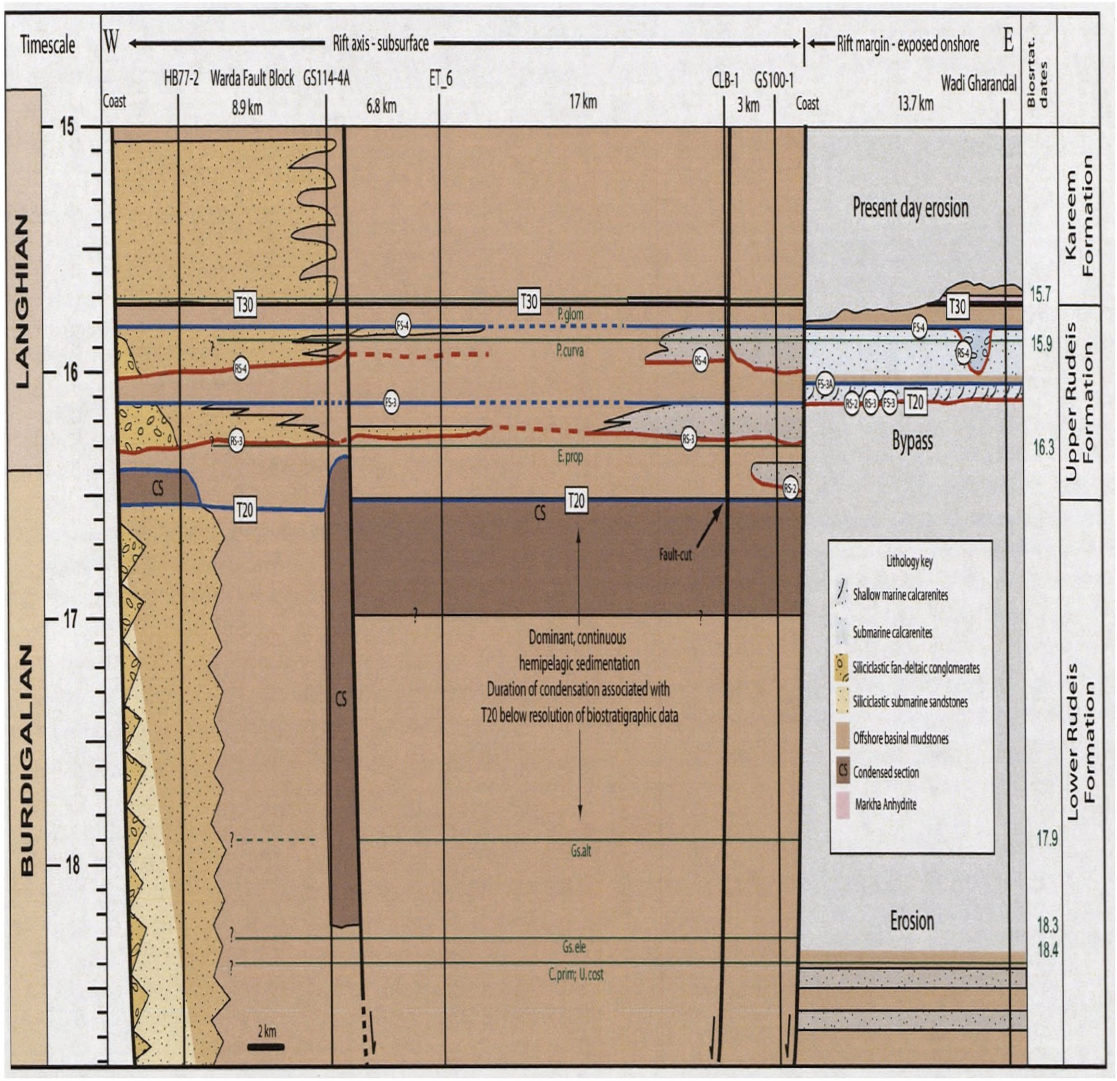

Figure 7.13. Cartoon chronostratigraphic correlation from west to east along the axis of the Zafarana Accommodation Zone (see Figure 7.1 for location). Two compositionally different clastic depositional systems are recognised entering the dominantly sediment starved rift axis from either margin. On the Warda Fault Block, stacked aggradational Lower Rudeis Formation fan-delta deposits (Elbaz and Handley, 1994) are suceeded by offshore basinal mudstones and progradational fan-delta units. This contrasts with the extensive erosion of the uppermost part of the Lower Rudies Formation at the western margin, and subsequent bypass of Upper Rudeis Formation Stratal Units 1 and 2. The mid-clysmic unconformity surface of Garfunkel and Bartov, (1977) represents an amalgamation of RS-2, RS-3, FS-3 and T20 surfaces. Timescale from Berggren et al., 1995, biostratigraphic ages from internal GUPCO database

7.7. SYNTHESIS AND DISCUSSION

Comparison of the sedimentary, stratigraphic and thickness variability of the Upper Rudeis Formation from the three tectono-stratigraphic domains (rift margin, rift axis and structural accommodation zone) allow a basinwide assessment of the nature and relative importance of the principal controls upon late rift climax sedimentation. This analysis allows a sequence stratigraphic model for the Upper Rudeis Formation to be developed and general implications for syn-rift sequence variability to be discussed.

7.7.1 Spatial variability and controls upon late rift climax stratigraphy and facies

The high-resolution correlation of the Upper Rudeis Formation from differing tectono-stratigraphic domains within the Suez Rift highlights the spatial variability of syn-rift depositional systems and their stratigraphic evolution. The principal spatial control recognised in this study is the nature of the structural configuration of the rift, which can be considered at both rift-wide and local, fault-block scales. This primary tectonic control directly impacts upon base-level within the rift, the nature of sediment sources along with subsequent supply and therefore the location of available accommodation space.

Figure 7.4 summarises the depositional synthesis for the Upper Rudeis Formation, with the Suez rift being characterised during late Burdigalian to early Langhian times by a relatively uplifted, emergent rift shoulder, a partially submerged rift margin, and a wholly submerged rift axis. Areas of relative uplift associated both with the rift shoulder, and local footwall crests, provided source areas for depositional systems. In the Upper Rudeis Formation, rift-wide depositional systems, sourced from the rift shoulder were volumetrically much more significant compared to those sourced from smaller, intra-basinal footwall crest sources. At the rift margin, large coarse-grained proximal depositional systems, sourced from the extensively exposed rift shoulder entered the rift via localised structurally controlled relay ramps and the tips of fault segments (e.g. Gebel Gawher at the northern tip of the Thal Fault) associated with the rift border fault. Particularly important in routing sediment into the rift were the broad zones of reduced subsidence associated with major structural accommodation zones (e.g. the Zafarana Accommodation Zone), as recognised in studies such as the East Africa Rift (e.g. Rosendahl, 1987; Morley et al., 1990). Once within the rift axis, the distribution of these regional sediment fluxes was controlled by both the regional dip of the

structural dip domains, and by the configuration of local fault zones. In the Upper Rudeis Formation, density-flow sand deposition was focussed within hangingwall depocentres, with large, regional-scale depositional systems intercalated with locally-sourced and volumetrically small depositional systems derived from adjacent footwall scarps. Typically footwall crests, being sediment starved were highly condensed (e.g. October Fault Zone), except where higher sediment supply rates associated with close proximity to major sediment input points was able to overcome structurally defined bathymetric relief (e.g. West July Fault Zone). The overall reduction in coarser-grained sediment from the rift margin to the rift axis is therefore a function of both increased distance from the important regional source hinterland of the rift shoulder, and the diminished importance of intra-rift axis uplifted footwall crests in yielding sediment.

The development of key surfaces and associated stratal units linked with these Upper Rudeis Formation depositional systems was primarily regional base-level controlled, but with considerable variability observed at the local fault-block scale (Fig.7.14). As a result of the difference in relative elevation of fault blocks from the rift margin to rift axis, due to increased overall subsidence, the relative importance of the role of base-level (and subsequent variations) was diminished within the axis compared to the margin. At the partially submerged rift margin there was increased potential for reworking of uplifted source areas and previously deposited syn-rift units. This is recorded in the nature of the lowermost bounding surface of the Upper Rudeis Formation being a highly composite, major sequence boundary, both upon hangingwall dip-slope and rift bounding fault tip locations. Within the wholly submerged rift axis, uplifted footwall crests were below the base of sea-level influence. Therefore deposition on hangingwall dip-slopes and footwall crest locations, whilst variable due to the nature of sediment supply, was typically characterised by condensed and thinned section and as a result, key surfaces on footwall crests therefore may be variably composite. This contrasts with the expanded sections observed in rift axis hangingwall depocentres, which are largely sediment starved, being dominated by offshore shelfal to basinal mudstones with intercalated density flow sand deposits, which may provide a complete record of individual key surfaces and intervening stratal units.

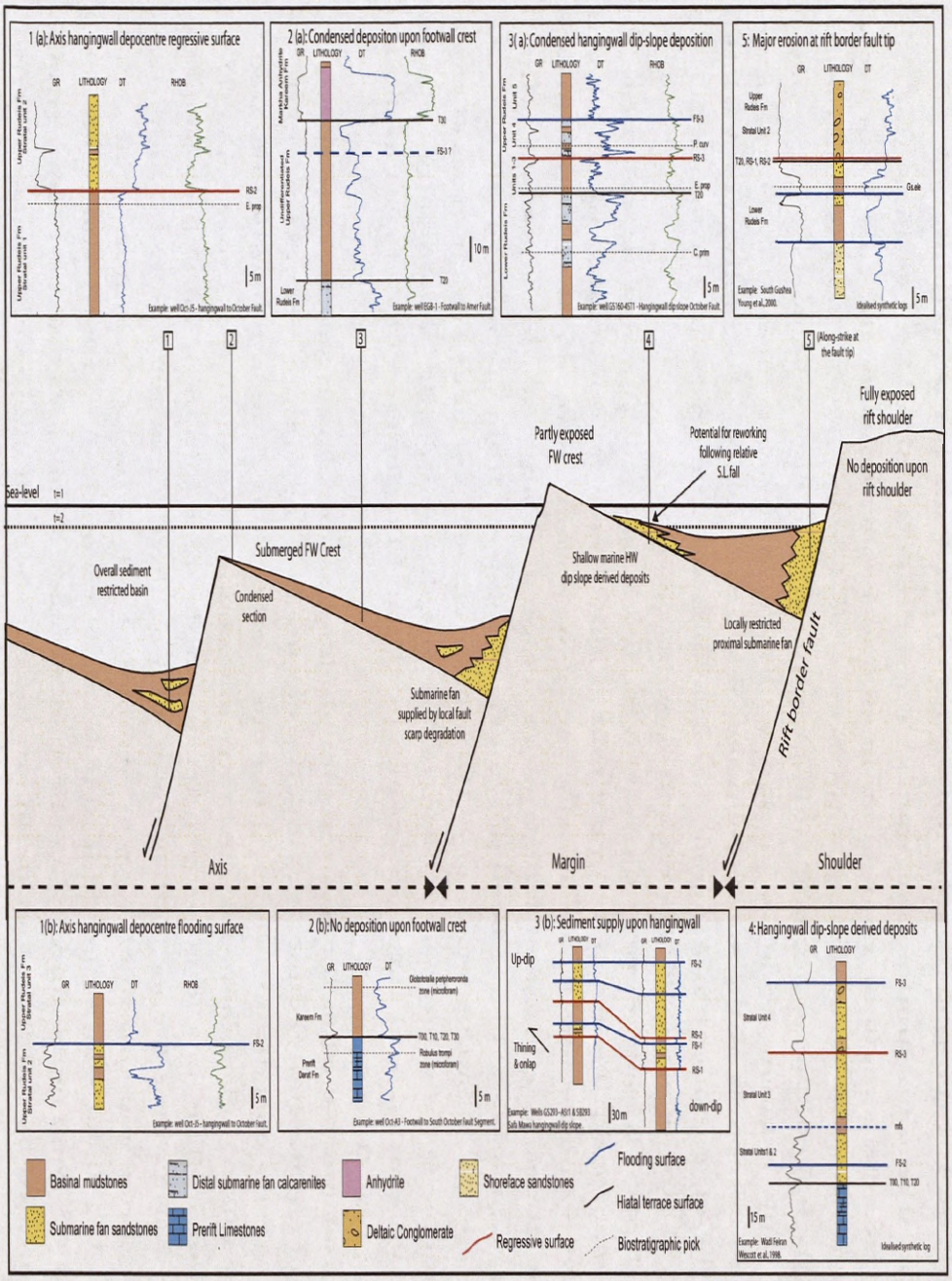

Figure 7.14. Conceptual 2D cross section through a series of tilted fault blocks during the climax phase of rifting, with type examples of key surfaces and associated facies for differing tectonostratigraphic settings examined in this study (locations 1-5). Rift climax deposits show an overall reduction in grainsize from the margin to the rift axis, reflecting both the increasing distance from the uplifted shoulder and reduced potential for locally derived sediment from increasingly submerged footwall crestal locations. Varability in facies and key surfaces depicted is fundamentally determined by the local basinal configuration. See Enclosure H for enlarged version.

7.7.2 Controls on the temporal evolution of the Upper Rudeis Formation

Conceptual tectono-stratigraphic models for rift basins typically suggest that during the rift climax phase, the structural configuration of the basin provides the major, first order control upon syn-rift sedimentation (e.g. Gawthorpe and Leeder, 2000). Localisation of strain onto increasingly linked, through-going fault arrays, results in high subsidence / uplift rates in the centre of fault segments and much lower displacement rates near the ends of fault segments. The interaction of the subsequent tectonic generated phyisography with variations in relative sea-level is thought to generate major sequence variations adjacent to normal fault zones (e.g. Gawthorpe et al., 1994; Hardy and Gawthorpe, 1998).

In the Upper Rudeis Formation however, the existence of rift-wide traceable key surfaces and synchronous facies shifts in both the highly structural dominated rift axis and rift margin, typified by major tilted fault blocks and also the more structurally diffuse rift wide accommodation zones, is consistent with a more regional, relative sea-level control. Similar rift-wide changes in sea-level have been previously recognised from marine syn-rift sediments in other rift basins, e.g. Surlyk et al. (1993), whilst regional surfaces which cross differing structural locations in rifts have also been documented, such as the tectonically-enhanced maximum flooding surfaces of Haywood et al. (1993); and Partington et al. (1993) in the Late Jurassic North Sea Rift.

The causal mechanisms for these regional changes in relative sea-level during Upper Rudeis times are potentially either regional tectonic (i.e. wholesale basinwide uplift and subsidence) or glacio-eustatic in origin. Previous workers have predominantly favoured the structural mechanism to account for a significant change between the Lower and Upper Rudeis Formations. This has largely been based on the recognition of an abrupt basinward shift in facies at base of the Upper Rudeis Formation on the rift margin, commonly referred to as the 'mid-Clysmic unconformity' (e.g. Garfunkel & Bartov, 1977; Patton et al., 1994). Related to the T_{20} hiatal biostratigraphic terrace of Wescott et al. (1996) and Krebs et al. (1997), the mid-Clysmic unconformity has been attributed to a major structural reorganisation of the rift, manifested by uplift and unroofing of the rift shoulder along with contemporaneous fault block rotation (e.g. Garfunkel & Bartov, 1977; Wescott et al., 1996) and has been linked to the initiation of a major regional tectonic episode associated with strike-slip movement

upon the Gulf of Aqaba trend (e.g. Patton et al., 1994). This study has demonstrated that the base of the Upper Rudeis Formation at the rift margin is a highly composite sequence boundary, contrasting with a series of independently preserved surfaces within the rift axis. Therefore, although yielding information specific to the tectono-stratigraphic evolution of the rift margin, correlation with data from the rift margin suggest that it is erroneous to interpret this highly composite surface as evidence for a single, major tectonic episode. Additionally recent reviews upon the timing of for such an event discount the initiation of the Aqaba trend as a possible mechanism (McClay & Bosworth, 2001), whilst published data from the rift also suggest continual rotation of fault blocks (Sharp et al., 2000) and progressive unroofing (Allen et al., 1984; Evans et al., 1990; Gawthorpe et al., 1990) rather than a specific, tectonic episode within the rift.

An alternative model for the basinwide stratigraphic signature is that high frequency variations in relative sea-level are driven by glacio-eustasy, against a background of late rift climax, waning tectonic subsidence. The presence of age calibrated key foraminiferal assemblages allows for the correlation of the Upper Rudeis Formation with proxy oxygen-isotope records for glacio-eustatic variation. Figure 7.15 illustrates how the Upper Rudeis Formation, approximately ranging from *ca.* 16.6 to 15.8 Ma coincides with a major glacio-eustatic fall in sea-level, with a ~ 30 m fall suggested by a positive inflection in oxygen isotope curves, *ca.* 16.3 Ma (of Miller et al. 1991, 2005; Abreu and Anderson. 1998), and a more significant, >100 m fall, *ca.* 15.9 M.a, in the proposed global eustatic curve of Haq et al (1987). Both datasets are suggestive of a shorter duration eustatic fall and a subsequent longer term eustatic rise. The correlation of these major glacio-eustatic variations as suggested in the curves of Haq et al (1987) and Miller et al (2005) provide an important constraint for the interpretation of regionally extensive key surfaces and intervening stratal units developed in the Upper Rudeis Formation (Fig.7.15). Both datasets are indicative of a single cycle glacio-eustatic event, associated with a late Burdigalian sea-level highstand followed by a major, early Langhian sea-level fall and a subsequent, prolonged, mid Langhian sea-level rise. In comparison, potential cycles observed in the Upper Rudeis Formation are suggestive of higher frequency glacio-eustatic variations with differential magnitudes.

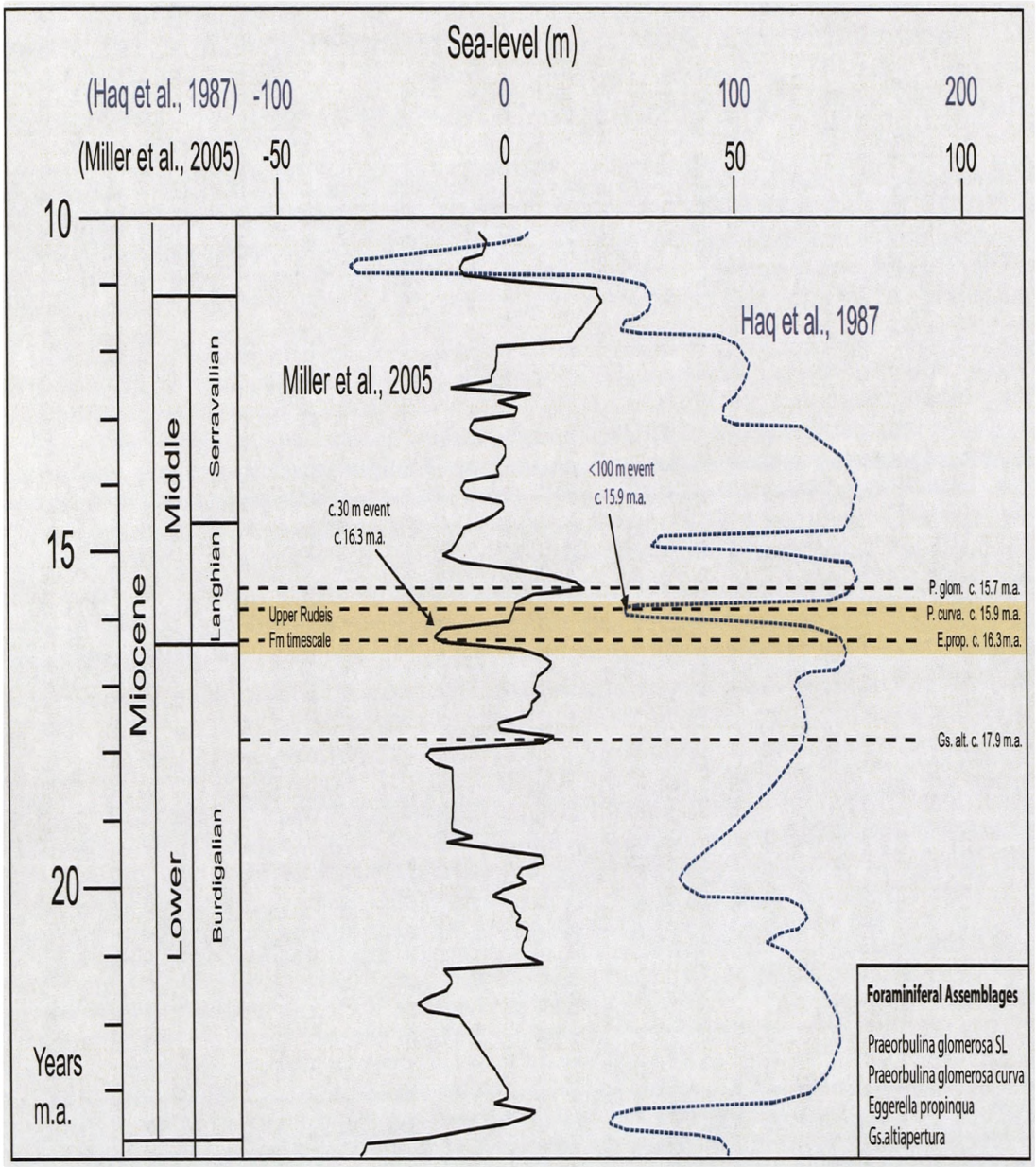

Figure 7.15. Proxy oxygen isotope record for glacio-eustatic variation after Miller et al., (2005) and the global eustatic curve of Haq et al., (1987) for the lower and Middle Miocene. Age information for key foraminiferal assemblages allows for the calibration of the Upper Rudeis Formation with significant eustatic variations, notably with a major sea-level fall proposed at 15.9 m.a. in the order of 100 m (Haq et al., 1987) or at 16.3 m.a. in the order of 30 m (Miller et al., 2005).

The characterisation of the T_{20} hiatal event within the rift axis as a maximum flooding surface within continuous section (Fig 7.2)), dated within biostratigraphic resolution as between ca.17.9 Ma and 16.3 Ma is consistent with the suggested late Burdigalian sea-level highstand. The three subsequent major influxes of sediment into the rift axis associated with regressive surfaces RS-2, RS-3 and RS-4 respectively, and capped by ensuing flooding surfaces (FS-2, FS-3 and FS-4) denotes three potential glacio-eustatic driven sea-level falls and subsequent rises. The volumetrically more significant clastic influx associated with RS-3 and Stratal Unit 2 is interpreted to be in response to the major sea-level fall suggested by both sea-level curves. the timing of which, represented in the Miller et al (2005) curve fits well within the biostratigraphic framework for surface RS-3, namely associated with the calibrated age of 16.3 Ma for the foraminiferal assemblage *Eggerella propinqua.* Correlation of the approximate timings for the relatively smaller influxes of sediment recorded in the rift axis associated with surfaces RS-2 and RS-4 with the glacio-eustatic curve of Miller et al (2005) indicates that they cannot be linked to a specific episode of sea-level fall. In fact, they are suggested to have occurred on the rising and falling limbs respectively of the major sea-level change associated with the 16.3 Ma event (Fig. 7.15). Thus, both these sediment influxes are interpreted to record higher-resolution eustatic sea-level variations against either the larger background fall or rise associated with the development of RS-3, as recorded in the Miller et al (2005) curve.

7.7.3 Model for the sequence stratigraphic development of the Upper Rudeis Formation

This section integrates observations for the presence of regionally extensive key surfaces across differing structural domains, and the spatial and temporal variability of intervening stratal units, with respect to thickness and the nature of principal facies associations, for the Upper Rudeis Formation, with correlated variations in glacio-eustasy. This allows for a model for the sequence stratigraphic development of the late rift climax, Upper Rudeis Formation to be proposed, in which four depositional sequences are identified.

Tectonically enhanced transgression: Lower Rudeis Formation

Both offshore borehole data within the rift axis and onshore exposures of the rift margin of the Lower Rudeis Formation are consistent with tectonostratigraphic and subsidence

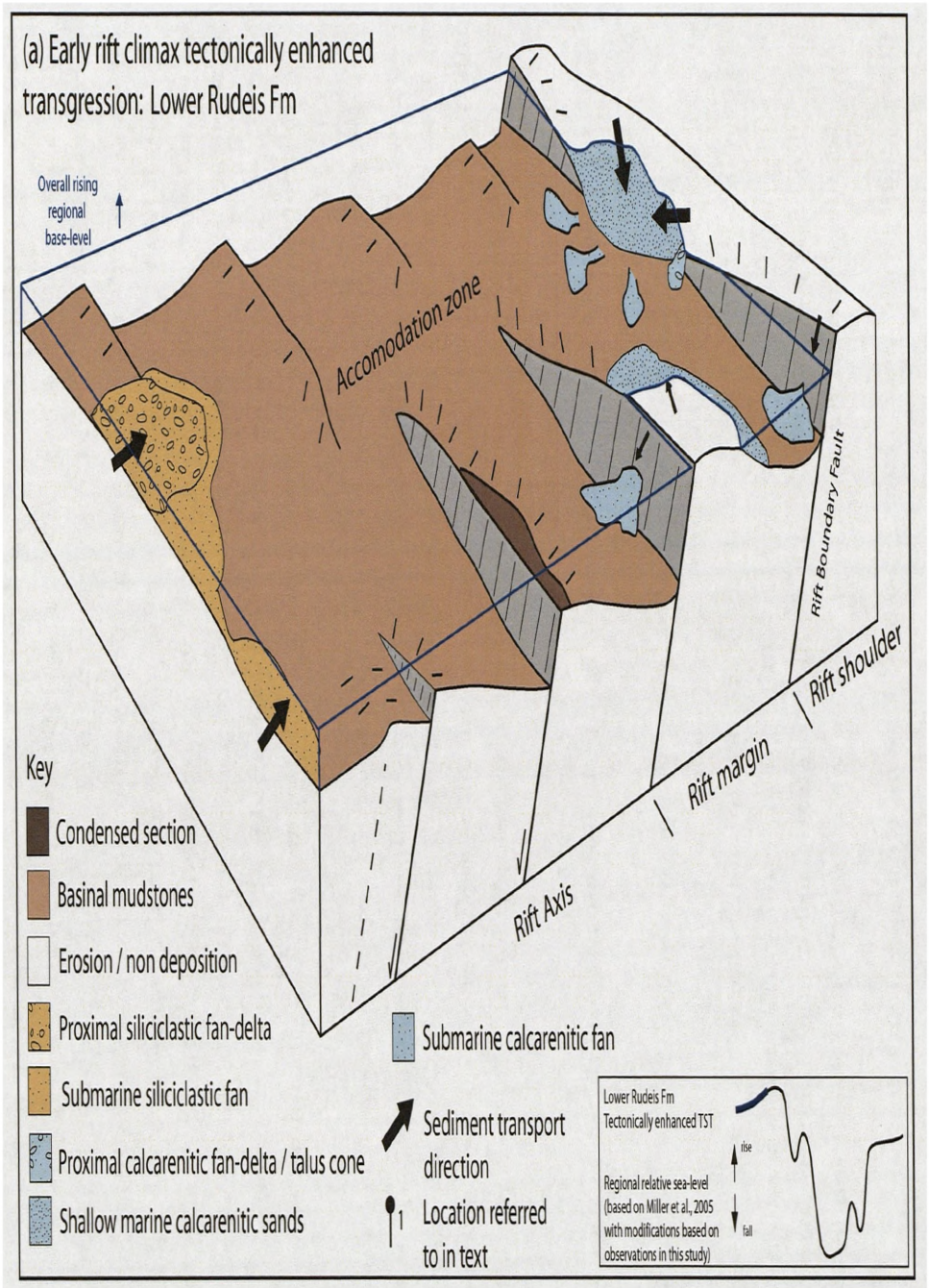

Figure 7.16. Schematic 3D model for evolution of the Suez Rift during the rift climax to late rift climax phase. (a) Maximum displacement rates during the rift climax phase associated with the Lower Rudeis Formation (c. 19.5 - 16.5 Ma) outpace any variations in eustasy and lead to the development of overall basinal conditions within the rift. Depositional systems sourced from the rift margin hinterland via structurally-controlled and antecedent drainage pathways in addition to those from intra-rift footwall highs are limited in extent. The rift is overall sediment starved, characterised by an overall transgressive sequence set.

models for the evolution of the Suez rift, which cite this period as the main climax phase of the rift (e.g. Garfunkel & Bartov, 1977; Patton et al., 1994; Steckler et al., 1988; Evans et al., 1988; Richardson and Arthur, 1988; Bosworth and McClay, 2001). Shoreface to offshore marine depositional systems, intercalated with proximal fan-delta and more distal submarine fan systems, displaying typically limited, aggradational (e.g. Gawthorpe et al., 1990; Elbaz and Handley 1994) to retrogradational stacking patterns (internal Gupco mapping) point towards a generally rift-wide, tectonically enhanced transgressive sequence set (Fig.7.16a). Within rift axis hangingwall depocentres (Fig.7.16a, point a), the end of Lower Rudeis deposition is typically characterised by the T_{20} marked flooding surface, associated with hiatal condensation. In comparison, footwall locations (Fig.7.16a, points b and c) may similarly be characterised by a flooding surface, condensed section or non-deposition, dependant upon varying fault-controlled bathymetry.

It is concluded that T_{20} within the rift represents a maximum flooding surface, developed as a response to high rates of relative sea-level rise caused by a combination of a peak in rift climax subsidence rates during a time of high eustatic sea-level (e.g. Haq et al., 1987; Miller et al., 2005). Along the rift margin, subsequent erosion of the uppermost parts of the Lower Rudeis Formation and bypass during the earliest stratal units of the Upper Rudeis Formation modified the expression of the T_{20} hiatal surface and created what is now observed as a composite sequence boundary, encompassing surfaces RS-2, RS-3 whilst also locally FS-4, and referred to as the 'mid-Clysmic' unconformity.

Basinwide highstand and subsequent regressions: Stratal Units 1 and 2

Following the T_{20} maximum flooding surface within the rift axis, initial deposition of Stratal Unit 1 continued to be dominated by offshore, basinal mudstone facies types, containing the foraminiferal assemblage *Eggerella propinqua*. Examination of sediment entry points into the rift axis indicates re-establishment of progradational clastic depositional systems, albeit not as extensive as those active prior to T_{20}, suggests a relative sea-level highstand within the rift axis (Fig. 7.16b, point a). Locally constrained to some rift axis hangingwall depocentres (Fig.7.16c point a), an influx of submarine fan sandstones into the rift axis is recorded during the latter part of Stratal Unit 1, intercalated within offshore basinal mudstones. Mapping of these depositional systems back towards interpreted rift axis sediment

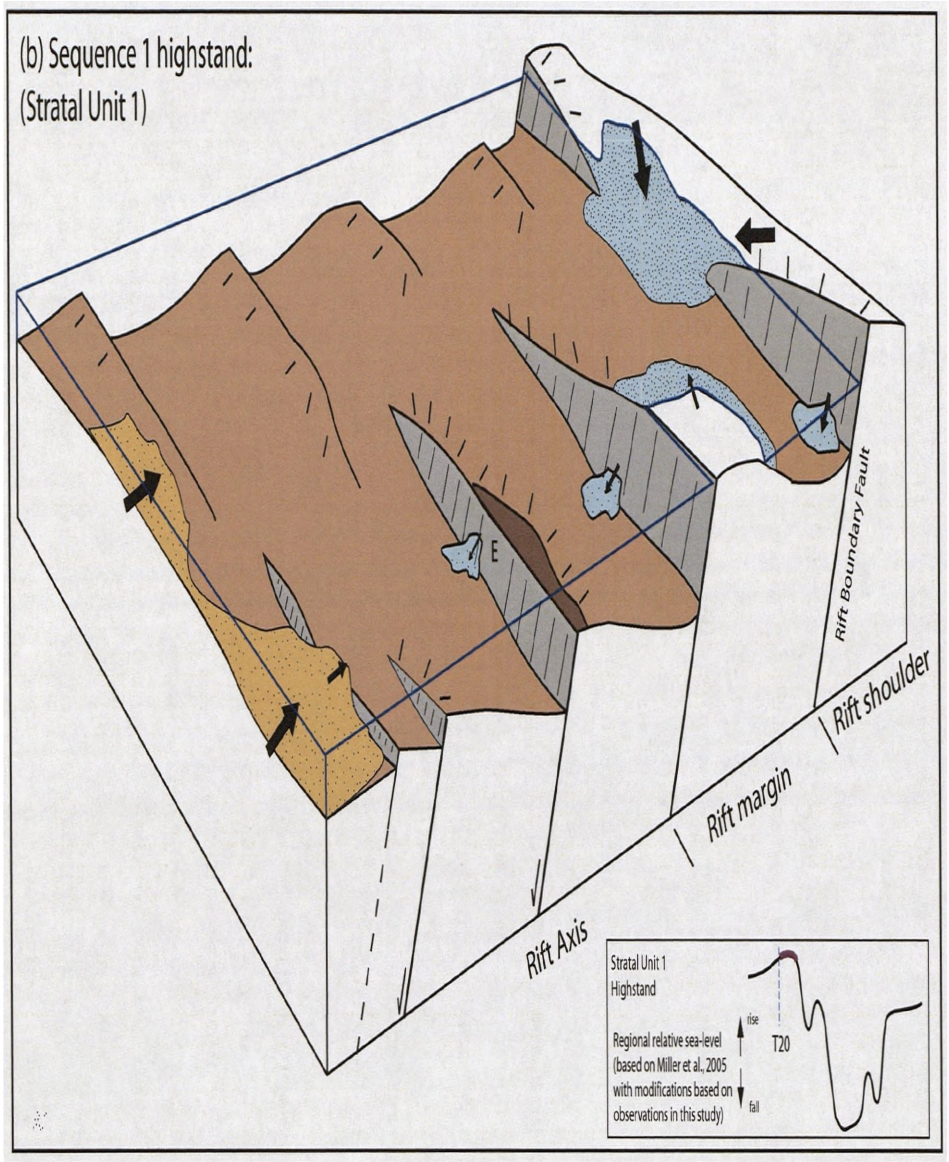

Figure 7.16 cont. (b) Towards the end of deposition of the Lower Rudeis Formation (c. 19.5 Ma), increasingly episodic fault activity reduced the rate of relative sea-level rise. This resulted in the development of the T20 maximum flooding surface within the rift axis and the development of highstand conditions associated with the base of the Upper Rudeis Formation. A renewed progradation of the clastic depositional systems entered into the rift, although this influx of sediment was spatially limited, with the rift axis still largely characterised by widespread offshore basinal mudstone deposition.

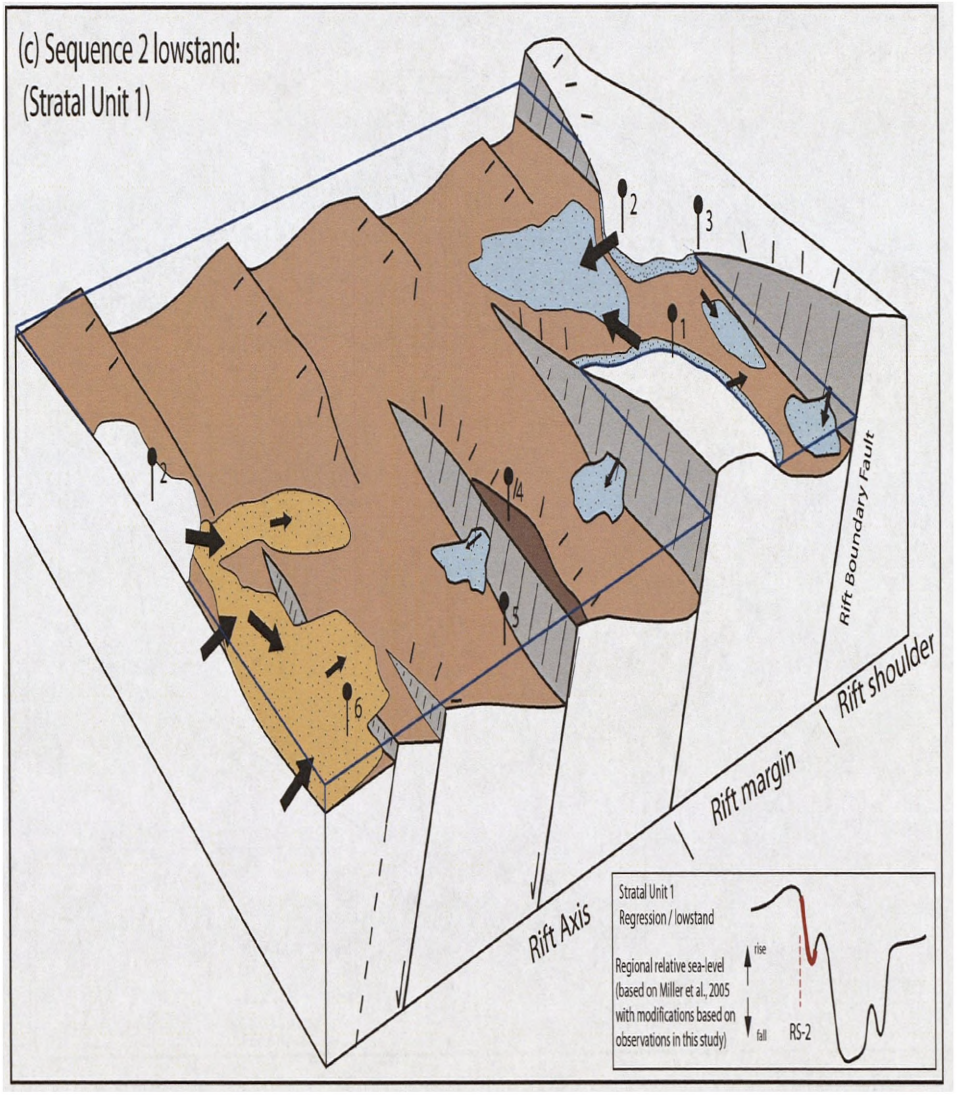

Figure 7.16 cont. (c) During the latter part of Stratal Unit 1, a regional fall in relative sea-level forced a marked influx of sediment into the rift, extending further than previous rift climax depositional systems. At areas of low subsidence at the rift margin, e.g. hangingwall dip-slopes (1), the proximal part of the accommodation zones (2) and rift border fault tip (3), significant erosion and bypass fed submarine fans extending into the rift axis. Rift axis footwall crests remain submerged (4), whilst rift axis hangingwall depocentres either remained relatively sediment starved (5) or experience this sediment influx (6).

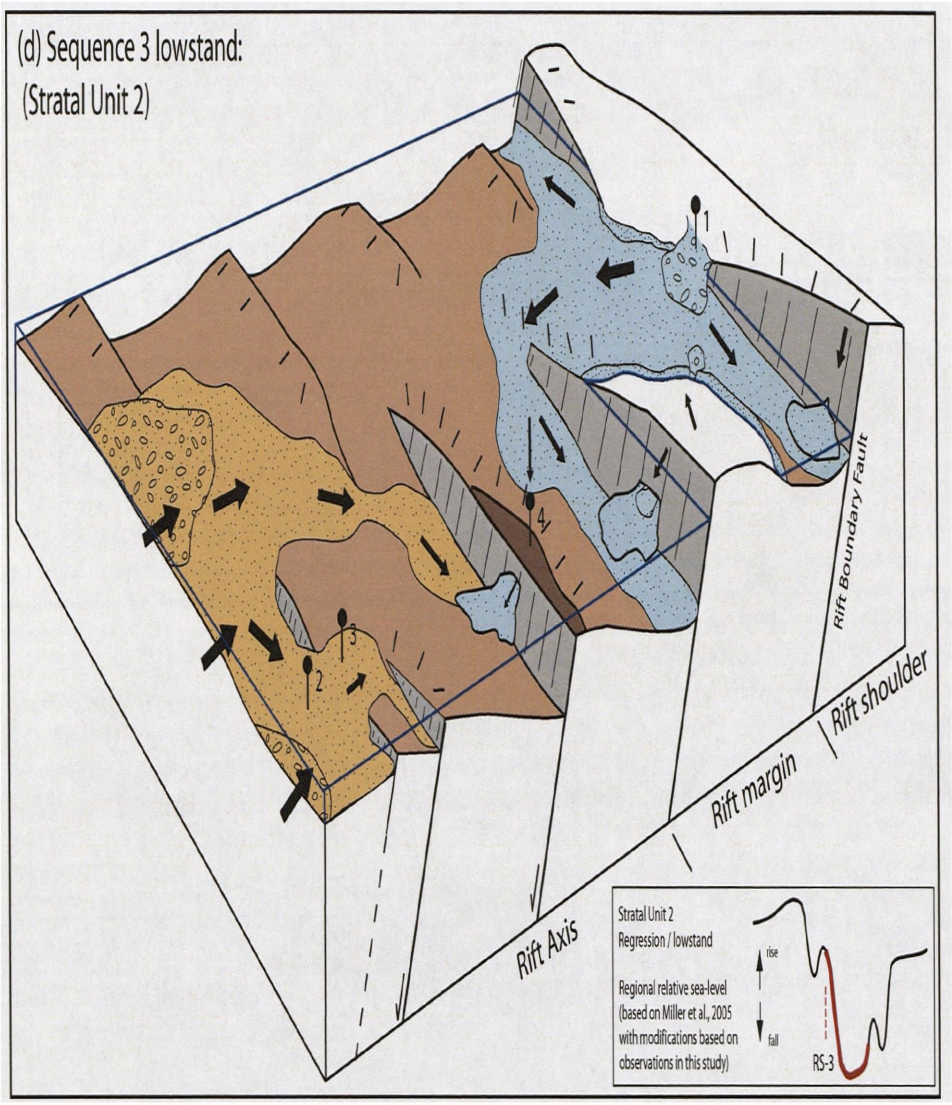

Figure 7.14 cont. (d) A regional lowstand in relative sea-level characterises Stratal Unit 2, with Upper Rudeis depositional systems attaining their maximum extent at this time. At the rift margin, coarse-grained fan-deltas infilled the erosional topography produced during Stratal Unit 1 (1) and fed submarine fan systems which extended into the rift axis, supplying material into hangingwall depocentres (2) and locally footwall crestal locations (3). Topographically higher footwall crests within the aix remained submerged, and characterised by condensed sedimentation (4). Compositional variations in pre-rift source provenance, allow for the discrimination of locally intra-rift and regional (>20 km) rift margin sourced depositional systems within the rift axis.

entry points shows either thinning and onlap towards otherwise basinal mudstone dominated areas, e.g. the Warda Fault Block, or clear correlation to thicker, more proximal submarine fan deposits, e.g. within West July Fault hangingwall (Fig.7.16c points b and c). Combined with the lack of any deposits equivalent to Stratal Unit 1 on the rift margin, and incision and erosion into the underlying Lower Rudeis Formation at low accommodation settings on the rift margin, suggests considerable sediment bypass directly into the rift axis due to a fall in regional relative sea level. Stratal Unit 1 is therefore a composite of the highstand systems tract of an earlier depositional sequence, Sequence 1, the base of which is inferred to be within the Lower Rudeis Formation and a full second sequence with forced regressive to lowstand and trangressive components, Sequence 2 (Fig. 7.6).

Stratal Unit 2 is only locally preserved within the rift margin, for example, a proximal fan-deltaic conglomeratic incised valley fill cut into the underlying Lower Rudeis Formation at the tip of the Thal Fault (Fig.7.16d point a), and as hangingwall dip-slope shoreface deposits (e.g. Wadi Feiran; Fig.7.16d point b). Stratal Unit 2 is also absent within the rift margin component of the Zafarana Accommodation Zone (e.g. Wadi Gharandal; Fig.7.16d point c). However in the rift axis portion of the Zafarana Accommodation Zone, on the Warda Fault Block, Stratal Unit 2 is characterised by markedly progradational fan-deltaic deposits. Further basinward into the tilted-half graben settings within the rift axis, distally equivalent submarine fan depositional systems recorded their maximum extent, primarily being focussed within hangingwall depocentres (Fig.7.16d point a). Stratal Unit 2 is therefore interpreted to principally represent a forced regressive and lowstand systems tract of Sequence 3 (Fig. 7.6) associated with the major eustatic fall in sea-level, at *ca.* 16.3 M.a (Miller et al., 2005). A higher magnitude fall is suggested in comparison to that associated with Sequence 2, due to the larger thicknesses and greater spatial extent of the submarine fan depositional systems within the rift axis. The rift margin components of Stratal Unit 2 are associated with the onset of rising base-levels, and represent lowstand infilling of previously incised topography.

Basinwide transgression to highstand: Stratal Unit 3

A major switch off in sediment supply is recorded within the rift axis by the sharp change across FS-3 to regional hemipelagic deposition of basinal mudstones of Stratal Unit 3 (Fig. 7.16e, point a). This is consistent with observations of a candidate maximum flooding

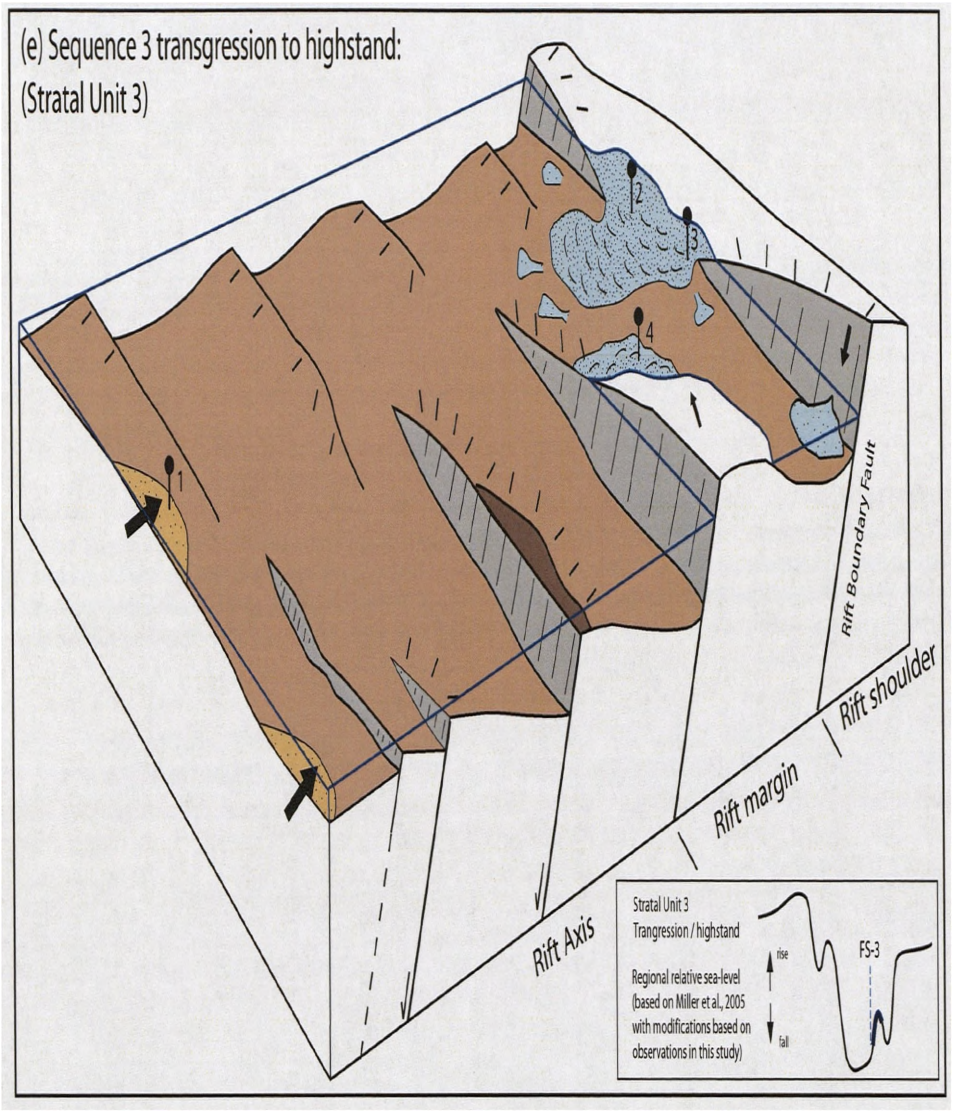

Figure 7.16 cont. (e) Following the lowstand of Stratal Unit 2, Stratal Unit 3 records the onset of widespread reduction in grainsize within the rift. Depositional systems entering the rift axis were locally restricted to sediment entry points (1), with the rift axis effectively sediment starved. At the rift margin, both the proximal accommodation zone (2), rift border fault tip (3) and rift margin hangingwall dip-slope (4) were characterised by trangression and the development of extensive tidally influenced shallow marine sandstones. At Wadi Gharandal (2), this facies forms the first preserved record of Upper Rudeis Formation deposition overlying the composite sequence boundary delineating the top of the Lower Rudeis Formation.

surface in some wells within the rift axis, characterised by a major, but thin high gamma-ray and equivalent low sonic log spike. Contemporaneous deposits within the rift margin are characterised by the widespread deposition of sheet-like, transgressive tidal marine sandwaves, observed within the rift margin part of the Zafarana Accommodation Zone and around the Rift Border Thal Fault tip (Fig. 7.16e, points b and c) and at the hangingwall dip-slope of the El Qaa Fault Block (Fig. 7.16e, point d). These deposits are capped by a distinctive flooding surface FS-3A and a switch to basinal mudstones, which have been observed to contain a condensed section associated with an interpreted maximum flooding surface (Wescott et al., 1998). Thus, Stratal Unit 3 is interpreted to reflect a regional relative sea-level rise associated with transgressive and early highstand systems tracts of Sequence 3 (Fig. 7.6).

Renewed regression: Stratal Unit 4

The onset of Stratal Unit 4 is characterised by local incision (RS-4) into Stratal Unit 3 at the rift margin component of the Zafarana Accommodation Zone and subsequent infill by fluvial conglomerates to shallow marine sandstones sourced from pre-rift units within the rift shoulder (Fig.7.16f, position a). On the hangingwall dip-slope of the El Qaa Fault Block at Wadi Feiran (Fig.7.16f, position b), RS-4 may be associated with the progradation of coarse-grained deltaic conglomerates. These rift marginal settings contrast with the rift axis, where RS-4 is characterised as a sharp regressive surface, denoting a switch to submarine fan sandstones from underlying basinal mudstones of Stratal Unit 3 (Fig.7.16f, position c). Renewed erosion at the rift shoulder and locally on the rift margin, characterised by incision into underlying Stratal Unit 3, provided for this renewed sediment influx into the rift axis. This renewed influx of sediment into the rift is interpreted to be associated with a relatively minor eustatic fall, against an overall background of relative sea-level rise. Stratal Unit 4 therefore forms the forced regressive to lowstand component of Sequence 4 (Fig. 7.6).

Renewed basinwide transgression: Stratal Unit 5

Stratal Unit 5 within the rift axis is characterised by a switch from the submarine fan facies association of Stratal Unit 4 to fine-grained calcareous marls rich in pelagic fauna indicative of sediment starvation. Coarser-grained, submarine fan depositional systems active during this stratal unit were locally restricted in extent, being located immediately adjacent to major sediment source entry points (Fig.7.16g, position A). On the rift margin, Stratal Unit 5 is similarly typified by fine-grained facies types with offshore to locally lacustrine mudstones

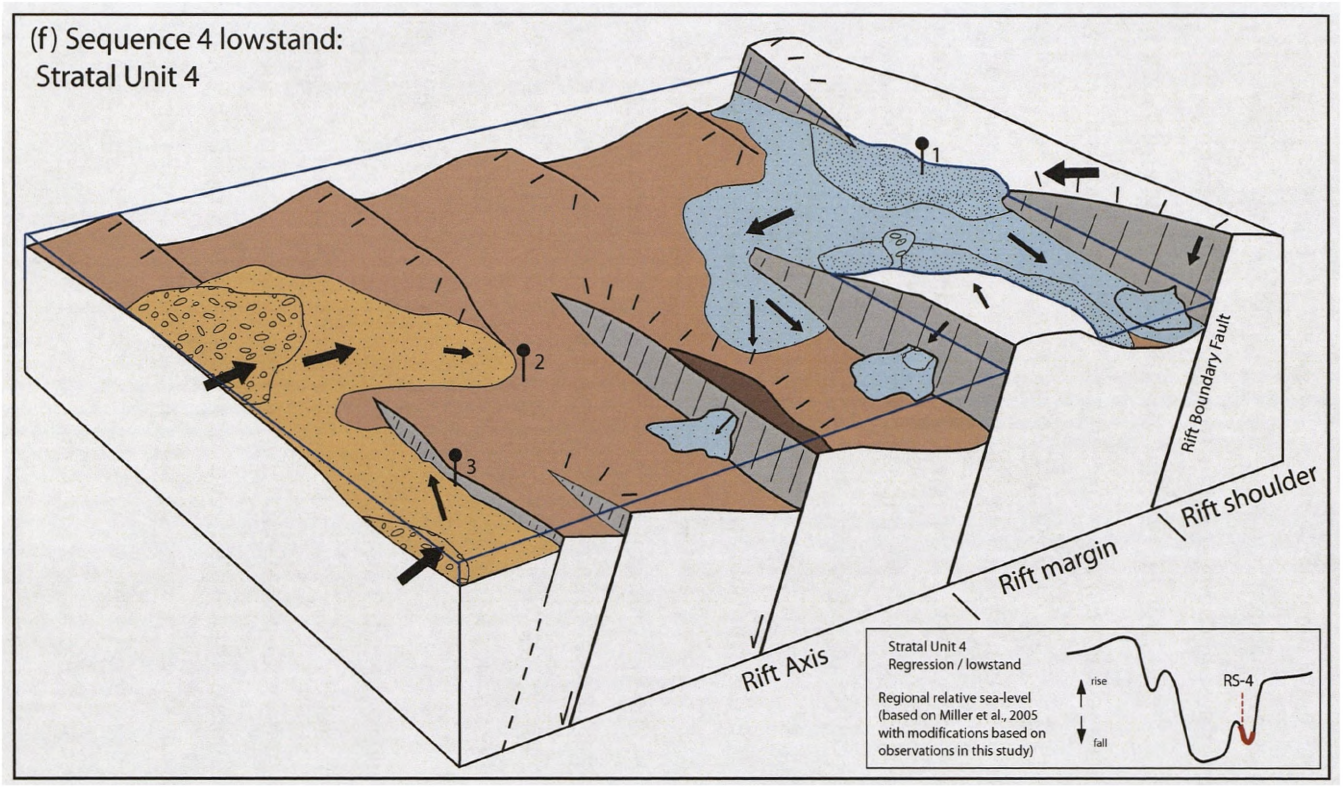

Figure 7.16 cont. (f) A relatively minor sea-level fall provided for the renewal of extensive clastic deposition within the rift axis during Stratal Unit 4. At the rift margin, a switch from retrogradational to progradational facies stacking is observed, and the onset of deposition of extensive shallow marine facies (1). The infilling of accommodation space at the rift margin allowed for the progradation of sediment into the rift axis; the sharp change in grain-size from underlying offshore basinal mudstones characterised by regressive surface RS-4. These depositional systems were not as extensive as those deposited during the Stratal Unit 2 lowstand (2), whilst continued fault development also provided a role in the location of specific sediment transfer pathways (3).

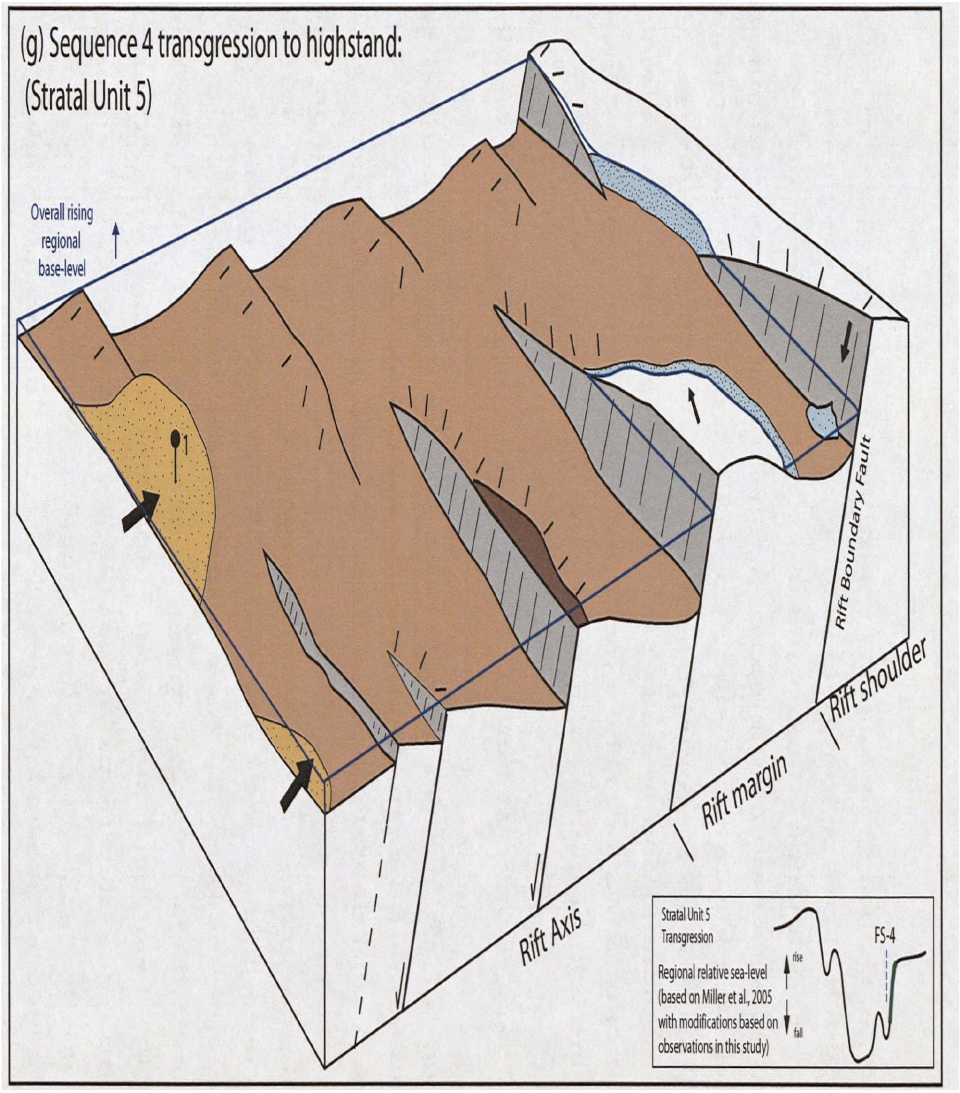

Figure 7.16 cont. (g) Stratal Unit 5 is characterised by a widespread overall shift to fine-grained deposition throughout the rift. Major depositional systems were locally restricted around principal sediment entry points (1), with the rift margin and rift axis largely typified by the deposition of offshore basinal mudstones and marls. This is interpreted as a renewed relative sea-level trangression to highstand.

and marls observed. Thus Stratal Unit 5 is interpreted to reflect a further period of relative sea-level rise associated with a period of prolonged transgression to hightand during Sequence 4 (Fig. 7.6).

7.8. CONCLUSIONS

This study demonstrates that during the final stages of the rift climax phase of rifting, waning fault activity may allow for variations in glacio-eustasy to provide a regional control upon the timing and magnitude of sedimentary fluxes and the sequence stratigraphic evolution of syn-rift deposits. However, the structural configuration of the rift, at both the regional and local scale, ultimately determines the location and size of primary sediment sources, transport pathways and depocentres. This is marked contrast to previously published models which have principally emphasised the potential dominance of the structural control, having typically focussed on the early to mid rift climax period. The examination of contemporaneous deposits from the main structural domains within the basin, namely rift margin, rift axis and rift-wide structural accommodation zone, allows for an assessment of the relative roles of structural configuration, eustasy and sediment supply, at both a regional rift-wide and local fault block scale (Fig.7.17).

Relative sea-level height, rift axis vs. rift margin: The interaction between global sea-level and the structural configuration of the rift determine the relative position of sea-level to tectonically generated topography and thus the availability of accommodation space. At the regional scale, the overall increase in subsidence towards the axis of the rift results in lower structural elevations and therefore overall increasing water depths. Thus whilst fault blocks at the rift margin may be locally emergent, as they intersect regional sea-level, the fault blocks within the rift axis may be wholly submerged. As a result, whereas variations in regional relative sea-level may have a direct impact upon rift marginal areas, effects within the rift axis may be relatively muted. At the local fault block scale, different lengths and gradients of tectonically-generated slopes influence the effects of variations in sea-level (e.g. Ranvas and Steel, 1998; McMurray and Gawthorpe, 2000). Short, steep footwall scarp slopes have a relatively narrow zone of influence of sea-level change, whereas longer hangingwall dip-slopes, with gentler gradients afford wider zones influenced by sea-level change, causing much greater lateral shifts in shoreline position during cycles of sea-level change.

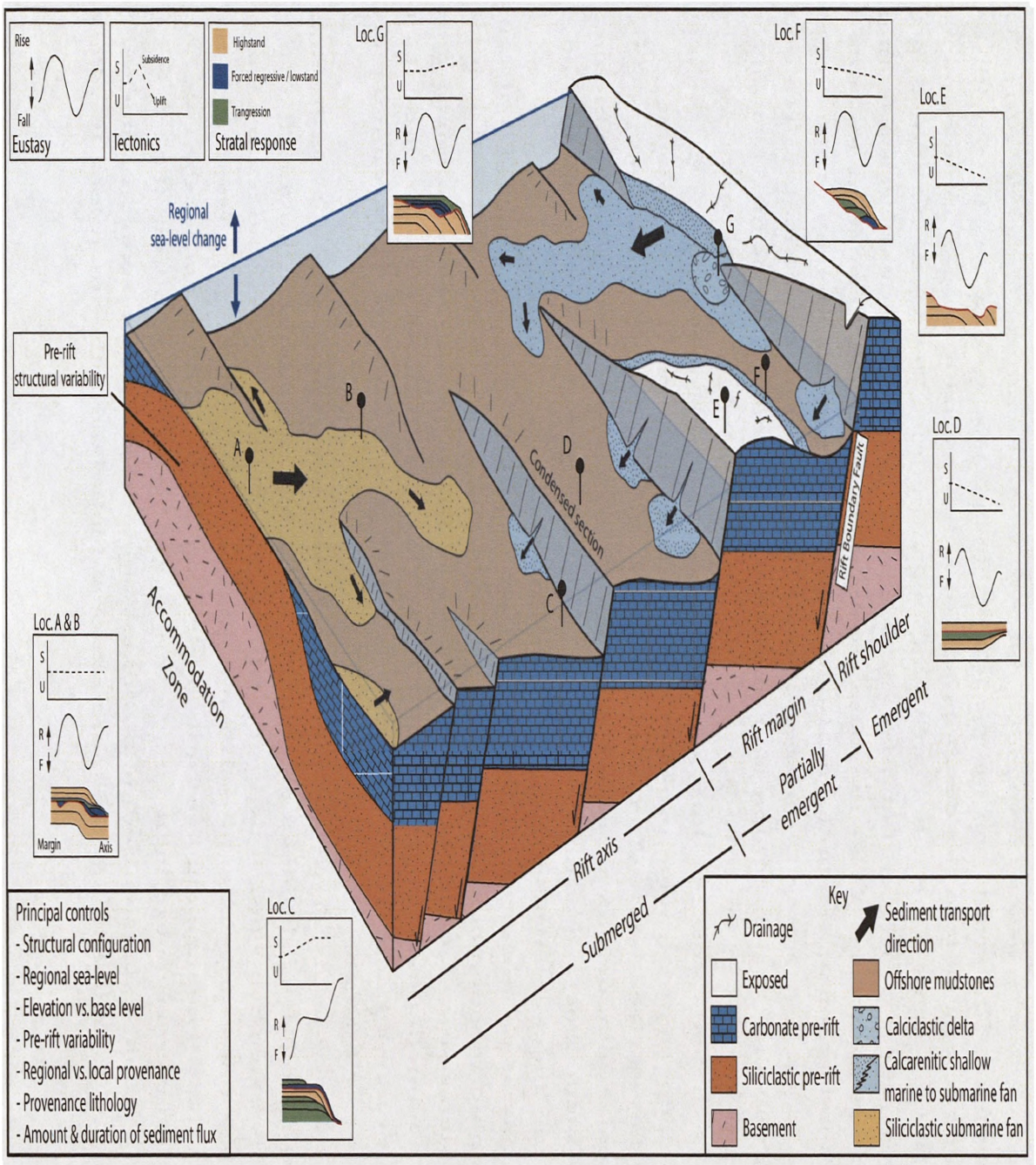

Figure 7.17. Schematic 3D model for the tectono-sedimentary and stratigraphic evolution of a rift during the main to late rift climax phase. Principal first order controls upon deposition include the evolving structural configuration of the rift, the role of relative sea-level change with structural elevation and pre-rift variability. Stratigraphic response for the interaction of structural uplift and subsidence with eustatic variations modelled after Gawthorpe et al., 1990.

Impact of regional sea-level change on late rift climax stratigraphic variability: Along the partially emergent rift margin, the interaction of changes in regional sea-level with local structural evolution may result in the development of highly variable stratigraphic sequences, surfaces and related systems tracts associated with late rift climax deposits. As shown in this study, a major regional sea-level fall may be recorded at rift marginal areas as highly composite sequence boundary, as at the base of the Upper Rudeis Formation towards the northern end of the Hammam Faraun Fault Block and rift marginal component of the Zafarana Accommodation Zone. As a result, surfaces at the rift margin may be difficult to regionally correlate throughout the rift. In comparison, the rift axis is typically associated with overall deeper bathymetry, with even fault block crests remaining submerged below storm wave base and relatively sediment starved during a relative sea-level lowstand. As a result, hangingingwall depocentres may provide a relatively full, preserved account of the development of key surfaces and systems tracts. Thus while key surfaces may be traced at a more regional scale, (although local condensation upon uplifted areas may prove problematic), variations in system tracts are only observed as subtle variations in stacking patterns associated with the distal elements of depositional systems.

A key conclusion therefore, is that extrapolating information for the regional linked tectono-stratigraphic development of a rift from potentially composite and locally variable surfaces and systems tracts at the rift margin may lead to erroneous interpretations. Direct comparison and reconciliation with data from the differing structural domains, in particular the potentially well preserved deposits of the rift axis, is required to construct an accurate picture of the evolution of a rift basin.

Sediment source areas: Two principal types of sediment source area are highlighted in this study. Large hinterland drainage catchments along the rift shoulder provide the source area for regionally extensive syn-rift depositional systems extending across the rift margin and into the rift axis, contrasting with intra-rift uplifted footwall sources associated with more limited sediment flux. The magnitude of this locally-derived flux differs across the rift, linked to the transition from emergent to increasingly submerged footwall crests from the rift margin to rift axis. As a result, extensive sediment fluxes within an otherwise sediment starved rift axis are likely to be associated with the more regional hinterland rather than locally adjacent footwall crests.

Sediment provenance: Variations in bedrock lithology within drainage catchments directly control the nature of erosional topography and also has a major impact on the magnitude and composition of resulting sediment fluxes. Contrasting siliciclastic and carbonate pre-rift lithologies have been linked to compositionally distinct depositional systems within both the Suez Rift, in the hanging wall of the October Fault Zone (Chapter 4) and in other extensional settings such as the Gulf of Corinth (e.g. Leeder et al., 2002). Variations in exposed pre-rift lithologies may be the result of differential uplift throughout a rift, or linked to inherent pre-rift structural variability. Furthermore, earlier syn-rift deposits may also become reworked due to the migration of fault activity and subsequent uplift, as documented in the Hammam Faraun Fault Block of the Suez Rift (Sharp et al., 2000b; Gawthorpe et al., 2003) and Gulf of Corinth (e.g. Zelilidis, 2000). In addition to spatial variations, temporal changes in provenance lithology have been recognised, associated with an ongoing roofing trend. For example, in the study of a major rift climax submarine fan system located in the Hammam Faraun Fault Block of the Suez Rift, Leppard and Gawthorpe (2006) recorded the apparent shutdown of coarse-clastic sediment supply associated with the onset of erosion of a major mudstone-dominated pre-rift unit within the rift shoulder. Accurately understanding the lithological nature of individual provenance areas along with potential variations, both spatially and temporally, is therefore important for both the delineation and prediction of the extent of competing syn-rift depositional systems

Sediment transport pathways: The input of sediment fluxes into the rift is the result of the structural configuration and variations in both relative base-level and climate. At both local and regional scales, sediment transfer pathways are controlled by the topographic and bathymetric gradients associated with evolving structures (e.g. Gawthorpe and Leeder, 2000). Locally fault block sediment pathways are typically provided by relay ramps and fault segment tips, with sediment being transported from areas of relative uplift to subsiding depocentres (e.g. Leeder and Gawthorpe 1987; Gawthorpe et al., 1990; Gawthorpe and Hurst, 1993; Leeder and Jackson, 1993; Eliet and Gawthorpe, 1995; Gupta et al., 1999; Gawthorpe and Leeder, 2000; Young et al., 2000). At the regional scale, diffuse structural accommodation zones may provide major sediment transfer pathways from rift marginal to rift axis areas, as in both rift-wide accommodation zones in the Suez Rift, with similar examples documented in other settings such as the East African Rift (e.g. Ebinger, 1989). Once within

the rift, contrasting regional dips associated within major structural domains, e.g. between the northern and central dip provinces in the Suez Rift, control the principal direction of major sediment fluxes away from the more structurally diffuse accommodation zones. Therefore the expression of sediment fairways into the rift is largely dependant upon distance away from the source area and tortuosity of the sediment transfer pathway provided by both regional and local structural configurations. The timing and magnitude of sediment fluxes however, have been shown in this study to be directly controlled by variations in base-level determined by changes in glacio-eustasy.

SECTION THREE
SYNTHESIS & DISCUSSION

CHAPTER EIGHT

CONTROLS ON LATE RIFT CLIMAX SEDIMENTATION: SYNTHESIS OF RESULTS FROM SUBSURFACE AND OUTCROP STUDIES IN THE SUEZ RIFT, EGYPT

CHAPTER 8: CONTROLS ON LATE RIFT CLIMAX SEDIMENTATION: SYNTHESIS OF RESULTS FROM SUBSURFACE AND OUTCROP STUDIES IN THE SUEZ RIFT, EGYPT

8.1. INTRODUCTION

The aims of this chapter are to: (1) summarise the observations, results and conclusions from Chapters Four to Seven which have examined late rift climax stratigraphy in different rift settings and at varying-length scales, (2) integrate the key results from the outcrop and subsurface studies, in order to discuss their implications for existing models of rift tectonics and syn-rift stratigraphy, (3) present the key conclusions of this thesis, and (4) provide some recommendations for future work.

8.2. THESIS SUMMARY

This thesis is composed of four individually themed research chapters (Section 2), which fall into three broad, late rift climax related topics a) controls upon sedimentation within a rift axis setting, b) controls upon sedimentation in a rift marginal, low accommodation setting and c) the integration of observations of late rift climax sedimentary and stratigraphic variability across differing structural domains within a rift.

8.2.1 Subsurface rift axis

Chapters Four and Five examined the nature of late rift climax sedimentation associated with the Upper Rudeis and Kareem Formations in the Central Dip Province, the Morgan Accommodation Zone and the northernmost part of the Southern Dip Province (Fig. 8.1). These studies have documented the facies, thickness variations and stratal architecture of these syn-rift deposits and determined the local structural and other more regional controls on the development and variability of syn-rift depositional systems within a rift axis setting. The key observations, results and conclusions from these chapters are summarised below.

Chapter Four: late rift climax tectono-stratigraphic evolution of the October Fault Zone

In Chapter Four, detailed sedimentary data obtained from a series of cores, wireline log and biostratigraphic data allowed for three contemporaneous Upper Rudeis depositional systems around the October Fault Zone to be identified: 1) a background offshore basinal

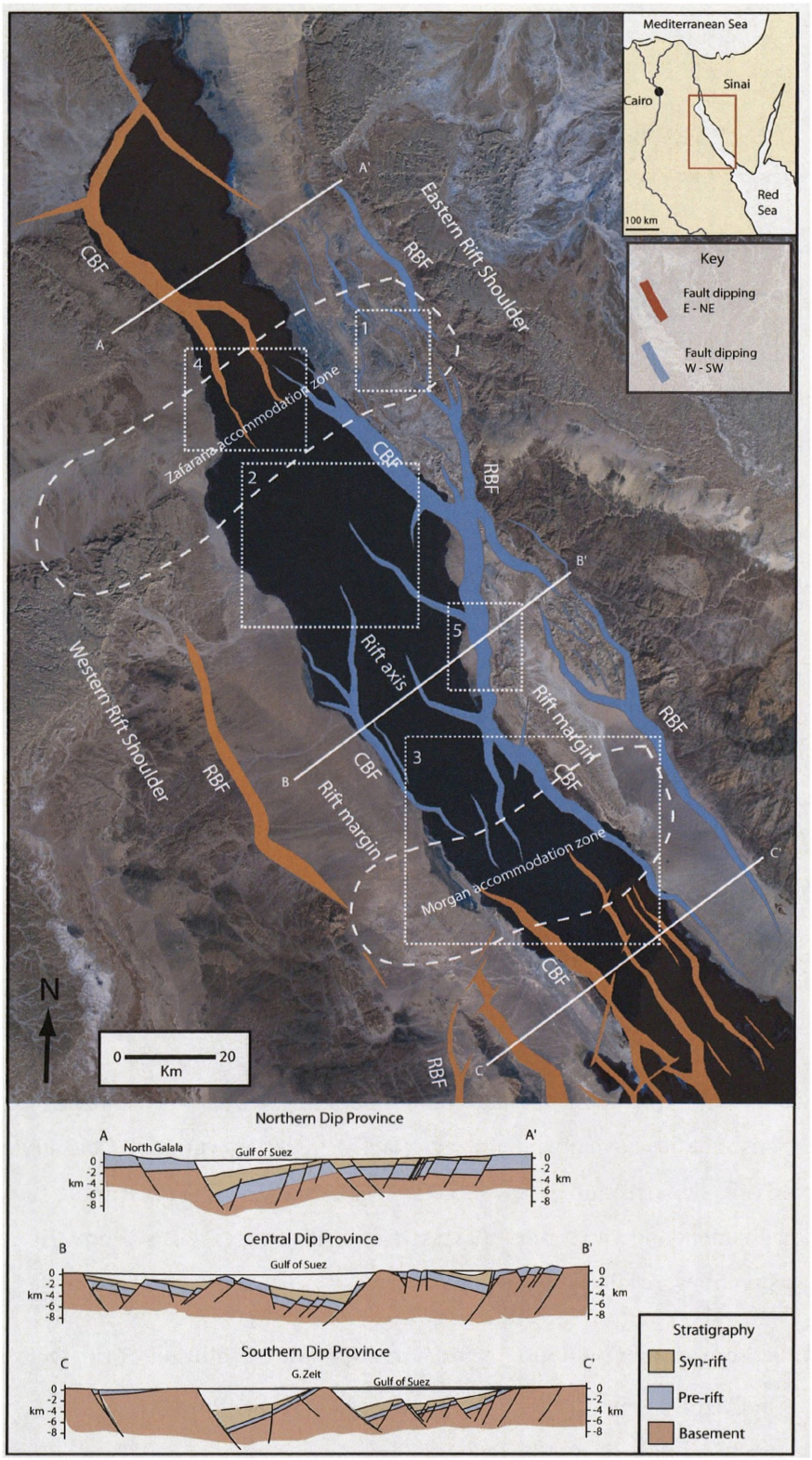

Figure 7.1. Simplified fault map of the Suez Rift showing faults with > 1km of displacement (modified after Younes and McClay, 2002) superimposed upon a regional landsat image. RBF= Rift Border Fault system; CBF = Coastal Boundary Fault system. Lines A-A', B-B' and C-C' refer to cross sections which highlight the change in dip between the three structural dip provinces (after Patton et al., 1994). Inset boxes 1-3 refer to areas specifically studied as part of this thesis: 1) Wadi Gharandal - Gebel Gushea area; 2) October area and 3) Offshore Morgan Accommodation Zone. Inset boxes 4 and 5 indicate other areas examined / referred to in this study: 4) Offshore Zafarana Accommodation Zone and 5) Wadi Feiran.

system, 2) a calcarenite-rich submarine fan system, and 3) a siliciclastic-rich submarine fan system. Key, regionally correlatable and biostratigraphically-constrained stratal surfaces within the succession define time equivalent stratal units, which when used to map thickness and facies variations, indicate that some 7.5 Ma after the onset of rifting, the October Fault Zone was active as a surface-breaking fault zone comprising a series of 1.5-10 km fault segments with intervening relay ramps. Continued fault interaction during an approximate period of 0.8 Myr led to the linkage of individual segments along the October Fault Zone, resulting in two large-scale fault segments (> 20 km in length). This structural evolution fundamentally controlled the location of principle sediment source areas, transport pathways and depocentres locally adjacent to the fault zone. Uplifted footwall crestal areas characterised by either condensed sedimentation, or alternatively non-deposition and erosion, whereas in hangingwall depocentres, locally-restricted fault scarp-derived slope apron deposits were intercalated with more regional submarine fan sandstones differentiated by marked compositional variations. A major calcarentic-rich submarine fan system, derived from Eocene pre-rift carbonates, extended from long-lived sediment entry points on the rift margin and prograded across the hangingwall dip-slopes to the Hammam Faraun Fault Zone and entered into the hangingwall of the October Fault Zone via a major 1.5 km wide relay ramp between two principle fault segments. Contemporaneously a siliciclastic submarine fan sourcing the exposed Nubia Formation within the Zafarana Accommodation Zone, some 57 km to the north, also extended into the study area.

Chapter Five: Upper Rudeis and Kareem depositional systems within the Morgan Accommodation Zone

Chapter Five focussed upon the extensive deposits of the Upper Rudeis and Kareem Formations within the rift axis component of the Morgan Accommodation Zone between the Central and Southern Dip Provinces (Fig. 8.1). The Upper Rudeis and Kareem Formations were subdivided into a series of stratal units based upon key chronostratigraphic significant surfaces, which mirror those identified in Chapter 4. Comparison of gross seismic isochores, borehole-derived individual stratal unit gross isopachs and sandstone isopachs with the present day structural configuration of the accommodation zone allowed: (1) the identification of principal stratigraphic thicks associated with major regional depositional systems, sourced

from a series of structurally–controlled sediment entry points located along the rift margin, and (2) comparison of areas of alternatively characterised by sediment thicks and thins to determine individual fault activity within the accommodation zone. The timing and magnitude of regional inputs of sediment into the axis of the rift were controlled by basinwide variations in relative sea-level, which contrast with more localised-scale, episodic control exerted by the evolution of individual faults. The interplay of the variable activity of faults with fluctuations in both rates of sediment supply and relative sea-level combine to determine the nature of available accommodation space, and thus the thickness and stratal geometry of coeval syn-rift depositional systems. A key example discussed in this chapter was the ability for the high rates of sediment supply associated with transverse orientated depositional systems to periodically outpace the rates of structurally generated accommodation space and completely infill the bathymetry associated with hangingwall depocentres.

8.2.2 Outcrop rift margin

Chapter Six documented the tectono-stratigraphic evolution of the main structures and linked-syn-rift depositional systems within the rift margin component of the Zafarana Accommodation Zone. Extensively preserved syn-rift deposits here contrast with the more spatially constrained syn-rift outcrops throughout the adjacent Hammam Faraun Fault Block, which has formed the basis of several pervious studies.

Chapter Six: Tectono-stratigraphic evolution of the Zafarana Accommodation Zone

This chapter documented the facies and stratigraphic variability of rift initiation to late rift climax deposits within a broad area of diffuse structural activity associated with the Zafarana Accommodation Zone between the northern and central dip provinces of the rift, exposed present day on the eastern rift margin. Whilst the stratigraphic and facies variability recorded there conforms to tectono-stratigraphic models for rift evolution, two main distinctions were made. (1) the important role that relative sea-level fluctuations played during the late rift climax period in this area of low accommodation space and (2), the relative timing of structural activity in comparison to other structural domains. This is shown by the continued role of mesoscale intra-block faults and propagation folding during the latter stages of the rift.

8.2.3 Rift-wide

Chapter Seven integrated the observations from previous Chapters Four to Six in addition to a further subsurface dataset within the offshore component of the Zafarana Accommodation Zone and several published studies documenting the nature of the Upper Rudeis Formation within the exposed eastern rift margin. This large, regionally-extensive dataset allows for the development of a rift-wide sequence stratigraphic model for the deposition of the late rift climax Upper Rudeis Formation.

Chapter Seven: Rift-wide sequence stratigraphy of late rift climax deposits

In Chapter Seven, a regional control on the sedimentological and stratigraphic nature of the late rift climax Upper Rudeis Formation, linked to variations in regional relative sea-level, is demonstrated by the regional consistency in the development of key stratal surfaces and facies shifts. These regional sea-level changes are interpreted to have determined the timing and magnitude of sediment flux into the rift. In contrast, the tectonically-generated physiography in each specific, yet different structural setting is shown to have a first order control in determining the nature of the sedimentological and sequence stratigraphic response to the more regional changes in base level. Previous studies have focussed upon outcrop data at the rift margin, (e.g. Garfunkel and Bartov, 1977; Patton et al., 1994) invoked a regional tectonic event linked to regional fault-block uplift to account for the observed facies and stratal variability associated with a marked basinward shift in facies from the Lower to Upper Rudeis Formations, termed the 'Mid-Clysmic' unconformity. This chapter in reconciling observations from both the rift axis and rift margin demonstrates that this model for a regional tectonic event, based solely on rift margin datasets fails to fully explain the rift-wide variability observed. An alternative mechanism is proposed, in which the previously identified regional changes in base level are attributed to a major glacio-eustatic event ca. 16.3 Ma occurring during a period of overall episodic and increasingly waning fault activity.

8.3. SYNTHESIS OF RESULTS

The aim of this section is to synthesise the results and key observations from Chapters Four to Seven of this thesis and to discuss their implications for the controls upon generic models for the development of syn-rift, and more specifically, late rift climax stratigraphy. This is achieved by considering the variability of the three issues that are central to this thesis:

(1) tectonics, (2) sea-level and (3) sediment sources, at both a local, fault block-scale and regional, rift-wide scale. Whilst other additional factors, such as the affects of climate are acknowledged to have a potential impact upon drainage evolution and sediment supply (e.g. Collier et al., 2000), evidence for a stable climatic regime during the deposition of the studied succession within the Suez Rift (e.g. Beialy and Ali, 2002), largely precludes this as a major contributing factor and are therefore not considered in this thesis. Thus, the sedimentological and stratigraphic variability of syn-rift deposits are interpreted to be largely the product of the complex interaction of the three main controlling factors outlined (Fig. 8.2).

Impact of tectonics

The spatial and temporal evolution of normal fault populations within a rift have been consistently shown in numerous outcrop, subsurface and numerical modelling based studies to provide a first order control upon the deposition of coeval syn-rift sediments. Differential areas of uplift and subsidence associated with the evolution of normal fault populations, ultimately determines the location and extent of sediment source areas, sediment transport pathways and depocentres. In this thesis, three specific issues relating to this dominant control are highlighted:

Evolving structural configuration

The results from this thesis are consistent with generic conceptual models for rift climax sedimentation (e.g. Leeder & Gawthorpe, 1987; Prosser, 1993; Ranvas et al., 2000; Gawthorpe and Leeder, 2000) in documenting the role of evolving normal fault populations in controlling the spatial and temporal nature and extent of coeval syn-rift depositional systems and resultant stratigraphic architectures. At a local scale, i.e. adjacent to a single fault zone, the distribution of facies, thicknesses and stratal surfaces is observed to vary from uplifted footwall locations to subsided hangingwalls. In Chapter Four, the footwalls of active segments of the October Fault Zone were characterised during the deposition of the Upper Rudeis Formation by dominantly fine-grained deposition to non-deposition or even submarine erosion; reflected in a markedly thinned to absent Upper Rudeis succession. In the adjacent hangingwalls, thick coarser-grained deposits reflected these locations as primary sediment depocentres. Along-strike variability associated within differential displacement along the fault zone is also recognised; hangingwall depocentres characterised by maximum

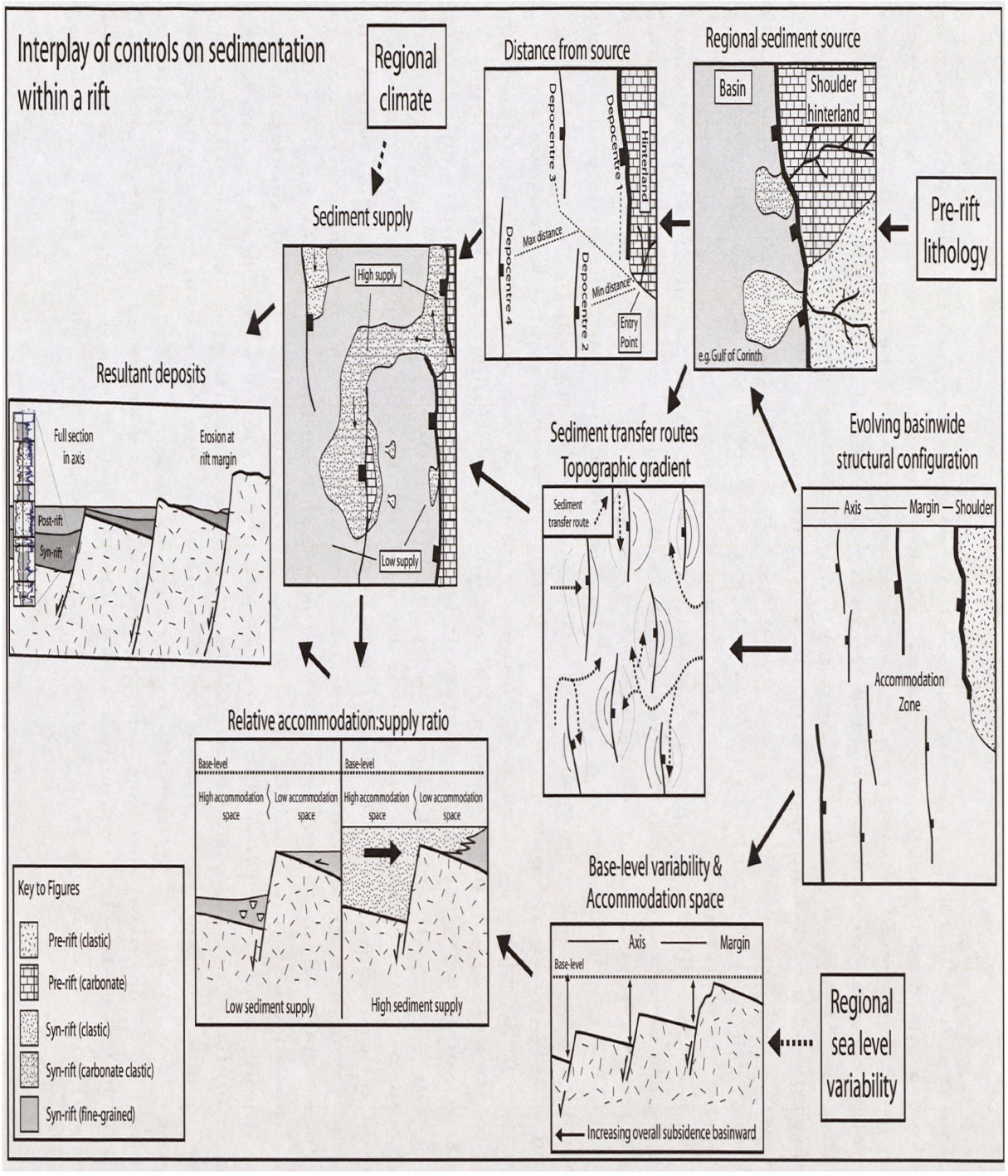

Figure 8.2. Summary diagram showing the some of the potential interplay of controlling factors upon sedimentation within extensional basins.

displacement and thus thicker syn-rift successions whereas intervening areas of displacement minima were characterised by relay ramps and fault perpendicular hangingwall anticlines, with a resultantly thinned syn-rift succession. The evolution of the individual fault zones such as the October Fault Zone, or those in the North July area examined in Chapter Five, allow for the migration of the location of principal depocentres, transport pathways and areas characterised by limited deposition. Additionally, the role of propagation folds above a blind fault at depth and syn-sedimentary growth or detachment faults in controlling the thickness variability of rift initiation to late rift climax deposits is observed at outcrop in the rift margin component of the Zafarana Accommodation Zone (Chapter Six).

At a more regional scale, the Suez Rift can be subdivided into a series of structural domains based upon the present day structural configuration, which were largely established by the late rift climax period which saw the deposition of the Upper Rudeis to Kareem Formations (Bosworth and McClay, 2001). The varying nature of these structural domains is an important factor in the response of late rift climax sedimentation to the interaction of sea-level and sediment source controls described below. Two main subdivisions are recognised: (1) a longitudinal orientated series of domains running approximately along-strike with the axis of the rift and (2) a transverse series of domains with varying structural elevation from the rift flank or shoulder to the centre of the rift (Fig 8.1). In the longitudinal sense, large dip domains characterised by tilted fault blocks, typically 10-40 km wide, with resultant half-graben geometries displaying a consistent dominant dip direction contrast with zones of more distributed deformation, typically 15-30 km wide which accommodate the switch in dip polarity between the dip domains. These accommodation zones are characterised by faults with reduced displacements and reduced widths of intervening fault blocks in comparison to those in the adjacent dip domains and increased observations of fault propagation folds associated with blind (i.e. non-surface breaking) faults. In a transverse section across the rift, three main domains are identified: rift shoulder, rift margin and rift axis. The present day rift shoulder is characterised by variable outcropping pre-rift units which are juxtaposed to downthrown pre-rift and syn-rift units by a series of large, 1-2 km displacement rift border fault zones. Moving basinward, the adjacent rift margin is comprised of a series of tilted fault blocks, 20 -30 km wide which contain a series of mesoscale, 100's m displacement intra-block fault zones. The rift margin is bounded on its basinward side by a series of large scale, up to 4

km displacement fault zones which largely form the present day coastal boundary of the Gulf of Suez. Whilst the majority of displacement along these faults is thought to have occurred during a latter renewed phase of rifting in the Pliocene, a relatively more structurally elevated rift margin, contrasting with a structurally lowered rift axis, is interpreted in Chapter Seven to have already existed by the late rift climax period associated with the Upper Rudeis Formation. Similar structural domains are observed from other intracontinental rifts such as the North Sea rift (e.g. Roberts et al., 1990), the East African Rift (e.g. Morley, 1999) and the Gulf of Thailand Rift (e.g. Kornsawan and Morley, 2002).

Structural control on sediment transport pathways

In Chapters Four to Seven, sediment transport pathways have been demonstrated to be largely controlled, at both the local individual fault-scale and more regional, structural domain scale, by the topographic and bathymetric gradients associated with tectonic evolution of a rift. Consistent with previous studies, local scale sediment pathways associated with individual fault zones and fault blocks are typically located through areas of minimum displacement, (relay ramps and around fault segment tips) with sediment being transported from relatively uplifted footwalls to subsided hangingwall depocentres (e.g. Leeder and Gawthorpe 1987; Leeder and Jackson, 1993; Eliet and Gawthorpe, 1995; Gawthorpe and Leeder, 2000). An example has been provided in this study (from Chapter Four), where during Sequences 1 and 2 of the Upper Rudeis Formation, a series of calcarenitic submarine fan lobes were sourced via a major, 1.5 km wide relay ramp across the October Fault Zone. The orientation of this relay ramp provided a dominant control on the dispersal patterns associated with this calcarenitic submarine fan system, focussing sediment into the hangingwall depocentre of the active South October Fault. This was in marked contrast to the active, yet sediment starved depocentres of a number of shorter fault segments of the North October Fault during this early phase of Upper Rudeis Formation deposition.

At the basinwide-scale, diffuse structural accommodation zones may provide major sediment transfer pathways from the rift shoulder and margin in to the rift axis. This is documented in this study in: (1) A long-lived sediment transport pathway identified to be active from rift initiation to the present day is documented within the rift margin component of the Zafarana Accommodation Zone, (Chapter Six) and (2) the documentation of regionally

extensive, late rift climax depositional systems within the rift axis part of the Morgan Accommodation Zone in Chapter Five. Similar examples of structural accommodation zones providing major sediment pathways are documented in other settings such as the East African Rift (e.g. Ebinger, 1989).

Rates of fault activity

The Upper Rudeis Formation (ca. 16.5 – 15.7 Ma), which forms the principal studied interval for this thesis, has been consistently referred to in previous studies as being deposited during the rift climax phase (e.g. Patton et al., 1994; Bosworth and McClay 2001). This classification is not wholly satisfactory given that: (1) the Upper Rudeis Formation displays a marked basinward shift in depositional systems and therefore is generally much coarser-grained than the immediately preceding Lower Rudeis Formation, which conforms to conceptual models for a basinal, fine-grained dominated succession during the main phase of rifting (e.g. Prosser, 1993); (2) subsidence studies for the rift show a clear switch from maximum subsidence rates during the deposition of the Lower Rudeis Formation (ca. 19.7 – 16.5 Ma) with estimates up to 400 m/Myr, whereas the Upper Rudeis is characterised by overall reduced rates, in the order of 100 -150 m/Myr, albeit with spatial variations linked to differing structural locations. Consequently, the Upper Rudeis Formation has been referred to in this thesis as constituting the syn-rift response to a late rift climax stage, characterised by waning tectonic subsidence and episodic normal faulting, before the transition to the Kareem Formation, when ca. 15.5 Ma, the majority of regional extension within the area was switched to the Aqaba Transform (e.g. Richardson and Arthur, 1988). Two major implications arising from the distinction of a late rift climax period are highlighted in this thesis. Firstly that rates of sediment supply, particularly those associated with transverse orientated systems, may outpace the rates of accommodation space generated by fault activity. As a result, some depositional systems during Upper Rudeis and Kareem time were able in areas of high sediment supply to rapidly infill hangingwall depocentres and prograde onto uplifted footwall crests. This is demonstrated in the Morgan Accommodation Zone study of Chapter 5, in which depositional systems sourced from the western rift margin crossed the active faults associated with the present day July Fault Block. The second implication is that the reduced rates of fault displacement may have had the potential to be outpaced by a regional glacio-

eustatic fall (*sensu* Gawthorpe et al., 1994), which typically average in the order of 1.5 mm/yr (or 1500 m/Myr) (e.g. Ranvas and Steel, 1998), and thus may provide a viable mechanism to account for the observed regional changes in relative sea-level from the late rift climax period onwards within the rift.

Impact of sea-level

Relative sea-level and therefore the accommodation space available for syn-rift sedimentation within a rift, is a function of tectonically generated uplift and subsidence with regional eustasy. Generic tectono-stratigraphic models for syn-rift sedimentation typically ascribe the maximum rates of displacement associated with the climax of the rift to be the dominant control upon relative sea-level and thus accommodation space within a rift (e.g. Gawthorpe and Leeder, 2000). This is consistent with studies which suggest that changes in glacio-eustasy may be largely masked within hangingwall depocentres of active faults (e.g. Gawthorpe et al., 1994; Howell and Flint, 1996). Changes in relative sea-level within a rift have thus been commonly attributed to uplift and subsidence which may be either associated with an individual fault block, or linked to more regional tectonic change, e.g. regional isostatic uplift. Two specific issues regarding relative sea-level have been addressed in Chapter Seven of this thesis: (1) The intersection of relative sea-level height with tectonically generated relief within differing structural domains and how sea-level change therefore may have differing expressions within the syn-rift succession. (2) The mechanisms by which regional, basinwide relative sea-level variations occur, which are identified by the regional shifts in late rift climax depositional systems described across differing structural domains.

Varying relative sea-level height reflective of differing structural domains

As outlined above, the interaction between global sea-level and the structural configuration of a rift determines the relative position of sea-level to tectonically generated relief and thus the availability of accommodation space. At the regional scale, the overall increase in subsidence towards the axis of a rift results in lower structural elevations and therefore overall increasing water depths. Thus whilst fault blocks at the rift margin may be locally emergent, as they intersect regional sea-level, the fault blocks within the rift axis may be wholly submerged. As a result, whereas variations in regional relative sea-level may have a direct impact upon rift marginal areas, effects within the rift axis may be relatively muted.

The distributed deformation associated with structural accommodation zones may result in reduced relief in contrast to adjacent tilted fault block dip provinces, and thus are a relatively low accommodation zone setting. Consequently, these areas may experience more marked shifts in depositional systems during periods of regional relative sea-level change, as within the Zafarana Accommodation Zone (Chapter Six).

At the local fault block scale, different lengths and gradients of tectonically-generated slopes influence the effects of variations in sea-level (e.g. Ranvas and Steel, 1998; McMurray and Gawthorpe, 2000). Short, steep footwall scarp slopes have a relatively narrow zone of influence of sea-level change, whereas longer hangingwall dip-slopes, with gentler gradients afford wider zones influenced by sea-level change, causing much greater lateral shifts in shoreline position during cycles of sea-level change.

Variations in regional sea-level

In Chapter Seven, the theme of basinwide fluctuations in relative sea-level controlling the deposition of late rift climax deposits within the Suez Rift was considered, at a scale independent of the evolution of local structures. This theme was developed drawing upon observations and interpretations for what most authors accept to be a markedly overall basinward shift in depositional systems during the deposition of the Upper Rudeis Formation (e.g. Garfunkel and Bartov, 1977; Evans, 1990; Patton et al., 1994), contrasting with the typically more basinal dominated nature of the preceding Lower Rudeis Formation, which conforms to classical models for syn-rift sedimentary response to the onset of the main, or rift climax phase of rifting (*sensu* Prosser, 1993). Evidence was included from the key study areas of the thesis, i.e. adjacent to the October Fault Zone in the central dip province (Chapter Four), the rift axis component of the Morgan Accommodation Zone (Chapter Five) and the rift margin component of the Zafarana Accommodation Zone (Chapter Six), with additional information incorporated from other published datasets from around the rift. The integration of these differing datasets allowed for the investigation of the nature of the sedimentary and stratigraphic response to these regional sea-level changes across the principal structural domains identified within the rift

Within the present day offshore axis of the rift, subsurface borehole data allowed for the identification of regionally consistent, biostratigraphically constrained key surfaces of

regression and flooding, which can be confidently correlated within the rift axis. Observed in Chapters Four and Five, markedly similar surfaces and associated facies shifts were observed in the October Fault Zone and Morgan Accommodation Zone study areas, which are in the order of 80 km apart. Initially identified in hangingwall depocentres, which may document the most continuous syn-rift succession within the rift axis, the nature of these surfaces and associated facies shifts varied in differing structural settings, e.g. upon footwall crests, where condensation and amalgamation of surfaces was commonly observed in conjunction with marked thinning of the Upper Rudeis Formation succession. Regionally extensive key surfaces have been identified in other rifts which cross differing structural locations, such as the tectonically-enhanced maximum flooding surfaces of Haywood et al. (1993) and Partington et al. (1993) in the Late Jurassic North Sea Rift. Potential maximum flooding surfaces were identified in this study, however the lack of consistent wireline log responses and accompanying biostratigraphic abundance and diversity data reduced the overall confidence in regional correlation away from key boreholes. At the rift margin, biostratigraphic data associated with key sections allowed for the correlation of surfaces and intervening stratal units to be correlated from the rift axis. In contrast to the rift axis, key surfaces bounding the Upper Rudeis Formation at the rift margin has been shown in this thesis to be typically highly composite and dominated by transgressive to highstand deposits; although key periods of regression are highlighted by the formation of incised valleys and subsequent lowstand infills.

Whilst the presence of regional, basinwide relative sea-level changes have been identified in other rift settings, e.g. the Jurassic North Sea and East Greenland Rifts, these have been linked to tectonic activity (e.g. Underhill, 1991; Surlyk et al., 1993). Thus the citing of a glacio-eustatic mechanism being the principal driving force behind the regional regional-sea-level fluctuations outlined in Chapter Seven is acknowledged to be potentially controversial. However, alternative explanations based on the observations at the rift margin, and referred to as the 'mid-Clysmic unconformity' (ca.f. Garfunkel and Bartov, 1977; Patton et al., 1994), have invoked various regional tectonic mechanisms which have largely been discounted in this thesis, based upon both updated timing of regional events and the integration of data from differing structural domains within the rift (c.f. Chapters Two and Seven). The glacio-eustatic mechanism proposed in Chapter Seven is identified in both the

controversial global sea-level curves of Haq et al (1987) and its updated forms (e.g. Abreu and Anderson, 1998), in addition to the more recent oxygen isotope proxy curves of Miller et al (2005). The Miller et al (2005) dataset suggest a major eustatic fall, in the order of 30 m, ca. 16.3 M.a, which is consistent with biostratigraphic calibrations for the timing of the Upper Rudeis Formation. The observations and subsequent interpretations presented in Chapter Seven point towards a high frequency set of eustatic falls and subsequent rises associated with this major episode identified in the oxygen isotope records. Conceptually, the role of a glacio-eustatic fall impacting a rift during a period of reduced and waning fault activity is wholly consistent with the models of Gawthorpe et al (1994) and Howell and Flint (1996); whilst the physical potential for eustatic variations to have been reflected during this period is also possible as during the preceding rift climax associated with the Lower Rudeis Formation, the Suez Rift has been consistently interpreted to have been linked to the world ocean to the south via the northern part of the Red Sea (e.g. Garfunkel and Bartov, 1977; Mart and Hall, 1984; Bosworth and McClay, 2001).

Impact of sediment sources

Marked compositional variations in the Upper Rudeis and Kareem Formations examined in Chapters Four to Six allowed for the impact of sediment sources to be addressed in this thesis. The compositional signature of a syn-rift deposit is a direct result of the lithology of a typically uplifted provenance area, whilst both the texture and the overall magnitude of the deposit are additionally influenced by the location, size and distance from sediment source to sink, and the nature of sediment transport processes. Thus two specific issues regarding sediment source arise from this thesis: (1) the controls upon composition of a source area and (2), the nature of the differing types of sediment source areas.

Compositional variations in sediment provenance

Variations in bedrock lithology within drainage catchments directly control the nature of erosional defined relief and also have a major impact on the magnitude and composition of resulting sediment fluxes. Contrasting siliciclastic and carbonate pre-rift lithologies have been linked to compositionally distinct late rift climax depositional systems within the Suez Rift in this study. The results of Chapter Four, focussed on the depositional systems adjacent to the October Fault Zone in the northern part of the central dip province document the existence of

calcarentic submarine fan systems, intercalated with more siliciclastic, subarkosic submarine fan deposits in the hanging wall of the October Fault Zone (Chapter Four). The interpretation for this variability within the studied succession was linked to the sourcing of differing pre-rift lithologies, which is mirrored in other extensional settings such as the Gulf of Corinth (e.g. Leeder et al., 2002). Variations in exposed pre-rift lithologies may be the result of differential uplift throughout a rift, or linked to inherent pre-rift structural variability. Furthermore, earlier syn-rift deposits may also become reworked due to the migration of fault activity and subsequent uplift, as documented in the Hammam Faraun Fault Block of the Suez Rift (Sharp et al., 2000b; Gawthorpe et al., 2003) and Gulf of Corinth (e.g. Zelilidis, 2000). In addition to spatial variations, broad temporal changes in provenance lithology have been recognised, associated with an ongoing roofing trend. As a result, the syn-rift units may record an inverse stratigraphy of the pre-rift succession being unroofed (e.g. Evans, 1990). Accurately understanding the lithological nature of individual provenance areas along with potential variations, both spatially and temporally, is therefore important for both the delineation and prediction of the extent of competing syn-rift depositional systems

Nature of sediment source area

Two principal types of sediment source area are highlighted in this study. Large hinterland drainage catchments along the rift shoulder provided the source area for regionally extensive syn-rift depositional systems extending across the rift margin and into the rift axis as identified in Chapters Four and Five in the October Fault Zone and Morgan Accommodation Zone areas. In marked contrast, intra-rift uplifted footwall sources within the axis of the rift are associated with more limited sediment fluxes. The magnitude of such locally-derived fluxes differs across the rift, linked to the transition from emergent to increasingly submerged footwall crests from the rift margin to rift axis. As a result, extensive sediment fluxes within an otherwise sediment starved rift axis are likely to be associated with the more regional hinterland rather than locally adjacent footwall crests.

8.4. CONCLUSIONS

The following conclusions relate to the specific objectives set out in Chapter One:

1) Deposition of the Upper Rudeis Formation associated with the October Fault Zone located in the rift axis was contained within three contemporaneous depositional systems: a background offshore basinal system, a calcarenite-rich submarine fan system, and a siliciclastic-rich submarine fan system. Within the background offshore depositional system was characterised by facies and thickness variations associated with the marked asymmetry of a tilted fault block setting, with thin condensed fine-grained section upon footwall crestal locations coeval to expanded, fine-grained and intercalated rarer coarser-grained, locally derived slope apron deposits in the immediate hangingwall of the fault zone. The calcarenitic submarine fan system was sourced from pre-rift Eocene carbonates on the eastern rift margin, and entered the hangingwall of the October Fault Zone via a 1.5 km wide relay ramp. In contrast, the distal elements of a siliciclastic submarine fan depositional system, sourced from exposed pre-rift Nubia Formation located at Wadi Araba in the western margin of the Zafarana Accommodation Zone, some 50 - 60 km to the north, were transported axially into the hangingwall of active segments of the North October Fault.

2) Thickness and facies variations associated with the high resolution stratal units defined in Chapter Four in the area of the October Fault Zone document the temporal structural evolution of the fault zone. During the latter stages of the rift climax phase, some 7.5 Ma after the onset of rifting, the October Fault Zone was active as a surface-breaking fault zone comprising a series of 1.5-20 km fault segments with intervening relay ramps and fault propagation folds characterising areas of minimum displacement. Continued fault interaction during an approximate period of 0.8 Myr led to the linkage of individual segments along the October Fault Zone, resulting in two large-scale fault segments (> 20 km in length). This progressive development of this fault array is consistent with models for the growth of normal fault zones by segment linkage.

3) Key stratal surfaces of regression and flooding, associated with marked basinward and landward shifts in facies in the late rift climax Upper Rudeis Formation, correlated within a biostratigraphic framework around the study area of the Morgan Accommodation Zone in Chapter Five, are markedly similar to those previously identified around the October Fault Zone located some 80 km towards the north. This similarity is contrasted by the differing nature of the two structural settings studied within the rift axis, i.e. a classic tilted fault block versus a more diffuse structural accommodation zone. This indicates that the deposition of the Upper Rudeis Formation, in addition to more local controls, records a role for a more regional control, independent of local structure, associated with the timing and magnitude of influxes of sediment into the axis of the rift.

4) Gross interval isopachs, sandstone isoliths and mapped facies variations within the offshore Morgan Accommodation Zone are indicative of a series of regionally extensive depositional systems entering the rift axis, via a consistent series of structurally controlled sediment entry points from the rift margin during the deposition of the late rift climax Upper Rudeis and Kareem Formations. Detailed analysis of fault activity, enabled through extensive well controls, indicates that activity upon individual structures was generally episodic, as demonstrated by a presented example for the North July and Ramadan areas. The evolution of fault activity provided a first order control upon the location of sediment transport pathways and depocentres, which may show marked temporal variability. Locally, the rate of accommodation space generated by waning subsidence upon individual structures was periodically outpaced by the rate of sediment supply, allowing for sedimentary depositional systems to prograde onto uplifted footwall crestal areas.

5) Examination of the sedimentology, stratigraphy and thickness variability of rift initiation to late rift climax deposits within the proximal part of the Zafarana Accommodation Zone., highlighted the increased role for fluctuations in relative to have pronounced facies shifts within a zone of limited structural relief, whilst the timing of structural activity also contrasts to what might be predicted in generic conceptual tectonostratigraphic models for rift development. As a result, geometries typically associated with the earliest syn-rift succession, as a response to fault-propagation folding and activity along low-displacement

faults, may be observed within the rift climax to late rift climax succession within an accommodation zone.

6) Integration of observations and interpretations for key study areas documented in this thesis in addition to previously published studies have allowed for a regional, basinwide sequence stratigraphic synthesis to be developed, independent of local structural evolution, for the late rift climax Upper Rudeis Formation. Regional shifts in facies and associated key, chronostratigraphic surfaces are interpreted to form a series of depositional sequences. The regional consistent nature of this stratigraphic model suggests that during the late rift climax phase, the dominant role provided by local structure was reduced from that experienced during the previous period of rift climax. A marked regional control is identified and interpreted to reflect marked variations in regional relative sea-level, which largely controlled the timing and magnitude of influxes of sediment into the rift; a glacio-eustatic, rather than tectonic model is suggested to account for these regional variations in relative sea-level. The nature of the syn-rift sedimentary and stratigraphic response to these regional fluctuations was still however dominantly controlled by the nature of tectonically generated relief throughout the rift.

7) This thesis has important implications for current models for the tectono-stratigraphic evolution of syn-rift deposits within intercontinental rifts. The Oligo-Miocene Suez Rift over a period of approximately 9.5 Ma experienced a relatively short episode of rifting (ca.f. the >30 Ma period of rifting of the Murchison-Statfjord Fault Zone in the Late Jurassic North Sea Rift, e.g. Young et al., 2001; or the polyphase rifting of the northeastern African plate, e.g. Guiraud and Bosworth, 1999). The Suez Rift experienced an initiation phase (23.5 to 19.7 Ma), climax phase (19.7 to 16.5 Ma) and a period of waning subsidence referred to in this study as late rift climax (16.5 – 15.7 Ma). This was succeeded by a period of tectonic acquiescence before renewed rifting began ca. 6 Ma ago. Subsequent models should take into account the latter stages of rift development, akin to previous work which has typically focussed upon the development of normal fault populations during the rift initiation period, and the nature of the transition to subsequent rift climax times.

8.5. RECOMMENDATIONS FOR FUTURE RESEARCH

The aim of this section is to suggest some recommendations for future work that can build upon and further develop the work presented in this thesis. In general there are three overall recommendations that are proposed, which can be subdivided between the subsurface rift axis and onshore rift margin components. Firstly, to obtain improved age constraints on the syn-rift succession studied by collecting improved data sets and/or finding more suitable sample locations. This would allow for an improved constraint upon the timing of deposition of the syn-rift sediments studied, further quantification of the timing of individual fault activity and overall regional fault displacement rates, in addition to an improved correlation of key stratigraphic intervals to more regional tectonic and glacio-eustatic events. Secondly, to extend this study to cover larger areas and encompass additional individual fault zones and larger fault blocks to enable comparisons to be made. Specifically, these recommendations are expanded upon below for both the subsurface rift axis and outcropping rift margin:

Subsurface rift axis

1) Improve the relative age constraints upon key stratal units within the Upper Rudeis Formation by using planktonic nannofossils, which are more reliable age indicators than the benthic forams which have been solely used to construct the present biostratigraphic database, which can be influenced by both facies variations and environment.
2) Improve the subsurface biostratigraphic database to include abundance and diversity data for key assemblages for a wider set of boreholes, thus allowing for the identification of biostratigraphic signatures associated with additional key chronostratigraphic surfaces, e.g. maximum flooding surfaces, to assist in correlation.
3) Utilise the break-though advances in the imaging of the subsalt section of the rift through multi-azimuth (MAZ) and ocean-bottom-cable (OBC) performed in recently acquired surveys conducted by GUPCO to update the understanding of the present day structural configuration and syn-rift thickness variability within the rift axis.
4) Extend the sequence stratigraphic subdivision of the Upper Rudeis Formation presented in this study into other areas of the rift axis, principally in the Offshore Belayim Oilfield area in the southern part of the Central Dip Provence, thus providing

a truly regional-scale, continuous rift axis study area extending across the Northern Central and Southern Dip Provinces.

5) Use a similar biostratigraphic supported key surface approach to subdivide the Lower Rudeis Formation. However, the presence of several localised, sediment starved depocentres within the axis of the rift may impede any attempts to do so.

Outcrop rift margin

1) Improve the age constraints on the studied succession in Chapter Six by adding to pre-existing biostratigraphic datasets, using both micro-fossils (e.g. from mudstone samples) and also from strontium isotope dating ($^{87}Sr/^{86}Sr$) of fauna, such as oysters. This would enable a more rigorous, higher resolution chronostratigraphy to be established within the study area, and also enhance the accuracy of jump-correlations between exposures.
2) Correlate key stratal surfaces and stratal units more extensively throughout all of the Upper Rudeis aged exposures in the adjacent Hammam Faraun and Sudr Fault Blocks (aided by the improved biostratigraphic constraints), to gain a more complete understanding of tectono-stratigraphic development of both these fault blocks. Specific areas of interest would include Gebel Sarbut El Gamal at the centre of the rift border Thal Fault and the downlapping cross bedded sandstones and calcarenitic conglomerates observed at Wadi Sudr (e.g. Patton et al., 1994). Furthermore, previous studies (e.g. Carr et al., 1999) which have investigated the along-strike variability of the extensive Upper Rudeis deposits located upon the hangingwall dip-slop of the El Qaa Fault Block should be wholly incorporated into the defined Upper Rudeis stratigraphic framework, and the framework modified as required.
3) Extend these tectono-stratigraphic analyses to the extensive subsurface datasets available within the western rift margin of the Central and Southern Dip Provinces, which have largely not been investigated in a detailed manner. These datasets could then be merged with the work presented in Chapter Six, providing a fully linked documentation of Upper Rudeis and Kareem high resolution variability across both the rift margin and axis components of the Morgan Accommodation Zone.

REFERENCES

Abreu, V.S & Anderson, J.B. 1998. Glacial eustasy during the Cenozoic; sequence stratigraphic applications, *AAPG Bulletin,* **82,** 7, 1385-1400

Abul-Nasr, R.A.A. 1987. Biostratigraphy and facies analysis of Paleogene rocks in the west-central Sinai (Egypt). *Unpublished Ph.D. thesis, University of South Carolina.*

Abul-Nasr, R.A.A. 1990. Re-evaluation of the Upper Eocene rock units in west Central Sinai, Egypt. *Ains Shams University, Earth Science Series*, **4**, 234-247.

Ackermann, R.V., Schlische, R.W., and Withjack, M.O., 2001. The geometric and statistical evolution of normal fault systems: an experimental study of the effects of mechanical layer thickness on scaling laws: Journal of Structural Geology, **23**, p. 1803-1819.

Alshahan, A. S. 2003. Petroleum Geology and potential hydrocarbon plays in the Gulf of Suez rift basin, Egypt. *AAPG Bulletin* **87**(1), 143-180

Allen, P. A. & Homewood, P. 1984. Evolution and mechanics of a Miocene tidal sandwave. *Sedimentology,* **28,** 369-379.

Allen, G., Ayyad, A., Desforges, G., Haddadi, N. & Pizon, J. 1984. Subsurface sedimentological study of the Rudeis Formation in Kareem, Ayun, Yisr and Sukheir Fields. *Egyptian General Petroleum Corporation, 6th exploration conference*,164-176.

Allen, P.A & ALLEN, J.R. 1990. *Basin Analysis, Principles & Applications*. Blackwell Science. pp 451.

Anders, M.H. & Schlische, R.W. 1994. Overlapping Faults, intrabasin highs, and the growth of normal Faults. *The Journal of Geology*, **102**, 165-180.

Ashley, G. M. 1990. Classification of large-scale subaqueous bedforms: a new look at an old problem. *J. Sedim. Petrol,* **60**, 160-172.

Barr, D. 1987. Structural/stratigraphic models for extensional basins of half-graben type, *Journal of Structural Geology*, **Vol. 9,** pp. 491 to 500

Beialy, S.Y.& Ali, A.S. 2002. *Journal of African Earth Sciences,* **35, 2,** 235-245

Beleity, A. 1982. The composite standard and definition of Palaeo events in the Gulf of Suez. From *6th EGPC conference.*

Bouma, A.H. 1962. Sedimentology of some Flysch deposits: A graphic approach to facies interpretation, 168. Elsevier, Amsterdam.

Burchette, T.P. 1988. Tectonic control on carbonate platform facies distribution and sequence development: Miocene, Gulf of Suez. *Sedimentary Geology*, **59**, 179-204.

Bosence, D., Cross, N. & Hardy, S. 1998. Architecture and depositional sequences of Tertiary fault-block carbonate platforms; an analyisis from outcrop (Miocene, Gulf of Suez) and computer modelling. *Marine and Petroleum Geology*, **15**, 203-221.

Bosworth, W. 1995 A high strain rift model for the southern Gulf of Suez (Egypt). In: *Hydrocarbon Habitat in Rift Basins* (Ed. by J.J. Lambiase), Geological Society of London Special Publication, **80**, 75-102.

Bosworth, W. & McClay, K.R. 2001. Structural and stratigraphic evolution of the Gulf of Suez Rift: A synthesis. In: *Peritethyan Rift/Wrench basins and passive margins. Memoirs du Museum National d'Histoire Naturelle de Paris*.

Bosworth, W., Huchon, P. & McClay, K. 2005. The Red Sea and Gulf of Aden Basins. *Journal of African Earth Sciences,* **43**, 334-378.

Bruhn, R. & Vagle, K. 2005. Relay ramp evolution and mass flow deposition (Upper Kimmeridgian-Lower Volgian) in the Tail End Graben, Danish North Sea. *Basin Research*, **17,** 551-567.

Burke, K. 1980. Intracontinental rifts and aulacogens. *In Continental Tectonics National Academy, Geophysics Research Board,* p.42-49.

Carr, I.D., Gawthorpe, R.L., Sharp, I.R. Underhill, J.R. et al, 1993. Sedimentology and sequence stratigraphy of the Nukhal and Asl Formation, Suez Rift. Unpublished University of Manchester Report.

Carr, I.D., Gawthorpe, R.L., Jackson, C.A.L., Sharp, I.R., Sadek, A., 2003. Sedimentology and sequence stratigraphy of early syn-rift tidal sediments: the Nukhul Formation, Suez Rift, Egypt. *Journal of Sedimentary Research,* **73,** 407-420.

Cartwright, J.A., Trudgill, B.D. & Mansfield, C.S. 1995. Fault growth by segment linkage: an explanation for scatter in maximum displacement and trace length data from the Canyonlands Graben of SE Utah. *Journal of Structural Geology*, **9**, 1319-1326.

Church, M. 1983. Patterns of instability in a a wandering gravel bed channel. In: *Modern and Ancient fluvial systems* (Ed. J. D. Collinson & J. Lewin) *Specl. Publ. int. Ass. Sediment*, p169-180.

Cochran, J. R. 1983. Effects of finite extension times on the development of sedimentary basins. *Earth and Planetary Science letters*, **66**, 289-302.

Coffield, D.Q. & Schamel, S. 1989. Surface expression of an accommodation zone within the Gulf of Suez rift, Egypt. *Geology*, **17**, 76-79.

Colletta, B. Le Quellec, P., Letouzey, J. & Moretti, I. 1988. Longitudinal evolution of the Suez rift structure (Egypt). *Tectonphysics*, **153**, 221-233.

Collier, R.E.LL. & Gawthorpe, R.L. 1995 Neotectonics drainage and sedimentation in central Greece: insights into coastal reservoir geometries in syn-rift sequences. Geological Society Special Publication, **80**, 165-181.

Collier, R.E.LL., Leeder, M.R., Trout, M., Ferentinos, G., Lyberis, E. & Papatheodorou, G. 2000. High sediment yields and cool, wet winters: test of last glacial palaeoclimates in the northern Mediterranean. *Geology*, **28**, 999-1002.

Contreras, J., Scholz, C.H. & King, G.C.P. (1997) A model of rift basin evolution constrained by first-order stratigraphic observations. *Journal of Geophysical Research*, **B102**, 7673-7690.

Corfield, S. & Sharp, I.R. 2000. Structural style and stratigraphic architecture of fault propagation folding in extensional settings: a seismic example from the Smorbukk area, Halten Terrace, Mid-Norway. *Basin Research*, **12**, 329-341.

Courtillot, V., Armijo, R., Tapponnier, P., 1987. Kinematics of the Sinai triple junction and a two phase model of Arabia–Africa rifting. In: Coward, M.P., Dewey, J.F., Hancock, P.L. (Eds.), *Continental Extensional Tectonics.* Geological Society Sp. Pub., London, pp. 559–573

Cowie, P.A. 1998. A healing-reloading feedback control on the growth rate of seismogenic faults. *Journal of Structural Geology*, **20**, 1075-1087.

Cowie, P.A. & Gupta, S. & Dawers, N.H. 2000. Implications of fault array evolution for synrift depocentre development: insights from a numerical fault growth model. *Basin Research*, **12**, 241-261.

Cowie, P.A. & Scholz, C.H. 1992a. Physical explanation for displacement-length relationship for faults using a post-yield fracture mechanics model. *Journal of Structural Geology*, **14**, 1133-1148.

Crone, A.J. & Haller, K.M. 1991. Segmentation and the coseismic behaviour of Basin and Range normal faults: examples from east-central Idaho and southwestern Montana, U.S.A. *Journal of Structural Geology*, **13**, 151-164.

Davies, S.J., Dawers, N.H., Mcleod, A.E. & Underhill, J.R. 2000. The structural and sedimentological evolution of early syn-rift successions: the middle Jurassic Tarbert Formation, North Sea. *Basin Research*, **12**, 343-365.

Dawers, N.H., Anders, M.H. & Scholz, C.H. 1993. Growth of normal faults: Displacement-length scaling. *Geology*, **21**, 1107-1110.

Dawers, N.H. & Anders. M.H. 1995. Displacement-length scaling and fault linkage. *Journal of Structural Geology,* **17**, 607-614.

Dawers, N.H. & Underhill, J.R. 2000. Role of fault interaction and 3inkage in controlling synrift stratigraphic sequences: Late Jurasic, Statfjord East Area, Northern North Sea. *AAPG Bulletin,* **84**(1), 45-64.

DePolo, C.M., Clark, D.G., Slemmons, D.B. & Ramelli, A.R. 1991. Historical surface faulting in the Basin and Range Province, western North America – implications for fault segmentation. *Journal of Structural Geology*, **13**, 123-136.

Dolson, J., El Gendi, O., Charmy, H., Fathalla, M. & Gaafar, I. 1996. Gulf of Suez rift basin sequence models-Part A. Miocene sequence stratigraphy and exploration significance in the Greater October Field Area, Northern Gulf of Suez. *Egyptian General Petroleum Corporation, 16th exploration conference*,227-241

Doresy, R.J. & Kidwell, S.M. 1999. Mixed carbonate-siliciclastic sedimentation on a tectonically active margin: examples from the Pliocene of Baja California Sur, Mexico. *Geology*, **27**, 935-938.

Ebinger, J. 1989. Tectonic Development of the Western Branch of the East African Rift System, Geological Society of America Bulletin, **1**, pp. 885-903.

Egyptian General Petroleum Company, stratigraphic committee Oligocene and Miocene Rock-Stratigraphy of the Gulf of Suez Region (EGPC, 1964).

El-Ashry, M. T. 1972. Source and dispersal of reservoir sands in El Morgan Field, Gulf of Suez, Egypt. *Sedimentary Geology,* 317-325.

El-Haddad, A., Aissaoui, D. M. & Soliman, M. A. 1984. Mixed carbonate-siliciclastic sedimentation on a Miocene fault-block, Gulf of Suez, Egypt. *Sedimentary Geology*, **37**, 185-202.

El-Heiny. I & Enani, N. 1990. Mioceneconglomeratic beds in Rudeis and Belyaim oil fields and their surface analogues. *Egyptian General Petroleum Corporation, 1oth exploration conference*,431-457.

Elbaz, M. R. & Handley, B. 1994. Reservoir description & depositional environment of the Miocene – Rudeis Formation, North Zaafarana, Warda Field, Gulf of Suez, Egypt. *Egyptian General Petroleum Corporation, 14th exploration conference*,327-354.

Eliet, P.P. & Gawthorpe, R.L. 1995. Drainage development and sediment supply within rifts, examples from the Sperchios Basin, central Greece. *Journal of Geological Society of London*, **152**, 883-893.

Emery, D. and Myers, K.L. 1996. *Sequence stratigraphy*, Blackwell, 297.

Evans, A.L. 1988. Neogene tectonics and stratigraphic events in the Gulf of Suez rift area, Egypt. *Tectonphysics*, **153**, 235-247.

Evans, A.L. 1990. Miocene Sandstone Provenance Relations in the Gulf of Suez: Insights into synrift Unroofing and Uplift History. *AAPG Bulletin*, **9**, 1386-1400.

Evans, A. L. and I. W. Moxon . 1986, Gebel Zeit chronostratigraphy: Egyptian General Petroleum Corporation, Eighth Exploration Seminar, 1986, 23 p.

Eyidoğan, H. & Jackson, J. 1985. A seismological study of normal faulting in the Demirci, Alaşehir and Gediz earthquakes of 1969-1970 in western turkey: implications for the nature and geometry of deformation in the continental crust. *Geophysical Journal of the Royal astronomical Society,* **81**, 569-607.

Galloway, W.E. 1989. Genetic Stratigraphic sequences in basin analysis: architecture and genesis of flooding surface bounded depositional units. *American Association of Petroleum Geology Bulletin*, **73**, 125-142.

Garfunkel, Z. & Bartov, Y. 1977. The Tectonics of the Suez Rift, *Geological Survey of Israel Bulletin,* **71**, 1-44.

Gawad, M. A. 1970. The Gulf of Suez: A brief Review of Stratigraphy and Structure. *Phil. Trans. Royal Soc. Lond,* **267, 41-48**

Gawthorpe, R. L., Hurst, J. M. & Sladen, C. P. 1990. Evolution of Miocene footwall-derived coarse-grained deltas, Gulf of Suez, Egypt: Implications for exploration. *AAPG Bulletin,* **74**, 1077-1086.

Gawthorpe, R.L., Jackson, C.A.L., Young, M.J., Sharp, I.R., Moustafa, A.R. & Leppard, C.W. 2003. Normal fault growth, displacement localisation and the evolution of normal fault populations: the Hamman Faraun fault block, Suez rift, Egypt. *Journal of Structural Geology*, **25**, 883-895.

Gawthorpe, R.L. & Hurst, J.M. 1993 Transfer zones in extensional basins: their structural style and influence on drainage development and stratigraphy. *Journal of the Geological Society of London*, **150**, 1137-1152.

Gawthorpe, R. L., Fraser, A. J. & Colier, R. E. Li. 1994. Sequence stratigraphy in active extensional basins: implications for the interpretation of ancient basin fills. *Marine & Petroleum Geology* **11**(6), 642-658.

Gawthorpe, R. L., Hardy, S. & Ritchie, B. 2003a. Numerical modelling of depositional sequences in half-graben rift basins. *Sedimentology* **50**, 169-185.

Gawthorpe, R. L. & Leeder, M. R. 2000. Tectono-sedimentary evolution of active extensional basins. *Basin Research* **12**, 195-218.

Gawthorpe, R.L., Sharp, I., Underhill, J.R. & Gupta, S. 1997. Linked sequence stratigraphic and structural evolution of propagating normal faults. *Geology*, **25**(9), 795-798.

Granier, T. 1985. Origin, damping and pattern of development of faults in granite. *Tectonics*, **4**, 721-737.

Gregory, J.W., 1894. Contributions to the physical geography of British East Africa. Geographical Journal, 4, 290-315, 408-424, 505 514.

Gudmundsson, A. 1987a. Geometry, formation and development of tectonic fractures on the Reykjanes Peninsula, southwest Iceland. *Tectonophysics*, **139**, 295-308.

Gudmundsson, A. 1992. Formation and growth of normal faults at the divergent plate boundary in Icleland. *Terra Nova*, **4**, 464-471.

Gupta, S., Cowie, P.A., Dawers, N.H. & Underhill, J.R. 1998. A mechanism to explain rift-basin subsidence and stratigraphic patterns through fault-array evolution. *Geology*, **26**(7), 595-598.

Gupta, S. Cowie, P. 2000. Processes and controls in the stratigraphic development of extensional basins. *Basin Research* **12**, 185-194.

Gupta, S., Underhill, J.R., Sharp, I.R. & Gawthorpe, R.L. 1999. Role of fault interactions in controlling synrift sediment dispersal patterns: Miocene, Abu Alaqa Group, Suez Rift, Sinai, Egypt. *Basin Research,* **11**, 167-189.

Guirad, R. & Bosworth, W. 1999. Phanerozoic geodynamic evolution of northeastern Africa and the northwestern Arabian platform. *Tectonophyshics,* **315**, 73-108.

Hamblin, A. P. & Walker, R. G. 1979. Storm-dominated shallow marine deposits: the Fernie-Kootenay (Jurassic) transition, southern Rocky Mountains. *Can. J. Earth Sci,* **16,** 1673-1690.

Hansen and Kamp, 2004 Late Mio to early plio stratigraphic record in northern taranaki basin: condensed sedimentation ahead of northern Graben extension and progradation of the modern continental margin. New Zealand Journal of Geology and Geophysics, 2004 VOL 47 645-622.

Haq, B.U., Hardenbol, J. & Vail, P.R. 1987. Chronology of fluctuating sea levels since the Triassic. *Science*, **235**, 1156-1167.

Hardy, S. & Gawthorpe, R.L. 1998. Normal fault control on along-strike sequence variability: insights from 3D numerical modelling. *Geology*, **26**, 911-914.

Hardy, S. & Mcclay, K. 1999. Kinematic modelling of extensional fault-propagation folding. *Journal of Structural Geology*, **21**, 695-702.

Helmy, H.M. 1993. Southern Gulf of Suez, Egypt: structural geology of the B-trend oil fields, *Geology Society, London,* **50:** 353-363

Howell, J.A. & Flint, S.S. 1996. A model for high resolution sequence stratigraphy within extensional basins. *In: High Resolution Sequence Stratigraphy: Innovations and Applications* (Ed. by Howell, J.A. & Aitken, J.F.) Geological Society Special Publication, **104,** 129-137.

Houbolt, J. H. C. 1968. Recent sediments in the southern bight of the North Sea. *Geol. Mijnbouw,* **47,** 254-273.

Hunt, D.W. and Tucker, M.E. 1992. Stranded parasequences and the forced regressive wedge systems tract: deposition during sea-level fall, *Sedimentary Geology*, **Vol. 81,** pp. 1 to 9

Hussein, H. M., Marzouk, I., Moustafa, A. R. & Hurukawa. 2006. Preiminary seismicity and focal mechanisms in the Southern Gulf of Suez: August 1994 through December 1997. *Journal of African Earth Sciences*, **45**, 48-60.

Jackson, C.A.L. 2002. Unpublished phd thesis, University of Manchester.

Jackson, C.A.L., Gawthorpe, R.L. & Sharp, I.R. 2002. Growth and linkage of the East Tanka fault zone, Suez rift: structural style and syn-rift stratigraphic response. *Journal of the Geological Society, London*, **159**, 175-187.

Jackson, C.A.L., Gawthorpe, R. L., Carr, I. D. & Sharp, I. R. 2005. Normal faulting as a control on the stratigraphic development of shallow marine syn-rift sequences: the Nukhul and Lower Rudeis Formations, Hammam Faraun Fault Block, Suez Rift, Egypt, *Sedimentology*, **52**, 313-338.

Jackson, C.A.L., Gawthorpe, R.L., Leppard, C.W. & Sharp, I. R. 2006. Rift-initiation development of normal fault blocks: insights from the Hammam Fararun Fault Block. *Journal of the Geological Society, London*, **163**, 165-183.

Jackson, J.A. & Leeder, M.R. 1994. Drainage systems and the development of normal faults: an example from Pleasant Valley, Nevada. *Journal of Structural Geology,* **16**, 1041-1059.

Jackson, J.A. 1987. Active normal faulting and crustal extension. In: *Continental Extensional Tectonics* (Ed. by M.P. Coward., J.F. Dewey. & P.L. Hancock), Geological Society of London Special Publication, **28**, 1-17.

Jackson, J.A., White, N.J., Garfunkel, Z., and Anderson, H., 1988: Relations between normal fault geometry, tilting and vertical motions in extensional terrains, an example from the southern Gulf of Suez, *J. Struct. Geol.* **10,** pp. 155 to 170

Jackson, J. 1994. Drainage systems and the development of normal faults: an example from Pleasant Valley, Nevada. *Journal of Structural Geology*, **16**, 1041-1059.

Jackson, J.A., White, N.J., Garfunkel, Z. & Anderson, H. 1988. Relations between normal fault geometry, tilting and vertical motions in extensional terrains: an example from the southern Gulf of Suez. *Journal of Structural Geology*, **10**, 155-170.

Jarrige, J., P. Ott d'Estevou, and P. Sehans, 1986. Etude structurale sur la marge occidentale de la Mer Rouge: Le secteur du Gebel Duwi pres de Quseir (Egypte): Documents et Travaux, Institut Geologique Albert De Lapparent, no. 10, p. 117-127.

Jarrige, P. Ott d'Estevou, P. F. Burollet, C. Montenat, P. Prat, J. Richert, and J. Thiriet, 1990, The multistage tectonic evolution of the Gulf of Suez and northern Red Sea continental rift from field observations: Tectonics, v. 9, p. 441-465.

Jervey, M.Y. 1988. Quantitative geological modelling of siliciclastic rock sequences and their seismic expressions. In: *Sea-level changes: an integrated approach* (Ed. by C.K. Wilgus, B.S. [Hastings, C.G.St.C. Kendall, H.W. Posamentier, C.A. Ross. & J.C. Van Wagoner), Society of Economic Palaeontologists and Mineralogists Special Publication, **42**, 47-69.

Katz, B.J. 1995. A survey of rift basin source rocks. In: *Hydrocarbon Habitat in Rift Basins* (Ed. By J.J. Lambiase), pp.213-242. *Spec. Publ. geol. Soc. Lond* **80.4.17**

Kendall, A. C. & Harwood, G. M. 1996, Marine evaporites; arid shorelines and basins. In: *Sedimentary environments; processes, facies and stratigraphy* (Ed H.G.Reading), 281-324.

Khalil, S. M. & McClay, K. R. 2001. Tectonic evolution of the NW Red Sea-Gulf of Suez rift system.. In: *Non-Volcanic Rifting of Continental Margins: A Comparison of Evidence from Land and Sea* (eds Wilson, R.C.L., Whitmarsh, R.B., Taylor, B. & Proitzheim, N.) Geological Society Special Publication, **187**, 453-473.

Kornsawan, A. & Morley, C. K. 2002. The origin and evolution of complex transfer zones (graben shifts) in conjugate fault systems around the Funan Field, Pattani basin, Gulf of Thailand, *Journal of Structural Geology,* **24**, 435–449.

Krebs, W. N., Wescott, W. A., Nummenadal, D., Gaafar, I., Azazi, G. & Karamat. S. 1997. Graphic correlation and sequence stratigraphy of Negoene rocks in the Gulf of Suez, *Bulletin of the Geological Society of France,* **168**, 63-71.

Krenkel, E. 1925. Geologie Afrikas, Borntrager, Berlin, Germany.

Lambiase, J.J. 1990. A model for tectonic control of lacustrine stratigraphic sequences in continental rift basins. *In: Lacustrine basin exploration: case studies and modern analogs* (Ed. by Katz, B.J.) American Association of Petroleum Geologists memoir, **50**, 265-276

Lambiase, J.J and Bosworth, W. 1995. Structural Controls on sedimentation in continental rifts, *in* J.J. Lambiase, ed., Hydrocarbon habitat in rift basins: London, Geological Society of London, p.117-144.

Landon, S. M. 1994. Introduction. In: *Interior rift basins* (edited by Landon, S. M.). The American Association of Petroleum Geologists, Tulsa, Oklahoma.

Leeder, M.R., Seger, M. & Stark. C. P. 1991. Sedimentology and tectonic geomorphology adjacent to active and inactive normal fault faults in the Megara Basin and Alkonides Gulf, Central Greece. *Journal Geol. Soc. Lond.* **148**. 331-343.

Leeder, M. R., Collier, R. E. Li., Aziz, A., Trout, M, Ferentinos, G., Papatheodorou, G. & Lyberis, E. 2002. Tectono-sedimentary processes along an active marine/lacustrine half-graben margin: Alkyonides Gulf, E. Gulf of Corinth, Greece. *Basin Research* **14**, 25-41.

Leeder, M. R. Gawthorpe, R. L. 1987. Sedimentary-models for extensional tilt-block/half graben basins. In: *Contiental Extensional Tectonics* (edited by Coward, M. P., Dewey, J. F. & Hanock, P. L). Geological Society Special Publication.

Leeder, M.R. & Jackson, J.A. 1993. The interaction between normal faulting and drainage in active extensional basins, with examples from the western United States and central Greece. *Basin Research*, **5**, 79-102.

Lelek, J. J., Shepherd, D. B., Stone, D. M. & Abdine, A. S. 1990. October Field: The Latest Giant under development in Egypt's Gulf of Suez. In: *Giant oil and Gas Fields of the Decade 1978 - 1988* (edited by Halbouty, M. T.). The American Association of Petroleum Geologists., Tulsa, Oklahoma.

Leppard, C. W. & Gawthorpe, R. L. 2006. Sedimentology of rift climax deep water systems: Lower Rudeis Formation, Hammam Faraun Fault Block, Suez Rift, Egypt. *Sedimentary Geology,* **191**, 67-87.

Lowe, D. R. 1982. Sediment Gravity flows:II. Depositional Models with special reference to the deposits of high-density turbidity currents. *J.Sedim. Petrol., **52**, 279-297.*

Lyberis, N. 1988. Tectonic evolution of the Gulf of Suez and the Gulf of Aqaba. *Tectonophysics*, **153**, 209-220.

Machette, M.N., Personius, S.F., Nelson, A.R., Schwarz, D.P., & Lund, W.R. 1991. The Wasatch fault zone, Utah: Segmentation and history of Holocene earthquakes. *Journal of Structural Geology*, **13**, 137-149.

Mahmoud. S, Reilinger, R., McClusky, S., Vernant, P. & Tealeb, A. 2005. GPS evidence for northward motion of the Sinai Block: implications for E. Mediterranean tectonics. *Earth and Planetary Science Letters*, **238**, 217–224.

Mansfield, C. & Cartwright, J. 2001. Fault growth by linkage: observations and implications from analogue models. *Journal of Structural Geology*, **23**, 745-763.

Manzocchi, T., Walsh, J.J. & Nicol, A. 2006. Displacement accumulation from earthquakes on isolated normal faults. *Journal of Structural Geology* **28**, 1685-1693.

Marrett, R., and Allmendinger, R.W., 1991. Estimates of strain due to brittle faulting: sampling of fault populations, *J. Struct. Geol.,* **13,** pp. 735 to 737

Mart, Y. & Hall, J. 1984. Structural trends in the northern Red Sea. *Journal of Geophysical Research*, **89**, 352-364.

Martel, S. J., Pollard, D.D. & Segall, P. 1988. Development of simple strike-slip fault zones, Mount Abott Quadrangle, Sierra Nevada, California. *Geological Society of America Bulletin,* **100**, 1451-1465.

Mellere, D & Steel, R.J. 1996. Tidal Sedimentation in Inner Hebrides half grabens, Scotland: the Mid-Jurassic Bearreraig Sandstone Formation. In: *Geology of Siliciclastic Shelf Seas,* (Eds, De Batist, M. & Jacobs, P. Geological Society Special Publication No. **117**, 49-79.

McClay, K. R., Nichols, G.J., Khalil, S. M., Darwish, M. & Bosworth, W. 1998. In: *Sedimentation and Tectonics of Rift Basins: Red Sea-Gulf of Aden* (edited by Purser, B.H. and Bosence, D.W.J.)223-238.

McClay, K. & Khalil, S. 1998. Extensional hard linkages, eastern Gulf of Suez, Egypt. *Geology*, **26**(6), 563-566.

McKenzie, D.P. 1978. Some remarks on the development of sedimentary basins. *Earth and planetary Science Letters,* **40**, 25-32.

Mcleod, A.E., Dawers, N.H. & Underhill, J.R. 2000. The propagation and linkage of normal faults: insights from the Strathspey-Brent-Statfjord fault array, northern North Sea. *Basin Research*, **12**, 263-284.

McMurray, L.S. & Gawthorpe, R.L. 2000. Along-strike variability of forced regressive deposits: late Quaternary, northern Peloponnesos, Greece. In: *Sedimentary responses to forced regressions* (Ed. by D. Hunt. & R.L. Gawthorpe), Geological Society of London Special Publication, **172**, 363-377.

Meshref W.M. and Khalil, B., 1990. Evidence for northerly propagation in Suez rift. *Proc. 10th EGPC Explor. Semin. Cairo* **1**, pp. 55–77

Meyer, V., Nicol, A., Childs, C., Walsh, J.J. & Watterson, J. 2002. Progressive localisation of strain during the evolution of a normal fault population. *Journal of Structural Geology,* **24**, 1215-1231.

Miller, K.G., Wright, J.D., and Fairbanks, R.G., 1991. Unlocking the Ice House: Oligocene Miocene oxygen isotopes, eustasy, and margin erosion. *J. Geophys. Res.*, **96**, 6829-6848.

Miller, K. G.,. Kominz, M. A., Browning, J. A., Wright, J. D., Mountain, G. S., Katz, M. E., Sugarman, P. J., Cramer, B. S., Christie-Blick, N. & Pekar, S. F. 2005. The Phanerozoic Record of Global Sea-Level Change. *Science,* **310,** 1293-

Montenat, C., Ott D'Estevou, P., Purser, B., Burollet, P., Jarrige, J., Orszag-Sperber, F., Philobbos, E., Plaziat, J., Prat, P., Richert, J., Roussel, N. & Thiriet, J. 1988. tectonic and sedimentary evolution of the Gulf Suez and the northwestern Red Sea. *Tectonphysics*, **153**, 161-177.

Morley, C.K. 1995. Developments in the structural geology of rifts over the last decade and their impact on hydrocarbon exploration. *In: Hydrocarbon Habitat in Rift Basins* (Ed. by Lambiase, J.J.). Geological Society of London Special Publication, **80**, 1-32.

Morley, C.K. 1999. Patterns of Displacement Along Large Normal Faults: Implications for Basin Evolution and Fault Propagation, Based on Examples from East Africa. *AAPG Bulletin*, **83**, 613-634.

Morley, C.K. 2002. Evolution of large normal faults: Evidence from seismic reflection data. *AAPG Bulletin*, **86**(6), 961-978.

Morley, C.K., Nelson, R.A., Patton, T.L. & Munn, S.G. 1990. Transfer zones in the East African rift system and their relevance to hydrocarbon exploration in rifts. *AAPG Bulletin*, **74**, 1234-1253.

Moretti I., Colletta, B. 1987. Spatial and temporal evolution of the Suez rift subsidence. *J.Geodn.* **7** ,151-168.

Moussa, H.E. 1987. Geologic studies and genetic correlation of basaltic rocks in west central Sinai. *Unpublished PhD thesis, Ain Shams University, Egypt.*

Moustafa, A.R. 1976. Block faulting in the Gulf of Suez. *5th Egyptian General Petroleum Organisation exploration seminar.* 19pp.

Moustafa, A. R. 1993. Structural characteristics and tectonic evolution of the east-margin blocks of the Suez rift. *Tectonphysics* **223**, 381-399.

Moustafa, A.R. 1996. Structural setting and tectonic evolution of the northern Hammam Faraun Block (Wadi Wasit-Wadi Wardan area) eastern side of the Suez Rift. *Kuwait Journal of Science and Engineering*, **23**, 105-132.

Moustafa, A.R. 1996. Internal structure and deformation of an accommodation zone in the northern part of the Suez rift. *Journal of Structural Geology*, **18**, 93-107.

Moustafa, A.R. 1997. Structural characteristics of updip sides of half grabens and effect of pre-rift structures on rift geometry: northeastern part of the Suez rift. *Annales Tectonicae*, **XI**, 58-74.

Moustafa, A. R. 2002. Controls on the geometry of transfer zones in the Suez rift and northwest Red Sea: Implications for the structural geometry of rift systems. *AAPG Bulletin* **86**(6), 979-1002.

Moustafa, A.R. & El Shaarawy, D.A. 1987. Tectonic setting of the northern Gulf of Suez. *Proceedings of the 5th Annual Meeting of the Egyptian Geophysical Society*, 339-368.

Moustafa, A.R. & Abdeen, M.M. 1992. Structural setting of the Hammam Faraun block, eastern side of the Suez rift, *Journal of the University of Kuwait,* **19**, 291-310.

Moustafa, A. R., and M. H. Khalil, 1987, The Durba-Araba fault, southwest Sinai: Egyptian Journal of Geology, **31**, 1-12.

Moustafa, A. R., and M. H. Khalil, 1995, Superposed deformation in the northern Suez rift, Egypt: relevance to hydrocarbon exploration: Journal of Petroleum Geology, v. 18, p. 245-266.

Mulder, T. & Alexander, J. 2001. The physical character of subaqueous sedimentary density flows and their deposits. *Sedimentology* **48**, 269-299

Mutti, E., Remacha, E. Sgavetti, M. Rosell, J. Valloni, R. & Zamorano, M. 1985. Stratigraphy and facies characteristics of the Eocene Hecho Group turbidite systems, South-Central Pyrenees. *In*: Mila, M.D. & Rosell, J. (eds) *International Association of Sedimentologists 6th European Regional Meeting, Excursion Guidebook,* **12**, 521–576, Lerida, Spain.

National Stratigraphic Sub-committee of the Geological Sciences of Egypt, 1974. Miocene rock stratigraphy of Egypt: Egyptian Journal of Geology, **18**, p.1-69

Nelson, R.A., Patton, T.L., Morley, C.K., 1992. Rift segment interaction and its relation to hydrocarbon exploration in rift systems. American Association of Petroleum Geologists Bulletin 76, 1153-1169.

Nemec, W. & Postma, G. 1993. Quaternary alluvial fans in southwestern Crete: sedimentation processes and geomorphic evolution. In: *Alluvial Sedimentation* (Eds. M. Marzo & C. Puigdefabregras), 235-276.

Nemec, W. & Steel, R.J. (1984) Alluvial and coastal conglomerates: Their significance and some comments on gravelly mass-flow deposits. In: *Sedimentology of Gravels and Conglomerates* (Ed. by E.H. Koster & R.J. Steel), *Memoirs of the Canadian Society of Petroleum Geology*, **10**, 1-31.

Nicol, A., Walsh, J.J., Watterson, J. & Underhill, J.R. 1997. Displacement rates of normal faults. *Nature*, **390**, 157-159.

Nicol, A., Walsh, J.J., Manzocchi, T. & Morewood, N. 2005. Displacement rates and average earthquake recurrence intervals on normal faults. *Journal of Structural Geology* **27**, 327-342.

Nøttvedt, A., Gabrielsen, R.H. & Steel, R.J. (1995) Tectonostratigraphy and sedimentary architecture of rift basins, with reference to the northern North Sea. *Marine and Petroleum Geology*, **12**, 881-901.

Orszag-Sperber, F., Harwood, G., Kendall, A. & Purser, B.H. 1998. A Review of hte evaporites of the Red Sea and Suez Rift. In: *Sedimentation and Tectonics of Rift Basins: Red Sea-Gulf of Aden* (edited by Purser, B.H. and Bosence, D.W.J.) 211-222.

Olariu, C., Steel, R. J., Dalrymple, R.W., Gingras, M. & Rubino, J-L. 2008. Tidal Dunes of the Eocene Baronia Sandstone, Ager Basin, Spain: Distinguishing Tidal Dunes from Tidal Bars; Why Bother? 2008 AAPG Annual Convention, San Antonio, Texas.

Orton, G. J. 1988. A spectrum of Middle Ordovician fan deltas and braid plain deltas North Wales: a consequence of varying fluvial clastic input. In: *Fan Deltas: Sedimentology and Tectonic settings* (Eds W. Nemec & R.J. Steel) 23-49. Blackie, London.

Patton, T. L., Moustafa, A. R., Nelson, R. A. & Abdine, S. A. 1994. Tectonic Evolution and Structural Setting of the Suez Rift. In: *Interior rift basins* (edited by Landon, S. M.). The American Association of Petroleum Geologists, Tulsa, Oklahoma.

Partington, M.A., Copestake, P., Mitchener, B. C. and Underhill, J.R, 1993. Biostratigraphic calibration of genetic stratigraphic sequences in the Jurassic-lowermost Cretaceous (Hettangian to Ryazanian) of the North Sea and adjacent areas. *In*: Petroleum Geology of Northwest Europe, Proceedings of the 4th Conference, (Ed. By J. R. Parker), p.371-386. Geological Society, London.

Peacock, D.C.P. & Sanderson, D.J. 1991. Displacements, segment linkage and relay ramps in normal fault zones. *Journal of Structural Geology*, **13**, 721-733.

Pivnik, D. A., Ramzy, M. Steer, B.L., Thorseth, J., El Sisi, Z., Gaafar, I., Garing, J.D. & Tucker, R.S. 2003. Episodic growth of normal faults as recorded by syntectonic sediments, July oil field, Suez rift, Egypt. *AAPG Bulletin*, **87**(6), 1015-1030.

Plaziat, J. C., Montenat, C., Barrier, P., Janin, M. C., Orszag-Sperber, F. & Philobbos, E. 1998. Stratigraphy of the Egyptian syn-rift deposits: correlations bewteen axial and peripheral sequences of the northwestern Red Sea and Gulf of Suez and their relations with tectonics and eustacy. In: *Sedimentation and Tectonics of Rift Basins: Red Sea-Gulf of Aden* (Ed. by Purser, B.H. and Bosence, D.W.J.) 211-222.

Pollard, D.D. and Aydin, A., 1984, Propagation and linkage of oceanic ridge segments: *Journal of Geophysical Research*, **89**, 10,017-10,028.

Posamentier, H.W. & Vail, P.R. 1988. Eustatic controls on clastic deposition II – sequence and systems tract models. In: *Sea-level changes: an integrated approach* (Ed. by C.K. Wilgus,

B.S. Hastings, C.G.St.C. Kendall, H.W. Posamentier, C.A. Ross. & J.C. Van Wagoner), Society of Economic Palaeontologists and Mineralogists Special Publication, **42**, 110-124.

Posamentier, H.W. & Allen, G.P. 1993a. Siliciclastic sequence stratigraphic patterns in foreland ramp-type basins. *Geology*, **21**, 455-458.

Posamentier, H.W. & Allen, G.P. 1993b. Variability of the sequence stratigraphic model: effects of local basin factors. *Sedimentary Geology*, **86**, 91-109.

Postama, G., Nemec, W. & Kleinspehn, K.L. 1988. Large floating clasts in turbidites: a mechanism for their emplacement, *Sedim. Geol.* **58**, 47-61.

Prosser, S. 1993. Rift-related linked depositional systems and their seismic expression. In: *Tectonics and Seismic Sequence Stratigraphy* (eds Williams, G.D. & Dobb, A.) Geological Society Special Publication No. 71, 35-66.

Ramzy, M., Steer, B., Abu-Shadi, F., Schlorholtz, M. & Mika, J. 1996. Gulf of Suez rift basin sequence models-Part B. Miocene Sequence stratigraphy and exploration significance in the central and southern Gulf of Suez. *Egyptian General Petroleum Corporation, 16th exploration conference*, 242-256.

Rattey, R. P., and A. B. Haywood, 1993, Sequence stratigraphy of a failed rift system: the Middle Jurassic to Late Cretaceous basin evolution of the central and northern North Sea, in J. R. Parker, ed., Petroleum geology of northwest Europe: Proceedings of the 4th Conference, Geological Society of London, v. 1, p. 215-251.

Ravnås, R. & Steel, R. J. 1997 Architecture of marine rift-basin successions. *AAPG Bulletin, 82, 110-146.*

Ravnås, R. & Bondevik, K. 1997. Architecture and controls on Bathonian to Kimmeridgian shallow-marine synrift wedges in the Oseberg-Brage area, northern North Sea. *Basin Research*, **9**, 197-226.

Ravnås, R., Bondevik, K., Helland-Hansen, W., Lømo, L., Ryseth, A. and Steel, R.J. 1997. Sedimentation history as an indicator of rift initiation and development: The Late Bajocian-Bathonian evolution of the Oseberg-Brage area, northern North Sea. *Norsk Tidsskrift,* **77**, 205-232.

Ravnås, R., Nøttvedt, A., Steel, R.J. & Windlestad, J. 2000. Syn-rift sedimentary architectures in the Northern North Sea. *In: Dynamics of the Norwegian margin* (Ed. by Nøttvedt, A.). Geological Society of London Special Publication, **167**, 133-177.

Refaat, A.A. & Imam, M.M. 1999. The Tayiba Red Beds: transitional marine-continental deposits in the precursor Suez rift, Sinai, Egypt. *Journal African Earth Science*, **28**, 487-506.

Retallack, G.J. (1986) The fossil record of soils. In: *Paleosols: Their Recognition and Interpretation* (Ed. by V.P. Wright), 1-57.

Richards, M., Bowman, M. & Reading, H. 1998. Submarine fan systems I characterization and stratigraphic prediction. *Marine & Petroleum Geology*, **15**, 689-717.

Reading, H. G. & Collinson, J. D. 1996. Clastic coasts. In: *Sedimentary environments; processes, facies and stratigraphy* (Ed H.G.Reading), 281-324.

Richardson, M. Arthur, M. A. 1988. The Gulf of Suez - northern Red Sea Neogene rift: a quantitive basin analysis. *Marine & Petroleum Geology* **5**, 247-270.

Rine, J. M., Hassouba, A. B. H., Shishkevish, L., Shafi, A.A., Azazi, G., Nashaat, H., Badawy, A. and El Sisi, Z. 1988. Evolution of a Miocene fan delta: a giant oli field in the Gulf of Suez, Egypt. In: *Fan Deltas: Sedimentology and Tectonic Settings* (edited by Nemec, W. & Steel, R. J.) Blackie and Son.

Roberts, H.H. 1987. Modern carbonate-siliciclastic transition: humid and arid tropical examples. *Sedimentary Geology*, **50**, 25-65.

Roberts, G.P. 1996. Variation in fault-slip directions along active and segmented normal fault-systems. *Journal of Structural Geology*, **18**, 835-846.

Roberts, S., and Jackson, J.A. 1991: Active normal faulting in central Greece: an overview, *in* Roberts, A.M., Yeilding, G., and Freemen, B. eds., The Geometry of Normal Faults, *Geological Society of London Special Publication, **No. 56,*** pp. 125 to 142

Roberts, D. A. 1990. Modern carbonate-siliciclastic transitions: humid and arid tropical examples: *Sedimentary Geology*, **53**, 247-267.

Robson, D.A. 1971. The structure of the Gulf of Suez (Clysmic) rift, with special reference to the eastern side. *Journal of the Geological Society, London,* **127**, 247-276.

Rosendahl, B.R. 1987. Architecture of continental rifts with special reference to East Africa. *Ann. Rev. Earth Planet. Sci.*, **15,** pp. 445 to 503

Rosendahl, B.R., Reynolds, D.J., Lorber, P.M., Burgess, C.F., McGill, J, Scott, D, Lambiase, J.J. and Derksen, S.J., 1986. Structural expressions of rifting; lessons from Lake Tanganyika, Africa. *In*: Frostick, L.E., Renaut, R.W., Reid, I. and Tiercelin, J.J. (Eds), *Sedimentation in the African rifts. Geol. Soc. Spec. Pub.* **25,** pp. 29 to 43

Salah, M. G. & Alsharhan, A. S. 1997. The Miocene Kareem Formnation in the Southern Gulf of Suez, Egypt: A review of the stratigraphy and petroleum geology. *Journal of Petroleum Geology,* **20**(3), 327-346.

Saoudi, A., and B. Khalil, 1984, Distribution and hydrocarbon potential of Nukhul sediments in the Gulf of Suez: Proceedings of the 7th Exploration Conference, Egyptian General Petroleum Corporation, p. 75-96.

Scheibner, C., Marzouk, A.M. and Kuss, J., 2001. Maastrichtian–Early Eocene lithostratigraphy and palaeogeography of the N Gulf of Suez Region, Egypt. *J. Afr. Earth Sci.* **32**, 201-222.

Schlager, W. 1993. Accommodation and supply; a dual control on stratigraphic sequences. *Sedimentary Geology*, **86**, 111-136.

Schlische, R.W. 1995. Geometry and origin of fault-related folds in extensional settings. *American Association of Petroleum Geologists Bulletin*, **79**, 1661-1678.

Schlische, R.W. & Olsen, P.E. 1990. Quantitative filling models for continental extensional basins with applications to early Mesozoic rifts of North America. *Journal of Geology*, **98**, 135-155.

Schlische, R.W., Young, S.S., Ackermann, R.V. and Gupta, A., 1996. Geometry and scaling relations of a population of very small rift-related normal faults, *Geology,* **24, 8,** pp. 683 to 686

Scholz, C.A., Rosendahl, B.R. And Scott, D.L. 1990. Development of coarse grained facies in rift basins: examples from East Africa. *Geology*, **18**, 140-144.

Schulze, K. I. 1994. Structure and Stratigraphy of the Gulf of Suez, Egypt. In: *Interior rift basins* (edited by Landon, S. M.). *World Petroleum Basins*. The American Association of Petroleum Geologists, Tulsa, Oklahoma.

Schwartz, D.P. & Coppersmith, K.J. 1984. Fault behaviour and characteristic earthquakes – examples from the Wasatch and San Andreas fault zones. *Journal of Geophysical Research*, **89**, 5681-5698.

Scott, R.W and Govean, F.M. 1986. Early depositional history of a rift basin: Miocene in western Sinai. PPP, **52**, 143-152

Segall, P. 1984. Formation and growth of extensional fracture sets. *Geological Society of America Bulletin*, **95**, 454-462.

Segall, P. & Pollard, D.D. 1980. Mechanics of discontinuous faults. *Journal of Geophysical research*, **85**, 4337-4350.

Sercombe, W. J., Golob, B. R., Kamel, M., Stewart, J. W., Smith, G. W. & Morse, J. D. 1997. Significant structural reinterpretation of the subsalt, giant October Field, Gulf of Suez, Egypt, Using SCAT, isogon-based sections and maps, and 3D seismic. *The Leading Edge* **16**(8), 1143-1150.

Segnor, A.M.C. & Burke, K. 1978. Relative timing of rifting and volcanism on earth and its tectonic implications. *Geophysical Research Letters*, **5** , 419–421.

Sharp, I.R., Gawthorpe, R.L., Armstrong, B. & Underhill, J.R. 2000a. Propagation history and passive rotation of mesoscale normal faults: implications for synrift stratigraphic development. *Basin Research*, **12**, 285-305.

Sharp, I.R., Gawthorpe, R.L., Underhill, J.R. & Gupta, S. 2000b. Fault-propagation folding in extensional settings: Examples of structural style and synrift sedimentary response from the Suez rift, Sinai, Egypt. *AAPG Bulletin*, **112**(12), 1877-1899.

Shaw, A.B. 1964. *Time in stratigraphy*. McGraw-Hill, New York, 365.

Smale, J.L. & Thurnell, R.C. 1988. Sedimentological evidence for early Miocene fault reactivation in the Gulf of Suez. *Geology,* **16**, 113-116.

Souaya, F. J. 1966. Miocene Foraminifera of the Gulf of Suez Region, U.A.R. Part 4: Palaeocology and Age. *Micropaleontology*, **12**, 493-504.

Steckler, M.S. 1985. Uplift and extension at the Gulf of Suez: indications of induced mantle convection. *Nature*, **317**, 153-139.

Steckler, M.S., Berthelot, F., Lyberis, N. & Le Pichon, X. 1988. Subsidence in the Gulf of Suez: implications for rifting and plate kinematics. *Tectonphysics*, **153**, 249-270.

Steckler, M.S. & Omar, G.I. 1994. Controls on eropsinal retreat of uplifted flanks at the Gulf of Suez and northern Red Sea. *American Geophysical Union*, VOL 1-9.

Steen, G. 1984. Radiometric age dating and tectonic significance of some Gulf of Suez igneous rocks. *Egyptian General Petroleum Corporation, 6th Exploration Seminar*, 199-211.

Stein, R.S. & Barrientos, S.E. 1985. Planar high-angle faulting in the Basin and Range: Geodetic analysis of the 1983 Borah Peak, Idaho, earthquake. *Journal of Geophysical Research*, **90**, 11355-11366.

Stow, D.A.V., 1994. Deep sea processes of sediment transport and deposition. In: *Sediment transport and Depositional processes* (Ed K Pye), 257-291.

Surlyk, F., Noe-Nygaard, N. & Dam, G. 1993. High and low resolution sequence stratigraphy in lithological prediction – examples from the Mesozoic around the northern North Atlantic. In: *Petroleum Geology of northwest Europe: Proceedings of the 4th Conference: London* (edited by Parker, J.R.) The Geological Society, 199-214.

Taylor, A. & Goldring, R. 1993. Description and anaylsis of bioturbation and ichnofabric. *Journal of the Geological Society, London* **150**, 141-148.

Taylor, A., Goldring, R. & Gowland, S. 2003. Anaylsis and applications of ichnofabric. *Earth Science reviews* **60**, 227-259.

Thiebaud, C.E. & Robson, D.A. 1979. The geology of the area between Wadi Wardan and Wadi Gharandal, East Clysmic Rift, Sinai, Egypt. *Journal of the Petroleum Geology*, **1**(4), 63-75.

Trudgill, B.D. 2002. Structural controls on drainage development in the Cayonlands grabens of southeast Utah. *AAPG Bulletin,* **86**(6), 1095-1112.

Trudgill, B.D. & Cartwright, J.A. 1994. Relay-ramp forms and normal fault linkages, Canyonlands National Park, Utah. *American Association of Petroleum Geologists Bulletin,* **106**, 1143-1157.

Trudgill, B.D. & Underhill, J.R. 2002. Introduction to the structure and stratigraphy of rift systems. *AAPG Bulletin*, **86** (6), 931-933.

Turcotte, D.L. & Emerman, S.H. 1983. Mechanisms of active and passive rifting. *Tectonophysics*, **94**, 39-50.

Underhill, J.R. 1991., Controls on Late Jurassic seismic sequences, Inner Moray, Firth, U.K. North Sea, A critical test of a key segment of Exxon's original global cycle chart. *Basin Research,* **3,** 79-98

Underhill. J.R. & Partington, M.A. 1993. Jurassic thermal doming and deflation in the North Sea: implications of the sequence stratigraphic evidence. *In: Petroleum Geology of northwest Europe: Proceedings of the 4th conference* (Ed. by Parker, J.R.). Geological Society of London, 337-346

Underhill, J.R., Sawyer, M.J., Hodgson, P., Shallcross, M.D., and Gawthorpe, R.L., 1997. Implications of Fault Scarp Degradation for Brent Group Prospectivity, Ninian Field, Northern North Sea, *Bulletin of the American Association of Petroleum Geologists*, **81,** pp. 999 to1022

Vail, P.R., Mitchum, R.M., Todd, R.G., Widmier, J.M., Thompson, S., III, Sangree, J.B., Bubb, J.N. & Hatleid, W.G. 1977. Seismic Stratigraphy and global changes in sea level. *In: Seismic Stratigraphy – Applications to Hydrocarbon Exploration* (Ed. By Paton, C. E.). Memoir of the American Association of Petroleum Geologists, **26**, 49-97.

Vail , P.R., Hardenbol, J., and Todd, R.G., 1984. Jurassic unconformities, chronostratigraphy, and sea-level changes from seismic stratigraphy and biostratigraphy. *In* Schlee, J.S. (Ed.), Interregional unconformities and Hydrocarbon Accumulation, *AAPG Mem.*, **36,** 129-144.
Vanderbeek, J. W. 1994. Introduction to Exploration in the gulf of Suez. In: *Interior rift basins* (edited by Landon, S. M.). *World Petroleum Basin.* The American Association of Petroleum Geologists, Tulsa, Oklahoma.

Van Wagoner, J.C., Posamentier, H.W., Mitchum, R.M., Vail, P.R., Sarg, J.F., Loutit, T.S. & Handenbol, J. 1988. An overview of the fundamentals of sequence stratigraphy and key definitions. *In: Sea Level Changes: an integrated Approach, Spec.* Special Publication, Society of Economic Palaeontologists and Mineralogists, **42**, 39-45.

Van Wagoner, J.C., Mitchum, JR, R.M., Campion, K.M. & Rahmanian, V.D. 1990. Siliciclastic sequence stratigraphy in well logs, cores and outcrops: concepts for high-resolution correlation of time and facies. *American Association of Petroleum Geologists, Methods in Exploration,* **Series 7**.

Walsh, J.J., Bailey, W.R., Childs, C., Nicol, A. & Bonson, C.G. Formation of segmented normal faults: a 3-D perspective. 2003. *Journal of Structural Geology*, **25**, 1251-1262.

Walsh, J.J., Childs, A., Imber, J., Manzocchi, T., Watterson, J. & Nell, P.A.R. 2003. Strain localisation and population changes during fault system growth within the Inner Moray Firth, Northern North Sea. *Journal of Structural Geology,* **25**, 307-315.

Walsh, J.J., Nicol, A. & Childs, C. 2002. An alternative model for the growth of faults. *Journal of Structural Geology*, **24**, 1669-1675.

Walsh, J.J. & Watterson, J. 1988. Analysis of the relationship between displacements and dimensions of faults. *Journal of Structural Geology*, **10**, 239-247.

Watterson, J. 1986. Fault dimensions, displacements and growth. *Pure and Applied Geophysics*, **124**, 365-363.

Wescott, W. A., Krebs, W. N., Dolson, J. C., Karamat, S. A. & Nummendal, D. 1996. Rift basin sequency stratigraphy: some examples from the Gulf of Suez. *GeoArabia,* **1**(2), 343-357.

Wescott, W.A., Nummedal, D., Krebs, W.N and Karamat, S.A. 1998. Depositional Facies of the early synrift strata on the Sinai margin of the Gulf of Suez, *In* Proceedings of te 13th Petroleum Conference: Cairo, Egyptian General Petroleum Corporation, 297-312

Wescott, W.A., Krebs, W.N., Bentham, P.A. & Pocknall, D.T. 2000. Miocene Brackish Water and Lacustrine Deposition in the Suez Rift, Sinai, Egypt. *Palaios*, **15**, 65-72.

Wernicke, B., 1981. Low-angle faulting in the Basin and Range Province: nappe tectonics in an extending orogen, *Nature*, **291**, 645 to 648

Wilson, M. 1989. *Igneous Petrogenesis* , 466 pp. Unwinn Hymann, London. **12.2.2**

Winn Jr, R.D., Crevello, P.D. & Bosworth, W. 2001. Lower Miocene Nukhul Formation, Gebel el Zeit, Egypt: Model for structural control on early synrift strata and reservoirs, Gulf of Suez. *AAPG Bulletin*, **85**(10), 1871-1890

Withjack, M.O., Olson, J. & Peterson, E. 1990. Experimental models of extensional forced folds. *American Association of Petroleum Geologists Bulletin*, **74**, 1038-1054.

Younes, A. I., and McClay, K.R. 2002. Development of accommodation zones in the Gulf of Suez – Red Sea rift, Egypt: AAPG Bulletin, **85** 1003-1026.

Young. M.J., Gawthorpe.R.L. & Sharp. I.R. 2000. Sedimentology and sequence stratigraphy of a transfer zone coarse-grained delta, Miocene Suez Rift, Egypt. *Sedimentology,* **47**, 1081-1104.

Young, M.J., Gawthorpe, R.L. & Hardy, S. 2001. Growth and linkage of a segmented normal fault zone; the Late Jurassic Murchison-Statfjord North Fault, northern North Sea. *Journal of Structural Geology,* **23**, 1933-1952.

Young, M.J, Gawthorpe, R.L. & Sharp, I.R. 2002. Architecture and evolution of the syn-rift clastic depositional systems towards the tip of a major fault segment, Suez Rift, Egypt. *Basin Research*, **14**, 1-23.

Young, M.J., Gawthorpe, R.L. & Sharp, I.R. 2003. Normal fault growth and early synrift sedimentology and sequence stratigraphy: Thal Fault, Suez Rift, Egypt. *Basin Research* **15**, 479-502.

Zahran, M. E. &. Meshref, W. 1988. The northern Gulf of Suez basin evolution, stratigraphy and facies relationship. *9th Egyptian General Petroleum Corporation, Petroleum Exploration and Production Conference*, **1**, 110-126.

Zelilidis, A. 2000. The geometry of fan-deltas and related turbidites in narrow linear basins. *Geological Journal,* **38**, 31-46.

Zhang, P. Slemmons, D.B. & Mao, F. 1991. Geometric pattern, rupture termination and fault segmentation of the Dixie Walley-Pleasant Valley active normal fault system, Nevada, U.S.A. *Journal of Structural Geology*, **13**, 165-176.

Zaki, R., McDowell, H., Threadgold, I. & Oldfield, O. 1990. Sub-salt imaging in the Gulf of Suez. In: (Ed. J. Brooks) *Classic Petroleum Provinces,* Geol. Soc. Spec. Publ, **50** Saoudi, A., and B. Khalil, 1986, Distribution and hydrocarbon potential of Nukhul sediments in the Gulf of Suez: Proceedings of the 7th Exploration Conference, Egyptian General Petroleum Corporation, p. 75-96., 341-551.

Ziegler, P.A. and Cloetingh, S. 2004. Dynamic Processes controlling evolution of rifted basins, *Earth Science Reviews*, **64,** 1-50

APPENDIX 1

Cored well intervals utilised in this study

Northern central dip province – October Fault Block

Well	Top MD (ft)	Base MD (ft)	MD Thickness (ft)	(m)
OCT-J5	10951	11235	284	85.56
ET-A3	9400	9488	88	26.82
TANKA-3	9950	10119	169	51.51
GS184-4A	11330	11510	180	54.86
GS195-3	12250	12331	81	24.69
OCT-F3B	13181	13240	59	17.98
OCT-J7A	12335	12383	48	14.63
GS 216-1*	9486	9546	60	18.28

* Core not located in the hangingwall of the October Fault Zone. Located in the distal portion of a submarine fan sourced from the east at the Abu Rudeis entry point.

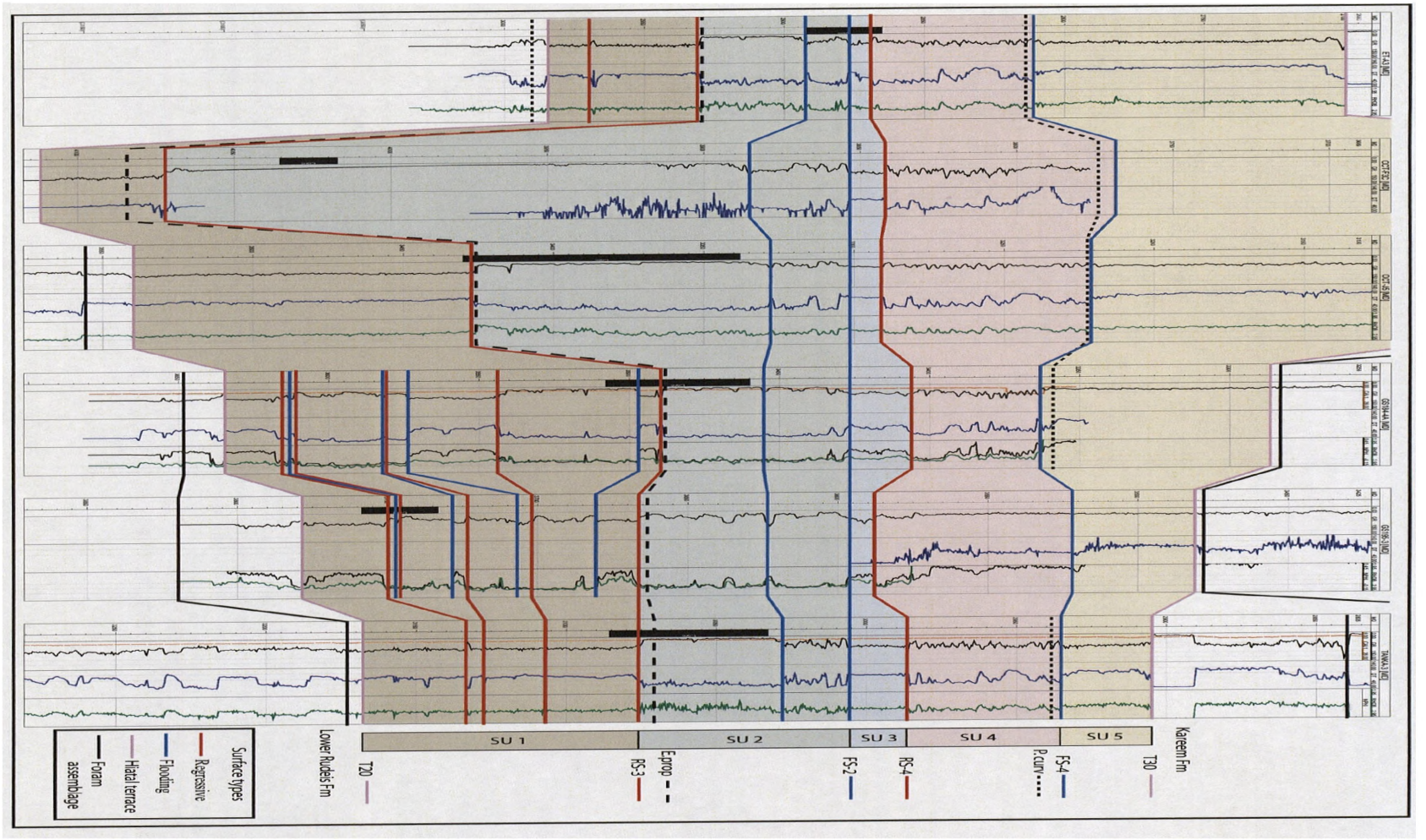
Surface types
Regressive
Flooding
Hiatal terrace
Foram assemblage
Lower Rudeis Fm
T20
SU 1
SU 2
SU 3
SU 4
SU 5
RS-3
E.prop
FS-2
RS-4
P.curv
FS-4
T30
Kareem Fm

Appendix 1: Key to core logs enclosures

Key to Facies Associations

Offshore basinal depositional system

A) Fault block crest Facies Association
- Facies A1: Condensed section (Not encountered in core)

B) Passive basinal infill Facies Association
- Facies B1: Laminated and massive mudstone
- Facies B2: Calcareous marl (Not encountered in core)
- Facies B3: Massive anhydrite (Not encountered in core)

C) Slope Apron Facies Association
- Facies C1: Bioclastic breccia

Carbonate-rich submarine fan

D) Proximal to mid fan
- Facies D1: Normal graded bioclastic grainstones, packstones and calcarenites
- Facies D2: Cross bedded bioclastic grainstones and calcarenites
- Facies D3: Laminated packstone

E) Distal fan
- Facies E1: Bioturbated packstones and calcarenites
- Facies E2: Reverse graded siltstone and wackestone

F) Pro fan turbidite
- Facies F1: Thin, sharp based calcarenites

Silciclastic submarine fan

G) Proximal to mid axial sheet
- Facies G1: Coarse to very fine normal graded sandstones
- Facies G2: Cross bedded sandstones
- Facies G3: Thinnly bedded sandstones
- Subfacies G3 i: Dewatering disrupted thinnly bedded sandstones
- Facies G4: Convoluted bedded sandstones

(H) Distal sheet
- Facies H1: Thin, sharp and erosive based sandstones

Key to log symbols and lithofacies

Sedimentary Structures
- Clast stringers
- Outsized clasts
- Tabular cross-bedding
- Low angle cross-bedding
- Current ripples
- Lamination
- Disrupted Lamination / dewatering structures
- Convoluted bedding / laminae

Surfaces
- FS Flooding surface
- RS Regressive surface

Trace Fossils
- *Thalassinoides*
- *Planolites*
- *Schaubcylindrichus*
- *Ophiomorpha Nodosa*
- *Ophiomorpha Irregulaire*
- *Palaeophycus*
- *Teichichnus*
- *Phycosiphon*
- *Unknown ichnotaxa*

Bioclasts
- Shell debris
- Bryzoa

APPENDIX 2

Description notes of thin sections taken from October Hangingwall wells.

WELL	Depth (MD Feet)	DESCRIPTION
OCT-J5	11218	Quartz dominated sandstone. Well sorted, sub angular to sub-rounded and typically fine-grained. Feldspar, >5% and biotite <5%. Rare carbonate forams. Good inter-granular porosity (10-15%)
	11204	: Dominated by angular to sub-rounded clasts of undulose quartz, fine-grained. 5-10% of Plagioclase feldspar grains – similarly shaped & sized, often showing laminellar twinning – Microcline. Grains well sorted. Relatively little carbonate (5-10%) with small carbonate grains and identifiable shells. Inter-granular porosity very good. Rare glauconitic grains. Good example.
	11193	Coarse (x-bedded facies) Quartz sandstone. Quartz dominated, moderately – poorly sorted, f-c size, sub-angular – very round. Porosity good. Biotite, glauconite present. Feldspar 5-10%, patches of calcite cement. Forams main bioclast.
	11191	Fine grained – silt silic sandstone. Same as log. No porosity. Very fine – so shows that calc cement is not the preserve of coarser units as in previous slide.
	11185	>25% quartz grains, varying sizes and shapes (well rounded – angular) and poorly sorted. Similar natured feldspar visible. Very little/no intergrain pore spaces – calcite cement. Glauconite present. Increased number of bioclasts – shells and Bryzoa.
	11170	Dominated by quartz and feldspar. Angular – sub angular grains. Moderately sorted. Calc grain rare – no more than 5-10% Glauconite present, good intergrain porosity.
	11146	75% quartz grains and felds, angular and sub-rounded. Varying in size and moderate sorted. Mainly dominated by bioclasts, calc grains and calc cement. No intergrain porosity.
	11095	Carb rich. Quartz grains (angular and sub rounded, similar size and moderate sorted. No more than 10%, little evidence of feldspar, glauconite present, calc cement and neoformed Calcite crystals and shell material. Little inter grain porosity, main porosity from within dissolved shell.
	11075	In packstone. Quartz grains widely vary in size and shape. Poorly sorted but no more than 5%. Mainly fine grained carbonate with Bryzoa and skeletal shell debris.
	11047	Quartz grains – fine sand – small pebble, angular to sub rounded. No feldspar. Glauconite present. Full of bioclastic material, little/no porosity spaces between grains – calcite cement – fine grained groundmass. Matrix supported.
	11043.9	Dominated by quartz: 50%. Little evidence of feldspar. Moderately sorted, angular – sub rounded, similar grainsize. Areas of good inter grain porosity. Some glauconite grains, and bioclasts/shell debris. Areas of carbonate cement.
	11031	Skeletal packestone – grain stone. Few quartz grains <1%. Bioclast dominant. Bryzoa fragments – up to 4mm. Also present red algae, echinoid spines and shell fragments and sparite cement.
	11021	Packestone – very poor, sorted quartz, angular – rounded, course – fine, 2-5%. Micritic matrix. Skeletal grains – red algae, bryzoa etc, shell debris.
	11000	Grain stone – Quartz grains = 1-2%. Very poorly sorted, very fine – m size, sub-angular – sub-rounded. Skeletal grains – echinoid spines, Bryzoa and forams. Range in sizes – very fine to medium.
	10966	Thin quartz rich bed. Quartz grains = >50%, moderately sorted, Sub.Ang – Sub .Rnd, m-c sandstone. Little evidence of feldspar, good inter porosity in places, glauconite grains. Areas of carb cement, bioclasts mainly echinoid

		spines and shell debris.
GS184-4A	11510	Quartz grains 10%. Angular –sub-rounded, poorly sorted. Fine – medium size. Same suite of bioclasts as OCT-J5 samples. Micrite mud. Very little/no porosity.
	11405	From log – Grainstone/packestone. G/Packestone coral bioclasts and red algae. Very low porosity – mouldic. Some glauconite. Qtz 1-2% moderate sorted, sub angular – sub rounded, f-m size.
	11345	(Bioturbated packestone) Qtz 5-10% Sub-round – round. Little/no porosity. Well- moderate sorted. F-m size. Clear laminations and variations in Qtz and bioclast grainsize. Separate depositional events. Small, very fine bioclasts. Increased mud contact.
	11374.5	From log – grainstone – packstone boundary. Grainstone – bioclast rich – red algae, echinoids, shell debris, forams etc. Neoformed calcite – not too much mud. Calcite cement. No porosity. Qtz 1-2% poorly sorted, f-m/c, sub angular – sub-round. Slight grading, F.U in section of Quartz and bioclasts.
ET-A3	9486	Quartz grains – poor-moderately sorted. Angular – sub-rounded, fine to very fine 30%/ Calcite cement, bioclasts include shell debris and echinoid spines, forams and bryzoa – small/fine size. Glauconite grains. Very low inter grain porosity.
	9475	Quartz grains- sub-angular – sub-rounded, poorly sorted, very fine to fine/medium 10-15%. More (than 9486) bioclastic rich, and coarser bioclasts. A lot of bryzoa fragments, shell debris, echinoid spines, forams, some carbonate mud/micite. Very low inter grain porosity.
	9469	Quartz – sub-angular – sub-rounded. Poor-moderately sorted, fine – medium, >50%. Finer bioclastic material – mainly forams, bryzoa and shells. Carb mud and glauconite grains. Calc sandstone.
	9463	Very fine, sub-angular – sub-rounded, well sorted grains of quartz and calcite. Quartz – 10%. Bioclastic material is very fine: shell debris and forams. Carb silt mud matrix.
	9442	Foram rich, very fine grained pack – wackestone. 1-2% well-sorted, very fine, angular – sub-angular quartz grains. (More coarser grains). Other bioclasts include shell fragments. Also, some angular – sub-angular sandy/yellow grains, quite rare isotropic. Mud/micrite matrix. Cement - no visible porosity. Foram Pack –wackestone.
	9437	25% quartz grains – poorly sorted, sub-angular – rounded. Grainsize ranging from very fine – medium, other parts = bioclasts and mitic mud. Bioclasts – m-c sized, red algae, shell fragments dominate, some bryzoa fragments. Bioclastic Sandstone
	9433	Quartz grains dominate >50%. Poor – moderately sorted, generally sub-rounded. Size = fine – coarse. Good inter granular porosity – no calc cement. 5% Bioclasts, mainly fragments, shell, Bryzoa and Red Algae and Forams. Mouldic porosity due to bioclastic dissolution. Quartz arenite.
	9428	Quartz grains: poorly sorted, sub-angular – sub-rounded, medium – very fine 50%. Forams, shell debris Red Algae and Bryzoa fragments as bioclasts. Moderate inter grain porosity. Areas of glauconite present. Quartz Sandstone.
	9412	Very fine quartz grains- rare fine sized. Moderately sorted, sub-angular – sub-rounded >25%. Also mud matrix and foram bioclasts and very fine shell material. Glauconite grains present. Very fine sandstone – siltstone.
Tanka-3	10073	Dominated by very fine quartz. Generally sub-rounded and well-sorted therefore areas of good inter grain porosity. Rare carbonate grains and rare feldspar grains. Main bioclasts = forams and shell debris with areas of carbonate cement. Very fine quartz sandstone.
	10068	Dominated by quartz, fine grained, sub-rounded – rounded, moderately sorted >50%. Good inter grain porosity, glauconite grains – generally amorphous. Bioclasts – fine grained, Bryzoa and shell fragments. Very fine quartz sandstone.
	10064	Similar facies as 10068 – the only main difference is partial areas of calcite

		concentration.
	10055	Mainly similar to 10068 and 10064 BUT coarser quartz grains, rounded, poorly sorted, increased bioclasts and carbonate cement.
	10048	Very much more bioclast rich. Quartz grains: fine – very fine, more sorted, sub-angular – rounded 25%. Echinoid spines - Bryzoa, Red Algae shell debris, shell debris, forams, etc aplenty. Carbonate cement – mouldic porosity only. Carbonate/calcarite
	10012	>50% quartz grain, medium size, sub-rounded – rounded, moderately sorted. Good inter grain porosity – little cement. Bioclasts relatively rare, red algae, shell and Bryzoa. Glauconite grains 1-2%.
	9990	5-10% quartz grains. Rounded - sub-rounded, moderately sorted, fine grained. Bioclasts and mud matrix dominate. Bioclasts include: Bryzoa and shell debris, forams etc. Areas of sparite cement. Mouldic porosity only. Packstone.
	9952	Quartz grains, sub-angular – sub-rounded, size range medium – very fine. Poorly sorted. >30% pockets of inter grain porosity, but mainly carbonate cement, bioclasts and glauconite grains. Calc aremite.
	9979.5	Quartz 5-10% Moderately/poorly sorted. Sub-rounded – sub-angular, medium – fine. Bioclasts dominate, thin shells, bryzoa fragments, red algae, echinoid spines and forams. Micritic matrix.
GS 195-3	12274-75	Fining up calcareite sst – siltst very fine – fine. with lamination. Poorly sorted quartz and bioclasts, sub angular at base. All – sub round at base of slide towards top. Less quartz, mud finer, bioclast dominated. All sub angular – sub rounded – much more mud/silt layers. Foram dominated. Base – 15-20% quartz. Looks like 1 deposition event. No evidence of increased grain size or erosive beds
	12272.73	Calc sst. Qtz 30%. Calcite and bioclast dominated. Very poorly sorted, range of grain sizes, coarse to very fine. Sub angular – sub rounded. Little porosity – most bioclasts, Bryzoa etc, altered to meoformed calcite crystals. Similar small amount of glauconite.
	12269-5	Quartz sst from log. Quartz dominated up to 60%. Very poorly sorted – course to very fine. Sub angular – rounded. Bioclasts and patcy calc cement. Better porosity – intragranular . Some quite large bioclasts – Bryzoa. 2% glauconite.
	12264	Log – lam, fine grained – BT area. Qtz dominated > 60% sub angular, sub meld. The rest is calc cement moderate sorted. Bioclastic <5%, glauconite 5%, also rare Biotite. Also Forams and shell debris. Calc cement low porosity.
	11264	Still quartz dominated, but much finer. Very fine sand – silt grade. Qtz = 40-50%. Sb angular – rounded, moderate sorted. Forams, shells etc – see above. BT glauconite. Calc cement low porosity.
	11254-11255	Log facies = calc sst. Bioclastic dom, >25% Qtz. Forams, shell frag – very poorly sorted. Bryzoa – very angular, sub angular. Very rare mouldic porosity. Calcite cement. 1-2% glauconite.

APPENDIX 3: NORTH CENTRAL DIP PROVINCE – OCTOBER AREA

Table 1: Upper Rudeis Stratal Unit 1 Gross Interval thickness (metres)

Well name	X	Y	MDT (M)
ARM-2	824637.0000	686609.0000	20
ARM-3	824679.0000	685233.0000	15
ARS-6	827349.0000	685099.0000	12
AZ13-1	826186.1030	691987.3488	63
C4NA-1	793007.0000	701540.0000	71
C4NA-2	794715.0000	702376.0000	73
C5C-1	798390.9980	674610.0020	48
CLB-1	798869.0000	722662.0000	43
EE81-1	786529.0000	690077.0000	50
EE85-4	822999.0000	698455.0000	20
ET_6	793065.4979	713621.2811	39
ET-2	820207.4337	679008.4599	8
ET-4	821516.9913	678742.3176	106
ET-5	815331.5269	705810.9903	39
ET-5A	815361.1412	705057.5817	102
ET-5A	815361.2361	705056.5587	105
ET-A1	804546.3079	698996.7891	86
ET-A2	804059.4372	699940.4244	82
ET-A3	804786.6990	699949.4937	47
GG83-2	802685.0000	674464.0000	58
GG83-3	802152.0000	670136.0000	58
GH82-6	826201.0000	677017.0000	85
GH82-6	826201.0000	677017.0000	85
GI78-1A	788227.0000	686795.0000	81
GI78-1B	788227.0000	686795.0000	96
GJ78-3	784931.3200	697965.5000	15
GJ79-4	790613.7200	693106.9000	258
GS100-1	794782.0000	728187.0000	119
GS114-1A	788166.0000	717790.0000	13
GS138-1A	810431.8753	705348.2032	177
GS138-1B	810486.0377	705352.8365	175
GS148-1	806051.6331	700338.1113	92
GS160-1	806425.6088	696019.2740	3
GS160-2	806052.3968	695628.0224	3
GS160-4A	807837.3356	695697.2915	41
GS160-4ST1	809174.1600	695255.6000	9
GS172-3	808791.0882	690815.7410	3
GS172-3ST1	810054.0000	690449.0000	0
GS172-4ST1	810053.0000	690460.0000	70
GS173-2	811040.2109	690868.5316	59
GS173-3	811313.6955	692863.0829	80
GS184-4A	812256.1517	687025.4835	143
GS195-3	815513.1782	684528.4996	92
GS196-1	821018.8693	684197.8618	8
GS196-2	820636.0000	680414.0000	4
GS196-3	822155.3821	681752.0371	3
GS197-1	826458.8209	680406.2182	55

GS197-2	825257.6124	681100.9187	46
GS206-1	821047.4851	678430.7982	38
GS206-1A	821044.4915	678431.2164	37
GS207-1	825177.6898	678712.6396	70
GS207-1A	825136.2651	678953.4865	42
GS216-1	829073.0000	674060.0000	118
HA78-5	784813.7800	701300.2300	3
HB77-1	779968.7580	720044.6010	43
HB77-2	779302.0000	718128.0000	7
HB77-3	777394.7600	721689.7900	18
HB77-4	779381.0500	720648.1260	22
HB77-5	780060.4100	720301.9660	24
HB78-2	780561.2680	720726.1540	18
HB78-3	782222.0000	720229.0000	16
HC78-1	786889.7000	726977.9000	95
HH84-1	820277.0000	667558.0000	33
LAGIA-2	799309.0000	725690.0000	93
NEBWI81-1	786481.0000	744838.0000	111
NO124-1	793601.0000	714143.0000	68
NO147-1ST1	801105.6940	703395.6196	110
NO159-1	803889.1276	696300.3368	60
NO159-2	804541.7022	697309.3895	5
NO159-4	804548.5691	697921.1399	67
NO159-5	804772.6885	698130.3234	27
NO159-6ST1	804594.0000	699000.0000	75
NO183-1	809342.0150	689565.4131	132
OCT-B6	816671.9938	685317.1028	46
OCT-C2	815007.1512	688071.5348	75
OCT-C3	816094.0785	686397.9429	37
OCT-C5	815389.7280	687389.9095	52
OCT-C6	816222.2984	685951.8073	10
OCT-C7	815599.1800	686839.7120	45
OCT-D1	810111.3108	690454.0401	2
OCT-D2	809457.0946	690977.6180	19
OCT-D3A	810671.5215	689904.8746	47
OCT-D4	809789.1167	690883.5308	44
OCT-D5	811684.9501	689267.5211	30
OCT-D5A	811299.2392	689643.6187	63
OCT-D6	807948.5493	692182.8537	48
OCT-D9B	812340.1954	687599.6615	98
OCT-D9ST1A	810054.8000	690463.5000	13
OCT-E2	821603.3849	678802.4900	34
OCT-E3	820429.2077	679500.1220	3
OCT-F1	809200.1940	695217.7759	25
OCT-F2	809987.9678	695108.5923	35
OCT-F3	808126.9487	693723.7607	6
OCT-F3B	807483.4411	693345.0830	16
OCT-F3C	807469.4769	693336.3238	16
OCT-G1	817963.0377	681279.5391	30
OCT-G2	817934.4549	681284.9680	42
OCT-G2ST1	817926.7200	681185.1300	59
OCT-G3	818260.2581	680748.4315	12
OCT-G4	817308.1259	682150.8023	41
OCT-G4ST1	817926.7200	681185.1300	49

OCT-G6	818649.3099	680615.3214	18
OCT-G8	817525.5088	681678.3261	19
OCT-H3	817021.5394	682721.6816	78
OCT-H4	816391.2354	684873.8192	61
OCT-H4A	816614.7208	684958.5781	42
OCT-H5	816819.6195	683067.5109	61
OCT-H5BST1	817036.3800	684451.6800	51
OCT-H7	816906.1375	683820.5446	12
OCT-J2ST1	806127.6100	694500.0100	46
OCT-J4ST2	806127.6100	694500.0100	149
OCT-J4ST2A	806127.6100	694500.0100	166
OCT-J5	806948.2013	693418.8802	89
OCT-J6	805137.3847	695552.1040	138
OCT-J6A	805149.8248	695552.8705	134
OCT-J7A	806319.1038	692711.3330	109
SABIL-1	789264.5630	701960.1951	97
TANKA-1	806030.0000	684492.0000	126
TANKA-3	809098.0000	678121.0000	109
TANKA-4	806190.7819	670619.8965	64
THELEMET_NW-1	787624.0000	701336.0000	90
OCT-A1	818537.0000	682966.0000	0
OCT-A10	819339.0000	682645.0000	0
OCT-A11	819311.0000	682937.0000	0
OCT-A2B	817898.0000	683187.0000	0
OCT-A3	817986.0000	682373.0000	0
OCT-A4A	818923.0000	682319.0000	0
OCT-A5B	817673.0000	682826.0000	0
OCT-A6	818225.0000	682188.0000	0
OCT-A7	818504.0000	682523.0000	0
OCT-A8ST1	818534.0000	682871.0000	0
OCT-A9	817931.0000	682880.0000	0
OCT-B1	817608.0000	684770.0000	0
OCT-B2	816963.0000	685616.0000	0
OCT-B3	817533.0000	684110.0000	0
OCT-B4	816873.0000	684716.0000	0
OCT-B5C	817298.0000	683735.0000	0
OCT-B7	817047.0000	684126.0000	0
OCT-B8	817942.0000	684247.0000	0
OCT-B9	818009.0000	683949.0000	0
OCT-B9ST1	817499.0000	684683.0000	0
OCT-C1ST1	816339.0000	687256.0000	0
OCT-K2ST2	818354.0000	682011.0000	0
OCT-K3	818034.0000	681656.0000	0
OCT-K4	818036.0000	682038.0000	0
OCT-K5	818400.0000	681193.0000	0
OCT-K6	818315.0000	682093.0000	0
OCT-K7	818697.0000	681299.0000	0

Table 2: Upper Rudeis Stratal Unit 2 Gross Interval thickness (metres)

Well name	X	Y	MDT (m)
ABU_ZENIMA-1	816765.4097	706799.6446	74
ARM-2	824637.0000	686609.0000	50
ARM-3	824679.0000	685233.0000	51
ARS-6	827349.0000	685099.0000	67
AZ11-1	818864.1348	690110.6435	28
AZ13-1	826187.8037	691988.0353	47
C4NA-1	793007.0000	701540.0000	44
C4NA-2	794715.0000	702376.0000	47
C5C-1	798390.9980	674610.0020	27
CLB-1	798869.0000	722662.0000	16
EE81-1	786529.0000	690077.0000	90
EE85-4	822999.0000	698455.0000	30
ET_6	793076.6243	713629.0458	16
ET-5	815330.4162	705811.9237	27
ET-5A	815357.5809	705093.7222	22
ET-A1	804553.8638	698997.3306	29
ET-A2	804060.9794	699938.9131	47
ET-A3	804780.1638	699922.9516	46
GG83-2	802685.0000	674464.0000	26
GG83-3	802152.0000	670136.0000	13
GH82-6	826201.0000	677017.0000	66
GI78-1	788227.0000	686795.0000	52
GI78-1A	788227.0000	686795.0000	62
GI78-1B	788227.0000	686795.0000	54
GJ78-3	784931.3200	697965.5000	22
GJ79-4	790613.7200	693106.9000	131
GS100-1	794782.0000	728187.0000	53
GS114-1A	788166.0000	717790.0000	15
GS138-1A	810432.9186	705348.7569	46
GS138-1B	810478.9178	705347.4264	49
GS148-1	806052.0071	700340.5100	31
GS160-4A	807854.5250	695696.9301	31
GS172-3A	808116.3318	690343.3140	55
GS172-4ST1	810053.0000	690460.0000	62
GS173-2	811040.6638	690870.8816	21
GS173-3	811313.4421	692863.4356	20
GS184-4A	812239.7612	687014.1611	61
GS195-3	815564.7509	684526.5259	58
GS196-1	821018.9207	684198.0148	13
GS197-1	826458.7138	680404.6471	30
GS197-2	825257.7116	681100.9725	7
GS207-1	825177.6051	678712.1508	15
GS207-1A	825136.6304	678942.5850	18
GS216-1	829073.0000	674060.0000	85
HA78-5	784813.7800	701300.2300	98
HB77-1	779968.7580	720044.6010	130
HB77-2	779302.0000	718128.0000	80
HB77-3	777394.7600	721689.7900	135
HB77-4	779381.0500	720648.1260	127
HB77-5	780060.4100	720301.9660	24
HB78-2	780561.2680	720726.1540	104
HB78-3	782222.0000	720229.0000	115

HC78-1	786889.7000	726977.9000	36
HH84-1	820277.0000	667558.0000	18
NEBWI81-1	786481.0000	744838.0000	73
NO124-1	793601.0000	714143.0000	11
NO147-1ST1	801100.5917	703396.5152	63
NO159-1	803890.1610	696296.5137	82
NO159-4	804548.0337	697919.8333	70
NO159-5	804769.6459	698141.5998	24
NO159-6ST1	804594.0000	699000.0000	27
NO183-1	809364.3016	689613.6660	101
OCT-C2	815032.0609	688050.9214	33
OCT-D2	809463.7931	690972.6036	17
OCT-D6	807988.5459	692150.4614	26
OCT-D9B	812319.4398	687684.0303	32
OCT-E2	821603.6545	678808.9833	9
OCT-F1	809198.8569	695216.1300	12
OCT-F2	809980.3344	695112.9779	9
OCT-F3C	807555.2177	693413.8275	107
OCT-G2ST1	817926.7200	681185.1300	28
OCT-J5	806898.1044	693473.6497	98
OCT-J6	805179.3923	695497.6825	56
OCT-J7A	806321.4832	692754.6257	70
SABIL-1	789265.6531	701964.9197	102
TANKA-1	806030.0000	684492.0000	70
TANKA-2	803269.3617	694118.9474	46
TANKA-3	809098.0000	678121.0000	70
TANKA-4	806192.6185	670620.0308	2
THELEMET_NW-1	787624.0000	701336.0000	87
OCT-A1	818537.0000	682966.0000	0
OCT-A10	819339.0000	682645.0000	0
OCT-A11	819311.0000	682937.0000	0
OCT-A2B	817898.0000	683187.0000	0
OCT-A3	817986.0000	682373.0000	0
OCT-A4A	818923.0000	682319.0000	0
OCT-A5B	817673.0000	682826.0000	0
OCT-A6	818225.0000	682188.0000	0
OCT-A7	818504.0000	682523.0000	0
OCT-A8ST1	818534.0000	682871.0000	0
OCT-A9	817931.0000	682880.0000	0
OCT-B1	817608.0000	684770.0000	0
OCT-B2	816963.0000	685616.0000	0
OCT-B3	817533.0000	684110.0000	0
OCT-B4	816873.0000	684716.0000	0
OCT-B5C	817298.0000	683735.0000	0
OCT-B7	817047.0000	684126.0000	0
OCT-B8	817942.0000	684247.0000	0
OCT-B9	818009.0000	683949.0000	0
OCT-B9ST1	817499.0000	684683.0000	0
OCT-C1ST1	816339.0000	687256.0000	0
OCT-K2ST2	818354.0000	682011.0000	0
OCT-K3	818034.0000	681656.0000	0
OCT-K4	818036.0000	682038.0000	0
OCT-K5	818400.0000	681193.0000	0
OCT-K6	818315.0000	682093.0000	0

OCT-K7	818697.0000	681299.0000	0

Table 3: Upper Rudeis Stratal Unit 3 Gross Interval thickness (metres)

Well name	X	Y	MDT (m)
ABU_ZENIMA-1	816771.6221	706802.4105	2
ARM-2	824637.0000	686609.0000	19
ARM-3	824679.0000	685233.0000	19
ARS-6	827349.0000	685099.0000	12
AZ11-1	818864.4421	690110.6811	11
AZ13-1	826188.9664	691988.4243	27
C4NA-1	793007.0000	701540.0000	15
C4NA-2	794715.0000	702376.0000	19
C5C-1	798390.9980	674610.0020	25
CLB-1	798869.0000	722662.0000	23
EE81-1	786529.0000	690077.0000	4
EE85-4	822999.0000	698455.0000	24
ET_6	793089.4624	713637.9002	47
ET-5	815329.8190	705812.4507	8
ET-5A	815356.4695	705103.9472	13
ET-A1	804556.1054	698997.3115	5
ET-A2	804061.6265	699938.2493	5
ET-A3	804776.4435	699907.4649	7
GG83-2	802685.0000	674464.0000	7
GH82-6	826201.0000	677017.0000	19
GI78-1	788227.0000	686795.0000	20
GI78-1A	788227.0000	686795.0000	9
GI78-1B	788227.0000	686795.0000	16
GJ78-3	784931.3200	697965.5000	9
GJ79-4	790613.7200	693106.9000	9
GS100-1	794782.0000	728187.0000	4
GS114-1A	788166.0000	717790.0000	35
GS138-1A	810433.1664	705348.8802	4
GS138-1B	810477.5089	705346.4362	3
GS148-1	806052.1528	700341.3957	13
GS160-4A	807863.1624	695696.6737	5
GS172-3A	808146.6951	690345.4372	15
GS172-4ST1	810053.0000	690460.0000	29
GS173-2	811040.7796	690871.7052	10
GS173-3	811313.3511	692863.6202	17
GS184-3AST1	816340.0000	687255.0000	3
GS184-4A	812233.2853	687010.1429	21
GS195-3	815587.1076	684525.7684	7
GS196-1	821018.9728	684198.1699	9
GS197-1	826458.4702	680403.3722	40
GS197-2	825257.7589	681100.9876	17
GS207-1	825177.5009	678711.3323	75
GS207-1A	825136.9300	678935.6009	21
GS216-1	829073.0000	674060.0000	15
HA78-5	784813.7800	701300.2300	23
HB77-1	779968.7580	720044.6010	17
HB77-2	779302.0000	718128.0000	16
HB77-3	777394.7600	721689.7900	9
HB77-4	779381.0500	720648.1260	19
HB77-5	780060.4100	720301.9660	16

HB78-2	780561.2680	720726.1540	21
HB78-3	782222.0000	720229.0000	27
HC78-1	786889.7000	726977.9000	49
NEBWI81-1	786481.0000	744838.0000	8
NO124-1	793601.0000	714143.0000	47
NO147-1ST1	801098.2832	703397.1043	8
NO159-1	803890.8010	696294.3863	4
NO159-4	804547.7394	697919.1152	6
NO159-5	804767.7744	698148.4857	7
NO183-1	809375.4947	689637.8927	14
OCT-C2	815040.5306	688044.0038	3
OCT-D2	809469.3447	690968.4897	12
OCT-D9B	812311.2051	687716.7182	14
OCT-E2	821603.7513	678812.6852	15
OCT-F1	809197.9524	695215.1171	13
OCT-F2	809975.8853	695115.5777	17
OCT-F3C	807630.2020	693476.1455	6
OCT-G2ST1	817926.7200	681185.1300	20
OCT-J5	806869.9958	693505.4788	9
OCT-J6	805194.7082	695478.2909	12
SABIL-1	789266.7292	701966.6773	17
TANKA-1	806030.0000	684492.0000	17
TANKA-2	803324.6257	694119.2368	10
TANKA-3	809098.0000	678121.0000	20
THELEMET_NW-1	787624.0000	701336.0000	11
OCT-A1	818537.0000	682966.0000	0
OCT-A10	819339.0000	682645.0000	0
OCT-A11	819311.0000	682937.0000	0
OCT-A2B	817898.0000	683187.0000	0
OCT-A3	817986.0000	682373.0000	0
OCT-A4A	818923.0000	682319.0000	0
OCT-A5B	817673.0000	682826.0000	0
OCT-A6	818225.0000	682188.0000	0
OCT-A7	818504.0000	682523.0000	0
OCT-A8ST1	818534.0000	682871.0000	0
OCT-A9	817931.0000	682880.0000	0
OCT-B1	817608.0000	684770.0000	0
OCT-B2	816963.0000	685616.0000	0
OCT-B3	817533.0000	684110.0000	0
OCT-B4	816873.0000	684716.0000	0
OCT-B5C	817298.0000	683735.0000	0
OCT-B7	817047.0000	684126.0000	0
OCT-B8	817942.0000	684247.0000	0
OCT-B9	818009.0000	683949.0000	0
OCT-B9ST1	817499.0000	684683.0000	0
OCT-C1ST1	816339.0000	687256.0000	0
OCT-K2ST2	818354.0000	682011.0000	0
OCT-K3	818034.0000	681656.0000	0
OCT-K4	818036.0000	682038.0000	0
OCT-K5	818400.0000	681193.0000	0
OCT-K6	818315.0000	682093.0000	0
OCT-K7	818697.0000	681299.0000	0

Table 4: Upper Rudeis Stratal Unit 4 Gross Interval thickness (metres)

Well name	X	Y	MDT (m)
ABU_ZENIMA-1	816776.9032	706804.7618	62
ARM-2	824637.0000	686609.0000	37
ARM-3	824679.0000	685233.0000	60
ARS-6	827349.0000	685099.0000	44
AZ11-1	818864.8241	690110.7228	32
AZ13-1	826191.0458	691989.2101	108
C4NA-1	793007.0000	701540.0000	78
C4NA-2	794715.0000	702376.0000	83
C5C-1	798390.9980	674610.0020	21
CLB-1	798869.0000	722662.0000	14
EE81-1	786529.0000	690077.0000	50
EE85-4	822999.0000	698455.0000	75
ET_6	793102.4448	713646.9326	16
ET-5	815329.2778	705812.9365	24
ET-5A	815355.5546	705112.2333	16
ET-A1	804558.8232	698997.2584	37
ET-A2	804062.2930	699937.5656	48
ET-A3	804772.4691	699890.9463	49
GG83-2	802685.0000	674464.0000	12
GH82-6	826201.0000	677017.0000	26
GI78-1	788227.0000	686795.0000	60
GI78-1A	788227.0000	686795.0000	62
GI78-1B	788227.0000	686795.0000	35
GJ78-3	784931.3200	697965.5000	39
GJ79-4	790613.7200	693106.9000	13
GS100-1	794782.0000	728187.0000	96
GS114-1A	788166.0000	717790.0000	22
GS138-1A	810433.4171	705349.0112	36
GS138-1B	810476.5733	705345.9150	36
GS148-1	806052.2465	700342.4653	34
GS160-4A	807869.4181	695696.4839	21
GS172-3A	808162.6969	690346.5561	22
GS172-4ST1	810053.0000	690460.0000	23
GS173-2	811040.8833	690872.9140	35
GS173-3	811313.2489	692863.8691	23
GS184-3AST1	816340.0000	687255.0000	27
GS184-4A	812228.4643	687007.3965	42
GS195-3	815609.5748	684525.0967	59
GS196-1	821019.0150	684198.2473	10
GS197-1	826458.2459	680402.4082	16
GS197-2	825257.8321	681101.0064	22
GS207-1	825177.3429	678709.9801	15
GS207-1A	825137.2368	678929.2009	15
GS216-1	829073.0000	674060.0000	72
HA78-5	784813.7800	701300.2300	77
HB77-1	779968.7580	720044.6010	50
HB77-2	779302.0000	718128.0000	24
HB77-3	777394.7600	721689.7900	44
HB77-4	779381.0500	720648.1260	38
HB77-5	780060.4100	720301.9660	8
HB78-2	780561.2680	720726.1540	47

HB78-3	782222.0000	720229.0000	25
HC78-1	786889.7000	726977.9000	6
NEBWI81-1	786481.0000	744838.0000	96
NO124-1	793601.0000	714143.0000	8
NO147-1ST1	801096.0035	703397.7214	63
NO159-1	803891.4627	696292.7294	67
NO159-2	804537.3749	697301.3104	73
NO159-4	804547.4997	697918.5304	56
NO159-5	804766.5721	698152.8807	12
NO183-1	809382.6253	689653.0069	56
OCT-C2	815043.2351	688041.7663	8
OCT-D2	809475.4853	690963.9753	20
OCT-D9B	812304.0692	687744.6511	24
OCT-E2	821603.8363	678815.9355	6
OCT-F1	809196.4057	695213.8479	30
OCT-F2	809971.1352	695118.4147	11
OCT-F3C	807657.1140	693499.3520	40
OCT-G2ST1	817926.7200	681185.1300	5
OCT-J5	806853.5030	693524.7760	53
OCT-J6	805199.3409	695472.4255	9
SABIL-1	789267.9574	701967.9456	87
TANKA-1	806030.0000	684492.0000	62
TANKA-2	803375.6986	694119.5042	42
TANKA-3	809098.0000	678121.0000	51
THELEMET_NW-1	787624.0000	701336.0000	133
OCT-A1	818537.0000	682966.0000	0
OCT-A10	819339.0000	682645.0000	0
OCT-A11	819311.0000	682937.0000	0
OCT-A2B	817898.0000	683187.0000	0
OCT-A3	817986.0000	682373.0000	0
OCT-A4A	818923.0000	682319.0000	0
OCT-A5B	817673.0000	682826.0000	0
OCT-A6	818225.0000	682188.0000	0
OCT-A7	818504.0000	682523.0000	0
OCT-A8ST1	818534.0000	682871.0000	0
OCT-A9	817931.0000	682880.0000	0
OCT-B1	817608.0000	684770.0000	0
OCT-B2	816963.0000	685616.0000	0
OCT-B3	817533.0000	684110.0000	0
OCT-B4	816873.0000	684716.0000	0
OCT-B5C	817298.0000	683735.0000	0
OCT-B7	817047.0000	684126.0000	0
OCT-B8	817942.0000	684247.0000	0
OCT-B9	818009.0000	683949.0000	0
OCT-B9ST1	817499.0000	684683.0000	0
OCT-C1ST1	816339.0000	687256.0000	0
OCT-K2ST2	818354.0000	682011.0000	0
OCT-K3	818034.0000	681656.0000	0
OCT-K4	818036.0000	682038.0000	0
OCT-K5	818400.0000	681193.0000	0
OCT-K6	818315.0000	682093.0000	0
OCT-K7	818697.0000	681299.0000	0

Table 5: Upper Rudeis Stratal Unit 5 Gross Interval thickness (metres)

Well name	X	Y	MDT (m)
ABU_ZENIMA-1	816788.7366	706810.0071	64
ARM-2	824637.0000	686609.0000	43
ARM-3	824679.0000	685233.0000	28
ARS-6	827349.0000	685099.0000	26
AZ11-1	818865.4707	690110.7459	37
AZ13-1	826194.2647	691990.4216	105
C2A-1	792147.0000	727847.0000	77
C4NA-1	793007.0000	701540.0000	49
C4NA-2	794715.0000	702376.0000	39
C5C-1	798390.9980	674610.0020	63
CLB-1	798869.0000	722662.0000	41
EE81-1	786529.0000	690077.0000	42
EE82-1A	795154.0000	692845.0000	36
EE85-4	822999.0000	698455.0000	78
EGB-1	793721.0000	693212.0000	11
EGB-2	794727.0000	692618.0000	17
ET_6	793110.2448	713652.4697	22
ET-5	815328.0902	705814.0550	50
ET-5A	815352.8870	705136.0666	67
ET-A1	804564.6161	698997.1417	51
ET-A2	804063.6862	699935.8949	59
ET-A3	804763.0018	699849.7092	97
GG83-2	802685.0000	674464.0000	35
GG83-3	802152.0000	670136.0000	55
GH82-6	826201.0000	677017.0000	26
GI78-1	788227.0000	686795.0000	11
GI78-1A	788227.0000	686795.0000	9
GI78-1B	788227.0000	686795.0000	13
GJ78-2	784412.4000	693761.6000	13
GJ78-3	784931.3200	697965.5000	61
GJ79-4	790613.7200	693106.9000	20
GS100-1	794782.0000	728187.0000	189
GS114-1A	788166.0000	717790.0000	17
GS138-1A	810434.0754	705349.5081	62
GS138-1B	810474.2224	705345.2570	63
GS148-1	806052.3955	700344.7753	61
GS160-1	806426.3166	696022.1792	97
GS160-2	806050.2650	695629.8360	54
GS160-4A	807889.6579	695695.7472	62
GS160-4ST1	809174.1600	695255.6000	176
GS172-3	808802.5493	690814.8497	38
GS172-3A	808260.7111	690354.5561	203
GS172-3ST1	810054.0000	690449.0000	40
GS172-4ST1	810053.0000	690460.0000	241
GS173-2	811041.0990	690876.0875	83
GS173-3	811312.9919	692864.4886	67
GS184-3	814127.9770	687372.1984	30
GS184-3AST1	816340.0000	687255.0000	61
GS184-4A	812219.4845	687002.3074	76
GS195-3	815639.5068	684524.3844	29
GS196-1	821019.0513	684198.2879	7

GS196-3	822156.4027	681750.9046	2
GS197-1	826457.9975	680401.4272	42
GS197-2	825257.8865	681101.0131	10
GS206-1	821048.6548	678429.6961	1
GS206-1A	821045.0265	678430.5839	0
GS207-1	825177.1982	678708.7826	49
GS207-1A	825137.9542	678917.8847	49
GS216-1	829073.0000	674060.0000	39
HA78-4	787644.4220	708533.0120	10
HA78-5	784813.7800	701300.2300	60
HB77-1	779968.7580	720044.6010	10
HB77-2	779302.0000	718128.0000	9
HB77-3	777394.7600	721689.7900	11
HB77-4	779381.0500	720648.1260	12
HB77-5	780060.4100	720301.9660	8
HB78-2	780561.2680	720726.1540	8
HB78-3	782222.0000	720229.0000	7
HC78-1	786889.7000	726977.9000	60
LAGIA-2	799309.0000	725690.0000	132
NEBWI81-1	786481.0000	744838.0000	202
NO124-1	793601.0000	714143.0000	11
NO147-1ST1	801090.8348	703399.1069	87
NO159-1	803893.6538	696289.3311	127
NO159-2	804533.5627	697295.7326	113
NO159-4	804546.8027	697916.8297	122
NO159-5	804762.6561	698166.9812	51
NO159-6ST1	804594.0000	699000.0000	17
NO183-1	809399.1564	689686.3823	95
OCT-B6	816691.8761	685299.6002	35
OCT-C2	815047.6945	688038.0768	10
OCT-C3	816109.3418	686416.0686	11
OCT-C5	815422.5056	687362.8236	7
OCT-C6	816220.7181	685972.9120	21
OCT-C7	815624.7196	686855.5705	27
OCT-D2	809483.2674	690958.2065	19
OCT-D3A	810657.8616	689922.1546	62
OCT-D4	809795.0497	690866.5094	31
OCT-D5A	811260.7631	689666.4409	17
OCT-D6	808002.8891	692139.4157	0
OCT-D7	808467.3492	692594.5235	58
OCT-D7ST2	810053.0000	690460.0000	95
OCT-D8ST1	810053.3600	690460.3600	70
OCT-D9B	812283.9439	687823.1192	82
OCT-D9ST1	810054.8000	690463.5000	164
OCT-E2	821603.8010	678821.2952	26
OCT-F1	809193.8021	695214.3723	76
OCT-F2	809954.3435	695128.4858	84
OCT-F3	808204.7380	693810.1198	99
OCT-F3A	807913.5111	693541.2973	74
OCT-F3AST1	809172.5000	695254.3000	141
OCT-F3B	807727.8367	693571.8346	84
OCT-F3BST1	809172.5000	695254.3000	163
OCT-F3C	807727.8938	693571.7177	85
OCT-G1	817960.0283	681282.8602	3

OCT-G2	817934.5474	681283.1407	23
OCT-G2ST1	817926.7200	681185.1300	5
OCT-G3	818244.0753	680767.3791	19
OCT-G4	817320.9997	682136.0072	14
OCT-G6	818627.0783	680619.1333	8
OCT-H3	817018.9022	682770.0066	16
OCT-H4	816420.8238	684862.1976	20
OCT-H5BST1	817036.3800	684451.6800	3
OCT-J2ST1	806127.6100	694500.0100	105
OCT-J3	806268.4657	694055.1035	102
OCT-J3A	806336.5878	694117.7158	119
OCT-J4ST1	806127.6100	694500.0100	207
OCT-J4ST2	806127.6100	694500.0100	155
OCT-J4ST2A	806127.6100	694500.0100	153
OCT-J4ST2B	806127.6000	694500.0000	55
OCT-J5	806811.3795	693574.0612	101
OCT-J5A	806426.2944	694212.9001	84
OCT-J6	805221.7854	695444.9298	89
OCT-J6A	805222.1877	695444.4444	87
OCT-J7	806728.0359	692033.4896	172
OCT-J7A	806328.6209	692863.3982	144
OCT-J7ST1	806127.6100	694500.0100	243
OCT-J7ST2	806127.6100	694500.0100	231
OCT-J8	806183.2717	694511.9440	38
OCT-J8A	806183.2478	694511.6340	38
OCT-J9	805787.5223	695249.5282	0
SABIL-1	789269.4179	701969.1727	52
TANKA-1	806030.0000	684492.0000	112
TANKA-2	803519.3348	694119.7544	102
TANKA-3	809098.0000	678121.0000	30
TANKA-4	806194.2521	670620.1193	46
THELEMET_NW-1	787624.0000	701336.0000	53
OCT-A1	818537.0000	682966.0000	0
OCT-A10	819339.0000	682645.0000	0
OCT-A11	819311.0000	682937.0000	0
OCT-A2B	817898.0000	683187.0000	0
OCT-A3	817986.0000	682373.0000	0
OCT-A4A	818923.0000	682319.0000	0
OCT-A5B	817673.0000	682826.0000	0
OCT-A6	818225.0000	682188.0000	0
OCT-A7	818504.0000	682523.0000	0
OCT-A8ST1	818534.0000	682871.0000	0
OCT-A9	817931.0000	682880.0000	0
OCT-B1	817608.0000	684770.0000	0
OCT-B2	816963.0000	685616.0000	0
OCT-B3	817533.0000	684110.0000	0
OCT-B4	816873.0000	684716.0000	0
OCT-B5C	817298.0000	683735.0000	0
OCT-B7	817047.0000	684126.0000	0
OCT-B8	817942.0000	684247.0000	0
OCT-B9	818009.0000	683949.0000	0
OCT-B9ST1	817499.0000	684683.0000	0
OCT-C1ST1	816339.0000	687256.0000	0
OCT-K2ST2	818354.0000	682011.0000	0

OCT-K3	818034.0000	681656.0000	0
OCT-K4	818036.0000	682038.0000	0
OCT-K5	818400.0000	681193.0000	0
OCT-K6	818315.0000	682093.0000	0
OCT-K7	818697.0000	681299.0000	0

Table 7: Upper Rudeis Formation gross interval thickness and the presence and thickness of siliciclastic sandstone lithofacies (metres).

(-999 = null value – represents no data coverage)

WELL	X	Y	Upper Rudeis MDT	Silic sand presence (Y/N)	Upper Rudeis Sand MDT
ABU-ZENIMA-1	817870.9993	707759.9973	197	N	0
ARM-2	824637.0000	686609.0000	170	N	0
ARM-3	824679.0000	685233.0000	173	N	0
AZ11-1	818865.0000	690111.0000	108	N	0
AZ13-1	826191.0000	691989.0000	350	N	0
C4NA-1	793007.0000	701540.0000	257	Y	107
C4NA-2	794715.0000	702376.0000	259	Y	186
C5C-1	798391.0000	674610.0000	184	N	0
CLB-1	798869.0000	722662.0000	137	N	0
EE81-1	786529.0000	690077.0000	237	N	0
EE82-1A	795154.0000	692845.0000	201	N	0
EE85-4	822999.0000	698455.0000	227	N	0
EGB-1	793721.0000	693212.0000	55	N	0
EGB-2	794727.0000	692618.0000	113	N	0
ET_6	793086.0000	713636.0000	139	Y	1
ET-4	821521.0000	678746.0000	120	N	0
ET-5	815330.0000	705813.0000	148	N	0
ET-5A	815358.0000	705092.0000	219	N	0
ET-A1	804554.0000	698997.0000	208	-999	-999
ET-A2	804061.0000	699939.0000	241	-999	-999
ET-A3	804773.0000	699892.0000	246	Y	12
GG83-1	803008.0000	676958.0000	100	-999	-999
GG83-2	802685.0000	674464.0000	138	Y	15
GG83-3	802152.0000	670136.0000	134	Y	9

GH82-6	826201.0000	677017.0000	223	-999	-999
GI78-1A	788227.0000	686795.0000	223	-999	-999
GI78-1B	788227.0000	686795.0000	214	-999	-999
GJ78-3	784931.0000	697966.0000	147	Y	16
GJ79-4	790614.0000	693107.0000	430	Y	88
GS100-1	794782.0000	728187.0000	461	N	0
GS101-1	795226.0000	725332.0000	97	N	0
GS114-1A	788166.0000	717790.0000	102	Y	16
GS132-1	781004.0000	706556.0000	2	N	0
GS138-1A	810433.0000	705349.0000	325	N	0
GS138-1B	810481.0000	705349.0000	326	N	0
GS148-1	806052.0000	700341.0000	231	N	0
GS160-1	806426.0000	696022.0000	109	N	0
GS160-2	806051.0000	695629.0000	73	N	0
GS160-4A	807866.0000	695697.0000	160	N	0
GS160-4ST1	809174.0000	695256.0000	199	N	0
GS172-3	808801.0000	690815.0000	45	N	0
GS172-3A	808349.0000	690366.0000	336	N	0
GS172-3ST1	810054.0000	690449.0000	40	N	0
GS172-4ST1	810053.0000	690460.0000	425	N	0
GS173-2	811041.0000	690873.0000	208	N	0
GS173-3	811313.0000	692864.0000	208	N	0
GS184-4A	812240.0000	687014.0000	342	Y	2
GS195-3	815566.0000	684526.0000	245	N	0
GS196-1	821019.0000	684198.0000	47	N	0
GS196-3	822156.0000	681751.0000	29	N	0
GS197-1	826459.0000	680404.0000	184	N	0
GS197-2	825258.0000	681101.0000	102	N	0
GS206-1	821048.0000	678431.0000	62	N	0
GS206-1A	821045.0000	678431.0000	51	N	0
GS207-1	825178.0	678712.0	223	N	0

	000	000			
GS207-1A	825137.000	678935.000	144	N	0
GS216-1	829073.000	674060.000	328	N	0
HA78-4	787644.000	708533.000	294	N	0
HA78-5	784814.000	701300.000	261	Y	79
HB77-1	779969.000	720045.000	251	Y	51
HB77-2	779302.000	718128.000	136	Y	60
HB77-3	777395.000	721690.000	217	Y	49
HB77-4	779381.000	720648.000	219	N	0
HB77-5	780060.000	720302.000	81	N	0
HB78-2	780561.000	720726.000	198	Y	68
HB78-3	782222.000	720229.000	189	N	0
HC78-1	786890.000	726978.000	246	Y	8
HH84-1	820277.000	667558.000	73	-999	-999
LAGIA-2	799309.000	725690.000	369	-999	-999
LAGIA-4	800491.000	728250.000	104	-999	-999
NO124-1	793601.000	714143.000	145	N	0
NO147-1ST1	801099.000	703397.000	331	Y	2
NO159-1	803891.000	696293.000	341	Y	95
NO159-2	804537.000	697301.000	293	Y	13
NO159-4	804548.000	697919.000	320	Y	5
NO159-5	804765.000	698159.000	122	N	0
NO159-6ST1	804594.000	699000.000	127	Y	6
NO183-1	809368.000	689621.000	398	Y	3
OCT-A1	818537.000	682966.000	0	N	0
OCT-A10	819339.000	682645.000	0	N	0
OCT-A11	819311.000	682937.000	0	N	0
OCT-A2B	817898.000	683187.000	0	N	0
OCT-A3	817986.000	682373.000	0	N	0
OCT-A4A	818923.000	682319.000	0	N	0
OCT-A5B	817673.000	682826.000	0	N	0

OCT-A6	818225.0000	682188.0000	0	N	0
OCT-A7	818504.0000	682523.0000	0	N	0
OCT-A8ST1	818534.0000	682871.0000	0	N	0
OCT-A9	817931.0000	682880.0000	0	N	0
OCT-B1	817608.0000	684770.0000	4	N	0
OCT-B2	816963.0000	685616.0000	0	N	0
OCT-B3	817533.0000	684110.0000	0	N	0
OCT-B4	816873.0000	684716.0000	0	N	0
OCT-B5C	817298.0000	683735.0000	0	N	0
OCT-B7	817047.0000	684126.0000	0	N	0
OCT-B8	817942.0000	684247.0000	0	N	0
OCT-B9	818009.0000	683949.0000	0	N	0
OCT-B9ST1	817499.0000	684683.0000	0	N	0
OCT-C1ST1	816339.0000	687256.0000	2	N	0
OCT-C2	815022.0000	688059.0000	128	N	0
OCT-C3	816100.0000	686405.0000	76	N	0
OCT-C5	815401.0000	687380.0000	103	N	0
OCT-C6	816221.0000	685965.0000	41	N	0
OCT-C7	815610.0000	686846.0000	101	N	0
OCT-D1	810111.0000	690454.0000	3	N	0
OCT-D2	809470.0000	690968.0000	87	N	0
OCT-D3A	810664.0000	689914.0000	136	N	0
OCT-D4	809792.0000	690876.0000	96	N	0
OCT-D5A	811285.0000	689652.0000	140	N	0
OCT-D6	807963.0000	692171.0000	75	N	0
OCT-E2	821604.0000	678811.0000	89	N	0
OCT-E3	820430.0000	679500.0000	7	N	0
OCT-F1	809196.0000	695214.0000	156	N	0
OCT-F2	809967.0000	695121.0000	156	N	0
OCT-F3C	807624.0000	693471.0000	254	Y	22
OCT-G2ST1	817927.0	681185.0	117	N	0

	000	000			
OCT-J5	806878.000	693497.000	350	Y	31
OCT-J6A	805174.000	695504.000	304	-999	-999
OCT-J7A	806324.000	692786.000	296	-999	-999
OCT-K2ST2	818354.000	682011.000	383	N	Absent
OCT-K3	818034.000	681656.000	0	N	Absent
OCT-K4	818036.000	682038.000	9	N	Absent
OCT-K5	818400.000	681193.000	0	N	Absent
OCT-K6	818315.000	682093.000	0	N	Absent
OCT-K7	818697.000	681299.000	0	N	Absent
SABIL-1	789266.000	701966.000	356	Y	210
TANKA-1	806030.000	684492.000	388	Y	15
TANKA-2	803224.000	694119.000	-999	Y	4
TANKA-3	809098.000	678121.000	280	Y	8
TANKA-4	806192.000	670620.000	119	N	0
THELEMET_NW-1	787624.000	701336.000	374	Y	134
NEBWI181-1	786481.000	744838.000	491	N	0

Table 8: Upper Rudeis Formation gross depositional environments postings. See Chapter 4 (Table 4.2) for facies key)

(SU = Stratal Unit; -999 = null value – represents no data coverage)

WELL	SU1 FACIES	SU2 FACIES	SU3 FACIES	SU4 FACIES	SU5 FACIES	Markha Anhydrite or equivalent facies
ABU-ZENIMA-1	B1	D	Eroded?	D	D	B3
ARM-2	E	D	F	F	B2	B3
ARM-3	E	D	F	F	B2	B3
AZ11-1	F	F	F	F	B2	B3
AZ13-1	F	D	E	E	B2	B3
C4NA-1	H	G	H	G	H	B3
C4NA-2	H	G	H	G	H	B3
C5C-1	H	G	H	H	B2	B3
CLB-1	F	D	F	F	B2	B3
EE81-1	F	G/D	B1	G/D	F	D
EE82-1A	A1/H	A1/H	A1/H	A1/H	A1/H	B3
EE85-4	F	E	F	F	B2	B3
EGB-1	A	A	A	A1	A1	B3
EGB-2	A	A	A	A1	A1	B3
ET_6	B1	H	B1	B1	B1	B1
ET-4	-999	-999	-999	-999	-999	B3

ET-5	D	D	F	D	F	B3
ET-5A	D	D	F	D	F	B3
ET-A1	F	D	B1	F	B2	B3
ET-A2	F	D	B1	F	B2	B3
ET-A3	F	D	B1	F	B2	B3
GG83-1	-999	-999	-999	-999	-999	-999
GG83-2	B1	G	B1	H	B1	B3
GG83-3	H	G	B1	B1	B2	B3
GH82-6	D	D	B1	F	B2	B3
GI78-1A	H	G	H	G	H	B3
GI78-1B	H	G	H	G	H	B3
GJ78-3	B1	G	H	G	B1	I
GJ79-4	H	G	B1	G	B1	B3
GS100-1	D	D	B1	D	B2	F
GS101-1	-999	-999	-999	-999	-999	E
GS114-1A	B1/A1	G	B1	G	H	G
GS132-1	0	0	0	0	0	0
GS138-1A	D	D	F	E	F	F
GS138-1B	D	D	F	E	F	F
GS148-1	D	D	F	E	B2	B3
GS160-1	A1	A1	A1	A1	B2	B3
GS160-2	A1	A1	A1	A1/F	B1	B3
GS160-4A	E	D	B1	D	B2	A1
GS160-4ST1	B1	E/B2	E/B2	E/B2	B2	B3
GS172-3	A1	A1	A1	A1	B2	B3
GS172-3A	B1	F	B1	F	B2	B3
GS172-3ST1	A1	A1	A1	A1	B2	B3
GS172-4ST1	F	F	B1	F	B2	B3
GS173-2	F	D	H	D	B2	D
GS173-3	F	D	H	D	B2	D
GS184-4A	D	D	F	E	B2	D
GS195-3	D	D	F	E	B2	D
GS196-1	A	A	A	A	A	B3
GS196-3	A/D	A/D	A/D	A/D	A/D	E
GS197-1	E	E	B1	F	B2	B3
GS197-2	E	E	B1	F	B2	B3
GS206-1	B1	D	D	D	D	E
GS206-1A	B1	D	D	D	D	E
GS207-1	B1	F	F	D	B2	B3
GS207-1A	B1	F	F	D	B2	B3
GS216-1	D	D	F	E	B2	B3
HA78-4	-999	-999	-999	-999	-999	G
HA78-5	B1	Fan Delta	B1	Fan Delta	G	G
HB77-1	B1	Fan Delta	B1	Fan Delta	G	Fan delta
HB77-2	A/B1	Fan Delta	H	Fan Delta	G	Fan delta
HB77-3	B1	Fan Delta	B1	Fan Delta	G	Fan delta
HB77-4	B1	Fan Delta	B1	Fan Delta	G	Fan delta
HB77-5	H	Fan	B1	G	B1	Fan delta

		Delta				
HB78-2	H	Fan Delta	B1	Fan Delta	G	Fan delta
HB78-3	H	Fan Delta	B1	Fan Delta	B1	Fan delta
HC78-1	B1	F/H	B1	B1	B1	B1
HH84-1	B1	F	B1	B1	B1	B1
LAGIA-2	-999	-999	-999	-999	-999	-999
LAGIA-4	-999	-999	-999	-999	-999	-999
NO124-1	B1	H	B1	B1	B1	B1
NO147-1ST1	F	D	B1	F	B2	B3
NO159-1	D/H	D/G	B1	E	G	B3
NO159-2	E/B2	E/B2	B1	E/F	B2	B3
NO159-4	B1	D/G	B1	F	B1	B3
NO159-5	F	F	B1	F	B1	B3
NO159-6ST1	B1	G	F	F	B2	B3
NO183-1	D	D	F	E	B2	B3
OCT-A1	Absent	Absent	Absent	Absent	Absent	A1
OCT-A10	Absent	Absent	Absent	Absent	Absent	A1
OCT-A11	Absent	Absent	Absent	Absent	Absent	A1
OCT-A2B	Absent	Absent	Absent	Absent	Absent	A1
OCT-A3	Absent	Absent	Absent	Absent	Absent	A1
OCT-A4A	Absent	Absent	Absent	Absent	Absent	A1
OCT-A5B	Absent	Absent	Absent	Absent	Absent	A1
OCT-A6	Absent	Absent	Absent	Absent	Absent	A1
OCT-A7	Absent	Absent	Absent	Absent	Absent	A1
OCT-A8ST1	Absent	Absent	Absent	Absent	Absent	A1
OCT-A9	Absent	Absent	Absent	Absent	Absent	A1
OCT-B1	Absent	Absent	Absent	Absent	Absent	A1
OCT-B2	Absent	Absent	Absent	Absent	Absent	A1
OCT-B3	Absent	Absent	Absent	Absent	Absent	A1
OCT-B4	Absent	Absent	Absent	Absent	Absent	A1
OCT-B5C	Absent	Absent	Absent	Absent	Absent	A1
OCT-B7	Absent	Absent	Absent	Absent	Absent	A1
OCT-B8	Absent	Absent	Absent	Absent	Absent	A1
OCT-B9	Absent	Absent	Absent	Absent	Absent	A1
OCT-B9ST1	Absent	Absent	Absent	Absent	Absent	A1
OCT-C1ST1	Absent	Absent	Absent	Absent	Absent	A1
OCT-C2	E	D	F	E	A	F
OCT-C3	E	D	F	E	A	F
OCT-C5	E	D	F	E	A	F
OCT-C6	E	D	F	E	A	F
OCT-C7	E	D	F	E	A	F
OCT-D1	0	0	0	0	0	A1
OCT-D2	E	E	E	E	B2	B3
OCT-D3A	-999	-999	-999	-999	-999	-999
OCT-D4	D	D	E/B2	E/B2	D	D
OCT-D5A	-999	-999	-999	-999	-999	-999
OCT-D6	B1	F	E/B2	E/B2	E/B2	Fault cut
OCT-E2	E	D	F	D	D	D
OCT-E3	A1	A1	A1	A1	A1	A1
OCT-F1	B1	D	B1	D	B2	D
OCT-F2	B1	F	B1	F	F	F

OCT-F3C	B1	F	B1	F	F	F
OCT-G2ST1	D	D	B1	E	F	F
OCT-J5	B1	D/G	F	F	B2	B3
OCT-J6A	B1	D/G	F	F	B2	-999
OCT-J7A	B1	D/G	B1	F	B2	B3
OCT-K2ST2	Absent	Absent	Absent	Absent	Absent	A1
OCT-K3	Absent	Absent	Absent	Absent	Absent	A1
OCT-K4	Absent	Absent	Absent	Absent	Absent	A1
OCT-K5	Absent	Absent	Absent	Absent	Absent	A1
OCT-K6	Absent	Absent	Absent	Absent	Absent	A1
OCT-K7	Absent	Absent	Absent	Absent	Absent	A1
SABIL-1	H	G	B1	G	B1	G
TANKA-1	B1	D/H	F	F	B2	B3
TANKA-2	B1	D/H	B1	F	B2	B3
TANKA-3	B1	D/H	B1	F	B1	B3
TANKA-4	B1	F	F	B1	B1	B3
THELEMET_NW-1	H	G	H	G	B1	G
NEBWI181-1	D	D	F	D/E	B1	B3

APPENDIX 4: MORGAN ACCOMMODATION ZONE DATASHEET

Tables 1-4: Borehole data for the Upper Rudeis Formation within the Morgan Accommodation Zone Study (Chapter 5)

Tables 5 & 6: Borehole data for the Kareem Formation within the Morgan Accommodation Zone Study (Chapter 5)

Table 1: Borehole dip data Upper Rudeis Fm

Well	Fm Azimuth	Fm Dip	Wellbore azimuth	Angle from vertical
Abu Durba-1	N/A	N/A	N/A	N/A
Abu Durba115-1	N/A	N/A	N/A	N/A
ALEF-1	045	10	000	0
BDR-A1	270	5	215	1.9
BDR-B1	270	5	268	1.25
BDR-B7	270	5	344	26.4
BDR-B8	250	5	236	8.3
BDR-E1	150	3	5	1.8
EG-2	65	12	253	42
EGJ-1	310	10	091	2.5
EGJ-2	320	6	000	0
EGJ-3	025	10	000	0
ERDMA_W-1	005	17	000	0
ERDMA_W-2	340	18	000	0
ERDMA-1	165	5	300	2
ERDMA-2	N/A	N/A	360	0
ERDMA-4	270	5	160	1
ESM-1	250	10	12	3.2
ESO344-3	220	12	10	1
ESO352-2A	70	20	232	36
ESO352-3	70	20	122	9.2
FARAH-1	270	10	80	17
G-1	0	0	0	0
G-2	0	0	0	0
GA84-10M	270	15	0	0
GA84-12M	215	15	0	0

GA84-13M	300	10	60	32
GAMMA-3	270	17	0	0
GB85-8	220	10	30	21
GB86-7	300	7	177	1.5
Gihan-1	N/A	N/A	000	000
GS269-1	130	20	351	4.2
GS277-1	085	5	263	9
GS277-A1ST1	085	5	N/A	N/A
GS277-A2	N/A	N/A	N/A	N/A
GS277-A3	N/A	N/A	N/A	N/A
GS277-A3A	N/A	N/A	N/A	N/A
GS277-A3ST1	N/A	N/A	N/A	N/A
GS278-1	245	6	49	3
GS285-1	90	12	183	27
GS293-2AST1	050	10	280	30
GS301-1	300	8	321	56
GS302-1	210	10	035	26
GS302-2	075	15	178	19
GS302-3	061	7.5	266	36
GS302-4	082	15	268	40
GS302-5	116	9	264	32
GS302-8	090	10	257	58
GS304-1	060	8	000	0
GS305-2	230	5	39	2
GS306-1	060	5	237	2
GS306-2	095	8	287	3.6
GS311-2ST1	60	25	50	33
GS313-1	260	7	120	3
GS313-2	035	10	087	1.2
GS313-3	250	25	053	6.2
GS316-1	40	6	4	1
GS317-1	340	10	165	1.6
GS323-1	250	28	55.3	46
GS324-2(A1)	240	5	157	5
GS325-2	45	20	233	2.6
GS326-1	220	10	137	1
GS326-2	270	10	60	1.5
GS326-3	240	15	44	36
GS327-1	70	10	267	0.8
GS327-2	260	6	217	1
GS327-A3	N/A	N/A	N/A	N/A

GS327-A5ST1	N/A	N/A	N/A	N/A
GS327-A6	N/A	N/A	N/A	N/A
GS327-A7	N/A	N/A	N/A	N/A
GS334-2	220	15	111	5.1
GS334-3	180	8	0	0
GS334-4ST2	180	8	142	2
GS337-1A	340	17	231	17
GS337-2	230	7	225	1.2
GS344-1AST2	240	10	201	15
GS344-2	225	18	15	7
GS345-1	270	7	348	1
GS345-2(A1)	270	7	85	1
GS345-A2	250	12	52	23
GS345-A4	310	14	93	58
GS346-1	40	10	172	1
GS352-1	90	5	210	1.5
H-1	240	15	0	0
J10-12A	100	21	123	14
J10-14	290	17	096	18
J10-16	075	50	031	28
J10-19	110	25	073	14
J10-33	045	20	104	23
J10-33A	045	20	062	25
J10-33C	060	30	078	18
J10-38A	100	30	002	12
J10-44	090	15	284	19
J10-55	210	10	302	20
J10-55A	210	10	302	20
J10-55B	210	10	195	20
J10-70	060	25	358	26
J10-72	140	20	357	27
J10-88B	270	15	288	23
J10-89	050	25	093	13
J15-18	090	7	211	7
J15-18A	090	7	170	8
J15-24	025	20	310	19
J15-48	065	6	325	19
J15-56	063	30	310	20
J15-56A	055	24	325	21
J15-95	055	20	222	38
J15-97	045	15	255	58
J15-97A	045	15	257	55

J15-97ST	045	15	255	50
J15-98	045	15	250	39
J22-22	060	35	275	4
J22-22A	060	25	274	4
J22-22ST1	065	23	275	4
J22-23B	065	25	338	16.5
J29-29A	045	15	040	30
J3	043	28	087	3
J37-37	165	14	197	8.75
J37-37A	165	14	268	17
J37-40	210	15	085	14
J37-42	160	25	000	0
J37-42A	160	25	000	0
J37-42B	160	25	248	38
J37-43A	090	10	280	24
J37-93	049	28	336	39
J4-47	050	30	275	10
J4-5	N/A	N/A	N/A	N/A
J4-5A	010	50	326	19
J4-71	060	25	112	18
J4-99	140	15	223	52
J53	145	8	340	13
J58-50	090	20	184	20
J58-51	030	8	097	12
J58-52A	230	20	270	31
J58-54	050	25	176	31
J58-58A	047	15	161	4
J58-73	310	12	357	32
J58-73A	350	20	332	27
J58-73B	350	20	333	24
J58-74	075	12	136	31
J58-77	060	15	333	20
J58-77A	060	6	320	49
J58-81	030	9	030	17
J58-81A	030	9	338	13
J58-82	250	25	233	27
J58-84	340	8	299	40
J58-84ST1	340	8	293	36
J58-85	060	15	008	35
J58-87	360	10	304	22
J58-90	355	10	325	41
J58-90A	355	10	323	43
J58-90AST1	014	12	323	48
J62-62	065	30	290	5
J62-63	045	33	128	18

J62-64	090	30	274	12
J62-64A	053	26	267	29
J62-64AST1	053	26	267	28
J62-65	146	41	027	11
J62-66	090	20	326	38
J62-67	135	20	163	22
J62-67A	090	15	230	5
J62-68	060	35	297	28
J62-69	050	20	257	46.5
J62-86	130	10	266	23
J6-34	035	20	009	9
J6-34A	035	20	339	14
J6-34AST	035	20	329	9.5
J6-36	075	25	020	65
J6-36A	090	15	073	15
J6-61	090	10	055	23
J6-7	135	10	340	6
J6-9	100	10	330	10
J6-9A	070	15	336	11
J8-13	070	10	000	0
J8-39	050	25	200	2
J8-41	110	20	302	3
J8-49	070	10	153	7
J8-8	040	20	207	4
J92	045	15	246	42
KK85-1	65	12	000	0
KK86-1A	050	10	090	0.5
LL87-2	045	13	040	8
LL87-3	240	8	1	1
LL87-4	250	15	055	13
LL87-5	260	15	280	2
LL87-6A	290	18	208	12
LL87-SE1	225	5	000	0
M100-132 (GS325-	220	25	203	24
M100-236	220	10	347	51
M1-1	240	15	338	1
M1-121	250	10	40	20
M120-206	220	10	46	21
M120-206A	220	10	39	17
M120-208ST3	300	15	67	24
M1-207	205	8	290	33
M36-70	220	10	90	16
M5-130	350	8	176	14
M-52	210	15	0	0

M-53	45	7	0	0
M5-5	N/A	N/A	58	6.5
M8-8	60	12	262	3
MM86-1A	90	25	235	10
MOUKHTA FY-1	N/A	N/A	0	0
NJ-1	310	10	296	18
NSM-A1	230	15	252	3.5
NSM-A1A	230	15	238	12
NSM-A2	270	10	298	24
NSM-A3A	230	10	288	3
NSM-A4	240	10	163	33
NSM-A5	240	10	294	38
R0-18A	250	35	077	6
R0-19	270	22	046	5
R0-19A	270	25	040	7.5
R1-1	250	12	200	4
R1-2	070	10	157	35.5
R1-21	045	15	054	26.5
R1-29	030	10	200	18
R1-2A	070	10	162	26
R1-34	035	8	284	15.3
R1-42	340	10	275	17.5
R1-49	250	20	262	14
R1-50	250	12	191	4
R1-51	250	12	180	2
R1-52A	050	10	148	24
R22-22	230	20	035	2.5
R24-24	240	14	030	5
R24-26	298	10.2	130	17.5
R24-27	250	20	015	22.7
R24-27A	230	32	015	7.5
R24-28	N/A	N/A	280	19
R24-36	050	10	326	24
R3-11	270	20	130	30
R3-3	270	25	075	7.1
R3-31	280	20	120	34
R3-57	280	35	175	16.5
R4-12	275	15	170	17.5
R4-44	280	12	235	20
R4-47	300	15	196	21
R4-7	305	15	110	4
R5-16	250	13	034	22
R5-17A	250	12	090	25
R5-30	270	15	130	22
R5-37	250	41	180	26

R5-5A	225	20	065	8
R5-5C	225	20	150	7
R5-60	060	5	047	10
R5-9	025	15	039	30
R6-10A	070	5	000	0
R6-20B	070	8	110	34
R6-23A	050	6	095	16.5
R6-32	095	5	347	20
R6-33	050	10	059	10.5
R6-35	050	10	105	16
R6-39	230	10	255	29
R6-40ST1	240	8	215	23
R6-43	290	15	175	14
R6-45	230	15	246	20
R6-53	230	15	240	4
R6-55ST1	200	15	172	21
R6-56A	060	11	094	35
R6-6	063	10	060	5
R6-61	N/A	N/A	N/A	N/A
R6-8	030	10	354	16
R6-8A	030	10	011	23
SB268-1	N/A	N/A	N/A	N/A
SB268-1A	350	15	325	4
SB268-2	N/A	N/A	N/A	N/A
SB276-1A	260	15	78	4
SB276-2	330	18	234	28
SB276-2A	330	18	233	25
SB276-2B	330	18	229	19
SB276-3ST1	N/A	N/A	333	37
SB284-1	290	20	318	3
SB293-1	240	15	330	33
SB293-2	070	18	274	43
SB293-3	070	18	276	52
SB294-1	320	12	252	4
SB294-2	270	12	299	20
SB294-3	280	12	038	6
SB294-4	050	20	320	11
SB296-1	001	12	180	6
SB296-2	050	15	313	18
SB297-1	045	10	066	21
SB305-A1	60	10	238	3
SG120-3	N/A	N/A	000	0
SG300-11	090	35	305	28
SG300-12	090	35	260	34
SG300-4	080	30	228	2.9

SG300-5	040	12	306	47
SG300-7	120	25	337	30
SG300-8	115	25	044	16.5
SG300-8ST1	115	25	040	18
SG300-9	100	10	355	36
SG300-9A	100	20	019	26
SG300-9B	100	20	051	32
SG310-10AST1	050	30	267	25
SG310-11	090	30	275	41
SG310-1B	045	25	211	17
SG310-2	063	24	216	8
SG310-3ST2	300	15	278	33
SG310-4	080	18	254	32
SG310-5	055	15	214	40
SG310-5A	055	15	235	4.8
SG310-5C	055	15	244	30
SG310-6	065	30	252	55
SG310-6A	065	30	246	59
SG310-7	230	30	243	43.3
SG310-7A	060	25	238	25.6
SG310-8	080	18	234	32
SG310-9ST1	065	30	253	53
SGOFFSH-2	090	45	225	9
SHM-1A	215	10	0	0
SHM-2	90	15	0	0
SHM-3	160	20	0	0
SHM-4	75	4	0	0
SHM-4A	75	4	0	0
SRM-1A	250	15	000	0
SRM-2	310	12	130	1.4
WADI_DARA_M-1	280	35	0	0
WADI_DARA_M-2	280	35	0	0

Table 2: Upper Rudeis Fm Stratal Unit A: Gross interval and net reservoir (metres)

			Gross Interval		PHIE>10% NetRes
Well	X	Y	MDT	TST	TST
ALEF-1	843566.7500	623793.4380	82	80	-999
BDR-B1	856936.7500	616776.7500	23	23	0
BDR-B7	856751.1250	617674.6880	28	25	-999
BDR-B8	856276.8750	616469.4380	23	22	0
BDR-E1	855321.2500	616735.6250	13	13	0
EG-2	829387.0620	627781.5000	0	0	0
EGJ-1	833345.9380	625927.6250	42	41	0
EGJ-2	832933.6250	627019.8750	49	48	0
EGJ-3	831885.2500	626242.4380	19	19	0
ERDMA_W-2	841041.0000	613039.0000	130	124	0
ERDMA-1	844498.7500	612521.5000	135	135	2
ESM-1	851076.6250	607125.8750	101	99	10
ESO344-3	859484.3750	602965.8120	35	34	0
ESO352-2A	852968.1250	598128.4380	31	30	-999
ESO352-3	849178.2500	599836.8120	14	12	0
FARAH-1	849678.7500	604396.8120	84	83	0
G-1	873268.0000	605534.0000	0	0	0
G-2	871086.0000	606302.0000	0	0	0
GA84-10M	849454.0000	598021.0000	17	16	-999
GA84-12M	850253.0000	596132.0000	29	28	0
GA84-13M	849680.5000	598125.3750	18	16	-999
GAMMA-3	849421.5000	598246.5000	20	19	-999
GB85-8	859258.9380	604091.8750	37	37	8
GB86-7	864515.5620	612616.3750	5	5	1
GS269-1	841650.5000	641732.2500	34	33	3
GS277-1	840407.4380	636177.3120	95	95	13
GS278-1	846691.8120	636636.1880	78	78	3
GS285-1	840319.3750	634801.6880	125	110	7
GS293-2AST1	835972.5620	626677.9380	69	63	2
GS301-1	833149.3120	624564.1250	44	20	0
GS302-1	836131.7500	624064.7500	27	26	0
GS302-2	837774.8750	625004.6250	55	51	0
GS302-3	838913.3120	623482.8750	82	71	0
GS302-4	839766.5000	622879.6250	100	91	3
GS302-5	839996.1880	621575.4380	55	50	0
GS302-8	837956.5000	624389.8120	101	67	0
GS304-1	845194.0000	620380.5620	148	147	-999
GS305-2	853527.3750	620947.6250	15	15	0

GS311-2ST1	838969.2500	617979.2500	143	76	0
GS313-1	846599.5620	618426.3750	135	134	-999
GS313-2	845109.8750	618542.9380	73	72	-999
GS313-3	847006.3120	615989.1250	33	31	0
GS316-1	860672.4380	617208.9380	10	10	0
GS317-1	868471.3750	618661.5620	4	4	0
GS323-1	847333.5000	613326.6250	137	128	-999
GS324-2(A1)	850825.7500	614264.7500	21	21	0
GS326-1	860577.8750	614762.3120	16	15	4
GS326-3	864323.9380	610933.1250	73	68	17
GS327-1	867419.1250	612134.0000	13	13	0
GS327-2	867763.5000	613547.3750	29	29	3
GS327-A3	867074.5000	614594.1880	15	-999	-999
GS327-A5ST1	867037.6250	615242.8120	16	-999	-999
GS327-A6	866683.5620	612002.5000	14	-999	-999
GS327-A7	867498.8750	613172.8750	22	-999	-999
GS334-2	853498.1880	607799.1250	150	145	3
GS334-3	853007.0000	606616.0000	135	134	-999
GS334-4ST2	851364.7500	610033.8120	138	136	0
GS337-1A	869407.6880	606204.6250	81	77	0
GS337-2	865627.4380	607284.0000	53	52	2
GS344-1AST2	858892.5620	602373.8750	40	36	-999
GS344-2	858493.4380	600712.7500	18	18	0
GS345-1	860820.0620	603022.9380	34	34	0
GS345-A2	865279.5000	601242.3120	20	19	1
GS345-A4	866665.5000	600447.6880	23	16	0
GS346-1	866607.8750	601133.4380	23	22	0
GS352-1	851349.1880	598058.8750	88	88	-999
H-1	865772.0000	612827.0000	9	9	-999
J10-16	836637.8750	618752.3750	64	20	0
J10-33	837404.0620	617761.3120	86	69	0
J10-33A	837419.3750	617947.0000	52	37	-999
J10-33C	837365.6880	617912.6250	60	41	0
J10-44	835327.7500	617938.8120	65	65	0
J10-70	836634.1250	618654.0620	30	22	0
J10-72	836290.0000	618760.2500	53	51	0
J15-18	835776.9380	619536.9380	48	47	-999
J15-18A	835834.9380	619523.8750	32	32	0
J15-24	835569.0000	620318.6880	49	42	-999
J15-48	835587.3120	620978.3750	54	51	0
J15-56	835659.0000	620455.1880	40	35	-999
J15-56A	835793.9380	620602.1250	88	75	0
J15-97	835621.5000	619380.1880	131	92	-999

J22-22	837178.6250	619496.1880	36	31	-999
J22-22A	837179.4380	619497.1250	37	35	-999
J22-22ST1	837179.4380	619497.1250	37	34	0
J22-23B	836894.9380	620146.7500	39	34	0
J29-29A	835098.8120	619024.7500	54	38	0
J3	834776.1880	626244.5620	60	52	0
J37-37A	834804.8120	618238.2500	52	49	0
J37-42B	835873.7500	618701.8120	37	26	-999
J37-43A	834144.9380	618764.4380	59	57	0
J4-71	836794.4380	619396.6250	34	27	0
J53	834915.0000	620126.0620	30	30	0
J58-50	835043.6880	621894.1250	8	7	0
J58-51	835527.8120	622477.5000	42	40	0
J58-52A	834154.0000	622445.9380	41	28	5
J58-58A	835048.3120	622561.5620	47	45	0
J58-73	835026.3750	623538.3120	19	14	1
J58-73B	834713.4380	623389.6250	18	13	0
J58-74	836106.8750	621895.1250	53	42	0
J58-77	834786.8120	623045.2500	27	24	0
J58-81	835421.3750	622993.3120	34	31	0
J58-84	833974.3750	623051.9380	50	34	-999
J58-84ST1	833988.3120	623033.5620	42	32	0
J58-85	835357.9380	623797.5000	35	25	0
J58-87	834390.8120	622665.0000	28	24	0
J58-90AST1	833724.1880	623472.1880	62	34	5
J62-63	839372.7500	616417.6880	19	15	0
J62-64	838294.5620	617345.1880	49	47	0
J62-64A	838061.0000	617277.9380	37	35	0
J62-64AST1	838061.1250	617277.9380	37	35	-999
J62-65	838797.5000	617396.3750	55	44	0
J62-66	837905.9380	618348.9380	57	49	-999
J62-67	838860.1880	616575.9380	18	14	0
J6-34	837373.6250	617630.8120	75	66	0
J6-34A	837347.5620	617633.0620	72	62	0
J6-34AST	837324.8120	617620.6250	143	129	-999
J6-36A	837768.0620	617408.0620	55	48	-999
J6-61	838086.2500	617949.8750	103	88	0
J8-39	836780.4380	617661.0620	34	31	0
J8-41	836970.5000	618334.6880	52	50	0
J8-49	837089.8120	618245.1880	65	64	0
KK85-1	829973.6250	627893.5000	0	0	0
KK86-1A	835453.5000	626654.9380	56	55	0
LL87-2	843914.5620	619787.1250	183	170	0

LL87-4	846507.6880	614919.6250	103	102	2
LL87-5	848302.5620	612120.3750	125	119	15
LL87-6A	844027.5620	616811.6250	159	147	2
LL87-SE1	845988.0000	614302.0000	139	139	21
M100-132 (GS325-	855433.7500	613015.0000	16	10	0
M100-236	855150.7500	615109.4380	8	5	0
M1-1	853976.1250	615926.8120	19	18	-999
M120-206	854281.5000	616095.1250	16	16	-999
M120-206A	854240.6250	616073.7500	16	16	0
M120-208ST3	854777.7500	616011.4380	9	8	0
M36-70	856798.3750	610857.4380	10	10	3
M5-130	852608.6880	614963.6250	9	9	0
M-52	861858.0000	608519.0000	10	9	0
M-53	858058.0000	615839.0000	3	3	0
M8-8	858241.5000	611573.8750	7	7	4
MM86-1A	841910.3750	607179.0000	28	27	0
MOUKHTAFY-1	823247.4380	645284.5000	67	-999	-999
NJ-1	833381.1250	625860.3750	44	39	0
NSM-A1	863249.6250	606946.8120	89	84	42
R0-18A	840600.5620	623877.2500	89	78	5
R0-19	840821.5000	622196.6880	98	93	-999
R0-19A	840823.8750	622200.2500	119	112	0
R1-1	842104.8120	623034.0620	148	143	0
R1-2	843052.6880	621774.6250	154	123	-999
R1-29	842008.3120	622835.9380	117	116	-999
R1-34	841946.6880	623086.0620	34	34	-999
R1-42	841637.3750	623085.3120	127	117	-999
R1-49	841059.8120	622657.5620	174	144	9
R1-52A	842740.5000	622461.4380	180	164	20
R22-22	842822.4380	620964.9380	62	59	0
R24-27	841015.3750	622420.0000	72	68	-999
R24-27A	841311.1880	622553.8750	73	65	0
R24-28	841486.1250	621974.4380	71	-999	-999
R24-36	841555.8750	622111.5620	43	38	0
R3-11	841291.5620	623558.5000	37	35	0
R3-3	841099.5620	623713.1880	69	66	0
R3-31	841177.0000	623703.5000	83	80	0
R3-57	841296.5000	622983.2500	97	80	1
R4-12	841248.8120	624586.6250	134	126	0
R4-44	841111.5620	624751.3120	124	108	0
R4-47	841163.3750	624525.5000	123	113	0
R4-7	841261.1880	624840.5620	74	73	0

R5-16	841781.3750	622855.5000	192	187	-999
R5-17A	841896.3750	622501.5620	206	200	0
R5-30	841878.9380	622220.1250	132	128	0
R5-37	841497.0000	621852.6880	119	69	-999
R5-5A	841681.8120	622407.6880	126	123	0
R5-5C	841682.1880	622389.8750	129	119	0
R5-60	842337.2500	622732.4380	87	84	-999
R5-9	841858.6880	623194.6250	245	175	-999
R6-10A	842788.5000	621531.0000	139	138	0
R6-20B	842950.5000	621469.1880	217	165	-999
R6-23A	843379.6880	621347.5620	179	167	16
R6-32	842586.0000	621923.5620	173	164	0
R6-33	842734.0000	621706.5620	162	152	0
R6-35	842956.3750	621634.5000	179	165	0
R6-39	841764.8750	621004.0000	77	60	-999
R6-40ST1	842141.8120	620820.5000	4	3	0
R6-43	842450.6880	620606.9380	39	38	0
R6-45	841970.2500	620954.6250	56	46	-999
R6-53	843006.3750	621527.1880	168	159	-999
R6-55ST1	843062.2500	620771.5620	161	132	0
R6-56A	844231.8750	621171.8120	179	127	-999
R6-6	842766.5000	621598.5000	157	151	0
R6-8	842656.6250	621793.5000	166	151	-999
R6-8A	842717.6250	621731.1250	179	151	0
SB268-1A	837366.3750	642579.5000	119	113	-999
SB276-1A	839823.1880	635831.4380	78	76	2
SB276-2	838907.3750	635098.7500	57	49	-999
SB276-2B	838933.6250	635115.5000	56	52	11
SB284-1	839993.1250	632842.9380	80	74	2
SB293-1	840065.0000	625707.4380	145	117	0
SB293-2	838570.1880	625187.4380	72	64	9
SB293-3	837858.6880	625171.5620	79	63	0
SB294-1	840355.3750	627375.4380	130	126	0
SB294-2	840565.0000	625397.9380	110	94	4
SB294-3	840528.7500	625154.3750	65	64	-999
SB294-4	840813.0620	625174.7500	76	70	0
SB296-1	851151.9380	629282.3750	53	52	0
SB296-2	853378.8120	625142.8750	4	4	-999
SB297-1	856243.7500	625654.2500	83	72	12
SB305-A1	854577.1880	624478.5620	16	16	0
SG120-3	831296.0000	613089.0000	213	-999	-999
SG300-12	825513.4380	624387.3120	12	11	-999
SG300-1A	825896.8120	624473.4380	0	0	0

SG300-2B	825941.8120	624502.4380	0	0	0
SG300-5	825077.3120	624968.8750	0	0	0
SG300-6A	825861.5620	624204.0000	0	0	0
SG300-7	825550.7500	624988.7500	1	1	0
SG310-10AST1	833089.8750	618962.8750	51	49	4
SG310-11	832952.2500	619198.1250	59	58	10
SG310-4	833404.1250	618334.3750	57	55	0
SG310-5A	833909.8750	617820.6250	73	72	11
SG310-5C	833389.3120	617974.9380	73	70	-999
SG310-6	832285.0000	618097.5000	183	166	20
SG310-7	834651.3120	616935.4380	37	37	0
SG310-7A	834763.4380	616970.3750	46	46	0
SGOFFSH-2	828256.6880	622238.0000	2	2	0
SHM-1A	839965.1250	607018.3120	23	22	-999
SHM-2	838491.0000	608806.0000	66	64	0
SHM-3	837050.0000	607100.0000	82	77	-999
SHM-4	841175.0000	606675.0000	18	18	-999
SHM-4A	841126.0000	606671.0000	22	22	-999
SRM-1A	845737.0000	616179.0000	162	156	10
SRM-2	845345.9380	617259.4380	139	137	1
WADI_DARA_M-1	848196.0000	598946.0000	21	17	0
WADI_DARA_M-2	848599.8750	599093.0000	24	20	0

Table 3: Upper Rudeis Fm Stratal Unit B: Gross Interval and Net reservoir (metres)

			Gross Interval		PHIE>10 % NetRes
Well	X	Y	MDT	TST	TST
ALEF-1	843567.0000	623797.0000	31	30	-999
BDR-A1	855152.0000	618351.0000	45	45	12
BDR-B1	856938.0000	616777.0000	51	50	10
BDR-B7	856764.0000	617629.0000	104	91	-999
BDR-B8	856280.0000	616472.0000	27	27	5
BDR-E1	855321.0000	616734.0000	70	70	14
EG-2	829395.0000	627784.0000	0	0	0
EGJ-1	833345.0000	625928.0000	21	20	7
EGJ-2	832931.0000	627021.0000	28	28	5
EGJ-3	831885.0000	626243.0000	13	13	2
ERDMA_W-2	841041.0000	613039.0000	50	48	-999
ERDMA-1	844500.0000	612520.0000	101	101	2
ERDMA-2	866253.0000	586057.0000	43	-999	-999
ESM-1	851076.0000	607123.0000	48	48	0
ESO344-3	859484.0000	602963.0000	91	89	26
ESO352-2A	852974.0000	598134.0000	18	17	-999
ESO352-3	849171.0000	599840.0000	57	51	5
FARAH-1	849668.0000	604395.0000	39	39	0
G-1	873268.0000	605534.0000	0	0	0
G-2	871086.0000	606302.0000	0	0	0
GA84-10M	849454.0000	598021.0000	30	29	-999
GA84-12M	850253.0000	596132.0000	18	17	0
GA84-13M	849666.0000	598119.0000	30	27	-999
GAMMA-3	849425.0000	598235.0000	31	30	-999
GB85-8	859231.0000	604043.0000	149	146	107
GB86-7	864516.0000	612618.0000	74	74	67
GS269-1	841650.0000	641726.0000	48	46	4
GS277-1	840408.0000	636178.0000	27	27	2
GS278-1	846690.0000	636636.0000	31	31	-999
GS285-1	840322.0000	634815.0000	30	27	10
GS293-2AST1	835984.0000	626676.0000	24	22	0
GS301-1	833162.0000	624548.0000	25	11	1
GS302-1	836126.0000	624057.0000	24	23	0
GS302-2	837775.0000	625014.0000	29	27	13
GS302-3	838935.0000	623484.0000	38	33	15
GS302-4	839816.0000	622881.0000	75	68	13
GS302-5	840026.0000	621578.0000	60	54	5
GS302-8	837980.0000	624395.0000	28	19	-999

GS305-2	853527.0000	620947.0000	32	32	5
GS311-2ST1	838969.0000	617979.0000	27	14	-999
GS313-1	846595.0000	618431.0000	88	87	-999
GS313-2	845110.0000	618546.0000	74	73	0
GS313-3	847000.0000	615985.0000	56	53	0
GS316-1	860672.0000	617207.0000	113	112	87
GS317-1	868471.0000	618663.0000	54	54	15
GS323-1	847281.0000	613294.0000	88	82	-999
GS324-2(A1)	850823.0000	614270.0000	69	68	2
GS326-1	860576.0000	614765.0000	154	151	105
GS326-3	864291.0000	610899.0000	81	75	54
GS327-1	867420.0000	612134.0000	28	28	0
GS327-2	867764.0000	613548.0000	36	36	15
GS327-A3	867102.0000	614549.0000	73	-999	-999
GS327-A5ST1	867076.0000	615162.0000	104	-999	-999
GS327-A6	866710.0000	612042.0000	57	-999	-999
GS327-A7	867505.0000	613181.0000	44	-999	-999
GS334-2	853493.0000	607800.0000	64	62	21
GS334-3	853007.0000	606616.0000	53	52	-999
GS334-4ST2	851364.0000	610035.0000	38	37	0
GS337-1A	869418.0000	606213.0000	55	52	15
GS337-2	865628.0000	607284.0000	73	72	44
GS344-1AST2	858897.0000	602391.0000	107	98	-999
GS344-2	858486.0000	600693.0000	124	121	13
GS345-1	860820.0000	603021.0000	97	96	53
GS345-A2	865274.0000	601239.0000	25	24	6
GS345-A4	866658.0000	600450.0000	19	13	2
GS346-1	866608.0000	601134.0000	21	21	4
GS352-1	851349.0000	598059.0000	57	57	-999
H-1	865772.0000	612827.0000	46	45	-999
J10-12A	837577.0000	617982.0000	79	65	-999
J10-14	836921.0000	617930.0000	55	55	-999
J10-16	836634.0000	618745.0000	18	5	0
J10-33	837361.0000	617774.0000	120	95	54
J10-33A	837371.0000	617921.0000	129	92	-999
J10-33C	837336.0000	617908.0000	109	74	0
J10-44	835346.0000	617934.0000	58	58	17
J10-55B	835438.0000	617570.0000	76	66	37
J10-70	836633.0000	618651.0000	9	7	0
J10-72	836290.0000	618744.0000	36	34	0
J15-18	835778.0000	619539.0000	23	23	0
J15-18A	835834.0000	619527.0000	27	26	0
J15-24	835578.0000	620311.0000	34	29	-999

J15-48	835590.0000	620974.0000	18	17	0
J15-56	835665.0000	620450.0000	23	21	-999
J15-56A	835798.0000	620597.0000	19	16	0
J15-97	835662.0000	619388.0000	45	32	-999
J15-97A	835629.0000	619808.0000	105	77	-999
J15-97ST	835685.0000	619402.0000	29	23	-999
J15-98	835747.0000	619815.0000	15	14	-999
J22-22	837179.0000	619496.0000	6	5	-999
J22-22A	837180.0000	619497.0000	7	6	-999
J22-22ST1	837180.0000	619497.0000	7	6	0
J22-23B	836896.0000	620145.0000	8	7	0
J29-29A	835093.0000	619017.0000	19	14	0
J3	834776.0000	626244.0000	15	13	0
J37-37	835143.0000	618355.0000	11	10	-999
J37-37A	834821.0000	618238.0000	58	54	21
J37-40	836125.0000	619119.0000	13	13	-999
J37-42B	835889.0000	618708.0000	29	2	-999
J37-43A	834166.0000	618761.0000	59	57	21
J37-93	835068.0000	620145.0000	35	21	-999
J4-71	836790.0000	619398.0000	15	12	0
J53	834917.0000	620122.0000	19	19	7
J58-50	835044.0000	621901.0000	20	18	2
J58-51	835525.0000	622478.0000	14	14	0
J58-52A	834173.0000	622446.0000	26	17	10
J58-58A	835048.0000	622563.0000	14	14	1
J58-73	835027.0000	623521.0000	23	17	2
J58-73B	834717.0000	623383.0000	18	13	0
J58-74	836103.0000	621899.0000	10	8	0
J58-77	834789.0000	623041.0000	15	14	1
J58-77A	833761.0000	623918.0000	22	15	2
J58-81	835419.0000	622989.0000	17	15	3
J58-84	833990.0000	623043.0000	26	18	13
J58-84ST1	833999.0000	623029.0000	23	17	11
J58-85	835356.0000	623786.0000	21	15	2
J58-87	834397.0000	622661.0000	18	16	6
J58-90A	833821.0000	623347.0000	38	23	12
J58-90AST1	833743.0000	623448.0000	41	23	12
J62-63	839371.0000	616419.0000	7	5	0
J62-64	838297.0000	617345.0000	12	12	0
J62-64A	838099.0000	617280.0000	79	76	31
J62-64AST1	838099.0000	617280.0000	79	76	-999
J62-65	838795.0000	617392.0000	26	21	0
J62-66	837927.0000	618317.0000	72	62	-999

J62-67	838857.0000	616587.0000	30	23	0
J6-34	837372.0000	617618.0000	73	65	-999
J6-34A	837354.0000	617614.0000	73	63	-999
J6-34AST	837329.0000	617614.0000	45	41	-999
J6-36A	837737.0000	617399.0000	109	95	47
J6-61	838077.0000	617943.0000	30	26	20
J6-7	836668.0000	616453.0000	77	77	20
J8-41	836972.0000	618334.0000	34	32	25
J8-49	837087.0000	618252.0000	59	58	-999
J92	835267.0000	619655.0000	20	18	-999
KK85-1	829974.0000	627896.0000	0	0	0
KK86-1A	835453.0000	626655.0000	23	22	2
LL87-2	843910.0000	619781.0000	85	79	0
LL87-4	846496.0000	614911.0000	66	65	2
LL87-5	848306.0000	612122.0000	76	73	-999
LL87-6A	844028.0000	616824.0000	88	81	1
LL87-SE1	845988.0000	614302.0000	87	87	25
M100-132 (GS325-	855440.0000	613041.0000	69	46	2
M100-236	855169.0000	615034.0000	100	70	8
M1-1	853977.0000	615926.0000	67	64	-999
M1-121	854845.0000	617160.0000	-999	-999	-999
M120-206	854266.0000	616081.0000	62	61	-999
M120-206A	854227.0000	616058.0000	70	70	4
M120-208ST3	854748.0000	615999.0000	69	66	21
M1-207	852977.0000	616429.0000	89	73	4
M36-70	856771.0000	610858.0000	102	100	60
M5-130	852608.0000	614967.0000	16	16	-999
M-52	861858.0000	608519.0000	84	81	-999
M-53	858058.0000	615839.0000	83	82	-999
M5-5	852686.0000	615633.0000	33	-999	-999
M8-8	858244.0000	611574.0000	67	66	-999
MM86-1A	841915.0000	607186.0000	37	35	0
MOUKHTAFY-1	823283.0000	645303.0000	97	-999	-999
NJ-1	833387.0000	625857.0000	22	19	5
NSM-A1	863259.0000	606949.0000	94	90	117
NSM-A1A	863232.0000	606985.0000	-999	-999	-999
NSM-A2	862827.0000	607461.0000	-999	-999	-999
NSM-A4	863651.0000	606511.0000	-999	-999	-999
R0-18A	840594.0000	623873.0000	72	63	2
R0-19	840817.0000	622193.0000	70	66	-999
R0-19A	840818.0000	622194.0000	70	66	2
R1-1	842107.0000	623038.0000	38	37	0
R1-2	843035.0000	621819.0000	83	66	-999

R1-29	842018.0000	622864.0000	87	86	-999
R1-2A	842998.0000	621905.0000	78	69	-999
R1-34	841960.0000	623083.0000	45	44	0
R1-42	841664.0000	623082.0000	85	78	0
R1-49	841086.0000	622663.0000	96	80	8
R1-52A	842721.0000	622492.0000	89	81	10
R22-22	842821.0000	620963.0000	55	52	5
R24-27	841019.0000	622417.0000	12	11	-999
R24-27A	841311.0000	622552.0000	11	10	0
R24-28	841494.0000	621973.0000	24	-999	-999
R24-36	841557.0000	622110.0000	5	5	0
R3-11	841289.0000	623561.0000	7	7	0
R3-57	841296.0000	622988.0000	18	15	5
R4-12	841250.0000	624606.0000	69	65	0
R4-44	841134.0000	624771.0000	82	71	0
R4-47	841170.0000	624549.0000	70	65	0
R4-7	841257.0000	624843.0000	72	70	0
R5-16	841772.0000	622834.0000	41	40	-999
R5-17A	841878.0000	622499.0000	49	48	0
R5-30	841860.0000	622238.0000	62	60	0
R5-37	841497.0000	621857.0000	10	6	0
R5-5A	841671.0000	622403.0000	28	27	0
R5-5C	841678.0000	622399.0000	30	27	0
R5-60	842327.0000	622722.0000	91	87	-999
R5-9	841833.0000	623163.0000	83	59	-999
R6-10A	842783.0000	621532.0000	73	72	0
R6-20B	842920.0000	621478.0000	69	52	2
R6-23A	843356.0000	621349.0000	75	70	8
R6-32	842592.0000	621897.0000	80	75	0
R6-33	842721.0000	621698.0000	76	71	0
R6-35	842936.0000	621644.0000	76	69	0
R6-39	841785.0000	621009.0000	24	19	-999
R6-40ST1	842146.0000	620826.0000	20	17	0
R6-43	842450.0000	620614.0000	26	25	0
R6-45	841985.0000	620961.0000	47	39	-999
R6-53	843006.0000	621529.0000	71	68	-999
R6-55ST1	843059.0000	620796.0000	67	55	0
R6-56A	844175.0000	621172.0000	89	63	-999
R6-6	842762.0000	621594.0000	70	67	0
R6-8	842658.0000	621771.0000	78	70	-999
R6-8A	842710.0000	621691.0000	100	84	0
SB268-1A	837370.0000	642576.0000	67	64	39
SB276-1A	839822.0000	635831.0000	24	24	9

SB276-2	838920.0000	635109.0000	37	32	-999
SB276-2B	838939.0000	635120.0000	30	27	7
SB276-3ST1	839529.0000	637685.0000	41	-999	-999
SB284-1	839993.0000	632843.0000	12	12	0
SB293-1	840074.0000	625690.0000	37	30	0
SB293-2	838609.0000	625185.0000	57	51	22
SB293-3	837900.0000	625167.0000	53	43	24
SB294-1	840357.0000	627374.0000	70	68	0
SB294-2	840573.0000	625393.0000	28	24	9
SB294-3	840525.0000	625151.0000	18	18	0
SB294-4	840820.0000	625170.0000	42	39	0
SB296-1	851152.0000	629290.0000	69	68	0
SB296-2	853381.0000	625140.0000	12	11	0
SB297-1	856219.0000	625644.0000	81	70	8
SB305-A1	854578.0000	624479.0000	21	21	2
SG120-3	831296.0000	613089.0000	181	-999	-999
SG300-12	825515.0000	624388.0000	3	3	1
SG300-1A	825897.0000	624473.0000	0	0	0
SG300-2B	825942.0000	624502.0000	0	0	0
SG300-4	826694.0000	625144.0000	0	0	0
SG300-6A	825862.0000	624204.0000	0	0	0
SG300-7	825551.0000	624989.0000	0	0	0
SG310-10AST1	833119.0000	618963.0000	69	66	19
SG310-11	833024.0000	619192.0000	85	83	27
SG310-4	833447.0000	618347.0000	85	82	48
SG310-5A	833914.0000	617824.0000	64	63	34
SG310-5C	833436.0000	617997.0000	97	94	-999
SG310-6	832392.0000	618119.0000	135	122	61
SG310-6A	832229.0000	618040.0000	124	109	98
SG310-7A	834784.0000	616983.0000	57	57	23
SG310-9ST1	832347.0000	617620.0000	-999	-999	-999
SGOFFSH-2	828257.0000	622239.0000	5	4	2
SHM-1A	839962.0000	607021.0000	109	107	-999
SHM-2	838491.0000	608806.0000	75	73	6
SHM-3	837050.0000	607100.0000	37	34	-999
SHM-4	841175.0000	606675.0000	93	93	-999
SHM-4A	841126.0000	606671.0000	38	38	-999
SRM-1A	845737.0000	616179.0000	96	93	3
SRM-2	845345.0000	617261.0000	78	77	0
WADI_DARA_M-1	848196.0000	598946.0000	37	30	6
WADI_DARA_M-2	848597.0000	599093.0000	23	19	7

Table 4: Upper Rudeis Fm Stratal Unit D: Gross interval and net reservoir (metres)

			Gross Interval		PHIE>10% NetRes
Well	X	Y	MDT	TST	TST
ALEF-1	843569.0000	623800.0000	32	32	0
BDR-A1	855152.0000	618353.0000	37	37	0
BDR-B1	856939.0000	616777.0000	52	53	27
BDR-B7	856772.0000	617603.0000	37	42	-999
BDR-B8	856291.0000	616478.0000	65	67	47
BDR-E1	855321.0000	616731.0000	80	80	66
EG-2	829432.0000	627795.0000	41	47	7
EGJ-1	833342.0000	625928.0000	41	41	0
EGJ-2	832923.0000	627021.0000	46	46	0
EGJ-3	831878.0000	626247.0000	73	74	60
ERDMA_W-1	840539.0000	612621.0000	44	46	-999
ERDMA_W-2	841041.0000	613039.0000	35	37	-999
ERDMA-1	844501.0000	612520.0000	32	32	0
ERDMA-2	866253.0000	586057.0000	-999	12	-999
ERDMA-4	843736.0000	614101.0000	28	28	0
ESM-1	851074.0000	607117.0000	73	74	0
ESO344-3	859484.0000	602961.0000	40	41	2
ESO352-2A	852992.0000	598153.0000	20	21	-999
ESO352-3	849163.0000	599843.0000	63	70	5
FARAH-1	849639.0000	604391.0000	101	101	0
G-1	873268.0000	605534.0000	0	0	0
G-2	871086.0000	606302.0000	0	0	0
GA84-10M	849454.0000	598021.0000	59	62	-999
GA84-12M	850253.0000	596132.0000	49	51	0
GA84-13M	849636.0000	598107.0000	47	53	-999
GAMMA-3	849429.0000	598210.0000	56	59	-999
GB85-8	859219.0000	604021.0000	33	34	8
GB86-7	864515.0000	612620.0000	62	62	56
GS269-1	841650.0000	641715.0000	71	74	16
GS277-1	840409.0000	636178.0000	64	64	2
GS278-1	846685.0000	636632.0000	87	87	-999
GS285-1	840329.0000	634854.0000	46	53	0
GS293-2AST1	836014.0000	626673.0000	39	43	1
GS301-1	833200.0000	624501.0000	20	45	10
GS302-1	836109.0000	624035.0000	45	47	-999
GS302-2	837775.0000	625018.0000	7	7	-999
GS302-3	838984.0000	623488.0000	56	64	-999
GS302-4	839864.0000	622882.0000	59	65	0
GS302-5	840069.0000	621582.0000	66	73	-999

GS302-8	838022.0000	624406.0000	30	44	-999
GS305-2	853526.0000	620946.0000	53	53	16
GS311-2ST1	838969.0000	617979.0000	16	31	0
GS313-1	846592.0000	618434.0000	23	23	-999
GS313-2	845109.0000	618548.0000	32	32	0
GS313-3	846993.0000	615981.0000	38	41	1
GS316-1	860671.0000	617206.0000	66	67	38
GS317-1	868469.0000	618663.0000	46	47	0
GS323-1	847236.0000	613269.0000	45	48	-999
GS324-2(A1)	850822.0000	614274.0000	39	39	0
GS326-1	860576.0000	614766.0000	47	48	41
GS326-2	864297.0000	613668.0000	59	59	47
GS326-3	864260.0000	610868.0000	68	73	30
GS327-1	867420.0000	612134.0000	55	55	29
GS327-2	867764.0000	613548.0000	32	32	3
GS327-A3	867115.0000	614527.0000	-999	24	-999
GS327-A5ST1	867106.0000	615098.0000	-999	53	-999
GS327-A6	866755.0000	612109.0000	-999	88	-999
GS327-A7	867511.0000	613189.0000	-999	34	-999
GS334-2	853489.0000	607800.0000	38	39	1
GS334-4ST2	851363.0000	610038.0000	78	79	2
GS337-1A	869441.0000	606232.0000	92	98	37
GS337-2	865629.0000	607286.0000	91	91	53
GS344-1AST2	858898.0000	602395.0000	40	43	-999
GS344-2	858482.0000	600682.0000	31	31	0
GS345-1	860819.0000	603020.0000	56	56	5
GS345-2(A1)	864596.0000	600711.0000	36	36	-999
GS345-A2	865263.0000	601234.0000	38	39	12
GS345-A4	866637.0000	600454.0000	25	36	4
GS346-1	866608.0000	601135.0000	50	51	10
GS352-1	851350.0000	598060.0000	52	52	-999
H-1	865772.0000	612827.0000	82	85	2
J10-12A	837559.0000	617991.0000	39	47	-999
J10-14	836907.0000	617931.0000	30	30	0
J10-19	836891.0000	618251.0000	16	20	0
J10-33	837344.0000	617779.0000	26	33	0
J10-33A	837343.0000	617906.0000	32	45	-999
J10-33C	837317.0000	617902.0000	30	45	0
J10-44	835361.0000	617931.0000	27	27	0
J10-55	834738.0000	618666.0000	27	29	-999
J10-55B	835443.0000	617588.0000	27	31	0
J10-72	836292.0000	618709.0000	49	52	0
J10-88B	834638.0000	617997.0000	34	44	0

J15-18	835783.0000	619546.0000	41	41	0
J15-18A	835833.0000	619537.0000	50	51	0
J15-24	835584.0000	620306.0000	0	0	-999
J15-48	835606.0000	620952.0000	46	48	0
J15-56	835687.0000	620432.0000	42	48	-999
J15-56A	835813.0000	620574.0000	30	35	0
J15-95	835949.0000	619474.0000	52	55	-999
J15-97	835755.0000	619412.0000	35	50	-999
J15-97ST	835761.0000	619419.0000	46	58	-999
J15-98	835803.0000	619836.0000	52	58	-999
J22-22	837182.0000	619496.0000	16	19	-999
J22-22A	837183.0000	619497.0000	18	19	-999
J22-22ST1	837183.0000	619497.0000	18	19	0
J22-23B	836901.0000	620132.0000	25	29	0
J3	834777.0000	626242.0000	31	36	0
J37-37	835135.0000	618335.0000	9	10	0
J37-37A	834843.0000	618240.0000	42	45	0
J37-40	836110.0000	619118.0000	47	48	-999
J37-42	836336.0000	618542.0000	44	48	0
J37-43A	834191.0000	618756.0000	32	33	0
J37-93	835081.0000	620116.0000	21	35	0
J4-5A	836099.0000	620327.0000	13	32	-999
J4-71	836789.0000	619399.0000	4	5	0
J53	834920.0000	620114.0000	23	23	0
J58-50	835045.0000	621905.0000	5	5	0
J58-51	835514.0000	622479.0000	25	26	0
J58-52A	834205.0000	622445.0000	26	39	0
J58-54	835250.0000	621558.0000	55	61	0
J58-58A	835046.0000	622567.0000	39	40	0
J58-73	835028.0000	623473.0000	34	46	0
J58-73B	834730.0000	623356.0000	28	39	-999
J58-74	836076.0000	621927.0000	33	42	0
J58-77	834800.0000	623020.0000	35	39	-999
J58-77A	833834.0000	623830.0000	62	94	8
J58-81	835408.0000	622969.0000	37	41	0
J58-84	834037.0000	623016.0000	40	58	-999
J58-84ST1	834038.0000	623011.0000	38	51	4
J58-85	835350.0000	623742.0000	30	42	-999
J58-87	834410.0000	622652.0000	23	26	1
J58-90A	833864.0000	623291.0000	40	65	5
J58-90AST1	833794.0000	623378.0000	44	78	11
J62-63	839368.0000	616421.0000	8	10	0
J62-64	838305.0000	617344.0000	27	29	0

J62-64A	838113.0000	617280.0000	17	18	0
J62-64AST1	838113.0000	617280.0000	20	21	0
J62-65	838789.0000	617380.0000	29	36	0
J62-66	837946.0000	618289.0000	25	29	-999
J62-67	837034.0000	617537.0000	19	25	0
J62-67A	838749.0000	616733.0000	8	8	0
J62-68	838511.0000	617142.0000	15	17	-999
J6-36	837728.0000	617409.0000	5	34	0
J6-36A	837723.0000	617395.0000	31	36	0
J6-61	838052.0000	617926.0000	39	46	0
J6-7	836669.0000	616450.0000	17	17	0
J8-13	837001.0000	618350.0000	66	67	-999
J8-41	836972.0000	618334.0000	6	6	0
J8-49	837085.0000	618256.0000	22	22	-999
J92	835316.0000	619677.0000	41	46	0
KK85-1	829978.0000	627906.0000	83	84	52
KK86-1A	835453.0000	626655.0000	33	33	1
LL87-2	843908.0000	619778.0000	30	33	0
LL87-4	846483.0000	614903.0000	38	39	0
LL87-6A	844024.0000	616828.0000	30	32	0
LL87-SE1	845988.0000	614302.0000	32	32	2
M100-132 (GS325-	861858.0000	608519.0000	18	27	13
M100-236	858058.0000	615839.0000	37	53	4
M1-1	853977.0000	615924.0000	57	59	-999
M1-121	854832.0000	617146.0000	47	48	-999
M120-206	853008.0000	616416.0000	68	69	-999
M120-206A	855443.0000	613056.0000	63	64	35
M120-208ST3	855182.0000	614983.0000	51	54	27
M1-207	854244.0000	616060.0000	41	50	17
M36-70	854212.0000	616042.0000	42	43	39
M5-130	854721.0000	615986.0000	28	28	-999
M-52	856753.0000	610858.0000	48	50	-999
M-53	852607.0000	614974.0000	57	57	-999
M5-5	852682.0000	615629.0000	-999	34	-999
M8-8	858246.0000	611574.0000	30	31	-999
MM86-1A	841925.0000	607194.0000	63	66	0
MOUKHTAFY-1	823299.0000	645313.0000	-999	23	-999
NJ-1	833413.0000	625844.0000	46	52	0
NSM-A1	863265.0000	606952.0000	67	70	39
NSM-A1A	863237.0000	606986.0000	44	49	35
NSM-A2	862850.0000	607447.0000	54	64	41
NSM-A3A	862945.0000	606837.0000	-999	-999	-999
NSM-A4	863641.0000	606544.0000	40	49	27

NSM-A5	862287.0000	607529.0000	-999	-999	-999
R0-18A	840590.0000	623871.0000	32	37	0
R0-19	840814.0000	622190.0000	30	31	-999
R0-19A	840814.0000	622191.0000	30	32	-999
R1-1	842109.0000	623045.0000	44	45	-999
R1-2	843020.0000	621856.0000	33	41	-999
R1-29	842027.0000	622889.0000	44	45	-999
R1-2A	842988.0000	621929.0000	34	38	-999
R1-34	841979.0000	623079.0000	41	43	0
R1-42	841681.0000	623080.0000	33	36	0
R1-49	841104.0000	622666.0000	31	37	0
R1-50	842230.0000	623100.0000	43	45	-999
R1-51	842291.0000	622996.0000	45	45	0
R1-52A	842704.0000	622518.0000	42	46	5
R22-22	842821.0000	620962.0000	9	9	1
R24-27	841024.0000	622413.0000	12	12	-999
R24-27A	841311.0000	622550.0000	12	13	0
R24-28	841508.0000	621970.0000	-999	24	-999
R24-36	841563.0000	622102.0000	14	16	0
R3-11	841282.0000	623567.0000	19	20	0
R3-57	841295.0000	622994.0000	8	10	0
R4-12	841248.0000	624620.0000	32	34	0
R4-44	841151.0000	624786.0000	36	41	0
R4-47	841175.0000	624566.0000	33	35	0
R4-7	841255.0000	624844.0000	23	23	0
R5-16	841758.0000	622804.0000	55	56	-999
R5-17A	841862.0000	622496.0000	27	27	0
R5-30	841844.0000	622252.0000	29	30	0
R5-37	841498.0000	621873.0000	18	30	0
R5-5A	841666.0000	622401.0000	37	38	0
R5-5C	841676.0000	622401.0000	25	27	0
R5-60	842316.0000	622712.0000	43	44	-999
R5-9	841808.0000	623131.0000	37	52	-999
R6-10A	842779.0000	621533.0000	28	28	0
R6-20B	842894.0000	621486.0000	25	34	-999
R6-23A	843337.0000	621350.0000	35	38	0
R6-32	842596.0000	621878.0000	33	35	0
R6-33	842713.0000	621692.0000	28	30	0
R6-35	842924.0000	621648.0000	24	26	0
R6-39	841790.0000	621010.0000	7	9	-999
R6-40ST1	842151.0000	620833.0000	14	16	0
R6-43	842449.0000	620624.0000	33	34	0
R6-45	841997.0000	620967.0000	24	30	-999

R6-53	843005.0000	621529.0000	20	21	-999
R6-55ST1	843056.0000	620816.0000	26	31	0
R6-56A	844158.0000	621171.0000	10	14	-999
R6-6	842759.0000	621589.0000	34	35	0
R6-8	842660.0000	621754.0000	31	34	0
R6-8A	842708.0000	621676.0000	19	22	0
SB268-1A	837372.0000	642573.0000	71	74	67
SB276-1A	839816.0000	635830.0000	69	70	60
SB276-2	838952.0000	635133.0000	50	59	-999
SB276-2B	838957.0000	635136.0000	52	56	0
SB276-3ST1	839556.0000	637631.0000	-999	75	-999
SB284-1	839989.0000	632842.0000	47	51	2
SB293-1	840101.0000	625643.0000	69	85	0
SB293-2	838676.0000	625177.0000	67	75	-999
SB293-3	837978.0000	625160.0000	56	70	-999
SB294-1	840355.0000	627372.0000	47	48	0
SB294-2	840587.0000	625381.0000	40	47	1
SB294-3	840523.0000	625148.0000	33	34	-999
SB294-4	840823.0000	625166.0000	17	18	-999
SB296-1	851153.0000	629296.0000	55	55	1
SB296-2	853388.0000	625135.0000	12	13	0
SB297-1	856206.0000	625639.0000	18	21	5
SB305-A1	854580.0000	624480.0000	38	39	1
SG120-3	831296.0000	613089.0000	-999	158	-999
SG300-12	825525.0000	624389.0000	9	10	-999
SG300-1A	825897.0000	624473.0000	-999	0	0
SG300-2B	825942.0000	624502.0000	-999	0	0
SG300-4	826694.0000	625144.0000	0	0	0
SG300-5	825077.0000	624969.0000	0	0	0
SG300-7	825557.0000	624973.0000	31	33	13
SG300-9	825868.0000	625142.0000	45	55	-999
SG300-9A	825949.0000	625039.0000	12	15	-999
SG300-9B	825987.0000	625016.0000	24	35	-999
SG310-10AST1	833154.0000	618967.0000	64	67	19
SG310-11	833102.0000	619184.0000	102	104	25
SG310-1B	833208.0000	617442.0000	180	183	83
SG310-2	832766.0000	618334.0000	152	159	47
SG310-4	833494.0000	618361.0000	72	74	31
SG310-5A	833920.0000	617828.0000	52	53	8
SG310-5C	833472.0000	618015.0000	66	68	-999
SG310-6	832541.0000	618156.0000	164	181	85
SG310-6A	832391.0000	618109.0000	169	194	101
SG310-8	833471.0000	618430.0000	68	72	34
SG310-9ST1	832530.0000	617675.0000	180	197	-999
SGOFFSH-2	828260.0000	622242.0000	16	20	12

SHM-1A	839961.0000	607023.0000	27	28	-999
SHM-2	838491.0000	608806.0000	31	32	4
SHM-3	837050.0000	607100.0000	53	56	-999
SHM-4	841175.0000	606675.0000	62	63	-999
SHM-4A	841126.0000	606671.0000	75	75	0
SRM-1A	845737.0000	616179.0000	41	43	0
SRM-2	845344.0000	617263.0000	34	35	0
WADI_DARA_M-1	848196.0000	598946.0000	44	54	17
WADI_DARA_M-2	848590.0000	599092.0000	35	43	1

Table 5: Borehole dip data Upper Rudeis Fm

Well	Fm Azimuth	Fm Dip	Wellbore azimuth	Angle from vertical
ALEF-1	045	10	000	0
BDR-A1	270	5	235	3
BDR-B1	270	5	221	3
BDR-B4	180	3	275	40
BDR-B7	NA	NA	343	28
BDR-B8	250	5	239	16
BDR-C1	280	3	255	5
BDR-C10	280	8	016	44
BDR-C11	\	\	032	49
BDR-E1	180	3	014	1
BDR-E4	NA	NA	214	14
D-1	NA	NA	000	0
DARA-BAY-1	NA	NA	227	9
E_GHARIB-M1	NA	NA	000	0
EG-2	045	12	254	41
EGJ-1	310	10	086	5
EGJ-2	320	6	000	0
EGJ-3	025	10	000	0
EL_KHALIG-1	NA	NA	000	0
ERDMA_W-1	085	10	000	0
ERDMA_W-2	085	10	000	0
ERDMA-1(ESMA-2)	165	10	207	2
ERDMA-3	145	5	000	0
ERDMA-4	250	5	003	0
ESM-1	250	10	014	3
ESMA-9	010	15	000	0
ESO344-3	230	10	034	1
ESO352-2	040	15	211	6
FARAH-1	270	10	078	2
G-1	240	15	190	2
G-2	000	0	000	0
GA84-10M	250	15	000	0
GA84-12M	220	10	000	0
GA84-13M	300	8	064	29
GAMMA-3	260	12	000	0
GB85-8	200	8	025	21
GB86-7	280	10	178	1.3
GS269-1	140	15	357	4
GS277-1	065	8	050	1
GS278-1	215	25	358	4
GS285-1	065	10	182	25
GS293-2AST1	NA	NA	276	32

GS301-1	300	8	318	44
GS302-1	126	9	032	28
GS302-2	070	15	103	3
GS302-3	061	7.5	266	36
GS302-4	082	15	268	40
GS302-5	116	9	264	32
GS302-8	090	10	257	58
GS305-2	225	10	000	0
GS306-1	060	5	237	2
GS306-2	095	8	293	4
GS313-1	260	7	120	3
GS313-2	035	10	087	1.2
GS313-3	250	25	053	6.2
GS316-1	070	5	054	0.8
GS317-1	340	10	037	1.6
GS323-1	250	28	062	42.3
GS324-2(A1)	240	5	154	5
GS324-3(A2)	250	5	135	8
GS324-4(A3)	250	5	041	10.5
GS325-2	045	20	101	8
GS326-1	240	15	204	0.6
GS326-2	270	10	049	1.6
GS327-1	060	10	239	0.5
GS327-2	260	10	233	2.25
GS327-A1ST1	260	10	155	10.2
GS327-A2A	260	10	336	27
GS327-A2B	260	10	034	3.8
GS327-A3	260	10	329	45
GS327-A4	260	10	304	16
GS327-A5ST1	260	10	334	53
GS327-A6	260	10	212	60
GS327-A7	260	10	215	14
GS334-2	240	5	144	1
GS334-3	160	10	000	0
GS334-4	180	5	000	0
GS334-4ST2	180	5	031	3
GS337-1	270	15	105	8
GS337-1A	340	13	230	21
GS337-2	220	5	204	2.4
GS338-1	270	5	320	34
GS344-1	140	5	004	3
GS344-1A	140	5	030	3
GS344-1AST2	140	5	030	3
GS344-2	215	15	007	7
GS345-1	290	35	057	0
GS345-2(A1)	NA	NA	106	1
GS345-A2	300	20	056	17

GS345-A3	240	10	060	24
GS345-A4	300	20	099	28
GS346-1	010	10	121	2
GS346-2	010	10	067	56
GS346-2A	010	10	054	66
GS346-2BST1	010	10	095	31
GS348-1	190	30	122	58
GS352-1	065	10	186	3
H-1	240	12	000	0
J10-11	220	20	115	16
J10-19	090	10	074	18
J10-38A	\	\	004	20
J10-44	080	15	282	25
J10-55	\	\	298	26
J10-55A	\	\	298	26
J10-55B	\	\	195	22
J10-70	\	\	016	25
J10-72	\	\	356	28
J10-88B	330	12	290	26
J15-18	\	\	210	8
J15-18A	\	\	165	8
J15-56	350	15	325	22
J22-22	060	25	285	3
J22-22A	060	25	285	3
J22-22ST1	060	25	285	3
J22-23B	060	25	340	20
J3	045	20	088	4
J37-37	\	\	199	11
J37-37A	160	15	232	16
J37-40	\	\	081	22
J37-43A	060	10	283	25
J37-93	\	\	336	37
J4-47	025	60	289	12
J58-51	060	8	088	19
J58-54	\	\	174	33
J58-58A	047	7	143	3
J58-73	310	12	356	34
J58-73B	350	20	335	31
J58-74	075	12	134	29
J58-77	025	8	332	22
J58-81	030	9	030	19
J58-84	340	8	300	37
J58-84ST1	340	8	300	37
J58-85	060	15	005	37
J58-87	000	10	289	25
J58-90A	355	10	319	39
J62-64	\	\	291	13

J62-64A	\	\	271	29
J62-64AST1	\	\	271	29
J62-67	135	20	163	22
J62-67A	090	15	230	5
J62-68	060	35	297	28
J6-36	110	15	061	20
J6-36A	110	15	068	18
J6-7	135	10	340	6
J6-9	\	\	322	14
J6-9A	\	\	336	11
J8-41	\	\	294	2
J8-49	210	15	149	8
KHEFREN-1	\	\	041	2
KHEFREN-1_ST1	\	\	041	2
KHEFREN-1_ST2	\	\	041	2
KK84-1	\	\	000	0
KK85-1	065	20	164	4
KK86-1A	045	10	117	1
LL87-2	045	13	040	8
LL87-3	240	8	010	1
LL87-4	250	15	055	13
LL87-6A	290	18	208	12
LL87-SE1	225	5	000	0
M0-52	160	12	000	0
M0-53	\	\	000	0
M100-132 (GS325-	\	\	191	21
M100-236	\	\	347	52
M1-1	\	\	339	1
M1-118	\	\	167	11
M1-121	250	10	040	30
M1-12A	\	\	152	9
M120-156	\	\	226	11
M120-187	\	\	157	23
M120-206	\	\	042	26
M120-206A	220	10	042	26
M1-207	205	8	292	32
M1-212	\	\	152	40
M15-15	240	8	000	0
M160-160	\	\	068	1
M160-161	\	\	041	42
M160-163	\	\	058	30
M160-168	\	\	054	41
M170-171	\	\	210	16
M190-190	\	\	014	8
M190-194	\	\	109	28
M2-2	\	\	020	3
M24-81	\	\	156	17

M3-117A	\	\	125	27
M3-135	\	\	331	21
M3-136	\	\	224	18
M36-70	210	12	101	15
M5-129	\	\	342	20
M5-130	\	\	171	17
M5-131	\	\	159	48
M55-142	\	\	356	15
M55-146	\	\	288	34
M55-80	\	\	160	34
M5-5A	\	\	000	0
M6-6	\	\	224	5
M7-7	\	\	359	0
M8-126	\	\	322	25
M8-149A	\	\	194	7
M8-35	\	\	012	32
M85-181	\	\	082	14
M85-99	\	\	085	15
M8-8	270	12	217	1
MM86-1A	090	25	222	5
MOUKHTAFY-1	\	\	000	0
NN88-1	045	20	231	3
NN89-1	215	8	044	13
NSM-A1A	230	15	249	6
NSM-A2	270	10	299	21.5
NSM-A3	230	15	254	19
NSM-A3A	230	10	286	3.2
NSM-A4	240	10	161	35
NSM-A5	240	10	295	38.4
R0-19	270	22	049	5
R0-19A	270	22	047	5
R1-1	\	\	232	1
R1-2	\	\	159	26
R1-21	\	\	049	22
R1-29	030	10	194	20
R1-2A	\	\	159	26
R1-34	040	8	286	14
R1-42	\	\	278	14
R1-49	250	20	257	26
R1-50	\	\	108	1
R1-51	\	\	029	1
R1-52A	\	\	146	24
R22-22	250	15	035	3
R24-27	250	20	356	9
R24-27A	250	20	356	9
R24-28	\	\	280	20
R24-36	\	\	326	24

R3-11	\	\	119	24
R3-57	\	\	161	16
R4-12	\	\	165	19
R4-47	\	\	186	22
R4-7	300	15	108	3
R5-17A	\	\	081	23
R5-30	305	15	123	27
R5-37	\	\	183	27
R5-5A	\	\	080	6
R5-5C	\	\	096	5
R5-60	\	\	048	16
R5-9	020	15	036	31
R6-32	\	\	350	20
R6-33	\	\	057	12
R6-35	\	\	097	15
R6-39	270	10	253	29
R6-45	\	\	246	20
R6-53	\	\	095	5
R6-6	090	5	037	7
R6-8	065	5	354	16
SABRA-1	\	\	000	0
SB268-1	330	12	000	0
SB268-1A	330	12	250	3
SB276-1A	300	10	080	5
SB276-2	300	15	236	35
SB276-2A	330	18	233	25
SB276-2B	300	15	236	35
SB284-1	270	15	003	84
SB293-1	230	15	325	30
SB293-2	060	18	276	41
SB293-3	070	18	276	52
SB294-1	320	12	252	4
SB294-2	270	10	314	22
SB294-3	280	12	021	5
SB294-4	050	20	351	6
SB296-1	001	12	184	4
SB296-2	050	15	313	18
SB297-1	045	10	059	33
SB305-A1	045	10	182	2
SB339-1	270	5	062	7.9
SB339-1A				
SG_SW-1	060	15	230	2
SG120-3	\	\	000	0
SG300-4	080	10	221	3
SG300-5	040	12	304	41
SG300-7	180	15	336	31
SG300-8	115	25	044	16.5

SG300-8ST1	115	25	040	18
SG300-9	110	10	335	37
SG300-9A	100	10	016	26
SG300-9B	330	20	027	26
SG310-10AST1	050	30	267	25
SG310-11	090	30	275	41
SG310-1B	060	25	227	3
SG310-2	060	25	071	6
SG310-3ST2	250	7	261	36
SG310-4	080	18	254	32
SG310-5	050	10	213	39
SG310-5A	055	15	235	4.8
SG310-5C	055	15	244	30
SG310-6	060	25	259	50
SG310-6A	060	25	258	58
SG310-7	230	30	243	43.3
SG310-7A	060	25	238	25.6
SG310-8	080	18	234	32
SG310-9ST1	065	30	253	53
SGOFFSH-2	090	45	181	2
SHM-1A	120	15	090	4
SHM-2	090	12	000	0
SHM-3	000	0	000	0
SHM-4	075	4	000	0
SHM-4A	075	4	000	0
SRM-1A	250	15	000	0
SRM-2	310	12	130	1.4
WADI_DARA_G-1	\	\	000	0
WADI_DARA_M-1	260	15	000	0
WADI_DARA_M-2	260	15	000	0
YARON-1		NA	000	0
YNS-A1	215	5	159	0
YNS-A10ST1	110	5	174	54
YNS-A2	NA	NA	006	30
YNS-A3	090	8	154	39
YNS-A4	250	50	031	32
YNS-A5	090	8	255	35
YNS-A6A	315	20	179	34

Table 6. Gross interval and net reservoir thickness (MDT) metres

Well	X	Y	S40 / Stratal Unit E		S50 / Stratal Unit G	
			Gross MDT	PHIE>10% NetRes MDT	Gross MDT	PHIE>10% NetRes MDT
ALEF-1	843567.9	623805.3	288	-999	73	3
BDR-A1	855159.9	618358.8	974	0	190	49
BDR-B1	856947.3	616786.8	1102	393	87	10
BDR-B4	855646.6	616444	1178	864	63	52
BDR-B7	856844.1	617371.3	1420	593	193	98
BDR-B8	856355.8	616519.1	998	733	197	106
BDR-C1	857794.5	615174.8	922	540	196	69
BDR-C10	858419.6	617343.9	1300	1035	210	109
BDR-C11	859069.3	616869.2	well TD	320+	255	32
BDR-E1	855319.8	616727.8	461	204	360	213
BDR-E4	855153.3	616255	827	5	162	-999
D-1	855068	607968	632	65	164	0
DARA-BAY-1	844638.5	594963	357	-999	380	-999
E_GHARIB-M1	823905	634105	258	-999	53	-999
EG-2	829488.6	627811	197	0	314	-999
EGJ-1	833337.6	625927.8	172	0	214	3
EGJ-2	832913.6	627020.6	234	0	461	0
EGJ-3	831870	626248.6	218	-999	357	0
EL_KHALIG-1	825200	620450	386	-999	620	-999
ERDMA_W-1	840539	612621	219	-999	264	-999
ERDMA_W-2	841041	613039	218	0	278	0
ERDMA-1(ESMA-2)	844502.3	612519.8	230	143	315	4
ERDMA-3	846600	611133	144	54	284	1
ERDMA-4	843735.8	614102.4	206	132	243	26
ESM-1	851070.4	607106.9	496	0	227	0
ESMA-9	849760.6	601447.5	380	75	540	21
ESO344-3	859483.4	602960.4	262	61	30	0
ESO352-2	852993.8	598155.4	165	0	323	54
FARAH-1	849602.4	604389.9	590	211	307	138
G-1	873268	605534	5	0	69	0
G-2	871086	606302	0	0	0	-999
GA84-10M	849454	598021	349	-999	391	-999
GA84-12M	850253	596132	168	0	402	0
GA84-13M	849583.8	598083	306	-999	401	-999
GAMMA-3	849436.3	598161.3	369	-999	442	-999
GB85-8	859199.5	603982.1	324	177	176	68
GB86-7	864515.1	612621.5	146	98	278	0
GS269-1	841650.6	641707.3	251	8	698	147
GS277-1	840410.1	636178.4	163	6	670	120
GS278-1	846676.8	636617.8	440	117	467	16
GS285-1	840333.3	634887.1	161	0	491	17

GS293-2AST1	836048.7	626668.8	149	0	459	16
GS301-1	833280.8	624399.8	393	-999	853	-999
GS302-1	836088.8	624005.3	167	-999	397	-999
GS302-2	837774.6	625037.6	164	-999	10050	-999
GS302-3	839065.9	623492.8	320	-999	347	-999
GS305-2	853523.3	620945.3	216	40	195	1.5
GS306-1	857228.4	622772.3	49	13	127	3
GS306-2	857556.4	621318.4	202	141	245	98
GS313-1	846589.7	618442.1	269	-999	341	-999
GS313-2	845108.4	618549.4	154	22	418	27
GS313-3	846984.7	615974.2	274	74	365	23
GS316-1	860670.4	617205.3	323	181	187	17
GS317-1	868467.5	618661.3	274	141	204	0
GS323-1	847189.3	613244.5	100	-999	414	-999
GS324-2(A1)	850813.6	614285	425	213	165	21
GS324-3(A2)	850725.9	613871.7	482	-999	289	-999
GS324-4(A3)	850808.1	614342.6	416	-999	130	-999
GS325-2	855985.3	613770.5	300	255	225	158
GS326-1	860576.3	614767.7	277	231	165	105
GS326-2	864295.8	613667.4	182	86	202	60
GS327-1	867420.8	612134.6	116	0	181	1
GS327-2	867765.2	613549.3	155	0	193	2
GS327-A1ST1	867777	613525.6	143	0	5526	-999
GS327-A2A	867452.5	614484.5	99	50	195	14
GS327-A2B	867784.2	614119	172	50	6203	-999
GS327-A3	867147.7	614470.9	224	146	322	-999
GS327-A4	867442.2	613755.6	189	60	5771	-999
GS327-A5ST1	867137.7	615028.5	216	208	265	-999
GS327-A6	866791.7	612165	197	0	265	-999
GS327-A7	867518.3	613199.1	139	0	195	-999
GS334-2	853482.2	607802.9	545	304	420	-999
GS334-3	853007	606616	503	379	180	46
GS334-4	851360	609963	530	-999	7401	-999
GS334-4ST2	851361.1	610046.3	529	3	7401	0
GS337-1	869650.1	606368.2	86	0	290	9
GS337-1A	869462.7	606249.8	248	0	326	30
GS337-2	865630.2	607287.3	217	63	262	145
GS338-1	874797.9	606286	188	-999	109	-999
GS344-1	858904.8	602515.4	267	-999	187	-999
GS344-1A	858893.8	602397.2	367	-999	159	-999
GS344-1AST2	858895	602396.8	246	-999	193	-999
GS344-2	858479.5	600671.1	264	98	213	0
GS345-1	860818.1	603018.9	274	26	243	0
GS345-2(A1)	864595.3	600711.3	112	3	194	77
GS345-A2	865248.9	601224.8	151	77	87	18
GS345-A3	865944.3	601610.8	133	59	172	9
GS345-A4	866616.6	600458.3	53	38	140	0

GS346-1	866606.1	601136.4	139	59	125	0
GS346-2	866810.3	601399.6	53	28	336	19
GS346-2A	866906.1	601548.6	58	28	392	0
GS346-2BST1	866487.2	601132.2	97	59	168	8
GS348-1	875719.9	604927.4	738	-999	201	-999
GS352-1	851349.6	598060.8	92	-999	376	-999
H-1	865772	612827	146	10	185	41
J10-11	837045.6	617537.3	171	-999	178	-999
J10-19	836867.9	618244.1	173	-999	178	-999
J10-38A	836427.5	618907.1	189	-999	338	-999
J10-44	835411.8	617922.1	184	15	296	27
J10-55	834781.8	618640.3	348	-999	102	-999
J10-55A	834784	618638.7	345	-999	98	-999
J10-55B	835453.1	617623.6	225	-999	305	-999
J10-70	836627.6	618631	120	-999	279	-999
J10-72	836294.3	618672.8	154	-999	33	-999
J10-88B	834699.5	617976.4	360	9	304	-999
J15-18	835788.2	619556.4	164	-999	17	-999
J15-18A	835830.1	619549	174	-999	75	-999
J15-56	835711.3	620411.2	192	-999	71	-999
J22-22	837187.1	619494.8	158	-999	156	-999
J22-22A	837187.8	619495.8	152	-999	159	-999
J22-22ST1	837187.8	619495.8	156	0	159	0
J22-23B	836909.9	620107.4	170	-999	256	-999
J3	834775.9	626241.7	117	0	187	0
J37-37	835148.4	618372.8	282	0	163	-999
J37-37A	834876.6	618253	347	0	216	0
J37-40	836070.6	619114.7	330	-999	150	-999
J37-43A	834254.1	618743.3	347	-999	246	-999
J37-93	835096.9	620075.8	161	4.5	83	4
J4-47	836058.8	619636.6	429	-999	218	-999
J58-51	835493.6	622479.7	172	-999	307	-999
J58-54	835246.9	621601.2	155	-999	365	-999
J58-58A	835045.1	622569.9	127	0	300	0
J58-73	835032.1	623391	337	0	253	-999
J58-73B	834752.5	623313.3	252	-999	257	-999
J58-74	836029.6	621974.5	319	0	225	-999
J58-77	834818.1	622983.9	255	-999	201	-999
J58-81	835391.7	622941.2	248	0	233	-999
J58-84	834118.3	622972.3	324	0	209	-999
J58-84ST1	834117.1	622969.3	326	0	203	-999
J58-85	835340.9	623672.2	301	-999	259	-999
J58-87	834444.4	622628.9	258	11	186	0
J58-90A	833945.2	623181.6	443	2	306	0
J62-64	838325	617340.3	222	-999	251	-999
J62-64A	838163.1	617283.3	223	-999	192	-999
J62-64AST1	838163.1	617283.3	222	8	190	-999

J62-67	838836.1	616645.6	312	-999	291	-999
J62-67A	838753.6	616748.8	326	-999	243	-999
J62-68	838558.9	617116.8	299	-999	159	-999
J6-36	837697.5	617394.6	187	-999	23	-999
J6-36A	837695.5	617384.9	187	-999	21	-999
J6-7	836674	616445.9	198	-999	252	0
J6-9	837041.3	617524.9	174	-999	179	-999
J6-9A	837053.6	617506.9	163	-999	176	-999
J8-41	836973.6	618332.6	147	-999	331	-999
J8-49	837081.5	618261.1	127	-999	140	-999
KHEFREN-1	851136	608675.4	448	-999	345	6
KHEFREN-1_ST1	851135.7	608675.7	452	-999	347	-999
KHEFREN-1_ST2	851135.6	608675.7	454	-999	336	0
KK84-1	820367	632957	0	-999	0	0
KK85-1	829979.8	627916.8	203	0	359	-999
KK86-1A	835452.6	626655.1	39	0	369	-999
LL87-2	843902.2	619771.3	211	0	211	-999
LL87-3	846378.4	613152.4	126	35	298	9
LL87-4	846465.7	614890.6	159	74	74	9
LL87-6A	844017.4	616831.4	192	15	373	1
LL87-SE1	845988	614302	196	58	251	15
M0-52	861858	608519	248	-999	180	-999
M0-53	858058	615839	592	-999	96	-999
M100-132 (GS325-	855456.9	613114.3	467	242	418	100
M100-236	855225.4	614798.5	692	288	146	82
M1-1	853978.8	615919.9	727	-999	172	-999
M1-118	854165.4	615574.8	747	328	191	28
M1-121	854758.8	617056.2	943	757	225	110
M1-12A	854349.8	615862.3	766	-999	160	-999
M120-156	853341.7	614826.9	691	-999	161	27
M120-187	854036.9	614674.4	1129	-999	108	-999
M120-206	854172.3	615991.5	716	287	206	28
M120-206A	854172.1	615992.6	672	-999	213	-999
M1-207	853157.1	616349.3	917	356	178	12
M1-212	854697.9	614798.6	878	415	236	47
M15-15	856842	609588	1042	-999	159	-999
M160-160	857385.1	611974.7	471	-999	22	-999
M160-161	858223.4	612771.1	1182	-999	273	237
M160-163	857883	612312.8	900	-999	232	196
M160-168	858295.4	612521.8	1195	-999	94	67
M170-171	855336.1	611889.2	511	-999	164	64
M190-190	857437.3	613090.1	878	-999	155	-999
M190-194	858206.1	612781.7	1101	-999	24	-999
M2-2	854448.3	613433.6	618	-999	65	-999
M24-81	857644.5	612177.9	940	-999	1	-999
M3-117A	853627.5	617001.9	684	-999	190	-999
M3-135	852220.1	618305.2	747	258	123	2

M3-136	852635.8	616963.5	791	-999	121	10
M36-70	856676.3	610871.9	889	0	237	-999
M5-129	852238.9	616041.6	669	-999	147	-999
M5-130	852597.3	615019	539	-999	180	-999
M5-131	853098.5	614029.4	915	-999	104	-999
M55-142	859464.8	610710.1	466	-999	254	-999
M55-146	858596.3	610495.3	834	-999	173	-999
M55-80	860222.4	609399.1	593	-999	94	-999
M5-5A	852580	615498	737	-999	0	-999
M6-6	853947.9	617441.4	983	-999	0	-999
M7-7	855915	612332	1001	-999	1	-999
M8-126	857786.9	611907.9	902	-999	80	-999
M8-149A	858219.7	611264.5	859	-999	177	-999
M8-35	858315.1	612263	1083	-999	0	-999
M85-181	858070.6	612889.1	1023	-999	27	-999
M85-99	857959.7	612954.1	1059	-999	69	-999
M8-8	858255.9	611576.4	828	-999	47	-999
MM86-1A	841939.1	607204.8	279	26	537	106
MOUKHTAFY-1	823316.9	645322.8	143	67	322	-999
NN88-1	857833.5	592893.6	133	-999	149	-999
NN89-1	866735.4	593816.5	342	60	141	2
NSM-A1A	863240.4	606987.8	94	7	128	0
NSM-A2	862856.9	607443.1	91	2	113	0
NSM-A3	862665.8	606688.9	283	124	202	3
NSM-A3A	862949.5	606834.9	255	111	183	0
NSM-A4	863621.4	606602.3	285	139	72	0
NSM-A5	862352.6	607498.3	294	106	221	0
R0-19	840807.8	622184.6	242	-999	230	-999
R0-19A	840807.8	622184.5	240	-999	239	-999
R1-1	842111.7	623049.4	170	-999	347	-999
R1-2	842993.4	621917.1	279	-999	328	-999
R1-21	842240.9	623129.1	314	-999	337	-999
R1-29	842039.3	622927.4	233	-999	294	-999
R1-2A	842971	621973.7	269	-999	296	-999
R1-34	842004.4	623072.8	233	-999	277	-999
R1-42	841706.8	623077.3	218	-999	220	-999
R1-49	841137.9	622672.4	271	-999	273	-999
R1-50	842230.5	623105.4	245	-999	279	-999
R1-51	842290.1	622995.1	236	-999	282	-999
R1-52A	842681.7	622551.3	228	-999	296	-999
R22-22	842818.4	620958.9	183	-999	177	-999
R24-27	841040.4	622398.2	132	-999	143	-999
R24-27A	841311.4	622540.5	135	-999	137	-999
R24-28	841524	621967.7	123	-999	169	-999
R24-36	841575	622083.6	153	-999	196	-999
R3-11	841268.3	623578.1	107	-999	186	-999
R3-57	841291.6	623007.4	144	-999	170	-999

R4-12	841243.7	624637.1	140	-999	220	-999
R4-47	841183.2	624590.2	155	-999	254	-999
R4-7	841250.4	624845.9	129	-999	229	-999
R5-17A	841830.1	622488.6	207	-999	208	-999
R5-30	841818.6	622267.9	145	-999	270	-999
R5-37	841500.1	621904.4	193	-999	10010	-999
R5-5A	841659.4	622398.3	152	-999	227	-999
R5-5C	841668.4	622401.3	156	-999	212	-999
R5-60	842293.8	622693.3	232	-999	301	-999
R5-9	841773.4	623082.7	266	-999	292	-999
R6-32	842601.1	621851.9	169	-999	379	-999
R6-33	842698.4	621682.9	172	-999	163	-999
R6-35	842904.3	621650.9	171	-999	325	-999
R6-39	841838.1	621025.3	247	-999	444	-999
R6-45	842021.6	620979	199	-999	383	-999
R6-53	843000.2	621529.7	135	-999	214	-999
R6-6	842753.5	621582.1	173	-999	68	-999
R6-8	842662.8	621728.1	178	-999	202	-999
SABRA-1	854097	624355	568	18	178	0
SB268-1	837326	642485	366	-999	592	-999
SB268-1A	837374.8	642574.3	363	-999	594	-999
SB276-1A	839811.4	635830.1	169	0	204	24
SB276-2	838987.1	635156.8	209	-999	559	23
SB276-2A	838987.4	635156.9	211	-999	559	-999
SB276-2B	838987.3	635156.9	196	0	557	-999
SB284-1	839988.3	632841.7	40	0	16	0
SB293-1	840124.8	625601.8	207	0	364	0
SB293-2	838749.2	625168.1	295	-999	316	-999
SB293-3	838064.5	625151.4	276	-999	242	-999
SB294-2	840600.2	625367.8	102	10	280	31
SB294-3	840519.6	625142.7	152	-999	240	-999
SB294-4	840829.3	625154.4	169	-999	303	-999
SB296-1	851153.6	629301.2	234	6	271	9
SB296-2	853399.6	625124.6	78	0	199	3
SB297-1	856139.8	625606	315	39	261	0
SB305-A1	854583.6	624485.9	458	22	188	-999
SB339-1	875200	605897	0	0	216	0
SG_SW-1	824922.6	622296.2	429	-999	662	-999
SG300-4	826693.9	625144.4	0	-999	16	-999
SG300-5	825182.4	624893.7	338	-999	521	-999
SG300-8	825582.1	624913.9	265	-999	367	-999
SG300-9A	825872.4	625079.3	243	-999	390	-999
SG300-9B	825936.5	625001.1	216	-999	385	-999
SG310-10AST1	825955.3	624988.7	220	7	370	-999
SG310-2	833247.4	617498.3	776	124	650	5.5
SG310-3ST2	832771.3	618349.1	673	5	598	2
SG310-4	833050.1	618463.6	687	0	776	-999

SG310-5	833549.1	618377	10655	-999	-10243	-999
SG310-5A	833769.2	617568.3	679	-999	625	-999
SG310-5C	833922.6	617829.6	125	-999	288	-999
SG310-6A	832734.2	618199.8	648	-999	612	-999
SG310-8	-999	-999	10789	-999	-10363	-999
SGOFFSH-2	828271.2	622251.9	214	-999	602	-999
SHM-1A	839956.1	607024.4	264	64	552	154
SHM-2	838491	608806	234	0	182	0
SHM-3	837050	607100	0	0	5	-999
SHM-4	841175	606675	299	-999	469	-999
SHM-4A	841126	606671	298	-999	461	-999
SRM-1A	845737	616179	149	58	205	4
SRM-2	845342.9	617265.4	128	28	298	17
WADI_DARA_G-1	840335	591239	718	-999	390	-999
WADI_DARA_M-1	848196	598946	488	329	453	14
WADI_DARA_M-2	848589.8	599094.8	576	-999	269	0
YNS-A1	874074.3	604868.9	56	0	120	0
YNS-A10ST1	874227.9	603692.3	93	0	106	-999
YNS-A2	874083.6	605425.5	29	0	137	1
YNS-A3	874318.8	604452.8	72	0	150	21
YNS-A4	874395.7	605148.4	76	0	160	23
YNS-A5	873506.4	604763.4	17	0	104	0
YNS-A6A	874023.1	604283.4	63	0	127	2

APPENDIX 5

Palaeocurrent data for the onshore Zafarana Accommodation Zone

Unit	Notebook Locality	Facies	Palaeocurrent	Unidirectional or Bidirectional?
Early syn-rift Abu Zenima and Nukhul Fms (S10)				
Early syn-rift	15	Facies C1/C2	240	Unidirectional
Early syn-rift	15	Facies C1/C2	292	Unidirectional
Early syn-rift	15	Facies C1/C2	228	Unidirectional
Early syn-rift	15	Facies C1/C2	305	Unidirectional
Early syn-rift	15	Facies C1/C2	300	Unidirectional
Early syn-rift	15	Facies C1/C2	284	Unidirectional
Early syn-rift	15	Facies C1/C2	320	Unidirectional
Early syn-rift	15	Facies C1/C2	156	Unidirectional
Early syn-rift	15	Facies C1/C2	170	Unidirectional
Early syn-rift	40	Facies C1/C2	NE	Unidirectional
Early syn-rift	44	Facies C1/C2	180	Bidirectional
Early syn-rift	38	Facies C1/C2	160	Unidirectional
Early syn-rift	15	Facies C1/C2	162	Unidirectional
Early syn-rift	15	Facies C1/C2	124	Unidirectional
Early syn-rift	15	Facies C1/C2	132	Unidirectional
Early syn-rift	15	Facies C1/C2	146	Unidirectional
Early syn-rift	15	Facies C1/C2	288	Unidirectional
Early syn-rift	15	Facies C1/C2	126	Unidirectional
Early syn-rift	15	Facies C1/C2	318	Unidirectional
Early syn-rift	15	Facies C1/C2	316	Unidirectional
Early syn-rift	15	Facies C1/C2	120	Unidirectional
Early syn-rift	52	Facies C1/C2	090	Bidirectional
Early syn-rift	52	Facies C1/C2	218	Unidirectional
Early syn-rift	52	Facies C1/C2	168	Unidirectional
Early syn-rift	52	Facies C1/C2	320	Bidirectional
Early syn-rift	52	Facies C1/C2	170	Unidirectional
Early syn-rift	52	Facies C1/C2	200	Unidirectional
Early syn-rift	52	Facies C1/C2	208	Unidirectional
Early syn-rift	52	Facies C1/C2	158	Unidirectional
Early syn-rift	52	Facies C1/C2	210	Bidirectional
Early syn-rift	Wasit main rd	Facies C1/C2	064	Unidirectional
Early syn-rift	Wasit main rd	Facies C1/C2	186	Unidirectional
Early syn-rift	Wasit main rd	Facies C1/C2	350	Unidirectional
Early syn-rift	Wasit Nukhul	Facies C1/C2	342	Unidirectional
Early syn-rift	Wasit Nukhul	Facies C1/C2	300	Unidirectional
Early syn-rift	Wasit Nukhul	Facies C1/C2	282	Unidirectional
Early syn-rift	Wasit Nukhul	Facies C1/C2	318	Unidirectional
Early syn-rift	Wasit Nukhul	Facies C1/C2	242	Unidirectional
Early syn-rift	Wasit Nukhul	Facies C1/C2	301	Unidirectional
Early syn-rift	Wasit Nukhul	Facies C1/C2	272	Unidirectional
Early syn-rift	Wasit Nukhul	Facies C1/C2	011	Unidirectional
Early syn-rift	Wasit Nukhul	Facies C1/C2	018	Unidirectional
Early syn-rift	Wasit Nukhul	Facies C1/C2	012	Unidirectional
Early syn-rift	Wasit Nukhul	Facies C1/C2	280	Unidirectional
Early syn-rift	Wasit Nukhul	Facies C1	282	Unidirectional
Early syn-rift	Wasit Nukhul	Facies C1	284	Unidirectional

Early syn-rift	Wasit Nukhul	Facies C1	128	Unidirectional
Early syn-rift	Wasit Nukhul	Facies C1	296	Unidirectional
Early syn-rift	Wasit Nukhul	Facies C1	282	Unidirectional
Early syn-rift	Wasit Nukhul	Facies C2	290	Unidirectional
Early syn-rift	Wasit Nukhul	Facies C2	276	Unidirectional
Early syn-rift	Wasit Nukhul	Facies C2	290	Unidirectional
Early syn-rift	Wasit Nukhul	Facies C2	290	Unidirectional
Early syn-rift	Wasit Nukhul	Facies C2	292	Unidirectional
Early syn-rift	Wasit Nukhul	Facies C2	262	Unidirectional
Early syn-rift	40	Facies A3	310	Unidirectional
Early syn-rift	40	Facies A3	312	Unidirectional
Early syn-rift	40	Facies A3	138	Unidirectional
Early syn-rift	40	Facies A3	302	Unidirectional
Early syn-rift	40	Facies A3	314	Unidirectional
Early syn-rift	40	Facies A3	308	Unidirectional
Early syn-rift	40	Facies A3	312	Unidirectional
Early syn-rift	40	Facies A3	322	Unidirectional
Early syn-rift	40	Facies A3	158	Unidirectional
Early syn-rift	40	Facies A3	140	Bidirectional
Early syn-rift	117	Facies A3	126	Unidirectional
Early syn-rift	117	Facies A3	152	Unidirectional
Early syn-rift	117	Facies A3	168	Unidirectional
Early syn-rift	117	Facies A3	136	Unidirectional
Early syn-rift	117	Facies A3	322	Unidirectional
Early syn-rift	Wadi Wasit	Facies A3	045	Unidirectional
Early syn-rift	Wadi Wasit	Facies A3	225	Unidirectional
Early syn-rift	Wadi Wasit	Facies A2	162	Bidirectional
Early syn-rift	Wadi Wasit	Facies A2	342	Bidirectional
Early syn-rift	Wadi Wasit	Facies A2	192	Bidirectional
Early syn-rift	Wadi Wasit	Facies A2	144	Bidirectional
Early syn-rift	Wadi Wasit	Facies A2	360	Unidirectional
Early syn-rift	Wadi Wasit	Facies A2	352	Unidirectional
Early syn-rift	Wadi Wasit	Facies A2	004	Unidirectional
Early syn-rift	Wadi Wasit	Facies A2	008	Unidirectional
Lower Rudeis (S20)				
L. Rudeis	11	Facies E1	240	Unidirectional
L. Rudeis	11	Facies E1	290	Unidirectional
L. Rudeis	11	Facies E2	300	Unidirectional
L. Rudeis	12	Facies G2	078	Bidirectional
L. Rudeis	12	Facies G2	084	Bidirectional
L. Rudeis	12	Facies G2	058	Bidirectional
L. Rudeis	12	Facies G2	066	Bidirectional
L. Rudeis	21	Facies E1	260	Unidirectional
L. Rudeis	21	Facies E1	260	Unidirectional
L. Rudeis	24	Facies G2	026	Bidirectional
L. Rudeis	24	Facies G2	042	Bidirectional
L. Rudeis	24	Facies G2	040	Bidirectional
L. Rudeis	24	Facies G2	030	Bidirectional
L. Rudeis	24	Facies G2	026	Bidirectional
L. Rudeis	24	Facies G2	041	Bidirectional
L. Rudeis	24	Facies G2	038	Bidirectional
L. Rudeis	24	Facies G2	058	Bidirectional
L. Rudeis	24	Facies G2	020	Bidirectional
L. Rudeis	24	Facies G2	024	Bidirectional

L. Rudeis	24	Facies G2	018	Bidirectional
L. Rudeis	44	Facies G2	N-S	Bidirectional
L. Rudeis	38	Facies G2	SE	Unidirectional
Upper Rudeis (S30)				
U. Rudeis	10	Facies C2	280	Unidirectional
U. Rudeis	22	Facies C2	344	Unidirectional
U. Rudeis	22	Facies C2	288	Unidirectional
U. Rudeis	22	Facies C2	352	Unidirectional
U. Rudeis	22	Facies C2	258	Unidirectional
U. Rudeis	22	Facies C2	352	Unidirectional
U. Rudeis	22	Facies C2	352	Unidirectional
U. Rudeis	22	Facies C2	288	Unidirectional
U. Rudeis	22	Facies C2	258	Unidirectional
U. Rudeis	22	Facies C2	344	Unidirectional
U. Rudeis	22	Facies C2	245	Unidirectional
U. Rudeis	22	Facies C2	272	Unidirectional
U. Rudeis	22	Facies C2	308	Unidirectional
U. Rudeis	22	Facies C2	318	Unidirectional
U. Rudeis	22	Facies C2	308	Unidirectional
U. Rudeis	22	Facies C2	320	Unidirectional
U. Rudeis	70	Facies C2	N-NE	Unidirectional
U. Rudeis	55	Facies C2	355	Unidirectional
U. Rudeis	55	Facies C2	342	Unidirectional
U. Rudeis	55	Facies C2	312	Unidirectional
U. Rudeis	55	Facies C2	318	Unidirectional
U. Rudeis	55	Facies C2	300	Unidirectional
U. Rudeis	55	Facies C2	220	Unidirectional
U. Rudeis	55	Facies C2	318	Unidirectional
U. Rudeis	55	Facies C2	346	Unidirectional
U. Rudeis	55	Facies C2	345	Unidirectional
U. Rudeis	55	Facies C2	335	Unidirectional
U. Rudeis	55	Facies C2	312	Unidirectional
U. Rudeis	55	Facies C2	335	Unidirectional
U. Rudeis	55	Facies C2	330	Unidirectional
U. Rudeis	55	Facies C2	330	Unidirectional
U. Rudeis	55	Facies C2	298	Unidirectional
U. Rudeis	55	Facies C2	326	Unidirectional
U. Rudeis	55	Facies C2	328	Unidirectional
U. Rudeis	88	Facies C2	198	Unidirectional
U. Rudeis	100	Facies C2	050	Unidirectional
U. Rudeis	100	Facies C2	070	Unidirectional
U. Rudeis	100	Facies C2	032	Unidirectional
U. Rudeis	100	Facies C2	318	Unidirectional
U. Rudeis	100	Facies C2	038	Unidirectional
U. Rudeis	100	Facies C2	058	Unidirectional
U. Rudeis	100	Facies C2	032	Unidirectional
U. Rudeis	100	Facies C2	040	Unidirectional
U. Rudeis	100	Facies C2	356	Unidirectional
U. Rudeis	100	Facies C2	078	Unidirectional
U. Rudeis	100	Facies C2	240	Unidirectional
U. Rudeis	AG-11	Facies C2	268	Unidirectional
U. Rudeis	AG-11	Facies C2	284	Unidirectional
U. Rudeis	AG-11	Facies C2	286	Unidirectional
U. Rudeis	AG-11	Facies C2	278	Unidirectional

U. Rudeis	AG-11	Facies C2	276	Unidirectional
U. Rudeis	24	Facies C2	280	Unidirectional
U. Rudeis	10	Facies C2	320	Unidirectional
U. Rudeis	10	Facies C2	308	Unidirectional
U. Rudeis	10	Facies C2	290	Unidirectional
U. Rudeis	10	Facies C2	330	Unidirectional
U. Rudeis	79	Facies C2	060	Bidirectional
U. Rudeis	79	Facies C2	060	Bidirectional
U. Rudeis	79	Facies C2	035	Bidirectional
U. Rudeis	79	Facies C2	062	Bidirectional
U. Rudeis	79	Facies C2	052	Bidirectional
U. Rudeis	79	Facies C2	165	Unidirectional
U. Rudeis	79	Facies C2	132	Unidirectional
U. Rudeis	79	Facies C2	154	Unidirectional

Location co-ordinates

Location	Latitude	Longitude
15	29°18'10.88"N	33° 2'55.92"E
40	29°18'11.87"N	32°58'55.68"E
44	29°19'53.06"N	33° 1'50.30"E
38	29°15'26.49"N	32°56'52.20"E
52	29°15'7.84"N	32°57'35.24"E
Wasit Main Rd	29°14'0.31"N	32°57'16.31"E
Wasit Nukhul	29°14'12.96"N	32°57'44.58"E
117	29°21'32.20"N	33° 2'14.66"E
Wadi Wasit	29°14'6.01"N	32°57'40.95"E
11	29°19'28.36"N	33° 1'27.17"E
21	29°20'34.56"N	33° 0'41.34"E
22	29°19'6.52"N	32°59'21.72"E
24	29°16'11.13"N	33° 1'3.20"E
10	29°19'23.47"N	33° 1'11.45"E
70	29°16'28.89"N	33° 0'46.29"E
55	29°16'19.67"N	33° 0'52.20"E
88	29°17'50.88"N	32°57'48.21"E
100	29°15'16.14"N	32°55'0.66"E
AG-11	29°17'23.90"N	33° 2'42.39"E
79	29°20'45.47"N	33° 0'30.04"E